frontiers | Research Topics

# Disturbance, resilience and restoration of wetlands

**Edited by**
Chuanyu Gao, Klaus-Holger Knorr, Huai Chen and He Yixin

**Published in**
Frontiers in Ecology and Evolution
Frontiers in Environmental Science

ISSN 1664-8714
ISBN 978-2-8325-2551-7
DOI 10.3389/978-2-8325-2551-7

## About Frontiers

Frontiers is more than just an open access publisher of scholarly articles: it is a pioneering approach to the world of academia, radically improving the way scholarly research is managed. The grand vision of Frontiers is a world where all people have an equal opportunity to seek, share and generate knowledge. Frontiers provides immediate and permanent online open access to all its publications, but this alone is not enough to realize our grand goals.

## Frontiers journal series

The Frontiers journal series is a multi-tier and interdisciplinary set of open-access, online journals, promising a paradigm shift from the current review, selection and dissemination processes in academic publishing. All Frontiers journals are driven by researchers for researchers; therefore, they constitute a service to the scholarly community. At the same time, the *Frontiers journal series* operates on a revolutionary invention, the tiered publishing system, initially addressing specific communities of scholars, and gradually climbing up to broader public understanding, thus serving the interests of the lay society, too.

## Dedication to quality

Each Frontiers article is a landmark of the highest quality, thanks to genuinely collaborative interactions between authors and review editors, who include some of the world's best academicians. Research must be certified by peers before entering a stream of knowledge that may eventually reach the public - and shape society; therefore, Frontiers only applies the most rigorous and unbiased reviews. Frontiers revolutionizes research publishing by freely delivering the most outstanding research, evaluated with no bias from both the academic and social point of view. By applying the most advanced information technologies, Frontiers is catapulting scholarly publishing into a new generation.

## What are Frontiers Research Topics?

Frontiers Research Topics are very popular trademarks of the *Frontiers journals series*: they are collections of at least ten articles, all centered on a particular subject. With their unique mix of varied contributions from Original Research to Review Articles, Frontiers Research Topics unify the most influential researchers, the latest key findings and historical advances in a hot research area.

Find out more on how to host your own Frontiers Research Topic or contribute to one as an author by contacting the Frontiers editorial office: frontiersin.org/about/contact

# Disturbance, resilience and restoration of wetlands

**Topic editors**

Chuanyu Gao — Northeast Institute of Geography and Agroecology, Chinese Academy of Sciences (CAS), China

Klaus-Holger Knorr — University of Münster, Germany

Huai Chen — Chengdu Institute of Biology, Chinese Academy of Sciences (CAS), China

He Yixin — Key Laboratory of Mountain Ecological Rehabilitation and Biological Resource Utilization, Chengdu Institute of Biology, Chinese Academy of Sciences (CAS), China

**Citation**

Gao, C., Knorr, K.-H., Chen, H., Yixin, H., eds. (2023). *Disturbance, resilience and restoration of wetlands*. Lausanne: Frontiers Media SA.

doi: 10.3389/978-2-8325-2551-7

# Table of contents

frontiers | Frontiers in Ecology and Evolution

TYPE Editorial
PUBLISHED 11 May 2023
DOI 10.3389/fevo.2023.1166223



OPEN ACCESS

EDITED AND REVIEWED BY
Daniel M. Ricciuto,
Oak Ridge National Laboratory (DOE),
United States

*CORRESPONDENCE
Chuanyu Gao
✉ gaochuanyu@iga.ac.cn

RECEIVED 15 February 2023
ACCEPTED 17 April 2023
PUBLISHED 11 May 2023

CITATION
Gao C, Knorr K-H, Chen H and He Y (2023) Editorial: Disturbance, resilience, and restoration of wetlands.
*Front. Ecol. Evol.* 11:1166223.
doi: 10.3389/fevo.2023.1166223



# Editorial: Disturbance, resilience, and restoration of wetlands

Chuanyu Gao[1]*, Klaus-Holger Knorr[2], Huai Chen[3] and Yixin He[3]

[1]Key Laboratory of Wetland Ecology and Environment, Northeast Institute of Geography and Agroecology, Chinese Academy of Sciences, Changchun, China, [2]ILÖK, Ecohydrology and Biogeochemistry Group, University of Münster, Münster, Germany, [3]Key Laboratory of Mountain Ecological Restoration and Bioresource Utilization and Ecological Restoration Biodiversity Conservation Key Laboratory of Sichuan Province, Chengdu Institute of Biology, Chinese Academy of Sciences, Chengdu, China

KEYWORDS

**wetland, peatland, biogeochemistry, paleoecology, resilience, restoration**

Editorial on the Research Topic
Disturbance, resilience and restoration of wetlands

Wetlands, including peatlands, marshes, swamps, and coastal wetlands, contain more than 30% of terrestrial soil carbon on only 8% of the Earth's land surface (Mitsch and Gosselink, 2007). Due to their specific biodiversity and ecosystem function, and linking terrestrial and aquatic systems, wetlands are key players in the most important ecosystem services, especially water regulation, nutrient retention, and carbon cycling. The accumulation of peat in wetlands not only results in high carbon stocks in these systems but also provides invaluable archives of past wetland biomes and regional environmental conditions (Yu et al., 2010). However, in recent decades, the area of wetlands is decreasing due to land use change and the residual wetlands are prone to degradation globally (Davidson et al., 2018). The remaining wetland area is also sensitive to global climatic change and faces many natural and anthropogenic disturbances, such as drainage, global warming, fire, biological invasions, degradation, land use change, pollution impact, etc. (Battisti et al., 2016). However, the lack of clear definitions and limited data for the entire range of existing wetland ecosystems poses challenges to assessing ecosystem functions and biodiversity and thus limits our understanding of mitigating the numerous impacts. Thus, the purpose of this Research Topic is to bring together the latest research on wetland ecology and disturbance ecology to better understand wetland resilience, spanning over the entire range of possible wetland systems and allowing for an isolated view of individual systems.

Due to the high amount of carbon stored in wetlands, the ongoing degradation of wetlands causes an increased release of carbon into the atmosphere and further promotes global warming. In this Research Topic, Apori et al. present a scientometric analysis based on 522 documents to assess the status and the global trends of degraded peatlands and restoration research. Considering many countries have degraded more than half of their original peatland coverage for agriculture and energy use or peat harvest, the major aim of peatland restoration is to decrease greenhouse gas emissions and enhance biodiversity conservation. Great Britain and Germany are very active countries on this topic. Based on 12 sites in Zoige alpine wetlands with different degrees of degradation, Yang et al. found that the rate of carbon sequestration increased by 25.70% from natural wetlands to slightly degraded conditions. However, from slightly degraded wetlands to severely degraded wetlands, carbon accumulation sharply decreased by 81.67%. Returning systems to near-natural states will thus help to preserve their carbon sink function. Wetland degradation significantly reduced soil water content, soil organic carbon, microbial biomass carbon, and microbial biomass nitrogen, which were hypothesized as potential reasons that explain the decrease of carbon sequestration.

Climate, one of the direct driving factors of vegetation development, is expected to play a critical role in the spatiotemporal patterns of wetland vegetation communities and resulting carbon storage, especially in recent years under global warming. In this Research Topic, Yan focuses on revealing the association between climate factors and net primary productivity (NPP) of freshwater marsh wetlands in Sanjiang Plain, which is the largest freshwater marsh wetland distribution region in China. In the last 60 years, solar radiation had the largest explanatory power on the spatial distribution of NPP before 1985, and the temperature was the most important climate factor after 1985. Another study from Zong et al. aims to predict the distribution of suitable habitat areas for the *Deyeuxia angustifolia* community in the Tumen River Basin under the current and future BCC-CSM1-1 models combined with the MaxEnt model. They found that the areas of the high-fitness region are approximately 2,268.40 $km^2$ (10.03%) and that these areas are decreasing under both RCP2.6 and RCP8.5 scenarios and the center of the habitat will move to the eastern region of the Tumen River Basin.

Water-logged anoxic conditions are the most important factors that promote and sustain carbon accumulation in wetlands. Correspondingly, changes in the hydrological processes and dynamics under climate change and human activities have been attracting attention to these studies globally. In this Research Topic, Liu Y. et al. highlight the importance of hydrodynamic characteristics on the stability and self-maintenance of the inland saline-alkali wetland. The results show that water resources act as the major factor that affects the dynamic characteristics of the wetland surface water and groundwater. The observed differences in submerged areas of the studied wetland between the wet and dry seasons amounted to a total of 250 $km^2$. There are four papers that focus on evaluating the effects of the hydrological processes on delta wetlands in the Yellow River Delta, China. Wang X. et al. evaluate the effects of hydrological connectivity blocking on *Suaeda Salsa* development, and they found moderate burial was beneficial for seedling emergence; moderate salinity (10–20 g. $kg^{-1}$) and fluctuating water levels (0–10 cm water depth) were the most suitable conditions for seed germination and vegetation growth. The changes in hydrological gradients also caused differences in soil iron contents across different vegetation communities. Liu X. et al. found higher iron content in the *Spartina alterniflora* community in the upper intertidal zone and the *Phragmites australis* community in the lower intertidal zone. Sun et al. report that the soil quality decreased from inland areas to the coastline and from reclaimed wetlands to tidal flats along with the change in vegetation type. High hydrological connectivity and diverse micro-habitats in the tidal creek section of the river estuary was a driver of the structures of the bacterial communities in different habits. Wang Z. et al. found that the bacterial community diversities, as well as the dominant bacteria *Flavobacteriia* and *d-Proteobacteria* but in reverse to *Bacteroidetes* and *Gemmatimonadetes,* significantly decreased with distance away from tidal creeks.

With climate change and increasing human impact, more nutrients accumulate in wetland soils, which may increase carbon decomposition yet promote vegetation growth, thus altering the carbon turnover of wetlands. There are four studies that focus on evaluating changes in available nutrients in wetland soils and their effects on wetland vegetation growth or soil properties. Li, Zhang et al. evaluate changes in C/N/P stoichiometry and water use efficiency of *Messerschmidia sibirica* and the soil in the Yellow River Delta. They found that water use efficiency had a positive correlation with the leaf C and N content and a negative correlation with the leaf C/N ratio, which indicates that *M. sibirica* can compensate for the decline in N use efficiency through the improvement of water use efficiency. Li, Yuan et al. evaluate the short- (3 years) and long-term (10 years) effects of N and P fertilization on the physicochemical properties of peat and water in a bog-fen complex in northern China. They found that short-term fertilization increased *Sphagnum* moss cover, while the expansion of vascular plants was found owing to continuing long-term fertilization. However, the changes in carbon input and decomposition process constrained the variation in the soil C concentrations when the cumulative amount of external N and P increased. Changes in hydrogeochemical processes also control the salinity of water in specific saline-alkali wetlands. Cui et al. thus analyze the spatial distribution characteristics of water hydrochemistry and salinity in an inland saline-alkali wetland in northeast China. The results show that the water in the studied wetland is at a risk of salinization owing to a high rate of evaporation while the solutes in the water are primarily derived from aquifer leaching. Wetlands can also remove phosphorus from sewage, and constructed wetlands are widely used for water purification. Zhang J. et al. analyzed experimental data reported in 27 papers to evaluate the nitrogen and phosphorus removal characteristics of vegetated steel slag substrate-constructed wetlands. Combining steel slag with other substrate materials in constructed wetlands significantly increased the removal amount of total nitrogen and ammonium nitrogen but reduced the removal amount of total phosphorus. Moreover, changes in physicochemical parameters (e.g., temperature and pH) significantly affected the N and P removal capacity.

The increasing regional human activities not only cause changes in the hydrological dynamics and nutrient budgets but also cause direct effects on wetlands, such as reclaiming, burning, species invasion, and heavy metal pollution. In this Research Topic, Wei et al. aim to reveal the response of nutrient stoichiometry in helophyte species *Glyceria spiculosa* under agricultural intervention. They report the highest increase in plant leaf N/P ratio in nutrient-rich wetlands followed by that in drained and cultivated wetlands, but the N/P ratio in root and root hair showed no significant changes under different agricultural interventions. Gao et al. focus on evaluating the litter decomposition of *Calamagrostis angustifolia* and the loss of key elements from litters in burned wetland sites. They found that autumn burning promotes more mass loss and accelerates the decomposition of plant litter, whereas spring burning decreases the decomposition rates of plant litter. The N/P ratios in residual plant litter indicated that N acted as the limiting element for plant litter decomposition in *C. angustifolia* wetlands, and the limitation increased with increasing decomposition time. Jiang et al. focus on evaluating heavy metal pollution in lake sediments in Xingkai Lake and Xiaoxingkai Lake in hydrologically connected periods and disconnected periods in 2021. They found that the overall

contamination level and potential ecological risk of heavy metals in these two lakes were low but relatively higher in the small lake than those in the large lake based on the geo-accumulation index and potential ecological risk index, mainly driven by agricultural activities. Yuan et al. also focus on heavy metal pollution in a lake, and *in-situ* and high-resolution information on metals at the sediment-water interface under ice cover in Chagan Lake was obtained. The results show that the concentrations of Pb and As in Chagan Lake were a little higher even under the ice than in other freshwater rivers and lakes, and the diffusive fluxes showed that the sediments indeed acted as a sink for Pb and Cd, while Cu, Zn, Mn, and As were released from sediments into the overlying water.

Wetland restoration became a major task and mitigation measure to maintain or restore the ecological functions of wetlands in recent years. Therefore, developing a simple and effective strategy for wetland restoration has become an urgent global concern for ecologists. In this Research Topic, Zhang M. et al. focus on restoring salinized wetlands and evaluating the effects of Melatonin Priming on *Suaeda corniculata* seed germination, antioxidant defense, and reserve mobilization. They found the priming of *S. corniculata* seeds with 50 mM melatonin significantly improved the germination index, superoxide dismutase, and peroxidase activity. However, the stress tolerance ability of *S. corniculata* seeds was reduced by high melatonin concentrations. Kowal et al. evaluate the water clarity and submersed aquatic vegetation cover after the exclusion of invasive common carp from the Delta Marsh in Manitoba. They found that the exclusion of large carp from the delta wetland resulted in increased water clarity, higher submersed aquatic vegetation cover, and species richness. Besides large carp, the delta wetland was also threatened by other stressors (e.g., increasing nutrient loading, stabilized water levels, and invasive hybrid cattail), which will also necessitate an ongoing assessment of wetland conditions.

In summary, the Research Topic widely discusses the response of wetlands to both natural and anthropogenic disturbances. We recognize there were few contributions that evaluated the resilience of wetlands under disturbances. We thus want to encourage more research related to this topic and hope that this compilation of articles will stimulate further work and help researchers and government managers understand the response of wetland ecological functions to climate change and human activities.

## Author contributions

CG wrote the first draft of the manuscript, which was edited by all co-authors and approved. All authors contributed to the article and approved the submitted version.

## Acknowledgments

We thank all the contributing authors for their excellent manuscripts.

## Conflict of interest

The authors declare that the research was conducted in the absence of any commercial or financial relationships that could be construed as a potential conflict of interest.

## Publisher's note



## References

Battisti, C., Poeta, G., and Fanelli, G. (2016). *An Introduction to Disturbance Ecology*. New York City, NY: Springer International Publishing.

Davidson, N.C., Fluet-Chouinard, E., and Finlayson, C.M. (2018). Global extent and distribution of wetlands: trends and issues. *Marine Freshwater Res.* 69, 620. doi: 10.1071/mf17019

Mitsch, W.J., and Gosselink, J.G. (2007). *Wetlands*. Hoboken, NJ: John Wiley and Sons, Inc.

Yu, Z., Loisel, J., Brosseau, D.P., Beilman, D.W., and Hunt, S.J., (2010). Global peatland dynamics since the Last Glacial Maximum. *Geophys. Res. Lett.* 37, 1–5. doi: 10.1029/2010gl043584

frontiers | Frontiers in Ecology and Evolution

ORIGINAL RESEARCH
published: 17 June 2022
doi: 10.3389/fevo.2022.939431

# Determination of the Hydrodynamic Characteristics of a Typical Inland Saline-Alkali Wetland in Northeast China

*Yan Liu[1,2], Geng Cui[2]*, Shouzheng Tong[2], Shan Wang[1,2] and Xianguo Lu[2]*

*[1] School of Geographical Sciences, Changchun Normal University, Changchun, China, [2] Northeast Institute of Geography and Agroecology, Chinese Academy of Sciences, Changchun, China*

OPEN ACCESS

**Edited by:**
*He Yixin,*
*Key Laboratory of Mountain Ecological Rehabilitation and Biological Resource Utilization, Chengdu Institute of Biology (CAS), China*

**Reviewed by:**
*Zhiqiang Tan,*
*Nanjing Institute of Geography and Limnology (CAS), China*
*Wenjun Cai,*
*Taiyuan University of Technology, China*

***Correspondence:**
*Geng Cui*
*cuigeng@iga.ac.cn*

**Specialty section:**
*This article was submitted to Conservation and Restoration Ecology, a section of the journal Frontiers in Ecology and Evolution*

**Received:** *09 May 2022*
**Accepted:** *31 May 2022*
**Published:** *17 June 2022*

**Citation:**
*Liu Y, Cui G, Tong S, Wang S and Lu X (2022) Determination of the Hydrodynamic Characteristics of a Typical Inland Saline-Alkali Wetland in Northeast China. Front. Ecol. Evol. 10:939431. doi: 10.3389/fevo.2022.939431*

Hydrological connectivity in wetland ecosystems comprises a combination of hydrodynamic, hydrochemical, and biological characteristics. Hydrodynamic characteristics are important for the transmission of energy, matter, and information between surface water bodies and are critical for maintaining the health of wetland ecosystems. The hydrodynamic characteristics of wetlands are the temporal and spatial changes in the water level, flow direction, quantity, recharge, and discharge conditions of surface water and groundwater. Identifying wetland hydrodynamic characteristics is of great significance in revealing the hydrological patterns and biogeochemical phenomena of wetland ecosystems. The Momoge National Nature Reserve (MNNR) is a wetland located in the semi-arid region of northeast China, where the hydrodynamic characteristics are still unclear. In this study, water level monitoring of surface water and groundwater in MNNR was carried out, and wetland recharge and discharge were calculated according to a water balance analysis. The submerged wetland area was simulated based on an improved distributed hydrological model, SWAT-DSF, and compared with remote sensing data. The results showed that the dynamic characteristics of wetland surface water and groundwater are mostly affected by topography and recharge water sources. The water resources in the reserve are in a positive state of equilibrium in the wet season (September), with an equilibrium difference of $276.41 \times 10^4$ $m^3$/day. However, it displays a negative equilibrium state in dry (November) and other (June) seasons, with an equilibrium difference of $-12.84 \times 10^4$ $m^3$/day and $-9.11 \times 10^4$ $m^3$/d, respectively. The difference between the submerged areas of the MNNR wetland during the wet and dry seasons was 250 $km^2$.

**Keywords: wetland, hydrodynamic characteristic, water level monitoring, water balance, Momoge National Nature Reserve**

## INTRODUCTION

Wetlands, often vividly described as the "kidneys of the Earth" are a critical part of the surface covering of our planet. Wetlands, forests, and oceans are three major ecosystems with irreplaceable functions (Mitsch et al., 2009; Keddy, 2010). Unfortunately, the global wetland area has decreased by nearly 70% since the beginning of the 20th century (Davidson, 2014; Hu et al., 2017), resulting

in a sharp decline in the service functions of wetland ecosystems. Countries worldwide have signed the Ramsar Convention on Wetlands to deal with and prevent further deterioration. Therefore, the protection and restoration of wetlands have become crucial issues for global research (Wang Q. et al., 2021; Xi et al., 2021). Wetlands comprise interconnected terrestrial and aquatic ecosystems (Lu et al., 2020; Guo et al., 2021). Inevitably, water plays a critical role in the formation, development, succession, and extinction of wetlands. In particular, hydrological processes are essential for maintaining the balance of regional water resources and the health of wetland ecosystems (Johnston, 2020; Makungu and Hughes, 2021). Most of the transmission of matter, energy, and information is related to wetland hydrological processes and water cycles. Therefore, hydrodynamic characteristics govern the stability and self-maintenance of wetland ecosystems (Singh and Sinha, 2019).

The hydrodynamic characteristics of wetlands include temporal and spatial changes in the water level, flow direction, and water quantity, as well as the recharge and discharge conditions of wetland groundwater and surface water. Hydrodynamic processes are critical in the formation and development of wetland ecosystems and habitat patterns by reshaping wetland topography, changing habitat distribution structures, and disturbing the physical and chemical properties. They shape wetland topography and geomorphology mostly through the erosion and deposition of sediment carried by water flow. For example, the alternating distribution of shoals and deep troughs is caused by variations in flow velocity, erosion, and accumulation. While flow erosion creates the topography of deep water areas, accumulation creates the shoals (Eulie et al., 2021). Changes in hydrodynamics affect and control the distribution pattern and succession of the wetland plant community. At the local scale, water level, flow state, and other hydrological conditions cause water stress to plants in wetlands, affect plant growth, morphological characteristics, and biomass. In addition, it determines the spatial distribution pattern of wetland plants. Hydrological processes affect the evolution of wetland topography by regulating the distribution pattern of wetland plant communities and the interaction between nutrients and carbon fluxes. Hydrological processes determine the essential properties and specific ecosystem structure and function of wetlands (Evenson et al., 2018a; Qi et al., 2021; Wu et al., 2021).

Groundwater is an essential form of water and energy source for wetland ecosystems. In addition to precipitation, the groundwater spatial-temporal variability and groundwater table changes are usually driven by evaporation and transpiration (Roulet, 1990; Carlson Mazur et al., 2020; Galliari et al., 2021). Moreover, they are accompanied by changes in the structure, distribution, and development of wetland vegetation and biological communities (Budzisz et al., 2017; Chen et al., 2021). However, descriptions of underground hydrological processes are often ignored or simplified in traditional wetland research. As a result, the transformation and circulation of materials and energy between wetland and groundwater systems remain poorly understood. Thus, further research on their interaction and ecological effects is required.

The complex interactions of multi-element, multi-scale, and multi-process wetland ecosystems and the dynamic matching of hydrological, biological, and ecological processes from the viewpoint of hydrological connectivity are important problems to be solved in wetland science. Hydrodynamic processes are the basic elements of wetland ecosystems. Based on hydrogeological conditions, topographic features, and anthropogenic disturbances, the objectives of this study are as follows: (1) to analyze the characteristics of wetland surface water and groundwater levels and calculate wetland recharge and discharge based on water balance analysis, (2) to simulate the evolutionary process of submerged wetland areas, and (3) to clarify the horizontal and vertical hydrodynamic characteristics of the Momoge National Nature Reserve (MNNR). The results will provide an important basis for exploring the distribution and evolution of wetland hydrochemical characteristics to achieve the goal of a continuous process, complete structure, and stable function of wetland ecosystems.

# MATERIALS AND METHODS

## Study Area

Momoge National Nature Reserve is an inland wetland and water ecosystem reserve in the saline-alkali land of western Jilin Province, China, with a total area of 1,440 $km^2$ from 45°4225″ to 46°18″N and 123°27′0″ to 124°4′33.7″E, respectively. The Nenjiang River flows from north to south and serves as the eastern boundary of the MNNR (**Figure 1**). The altitude of the reserve is between 100 and 171 m, and the land is generally high in the northwest and low in the southeast. There are several small and large lakes surrounded by uplands in western MNNR. However, the eastern part is relatively flat with a relative elevation difference of only 2–5 m. The MNNR is located in a semi-arid region and has a temperate continental monsoon climate with an average annual temperature of 4.2°C. The highest temperature occurs in July, with an average temperature of 23.5°C, and the lowest temperature occurs in January, with an average temperature of −17.4°C. The average annual precipitation is 391.8 mm. Generally, precipitation is relatively concentrated from June to September, reaching 300 mm and accounting for 76.6% of the annual precipitation. The average annual evaporation was 1,585.1 mm, with the highest evaporation in May.

## Field Monitoring

To understand the water level fluctuation and hydrodynamic characteristics of natural water in the study area, a detailed hydrogeological survey was conducted in and around the MNNR. Sixty-one groundwater table monitoring points were arranged to cover the entire area using existing boreholes, civil wells, and exploration wells. Four water level gauges were arranged in the wetlands from west to east within the MNNR to monitor the surface water level continuously (**Figure 2**).

The groundwater table was measured in June, September, and November 2019. The specific work-monitoring means and frequencies are listed in **Table 1**. Combining continuous

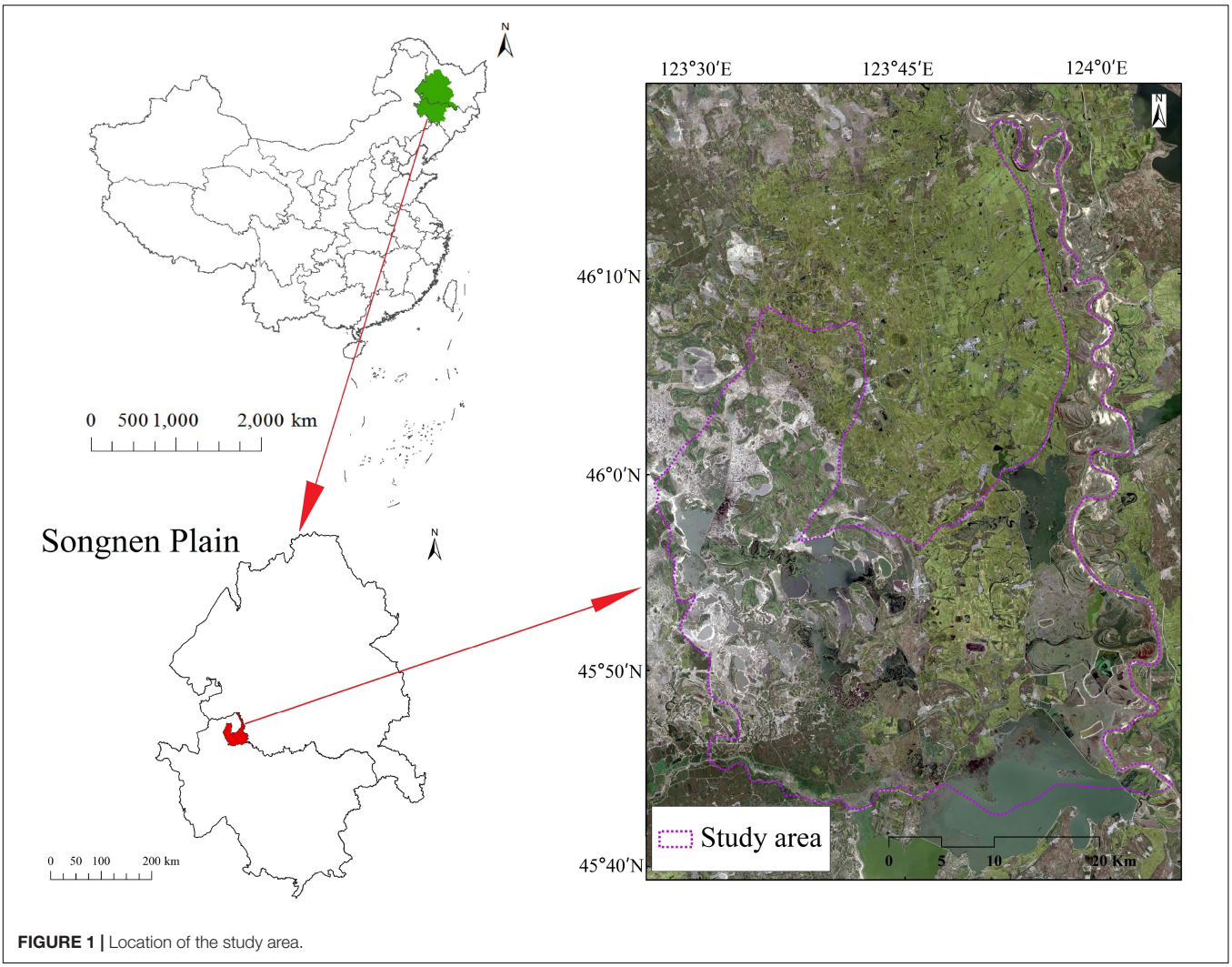


**FIGURE 1 |** Location of the study area.

groundwater table monitoring data collected from two monitoring points, Yinghua and Dongerlong, the regional multi-dimensional hydrodynamic characteristics were ascertained based on the hydrological and hydrogeological conditions and water level fluctuation at the above monitoring points.

## Analysis of Water Balance in Momoge National Nature Reserve

The water budget in the dry (November), wet (September), and other (June) seasons, including surface water and shallow groundwater, of the study area was calculated using the water balance equation:

$$\triangle Q = Q_{in} - Q_{out} \quad (1)$$

where, $\triangle Q$ is the variation in the water resources in the study area during the equilibrium period ($m^3$/day), $Q_{in}$ is the recharge of water resources during the equilibrium period ($m^3$/day), and $Q_{out}$ is the discharge of water resources during the equilibrium period ($m^3$/day).

According to the actual situation in the MNNR, the water balance equation can be specified as:

$$\triangle Q = Q_P + Q_C + Q_S - E_W - E_t - W \pm \mathrm{GW} \pm Q_{G-S} \quad (2)$$

where, $\triangle Q$ is the change in water resources storage in MNNR; $Q_P$ is the precipitation recharge; $Q_C$ is the recharge of farmland drainage; $Q_S$ is the recharge of river flooding; $E_W$ is the water surface evaporation; $E_t$ is transpiration; $W$ is groundwater extraction; GW is the lateral groundwater runoff; a positive value indicates that the groundwater recharge from the outside of the MNNR to the interior is greater than the groundwater discharge; on the contrary, a negative value indicates that the groundwater discharge is greater than the groundwater recharge; $Q_{G-S}$ is the exchange flux between groundwater and Nenjiang River; a positive value indicates that the groundwater recharges the river, and a negative value indicates that the river recharges the groundwater. The units of the above elements are $m^3$/day, and each element is calculated according to existing data and calculation formulas.

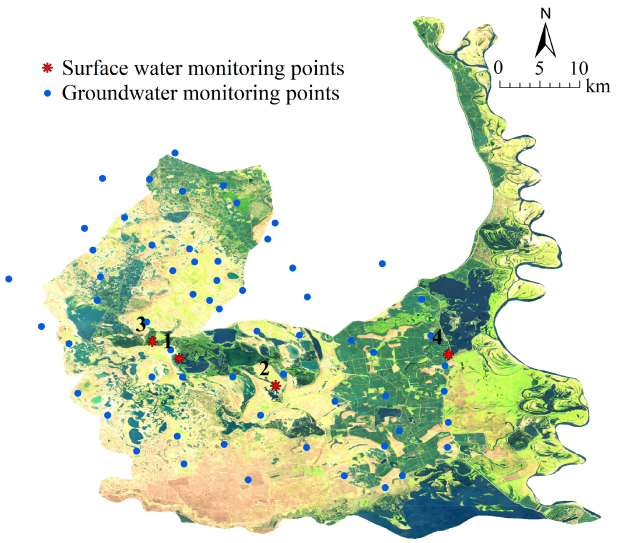


**FIGURE 2 |** Distribution of surface water level loggers and groundwater table monitoring sites (Image source: Landsat 8TM band 654 false-color combination, imaging date: June 20, 2019).

## Simulation of Wetland Hydrological Process

The improved distributed hydrological model SWAT-DSF (Depressional Storage and Flows, DSF; Evenson et al., 2018b) was utilized to simulate the wetland hydrological processes. Based on the improved SWAT model proposed by Evenson et al. (2016), three hydrological response units (HRUs) are established in the model: depressional HRUs, non-depressional HRUs discharged by the depression unit, and non-depressional HRUs discharged directly into the sub-basin. The wetland in the depression unit was simulated using the following water-balance equation:

$$\triangle V = P - \mathrm{ET} + Q_{Surf} - Q_{Spill} \pm Q_{local} \tag{3}$$

where, ΔV is the variation in wetland water storage ($m^3$/day), $P$ is the precipitation on the wetland submerged area that changes with time ($m^3$/day), ET is the evapotranspiration in the wetland submerged area ($m^3$/day), $Q_{\mathrm{Surf}}$ is the runoff flowing in from the non-depression unit in the higher terrain ($m^3$/day), $Q_{\mathrm{Spill}}$ is the surface water outflow ($m^3$/day) leaving the wetland *via* the delineated outlet for spillage (i.e., when wetland storage capacity is exceeded).

The upland portion of the depressional HRU (i.e., the upland area surrounding the wetland and contained within the HRU depressional boundary) was simulated as having the following water balance:

$$\triangle \mathrm{S} = P - \mathrm{ET} + Q_{\mathrm{lat,in}} - Q_{\mathrm{lat,\ out}} - Q_{\mathrm{gw}} \pm Q_{\mathrm{local}} \tag{4}$$

where, ΔS is the daily water volume change ($m^3$/day) in the HRU (in the soil profile, shallow aquifer, and deep aquifer), $P$ is precipitation ($m^3$/day) on the upland portion of the HRU, ET is evapotranspiration ($m^3$/day) from the upland portion of the HRU, $Q_{\mathrm{lat,in}}$ is subsurface inflow ($m^3$/day) entering the soil profile from upgradient HRUs, $Q_{\mathrm{lat,\ out}}$ is the subsurface outflow ($m^3$/day) leaving the HRU and entering either a downgradient depressional HRU or the reach, $Q_{\mathrm{gw}}$ is groundwater outflow ($m^3$/day) leaving shallow and deep aquifers and entering the reach, and $Q_{local}$ is the net subsurface flow ($m^3$/day) entering (+) or leaving (−) the upland portion *via* local exchange with a wetland.

$Q_{local}$ is simulated as:

$$Q_{local} = (\alpha \times K_{sat,w}) \times SA_{Darcy} \times \frac{|y_{wt} - y_{wet}|}{\beta \times r_{w,max}} \tag{5}$$

where, $K_{\mathrm{sat},w}$ is the saturated hydraulic conductivity (m/day) of the wetland sediments, $y_{\mathrm{wt}}$ is the upland groundwater height, $y_{\mathrm{wet}}$ is the wetland surface water level, $\mathrm{SA_{Darcy}}$ is the dynamic submerged area of the wetland, $r_{w,\mathrm{max}}$ is the radius at which the wetland reaches the maximum area, and α and β are the correction parameters.

Due to limitations of the runoff data, the data from June 2006 to June 2013 were selected to run the model (with June 2006 to June 2010 and July 2010 to June 2013 as the verification periods). Moreover, we utilized the water body coverage area, calculated by the algorithm based on the Google Earth Engine platform in our previous study (Cui et al., 2021) as the verification data.

The results directly reflected the applicability of the model to the study area. The relative error, percent bias (PBIAS), certainty coefficient, $R^2$, and Nash efficiency coefficient (NSE) were selected to evaluate the simulation results of the model in this study.

$$NSE = 1 - \left[ \frac{\sum_{i=1}^{n} \left( Q_i^{obs} - Q_i^{sim} \right)^2}{\sum_{i=1}^{n} \left( Q_i^{obs} - Q^{obs} \right)^2} \right] \tag{6}$$

$$PBIAS = \left[ \frac{\sum_{i=1}^{n} \left( Q_i^{obs} - Q_i^{sim} \right) \times 100}{\sum_{i=1}^{n} Q_i^{obs}} \right] \tag{7}$$

$$R^2 = \left[ \frac{\sum_{i=1}^{n} \left( Q_i^{obs} - Q^{obs} \right) \times \left( Q_i^{sim} - Q^{sim} \right)}{\sqrt{\sum_{i=1}^{n} \left( Q_i^{obs} - Q^{obs} \right)^2} \sqrt{\sum_{i=1}^{n} \left( Q_i^{sim} - Q^{sim} \right)^2}} \right]^2 \tag{8}$$

where, $Q_i^{\mathrm{obs}}$ is the observed value, $Q_i^{\mathrm{sim}}$ the simulated value, $Q^{\mathrm{obs}}$ is the average of the observed values, and $Q^{\mathrm{sim}}$ the average of the simulated values.

**TABLE 1 |** Water level monitoring details.

| Monitoring items | Number of monitoring points | Monitoring instruments | Monitoring frequency |
|---|---|---|---|
| Surface water level | 4 | Onset Hobo automatic recording water level gauge | Every 15 min |
| Groundwater table | 61 | Steel ruler water level gauge | Once in dry, wet and other seasons |

# RESULTS

## Changes in Surface Water Level

Water level gauges 1 and 2 were located on both sides of the road within the Baihe Lake. They lacked a surface hydraulic connection due to the presence of the road. **Figure 3** Displays that the water level at the two points fluctuated and decreased before May 17, showing the same trends, which were predominantly driven by atmospheric rainfall and evaporation. However, a water level difference of 20 cm existed at the two points due to water head loss during the underground connection formed by seepage across the road.

From May 17, the water level gradually increased when the Qianhang drainage station in the upper reaches of Baihe Lake opened its floodgates to discharge farmland irrigation water into the area where water level meter 1 was located. Furthermore, the water level at the point where water level meter 2 was located also increased because of the underground connectivity. In early August (the blue columnar area in **Figure 3**), the water in Baihe Lake overflowed and spread over the road around the Lake because of the continuous water level rise. As a result, the surface water inside and outside the road became partially connected, and the water level outside the road rose until it reached the same water level of 68 cm and further merged completely with the water inside the road.

On September 8, the sluice gate opened and water in Baihe Lake began to discharge downstream, resulting in the declination of water level. The water level outside Baihe Lake also decreased slowly due to the connection, and finally, the two tended to be consistent. The surface water inside and outside the road remained connected until it began to freeze in November. The change in surface connectivity was also caused by water level variation. Therefore, irrigation and drainage in farming are the major factors affecting water-level fluctuations from May to October. The water level variation near Baihe Lake was mostly affected by natural rainfall, evaporation, and underground connectivity when there was no irrigation water discharge. A photograph of the field is shown in **Figure 4**.

Water level gauge 3 was located on the island west of the MNNR, and water level gauge 4 was located in a pond outside the gate of the Harnao Reservoir in the northeastern part of the MNNR. As shown in **Figure 5**, although gauges 3 and 4 were geographically far apart, their fluctuation trends were very similar. Both demonstrated a good relationship with precipitation, indicating that the two points were affected by precipitation. In early August and early November 2019, the water level of gauge 4 increased with an increase in the water level of the Nenjiang River under the influence of two distinct inflow processes of the Nenjiang River. In addition, the rising range was greater than that of gauge 3. This trend reveals a minor head loss due to groundwater flow during the groundwater connection between the two points.

## Groundwater Dynamic Process

### Response of Groundwater to Precipitation

According to the precipitation data of MNNR from 2006 to 2012 and the relationship between the groundwater depth at monitoring points Yinghua and Dongerlong (**Figure 6**), precipitation indicated an overall upward trend. The groundwater depth at Yinghua also demonstrated an overall

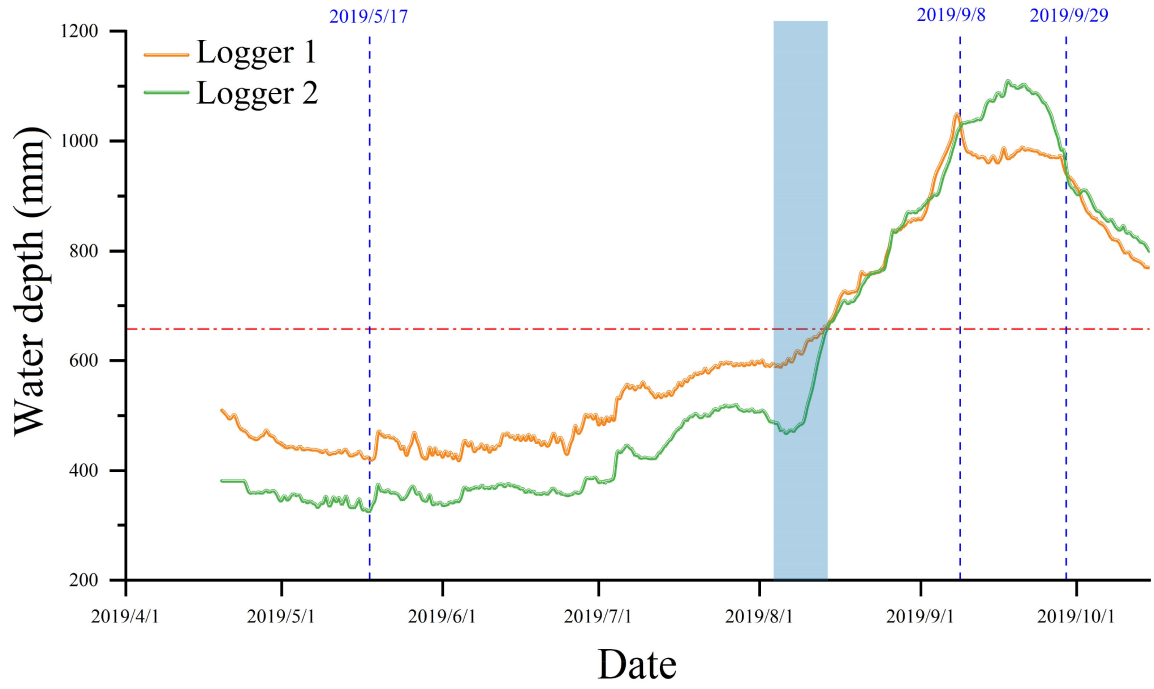


**FIGURE 3 |** Surface water level fluctuations under artificial regulation.

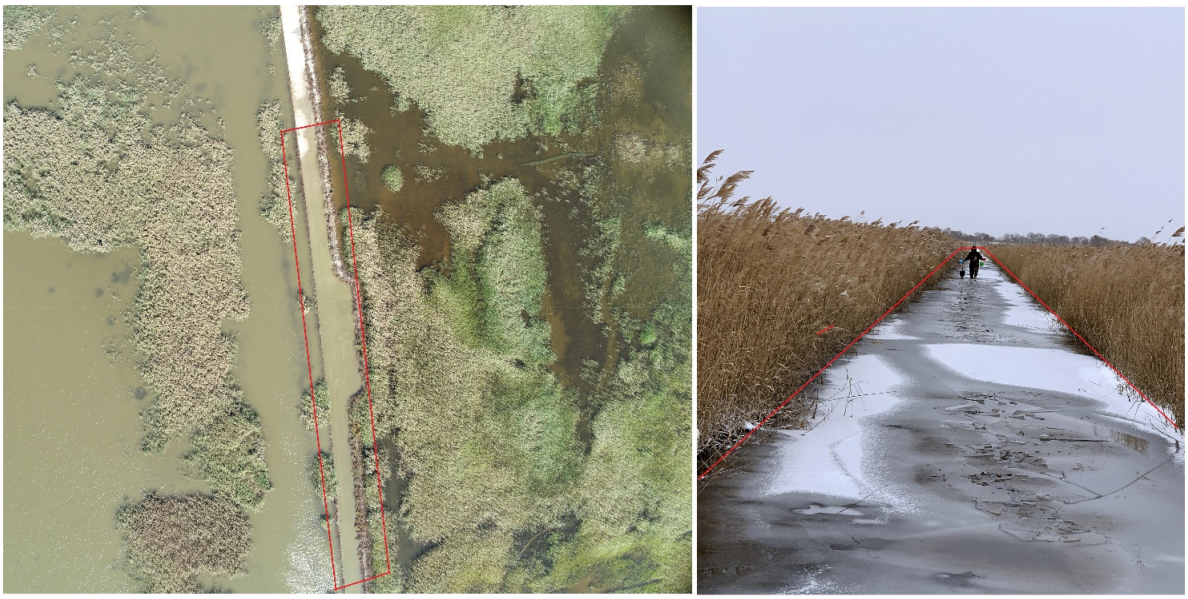

**FIGURE 4 |** Surface connection of Baihe Lake water on both sides of the road (within the red lines).

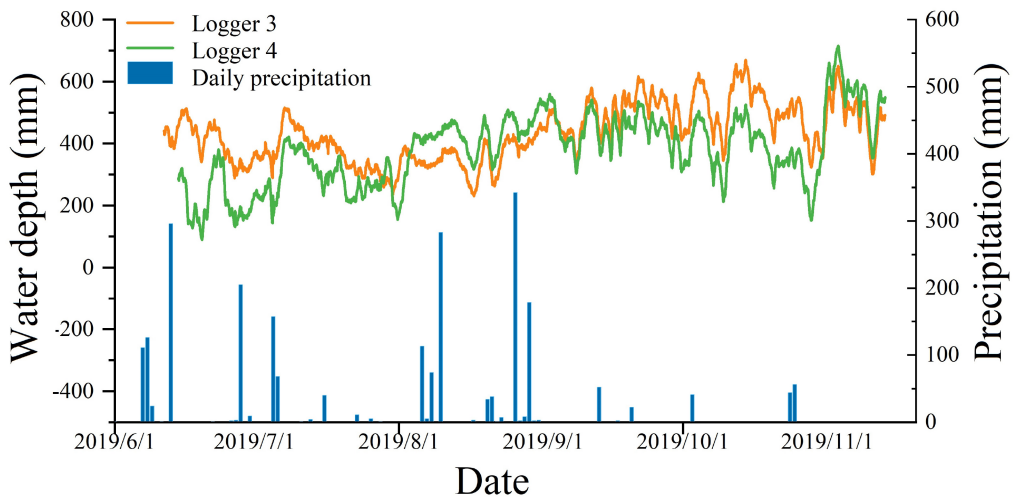


**FIGURE 5 |** Surface water level fluctuations affected by precipitation.

upward trend from 2 m in 2006 to 6 m in 2011. Although the groundwater depth in Dongerlong fluctuated, it remained at about 6 m. In the densely populated area of Yinghua, owing to the over-exploitation of groundwater, the groundwater table gradually decreased with the increase in precipitation. The decline in the groundwater level will affect the ecological environment of the wetlands, and it is necessary to explore the groundwater dynamics of MNNR further.

## Seasonal Variation of the Groundwater Flow Field

In the wet, dry and other seasons, groundwater in the MNNR generally flows from northwest to southeast, driven by the topography and aquifer floor gradient (**Figures 7**, **8**, **9**). In the northwest, groundwater flows from the uplands to the surrounding low-lying lakes, forming widely distributed isolated wetlands. In the central region, groundwater flows from west to east, and the hydraulic gradient is lower than that in the northwest. However, local differences in groundwater flow fields exist due to variations in hydrological conditions. Because of the rising water level of the Nenjiang River during the flood season, the floodplain on the west side of the Nenjiang River is submerged by the river water. Moreover, the infiltration of surface water increases the groundwater table, changing the direction of local groundwater that flows toward the west of the MNNR along the west bank of the Nenjiang River. Groundwater is discharged to the Nenjiang River the dry season and June. In the western

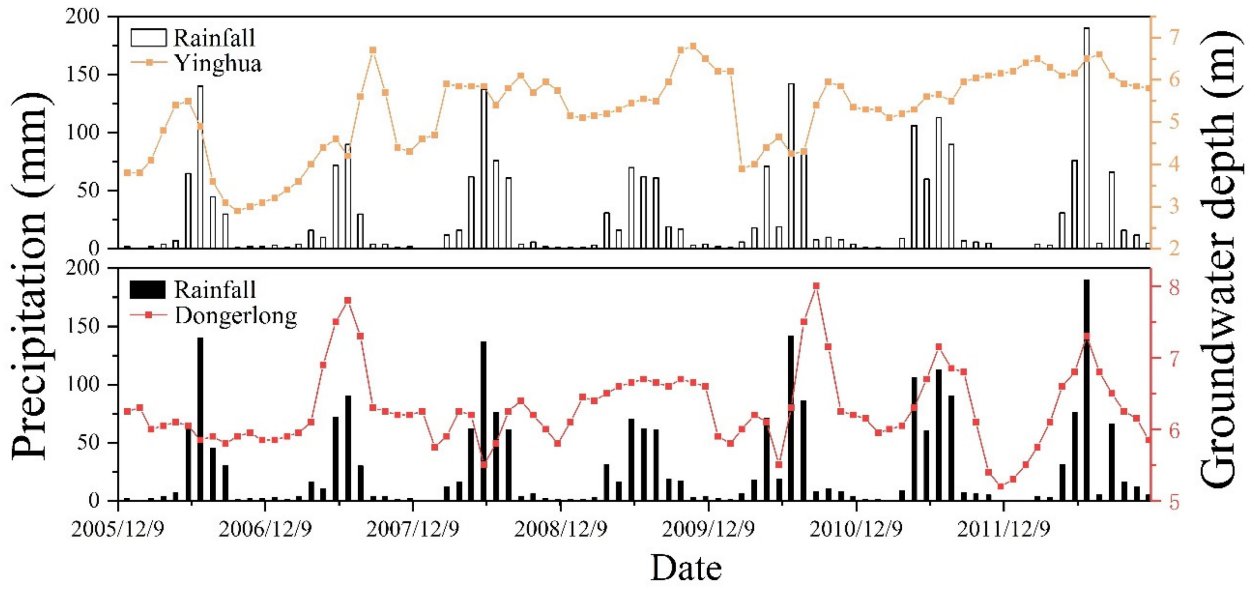


**FIGURE 6 |** Variations of groundwater depths in MNNR.

part of the reserve, there is groundwater recharge from outside the reserve in the northwest during the wet and dry seasons, which does not occur in the other season (June). In the middle of the reserve, except for the groundwater recharge to Baihe Lake from the uplands, the groundwater generally flows northwest to southeast. In the wet season, the groundwater table increases significantly, and the hydraulic gradient becomes higher due to the increase in precipitation and the rise in the river water level. By contrast, in the dry season and in June, the hydraulic gradient of groundwater is relatively low. In particular, a regional cone of groundwater depression forms in the west of the floodplain of the Nenjiang River in June.

Groundwater is a major factor maintaining the wetland water source, and the topography significantly affects the groundwater flow direction and hydraulic gradient. In addition to precipitation and artificial recharge, groundwater flows from the surrounding upland to the lake in the northwest. The evolution of groundwater flow fields in the central and eastern regions was mostly affected by the precipitation and hydrological conditions of the Nenjiang River.

## Water Balance Calculation

The primary water sources of MNNR include precipitation, surface runoff, irrigation drainage, groundwater lateral runoff, and river infiltration. The recharge and discharge of the MNNR water resources and equilibrium calculation results are listed in **Table 2**. The water resources in the MNNR were in negative equilibrium during the dry season and in the month of June, with equilibrium differences of $-12.84 \times 10^4$ and $-9.11 \times 10^4$ $m^3$/day, respectively. These results indicate that water surface evaporation significantly affects the volume of water resources in the MNNR. During the wet season, the water resources in MNNR were in positive equilibrium, and the equilibrium difference was $276.41 \times 10^4$ $m^3$/day. The increase in water resources mostly emerged from the floodplain submerged by the flood of the Nenjiang River.

## Simulation Results of Submerged Area in Momoge National Nature Reserve

The submerged area of the wetlands varied considerably between 2010 and 2013 (**Figure 10**). The extent was approximately 50 $km^2$ in the dry season, and a small peak occurred during the snowmelt period. While the area was generally approximately 300 $km^2$ in the wet season, it reached 400 $km^2$ in 2012. The simulation results were generally lower in the wet season and higher in the dry season than observed in the remote sensing observations. This trend was due to the influence of high vegetation coverage on remote sensing calculations and the calculation error of groundwater recharge by the SWAT-DSF. The water level and wetland discharge can be inferred based on their correlation with submerged areas.

As for the model simulation accuracy, PBIAS was within ±20%, NSE > 0.5, and $R^2$ > 0.6 (**Table 3**), which met the requirements of model simulation accuracy. In addition, the simulation result of the validation period was better than that of the calibration period. Therefore, the model results are reliable.

# DISCUSSION

## Horizontal Hydrodynamic Processes

The analysis of the surface water level fluctuation in the western part of the MNNR demonstrated that the lakes were mostly linked by hydrodynamic connections. The surface water area of the floodplain expands and shrinks with the seasons. When the level of the Nenjiang River exceeds the banks or

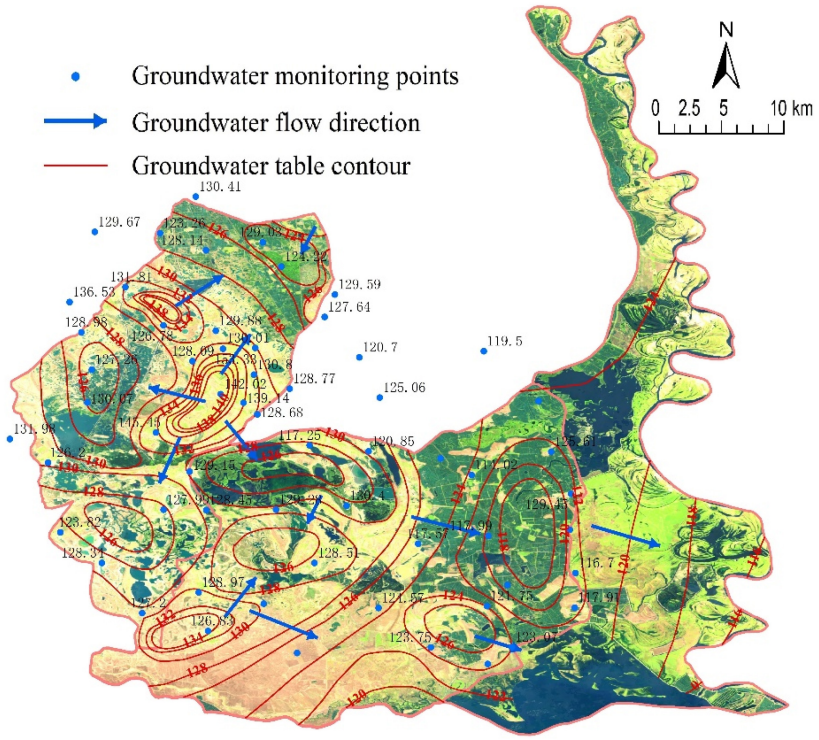


**FIGURE 7 |** Groundwater table contour in June 2019 (a.m.s.l).

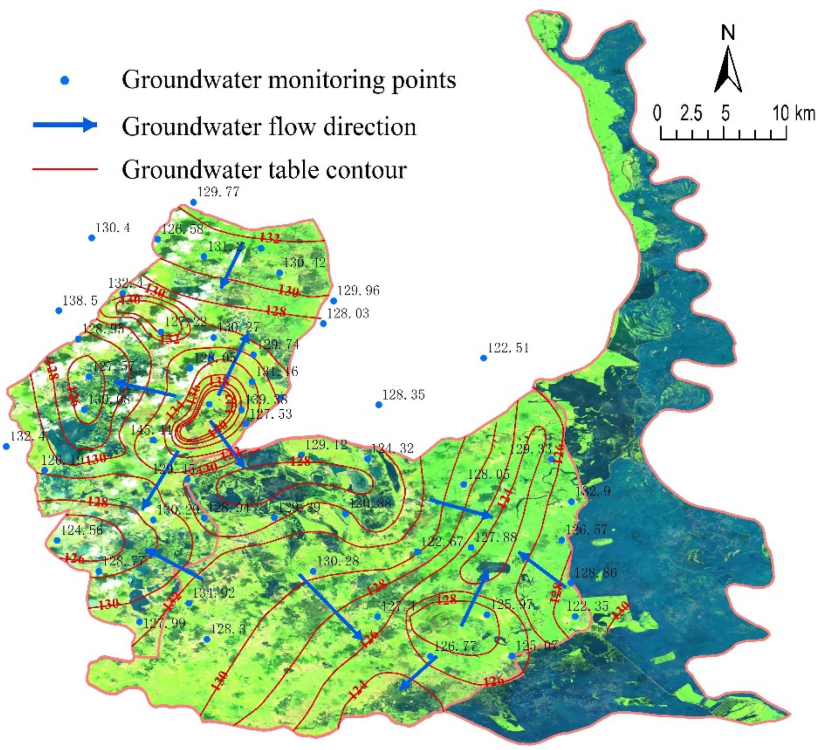


**FIGURE 8 |** Groundwater table contour in September 2019 (a.m.s.l).

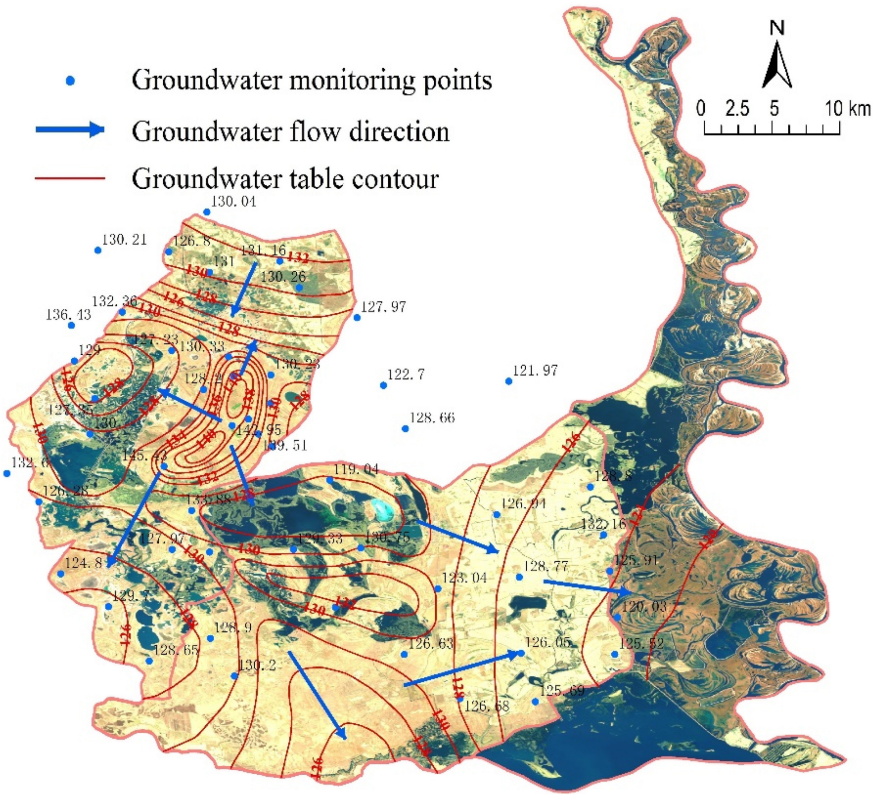


**FIGURE 9 |** Groundwater table contour in November 2019 (a.m.s.l).

**TABLE 2 |** Water balance calculation results of MNNR (Unit: $\times 10^4$ $m^3$/day).

| Source/sink term | | Jun. | Sep. | Nov. |
|---|---|---|---|---|
| Recharge | Precipitation | 18.95 | 5.45 | 0.95 |
| | Surface runoff | 0 | 359.33 | 0 |
| | Irrigation drainage | 5.06 | 8.55 | 0 |
| | Lateral groundwater runoff | 6.75 | 9.86 | 5.67 |
| | River infiltration | 0 | 9.65 | 0 |
| Total | | 30.77 | 392.85 | 6.63 |
| Discharge | Water surface evaporation | 29.85 | 109.87 | 14.71 |
| | Transpiration | 2.98 | 2.34 | 0 |
| | Groundwater exploitation | 1.00 | 0.75 | 0.55 |
| | Base flow | 2.60 | 0.88 | 1.64 |
| | Lateral groundwater runoff | 3.46 | 2.60 | 2.56 |
| Total | | 39.90 | 116.44 | 19.47 |
| Equilibrium difference | | −9.11 | 276.41 | −12.84 |

embankments, the floodplain is submerged. In depressions, the surface water forms permanent or seasonal wetlands when the river level drops. The surface water in the uplands flows back to the river or infiltrates the shallow aquifer. The horizontal hydrodynamic processes mostly occur on the surface. Previous research has shown that there are three mechanisms of horizontal hydrodynamic processes: fill-spill, fill-merge, and river-floodplain connections.

When the net inflow of an upland wetland exceeds its capacity, the water overflows into another lower-lying wetland, called a fill-spill (Spence and Woo, 2003; Tromp-van Meerveld and McDonnell, 2006; **Figure 11A**). Fill-merge occurs when the water depth of one depression exceeds the internal overflow point of another adjacent depression. In this case, the flow of material is bidirectional rather than the unidirectional flow occurring during fill-spill (Leibowitz et al., 2016; Grimm and Chu, 2020; **Figure 11B**). Although the wetland storage within the floodplain differs, the floodplain can reduce and delay flooding by storing the water overflow from the riverbank. The floodplain is a depression outside the natural river embankment, including perennial and seasonal wetlands, among which the seasonal wetlands are primarily controlled by periodic floods (**Figure 11C**). The surface water level monitoring results indicate that the wetlands west of the MNNR achieve hydraulic connection by fill-spill. In contrast, wetlands within the floodplain are hydraulically connected by fill-merge and river-floodplain connections.

## Vertical Hydrodynamic Processes

Wetlands may recharge or discharge groundwater due to variations in the hydrogeological conditions. The surface water-groundwater exchange flux is affected by the hydraulic gradient of the groundwater and wetland surface water along with the hydraulic conductivity of the aquifer and wetland sediment.

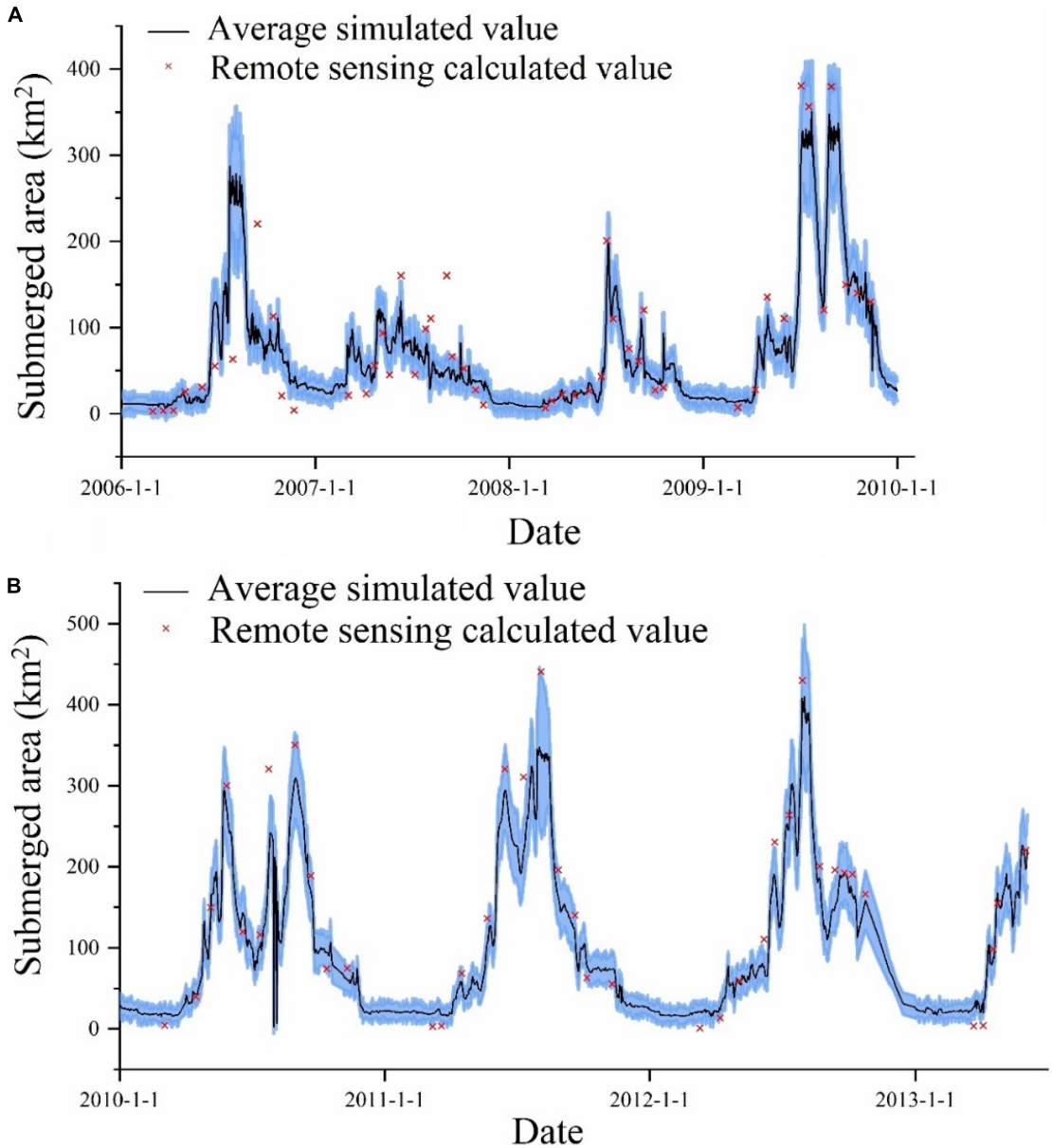


**FIGURE 10 |** Simulations and remote sensing observations of the total submerged area of wetland (**A:** calibration period; **B:** validation period; blue area represents the range given across all parameter sets as evaluated for the calibration period).

Precipitation, topography, and underground runoff are the major factors affecting the groundwater flow field in the study area. The hydrodynamic characteristics and seasonal variation of groundwater in the MNNR show that the upland topography around the lakes and the high permeability of the phreatic aquifer of Pleistocene sand and loess sub-sand provide favorable conditions for the flow of groundwater to the lakes. The regional groundwater flow field displays a hydraulic relationship between the wetland water and the surrounding groundwater in the uplands, which is predominantly affected by the shallow local groundwater flow system (**Figure 12**). However, the recharge mode (such as vertical or lateral recharge) and recharge intensity of groundwater to lake water differ, owing to the difference in hydraulic gradient and hydraulic conductivity of the sediment and aquifer. There may be an unsaturated zone of a certain thickness under the lake sediment due to very fine-grained silt with low permeability, which can affect the exchange flux between wetland surface water and groundwater.

Hydrodynamic processes are formed by surface-underground connectivity. In addition, a comprehensive analysis of topographic features and statistical characteristics of hydrological processes controlled by depressions will help reveal the internal relationship between them and improve watershed modeling.

**TABLE 3 |** Results of the model verification indices.

| | Calibration (2006.1–2009.12) | Validation (2010.1–2013.6) |
|---|---|---|
| NSE | 0.699 | 0.823 |
| R2 | 0.7 | 0.864 |
| PBIAS | −1.80% | −1.19% |

## Simulation of Hydrological Processes in Wetland

Under the premise of a known topography, there is a functional relationship between the volume of water resources and the wetland water level. The water level and volume directly affect the hydrodynamic characteristics. Therefore, it is important to obtain accurate water quantities and water levels. The hydrological processes of small-scale wetlands can be evaluated using on-site monitoring (Clilverd et al., 2013). However, it is impractical to explore the hydrological/hydraulic interactions between wetlands and other water bodies and aquifers in large catchment areas (Fan and Miguez-Macho, 2011). The application of hydrological models is a common method for studying the hydrological processes of large-scale wetlands and watersheds. Watershed hydrological models have been developed from lumped conceptual models to physics-based distribution models. Furthermore, wetlands are directly or indirectly included in watershed-scale models (Singh, 1997).

In the standard semi-distributed hydrological model, it is assumed that the entire area of the basin is well connected with its related outlet. In addition, the surface depression is usually concentrated at a depth to provide water storage and discharge functions for the entire basin. However, practically, the contribution area of the watershed is variable and can be significantly affected by the spatial distribution and dynamic connectivity of depressions (Wang N. et al., 2021). Direct water exchange between wetlands and other water bodies is limited. From the perspective of filling and overflow, wetlands can establish hydrological connectivity with downstream wetlands through local surface flow paths (Brierley et al., 2013). The recharge and discharge of wetlands and downstream water surface-groundwater exchange between wetlands and the surrounding uplands (Hayashi et al., 2016; Ameli and Creed, 2017) are important for the hydrological process of the depression, but they are not completely reflected in most watershed hydrological models. Therefore, a distributed hydrological model is required for improved simulations of

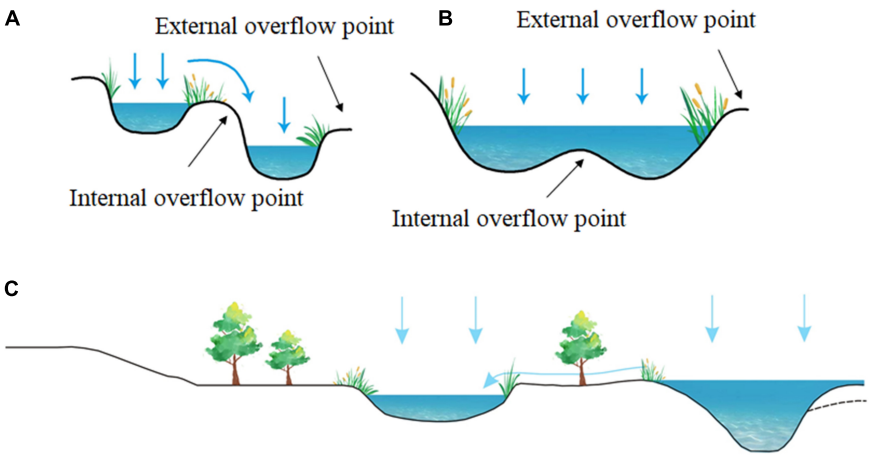


**FIGURE 11 |** Mechanisms and types of surface hydrodynamic process (**A**. fill-spill; **B**. fill-merge; and **C**. river-floodplain connections).

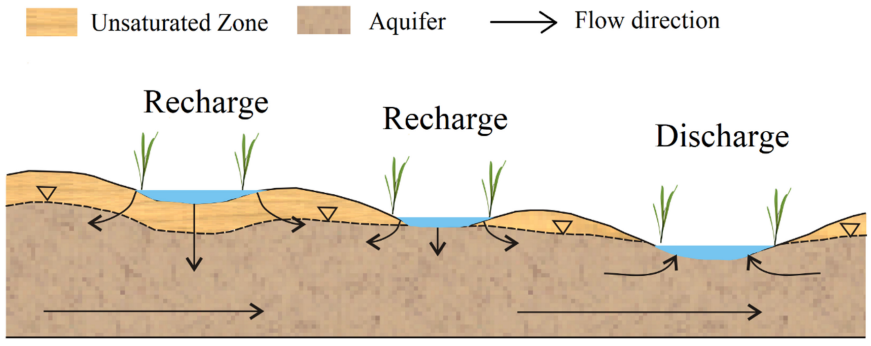


**FIGURE 12 |** Schematic diagram of local groundwater flow system in wetland (modified from Hayashi et al., 2016).

wetland hydrological processes. In addition, an improved spatial resolution is required to predict and manage hydrological, biogeochemical, and biological functions on a larger spatial scale.

The SWAT model provides a limited description of hydrological exchange in wetlands, especially in terms of the local underground exchange between wetlands and uplands and the surface connection between wetlands. The surface and groundwaters from a single HRU are presumed to flow to rivers. However, in reality, they flow to the wetlands of the HRU (considering the model limitations and the complexity of each wetland separately, it is assumed that there is only one wetland in each HRU, and each wetland represents a collection of all scattered wetlands in its HRU). The water stored in each wetland either flows directly into the sub-basin as surface overflow or returns to the HRU as seepage. This method limits the characterization of surface and underground exchange. Surface water flows directly from the wetland collection to the sub-basin reach; therefore, it is not possible to simulate the exchange between wetlands through fill-spill dynamics or surface drainage characteristics (such as agricultural ditches). For underground exchange, the original SWAT model largely determines the inflow and outflow of wetlands as a function of HRU conditions. This modeling method excludes the representation of the variation in the water head gradient between wetlands and their surrounding uplands, while the variation in the water head gradient drives the amplitude and direction of local underground exchange (inflow and outflow; McLaughlin et al., 2014).

In wetland hydrological simulations, the vertical underground-surface interaction cannot be ignored, and further nuanced dynamic characterization can be combined with the groundwater model in future research to study the impact of depressions on the entire hydrological system.

## CONCLUSION

The hydrodynamic characteristics of wetlands include the intensity, amplitude, period, and cycle characteristics of hydrological regime changes in wetlands. Furthermore, it explains the hydrological mechanism of hydrological connectivity in maintaining the structure and function of wetland systems. Therefore, groundwater plays a critical role in maintaining the integrity of wetland ecosystems.

The water balance of wetlands is controlled by the strong influence of watershed runoff and the exchange between wetland water and groundwater around wetlands. During the simulation of the hydrological processes of wetlands, the exchange of vertical groundwater should be completely considered to simulate the submerged area of wetlands more accurately. The dynamic change in the hydrodynamic characteristics should be further verified on a smaller scale and combined with hydrochemistry, isotope tracking, and other methods in future research.

## DATA AVAILABILITY STATEMENT

The original data presented in this study are included in the article further inquiries can be directed to the corresponding author.

## AUTHOR CONTRIBUTIONS

YL: investigation, data curation, writing – original draft preparation, and funding acquisition. GC: software, visualization, validation, and writing – review and editing. ST: conceptualization and methodology. SW: visualization and investigation. XL: supervision. All authors contributed to the article and approved the submitted version.

## FUNDING

This research was funded by the National Key Research and Development Program of China (2019YFC0409103), Chinese Academy of Sciences (XDA23060402), China Postdoctoral Science Foundation (2021M693154), Natural Science Foundation of Changchun Normal University (2021-009), and the Jilin Association of Science and Technology (QT202029). We express their deep gratitude to the funding agency for supporting this research.

## REFERENCES

Ameli, A. A., and Creed, I. F. (2017). Quantifying hydrologic connectivity of wetlands to surface water systems. *Hydrol. Earth Syst. Sci.* 21, 1791–1808. doi: 10.5194/hess-21-1791-2017

Brierley, G., Fryirs, K., Cullum, C., Tadaki, M., Huang, Q. H., and Blue, B. (2013). Reading the landscape: integrating the theory and practice of geomorphology to develop place-based understandings of river systems. *Prog. Phys. Geogr.* 37, 601–621. doi: 10.1177/0309133313490007

Budzisz, M., Cieśliński, R., and Woźniak, E. (2017). Effect of changes in groundwater levels on selected wetland plant communities. *Art. Subm.* XV, 19–29. doi: 10.5775/fg.2016.032.s

Carlson Mazur, M. L., Wilcox, D. A., and Wiley, M. J. (2020). Hydrogeology and landform morphology affect plant communities in a great lakes ridge-and-swale wetland complex. *Wetlands* 40, 2209–2224. doi: 10.1007/s13157-020-01312-6

Chen, G., Yue, D., Zhou, Y., Wang, D., Wang, H., Hui, C., et al. (2021). Driving factors of community-level plant functional traits and species distributions in the desert-wetland ecosystem of the Shule river basin, China. *Land Degrdn. Dev.* 32, 323–337. doi: 10.1002/ldr.3624

Clilverd, H. M., Thompson, J. R., Heppell, C. M., Sayer, C. D., and Axmacher, J. C. (2013). River–floodplain hydrology of an embanked lowland Chalk river and initial response to embankment removal. *Hydrol. Sci. J.* 58, 627–650. doi: 10.1080/02626667.2013.774089

Cui, G., Liu, Y., and Tong, S. (2021). Analysis of the causes of wetland landscape patterns and hydrological connectivity changes in Momoge National Nature Reserve based on the google earth engine platform. *Arab. J. Geosci.* 14:170. doi: 10.1007/s12517-021-06568-8

Davidson, N. C. (2014). How much wetland has the world lost? Long-term and recent trends in global wetland area. *Mar. Freshw. Res.* 65, 934–941. doi: 10.1071/MF14173

Eulie, D. O., Leonard, L., and Polk, M. (2021). Sediment deposition and availability in riparian wetlands. *J. Coast. Res.* 37, 302–315. doi: 10.2112/JCOASTRES-D-20-00020.1

Evenson, G. R., Golden, H. E., Lane, C. R., and Ellen, D. A. (2016). An improved representation of geographically isolated wetlands in a watershed-scale

hydrologic model. *Hydrol. Process.* 30, 4168–4184. doi: 10.1002/hyp.10930

Evenson, G. R., Golden, H. E., Lane, C. R., McLaughlin, D. L., and D'Amico, E. (2018a). Depressional wetlands affect watershed hydrological, biogeochemical, and ecological functions. *Ecol. Appl.* 28, 953–966. doi: 10.1002/eap.1701

Evenson, G. R., Jones, C. N., McLaughlin, D. L., Golden, H. E., Lane, C. R., DeVries, B., et al. (2018b). A watershed-scale model for depressional wetland-rich landscapes. *J. Hydrol. X* 1:100002. doi: 10.1016/j.hydroa.2018.10.002

Fan, Y., and Miguez-Macho, G. (2011). A simple hydrologic framework for simulating wetlands in climate and earth system models. *Clim. Dyn.* 37, 253–278. doi: 10.1007/s00382-010-0829-8

Galliari, J., Santucci, L., Misseri, L., Carol, E., and del Pilar Alvarez, M. (2021). Processes controlling groundwater salinity in coastal wetlands of the southern edge of South America. *Sci. Total Environ.* 754:141951. doi: 10.1016/j.scitotenv.2020.141951

Grimm, K., and Chu, X. (2020). Depression threshold control proxy to improve HEC-HMS modeling of depression-dominated watersheds. *Hydrol. Sci. J.* 65, 200–211. doi: 10.1080/02626667.2019.1690148

Guo, H., Cai, Y., Yang, Z., Zhu, Z., and Ouyang, Y. (2021). Dynamic simulation of coastal wetlands for Guangdong-Hong Kong-Macao Greater Bay area based on multi-temporal Landsat images and FLUS model. *Ecol. Ind.* 125:107559. doi: 10.1016/j.ecolind.2021.107559

Hayashi, M., Kamp, G. V. D., and Rosenberry, D. O. (2016). Hydrology of prairie wetlands: understanding the integrated surface-water and groundwater processes. *Wetlands* 36(Suppl. 2), 237–254. doi: 10.1007/s13157-016-0797-9

Hu, S., Niu, Z., Chen, Y., Li, L., and Zhang, H. (2017). Global wetlands: potential distribution, wetland loss, and status. *Sci. Total Environ.* 586, 319–327. doi: 10.1016/j.scitotenv.2017.02.001

Johnston, C. (2020). *Mechanisms of Wetland-Water Quality Interaction, Constructed Wetlands for Water Quality Improvement*. Boca Raton, FL: CRC Press, 293–299. doi: 10.1201/9781003069997-35

Keddy, P. A. (2010). *Wetland Ecology: Principles and Conservation*. Cambridge: Cambridge university press. doi: 10.1017/CBO9780511778179

Leibowitz, S. G., Mushet, D. M., and Newton, W. E. (2016). Intermittent surface water connectivity: fill and spill vs. fill and merge dynamics. *Wetlands* 36, 323–342. doi: 10.1007/s13157-016-0830-z

Lu, Q., Bai, J., Yan, D., Cui, B., and Wu, J. (2020). Sulfur forms in wetland soils with different flooding periods before and after flow-sediment regulation in the yellow river delta, China. *J. Clean. Prod.* 276:122969. doi: 10.1016/j.jclepro.2020.122969

Makungu, E., and Hughes, D. A. (2021). Understanding and modelling the effects of wetland on the hydrology and water resources of large African river basins. *J. Hydrol.* 603:127039. doi: 10.1016/j.jhydrol.2021.127039

McLaughlin, D. L., Kaplan, D. A., and Cohen, M. J. (2014). A significant nexus: geographically isolated wetlands influence landscape hydrology. *Water Resour. Res.* 50, 7153–7166. doi: 10.1002/2013wr015002

Mitsch, W. J., Gosselink, J. G., Zhang, L., and Anderson, C. J. (2009). *Wetland Ecosystems*. Hoboken, NJ: John Wiley & Sons.

Qi, Q., Zhang, D., Zhang, M., Tong, S., An, Y., Wang, X., et al. (2021). Hydrological and microtopographic effects on community ecological characteristics of Carex schmidtii tussock wetland. *Sci. Total Environ.* 780:146630. doi: 10.1016/j.scitotenv.2021.146630

Roulet, N. T. (1990). Hydrology of a headwater basin wetland: groundwater discharge and wetland maintenance. *Hydrol. Process.* 4, 387–400. doi: 10.1002/hyp.3360040408

Singh, M., and Sinha, R. (2019). Evaluating dynamic hydrological connectivity of a floodplain wetland in North Bihar, India using geostatistical methods. *Sci. Total Environ.* 651, 2473–2488. doi: 10.1016/j.scitotenv.2018.10.139

Singh, V. P. (1997). *Computer Models of Watershed Hydrology*. 443–476. Highlands Ranch: Water Resources Publications

Spence, C., and Woo, M.-K. (2003). Hydrology of subarctic Canadian shield: soil-filled valleys. *J. Hydrol.* 279, 151–166. doi: 10.1016/S0022-1694(03)00175-6

Tromp-van Meerveld, H., and McDonnell, J. (2006). Threshold relations in subsurface stormflow: 2. the fill and spill hypothesis. *Water Resour. Res.* 42:W02411. doi: 10.1029/2004WR003800

Wang, N., Chu, X., and Zhang, X. (2021). Functionalities of surface depressions in runoff routing and hydrologic connectivity modeling. *J. Hydrol.* 593:125870. doi: 10.1016/j.jhydrol.2020.125870

Wang, Q., Rogers, M. J., Ng, S. S., and He, J. (2021). Fixed nitrogen removal mechanisms associated with sulfur cycling in tropical wetlands. *Water Res.* 189:116619. doi: 10.1016/j.watres.2020.116619

Wu, S., Tetzlaff, D., Goldhammer, T., and Soulsby, C. (2021). Hydroclimatic variability and riparian wetland restoration control the hydrology and nutrient fluxes in a lowland agricultural catchment. *J. Hydrol.* 603:126904. doi: 10.1016/j.jhydrol.2021.126904

Xi, Y., Peng, S., Ciais, P., and Chen, Y. (2021). Future impacts of climate change on inland Ramsar wetlands. *Nat. Clim. Chang.* 11, 45–51. doi: 10.1371/journal.pone.0239945

**Conflict of Interest:** The authors declare that the research was conducted in the absence of any commercial or financial relationships that could be construed as a potential conflict of interest.

frontiers | Frontiers in Ecology and Evolution

ORIGINAL RESEARCH
published: 24 June 2022
doi: 10.3389/fevo.2022.948682

# Seasonal Variation Characteristics of C, N, and P Stoichiometry and Water Use Efficiency of *Messerschmidia sibirica* and Its Relationship With Soil Nutrients

*Tian Li[1], Zehao Zhang[1,2], Jingkuan Sun[1]*, Zhanyong Fu[1], Yinghan Zhao[1,2] and Wenjing Xu[1,2]*

[1] Shandong Key Laboratory of Eco-Environmental Science for Yellow River Delta, Binzhou University, Binzhou, China,
[2] College of Forestry, Shandong Agricultural University, Taian, China

OPEN ACCESS

**Edited by:**
Chuanyu Gao,
Northeast Institute of Geography and Agroecology (CAS), China

**Reviewed by:**
Zhongsheng Zhang,
Key Laboratory of Mollisols Agroecology, Northeast Institute of Geography and Agroecology (CAS), China
Guan Bo,
Ludong University, China

***Correspondence:**
Jingkuan Sun
sunjingkuan@126.com

**Specialty section:**
This article was submitted to Conservation and Restoration Ecology, a section of the journal Frontiers in Ecology and Evolution

**Received:** 20 May 2022
**Accepted:** 01 June 2022
**Published:** 24 June 2022

**Citation:**
Li T, Zhang Z, Sun J, Fu Z, Zhao Y and Xu W (2022) Seasonal Variation Characteristics of C, N, and P Stoichiometry and Water Use Efficiency of Messerschmidia sibirica and Its Relationship With Soil Nutrients. Front. Ecol. Evol. 10:948682. doi: 10.3389/fevo.2022.948682

The seasonal dynamic characteristics of C, N, and P stoichiometry and water use efficiency (WUE) of *Messerschmidia sibirica* and the soil in the Yellow River Delta (YRD) were studied. The correlations of stoichiometric characteristics and WUE between organs of *M. sibirica* and soil were analyzed. The results showed that: (1) the contents of C, N, and P and their stoichiometric ratios in various organs of *M. sibirica* varied with seasons. The seasonal dynamics of leaf N:P showed that the degree of nutrient restriction by N decreased in July and increased in September. (2) The contents of C, N, and P, as well as their stoichiometric ratio, showed a high correlation throughout the growing season, with N:P showing a significantly positive correlation among organs and the lowest stoichiometric correlation between leaf and root. (3) $C^{13}$ stable isotope analysis showed that the WUE of *M. sibirica* in May was significantly higher than that of other months (July and September). The WUE had a significantly positive correlation with leaf C and N content and a significantly negative correlation with leaf C:N, indicating that *M. sibirica* can compensate for the decline in N use efficiency through the improvement of WUE. The structural equation model (SEM) showed that the leaf N and P contents were affected by the joint effect of season and WUE, and the leaf C content was mainly directly affected by WUE. (4) Redundancy analysis (RDA) analysis showed that soil P content and soil N:P were the main factors affecting the variation of stoichiometry and WUE in various organs of *M. sibirica*. This study is helpful to deeply understand the adaptive mechanism of plant nutrient and water use, which provides a theoretical basis for vegetation protection and restoration in the study area.

**Keywords: stoichiometry, plant organ, stable carbon isotope, growing season, Yellow River Delta**

## INTRODUCTION

Change in plant stoichiometry not only reveal the nutrient uptake and utilization status of different plants but also indicate the constraint relationship between different nutrients, which is an important indicator to determine whether plants can renew themselves and recycle nutrients (Crous et al., 2019). Changes in plant carbon, nitrogen, and phosphorus stoichiometry are influenced not only by environmental factors and plant physiological processes but also by differences in structure and function in different organs of the same plant (Luo et al., 2021; Yang and Xu, 2021). Observing changes in environmental and plant stoichiometry can help identify nutrient-limiting factors for plant growth and is an important complement to investigating the relationships between ecosystem stoichiometry and plant function and environmental adaptation mechanisms (Cao and Chen, 2017; Tang et al., 2018).

Various factors influence plant stoichiometry, and the soil C: N: P ratio directly reflects the soil nutrient status and can be used indirectly as an indicator of plant nutrient status (Elser et al., 2010). Studying the stoichiometric characteristics of plants and soils and their interrelationships provides insight into their feedback processes in terms of nutrients and improves our understanding of the adaptation mechanisms of plants. However, due to the study scale, scope, plant species, and other reasons, there is no unified research conclusion on whether plant stoichiometry is influenced by soil stoichiometry (Wang et al., 2015). Therefore, the relationship between plant and soil stoichiometry needs to be further explored.

There is a close relationship between water and nutrient use by plants, and plants need to constantly coordinate the balance between nutrient and water use during growth to adapt to environmental influences (Li et al., 2021). In recent years, stable isotope $^{13}C$ has been widely used to characterize plant water use efficiency (WUE), which provides important technical support for the study of the plant WUE. Researching the relationship between plant water use and plant stoichiometry can enrich the theory of plant water-fertilizer relationship (Yan et al., 2016). However, studies on the relationship between plant nutrient use characteristics, WUE, and soil nutrients are still very limited.

*Messerschmidia sibirica* is a perennial herb with salt secretion characteristics and strong adaptability. It is a widely grown constructive species in the chenier of the Yellow River Delta (YRD) and plays an important role in species diversity and ecological function. Previous research on *M. sibirica* mainly focused on the distribution survey of plant communities, the growth and physiological characteristics under salt and sand burial stresses, and diversity of endophytic bacteria (Lee et al., 2007; Suzuki et al., 2011; Xie et al., 2015; Zhang et al., 2019a). The ecological stoichiometry and its dynamic change characteristics of *M. sibirica* are not clear, especially from the perspective of water and nutrient use. It is necessary to further strengthen the research on the adaptation strategies of *M. sibirica* to chenier habitats. Therefore, the seasonal changes of C, N, and P stoichiometry of *M. sibirica* and soils in the chenier of YRD and WUE of *M. sibirica* were analyzed to (1) clarify the nutrient characteristics and seasonal dynamics of nutrient use in different organs of *M. sibirica*; (2) reveal the seasonal characteristics of WUE and its relationship with leaf stoichiometry; and (3) explain the correlation between different organ stoichiometric characteristics and WUE of *M. sibirica* and soil nutrients. The results contribute to a better understanding of the adaptation of *M. sibirica* to the chenier coastal environment and provide a theoretical basis for the protection and restoration of vegetation in the coastal zone of YRD.

## MATERIALS AND METHODS

### Site Description

The study area is located in the chenier of the YRD in Wudi County, Shandong Province, China (37°35′∼38°12′ N, 118°33′∼119°20′ E), with a semi humid continental monsoon climate. The average annual temperature ranges from approximately 11.7 °C to 12.6 °C, and the average annual precipitation is 550 mm.

### Plot Setting and Sample Collection

Sample lines were set along the vertical coastline through grid distribution, that based on soil texture, geomorphology, and land use type of chenier of YRD and the distance from the coast. Three sample points were set on the sample ground wire, the spacing of each sample point was not less than 1 km, and three quadrats (each with a size of 5 m × 5 m) were set at each sampling point.

The samples were collected in May, July, and September on the seaward side, representing the seasons of spring, summer, and autumn, respectively. Representative *M. sibirica* communities were selected and a random sample method was used to collect three to five complete plant samples, including the root system, from each sample point, which were placed inside ventilated bags. A total of 36 plant samples were collected during the sampling period. The soil samples were collected by using a 4.5 cm diameter special earth drill in four soil depths: 0–10 cm, 10–20 cm, 20–40 cm, and 40–60 cm. Three parallel soil samples were taken at each sampling point adjacent to the plant. The soil was placed inside sealed bags and brought back to the lab. The soil samples were naturally air-dried, sieved, and stored for extraction and determination. The plant samples were separated into root, stem, and leaf, then dried at 105°C for 20 min, and then transferred to 70°C for 48 h. The dried samples were grinded, and then selected by 80 mesh sieving.

### Sample C, N, and P Content and $\delta^{13}C$ Determination

The leaf $\delta^{13}C$ determination was carried out by the Finnigan DELTAPlus XP stable isotope mass spectrometer (Thermo Electron Corp., Waltham, MA, United States). The value of plant leaf $\delta^{13}C$ was calculated by the following formula:

$$\delta^{13}C(‰) = ({}^{13}C/{}^{12}C_{sample} - {}^{13}C/{}^{12}C_{standard})/ ({}^{13}C/{}^{12}C_{standard}) \times 1000$$

in which $^{13}C/^{12}C_{sample}$ is the $^{13}C/^{12}C$ ratio of plant leaf samples, and $^{13}C/^{12}C_{standard}$ is the $^{13}C/^{12}C$ ratio of glycine in the determination process.

The total carbon (TC) and total nitrogen (TN) of soil and plant were determined by element analyzer (Vario EL III, Elementar, Germany), while total phosphorus (TP) was determined by molybdenum-antimony colorimetric method (Lu, 1999).

## Data Analysis

Excel 2010 (Microsoft Corp., Redmond, WA, United States) and SPSS19.0 (SPSS Inc., Chicago, IL, United States) were used to analyze the variance of the data. One-way ANOVAs were conducted on the C, N, and P contents and their stoichiometric ratios of soil and roots, stems and leaves of *M. sibirica*, respectively. Duncan's test, Pearson method and maximum likelihood method was used for multiple comparison, correlation analysis, and structural equation modeling, respectively.

# RESULTS

## C, N, and P Stoichiometry in *Messerschmidia sibirica*

### Seasonal Dynamics of the Stoichiometry of Different Organs of *Messerschmidia sibirica*

The C, N, and P contents of each organ of *M. sibirica* showed different variation patterns with seasonal changes (**Figure 1**). The C content of root was significantly higher than that of the stem and leaf ($P < 0.05$), and there was no significant difference between the stem and leaf ($P > 0.05$). The C content of the root did not change significantly with seasonal changes, while the C content of both stem and leaf showed a significant decrease with the increase of months ($P < 0.05$). The N content of all organs showed a similar change pattern in each month, that was leaf > stem > root, and the differences were significant ($P < 0.05$). The dynamic changes of N showed that N of both root and stem increased and then decreased with the increase of the month, and both had the highest value in July, which was significantly higher than that in May and September. The maximum leaf N content was in May, and decreased with the increase of the months, which was different from the change of root and stem N content. There were differences in the P changes of each organ of *M. sibirica*, in which the P showed leaf > stem > root in May and July ($P < 0.05$). In September, it showed stem > leaf > root ($P < 0.05$). In the whole growing season, P content showed stem = leaf > root. According to the dynamic change characteristics, the P content of the root and stem was highest in September, while the P content of the leaf decreased and then increased with the month, with the lowest in July and no significant difference between May and September.

The seasonal pattern of C:N:P stoichiometric ratio was different for each organ (**Figure 1**). The C: N ratio showed root > stem > leaf, and all the differences were significant ($P < 0.05$). The C: N of both root and stem tended to decrease and then increase with increasing months. The maximum of root C:N was in May, the maximum of stem C:N was in September, and the lowest of both root and stem occurred in July with 33.64 and 19.38, respectively. Leaf C:N showed an increasing trend with increasing months. Root C:P was significantly higher than that of both stem and leaf throughout the growing season ($P < 0.05$), and its C:P tended to decrease. Stem and leaf C:P showed similar trends, both increasing first and then decreasing. C:P of root, stem, and leaf was lowest in September and highest in May, July, and July, respectively. N:P in different organs showed that leaf > root > stem ($P < 0.05$), and the dynamic change pattern of N:P in different organs was similar. The N:P of root, stem, and leaf increased and then decreased with increasing months, with the highest in July and the lowest in September, respectively.

### Correlation Analysis of C, N, and P Contents and C:N:P Ratios in *Messerschmidia sibirica*

There were high correlations in C, N, P content and C:N:P ratios of *M. sibirica* (**Table 1**). The correlations were different between different seasons. In May, the correlations among all indicators were significant except for N:P. The correlations between July and May were similar, and N: P was significantly positively and negatively correlated with N content and C:N, respectively. In September, significant correlations were reduced. There was no correlation between C and N, N and P, N and C:P, P and C:N. In all months, there were no significant correlations among C, N, and P of *M. sibirica,* but there were significant correlations between C, N, and P contents and C:N, C:P, and N:P.

### Correlation Analysis of Stoichiometry Among Different Organs

The C, N, and P stoichiometric correlations among the organs of *M. sibirica* are shown in **Table 2**. Except for the C which was not significant between the stem and the root, the other indexes were significantly positively correlated, and the correlation coefficient was high, ranging from 0.843 to 0.983. C, P, C:P, and N:P were significantly and positively correlated between stem and leaf, and the correlation coefficient was 0.940, 0.744, 0.863, and 0.998, respectively. However, only N:P was significantly and positively correlated between leaf and root with a correlation of 0.989. N:P had the highest correlation in all organs and was most closely related to each organ.

## $\delta^{13}C$ Dynamics Analysis and Correlation Analysis Between $\delta^{13}C$ and Leaf Stoichiometry

The seasonal variation of WUE of *M. sibirica* leaf is shown in **Figure 2**. WUE in May was significantly higher than in July and September ($P < 0.05$). There was no significant difference between July and September. The average $\delta^{13}C$ during the growing season was $-29.98‰$, which was significantly lower than the global plant $\delta^{13}C$ average of $-28.74‰$.

Correlation analysis (**Table 3**) showed that the WUE of *M. sibirica* was significantly positively correlated with leaf C and leaf N ($P < 0.01$) and significantly negatively correlated with leaf C:N. In addition, WUE was positively correlated with leaf P content and N:P but did not reach a significant level.

Structural equation modeling was used to analyze the effect of water utilization and seasonal variation on C, N, and P nutrient

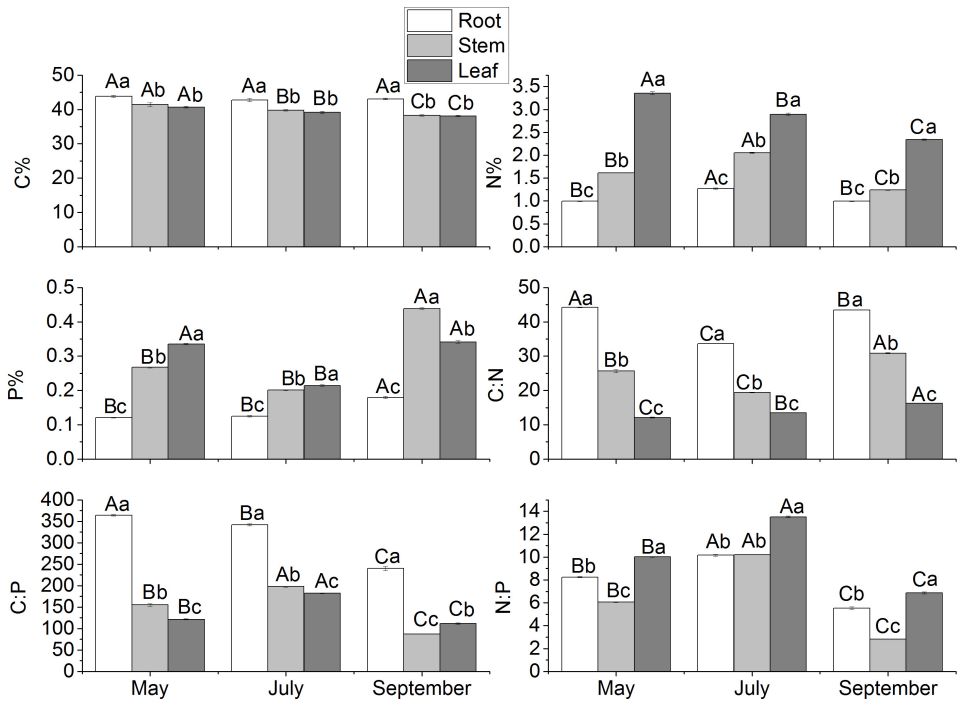


**FIGURE 1 |** Seasonal dynamics of C, N, and P stoichiometry in different organs of *M. sibirica*. Different capital letters indicate the significant difference in the same organ in different months, and different small letters indicate the significant difference between different organs in the same month.

**TABLE 1 |** Correlation of C, N, and P Stoichiometry in different months of *M. sibirica*.

| Month | Indexes | N% | P% | C:N | C:P | N:P |
|---|---|---|---|---|---|---|
| May | C% | −0.795* | −0.936** | 0.926** | 0.937** | −0.159 |
| | N% | 1 | 0.889** | −0.937** | −0.789* | 0.666 |
| | P% | | 1 | −0.993** | −0.983** | 0.251 |
| | C:N | | | 1 | 0.954** | −0.363 |
| | C:P | | | | 1 | −0.067 |
| July | C% | −0.871** | −0.928** | 0.946** | 0.944** | −0.621 |
| | N% | 1 | 0.918** | −0.966** | −0.896** | 0.880** |
| | P% | | 1 | −0.986** | −0.997** | 0.621 |
| | C:N | | | 1 | 0.980** | −0.733* |
| | C:P | | | | 1 | −0.581 |
| September | C% | −0.655 | −0.909** | 0.851** | 0.977** | 0.165 |
| | N% | 1 | 0.311 | −0.953** | −0.519 | 0.630 |
| | P% | | 1 | −0.584 | −0.973** | −0.542 |
| | C:N | | | 1 | 0.753* | −0.365 |
| | C:P | | | | 1 | 0.336 |
| Overall month | C% | −0.516 | −0.748 | 0.719** | 0.817** | 0.045 |
| | N% | 1 | 0.344 | −0.928** | −0.531** | 0.589** |
| | P% | | 1 | −0.465** | −0.921** | −0.501** |
| | C:N | | | 1 | 0.664** | −0.471* |
| | C:P | | | | 1 | 0.301 |

*$p < 0.05$, **$p < 0.01$.

characteristics (**Figure 3**). Seasonal variation had a significant direct negative effect on leaf P ($P < 0.001$) and a significant positive effect on leaf N ($P < 0.05$), while the effect on C content and $\delta^{13}C$ was not significant ($P > 0.05$). The direct effects of $\delta^{13}C$ on the C, N, and P content of leaves were positive. The results of structural equation modeling were consistent with the results of correlation analysis, and all the above effects reached a highly significant level. The effect coefficients showed that the

**TABLE 2 |** Correlation of C, N, and P stoichiometry among roots, stems and leaves of *M. sibirica*.

| Indexes | Organ | Stem | Leaf |
|---|---|---|---|
| C | Root | 0.533 | 0.615 |
| | Stem | | 0.940** |
| N | Root | 0.886** | 0.061 |
| | Stem | | 0.511 |
| P | Root | 0.934** | 0.472 |
| | Stem | | 0.744* |
| C:N | Root | 0.858** | 0.124 |
| | Stem | | 0.613 |
| C:P | Root | 0.843** | 0.462 |
| | Stem | | 0.863** |
| N:P | Root | 0.983** | 0.989** |
| | Stem | | 0.998** |

*$p < 0.05$, **$p < 0.01$.

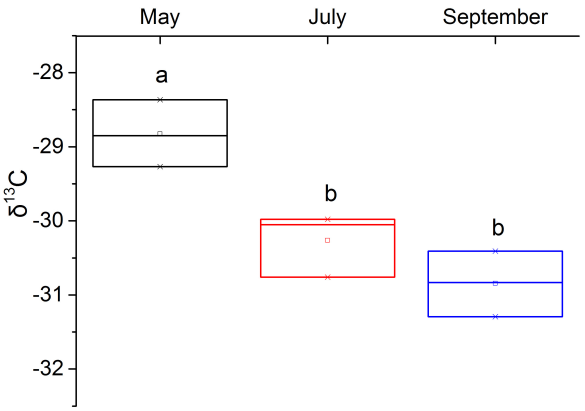


**FIGURE 2 |** Seasonal variation characteristics of $\delta^{13}C$ in leaves of *M. sibirica*.

negative effect of seasonal variation on the leaf stoichiometric P was greater than the positive effect of WUE on it, and the positive effect of WUE on the leaf N content was greater than the positive effect of seasonal variation on it. In addition, leaf C content was more significantly influenced by the direct effect of WUE. Leaf P content was influenced by the opposite effects of seasonal variation and WUE, while leaf N content was influenced by the same positive effect of both.

## Seasonal Dynamic Analysis of C, N, and P Stoichiometry in Different Soil Layers

The C, N, and P stoichiometric characteristics of each soil layer at different seasons are shown in **Figure 4**. Overall, there was no significant change in C content with seasonal change in the same soil layer. However, the C of different soil layers showed a trend of increasing and then decreasing with increasing depth. The highest C content was in the 20–40 cm soil layer, which was significantly higher than that in the 0–10 cm soil layer. In the same soil layer, the N of the 40–60 cm soil layer showed a trend of decreasing and then increasing with seasonal changes, while the differences of N content of other soil layers with seasonal changes were not significant. Vertically, the pattern of variation in N content between soil layers in each month was consistent, showing a decrease with increasing soil depth. P content tended to increase in the 10–20 cm soil layer with increasing months, and was significantly higher in September than in July, while there was no significant difference in P content between May and July. The overall P content variation in each soil layer was similar to the N variation characteristics.

In soil stoichiometric ratios, the seasonal variation of C:N in the same soil layer showed a general trend of increasing and then decreasing, but the seasonal variation in the same soil layer did not reach the level of significant difference. In the same month, the differences between soil layers were not significant. Similarly, both C:P and N:P did not reach significant levels of difference among months, but there were some differences among soil layers under the same month. In May, the C:P of 20–40 cm soil layer was significantly higher than that of the other three soil layers, and the N:P of 0–20 cm soil layer was significantly higher than that of 40–60 cm soil layer. In July, C:P and N:P were similar between different soil layers and were not significantly different. In September, C:P in 20–40 cm soil layer was significantly higher than that in 0–20 cm soil layer, and N:P in 0–40 cm soil layer was significantly higher than that in 40–60 cm soil layer.

## Correlation of C, N, and P Stoichiometry and Water Use Efficiency in *Messerschmidia sibirica* and Soils

Redundancy analysis (RDA) of stoichiometry, WUE in *M. sibirica* and soils are shown in **Figure 5**. The longer rays of soil N:P and soil P content suggested that both were important factors

**TABLE 3 |** Correlation between water use efficiency (WUE) and leaf stoichiometry.

| Indexes | C% | N% | P% | C:N | C:P | N:P | $\delta^{13}C$ |
|---|---|---|---|---|---|---|---|
| C% | 1 | 0.944** | 0.067 | −0.895** | 0.019 | 0.352 | 0.849** |
| N% | | 1 | −0.094 | −0.989** | 0.178 | 0.518 | 0.888** |
| P% | | | 1 | 0.226 | −0.996** | −0.900** | 0.171 |
| C:N | | | | 1 | −0.307 | −0.628 | −0.849** |
| C:P | | | | | 1 | 0.933** | −0.101 |
| N:P | | | | | | 1 | 0.238 |
| $\delta^{13}C$ | | | | | | | 1 |

**$p < 0.01$.

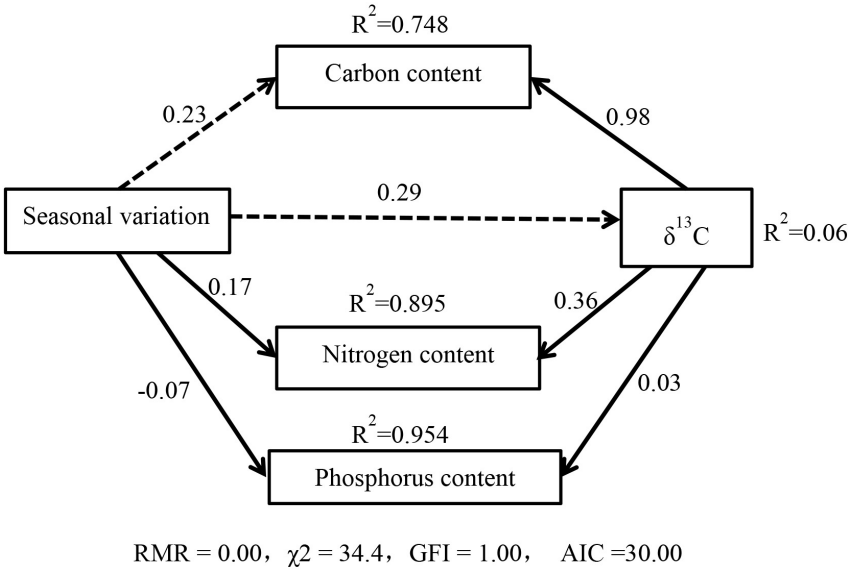


**FIGURE 3 |** Relationships between season, water use efficiency, and C, N, P content in the leaves of *M. sibirica.* Solid lines are statically different at $P < 0.001$, while dotted lines are not significant at $P > 0.05$.

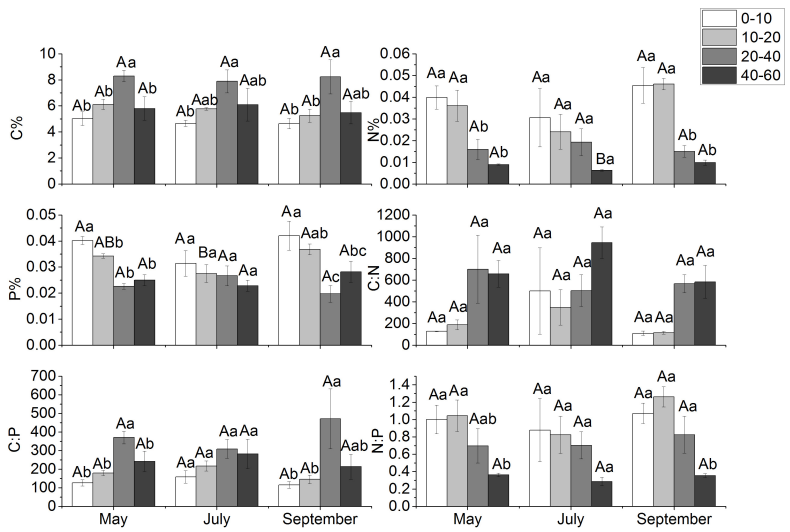


**FIGURE 4 |** Seasonal dynamics of C, N, and P stoichiometry in different soil layers. Different capital letters indicate the significant difference in the same soil layer in different months, and different small letters indicate the significant difference of different soil layers in the same month.

affecting the ecological stoichiometric characteristics and WUE of each organ of *M. sibirica.* In contrast, the ray of soil C, soil C:P, and soil C:N were shorter, indicated that the influences of these three factors were less. Soil P content was positively correlated with root C:N, root C content, stem C:N and leaf P content, and negatively correlated with root N content, stem N, C:P, N:P and leaf $\delta^{13}C$. Soil N:P was positively correlated with root P content, stem P content, and leaf C:N, and was negatively correlated with root C:P, stem C content, leaf C content, leaf N content, and leaf $\delta^{13}C$. The stoichiometric characteristics of root, stem, and leaf were greatly affected by soil N:P in September.

# DISCUSSION

## Stoichiometric Characteristics and Correlation of C, N, and P in Different Growing Seasons of *Messerschmidia sibirica*

The ecological stoichiometric characteristics of plants under seasonal changes reflect the inherent response and adaptation of plants to environmental changes. For example, a study on the dominant shrubs in a dry-hot valley showed that the contents

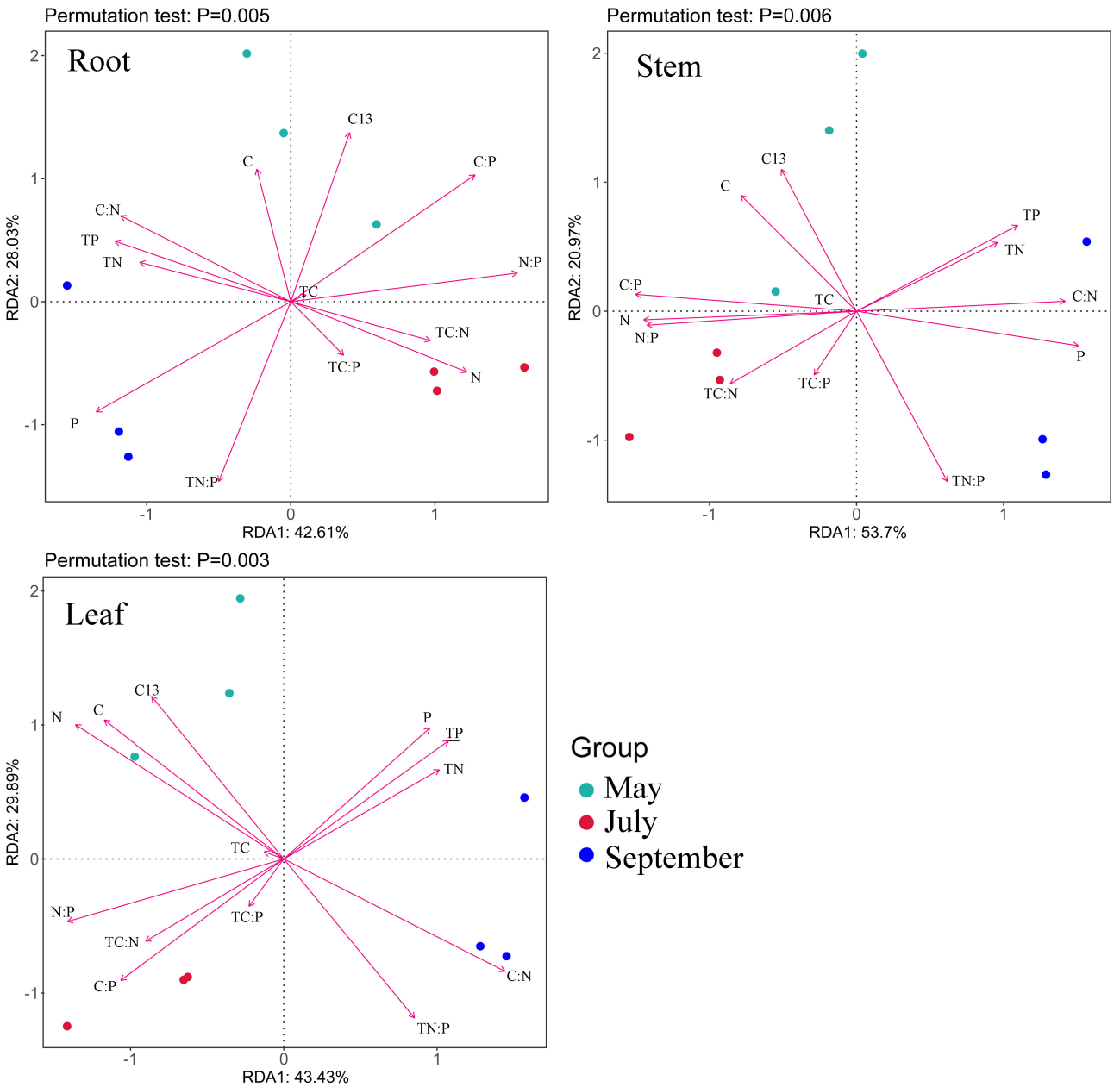


**FIGURE 5 |** Redundancy analysis of stoichiometry, WUE in *M. sibirica* and soil nutrients. C, Plant carbon content; N, Plant nitrogen content; P, Plant phosphorus content; C: N, Plant C: N; C:P, Plant C:P; N:P, Plant N:P; C13, Plant WUE; TC, Soil carbon content; TN, Soil nitrogen content; TP, Soil phosphorus content; TC:N, Soil C:N; TC:P, Soil C:P; TN:P, Soil N:P.

of C, N, and P in leaves varied with seasons, and the seasonal variation of C content was less than that of N and P content (Liu et al., 2020). Xiong et al. (2020) found that the leaf N and P contents of typical dicotyledons in the Mongolian steppe showed a decreasing trend throughout the growing season.

In this study, C content of root, stem and leaf of *M. sibirica* did not vary significantly with the seasons, but N and P contents of each organ showed significant variability with the seasons, with leaf N gradually decreasing and the P content first decreasing and then increasing with the seasons. This was consistent with some previous studies (Niu et al., 2013; Jing et al., 2020). N and P were regarded as the most important nutrient factors in limiting plant growth (Drinkwater and Snapp, 2007). With the change of seasons, plants optimized their growth as much as possible through the rational distribution and adjustment of nutrients in various tissues (Weih et al., 2016). In this study, the N content of *M. sibirica* was more distributed in the leaf during the early growth period, the N content of root and stem was

more dominant during the peak growth period, and N contents in stem and leaf were affected during the late period, with little effect on the root. The P content in each organ was the most in September, indicating that the accumulation of P in each organ had an advantage in the later growth stage. The response patterns of N and P content of each organ of *M. sibirica* with the seasons reflected the distribution and transfer characteristics of nutrients at different growth stages. In addition, the path analysis showed that seasonal changes had different effects on N and P contents in leaves, which was related to the element concentration pattern in plant was affected by plant developmental stage and weather (Weih et al., 2016; Zhang et al., 2016).

Plant C:N:P was an important physiological index, that reflected the growth rate of plants. Plant C:N and C:P were used to reflect plant utilization of nutrients (Wang et al., 2014). There was a significant correlation between the C, N, and P content and the stoichiometric ratios of C:N, C:P, and N:P in different seasons, which reflected one of the general laws of nutrient stoichiometry in higher terrestrial plants, that was, the dominant role of plant leaf N and P contents on leaf C:N and C:P (Sardans et al., 2012). It reflected the strong coupling mechanism between plant nutrients (Zhou et al., 2019). Previous studies have found that the distribution of N and P content in leaf followed a certain stoichiometric law. Plants maintained a dynamic balance of C:N:P through stoichiometric homeostasis mechanism. Leaf N:P increased with increasing plant age, reflecting the transition from N-limited to P-limited, a dynamic mechanism usually observed in both short- and long-term time series (Fan et al., 2015). Dynamic nutrient stoichiometry and limitation implied plant nutrition status at different growth stages (Bratt et al., 2020). In this research, the seasonal dynamics of leaf N:P reflected the variation of the N nutrient limitation degree of *M. sibirica*. In July, leaf N:P increased significantly compared with May, and N:P was close to 14, indicating that the nutrient limitation degree of N content was reduced in this period, and the growth of *M. sibirica* was in a relatively good nutritional state. In September, N:P was significantly lower than in May and July, indicating an increase in N limitation at the end of growth. This was consistent with the trend of increasing and then decreasing N:P in aboveground organs of *Imperata Cylindrica* with seasons (Niu et al., 2013).

Physiological differences in the structure and function of different organs may lead to differences in nutrient uptake and accumulation in different organs of plants (Feng et al., 2019; Li et al., 2019). In the present study, there was no significant correlation in C among the root, stem, and leave of *M. sibirica*, which was consistent with the results of Liu et al. (2020). And there was a correlation between the utilization of N and P nutrients by various plant organs (Han et al., 2005; Ping et al., 2014). In our study, the N:P between root and stem, stem and leaf, and leaf and root of *M. sibirica* showed highly significant positive correlations, which were consistent with the previous studies (Yuan et al., 2011), and reflected the uniformity of growth among plant organs. More correlations were seen between stem and leaf, root and stem than those between leaf and root, and this result was similar to that of *Platycladus Orientalis* (Feng et al., 2019).

## Relationship Between Water Use Efficiency and Leaf Stoichiometry of *Messerschmidia sibirica*

Plant nutrients regulated the plant's photosynthetic capacity by influencing leaf stomatal opening and photosynthetic rate, which in turn influenced plant $\delta^{13}C$ (Zhang et al., 2019b). In this study, the significant correlations of $\delta^{13}C$ with C, N contents, and C:N of leaf indicated that there were important effects of leaf WUE on stoichiometric characteristics. The WUE of *M. sibirica* was positively correlated with the leaf C content, which was consistent with the physiological characteristics that carbon fixation and WUE were closely related in the plant photosynthesis process, and reflected the relationship between them. The higher the plant WUE, the higher the amount of leaf carbon assimilated into organic matter (Basso and Ritchie, 2018). Within a certain range, the increase in plant N content promoted photosynthesis. The significant positive correlation between WUE and leaf N content in this study was due to a positive correlation of leaf N content with carboxylation efficiency and photosynthetic capacity, and therefore there was a positive correlation between $\delta^{13}C$ and leaf N content (Hamerlynck et al., 2004). The structural equation model (SEM) analysis showed that seasonal variation did not contribute to the leaf stoichiometry by directly affecting its WUE. This reflects the effect of plant growth stage on WUE, which mainly depends on the change of external environmental conditions, such as precipitation, temperature, and light.

Plant leaf C:N ratios were found to be an important indicator of N distribution and utilization, as well as C acquisition and assimilation (Hedges et al., 1986). Plants with higher WUE had lower nitrogen use efficiency in natural ecosystems (Sheng et al., 2011). Xia et al. (2020) studied two types of halophytes and found that $\delta^{13}C$ and C:N in the leaf of both salt-dilute halophyte and salt-repellent halophyte were significantly negatively correlated. This study showed that *M. sibirica* was similar to the other two types of halophyte in terms of growth adaptation strategies. Salt-secreting plants could also compensate for the reduced N use efficiency by increasing WUE, especially in barren environments, plant water and nutrient use efficiencies might compensate for each other (Salazar et al., 2018).

## Stoichiometry Correlations Between Different Organs of *Messerschmidia sibirica* and Soil

Soil was the main source of plant nutrients, and the C, N, and P content and stoichiometry of plants were influenced by soil fertility (Lambers et al., 2008). Plant leaf P content was dominated by soil P content, and Chinese plant leaf P content was lower than global plant leaf P content, which was probably due to the lower soil P content of China (He et al., 2008). Our study found that the leaf P content of *M. sibirica* was significantly and positively correlated with soil P content, suggesting that soil P content was one of the important factors affecting *M. sibirica* nutrient, which was consistent with the theory that low soil P content caused low leaf P content in plants (He et al., 2008). However, Geng et al. (2011) found that there was no significant correlation between

leaf P content and soil P content in Inner Mongolia grasslands. The same phenomenon was found between *Robinia pseudoacacia L.* and soil in the Loess Plateau (Li et al., 2013). This suggests that the plant–soil nutrient relationship varies depending on the region or species.

The C:N:P ratio in soil directly reflected soil fertility and nutrient status, and influenced plant growth to a certain extent. Studies on the leaf and soil nutrients of nearly two thousand plant species in China showed a positive correlation between the stoichiometry of soil and plant leaf (Han et al., 2011). Previous studies showed that the N:P of subtropical eucalyptus leaves was significantly correlated with soil N:P (Fan et al., 2015). Both C:P and N:P were positively correlated between soil and *Robinia pseudoacacia L.* in the Loess Plateau (Cao and Chen, 2017). In addition, in the YRD, C:P of *Phragmites communis* leaf and soil N:P were positively correlated, C:P of *Limonium bicolor* leaf and both C:P and N:P of soil were positively correlated, and C:P of *Suaeda salsa* leaf and soil N were positively correlated (Li et al., 2021). In this study, we found that the soil N:P in the chenier of YRD was significantly lower than the soil N:P of forest ecosystems in the country, indicating a soil N deficiency in this region. The leaf C:N of *M. sibirica* was strongly and positively correlated with soil N:P, indicating that N:P was more closely related to leaf building efficiency than N and P content in soil. Chen et al. (2016) found that the nutritional variation of different organs of *Cunninghamia lanceolata* had a relative consistency with that of soil, which ensured the stable growth and development of *Cunninghamia lanceolata*. In our work, the correlations between root N content and soil N: P, between root and stem C: N and soil N content, and between leaf P content and soil P content were significant and positive, indicating a good correlation between each organ of *M. sibirica* and soil stoichiometry, and embodying a close relationship between *M. sibirica* and soil nutrient environment with mutual constraints and interactions, which enhances the adaptability of *M. sibirica* to grow in this region.

## CONCLUSION

The accumulation of N and P by above-ground leaves and stem was higher than that by below-ground roots in various growing seasons of *M. sibirica*. The plant N was mainly distributed to the leaves in the early growth stage and to the roots and stem in the peak growth stage of *M. sibirica*. The accumulation of P in each organ was dominant in the later stages of growth. The ratio of C:N, C:P, N:P in different growing seasons showed the highest utilization efficiency of N and P in the root and the lowest limitation of N in the leaf. The degree of N restriction of *M. sibirica* decreased in July, and increased in September. The overall C, N, and P content and stoichiometric ratio of *M. sibirica* were strongly correlated, reflecting the coupling between plant nutrient elements. The N:P of root and stem, stem and leaf, and leaf and root were strongly significantly and positively correlated, indicating the same nutrient-limited growth of each organ. The stoichiometric correlations between stem and leaf and between root and stem were higher than those between leaf and root. The $\delta^{13}C$ of *M. sibirica* was significantly higher in May than in July and September, and it was strongly and positively correlated with leaf C and N content, indicating that WUE played an important role in nutrient accumulation. The highly significant negative correlation between WUE and leaf C:N indicated that *M. sibirica* could not optimize both water and nutrient use in the relatively poor soil habitat, and there was a compensatory effect between water and nutrient use. RDA showed that there was mutual influence and constraint between the root, stem, and leaf of *M. sibirica* and soil in terms of stoichiometry. Soil P content and soil N:P were the main factors affecting the ecological stoichiometric characteristics and WUE of *M. sibirica*. This study provides valuable information for the protection and restoration of *M. sibirica*.

## DATA AVAILABILITY STATEMENT

The original contributions presented in this study are included in the article/supplementary material, further inquiries can be directed to the corresponding author.

## AUTHOR CONTRIBUTIONS

TL completed data analysis and wrote the manuscript. ZZ was in charge of the modification of the manuscript. JS conceived and designed the study, and fund support. ZF conducted experiments and data sorting. YZ and WX participated in data sorting and revision of the manuscript. All authors contributed to the article and approved the submitted version.

## FUNDING

This funding was supported by the National Natural Science Foundation of China (41871089, 41971119, and 42171059), the "Collection, Conservation, and Accurate Identification of Forest Tree Germplasm Resources" of Shandong Provincial Agricultural Elite Varieties Project (2019LZGC01805), the Natural Science Foundation of Shandong Province (ZR2019MD024 and ZR2020QD004), and the Science and Technology Support Plan for Youth Innovation of Colleges and Universities (2019KJD010).

## REFERENCES

Basso, B., and Ritchie, J. T. (2018). Evapotranspiration in high-yielding maize and under increased vapor pressure deficit in the US Midwest. *Agricultural Environ. Lett.* 3:170039.

Bratt, A. R., Finlay, J. C., Welter, J. R., Vculek, B. A., and Van Allen, R. E. (2020). Co-limitation by N and P characterizes phytoplankton communities across nutrient availability and land Use. *Ecosystems* 23, 1121–1137. doi: 10.1007/s10021-019-00459-6

Cao, Y., and Chen, Y. M. (2017). Coupling of plant and soil C: N: P stoichiometry in black locust (*Robinia pseudoacacia*) plantations on the Loess Plateau. China. *Trees* 31, 1559–1570. doi: 10.1007/s00468-017-1569-8

Chen, C., Wang, G. J., Zhao, Y., Zhou, G. X., Li, L., and Gao, J. Q. (2016). Seasonal dynamics and allometric growth relationships of C, N, and P stoichiometry

in the organs of *Cunninghamia lanceolata* from Huitong. *Acta Ecol. Sinica* 36, 7614–7623.

Crous, K. Y., Wujeska, A., Jiang, M., Medlyn, B. E., and Ellsworth, D. (2019). Nitrogen and phosphorus retranslocation of leaves and stemwood in a mature eucalyptus forest exposed to 5 years of elevated CO2. *Front. Plant Sci.* 10:664. doi: 10.3389/fpls.2019.00664

Drinkwater, L. E., and Snapp, S. S. (2007). Nutrients in agroecosystems: rethinking the management paradigm. *Adv. Agronomy* 92, 163–186. doi: 10.1016/s0065-2113(04)92003-2

Elser, J. J., Fagan, W. F., Kerkhoff, A. J., Swenson, N. G., and Enquist, B. J. (2010). Biological stoichiometry of plant production: metabolism, scaling and ecological response to global change. *New Phytol.* 186, 593–608. doi: 10.1111/j.1469-8137.2010.03214.x

Fan, H. B., Wu, J. P., Liu, W. F., Yuan, Y. H., Hu, L., and Cai, Q. K. (2015). Linkages of plant and soil C:N:P stoichiometry and their relationships to forest growth in subtropical plantations. *Plant Soil.* 392, 127–138.

Feng, H. Y., Du, M. Y., Xin, X. B., Gao, X., Zhang, L. J., Kong, Q. Y., et al. (2019). Seasonal variation in C, N, and P stoichiometry of Platycladus orientalis plantation in the rocky mountainous areas of North China. *Acta Ecol. Sinica* 39, 1572–1582. doi: 10.5846/stxb201803120483

Geng, Y., Wu, Y., and He, J. S. (2011). Relationship between leaf phosphorus concentration and soil phosphorus availability across Inner Mongolia grassland. *Chinese J. Plant Ecol.* 35, 1–8.

Hamerlynck, E. P., Huxman, T. E., Mcauliffe, J. R., and Smith, S. D. (2004). Carbon isotope discrimination and foliar nutrient status of *Larrea tridentata* (creosote bush) in contrasting Mojave Desert soils. *Oecologia* 138, 210–215. doi: 10.1007/s00442-003-1437-7

Han, W. X., Fang, J. Y., Reich, P. B., Woodward, F. I., and Wang, Z. H. (2011). Biogeography and variability of eleven mineral elements in plant leaves across gradients of climate, soil and plant functional type in China. *Ecol. Lett.* 14, 788–796. doi: 10.1111/j.1461-0248.2011.01641.x

Han, W., Fang, J., Guo, D., and Zhang, Y. (2005). Leaf nitrogen and phosphorus stoichiometry across 753 terrestrial plant species in China. *New Phytol.* 168, 377–385. doi: 10.1111/j.1469-8137.2005.01530.x

He, J. S., Wang, L., Flynn, D. F. B., Wang, X. P., Ma, W. H., and Fang, J. Y. (2008). Leaf nitrogen: phosphorus stoichiometry across Chinese grassland biomes. *Oecologia* 155, 301–310. doi: 10.1007/s00442-007-0912-y

Hedges, J. I., Clark, W. A., Quay, P. D., Richey, J. E., Devol, A. H., and Santos, M. (1986). Compositions and fluxes of particulate organic material in the Amazon River. *Limnol. Oceanogr.* 31, 717–738.

Jing, H. X., Sun, N., Umair, M., Liu, C., and Du, H. (2020). Stoichiometric characteristics of soils and dominant shrub leaves and their responses to water addition in different seasons in degraded karst areas in southern yunnan of China. *Chinese J. Plant Ecol.* 44, 56–69.

Lambers, H., Raven, J. A., Shaver, G. R., and Smith, S. E. (2008). Plant nutrient-acquisition strategies change with soil age. *Trends Ecol. Evol.* 23, 95–103. doi: 10.1016/j.tree.2007.10.008

Lee, J. S., Ihm, B. S., Du, S. C., Son, D. Y., and Kim, J. W. (2007). Soil particle sizes and plant communities on coastal dunes. *J. Plant Biol.* 50, 475–479. doi: 10.1007/BF03030685

Li, H., Li, J., He, Y. L., Li, S. J., Liang, Z. S., Peng, C. H., et al. (2013). Changes in carbon, nutrients and stoichiometric relations under different soil depths, plant tissues and ages in black locust plantations. *Acta Physiol. Plan.* 35, 2951–2964. doi: 10.1007/s11738-013-1326-6

Li, M., Huang, C., Yang, T., Drosos, M., Wang, J. Z., Kang, X. M., et al. (2019). Role of plant species and soil phosphorus concentrations in determining phosphorus: nutrient stoichiometry in leaves and fine roots. *Plant Soil.* 445, 231–242.

Li, T., Sun, J. K., and Fu, Z. Y. (2021). Halophytes differ in their adaptation to soil environment in the Yellow River Delta: effects of water source, soil depth, and nutrient stoichiometry. *Front. Plant Sci.* 12:675921. doi: 10.3389/fpls.2021.675921

Liu, Y., He, J. W., Yu, H., Lin, Y. M., and Wang, D. J. (2020). Nutrients (C, N, P) contents and stoichiometric ratios of fine root, coarse root and leaf in dominant shrubs in dry-hot valley. *Mountain Res.* 38, 668–678.

Lu, R. K. (1999). *Analytical Methods for Soil and Agro-Chemistry*. Beijing: China Agricultural Science and Technology Press.

Luo, Y., Peng, Q., Li, K., Gong, Y., and Han, W. (2021). Patterns of nitrogen and phosphorus stoichiometry among leaf, stem and root of desert plants and responses to climate and soil factors in xinjiang, China. *Catena* 199:105100.

Niu, D. C., Li, Q., Jiang, S. G., Chang, P. J., and Fu, H. (2013). Seasonal variations of leaf C:N:P stoichiometry of six shrubs in desert of China's Alxa Plateau. *Chinese J. Plant Ecol.* 37, 317–325.

Ping, C., Wang, C. K., and Quan, X. K. (2014). Influence of environmental changes on stoichiometric traits of nitrogen and phosphorus for *Larix gmelinii* trees. *Acta Ecol Sinica* 34, 1965–1974. doi: 10.5846/stxb201306301805

Salazar, T. D., Castro, J., Villar, S. P., Vinegla, B., Matías, L., Michelsen, A., et al. (2018). The "isohydric trap": a proposed feedback between water shortage, stomatal regulation, and nutrient acquisition drives differential growth and survival of European pines under climatic dryness. *Global Change Biol.* 24, 4069–4083. doi: 10.1111/gcb.14311

Sardans, J., Rivas, A., and Penelas, J. (2012). The C: N: P stoichiometry of organisms and ecosystems in a changing world: a review and perspectives. *Perspect. Plant Ecol.* 14, 33–47.

Sheng, W. P., Ren, S. J., Yu, G. R., Fang, H. J., Jiang, C. M., and Zhang, M. (2011). Patterns and driving factors of WUE and NUE in natural forest ecosystems along the North-South Transect of Eastern China. *J. Geograph. Sci.* 21, 651–665. doi: 10.1007/s11442-011-0870-5

Suzuki, S., Abe, M., and Motokawa, M. (2011). Allometric comparison of skulls from two closely related weasels, *Mustela itatsi* and *M. sibirica*. *Zoology* 28, 676–688. doi: 10.2108/zsj.28.676

Tang, Z., Xu, W., Zhou, G., Bai, Y., Li, J., Tang, X., et al. (2018). Patterns of plant carbon, nitrogen, and phosphorus concentration in relation to productivity in China's terrestrial ecosystems. *Proc. Natl. Acad. Sci. U S A.* 115, 4033–4038.

Wang, M., Murphy, M. T., and Moore, T. R. (2014). Nutrient resorption of two evergreen shrubs in response to long-term fertilization in a bog. *Oecologia* 174, 365–377. doi: 10.1007/s00442-013-2784-7

Wang, Z. N., Lu, J. Y., Yang, H. M., and Zhang, Q. P. (2015). Stoichiometric characteristics of carbon, nitrogen, and phosphorus in leaves of differently aged lucerne (*Medicago sativa*) stands. *Front. Plant Sci.* 6:1062. doi: 10.3389/fpls.2015.01062

Weih, M., Pourazari, F., and Vico, G. (2016). Nutrient stoichiometry in winter wheat: element concentration pattern reflects developmental stage and weather. *Sci. Rep.* 6:35958. doi: 10.1038/srep35958

Xia, D. J., Liu, Q. R., Zou, L., Ge, Z. W., Xue, J. H., and Peng, S. L. (2020). Foliarδ13C correlates with elemental stoichiometry in halophytes of coastal wetlands. *Acta Ecol. Sinica* 40, 2215–2224. doi: 10.5846/stxb201901170140

Xie, W. H., Zhou, R. L., Liang, H. M., Qu, H., and Qiang, S. B. (2015). Physiological difference in *Messerschmidia sibirica* grown in inland and coastal sand land in nature environment and under sand burial. *J. Desert Res.* 35, 1538–1548.

Xiong, X. S., Cai, H. Y., Li, Y. Q., Ma, W. H., Niu, K. C., Chen, D. M., et al. (2020). Seasonal dynamics of leaf C, N and P stoichiometry in plants of typical steppe in Nei Mongol, China. *Chinese J. Plant Ecol.* 44, 1138–1153.

Yan, W. M., Zhong, Y. Q., Zheng, S. X., and Shangguan, Z. P. (2016). Linking plant leaf nutrients/stoichiometry to water use efficiency on the Loess Plateau in China. *Ecol. Eng.* 87, 124–131. doi: 10.1016/j.ecoleng.2015.11.034

Yang, C., and Xu, W. (2021). Seasonal variations in carbon, nitrogen, and phosphorus stoichiometry of a *Robinia pseudoacacia* plantation on the Loess Hilly Region. China. *Forests* 12:214. doi: 10.3390/f12020214

Yuan, Z. Y., Chen, H. Y. H., and Reich, P. B. (2011). Global-scale latitudinal patterns of plant fine-root nitrogen and phosphorus. *Nat. Commun.* 2:344. doi: 10.1038/ncomms1346

Zhang, P., Bakker, E. S., Zhang, M., and Xu, J. (2016). Effects of warming on *Potamogeton crispus* growth and tissue stoichiometry in the growing season. *Aquatic Botany* 128, 13–17.

Zhang, C. W., Tian, X. Y., and Zhang, C. S. (2019a). Diversity and probiotic activities of endophytic bacteria associated with the coastal halophyte *Messerschmidia sibirica*. *Appl. Soil Ecol.* 143, 35–44.

Zhang, X. S., Joachimski, M. M., Over, D. J., Ma, K. Y., Huang, C., and Gong, Y. M. (2019b). Late Devonian carbon isotope chemostratigraphy: a new record from the offshore facies of South China. *Global Planet. Change* 182:103024.

Zhou, T. C., Sun, J., Liu, M., Shi, P. L., and Tsunekawa, A. (2019). Coupling between plant nitrogen and phosphorus along water and heat gradients in alpine grassland. *Sci. Total Environ.* 701:134660. doi: 10.1016/j.scitotenv.2019.134660

**Conflict of Interest:** The authors declare that the research was conducted in the absence of any commercial or financial relationships that could be construed as a potential conflict of interest.

**Publisher's Note:** All claims expressed in this article are solely those of the authors and do not necessarily represent those of their affiliated organizations, or those of the publisher, the editors and the reviewers. Any product that may be evaluated in this article, or claim that may be made by its manufacturer, is not guaranteed or endorsed by the publisher.

frontiers | Frontiers in Ecology and Evolution

ORIGINAL RESEARCH
published: 04 July 2022
doi: 10.3389/fevo.2022.941032

# Effects of Melatonin Priming on *Suaeda corniculata* Seed Germination, Antioxidant Defense, and Reserve Mobilization: Implications for Salinized Wetland Restoration

*Mingye Zhang[1,2†], Shuchen Liu[3†], Shouzheng Tong[1*], Dongjie Zhang[4], Qing Qi[5], Yanji Wang[1,2], Xuehong Wang[6], Yu An[1] and Xianguo Lu[1]*

*[1] Key Laboratory of Wetland Ecology and Environment, Northeast Institute of Geography and Agroecology, Chinese Academy of Sciences, Changchun, China, [2] University of Chinese Academy of Sciences, Beijing, China, [3] School of Environment, Northeast Normal University, Changchun, China, [4] Shandong Key Laboratory of Eco-Environmental Science for the Yellow River Delta, Binzhou University, Binzhou, China, [5] Shijiazhuang University, Shijiazhuang, China, [6] The Institute for Advanced Study of Coastal Ecology, Key Laboratory of Ecological Restoration and Conservation of Coastal Wetlands in Universities of Shandong, Ludong University, Yantai, China*

OPEN ACCESS

**Edited by:**
*He Yixin,*
*Chengdu Institute of Biology (CAS), China*

**Reviewed by:**
*Junhong Bai,*
*Beijing Normal University, China*
*Jun You,*
*Oil Crops Research Institute (CAAS), China*

***Correspondence:**
*Shouzheng Tong*
*tongshouzheng@iga.ac.cn*

*† These authors have contributed equally to this work*

**Specialty section:**
*This article was submitted to Conservation and Restoration Ecology, a section of the journal Frontiers in Ecology and Evolution*

**Received:** *11 May 2022*
**Accepted:** *06 June 2022*
**Published:** *04 July 2022*

**Citation:**
*Zhang M, Liu S, Tong S, Zhang D, Qi Q, Wang Y, Wang X, An Y and Lu X (2022) Effects of Melatonin Priming on Suaeda corniculata Seed Germination, Antioxidant Defense, and Reserve Mobilization: Implications for Salinized Wetland Restoration. Front. Ecol. Evol. 10:941032. doi: 10.3389/fevo.2022.941032*

Melatonin priming has been widely reported to positively affect seed germination under abiotic stresses. However, there is still a gap in knowledge on how melatonin priming impacts the seed germination and physiological change of wetland plant species. We assessed the effects of different melatonin concentrations on germination characteristics, antioxidant defense, and reserve mobilization of *Suaeda corniculata* seeds. Priming of *S. corniculata* seeds with 50 μM melatonin significantly improved the germination rate, germination speed, germination index, superoxide dismutase and peroxidase activity, and soluble sugar content as compared with the control, and effectively reduced the malondialdehyde content, promoted starch, soluble protein, and fat mobilization. However, the stress tolerance ability of *S. corniculata* seeds was reduced by high melatonin concentration. The structural equation model indicated that the melatonin priming directly affects the seed germination, while also indirectly regulating the antioxidant defense system and reserve mobilization. In conclusion, melatonin priming affects the *S. corniculata* seed germination under salinization stress in a concentration-dependent manner via both direct and indirect regulatory pathways. Insights into these aspects will advance our understanding of how melatonin priming affects *S. corniculata* seed germination and provide invaluable information and technical support for the restoration of salinized wetlands in the Momoge National Nature Reserve.

**Keywords: antioxidant defense, melatonin priming, reserve mobilization, salinization stress, seed germination, *Suaeda corniculata*, wetland restoration**

## INTRODUCTION

Salinization causes major losses in the earth's ecosystem, with nearly 831 million hectares of land undergoing salinization globally (Ma et al., 2015; Zhao et al., 2021a). Salinization is becoming more widespread due to the interactions between the global climate change and anthropogenic hydrological modifications, especially in the wetland ecosystems in arid and semi-arid regions (An et al., 2019; Feghhenabi et al., 2020; Wang et al., 2021). Salinization not only changes the fundamental physicochemical properties of soil, but also negatively affects the seed germination and plant growth by disturbing the physio-biochemical processes including ionic imbalance, oxidative stress, and osmotic stress, thereby reducing the effective wetlands area, thereby resulting in gradual changes or even disappearance of wetland ecosystem services (Tahjib et al., 2018; Wang et al., 2019; Zhang et al., 2019). Therefore, the quick and effective restoration of salinity-degraded wetlands has become an urgent global concern.

Seeds are pivotal propagative organs which carry the genetic information and support the multifunctional evolution in plants (Kettenring and Tarsa, 2020). Employing strategic seed-based approaches in wetland restoration is key to faster and complete recovery of the targeted underlying vegetation structure and composition (James and Carrick, 2016; Zhang M. Y. et al., 2021). Besides being the beginning of the life cycle of higher plants, seed germination is also the most environmentally stress-sensitive stage of the plant's life history (Chen et al., 2021). Previous studies had identified that salinization weakens the seeds' ability to absorb water from the soil as well as inhibits the growth of the seed and the embryo (Li et al., 2019). Moreover, salinization disturbs the delicate balance between the intracellular ROS production and scavenging, and also reduces the ability of reserve mobilization in seeds (Ibrahim, 2016). The seed's stress-amelioration techniques, which can address limiting environmental constraints, are crucial for improving outcomes in degraded salinized wetlands (Kettenring and Tarsa, 2020). In recent decades, various strategies have been adopted to enhance the abiotic stress tolerance of seeds, such as genetic approach, genetic engineering, and plant breeding. However, these methods are complex, time-consuming, expensive, and have biosafety issues (Cao et al., 2019; Johnson and Puthur, 2021). Therefore, the development of a simple, effective, and economical strategy will be significant in improving the salinization stress tolerance of seeds.

Priming is a pretreatment technology which hydrates the seed in specific solutions for initiating specific metabolic processes before germination (Masondo et al., 2018). It is proven to be an effective and safe strategy for addressing the current and future issues of seed germination under abiotic stress conditions (Forti et al., 2021). The priming treatment enhances the inherent tolerance potential of seeds through many mediums, which, based on hormone, have been widely applied in the pretreatment of commercial seeds (Li et al., 2020; Zhang Y. et al., 2021). Melatonin (N-acetyl-5-methoxtryptamine), an endogenous indoleamine, is a highly evolutionarily conserved multifunctional molecule, which is proven to be an abiotic anti-stress hormone in seeds and is recently being considered as a research hotspot in the priming domain (Li et al., 2016; Arnao and Hernandez-Ruiz, 2019; Zhang T. G. et al., 2022). Recent studies have demonstrated that melatonin priming boosted the activities and transcript levels of antioxidant enzymes in seeds for effectively scavenging salinization stress-induced ROS, and consequently improving their salinization stress tolerance ability during seed germination (Yan et al., 2020). Additionally, melatonin priming also promotes seed germination under salinization stress by regulating carbohydrate metabolism and enhancing reserve mobilization (Zhao et al., 2015; Seneviratne et al., 2019). However, due to the differences in seed parameters, the most optimum effect of melatonin priming needs to be quantified according to the target seed. Additionally, most studies have focused only on how melatonin priming affects crops and fodder grasses, but little is known about their effect on wetland species under salinization stress.

The Ramsar-listed Momoge National Nature Reserve (MNNR), a vital stopover habitat on the migration route of East Asian-Australasian migratory birds, serves as an ecological barrier in preventing the soil salinization and desertification in the Songnen plain (Tang et al., 2021; Zhang M. Y. et al., 2022). Over the past 50 years, soil salinization due to climate change and anthropogenic activities has resulted in a loss of wetland area and severely limited the ecological service functions in the MNNR (Li X. Y. et al., 2017). As an indigenous species, *Suaeda corniculata* is widely distributed in the lake, river, and saline wetlands in MNNR. It was selected as the pioneer species for vegetation restoration in this region due to their ability to absorb soluble salt from soil and consequently increase their organic matter content (Zhao et al., 2003; Yang et al., 2017; Wang D. W. et al., 2020). Recently, the MNNR plans to not only implement the seed-based wetland restoration project, but also enhance the salinization stress tolerance ability of *S. corniculata* to improve their impact on wetland restoration. Therefore, studying the effect of melatonin priming on *S. corniculata* seed germination, antioxidant defense, and reserve mobilization is of great importance in achieving wetland restoration.

Due to the primary aim of restore degraded salinization wetlands, current studies have deepened our comprehension of sexual propagation-based restoration strategies. However, little is known about the positive effects of improve stress tolerance of germinating seeds by priming treatment (Wang X. Y. et al., 2020; Zhao et al., 2021b). In this study, laboratory experiment was carried out to investigate the effects of melatonin priming on *S. corniculata* seed germination, antioxidant enzyme activity, and reserve mobilization. The aims of this study are: (1) to examine the response of *S. corniculata* seed germination to melatonin priming; (2) to identify the effect of melatonin priming on *S. corniculata* seed's antioxidant enzyme activity and reserve mobilization; and (3) to reveal the tolerance regulatory pathways induced by melatonin priming during *S. corniculata* seed germination under salinization stress conditions. We hypothesized that the accelerating effect of exogenous melatonin happens in a concentration-dependent manner during *S. corniculata* seed germination under salinization stress. This study will assist facilitate the understanding of the

protective effects of seed priming under abiotic stress conditions, and also provide technique guidelines for salinized wetland restoration in the MNNR.

# MATERIALS AND METHODS

## Seed Materials

Matures seeds were collected in late September 2020 from the wild *S. corniculata* populations in the Ertou wetlands in the MNNR (45°53′ – 45°55′ N, 123°36′ – 123°41′ E). The collected seeds were air-dried indoors under dark conditions and then stored in cloth bags at 4°C until the start of the experiment in January 2022. Healthy *S. corniculata* seeds were surface-sterilized using 75% ethanol for 10 min and then rinsed 9 times with distilled water, and the water was wiped off the seeds surface with sterile filter paper in the super clean bench before being used in the experiments.

## Experimental Design

The experiment was conducted in the Key Laboratory of Wetland Ecology and Environment of the Northeast Institute of Geography and Agroecology, Chinese Academy of Sciences. We selected six priming treatments: MT10 (10 μM melatonin), MT20 (20 μM melatonin), MT50 (50 μM melatonin), MT100 (100 μM melatonin), MT200 (200 μM melatonin), and CK (distilled water). Seeds were incubated in each priming solution for 12 h. For each treatment, 25 seeds were evenly placed in Petri dishes (diameter 9 cm) containing double Whatman No. 1 filter paper soaked with 2 ml of 30 mM $NaHCO_3$ solution (the salt solution concentration data comes from the MNNR), and sealed with Parafilm® to prevent moisture evaporation. The seeds were then germinated in an artificial climate box (RDN-300B-4, China) under an alternating cycle of 12/12 h light and dark at an average temperature of 22.5/8.6°C (the climate data represents field conditions in May in the MNNR). For each germination treatment, five independent replicates were used (three petri dishes were used to test the germination rate of *S. corniculata* seeds, while two petri dishes were used to cultivate testable seed materials). Germinated seeds were recorded daily, and germination was considered having occurred when the radicle $\geq$ 2 mm. The entire experiment lasted for 7 days (from $6^{th}$ to $12^{th}$ January, 2022) and partial seeds were harvested on days 1, 3, 5, and 7, and immediately frozen in liquid nitrogen and stored at −80°C until further analysis of antioxidant enzymes and reserve substances.

## Determination of Germination

In order to describe seed germination changes, the germination rate (GR), germination speed (GS), and germination index (GI), were measured according to following Biju et al. (2017):

$$GR = \frac{n}{N} \times 100\% \quad (1)$$

$$GS = (N_1 + \frac{N_2 - N_1}{2} + \frac{N_3 - N_2}{3} + \ldots + \frac{N_t - N_{t-1}}{t}) \times 100 \quad (2)$$

$$GI = \sum \frac{G_t}{D_t} \quad (3)$$

where n is the number of germinated seeds, N is the total number of the tested seeds, Nt is the percentage of germinated seeds at the $t^{th}$ days, $G_t$ is the number of germinated seeds in t days, and Dt is the corresponding germination days.

## Determination of Antioxidant Enzyme Activity and Reserve Content

The activities of superoxide (SOD), peroxidase (POD), and the malondialdehyde (MDA) content were determined via WST-8, visible-spectrophotometry and TBA-spectrophotometry by using detection kits (M0102B, M0105B, M0106B, Michy Biomedical Technology Co., Ltd., Suzhou, China), respectively. The contents of starch (ST), soluble sugar (SS), and soluble protein (SP) were determined by detection kits (M1101B, M1503B, M1806B, Michy Biomedical Technology Co., Ltd., Suzhou, China) which are based on anthrone-sulfuric acid colorimetry, anthrone colorimetry, and Lowry's method, respectively. The fat content was determined by the supercritical fluid-Soxhlet extractor using petroleum ether as the extraction buffer (Soriano et al., 2011). All the samples were conducted in three independent biological replicates.

## Statistical Analysis

Statistical analysis was conducted using SPSS 22.0 (SPSS, Chicago, IL, United States) and Origin Pro 2022 (OriginLab, Northampton, MA, United States). The data normality and homogeneity were checked before further analyses; seed GR, SOD, and ST were log-transformed and square root transformed to meet the assumptions of homoscedasticity. Effects of melatonin priming on *S. corniculata* seeds under salinization stress were evaluated using one-way analysis of variance (ANOVA). Duncan's multiple comparison test was used to determine the significant differences at the 0.05 significance level. Pearson's correlation analysis was performed to identify the correlational relationship between antioxidant enzymes, reserve contents, as well as seed germination. Structural equation model (SEM) analysis was performed to evaluate the direct and indirect regulatory pathways of melatonin priming on *S. corniculata* seed germination in SPSSAU[1].

# RESULTS

## Seed Germination Characteristics

Among the different priming treatments, we observed significant differences in the *S. corniculata* seed GR ($F = 20.64$, $p < 0.05$), ranging from 51.33 to 87.33%, with the maximum and minimum being recorded in the M50 and M200 treatments, respectively (**Figure 1A**). Priming treatment significantly affected the GS ($F = 13.20$, $p < 0.05$), which peaked in M50 (7.47) and was 1.80 times greater than in the M200 treatment (**Figure 1B**). Additionally, the GI was significantly affected by the priming treatments ($F = 19.75$, $p < 0.05$). The GI values

[1] www.spssau.com

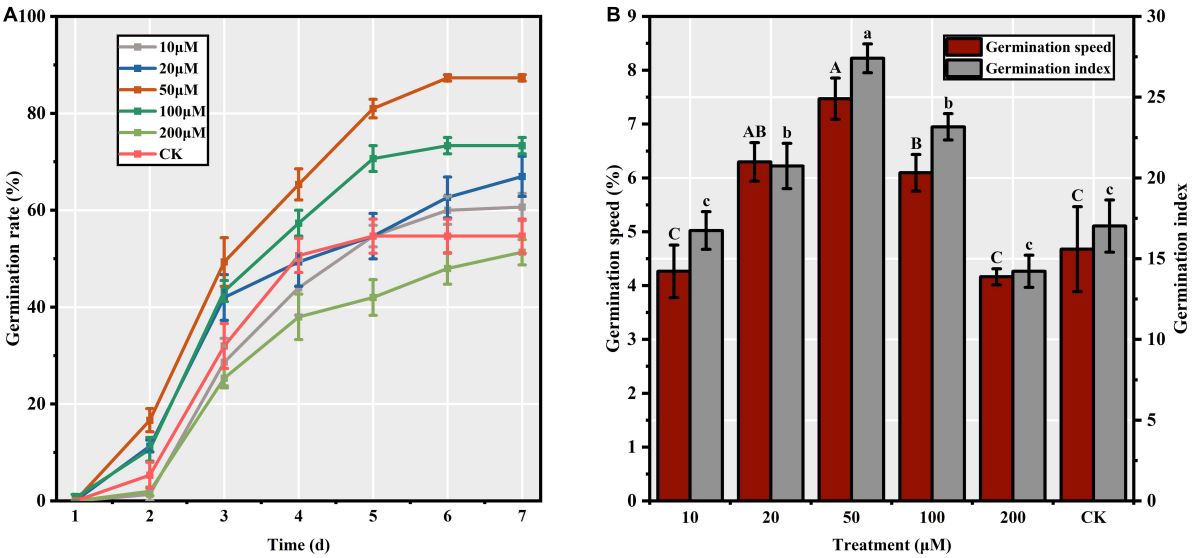


**FIGURE 1 |** Effect of melatonin priming on *Suaeda corniculata* seed germination (means ± standard errors, $n = 3$). **(A)** Germination rate of Suaeda corniculata seeds. **(B)** Germination speed and Germination index of Suaeda corniculata seeds. Different capital letters indicate the significant differences in GS at the 0.05 significance level. Different small letters indicate the significant differences in GI at the 0.05 significance level.

recorded in the M50 treatment (27.41 ± 0.89) were 61.05 and 92.28% higher than those in CK and M200 treatment, respectively (**Figure 1B**).

## Antioxidant Enzymes Activity and Malondialdehyde Content

We identified significant differences in the activities of antioxidant enzymes of *S. corniculata* seeds at each stage under different melatonin priming treatments (**Table 1** and **Figure 2**). The antioxidant enzymes activities showed a gradually increasing trend during germination stage, with both SOD and POD activities peaking in the M50 treatment on the 7$^{th}$ day, and which were 2.59 and 3.67 times greater than the M200 treatment during the same period (**Figures 2D,H**). The degree of membrane lipid peroxidation in *S. corniculata* seeds was significantly affected by the melatonin priming treatments (**Figure 2**). The MDA content gradually decreased with germination time, with its lowest value appearing in the M50 treatment on the 7$^{th}$ day, and it was 27.33% lower than that on the 1st day (**Figures 2I,L**).

## Reserve Mobilization

Melatonin priming significantly affected the reserve mobilization process in *S. corniculata* seeds (**Table 1**). The trend of changes in the starch and fat contents was basically uniform across each stage, i.e., they decreased significantly with the increase in germination days, where the seed starch and fat contents under M50 treatment decreasing up to 40.36 and 8.87%, respectively (**Figures 3A,D**). The soluble sugar content continuously increased with the germination stage, with the increase ranging from 13.90 to 56.11% under each melatonin treatment (**Figure 3B**). Additionally, the soluble protein content initially increased before decreasing during the process of *S. corniculata* seed germination (**Figure 3C**). By the 7$^{th}$ day, the soluble protein content of the M200 treatment was the highest, thus indicating that its mobilization level was significantly lower than in the other treatments.

## The Coupling Relationships of Seed Germination, Antioxidant Enzyme Activity, and Reserve Mobilization Under Melatonin Priming Treatments

We observed significant positive relationships between SOD, POD, and soluble sugar, while there were significant negative relationships with MDA, starch, soluble protein, and fat (**Figure 4**). Additionally, the GR was significantly correlated with antioxidant enzymes' activity and reserve mobilization. The SEM analysis showed that the differences in melatonin concentration priming were directly related to the antioxidant enzymes' activity, reserve mobilization, and seed germination (**Figure 5**). Meanwhile, melatonin priming also indirectly affected *S. corniculata* seed germination by affecting their antioxidant enzymes' activity and reserve mobilization. Additionally, the degree of reserve mobilization directly affected the level of antioxidant enzymes' activity.

# DISCUSSION

Since soil salinization had caused losses of ecological functions and also in wetland area in the MNNR, the process of effectively restoring degraded wetlands has attracted a lot of attention from the wetland manager and policymakers (Zhao et al., 2021a). Priming treatment, a key technique to alleviate the effects of abiotic stress on seed germination, had been attempted

**TABLE 1 |** Result (*F* and *p*-values) of one-way ANOVAs about the priming with melatonin effects on *Suaeda corniculata* seed antioxidant enzymes activity and reserve traits.

| Traits | 1st day | | 3rd day | | 5th day | | 7th day | |
|---|---|---|---|---|---|---|---|---|
| | F | *p* | F | *p* | F | *p* | F | *p* |
| SOD | 8.794 | 0.000*** | 32.911 | 0.000*** | 23.023 | 0.000*** | 9.898 | 0.000*** |
| POD | 9.319 | 0.000*** | 5.148 | 0.002** | 21.700 | 0.000*** | 20.397 | 0.000*** |
| MDA | 3.592 | 0.013* | 5.479 | 0.001** | 2.802 | 0.046* | 10.054 | 0.000*** |
| ST | 0.969 | 0.454 | 0.440 | 0.817 | 0.292 | 0.913 | 2.187 | 0.040* |
| SS | 3.802 | 0.010* | 0.525 | 0.755 | 0.618 | 0.687 | 3.316 | 0.039* |
| SP | 2.824 | 0.035* | 0.406 | 0.840 | 0.660 | 0.657 | 4.893 | 0.003** |
| FA | 1.409 | 0.253 | 1.090 | 0.388 | 1.774 | 0.152 | 8.189 | 0.000*** |

*SOD, superoxide dismutase; POD, peroxidase; MDA, malondialdehyde; ST, starch; SS, soluble sugar; SP, soluble protein; FA, fat; *p < 0.05; **p < 0.01; ***p < 0.001.*

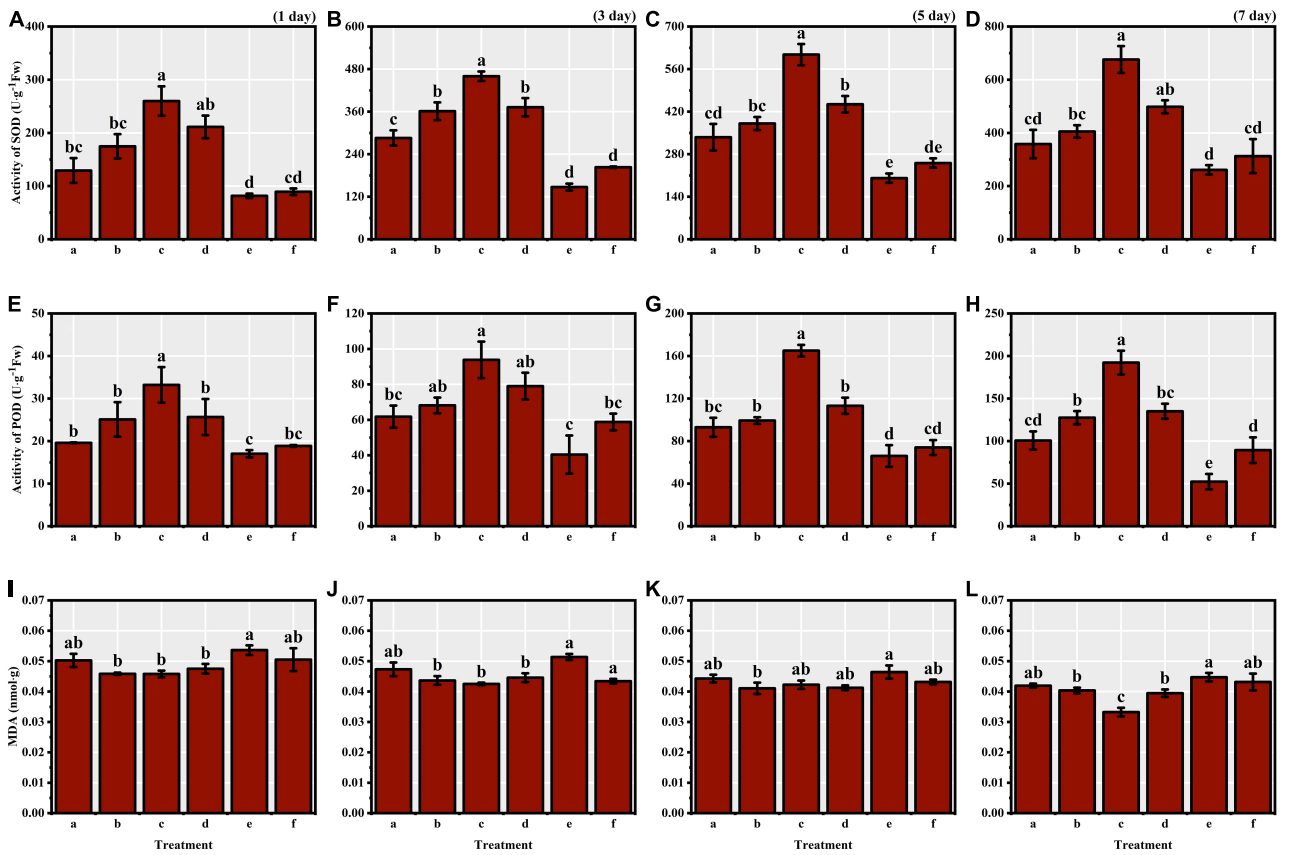


**FIGURE 2 |** The antioxidant enzymes' activity and MDA content of *Suaeda corniculata* seeds under melatonin priming during the entire germination period (means ± standard errors, *n* = 3). Different letters indicate the significant differences at the 0.05 significance level. SOD, superoxide dismutase; POD, peroxidase; MDA, malondialdehyde; (a) M10; (b) M20; (c) M50; (d) M100; (e) M200; (f) CK. **(A)** SOD of 1st day; **(B)** SOD of 3th day; **(C)** SOD of 5th day; **(D)** SOD of 7th day; **(E)** POD of 1st day; **(F)** POD of 3th day; **(G)** POD of 5th day; **(H)** POD of 7th day; **(I)** MDA of 1st day; **(J)** MDA of 3th day; **(K)** MDA of 5th day; **(L)** MDA of 7th day.

recently in wetland restoration engineering (Zhang M. Y. et al., 2021). It boosts the antioxidant and DNA repair systems, and also modulates the reserve mobilization for improving seed germination (Yan et al., 2020; Forti et al., 2021). Our results support the notion of effectively applying the priming treatment to wetland plant seed germination, and thus confirm the previously proposed hypothesis that melatonin priming had a concentration-dependent effect on *S. corniculata* seed germination during salinization stress. Priming with M50 had significantly positive effects on the seed germination, antioxidant defense, and reserve mobilization of *S. corniculata*.

## Effect of Melatonin Priming on the Seed Germination of *Suaeda corniculata*

Seed propagation is preferred for maintaining plant genetic variation, and it will also play an important role in the process of near-naturalized wetland restoration (Kim, 2019). The seed

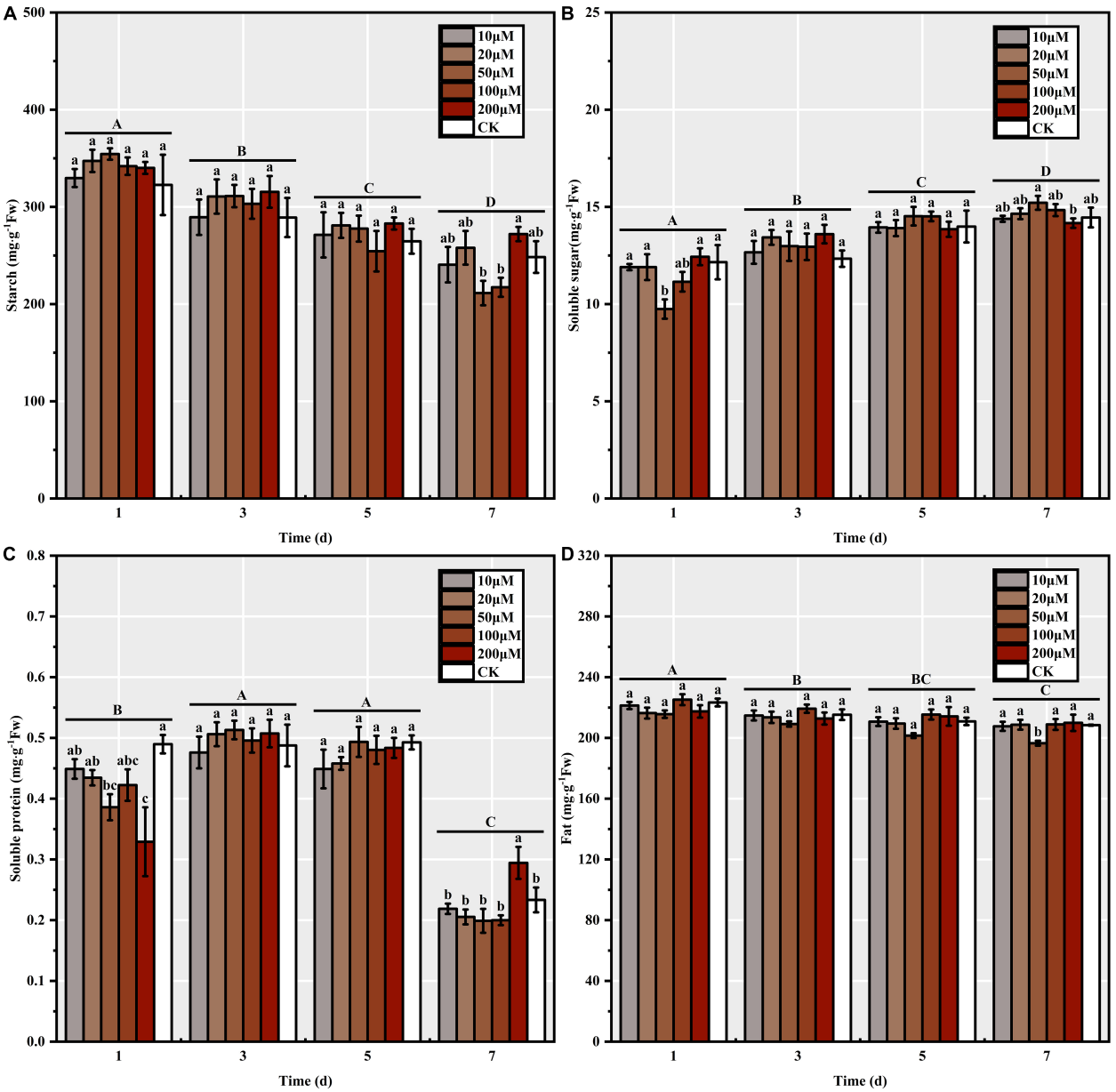


**FIGURE 3 |** The reserve mobilization of *Suaeda corniculata* seeds under melatonin priming during the entire germination period (means ± standard errors, $n = 3$). **(A)** Starch, **(B)** Soluble sugar, **(C)** Soluble protein, and **(D)** Fat of *Suaeda corniculata* seeds. Different capital letters indicate significant differences in the germination stages at the 0.05 significance level; different small letters indicate significant differences in the treatments at the 0.05 significance level.

germination process is usually affected by salinization stress, which leads to the decrease in germination quality and even results in an incomplete plant life cycle (Jia et al., 2018). Multiple studies have shown that melatonin is a major regulator not only involved in seed germination, but also in diverse physiological and biochemical processes like stress resistance-related gene expression, boosting the antioxidant defense system, and reserve mobilization (Cao et al., 2019; Chen et al., 2021; Zhang T. G. et al., 2022). Our results showed that melatonin priming positively affected seed germination of *S. corniculata* in a concentration-dependent manner, while significantly increasing the GR, GS, and GI of *S. corniculata* seed under the M50 treatment. This finding was consistent with Qin and Zeevaart (2002) and Ogawa et al. (2003), where they found that exogenous melatonin priming upregulates the expression of gibberellins (GA) biosynthesis genes (GA20ox and GA30ox), while downregulating the key abscisic acid (ABA) biosynthesis genes (LbNCED1 and LbNCED3), both of which affect seed germination. Additionally, the appropriate melatonin priming concentration activated the SOS pathway to improve the seed's

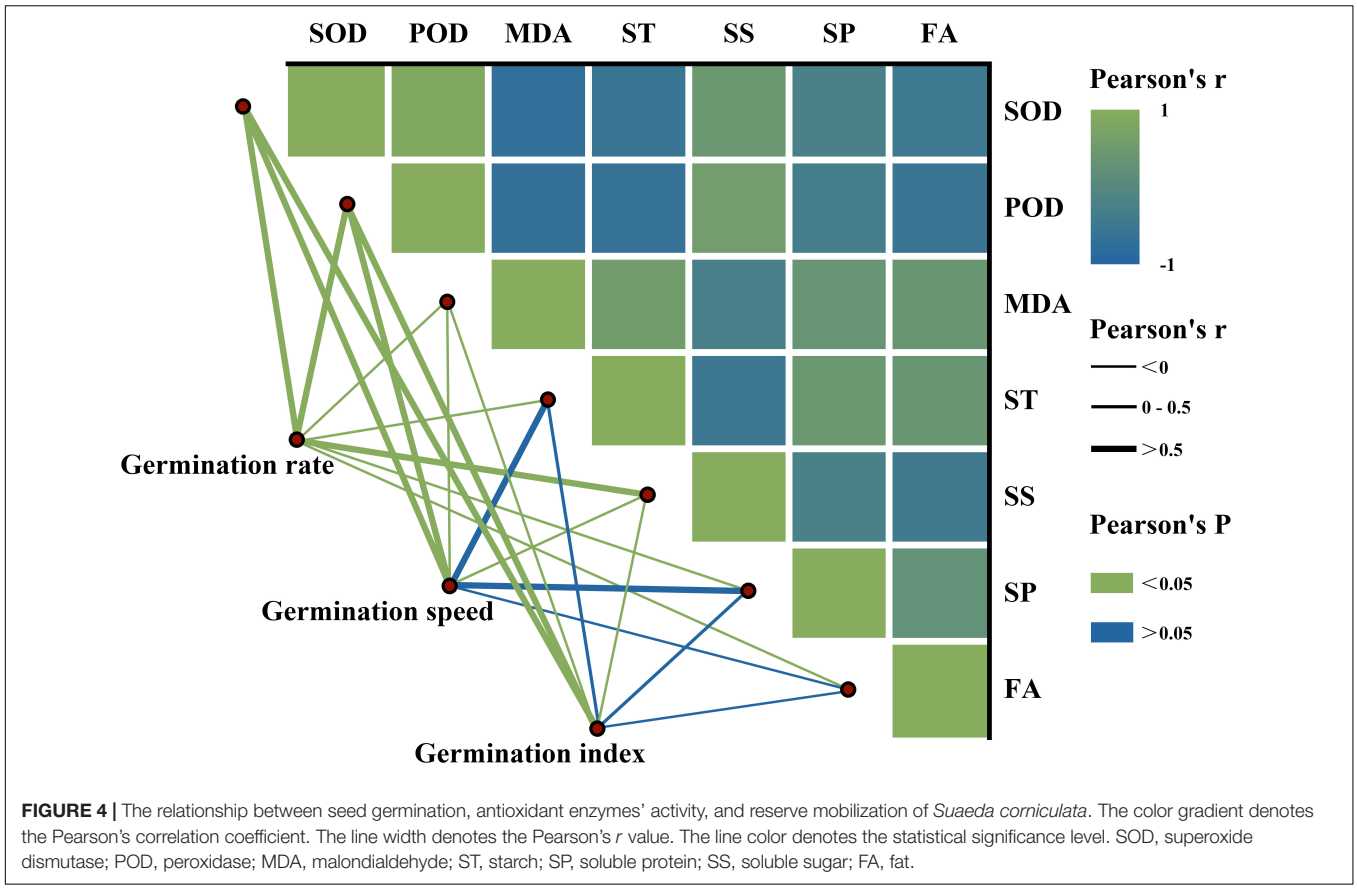


**FIGURE 4 |** The relationship between seed germination, antioxidant enzymes' activity, and reserve mobilization of *Suaeda corniculata*. The color gradient denotes the Pearson's correlation coefficient. The line width denotes the Pearson's *r* value. The line color denotes the statistical significance level. SOD, superoxide dismutase; POD, peroxidase; MDA, malondialdehyde; ST, starch; SP, soluble protein; SS, soluble sugar; FA, fat.

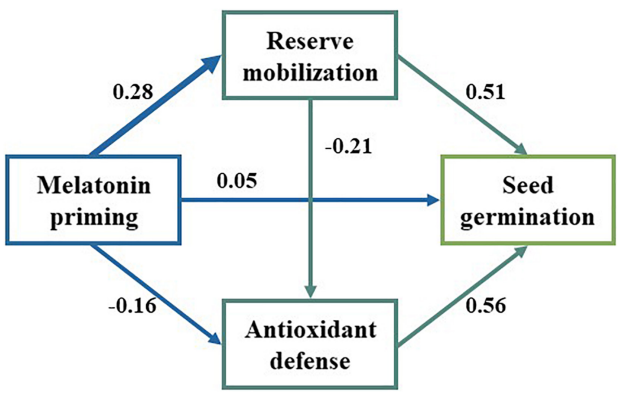


**FIGURE 5 |** The structural equation model (SEM) analysis was performed to evaluate the effect of the influential pathways of melatonin priming on reserve mobilization, antioxidant activity (SOD and POD) and seed germination. The arrows indicate the assumed pathways. The arrow width is proportional to the strength of the pathways. The number on the arrow is the path coefficients ($\chi^2$ = 4.311, dfp = 2, $p$ = 0.116, CFI = 0.995, RMSEA = 0.094).

salinity tolerance at the germination stage by upregulating the expression of chloride channel proteins (CLC1 and CLC2) (Li X. J. et al., 2017). Meanwhile, priming with the appropriate melatonin concentration could up-regulate the ethylene, kinetin, and brassinolide biosynthetic gene expression and the plant hormone signal pathways in response to salinization stress (Zhang Y. X. et al., 2021). However, the mitigative effect of melatonin priming treatment on salinization stress could be counterproductive at high concentration. Our results suggested that the M200 treatment inhibited the *S. corniculata* seed germination as compared with the CK treatment. This may be because high melatonin concentration promoted the synthesis of endogenous ABA, which regulated seed germination via ABI3, ABI4, and ABI5 and promotes dormancy via the response factors like SCHNARCHZAPFEN (SNZ) and ABA overly sensitive 5 (ABO5) (Liu et al., 2010; Zou et al., 2013). This explanation has been supported by the fact that 1,000 μM melatonin treatment significantly inhibited the *Arabidopsis* seed germination as compared with the untreated control in Lv et al. (2021).

## Effect of Melatonin Priming on Antioxidant Defense of *Suaeda corniculata* Seeds

The excessive accumulation of reactive oxygen species (ROS) not only has irreversible negative effects on seed germination, but also affects the future seedling growth (Goud and Kachole, 2011). Antioxidant system is one of the major physiological defense systems protecting against salinization-induced oxidative stress by improving the antioxidant enzyme activity and antioxidant contents (Ibrahim, 2016). In this sense, studying the antioxidant defense is crucial for a holistic understanding

of priming treatments. Previous studies have demonstrated that melatonin get through the free radical scavenging cascade, extends the free radical scavenging capacity of antioxidants to its multi-stage metabolites. Especially N1-acetyl-N2-formyl-5-methoxykynuramine, a primary metabolite derived from melatonin, also has strong antioxidant capacity, thus effectively protecting organisms from oxidative stress (Balabusta et al., 2016). Simultaneously, melatonin helps scavenge free radicals through its receptors by modulating the antioxidant enzymes in the cells and tissues in a dose-dependent manner (Li et al., 2018; Cao et al., 2019). Our results showed that the SOD and POD activities of *S. corniculata* seeds continued increasing with the germination stage, which was significantly higher than others in the M50 treatment. Exogenous melatonin priming may have indirectly upregulated the expression of antioxidant enzyme and related genes, which then improves their efficiency as antioxidants (Arora and Bhatla, 2017; Wang et al., 2017). However, other studies have demonstrated that exogenous melatonin priming did not change the antioxidant enzymes' activity of *Lolium perenne* (Zhang et al., 2016; Lu et al., 2022), and we suspect that melatonin possibly uses different physiological mechanisms to strengthen the antioxidant defense. MDA is the indicator of oxidative-stress induced membrane damage under salinization stress (Ibrahim, 2016). Our study results showed the MDA content in *S. corniculata* seeds continuously decreased during the experiment, and it decreased up to 27.33% in the M50 treatment. This result was in agreement with previous findings indicating that a negative correlation exists between the MDA content and the activity of antioxidant enzymes (Esfandiari et al., 2008; Younesi and Moradi, 2015). The possible explanation is that melatonin treatment increases the autophagy induction capacity and thereby reduces the accumulation of oxidized proteins, while also simultaneously controlling the ROS accumulation by upregulating the antioxidant enzymes activity and their transcript levels to mitigate membrane lipid peroxidation under salinization stress (Wang et al., 2015; Sun et al., 2020; Zhang T. G. et al., 2022). Additionally, it improves the activity of non-enzymatic antioxidants by regulating the activity of enzymes in the ASA-GSH cycle, thereby further improving the free radical scavenging capacity (Ni et al., 2018). Simultaneously, by up-regulating the genes related to glutathione metabolic pathway and activating the downstream signal transduction pathway, also may help explain how melatonin priming improves the antioxidant defense of seeds under salinization stress (Zhang Y. X. et al., 2021).

## Effect of Melatonin Priming on Reserve Mobilization of *Suaeda corniculata* Seeds

It is well known that the seed reserve is an important factor which affects germination characteristics, and reserve mobilization plays an important role in the energy supply and maintains osmotic balance (Zhao et al., 2018; Lei et al., 2021). Recent experimental data suggested that the priming treatment regulates the carbohydrate, protein, and fat metabolism, thereby resulting in increased seed germination (Li et al., 2019; Chen et al., 2021). However, the effect of melatonin priming treatment on reserve mobilization under abiotic stress still needs to be studied according to the target species. Our results showed that there is a strong negative correlation between starch and soluble sugar content variation. A plausible explanation for this phenomenon could be that melatonin priming upregulated the α-amylase gene expression, to ensure that starch is broken down into smaller and simpler molecules which will be used as an energy source by the organism for seed germination (Cao et al., 2019; Yan et al., 2020). Previous studies also found that the priming treatment induced a phased effect on the change of seed soluble protein content under abiotic stress (Adawy et al., 2003). Priming treatment induced seeds to adopt the defensive strategy of accumulating soluble protein for improving the cell's water holding capacity and protect its membrane (Li et al., 2010). During the later stage of germination, hydrolysis of storage proteins provides the energy for both the hypocotyl growth and new protein synthesis (Wahid and Bounoua, 2013). Meanwhile, the fat metabolism also pushed the seed's developmental switch from dormancy to germination (Footitt et al., 2002), which was similar to our data.

## Pathways of Melatonin Priming in *Suaeda corniculata* Seed Germination

The action pathway of priming treatment is the basis for revealing the driving mechanisms. The SEM analysis showed that there are both direct and indirect effect pathways of melatonin priming on the *S. corniculata* seed germination under salinization stress conditions (**Figure 5**). On the one hand, melatonin priming promoted seed germination by regulating the expression of stress tolerance, hormone synthesis, and metabolism-related genes (Zhang Y. et al., 2021). On the other hand, priming treatment also upregulated the antioxidant enzyme activities and accelerated the level of reserve mobilization, ultimately improving the seed germination (Arora and Bhatla, 2017; Cao et al., 2019; Lu et al., 2022). This study is the first to reveal the effect pathways of melatonin priming on the *S. corniculata* seed germination under salinization stress, and also proved the feasibility of melatonin priming in improving the germination of *S. corniculata* seeds. It is also worth noting that the positive effects of the melatonin priming we found were concentration-dependent, which reconfirms our hypothesis.

# CONCLUSION

In summary, we comprehensively assessed the effect of melatonin priming on the *S. corniculata* seed germination under salinization stress. Our results showed that the stress-alleviating effect of melatonin priming is concentration-dependent. The melatonin priming concentration of 50 μM significantly improved the germination characteristics of *S. corniculata* seeds, increased the activity of antioxidant enzymes to alleviate the salinity stress-induced membrane lipid peroxidation, and promoted the reserve mobilization during germination. However, the treatment of 200 μM melatonin inhibited the above mentioned physiological activities. Melatonin priming directly influences

the seed germination of *S. corniculata*, while also acting *via* indirect pathways to regulate the antioxidant defense and reserve mobilization. Our study is the first to explore the effects of exogenous melatonin on *S. corniculata* seed germination, antioxidant defense, and reserve mobilization under salinization stress, thereby providing invaluable information and technical support for the restoration of salinized wetlands. However, further studies are required to understand the synthetic effects of salinization stress intensity on the *S. corniculata* seed germination post-priming treatments, before a general conclusion can be drawn.

## DATA AVAILABILITY STATEMENT

The original contributions presented in this study are included in the article/**Supplementary Material**, further inquiries can be directed to the corresponding author.

## AUTHOR CONTRIBUTIONS

MZ, ST, and XW designed the study. MZ, SL, and YW collected the data. DZ, QQ, and YA analyzed the data. ST and XL lead the writing with all co-authors. All authors gave final approval for publication.

## FUNDING

This research was supported by the National Natural Science Foundation of China (No. 41871101) and the Strategic Priority Research Program of the Chinese Academy of Sciences (No. XDA23060402).

## ACKNOWLEDGMENTS

We would like to express their gratitude to EditSprings (https://www.editsprings.cn) for the expert linguistic services provided.

## SUPPLEMENTARY MATERIAL

The Supplementary Material for this article can be found online at: https://www.frontiersin.org/articles/10.3389/fevo.2022.941032/full#supplementary-material

## REFERENCES

Adawy, T. A. E., Rahma, E. H., Bedawey, A. A. E., and Beltagy, A. E. E. (2003). Nutritional potential and functional properties of germinated mung bean, pea and lentil seeds. *Plant Foods Hum. Nutr*. 58, 1–13. doi: 10.1023/b:qual.0000040339.48521.75

An, Y., Gao, Y., Zhang, Y., Tong, S. Z., and Liu, X. H. (2019). Early establishment of *Suaeda salsa* population as affected by soil moisture and salinity: implications for pioneer species introduction in saline-sodic wetlands in Songnen Plain, China. *Ecol. Indic*. 107:105654. doi: 10.1016/j.ecolind.2019.105654

Arnao, M. B., and Hernandez-Ruiz, J. (2019). Melatonin: a new plant hormone and/or a plant master regulator? *Trends Plant Sci*. 24, 38–48. doi: 10.1016/j.tplants.2018.10.010

Arora, D., and Bhatla, S. C. (2017). Melatonin and nitric oxide regulate sunflower seedling growth under salt stress accompanying differential expression of Cu/Zn SOD and Mn SOD. *Free Radic. Biol. Med.* 106, 315–328. doi: 10.1016/j.freeradbiomed.2017.02.042

Balabusta, M., Szafranska, K., and Posmyk, M. M. (2016). Exogenous melatonin improves antioxidant defensein Cucumber seeds (*Cucumis sativus* L.) germinated under chilling stress. *Front. Plant Sci.* 7:575. doi: 10.3389/fpls.2016.00575

Biju, S., Fuentes, S., and Gupta, D. (2017). Silicon improves seed germination and alleviates drought stress lentil crops by regulating osmolytes, hydrolytic enzymes and antioxidant defense system. *Plant Physiol. Biochem*. 119, 250–264. doi: 10.1016/j.plaphy.2017.09.001

Cao, Q. J., Li, G., Cui, Z. G., Yang, F. T., Jiang, X. L., Diallo, L., et al. (2019). Seed priming with melatonin improves the seed germination of waxy maize under chilling stress via promoting the antioxidant system and starch metabolism. *Sci. Rep*. 9:15044. doi: 10.1038/s41598-019-51122-y

Chen, L., Lu, B., Liu, L. T., Duan, W. J., Jiang, D., Li, J., et al. (2021). Melatonin promotes seed germination under salt stress by regulating ABA and GA(3) in cotton (*Gossypium hirsutum* L.). *Plant Physiol. Biochem*. 162, 506–516. doi: 10.1016/j.plaphy.2021.03.029

Esfandiari, E., Shakiba, M. R., Mahboob, S. A., Alyari, H., and Shahabivand, S. (2008). The effect of water stress on the antioxidant content, protective enzyme activities, proline content and lipid peroxidation in wheat seedling. *Pak. J. Biol. Sci*. 11, 1916–1922. doi: 10.3923/pjbs.2008.1916.1922

Feghhenabi, F., Hadi, H., Khodaverdiloo, H., and van Genuchten, M. T. (2020). Seed priming alleviated salinity stress during germination and emergence of wheat (*Triticum aestivum* L.). *Agric. Water Manage*. 231:106022. doi: 10.1016/j.agwat.2020.106022

Footitt, S., Slocombe, S. P., Larner, V., Kurup, S., Wu, Y. S., Larson, T., et al. (2002). Control of germination and lipid mobilization by COMATOSE, the Arabidopsis homologue of human ALDP. *EMBO J*. 21, 2912–2922. doi: 10.1093/emboj/cdf300

Forti, C., Ottobrino, V., Doria, E., Bassolino, L., Toppino, L., Rotino, G. L., et al. (2021). Hydropriming applied on fast germinating *Solanum villosum* miller seeds: impact on pre-germinative metabolism. *Front. Plant Sci*. 12:639336. doi: 10.3389/fpls.2021.639336

Goud, P. B., and Kachole, M. S. (2011). Effect of exogenous hydrogen peroxide on peroxidase and polyphenol oxidase activities in *Cajanus cajan* (L.) Millsp, Detached leaves. *Int. J. Curr. Res*. 3, 61–65.

Ibrahim, E. A. (2016). Seed priming to alleviate salinity stress in germinating seeds. *J. Plant Physiol*. 192, 38–46. doi: 10.1016/j.jplph.2015.12.011

James, J. J., and Carrick, P. J. (2016). Toward quantitative dryland restoration models. *Restor. Ecol*. 24, S85–S90. doi: 10.1111/rec.12393

Jia, J., Huang, C., Bai, J. H., Zhang, G. L., Zhao, Q. Q., and Wen, X. J. (2018). Effects of drought and salt stresses on growth characteristics of euhalophyte *Suaeda salsa* in cosatal wetlands. *Phys. Chem. Earth* 103, 68–74. doi: 10.1016/j.pce.2017.01.002

Johnson, R., and Puthur, J. T. (2021). Seed priming as a cost effective technique for developing plants with cross tolerance to salinity stress. *Plant Physiol. Biochem*. 162, 247–257. doi: 10.1016/j.plaphy.2021.02.034

Kettenring, K. M., and Tarsa, E. E. (2020). Need to seed? Ecological, genetic, and evolutionary keys to seed-based wetland restoration. *Front. Environ. Sci*. 8:109. doi: 10.3389/fenvs.2020.00109

Kim, D. H. (2019). Practical methods for rapid seed germination from seed coat-imposed dormancy of *Prunus yedoensis*. *Sci. Hortic*. 243, 451–456. doi: 10.1016/j.scienta.2018.08.039

Lei, K., Sun, S., Zhong, K., Li, S., Hu, H., Sun, C., et al. (2021). Seed soaking with melatonin promotes seed germination under chromium stress via enhancing reserve mobilization and antioxidant metabolism in wheat. *Ecotox. Environ. Safe*. 220:112241. doi: 10.1016/j.ecoenv.2021.112241

Li, D. X., Batchelor, W. D., Zhang, D., Miao, H. X., Li, H. Y., Song, S. J., et al. (2020). Analysis of melatonin regulation of germination and

antioxidant metabolism in different wheat cultivars under polyethylene glycol stress. *PLoS One* 15:e0237536. doi: 10.1371/journal.pone.0237536

Li, J. P., Zhao, C., Zhang, M. J., Yuan, F., and Chen, M. (2019). Exogenous melatonin improves seed germination in *Limonium bicolor* under salt stress. *Plant Signal. Behav*. 14:1659705. doi: 10.1080/15592324.2019.1659705

Li, X. J., Yang, M. F., Chen, H., Qu, L. Q., Chen, F., and Shen, S. H. (2010). Abscisic acid pretreatment enhances salt tolerance of rice seedlings: proteomic evidence. *Biochim. Biophys. Acta Proteins Proteom*. 1804, 929–940. doi: 10.1016/j.bbapap.2010.01.004

Li, X. J., Yu, B. J., Cui, Y. Q., and Yin, Y. F. (2017). Melatonin application confers enhanced salt tolerance by regulating $Na^+$ and $Cl^-$ accumulation in rice. *Plant Growth Regul*. 83, 441–454. doi: 10.1007/s10725-017-0310-3

Li, X. N., Brestic, M., Tan, D. X., Zivcak, M., Zhu, X. C., Liu, S. Q., et al. (2018). Melatonin alleviates low PS I-limited carbon assimilation under elevated $CO_2$ and enhances the cold tolerance of offspring in chlorophyll -deficient mutant wheat. *J. Pineal Res*. 64:12453. doi: 10.1111/jpi.12453

Li, X. N., Tan, D. X., Jiang, D., and Liu, F. L. (2016). Melatonin enhances cold tolerance in drought-primed wild-type and abscisic acid -deficient mutant barley. *J. Pineal Res*. 61, 328–339. doi: 10.1111/jpi.12350

Li, X. Y., Wen, B. L., Yang, F., Hartley, A., and Li, X. J. (2017). Effects of alternate flooding-drought conditions on degenerated *Phragmites australis* salt marsh in northeast China. *Restor. Ecol*. 25, 810–819. doi: 10.1111/rec.12500

Liu, Y., He, J. N., Chen, Z. Z., Ren, X. Z., Hong, X. H., and Gong, Z. Z. (2010). ABA overly-sensitive 5 (ABO5), encoding a pentatricopeptide repeat protein required for cis-splicing of mitochondrial nad2 intron 3, is involved in the abscisic acid response in Arabidopsis. *Plant J*. 63, 749–765. doi: 10.1111/j.1365-313x.2010.04280.x

Lu, X. P., Min, W. F., Shi, Y. F., Tian, L., Li, P. F., Ma, T. L., et al. (2022). Exogenous melatonin alleviates alkaline stress by removing reactive oxygen species and promoting antioxidant defence in rice seedlings. *Front. Plant Sci*. 13:849553. doi: 10.3389/fpls.2022.849553

Lv, Y., Pan, J. J., Wang, H. P., Reiter, R. J., Li, X., Mou, Z. M., et al. (2021). Melatonin inhibits seed germination by crosstalk with abscisic acid, gibberellin, and auxin in Arabidopsis. *J. Pineal Res*. 70, e12736. doi: 10.1111/jpi.12736

Ma, H. Y., Yang, H. Y., Lu, X. T., Pan, Y. P., Wu, H. T., Liang, Z. W., et al. (2015). Does high pH give a reliable assessment of the effect of alkaline soil on seed germination? A case study with *Leymus chinensis* (Poaceae). *Plant Soil* 394, 35–43. doi: 10.1007/s11104-015-2487-4

Masondo, N. A., Kulkarni, M. G., Finnie, J. F., and Van Staden, J. (2018). Influence of biostimulants-seed-priming on *Ceratotheca triloba* germination and seedling growth under low temperatures, low osmotic potential and salinity stress. *Ecotox. Environ. Safe*. 147, 43–48. doi: 10.1016/j.ecoenv.2017.08.017

Ni, J., Wang, Q. J., Shah, F. A., Liu, W. B., Wang, D. D., Huang, S. W., et al. (2018). Exogenous melatonin confers cadmium tolerance by counterbalancing the hydrogen peroxide homeostasis in wheat seedlings. *Molecules* 23:799. doi: 10.3390/molecules23040799

Ogawa, M., Hanada, A., Yamauchi, Y., Kuwahara, A., Kamiya, Y., and Yamaguchi, S. (2003). Gibberellin biosynthesis and response during Arabidopsis seed germination. *Plant Cell* 15, 1591–1604. doi: 10.1105/tpc.011650

Qin, X. Q., and Zeevaart, J. A. D. (2002). Overexpression of a 9-cis-epoxycarotenoid dioxygenase gene in *Nicotiana plumbaginifolia* increases abscisic acid and phaseic acid levels and enhances drought tolerance. *Plant Physiol*. 128, 544–551. doi: 10.1104/pp.010663

Seneviratne, M., Rajakaruna, N., Rizwan, M., Madawala, H. M. S. P., Ok, Y. S., and Vithanage, M. (2019). Heavy metal-induced oxidative stress on seed germination and seedling development: a critical review. *Environ. Geochem. Health* 41, 1813–1831. doi: 10.1007/s10653-017-0005-8

Soriano, D., Orozco-Segovia, A., Marquez-Guzman, J., Kitajima, K., Gamboa-de Buen, A., and Huante, P. (2011). Seed reserve composition in 19 tree species of a tropical deciduous forest in Mexico and its relationship to seed germination and seedling growth. *Ann. Bot*. 107, 939–951. doi: 10.1093/aob/mcr041

Sun, C. L., Lv, T., Huang, L., Liu, X. X., Jin, C. W., and Lin, X. Y. (2020). Melatonin ameliorates aluminum toxicity through enhancing aluminum exclusion and reestablishing redox homeostasis in roots of wheat. *J. Pineal Res*. 68:e12642. doi: 10.1111/jpi.12642

Tahjib, U. A., Roy, P. R., Sohag, A. A. M., Afrin, S., Rady, M. M., and Hossain, M. A. (2018). Exogenous calcium supplementation improves salinity tolerance in *BRRI Dhan*28; a salt susceptible high-yielding *Oryza Sativa* cultivar. *J. Crop Sci. Biotech*. 21, 383–394. doi: 10.1007/s12892-018-0098-0

Tang, H. R., Bai, J. S., Chen, F. Y., Liu, Y., and Lou, Y. J. (2021). Effects of salinity and temperature on tuber sprouting and growth of *Schoenoplectus nipponicus*. *Ecosphere* 12:e03448. doi: 10.1002/ecs2.3448

Wahid, N., and Bounoua, L. (2013). The relationship between seed weight, germination and biochemical reserves of maritime pine (*Pinus pinaster* Ait.) in Morocco. *New For*. 44, 385–397. doi: 10.1007/s11056-012-9348-2

Wang, D. W., Bai, J. H., Wang, W., Ma, X., Guan, Y. N., Gu, C. H., et al. (2020). Micro-topography manipulations facilitate *Suaeda Salsa* Marsh restoration along the lateral gradient of a tidal creek. *Wetlands* 40, 1657–1666. doi: 10.1007/s13157-020-01308-2

Wang, L., Feng, C., Zheng, X. D., Guo, Y., Zhou, F. F., Shan, D. Q., et al. (2017). Plant mitochondria synthesize melatonin and enhance the tolerance of plants to drought stress. *J. Pineal Res*. 63:e12429. doi: 10.1111/jpi.12429

Wang, P., Sun, X., Wang, N., Tan, D. X., and Ma, F. (2015). Melatonin enhances the occurrence of autophagy induced by oxidative stress in Arabidopsis seedlings. *J. Pineal Res*. 58, 479–489. doi: 10.1111/jpi.12233

Wang, Q., Xie, T., Luo, M., Bai, J. H., Chen, C., Ning, Z. H., et al. (2021). How hydrological connectivity regulates the plant recovery process in salt marshes. *J. Appl. Ecol*. 58, 1314–1324. doi: 10.1111/1365-2664.13879

Wang, X. H., Zhang, D. J., Qi, Q., Tong, S. Z., An, Y., Lu, X. G., et al. (2019). The restoration feasibility of degraded *Carex* tussock in soda-salinization area in arid region. *Ecol. Indic*. 98, 131–136. doi: 10.1016/j.ecolind.2018.08.066

Wang, X. Y., Cheng, R., Zhu, H., Cheng, X. W., Shutes, B., and Yan, B. X. (2020). Seed germination and early seedling growth of six wetland plant species in saline-alkaline environment. *Int. J. Phytoremediat*. 22, 1185–1194. doi: 10.1080/15226514.2020.1748565

Yan, H. F., Jia, S. G., and Mao, P. S. (2020). Melatonin priming alleviates aging-induced germination inhibition by regulating β-oxidation, protein translation, and antioxidant metabolism in oat (*Avena sativa* L.) seeds. *Int. J. Mol. Sci*. 21:1898. doi: 10.3390/ijms21051898

Yang, F., Baskin, J. M., Baskin, C. C., Yang, X. J., Cao, D. C., and Huang, Z. (2017). Divergence in life history traits between two populations of a seed-dimorphic halophyte in response to soil salinity. *Front. Plant Sci*. 8:1028. doi: 10.3389/fpls.2017.01028

Younesi, O., and Moradi, A. (2015). Effect of priming of seeds of *Medicago sativa* 'Bami' with gibberellic acid on germination, seedlings growth and antioxidant enzymes activity under salinity stress. *J. Hortic. Res*. 22, 167–174. doi: 10.2478/johr-2014-0034

Zhang, D. J., Qi, Q., Tong, S. Z., Wang, X. H., An, Y., Zhang, M. Y., et al. (2019). Soil degradation effects on plant diversity and nutrient in tussock meadow wetlands. *J. Soil Sci. Plant Nutr*. 19, 535–544. doi: 10.1007/s42729-019-00052-9

Zhang, J., Li, H. B., Xu, B., Li, J., and Huang, B. R. (2016). Exogenous melatonin suppresses dark-induced leaf senescence by activating the superoxide dismutase-catalase antioxidant pathway and down-regulating chlorophyll degradation in excised leaves of perennial ryegrass (*Lolium perenne* L.). *Front. Plant Sci*. 7:1500. doi: 10.3389/fpls.2016.01500

Zhang, M. Y., Qi, Q., Zhang, D. J., Tong, S. Z., Wang, X. H., An, Y., et al. (2021). Effect of priming on *Carex schmidtii* seed germination and seedling growth: implications for tussock wetland restoration. *Ecol. Eng*. 171:106389. doi: 10.1016/j.ecoleng.2021.106389

Zhang, M. Y., Zhang, D. J., Qi, Q., Tong, S. Z., Wang, X. H., An, Y., et al. (2022). Flooding effects on population and growth characteristics of *Bolboschoenus planiculmis* in Momoge wetland, northeast China. *Ecol. Indic*. 137:108730. doi: 10.1016/j.ecolind.2022.108730

Zhang, T. G., Wang, J., Sun, Y. P., Zhang, L., and Zheng, S. (2022). Versatile roles of melatonin in growth and stress tolerance in plants. *J. Plant Growth Regul*. 41, 507–523. doi: 10.1007/s00344-021-10317-2

Zhang, Y., Zhou, X. J., Dong, Y. T., Zhang, F., He, Q. L., Chen, J. H., et al. (2021). Seed priming with melatonin improves salt tolerance in cotton through regulating photosynthesis, scavenging reactive oxygen species and coordinating with phytohormone signal pathways. *Ind. Crop. Prod*. 169:113671. doi: 10.1016/j.indcrop.2021.113671

Zhang, Y. X., Fan, Y. P., Rui, C., Zhang, H., Xu, N., Dai, M. H., et al. (2021). Melatonin improves cotton salt tolerance by regulating ROS scavenging system

and $Ca^{2+}$ signal transduction. *Front. Plant Sci.* 12:693690. doi: 10.3389/fpls.2021.693690

Zhao, H. B., Xu, L. F., Su, T., Jiang, Y., Hu, L. Y., and Ma, F. W. (2015). Melatonin regulates carbohydrate metabolism and defenses against *Pseudomonas syringae* pv. *tomato DC3000* infection in *Arabidopsis thaliana*. *J. Pineal Res.* 59, 109–119. doi: 10.1111/jpi.12245

Zhao, K. F., Fan, H., Zhou, S., and Song, J. (2003). Study on the salt and drought tolerance of *Suaeda salsa* and *Kalanchoe claigremontiana* under iso-osmotic salt and water stress. *Plant Sci.* 165, 837–844. doi: 10.1016/s0168-9452(03)00282-6

Zhao, M., Zhang, H. X., Yan, H., Qiu, L., and Baskin, C. C. (2018). Mobilization and role of starch, protein, and fat reserves during seed germination of six wild grassland species. *Front. Plant Sci.* 9:234. doi: 10.3389/fpls.2018.00234

Zhao, Y. T., Wang, G. D., Zhao, M. L., Wang, M., and Jiang, M. (2021a). Direct and indirect effects of soil salinization on soil seed banks in salinizing wetlands in the Songnen Plain, China. *Sci. Total Environ.* 819:152035. doi: 10.1016/j.scitotenv.2021.152035

Zhao, Y. T., Wang, G. D., Zhao, M. L., Wang, M., Hu, N. L., Jiang, M., et al. (2021b). The potentials of wetland restoration after farming differ between community types due to their differences in seed limit and salt tolerances in the Songnen Plain. *China. Ecol. Indic.* 131:108145. doi: 10.1016/j.ecolind.2021.108145

Zou, Y. M., Wang, Y. N., Wang, L. X., Yang, L., Wang, R., and Li, X. (2013). miR172b controls the transition to autotrophic development inhibited by ABA in Arabidopsis. *PLoS One* 8:E64770. doi: 10.1371/journal.pone.0064770

**Conflict of Interest:** The authors declare that the research was conducted in the absence of any commercial or financial relationships that could be construed as a potential conflict of interest.

**Publisher's Note:** All claims expressed in this article are solely those of the authors and do not necessarily represent those of their affiliated organizations, or those of the publisher, the editors and the reviewers. Any product that may be evaluated in this article, or claim that may be made by its manufacturer, is not guaranteed or endorsed by the publisher.

frontiers | Frontiers in Ecology and Evolution

TYPE Original Research
PUBLISHED 14 July 2022
DOI 10.3389/fevo.2022.953349



OPEN ACCESS

EDITED BY
Arnaldo Marín,
University of Murcia, Spain

REVIEWED BY
Junhong Bai,
Beijing Normal University, China
Fengqin Yan,
Institute of Geographic Sciences and Natural Resources Research (CAS), China

*CORRESPONDENCE
Hongmei Zhao
zhaohongmei@iga.ac.cn

SPECIALTY SECTION
This article was submitted to Conservation and Restoration Ecology, a section of the journal Frontiers in Ecology and Evolution

RECEIVED 26 May 2022
ACCEPTED 28 June 2022
PUBLISHED 14 July 2022

CITATION
Gao C, Wang G, Cong J, Han D and Zhao H (2022) Burning alters the decomposition of residual plant litters in *Calamagrostis angustifolia* wetlands in the Sanjiang Plain (Northeast China). *Front. Ecol. Evol.* 10:953349. doi: 10.3389/fevo.2022.953349



# Burning alters the decomposition of residual plant litters in *Calamagrostis angustifolia* wetlands in the Sanjiang Plain (Northeast China)

Chuanyu Gao, Guoping Wang, Jinxin Cong, Dongxue Han and Hongmei Zhao*

Key Laboratory of Wetland Ecology and Environment, Northeast Institute of Geography and Agroecology, Chinese Academy of Sciences, Changchun, China

Wetlands store >30% of the global soil carbon pool, which is important for global carbon cycling. However, with global warming and the increase in regional human activities, an increasing number of wetlands are being threatened by fires, which have serious effects on carbon cycling in wetlands. Although plant litter decomposition is one of the key stages of carbon cycling in wetlands, it is still unclear whether fires affect residual plant litter decomposition in burnt wetlands and whether the fire season also causes different effects. To address these knowledge gaps, a plant litter decomposition experiment was conducted during the growing season in autumn burnt, spring burnt, and unburnt sites in a *Calamagrostis angustifolia* wetland in the Sanjiang Plain (Northeast China). The results show that autumn burning promotes more mass loss (i.e., 15.9 ± 1.6% in autumn burnt sites and 14.8 ± 1.7% in autumn unburnt sites) and accelerates the decomposition of plant litter, whereas spring burning decreases the decomposition rates of plant litter (i.e., 15.7 ± 1.7% in spring burnt sites and 22.0 ± 2.5% in spring unburnt sites). As the decomposition time increased, the accumulation index indicated that carbon was released from plant litter to the surrounding environment accompanied by mass loss and nutrient elements accumulated in the residual plant litter. The N/P ratio of plant litter decreased from ca. 20 on day 26th to ca. 9 on day 121st, indicating that N acts as the limiting element for plant litter decomposition in *C. angustifolia* wetlands, and the limitation increased with increasing decomposition time. Our results also suggest that the autumn burning may promote more carbon loss and nutrient elements accumulated in plant litter in *C. angustifolia* wetlands than the spring burning.

KEYWORDS

**wetland, plant litter, burning, litter decomposition, carbon**

## Introduction

Wetlands, which include both peatlands and other biomass accumulation-flooded environments, store more than 30% of the global soil carbon while covering only 8–10% of the world's land surface (Yu et al., 2010). Due to surface plant growth and an anaerobic soil environment, wetlands with high carbon accumulation rates acted as one of the most important carbon sink ecosystems during the Holocene (Nilsson et al., 2008). With the state of global warming in recent years, carbon storage in wetlands has been threatened by environmental disturbances. Wetlands have switched from carbon sinks to carbon source ecosystems, which have serious effects on global carbon cycling (Gallego-Sala et al., 2018; Loisel et al., 2020). Additionally, most of the carbon (C) in wetlands is stored in northern regions, which are located in mid-high latitude regions and are more sensitive to climate change than other regions (Yu et al., 2010). Global warming has also markedly increased the intensity and frequency of fires over the last century and which will continue to increase in the current century (Flannigan et al., 2013; Gao et al., 2018). Recently, nearly 4% of the earth's land surface has been burnt and this has serious consequences on wetlands and other ecosystems (Battisti et al., 2016; Just et al., 2017; van der Werf et al., 2017). Fires not only consume surface plants and emit ca. 2,200 Tg carbon to the atmosphere, but also cause serious effects on residual carbon cycling (i.e., soil carbon mineralization and residual litter decomposition) in natural ecosystems because they increase the accumulation of pyrogenic carbon and ash (Butler et al., 2017; Jones et al., 2019; Cong et al., 2020). Thus, fires have become an important disturbance factor for carbon cycling in wetland ecosystems (Flannigan et al., 2009; Turetsky et al., 2015).

For wetlands, fires increase the species diversity and abundance of plants in the next growing season and this has great potential to cause more carbon to accumulate in the soil carbon pool (Marrs et al., 2019; Gao et al., 2021). Apart from the amount of aboveground biomass, the decomposition of plant litter also acts as an important factor affecting the amount of carbon accumulated in wetlands. Most plant litter decomposes in the surface aerobic layers, and some residual plant litter acts as long-term carbon stored in the anaerobic layers (Reddy and DeLaune, 2008). Due to changes in available nutrients, microbial activities, and hydrological processes, fires also have great potential to influence the decomposition process of plant litter, which is closely related to these changing factors (Straková et al., 2012; Clarkson et al., 2013; Song et al., 2021). For example, in the *Eucalyptus pilularis* forest, fire frequency and intensity have serious effects on the decomposition process of plant litter and decrease the decomposition rates in long-term high-frequency burning sites (Brennan et al., 2009). Except for fire frequency and intensity, the fire season also causes serious effects on the microbial activities and soil moisture in burnt wetlands and had been proofed that leads to markedly different effects on plant growth and organic matter mineralization rates in autumn and spring burnt sites (Zhao et al., 2012; Gao et al., 2021). Although these effects of the fire season on plant litter decomposition may also differ, however, these effects remain uncertain.

Decomposition is not only important for carbon capture in wetlands but is also an important factor for nutrient element cycling in wetlands. Dynamic nutrient elements are influenced by the chemical properties of plant litter and available nutrients in the surrounding soil and water environment (Wang and Roulet, 2017; Song et al., 2018). Due to high temperatures during burning, fires promote nutrient element forms (e.g., P) in soils to change from organic to inorganic forms, which are more beneficial for plants and microbes (Wang et al., 2015). Residual fire products, such as ash and PyC, contain high amounts of available nutrients and accumulate on the surface of the burnt sites, which also increase the amount of available nutrients (Giardina et al., 2000; Pingree and DeLuca, 2018). Thus, the changes in available nutrients in burnt sites also act as major factors that influence the dynamics of nutrient elements in plant litter during decomposition. Compare to spring burning, autumn burning promotes the availability of more nutrient elements for plant growth in seasonally frozen regions, and the effects of autumn burning on plant growth are more direct than those of spring burning (Gao et al., 2021). However, it is unclear whether the burning season also has different effects on nutrient element dynamics in the decomposition process of plant litter in burnt and unburnt sites.

To address these knowledge gaps, we examined the effects of the burning season (i.e., spring burning and autumn burning) on plant litter decomposition in a typical *Calamagrostis angustifolia* wetland in the Sanjiang Plain (China) (Zhao et al., 2012). Based on a 121-day field decomposition experiment, the mass loss, carbon, and selected nutrient elements (i.e., N, P, and S) in residual plant litter in autumn, spring, and unburnt sites were analyzed in detail. The objective of this study was to provide insights into the impact of the fire season on plant litter mass loss during the decomposition process at burnt and unburnt sites. Second, we aimed to identify the differences in carbon loss and nutrient dynamics of plant litter during decomposition in burnt and unburnt sites. Third, the potential effects of nutrient elements on the mass loss of plant litter in the burnt and unburnt sites were also evaluated.

## Materials and methods

### Experiment design and sampling

The climate characteristics in the Sanjiang Plain are of a cold-temperate continental monsoon, with an annual mean temperature of 1.6°C and annual mean precipitation of 600 mm (Gao et al., 2014). The burnt wetland in the Sanjiang Plain is adjacent to farmland, and nine sites within a homogenous

area of *C. angustifolia* wetland were selected for the plant litter decomposition experiment (**Figure 1**). Details of the burnt experimental design and study sites are presented in our previous studies (Zhao et al., 2012; Gao et al., 2021). The plant litter for the decomposition experiment was collected in October 2007 in autumn-burnt sites and in May 2008 in spring-burnt sites before prescribed burning. Part of the plant litter was dried at 85°C for 48 h and used to analyze the original contents of water and elements. The remaining plant litter selected for plant litter decomposition experiments were cut into small pieces (ca. 10 cm), and every 10 g dry weight plant litter (calculated by water content and wet weight of fresh plant litters) was placed in a decomposition bag (Nylon, 20 cm × 20 cm, 100 mesh). For the autumn burnt and unburnt sites, the decomposition bags were placed on the surface of the soil on 20 October 2007. For the spring burnt and unburnt sites, the decomposition bags were placed on the surface of the soil on 11 May 2008. The plant litter of spring burnt and unburnt sites was collected before spring burning, and the litter was decomposed in the natural environment from autumn 2007 to spring 2008. Therefore, the decomposition times were the same as those for the decomposition bags at the autumn burnt and unburnt sites. Because all plant litter was collected from the same vegetation community, the original contents of carbon and nutrients in plant litter was similar for all sites. Considering the monthly average temperature in the Sanjiang Plain (**Figure 1**), the temperature from May to September is beneficial for microbial activity, and most of the mass loss occurred during this period (Fick and Hijmans, 2017). Thus, the start decomposition time in the present experiment was set on 11 May, when the plant decomposition bags were placed in the spring burnt and unburnt sites. The sampling times were June 6th (26 days), July 6th (56 days), August 10th (91 days), and September 9th (121 days). Three plant decomposition bags were collected from each site for further analysis.

## Element contents in plant litter

The total mass loss of plant litter in decomposition bags was calculated as the difference between the original dry weight and dry weight (85°C, 48 h) of residual plant litter. The carbon (C) content of the plant litter was determined using the external heating potassium dichromate oxidation method (Wu and Tao, 1993). The total nitrogen (N) content of the plant litter was measured after digestion (concentrated $H_2SO_4$ and catalytic) using a flow continuous chemistry analyzer (Cong et al., 2019). The total phosphate (P) and sulfur (S) contents of the plant litter after digestion ($HNO_3$/$HClO_4$/HF) were determined by atomic emission spectrometry with inductively coupled plasma (ICPS-7500) (Gao et al., 2014). The C contents in the origin plant litter was 441.5 ± 8.8 g $kg^{-1}$ and the N, P, and S contents of the original plant litter were 2,818.1 ± 331.2 mg $kg^{-1}$, 199.5 ± 8.5 mg $kg^{-1}$, and 538.9 ± 9.0 mg $kg^{-1}$, respectively.

## Accumulation index of elements

Accumulated or released carbon and selected elements were indicated by the accumulation index (AI), which was calculated as follows:

$$\mathrm{AI} = \frac{M_t \cdot X_t}{M_0 \cdot X_0} \times 100\%$$

where $M_t$ is the dry mass weight (g) of the plant litter at sampling time $t$, $X_t$ is the element content (mg $kg^{-1}$) of the plant litter at sampling time $t$, $M_0$ is the dry mass weight of the original plant litter, and $X_0$ is the element content (mg $kg^{-1}$) of the original plant litter. Because the decomposition starting time of plant litter in spring burnt and unburnt sites was similar to that in autumn burnt and unburnt sites, the $X_0$ used for litter bags in spring unburnt and burnt sites was the same as the elemental contents of the original plant litter collected in autumn. The AI lower than 100% indicates the selected elements released from the plant litter to the surrounding environment, and the AI higher than 100% indicates the selected elements accumulated in the plant litter.

## Two-way analysis of variance

A two-way analysis of variance (two-way ANOVA) *via* SPSS 22 (SPSS, Inc.) was used to evaluate whether the different burnt sites and sampling time were associated with significant differences in mass loss, AI of carbon and nutrients, and the mass ratio of selected elements in plant litters. Sampling time (i.e., day 26th, day 56th, day 91st, and day 121st) and site types (i.e., autumn burnt, autumn unburnt, spring burnt, and spring unburnt) were the factors tested. The ANOVA results were then applied with the different treatments being grouped by Tukey's honestly significant differences (Tukey-HSD) test, respectively. Significant differences are reported at the 0.05 probability level (i.e., $P < 0.05$).

# Results

## Litter decomposition and accumulation index-carbon

The variations in litter mass loss rates and AI-C at the four sampling times are shown in **Figure 2**. There were significant differences in mass loss rates and AI-C at different sampling times and sites (**Table 1**). As the sampling time increased, the mass loss rates increased from ca. 5% on day 26th to ca. 18% on day 121st. The mass loss rates in spring unburnt sites in

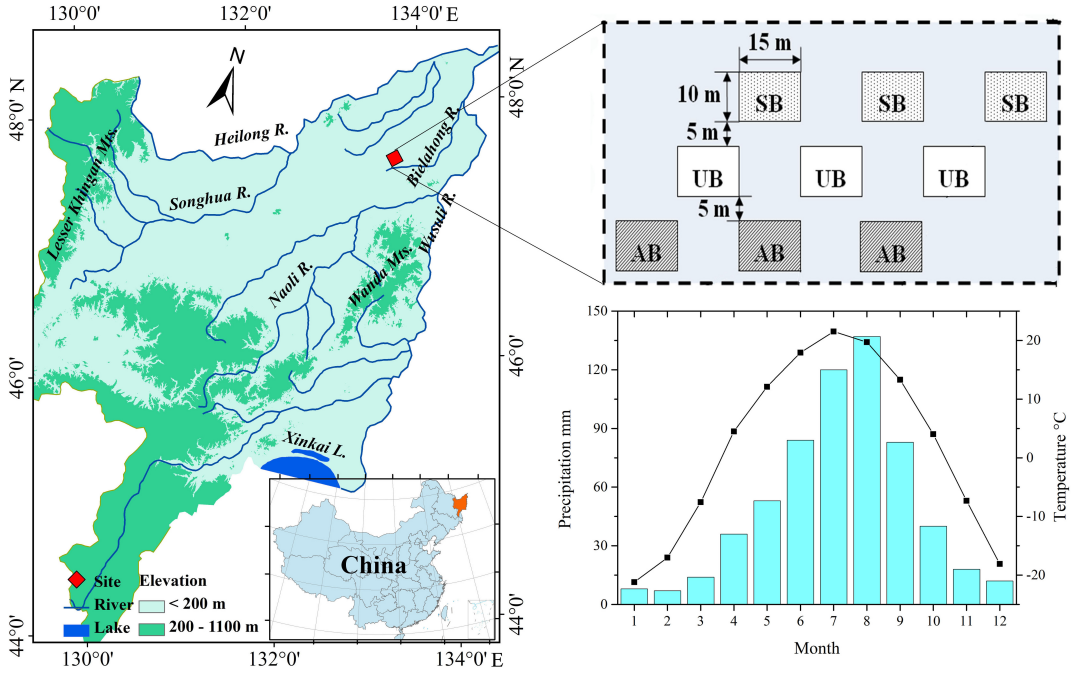


FIGURE 1
Location of the studied sites (i.e. spring burnt sites, SB; autumn burnt sites, AB; unburnt sites, UB) in Sanjiang Plain, Northeast China (Gao et al., 2021), and the average monthly temperature and precipitation in Sanjiang Plain (Fick and Hijmans, 2017).

the four sampling times were higher than those in the other three site types. The mass loss rate in spring unburnt sites was 21.95 ± 2.54% on day 121st and markedly higher than those in the other three site types, which were around 15%. The mass loss rates in the spring and autumn burnt sites were similar and slightly higher than those in the autumn unburnt sites. The AI-C of plant litter at the four sampling sites gradually decreased from ca. 97% on day 26th to ca. 85% on day 121st. The AI-C of plant litter in autumn-burnt sites was slightly higher than that in autumn-unburnt sites. However, except on day 26th, the AI-C of plant litter in the spring burnt sites was markedly higher than that in the spring unburnt sites. After 121 days of decomposition, the AI-C in spring unburnt sites was the lowest at 81.08 ± 2.86% and the AI-C in spring burnt sites were the highest (86.35 ± 1.96%). The AI-C in the autumn burnt and unburnt sites were in the middle and slightly close to those in the spring burnt sites.

## Accumulation index of nutrient elements

There were significant differences in AI-N, AI-P, and AI-S in the different types of burnt sites, and the sampling time only caused significant differences in AI-P and AI-S. The interaction between burn site type and sampling time also had significant effects on AI-P and AI-S (Figure 3). On day 26th, the AI-N in residual litter was slightly higher than 100% in burnt sites and markedly lower than those in unburnt sites, which were approximately 120%. In the spring unburnt sites, the AI-N decreased gradually from 122.93 ± 15.82% on day 26th to 96.15 ± 14.17% on day 121st. In contrast, in other site types, the AI-N increased, and the highest value appeared on day 56th or 91st, and then decreased gradually. The AI-P in residual plant litter decreased before day 56th, and the lowest AI-P was 63.52 ± 3.95% in spring unburnt sites on day 56th. On day 91st, the AI-P in autumn unburnt sites and spring burnt sites was higher than 200% and markedly higher than those in the other two site types. On day 121st, the AI-P gradually decreased and was similar in all four site types, ranging from 137.18 ± 8.39 to 166.76 ± 29.35%. Similar to the variation of AI-P, the AI-S in residual plant litter also decreased before day 56th, and then increased on days 91st and 121st. The AI-S in the spring burnt and unburnt sites was approximately 120% on day 56th and significantly higher than those in the autumn burnt and unburnt sites, which were around 73%.

## Mass ratio of typical elements in residual litters

The mass ratios of C/N, C/P, C/S, and N/P were selected as typical element ratios in this study (Figure 4), and the effects of sampling time and site type on these ratios were significant, with

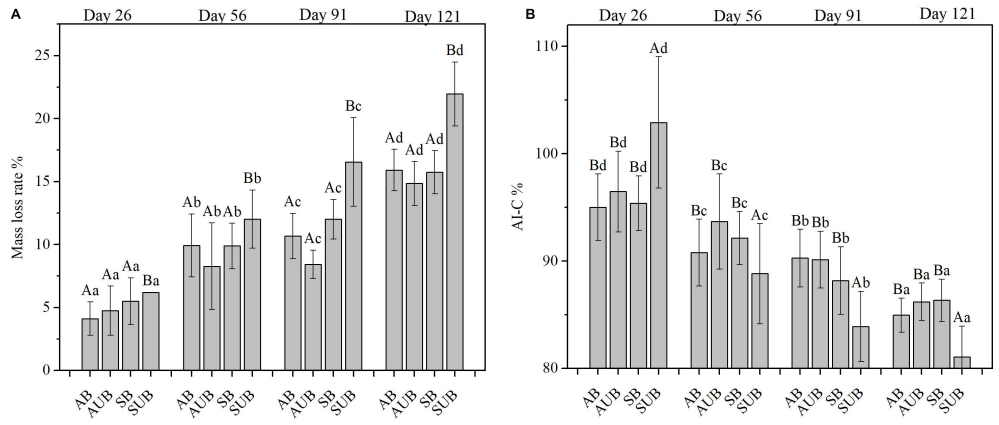


FIGURE 2
Mass loss **(A)** and the AI-C **(B)** in residual plant litters in autumn burnt (AB), autumn unburnt (AUB), spring burnt (SB), and spring unburnt (SUB) sites. Different lowercase letters **(a-d)** indicate significant differences (Tukey-HSD test) among sampling times and different uppercase letters **(A-B)** indicate significant differences (Tukey-HSD test) between site types.

TABLE 1 Two-way analysis of variance (ANOVA) of mass loss, AI of selected elements, and elements mass ratio.

| | Time | | Types | | Types × time | |
|---|---|---|---|---|---|---|
| | *F* | *P* | *F* | *P* | *F* | *P* |
| Mass loss | 53.432 | 0.000 | 8.974 | 0.000 | 1.074 | 0.395 |
| AI-C | 31.472 | 0.000 | 3.585 | 0.019 | 0.835 | 0.587 |
| AI-N | 1.665 | 0.184 | 10.730 | 0.000 | 1.684 | 0.113 |
| AI-P | 107.339 | 0.000 | 17.960 | 0.000 | 8.814 | 0.000 |
| AI-S | 21.209 | 0.000 | 5.147 | 0.003 | 4.837 | 0.000 |
| C/N ratio | 0.534 | 0.661 | 5.636 | 0.002 | 1.234 | 0.292 |
| C/P ratio | 125.420 | 0.000 | 9.519 | 0.000 | 2.917 | 0.006 |
| C/S ratio | 43.409 | 0.000 | 5.790 | 0.002 | 8.910 | 0.000 |
| N/P ratio | 90.594 | 0.000 | 3.022 | 0.037 | 1.943 | 0.063 |

Sampling time and types of burnt sites were regarded as two factors for the two-way ANOVA.

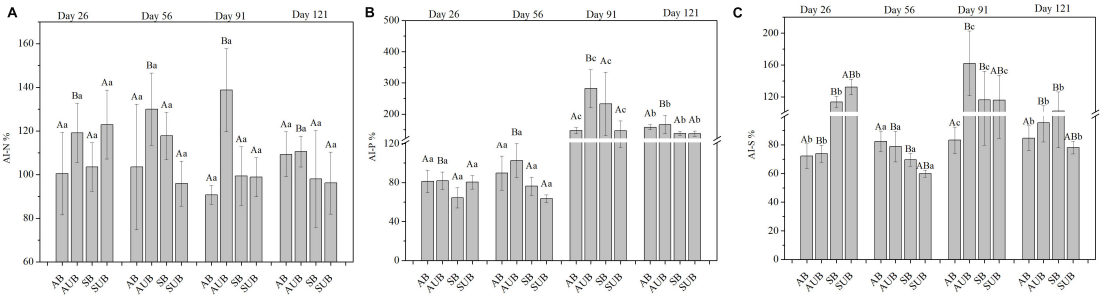


FIGURE 3
The AI-N **(A)**, AI-P **(B)**, and AI-S **(C)** in residual plant litters in autumn burnt (AB), autumn unburnt (AUB), spring burnt (SB), and spring unburnt (SUB) sites. Different lowercase letters **(a-c)** indicate significant differences (Tukey-HSD test) among sampling times and different uppercase letters **(A-B)** indicate significant differences (Tukey-HSD test) between site types.

the exception of the C/N ratio. Only site type had a significant effect on the C/N ratio, and there was no significant effect of sampling time on C/N ratios. The C/N ratio ranged from $103.6 \pm 14.8$ to $156.1 \pm 7.0\%$. Both the highest and lowest values occurred on day 91st at the autumn burnt site and autumn unburnt site, respectively. There was no obvious change in the

C/N ratio during the 121-day decomposition, and the C/N ratio fluctuated overall. Unlike the C/N ratio, the C/P ratio in all four site types decreased significantly from day 56th to day 91st. The C/P ratios on day 91st and 121st were approximately 1,000 and significantly lower than those on day 26th and 56th, which were approximately 3,000. Similar to the C/P ratios, the N/P ratio decreased from approximately 20 on day 56th to ca. 9 on day 121st. After 121 days of decomposition, the N/P ratios in all four site types were similar and ranged between 9.56 ± 1.33 and 10.00 ± 1.95. The range of the C/S ratio during the 121-day decomposition was between 472.3 ± 92.1 and 1,215.9 ± 50.6, which was slightly weaker than the changes in the C/P and N/P ratios. The C/S ratio decreased in autumn burnt and unburnt sites before day 91st, and then increased on day 121st. In the spring burnt and unburnt sites, the C/S ratio increased from day 26th to day 56th, and then decreased on day 91st. The lowest C/S ratio in the spring unburnt and burnt sites appeared on day 91st, and increased by a little on day 121st.

# Discussion

## Seasonal burning promotes biomass loss in plant litter

Comparing the mass loss rates in autumn burnt and unburnt sites, the mass loss rates in autumn burnt sites were higher than those in unburnt sites. However, the mass loss rates in the spring burnt sites were lower than those in the unburnt sites (**Figure 2**). These results showed that autumn burning increased plant litter decomposition rates and that spring burning decreased plant litter decomposition rates. Plant litter decomposition rates are mainly influenced by microbial activities, which are controlled by surrounding environmental factors (e.g., temperature, water table, available nutrients, aboveground plant community, and pH) (Ward et al., 2015; Wang et al., 2019; Yu et al., 2020). Burning also acts as an important factor that not only promotes the release of nutrients from the residual plant to the environment and increases nutrient availability, but can also promote microbial activities (Medvedeff et al., 2015; Wang et al., 2015; Singh et al., 2017). In our experimental sites, there was more DOC and MBC in burnt sites than in unburnt sites during the entire growing season from May to September (Zhao et al., 2012). The greater nutrient availability and greater activity of microbial metabolism in the surface soils not only promoted more soil carbon decomposition and aboveground plant growth, but also caused the decomposition rates of plant litter in autumn burnt sites to be higher than those in autumn unburnt sites. However, because the microbial activities in burnt sites decreased after burning and required several months for recovery (Medvedeff et al., 2013), the short time interval between burning and plant litter decomposition in spring burnt sites may lead to microbial activities not recovering. The weak activity of microbial metabolism in spring burnt sites was speculated to be the major reason why the plant litter decomposition rates in spring burnt sites were lower than those in the spring unburnt sites.

In addition to the direct effects of burning on microbial activity, the effects of burning on plant growth and soil moisture may also influence the decomposition rates of plant litter. Our previous study found that stem density in spring burnt sites was markedly higher than that in autumn burnt sites and unburnt sites, and the aboveground biomass and biomass per plant in autumn burnt sites were higher than those in spring burnt and unburnt sites (Gao et al., 2021). The temperature of surface soils is mainly influenced by micro-geomorphology and surface plants (Song et al., 2013; Goncharova et al., 2019). Because the decomposition process of plant litter mainly occurs during the growing season in the Sanjiang Plain, surface plants also directly influence the temperature of surface soils. The high density of aboveground vegetation communities in spring burnt sites decreases the solar radiation and surface soil temperature during the daytime, which is speculated to be another factor that decreases the decomposition rates of plant litter. The increase in aboveground plants also increases the underground biomass, which is the major oxygen source in rhizospheric soil under the water table and may increase the oxygen concentrations in the water and surface soil layers (Reddy and DeLaune, 2008). The higher aboveground biomass in autumn-burnt sites results in increased oxygen availability under the water table for microbial metabolism and accelerates the decomposition rates of plant litter. Except for the increase in aboveground biomass, burning also decreases the water-retention capacity of surface soils (Thompson and Waddington, 2013). This leads to lower soil moisture in the burnt sites, and higher available oxygen than that in the unburnt sites. Thus, burning not only alters the microbial activities directly, but also changes the aboveground plant growth and water retention capacity, which causes serious effects on the decomposition rates of plant litter indirectly. The enhanced microbial activities and high aboveground biomass resulted in greater oxygen availability in rhizospheric soil, which were speculated to be two major factors that increased the decomposition rates of plant litter in autumn-burnt sites.

Carbon is the most important element in residual plant litter, which contains a carbon content higher than 40%. The mass loss of plant litter leads to carbon release to the surrounding environment. The AI-C in residual plant litter decreased gradually with an increase in mass loss rates during the 121-day decomposition experiment, which was similar to the results of previous studies (Brennan et al., 2009; Gorecki et al., 2021). Due to the high mass loss of plant litter in autumn burnt sites, the AI-C in autumn burnt sites was also lower than that in autumn unburnt sites. Conversely trends were observed in the spring burnt/unburnt sites. Our results showed that autumn burning promoted the release of more carbon from residual plant litter to the surrounding environment. Additionally, autumn burning

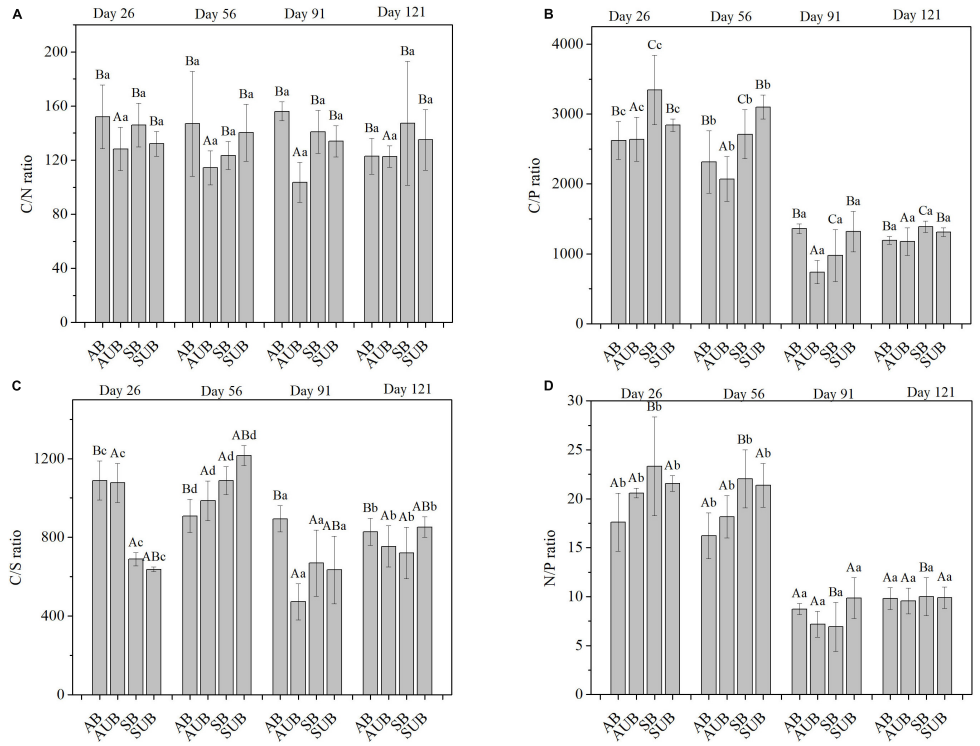


FIGURE 4
The mass ratio of C/N **(A)**, C/P **(B)**, N/P **(C)**, and C/S **(D)** in residual plant litters in autumn burnt (AB), autumn unburnt (AUB), spring burnt (SB), and spring unburnt (SUB) sites. Different lowercase letters **(a-d)** indicate significant differences (Tukey-HSD test) among sampling times and different uppercase letters **(A-C)** indicate significant differences (Tukey-HSD test) between site types.

also promotes the aboveground biomass and the mineralization rates of surface soils (Zhao et al., 2012; Gao et al., 2021). Thus, autumn burning increased all links of carbon cycling in the wetlands and accelerated carbon turnover rates. However, the effects of spring burning on carbon turnover in seasonally frozen wetlands were more complex than those of autumn burning, and it not only decreased the carbon loss rates in residual plant litter, but also caused no significant increase in aboveground biomass compared to unburnt sites (Gao et al., 2021). The potential reasons for this were similar to the reasons for the limitation of mass loss in the spring burnt sites, as previously discussed, and unrecovered microbial activities in the spring unburnt sites were speculated to be the major reason. Thus, similar to the results and potential reasons of mass loss in different sites, the autumn burnt sites were more beneficial for microbial activities and accelerated the release of carbon from plant litter to the surrounding environment.

## Dynamic of nutrient elements in residual plant litters

The dynamic changes in the selected nutrient elements in the residual plant litter are shown in **Figure 3**. Unlike the changes in AI-C, the AI of nutrient elements gradually increased with increasing decomposition time, and the highest AI of nutrient elements (i.e., AI-P) was higher than 300%, which means that the nutrient elements accumulated in the plant litter during the 121-day decomposition. Nutrients were also released to the surrounding environment during the mass loss of plant litter, which is similar to that seen for carbon loss in plant litter. In contrast, microbes can absorb nutrient elements from the surrounding environment (e.g., water and soils) for their metabolism and accumulate nutrient elements in the plant litter (Cui et al., 2021; Wang et al., 2022). More nutrients absorbed than nutrient loss in microbes accompany the decomposition of plant litter, which causes the AI of all selected nutrient elements (i.e., N, P, and S) to increase gradually during the 121-day decomposition period (**Figure 3**). Compared to that of unburnt sites, the AI of nutrient elements in residual plant litters in autumn burnt sites were lower than those in autumn unburnt sites. The AI of nutrient elements in residual plant litter in the spring burnt sites was higher than that in the spring unburnt sites. The AI of nutrients is not only controlled by microbial activity but is also influenced by the amount of available nutrients in the surrounding environment (Aerts and de Caluwe, 1997; Song et al., 2021). High mass loss rates of plant litter in autumn burnt sites and spring unburnt sites were also

found, indicating that the activity of microbial metabolism in these two site types was higher than that in other sites (**Figure 2**). The nutrients in the decomposed part of plant litter are more easily released into the surrounding environment, which was speculated to be the reason for the slightly lower AI of nutrients in high mass loss rates of plant litter than that in low mass loss rates of plant litter.

There are also several differences in the changing trends of the AI for different nutrient elements. For example, AI-N increased gradually before day 91st, and the average values of AI-N during this period were higher than 100%, which means that the N accumulation rates were higher than the loss rates at the beginning of decomposition. The AI-P decreased gradually, and the average values were lower than 100% before day 56th, which means that P was released from the plant litter to the surrounding environment before this day. Although N and P are both important nutrients for microbial metabolism, there are marked differences in biogeochemical cycling in natural ecosystems, especially in anaerobic environments. For example, microbes can fix N from the atmosphere and convert organic N to inorganic N in both aerobic and anaerobic environments (Reddy and DeLaune, 2008). The natural sources of inorganic P are mainly dust and rock weathering, and organic P from the decomposition of plant litter and organic matter. The transfer of organic to inorganic P through microbial metabolism occurs only in aerobic layers (Reddy and DeLaune, 2008). Differences in the biogeochemical processes of N and P lead to differences in the availability of microbial activities (Zhao et al., 2022). In particular, for plant litter decomposition experiment in the present study, which are located under the water table, the flooding environment causes difficulty in the conversion of organic P in surface soils to inorganic P; microbes cannot absorb organic P directly. Thus, the AI-P in the residual plant litter before day 56th was lower than 100%, and the P in the plant litter released to the surrounding environment was accompanied by mass loss. However, because microbes absorb N in an anaerobic environment more easily than P, the AI-N in the residual litter at the beginning of decomposition was higher than 100%. With increasing decomposition time, the mass loss rate gradually decreased, and the microbes adapted to the environment and gradually absorbed P from the surrounding environment. The AI-P markedly increased on days 91st and 121st, and the increasing trend was more obvious than that for AI-N. Previous studies also found that plant litter could accumulate P, and the AI-P was higher than 800% (Qualls and Richardson, 2000). The potential reason for this result was speculated to be that the N in plant litter may be released into the atmosphere as $N_2$ or $N_2O$ through the denitrification process, and the mobility of N is markedly higher than that of P (e Silva et al., 2007; Rubol et al., 2012). The loss of N in residual plant litter was easier than the loss of P, and there was no marked increase in N with increasing decomposition time. The biogeochemical cycling of S in an anaerobic environment was similar to that of P, and the transfer of organic S to inorganic S only occurred in the aerobic environment (Reddy and DeLaune, 2008). The AI-S in the residual plant litter before day 56th was lower than 100% in total, which means that the S released from plant litter to the surrounding environment was accompanied by mass loss. S may also be emitted to the atmosphere through $H_2S$ under the anaerobic environment, which is similar to the loss process of N. Thus, the biogeochemical character of S led to a marked increase in the AI-S in residual plant litter after day 56th, and the increasing trend was weaker than that of AI-P.

Shortly, the P and S were mainly released from plant litter to the surrounding environment before day 56th, and then accumulated in plant litter through the microbes absorbed from the surrounding environment. Because S could be released into the atmosphere through $H_2S$ under anaerobic conditions, the increasing trend of AI-P in the residual plant litter was more marked than that of AI-S. Compared to P and S, N was more easily utilized by microbes in anaerobic environments, and more N accumulated in the residual plant litter during the 121-day decomposition time in the present study.

## Direct effect of burning on element ratios in residual litters

The element ratios are widely used to evaluate the decomposition and nutrient changes of residual plant litter, and we selected C/N, C/P, N/P, and C/S to reflect the decomposition degree, nutrient limit, and acid stress, respectively (Güsewell and Verhoeven, 2006; Wang et al., 2019). The C/N ratio is a good indicator of the degree of decomposition because it reflects the ratio of carbohydrate to protein, and N is more stable than C during litter decomposition (Broder et al., 2012; Sun et al., 2012). As the C/N ratio decreased, the residual carbon decreased and the decomposition degree of plant litter increased. In the present study, the C/N ratio in the burnt sites was higher than that in the unburnt sites. The C/N ratio in the autumn burnt sites was higher than that in the spring burnt sites before day 91st, and then lower than that in the spring burnt sites on day 121st (**Figure 4**). Considering the variation trend of AI-N and AI-C, changes in the C/N ratio were mainly influenced by the accumulation of N, especially for the autumn burnt sites. The low N accumulation rates of residual plant litter in autumn-burnt sites was the major reason why the C/N ratio was higher than that in unburnt sites. Because N also accumulates through microbial activity at the initial stage of plant litter decomposition, the C/N ratio may not be a good indicator of carbon loss in plant litter.

In addition to the C/N ratio, the C/P ratio can be used to reflect the P available during the plant litter decomposition process. The C/P ratio of plant litter before day 56th was markedly higher than that after day 91st, and the C/P ratio of plant litter in the autumn burnt sites was markedly higher

than that in the autumn unburnt sites—especially on days 56th and 91st. Due to the small amount of P absorbed by microbes in the initial stage, the P in the plant litter was released to the surrounding environment, accompanied by mass loss. The low P content in the residual plant litter caused the C/P ratios to be higher than 3,000. Similar results were also found in a previous study in which litter decomposition was strongly limited by a high C/P ratio in the initial stage (Aerts and de Caluwe, 1997). After day 56th, the increase in AI-P in residual plant litter indicated the accumulation of P from the surrounding environment and a significant decrease in the C/P ratio. Compared to unburnt sites, autumn burning significantly increased the C/P ratio, which also indicated that the degree of P loss in the initial stage of litter decomposition was higher than that in unburnt sites. The potential reason for this is that microbial metabolism in autumn-burnt sites was more active than that in unburnt sites, and more C and P loss occur during decomposition. Compared to the loss of C, the loss of P in autumn burnt sites was more serious than that in unburnt sites, and thus increased the C/P ratios in total.

In addition to the amount of N and P, the N/P ratio is also important for the decomposition of plant litter. The critical N/P ratio (threshold between N and P limitation) was 25 for graminoid leaf litter (Güsewell and Verhoeven, 2006). In the present study, the N/P ratio was lower than 20, which indicates that the decomposition environment is the N limitation of litter decomposition, and bacteria were most abundant on cellulose (Güsewell and Gessner, 2009). Before day 56th, the N/P ratios ranged between 16.21 ± 2.33 and 23.32 ± 5.06, and the N/P ratios in unburnt sites were higher than those in autumn burnt sites, while they were lower than those in spring burnt sites. As the decomposition time increased, more P accumulated in the plant litter, and the N/P ratio decreased significantly and was lower than 10 (**Figure 4D**). The present results show that the plant litter decomposition process in the studied *C. angustifolia* litter was N limitation, and spring burning increased the N/P ratio and slightly decreased the N limitation effects on litter decomposition. Although P was lost at the initial stage of plant litter decomposition, the N/P ratio was still lower than 25, indicating that the residual P in plant litter was sufficient for microbial metabolism. As the AI-P increased significantly on day 91st, the N/P ratio significantly decreased, which means that the N limitation environment for litter decomposition was clearer and the changes in N content in residual plant litter were the major factors that influenced the decomposition rates of plant litter.

The release of S from plant litter to the surrounding environment may decrease the pH of the water environment and cause S stress on microbial activities for plant litter decomposition (Wang et al., 2019). As the decomposition time increased, the C/S ratio decreased, indicating that the loss rates of S were lower than the C loss rates. More S accumulated in plant litter and the marked decrease in the C/S ratio indicated that S stress on microbial metabolism increased and may become a stress factor that decreases the decomposition rates of plant litter. After 121 days of decomposition, the C/S ratios in plant litter in autumn burnt sites were higher than those in autumn unburnt sites; opposite trends were found in spring burnt sites. Autumn burning increased the C/S ratio in residual plant litter, which decreased the S stress for plant litter decomposition, and spring burning increased the S stress for plant litter decomposition. The difference of S stress may also explain why more plant litter was decomposed in autumn burnt sites than those in autumn unburnt sites.

The overall trends of selected element ratios in residual plant litter in burnt and unburnt sites were similar, and the ratio of C/P and C/S decreased significantly on day 91st. The N/P ratio during the entire decomposition process was lower than 25, indicating that the decomposition environment was limited by N. The accumulation of P after day 91st increased the importance of the N content in plant litter decomposition. Similar to the previous discussion, the nutrient element ratios also showed that autumn burning promoted a nutrient environment more suitable for plant litter decomposition, while spring burning slightly decreased the nutrient availability for plant litter decomposition.

## Conclusion

Based on a 121-day plant litter decomposition experiment in burnt and unburnt sites during the growing season, our results showed that the decomposition rates of plant litter in burnt and unburnt sites were markedly different, and that the burning season acts as a major factor that influences the decomposition process of residual plant litter. As the decomposition time increased, the carbon released to the surrounding environment was accompanied by mass loss, and nutrient elements accumulated in the residual plant litter. Autumn burning promoted carbon and mass loss from plant litter, whereas the mass loss rates of plant litter in spring burnt sites were lower than those in spring unburnt sites. P and S were released from plant litter to the surrounding environment before day 56th, and then accumulated more markedly in the plant litter. Unlike P and S, N accumulated in the residual plant litter during the 121-day decomposition period. The N/P ratio of plant litter in the spring burnt sites was significantly higher than that in other site types, and significantly decreased from ca. 20 on day 56th to ca. 9 on day 121st. A low N/P ratio indicates that N is the limiting nutrient element for plant litter decomposition in *C. angustifolia* wetlands, and the limitation of N became more serious as the decomposition time increased. Our results also suggest that the autumn burning accelerate the plant litter decomposed and nutrient elements accumulated in the residual plant litter, which may more benefit of elements cycling in *C. angustifolia* wetlands than the spring burning.

## Data availability statement

The raw data supporting the conclusions of this article will be made available by the authors, without undue reservation.

## Author contributions

CG, GW, and HZ designed the research and provided the funding. CG, JC, and HZ ran the experiment and data analysis. CG and HZ wrote the manuscript with input from GW, JC, and DH. All authors contributed to the article and approved the submitted version.

## Funding

Financial support was provided by the National Natural Science Foundation of China (Nos. 42171103 and 42101108), the Jilin Association for Science and Technology (QT202126), the Young Scientist Group Project of Northeast Institute of Geography and Agroecology, Chinese Academy of Sciences (2022QNXZ01), and the Youth Innovation Promotion Association CAS (No. 2020235).

## Acknowledgments

We thank Yuxia Zhang, Haiyang Zhao, and Shaoqing Zhang for sample analyses, and Yang Wang for help with the experimental burning. Assistance of the Sanjiang Mire Wetland Experimental Station, Chinese Academy of Sciences is also gratefully acknowledged.

## Conflict of interest

The authors declare that the research was conducted in the absence of any commercial or financial relationships that could be construed as a potential conflict of interest.

## Publisher's note



## References

Aerts, R., and de Caluwe, H. (1997). Nutritional and plant-mediated controls on leaf litter decomposition of *Carex species*. *Ecology* 78, 244–260

Battisti, C., Poeta, G., and Fanelli, G. (2016). *An Introduction to Disturbance Ecology*. Berlin: Springer International Publishing.

Brennan, K. E., Christie, F. J., and York, A. (2009). Global climate change and litter decomposition: more frequent fire slows decomposition and increases the functional importance of invertebrates. *Glob. Change Biol.* 15, 2958–2971. doi: 10.1111/j.1365-2486.2009.02011.x

Broder, T., Blodau, C., Biester, H., and Knorr, K. H. (2012). Peat decomposition records in three pristine ombrotrophic bogs in southern Patagonia. *Biogeosciences* 9, 1479–1491. doi: 10.5194/bg-9-1479-2012

Butler, O. M., Lewis, T., and Chen, C. (2017). Fire alters soil labile stoichiometry and litter nutrients in Australian eucalypt forests. *Int. J. Wildland Fire* 26, 783–788. doi: 10.1071/WF17072

Clarkson, B. R., Moore, T. R., Fitzgerald, N. B., Thornburrow, D., Watts, C. H., and Miller, S. (2013). Water Table Regime Regulates Litter Decomposition in Restiad Peatlands. *N. Zealand. Ecosyst.* 17, 317–326. doi: 10.1007/s10021-013-9726-4

Cong, J., Gao, C., Han, D., Li, Y., and Wang, G. (2020). Stability of the permafrost peatlands carbon pool under climate change and wildfires during the last 150 years in the northern Great Khingan Mountains, China. *Sci. Total Environ.* 712:136476. doi: 10.1016/j.scitotenv.2019.136476

Cong, J., Gao, C., Han, D., Liu, H., and Wang, G. (2019). History metal (Pb, Zn, and Cu) deposition and Pb isotope variability in multiple peatland sites in the northern Great Hinggan Mountains, Northeast China. *Environ. Sci. Pollut.* R. 26(21), 21784-21796. doi: 10.1007/s11356-019-04432-7

Cui, W., Mao, Y., Tian, K., and Wang, H. (2021). A Comparative Study of Manipulative and Natural Temperature Increases in Controlling Wetland Plant Litter Decomposition. *Wetlands* 41:48. doi: 10.1007/s13157-021-01445-2

e Silva, C. A. R., Oliveira, S. R., Rêgo, R. D., and Mozeto, A. A. (2007). Dynamics of phosphorus and nitrogen through litter fall and decomposition in a tropical mangrove forest. *Mar. Environ. Res.* 64, 524–534. doi: 10.1016/j.marenvres.2007.04.007

Fick, S. E., and Hijmans, R. J. (2017). WorldClim 2: new 1-km spatial resolution climate surfaces for global land areas. *Int. J. Climatol.* 37, 4302–4315. doi: 10.1002/joc.5086

Flannigan, M., Cantin, A. S., De Groot, W. J., Wotton, M., Newbery, A., and Gowman, L. M. (2013). Global wildland fire season severity in the 21st century. *Forest Ecol. Manag.* 294, 54–61. doi: 10.1016/j.foreco.2012.10.022

Flannigan, M. D., Krawchuk, M. A., de Groot, W. J., Wotton, B. M., and Gowman, L. M. (2009). Implications of changing climate for global wildland fire. *Int. J. Wildland Fire* 18, 483–507. doi: 10.1071/WF08187

Gallego-Sala, A. V., Charman, D. J., Brewer, S., Page, S. E., Prentice, I. C., Friedlingstein, P., et al. (2018). Latitudinal limits to the predicted increase of the peatland carbon sink with warming. *Nat. Clim. Change* 8, 907–913. doi: 10.1038/s41558-018-0271-1

Gao, C., Bao, K., Lin, Q., Zhao, H., Zhang, Z., Xing, W., et al. (2014). Characterizing trace and major elemental distribution in late Holocene in Sanjiang Plain, Northeast China: Paleoenvironmental implications. *Quatern. Int.* 349, 376–383. doi: 10.1016/j.quaint.2014.01.022

Gao, C., He, J., Cong, J., Zhang, S., and Wang, G. (2018). Impact of forest fires generated black carbon deposition fluxes in Great Hinggan Mountains (China). *Land Degrad. Dev.* 29, 2073–2081. doi: 10.1002/ldr.2837

Gao, C., Wang, G., Santin, C., Doerr, S. H., Cong, J., and Zhao, H. (2021). Response of Calamagrostis angustifolia to burn frequency and seasonality in the Sanjiang Plain wetlands (Northeast China). *J. Environ. Manage.* 300:113759. doi: 10.1016/j.jenvman.2021.113759

Giardina, C. P., Sanford, R. L., Døckersmith, I. C., and Jaramillo, V. J. (2000). The effects of slash burning on ecosystem nutrients during the land preparation phase of shifting cultivation. *Plant Soil* 220, 247–260. doi: 10.1023/A:1004741125636

Goncharova, O. Y., Matyshak, G. V., Epstein, H. E., Sefilian, A. R., and Bobrik, A. A. (2019). Influence of snow cover on soil temperatures: Meso- and micro-scale topographic effects (a case study from the northern West Siberia discontinuous permafrost zone). *Catena* 183:104224. doi: 10.1016/j.catena.2019.104224

Gorecki, K., Rastogi, A., Strozecki, M., Gabka, M., Lamentowicz, M., Lucow, D., et al. (2021). Water table depth, experimental warming, and reduced precipitation impact on litter decomposition in a temperate Sphagnum-peatland. *Sci. Total Environ.* 771:145452. doi: 10.1016/j.scitotenv.2021.145452

Güsewell, S., and Gessner, M. O. (2009). N : P ratios influence litter decomposition and colonization by fungi and bacteria in microcosms. *Funct. Ecol.* 23, 211–219. doi: 10.1111/j.1365-2435.2008.01478.x

Güsewell, S., and Verhoeven, J. T. A. (2006). Litter N:P ratios indicate whether N or P limits the decomposability of graminoid leaf litter. *Plant Soil* 287, 131–143. doi: 10.1007/s11104-006-9050-2

Jones, M. W., Santín, C., van der Werf, G. R., and Doerr, S. H. (2019). Global fire emissions buffered by the production of pyrogenic carbon. *Nat. Geosci.* 12, 742–747. doi: 10.1038/s41561-019-0403-x

Just, M. G., Hohmann, M. G., and Hoffmann, W. A. (2017). Invasibility of a fire-maintained savanna–wetland gradient by non-native, woody plant species. *Forest Ecol. Manag.* 405, 229–237. doi: 10.1016/j.foreco.2017.09.052

Loisel, J., Gallego-Sala, A. V., Amesbury, M. J., Magnan, G., Anshari, G., Beilman, D. W., et al. (2020). Expert assessment of future vulnerability of the global peatland carbon sink. *Nat. Clim. Change* 70–77. doi: 10.1038/s41558-020-00944-0

Marrs, R., Marsland, E.-L., Lingard, R., Appleby, P., Piliposyan, G., Rose, R., et al. (2019). Experimental evidence for sustained carbon sequestration in fire-managed, peat moorlands. *Nat. Geosci.* 12, 108–112. doi: 10.1038/s41561-018-0266-6

Medvedeff, C. A., Inglett, K. S., and Inglett, P. W. (2015). Can Fire Residues (Ash and Char) Affect Microbial Decomposition in Wetland Soils? *Wetlands* 35, 1165–1173. doi: 10.1007/s13157-015-0703-x

Medvedeff, C. A., Inglett, K. S., Kobziar, L. N., and Inglett, P. W. (2013). Impacts of Fire on Microbial Carbon Cycling in Subtropical Wetlands. *Fire Ecol.* 9, 21–37. doi: 10.4996/fireecology.0901021

Nilsson, M., Sagerfors, J., Buffam, I., Laudon, H., Eriksson, T., Grelle, A., et al. (2008). Contemporary carbon accumulation in a boreal oligotrophic minerogenic mire - a significant sink after accounting for all C-fluxes. *Global Change Biol.* 14, 2317–2332. doi: 10.1111/j.1365-2486.2008.01654.x

Pingree, M. R. A., and DeLuca, T. H. (2018). The influence of fire history on soil nutrients and vegetation cover in mixed-severity fire regime forests of the eastern Olympic Peninsula. *Washington, USA. Forest Ecol. Manag.* 422, 95–107. doi: 10.1016/j.foreco.2018.03.037

Qualls, R. G., and Richardson, C. J. (2000). Phosphorus enrichment affects litter decomposition, immobilization, and soil microbial phosphorus in wetland mesocosms. *Soil Sci. Soc. Am. J.* 64, 799–808. doi: 10.2136/sssaj2000.642799x

Reddy, K. R., and DeLaune, R. D. (2008). *Biogeochemistry of Wetlands: Science and Applications*. Boca Raton: CRC press.

Rubol, S., Silver, W. L., and Bellin, A. (2012). Hydrologic control on redox and nitrogen dynamics in a peatland soil. *Sci. Total Environ.* 432, 37–46. doi: 10.1016/j.scitotenv.2012.05.073

Singh, A. K., Kushwaha, M., Rai, A., and Singh, N. (2017). Changes in soil microbial response across year following a wildfire in tropical dry forest. *Forest Ecol. Manag.* 391, 458–468. doi: 10.1016/j.foreco.2017.02.042

Song, Y., Song, C., Ren, J., Tan, W., Jin, S., and Jiang, L. (2018). Influence of nitrogen additions on litter decomposition, nutrient dynamics, and enzymatic activity of two plant species in a peatland in Northeast China. *Sci. Total Environ.* 625, 640–646. doi: 10.1016/j.scitotenv.2017.12.311

Song, Y., Zhou, D., Zhang, H., Li, G., Jin, Y., and Li, Q. (2013). Effects of vegetation height and density on soil temperature variations. *Chin. Sci. Bull.* 58, 907–912. doi: 10.1007/s11434-012-5596-y

Song, Y.-B., Zhou, M.-Y., Qin, Y.-L., Cornelissen, J. H. C., and Dong, M. (2021). Nutrient effects on aquatic litter decomposition of free-floating plants are species dependent. *Glob. Ecol. Conserv.* 30:e01748. doi: 10.1016/j.gecco.2021.e01748

Straková, P., Penttilä, T., Laine, J., and Laiho, R. (2012). Disentangling direct and indirect effects of water table drawdown on above- and belowground plant litter decomposition: consequences for accumulation of organic matter in boreal peatlands. *Glob. Change Biol.* 18, 322–335. doi: 10.1111/j.1365-2486.2011.02503.x

Sun, Z., Mou, X., and Liu, J. S. (2012). Effects of flooding regimes on the decomposition and nutrient dynamics of Calamagrostis angustifolia litter in the Sanjiang Plain of China. *Environ. Earth Sci.* 66, 2235–2246. doi: 10.1007/s12665-011-1444-7

Thompson, D. K., and Waddington, J. M. (2013). Peat properties and water retention in boreal forested peatlands subject to wildfire. *Water Resour. Res.* 49, 3651–3658. doi: 10.1002/wrcr.20278

Turetsky, M. R., Benscoter, B., Page, S., Rein, G., van der Werf, G. R., and Watts, A. (2015). Global vulnerability of peatlands to fire and carbon loss. *Nat. Geosci.* 8, 11–14. doi: 10.1038/ngeo2325

van der Werf, G. R., Randerson, J. T., Giglio, L., van Leeuwen, T. T., Chen, Y., Rogers, B. M., et al. (2017). Global fire emissions estimates during 1997–2016. *Earth Syst. Sci. Data* 9, 697–720. doi: 10.5194/essd-9-697-2017

Wang, G., Yu, X., Bao, K., Xing, W., Gao, C., Lin, Q., et al. (2015). Effect of fire on phosphorus forms in Sphagnum moss and peat soils of ombrotrophic bogs. *Chemosphere* 119, 1329–1334. doi: 10.1016/j.chemosphere.2014.01.084

Wang, J., Ge, Y., Cornelissen, J. H. C., Wang, X. Y., Gao, S., Bai, Y., et al. (2022). Litter nitrogen concentration changes mediate effects of drought and plant species richness on litter decomposition. *Oecologia* 198, 507–518. doi: 10.1007/s00442-022-05105-y

Wang, Q., Kwak, J. H., Choi, W. J., and Chang, S. X. (2019). Long-term N and S addition and changed litter chemistry do not affect trembling aspen leaf litter decomposition, elemental composition and enzyme activity in a boreal forest. *Environ. Pollut.* 250, 143–154. doi: 10.1016/j.envpol.2019.04.007

Wang, Z., and Roulet, N. (2017). Comparison of plant litter and peat decomposition changes with permafrost thaw in a subarctic peatland. *Plant Soil* 417, 197–216. doi: 10.1007/s11104-017-3252-7

Ward, S. E., Orwin, K. H., Ostle, N. J., Briones, M. J., Thomson, B. C., Griffiths, R. I., et al. (2015). Vegetation exerts a greater control on litter decomposition than climate warming in peatlands. *Ecology* 96, 113–123. doi: 10.1890/14-0292.1

Wu, L., and Tao, Q. (1993). The improved method on quantify organic carbon in plant. *Chin. J. Soil Sci.* 24, 286–287. doi: 10.19336/j.cnki.trtb.1993.06.018

Yu, X., Ding, S., Lin, Q., Wang, G., Wang, C., Zheng, S., et al. (2020). Wetland plant litter decomposition occurring during the freeze season under disparate flooded conditions. *Sci. Total Environ.* 706:136091. doi: 10.1016/j.scitotenv.2019.136091

Yu, Z., Loisel, J., Brosseau, D. P., Beilman, D. W., and Hunt, S. J. (2010). Global peatland dynamics since the Last Glacial Maximum. *Geophys. Res. Lett.* 37, 1–5. doi: 10.1029/2010gl043584

Zhao, H., Tong, D. Q., Lin, Q., Lu, X., and Wang, G. (2012). Effect of fires on soil organic carbon pool and mineralization in a Northeastern China wetland. *Geoderma* 18, 532–539. doi: 10.1016/j.geoderma.2012.05.013

Zhao, X., Chen, J., Guo, M., Li, C., Hou, N., and Bai, S. (2022). Constructed wetlands treating synthetic wastewater in response to day-night alterations: Performance and mechanisms. *Chem. Eng. J.* 446:137460. doi: 10.1016/j.cej.2022.137460

frontiers | Frontiers in Ecology and Evolution

TYPE Original Research
PUBLISHED 25 July 2022
DOI 10.3389/fevo.2022.973626



OPEN ACCESS

EDITED BY
Chuanyu Gao,
Northeast Institute of Geography and Agroecology (CAS), China

REVIEWED BY
Yuanchun Zou,
Northeast Institute of Geography and Agroecology (CAS), China
Xiaoming Kang,
Institute of Wetland Research, Chinese Academy of Forestry, China

*CORRESPONDENCE
Meng Wang
meng.wang3@mail.mcgill.ca

SPECIALTY SECTION
This article was submitted to Conservation and Restoration Ecology, a section of the journal Frontiers in Ecology and Evolution

RECEIVED 20 June 2022
ACCEPTED 07 July 2022
PUBLISHED 25 July 2022

CITATION
Li T, Yuan X, Ge L, Cao C, Suo Y, Bu Z-J, Peng C, Song H, Liu Z, Liu S and Wang M (2022) Weak impact of nutrient enrichment on peat: Evidence from physicochemical properties.
*Front. Ecol. Evol.* 10:973626.
doi: 10.3389/fevo.2022.973626



# Weak impact of nutrient enrichment on peat: Evidence from physicochemical properties

Tong Li[1,2,3], Xin Yuan[4], Leming Ge[1,2], Chenhao Cao[1,2], Yuchen Suo[1,2], Zhao-Jun Bu[1,2,5], Changhui Peng[3,6], Hanxiong Song[6], Ziping Liu[1], Shasha Liu[1] and Meng Wang[1,2,5]*

[1]Key Laboratory of Geographical Processes and Ecological Security in Changbai Mountains, Ministry of Education, School of Geographical Sciences, Northeast Normal University, Changchun, China, [2]State Environmental Protection Key Laboratory of Wetland Ecology and Vegetation Restoration, Institute for Peat and Mire Research, Northeast Normal University, Changchun, China, [3]School of Geographic Sciences, Hunan Normal University, Changsha, China, [4]Center for Ecological Forecasting and Global Change, College of Forestry, Northwest A&F University, Yangling, China, [5]Jilin Provincial Key Laboratory for Wetland Ecological Processes and Environmental Change in the Changbai Mountains, Changchun, China, [6]Department of Biology Sciences, Institute of Environment Sciences, University of Quebec at Montreal, Montreal, QC, Canada

Atmospheric deposition of nitrogen (N) and phosphorus (P) far exceeding the pre-industrial levels have the potential to change carbon (C) dynamics in northern peatlands. However, the responses of soil C concentration and organo-chemical composition to different rates and durations of nutrient enrichment are still unclear. Here, we compared the short- (3 years) and long-term (10 years) effects of N and P fertilizations on the physicochemical properties of peat and porewater in a bog-fen complex in northern China. Our results showed that the short-term fertilization increased *Sphagnum* moss cover, while the expansion of vascular plants was observed owing to the long-term fertilization. The preserved soil C did not vary considerably after the short- and long-term fertilizations. The harsh soil conditions may impede the decomposition of organic matters by soil microorganisms during the short-term fertilization. For the long-term fertilization, the input of high-phenolic litters owing to vascular plant expansion likely exerted an important control on soil C dynamics. These processes constrained the variation in soil C concentrations when the addition rate and cumulative amount of external N and P increased, which will advance our understanding and prediction of the resilience of soil C storage to imbalanced nutrient enrichment of N and P in northern peatlands.

KEYWORDS

**fen, bog, fertilization, FTIR, humification indices**

## Introduction

Peatlands are important carbon (C) sinks which store 500–700 Gt of soil organic C, but only comprise about 3% of the land surface (Gorham, 1991; Yu et al., 2010). These massive C sequestrations result from the imbalance between production and decomposition under waterlogged, acid and nutrient-deficient conditions (Schothorst, 1977; Rydin and Jeglum, 2013). Nutrient deposition may have unforeseen effects on global peatlands, for example increase soil C release, leading to a catastrophic impact on future climate (Dash et al., 2020; Wang et al., 2021). Unfortunately, significant increase in atmospheric deposition of reactive nitrogen (N) and phosphorus (P) have been observed due to fertilization, mining, and fossil fuel combustion in recent decades (Rice and Herman, 2012; Tipping et al., 2014; Ackerman et al., 2019). Furthermore, considering the possibly faster increase of N input than P input, the imbalance of N and P enrichment was expected to deteriorate (Peñuelas et al., 2013), which may change plant community composition and present a substantial threat to soil C stock (Moore et al., 2019; Schlesinger and Bernhardt, 2020).

Numerous nutrient manipulation experiments have been established in global peatlands to gain insight into the effects of nutrient enrichment on soil C decomposition, but these studies usually produced different or even contrasting results (e.g., Bubier et al., 2007; Li et al., 2019; Moore et al., 2019). These discrepancies might result from various biotic controls associated with shift in plant community compositions on soil C mineralization. For example, long-term fertilization might stimulate vascular plant growth at the expense of moss (Moore et al., 2019; Schlesinger and Bernhardt, 2020), and this change may have complex effects on preserved soil C.

As for the negative effect, the expansion of vascular plants, especially by the extended root network, would raise peat surface, and further contribute to the hummock-hollow microtopography to ameliorate waterlogged stress (Moore et al., 2002; Schlesinger and Bernhardt, 2020). Subsequently, this may further enhance ecosystem respiration and change nutrient storage and enzyme activity (Larmola et al., 2013; Li et al., 2020). This vascular plant-mediated effect could be reflected not only in peat quality, but also in porewater chemistry (Moore et al., 2019). For example, the concentrations of dissolved N and P in porewater were positively related to proteins or protein precursors exuded by plant roots and microorganisms but negatively related to the "capacity of the 'filter'" function of *Sphagnum* moss (Limpens et al., 2004; Chiwa et al., 2016; Moore et al., 2019).

As for the positive effect, a series of cascading effects caused by increased vascular plant growth might retard organic matter decomposition and obscure microbial response to nutrient inputs (Li et al., 2019; Fenner and Freeman, 2020; Wang et al., 2021). Microbial decomposers might be much less responsive to the enrichment of external nutrients in shrub-dominated peatlands (e.g., Wang et al., 2015; Fenner and Freeman, 2020), because the improved litter quality and increased tannin production, associated with shift in the dominance of vascular plants, could effectively bind protein and inhibit enzyme activity by oxidative degradation and biotoxicity (Freeman et al., 2001; Wang et al., 2015). This was supported by a long-term decomposition experiment conducted by Fenner and Freeman (2020), in which the water-soluble phenolics leached from wood trunks inhibited both the extracellular and intracellular metabolism and lowered nutrient mobilization. Besides, vascular plants could strongly compete with soil microorganisms for available nutrients through extended root and releasing allelopathic compounds (van Breemen, 1995; Schlesinger and Bernhardt, 2020). In both cases, because the activities of microbial decomposers were inhibited by protein-binding phenolic compounds from the litters of vascular plants, the expansion of vascular plants may eventually counteract the negative effects of nutrient enrichment on soil C stock (Freeman et al., 2001; Wang et al., 2015; Fenner and Freeman, 2020). The above-mentioned confounding effects make it difficult for the results of current studies to reach a consensus (Rousk et al., 2013; Wang et al., 2015). Therefore, the interactive effect of N and P enrichment on soil C decomposition is still under-investigated, especially in northern peatlands where to the shift in plant community composition occurs under cumulative nutrient fertilization.

The absorption bands of Fourier transform infrared (FTIR) spectroscopy can indicate the composition of major peat chemical moieties, such as polysaccharides, lignin, phenolics, and carboxylates (Biester et al., 2014; Moore et al., 2019; Drollinger et al., 2020). With regard to the peak intensity ratios, the relative contributions of refractory organic compounds increased compared to labile polysaccharides can be identified as an increase in the degree of organic matter decomposition, considering that the liberated monomers from carbohydrates are easily assimilated by microorganisms or oxidized to generate metabolic energy (Niemeyer et al., 1992; Cocozza et al., 2003; Broder et al., 2012). In this study, we evaluated whether and how the interrelated chemical properties of peat and porewater and plant community composition were changed by N and P enrichment that ultimately affected C storage under short- (3 years) and long-term fertilization (10 years) at Hani peatland, northeastern China. Specifically, we quantified the total concentrations of C, N, P, and metals in peat, and the concentrations of dissolved C, N, and P in porewater, as well as four humification indices of surface peat *via* FTIR spectroscopic analysis. We intended to test the following two hypotheses: (1) in *Sphagnum* moss-dominated plots, the strong changes in chemical moieties in peat and/or porewater due to short-term fertilization could threaten the reservoir of soil organic C and (2) the increased phenolics input due to the loss of *Sphagnum* and the expansion of vascular plants would protect soil C stock during long-term N and P additions.

# Materials and methods

## Study site and fertilization experiments

This study was conducted at Hani peatland (42°13′N, 126°31′E) in Changbai Mountains, northeastern China. Hani peatland is a bog-fen complex with a mean annual precipitation of 757–930 mm and a mean annual temperature of 2.5–3.6°C (Bu et al., 2011). The average peat depth in the area is 4 m with a maximum depth of 9.6 m (Qiao, 1993; Bu et al., 2011). The short- (since 2018) and long-term (since 2007) N and P fertilization experiments were both established on large hummocks in the open bog region of Hani peatland. A factorial design was used with three levels of N addition (0, 5, and 10 g N $m^{-2}$ $year^{-1}$; i.e., 0N, 5N, 10N) and in combination with P addition (0, 0.5, and 10 g P $m^{-2}$ $year^{-1}$; i.e., 0P, 0.5P, 1P). There were four replicates for each treatment combination, and the size of fertilized plot was 1.2 m × 1.2 m for the short-term experiment and 0.8 m × 0.8 m for the long-term experiment. In total, there were 72 plots (9 treatment combinations × 4 replicates × 2 fertilization experiments). Nitrogen and P was applied as ammonium nitrate ($NH_4NO_3$) and sodium dihydrogen phosphate ($NaH_2PO_4{\cdot}2H_2O$), respectively, and the control plots were supplied with deionized water. The dominant shrubs are *Betyla ovalifolia* Rupr., *Rhododendron parvifolium* Adams, and *Potentilla fruticose* Linn., and the dominant herbaceous plants are *Carex lasiocarpa* Ehrh., *Eriophorum polystachion* L., and *Smilacina japonica* A. Gray. The underlying moss layer is dominated by *Sphagnum palustre* Linn. and *Polytrichum commune* Linn. ex Hedw.

## Vegetation measurements

We used point intercept method to determine the abundances of *Sphagnum* moss and vascular plants in the fertilized plots (Larmola et al., 2013). Briefly, a customized stain-steel frame (60 cm × 60 cm) with 61 grid points was used for the measurement. The number of times (i.e., "hits") were recorded when the leaves of vascular plants at different height or *Sphagnum* capitula on the ground contacted a carbon fiber rod (2 mm in diameter) over the grid points. *Sphagnum* moss abundance (i.e., cover) was calculated by the total number of hits divided by 61. Vascular plant abundance (not identical to plant cover) was approximated by the total number of hits per unit area (i.e., hits $m^{-2}$).

## Physicochemical properties of peat and porewater

Peat samples (20 g of fresh peat) at 0–5 cm from the long-term and short-term fertilized plots were collected in August 2017 and 2020, respectively. Living mosses were removed and the remaining peat samples were stored at 4°C prior to analyses within seven days. A subset of fresh peat samples was dried at 65°C and ground with a ball mill (MM400, Retsch GmbH, Haan, Germany). Total carbon (TC) and total nitrogen (TN) concentrations were measured on an elemental analyzer (vario MACRO cube, elementar, Germany). The remaining samples of the ground peat were digested in concentrated sulfuric acid and hydrogen peroxide with selenium and lithium sulfate as catalysts (Parkinson and Allen, 2008). Total phosphorus (TP) concentration of samples from the long-term fertilized plots was determined colorimetrically using the ammonium molybdate-ascorbic acid method (Murphy and Riley, 1962) on a continuous flow analyzer (San + +, Skalar Analytical B.V., Breda, Netherlands). Total P concentration of samples from the short-term fertilized plots was determined by the malachite green method against calibration standard (Ohno and Zibilske, 1991) on a full-wavelength microplate reader (Multiskan GO, Thermo Fisher, Finland). Potassium (K), calcium (Ca), and magnesium (Mg) concentrations were measured on an atomic absorption spectrophotometer (AA-7003A, EWAI company, China), with the calibration standards of potassium chloride, calcium carbonate, and magnesium sheet, respectively. The data of TC, TN, and TP concentrations in the long-term fertilized plots were derived from our previous study (Li et al., 2019).

In August 2020, we collected porewater samples (∼30 mL) from the short- and long-term fertilized plots with MacroRhizons tubes (Rhizosphere Research Products B.V., Wageningen, Netherlands). Concentration of dissolved organic carbon (DOC) was measured on a TOC analyzer (TOC-L, SHIMADZU, Japan). The concentrations of $NH_4^+$-N, $NO_3^-$-N, and $PO_4^{3-}$ [i.e., dissolved inorganic phosphorus (DIP)] in porewater were measured on a continuous flow analyzer (San + +, Skalar Analytical B.V., Breda, Netherlands). The concentration of dissolved inorganic nitrogen (DIN) was calculated as the sum of $NH_4^+$-N and $NO_3^-$-N concentrations. The remaining porewater samples were then digested with potassium persulfate at 120°C for 1 h to quantify the total dissolved N and P concentrations (TDN and TDP). The concentration of dissolved organic nitrogen (DON) was calculated as the difference between the concentrations of TDN and DIN. Similarly, the concentration of dissolved organic phosphorus (DOP) was calculated as the difference between the concentrations of TDP and DIP.

## Organic chemistry analysis

The organo-chemical composition of dried peat samples was measured on a FTIR spectrometer (Vetex70, BRUKER, Germany) with absorption mode. Specifically, 2 mg of ground and oven-dried peat sample was mixed with 200 mg of potassium bromide, and then pressed to translucent pellets. The range of the wavenumber was 4,000 to 400 $cm^{-1}$ with a resolution of 2 $cm^{-1}$ and 16 scans per sample were collected.

The background of potassium bromide was removed from the spectra, and then atmospheric compensation and baseline correction was performed (see section "statistical analyses"). To determine the degree of humification of peat samples, spectra peaks around the following wavenumbers were recorded: 1,090 $cm^{-1}$ (polysaccharide), 1,420 $cm^{-1}$ (carboxylates and humic acids), 1,510 $cm^{-1}$ (lignin and phenolics), 1,630 $cm^{-1}$ (mainly aromatics), and 1,720 $cm^{-1}$ (carboxylates–acids) (Niemeyer et al., 1992; Moore et al., 2019; Drollinger et al., 2020). Humification indices were calculated as the ratios of the absorption at corresponding wavenumbers, i.e., 1,420/1,090, 1,510/1,090, 1,630/1,090, and 1,720/1,090 (Niemeyer et al., 1992; Cocozza et al., 2003; Broder et al., 2012). The decreases in these humification indices were considered to reflect the enhanced degree of organic matter decomposition (Niemeyer et al., 1992; Broder et al., 2012).

## Statistical analyses

Statistical analyses were performed using R 4.0.4 (R Core Team, 2021). Data normality and the homogeneity of variance were examined with Shapiro–Wilk tests and Levene's tests, respectively. Two-way ANOVAs were used to test the fertilization effect on plant abundance, physicochemical properties, and humification indices using the addition rates of N, P, and their combination as fixed factors for the short- and long-term fertilization experiments separately. *Post hoc* multiple comparisons were conducted using Tukey's test at the significance level of $P < 0.05$. Two-sample *t*-test was used to compare the results of plant abundance, physicochemical properties, and humification indices between the short- and long-term fertilization under the same N or P addition rate. The *ir* (Teickner, 2022) and *irpeat* (Teickner and Hodgkins, 2022) packages in R were used to process the spectra of FTIR, including baseline correction, normalization, and calculation of humification indices. Spearman's correlation analysis was conducted to detect the relationships between plant species abundance and physicochemical properties of peat and porewater. Hierarchical partitioning was employed to assess the contribution of physicochemical properties of peat and porewater on organic matter decomposition as indicated by four humification indices using the *rdacca.hp* package in R (Lai et al., 2022).

# Result

## Peat and porewater chemistry

We did not observe any significant change in TC concentration in peat under neither fertilization experiment (**Table 1**). For the short-term fertilization, without significant N by P interaction, N and P additions significantly increased TN and TP concentrations, respectively. However, for the long-term fertilization, the effect of N and P interaction on nutrient concentrations was significant. Specifically, under the same rate of P addition, N addition increased TN ($P < 0.001$) and TP concentrations ($P = 0.034$); under the same rate of N addition, P addition increased TP concentration (**Table 1**). In combination with the highest rate of N addition (i.e., 10 g N $m^{-2}$ $year^{-1}$), P addition ultimately increased TN concentration by 54% ($P < 0.001$). Short-term fertilization had little effect on K, Ca, and Mg concentrations, while long-term N addition significantly decreased K concentration ($P < 0.001$; **Table 1**). Compared to the short-term fertilization, long-term N and/or P additions significantly decreased Ca and Mg concentrations.

As for porewater chemistry, the concentrations of dissolved nutrients only showed weak responses to N and/or P additions in both experiments (**Table 2**). Specifically, the short- or long-term fertilization did not show significant effect on DOC concentration (**Table 2**). Nitrogen addition significantly increased the concentrations of $NH_4^+$-N (short-term, $P = 0.017$; long-term, $P < 0.001$) and DON (short-term, $P = 0.045$; long-term, $P = 0.038$; **Table 2**). In particular, the long-term N addition significantly increased DON concentration compared to the short-term fertilization. We did not observe significant change in dissolved P concentrations (i.e., DIP and DOP) in neither experiment (**Table 2**).

## Variation in plant abundance

For the short-term fertilization, the abundance of *Sphagnum* moss was increased by 25–70% compared to the control (i.e., 0N0P treatment; **Figure 1A**). The total abundance of vascular plants was substantially reduced by N-only addition and the combination of N and P additions (**Figure 1B**). Strong and positive correlation between *Sphagnum* moss abundance and TP concentration was observed after short-term fertilization (Spearman's $\rho = 0.55$, $P < 0.001$; **Figure 2A**). For the long-term fertilization, the abundance of *Sphagnum* moss was decreased by 21–55%, while the abundance of vascular plants was increased by 0.4–28% (**Figures 1C, D**). Results of Spearman's correlation analysis indicated that the abundance of vascular plants was significantly and negatively correlated with *Sphagnum* moss abundance ($\rho = -0.39$, $P = 0.013$), and significantly and positively correlated with TP concentration under the long-term fertilization ($\rho = 0.48$, $P = 0.014$; **Figure 2C**).

## Humification indices and the contributions of physicochemical properties

The additions of N and P did not remarkably increase the degree decomposition of organic matter as indicated

TABLE 1 Peat chemical properties under different treatments in the short- and long-term fertilizations.

| Treatment | TC (mg $g^{-1}$) | TN (mg $g^{-1}$) | TP (mg $g^{-1}$) | K (mg $g^{-1}$) | Ca (mg $g^{-1}$) | Mg (mg $g^{-1}$) |
|---|---|---|---|---|---|---|
| **Short-term fertilization** | | | | | | |
| 0N0P | 424.7 ± 2.8 | 8.9 ± 0.5$^{a}$ | 1.8 ± 0.1$^{A}$ | 2.0 ± 0.1* | 4.6 ± 0.2* | 1.3 ± 0.3 |
| 5N0P | 416.6 ± 4.8 | 11.2 ± 0.4$^{b}$ | 1.9 ± 0.2$^{A}$ | 2.0 ± 0.1 | 4.3 ± 0.2* | 0.9 ± 0.1* |
| 10N0P | 422.0 ± 2.9* | 12.7 ± 0.8$^{c}$* | 2.3 ± 0.2$^{A}$ | 1.5 ± 0.1* | 4.0 ± 0.6* | 0.9 ± 0.1* |
| 0N0.5P | 420.2 ± 5.1 | 8.8 ± 0.3$^{a}$ | 2.8 ± 0.1$^{B}$ | 2.1 ± 0.1* | 5.5 ± 0.2* | 0.9 ± 0.0* |
| 0N1P | 408.6 ± 0.8 | 8.9 ± 0.4$^{a}$ | 4.1 ± 0.1$^{C}$ | 1.8 ± 0.1* | 4.8 ± 0.3* | 0.8 ± 0.0* |
| 5N0.5P | 433.6 ± 3.1 | 11.6 ± 0.5$^{b}$ | 2.9 ± 0.1$^{B}$ | 1.9 ± 0.2 | 4.3 ± 0.3* | 1.0 ± 0.1* |
| 10N0.5P | 416.1 ± 5.0 | 13.4 ± 0.5$^{c}$ | 3.1 ± 0.1$^{B}$ | 1.5 ± 0.3 | 5.3 ± 0.2* | 0.9 ± 0.0* |
| 5N1P | 413.5 ± 6.6 | 11.7 ± 0.1$^{b}$ | 4.1 ± 0.0$^{C}$ | 1.9 ± 0.2 | 4.6 ± 0.1* | 0.8 ± 0.0* |
| 10N1P | 418.6 ± 8.9 | 12.6 ± 0.5$^{c}$* | 3.9 ± 0.0$^{C}$ | 2.1 ± 0.2 | 4.2 ± 0.1* | 0.8 ± 0.0* |
| **Long-term fertilization** | | | | | | |
| 0N0P | 411.0 ± 3.8 | 9.8 ± 0.7$^{aA}$ | 0.5 ± 0.1$^{aA}$ | 4.4 ± 0.3$^{b}$* | 0.2 ± 0.0* | 0.1 ± 0.0$^{a}$ |
| 5N0P | 423.7 ± 4.7 | 12.8 ± 0.8$^{aA}$ | 0.5 ± 0.0$^{aA}$ | 2.8 ± 0.2$^{a}$ | 0.3 ± 0.2* | 0.2 ± 0.1$^{ab}$* |
| 10N0P | 387.2 ± 4.3* | 16.6 ± 0.4$^{bB}$* | 0.6 ± 0.0$^{aA}$ | 3.4 ± 0.1$^{a}$* | 0.4 ± 0.1* | 0.3 ± 0.0$^{b}$* |
| 0N0.5P | 412.8 ± 9.9 | 10.0 ± 1.1$^{aA}$ | 0.8 ± 0.1$^{aB}$ | 6.0 ± 0.1$^{b}$* | 0.2 ± 0.0* | 0.1 ± 0.0$^{a}$* |
| 0N1P | 421.2 ± 10.2 | 10.0 ± 1.1$^{aA}$ | 0.9 ± 0.0$^{aB}$ | 4.5 ± 0.7$^{b}$* | 0.1 ± 0.1* | 0.1 ± 0.0$^{a}$* |
| 5N0.5P | 425.0 ± 5.3 | 11.8 ± 0.8$^{aA}$ | 0.7 ± 0.1$^{aB}$ | 3.3 ± 0.7$^{a}$ | 0.3 ± 0.0* | 0.2 ± 0.0$^{ab}$* |
| 10N0.5P | 393.6 ± 14.9 | 12.9 ± 1.5$^{bA}$ | 0.8 ± 0.1$^{aB}$ | 3.5 ± 0.5$^{a}$ | 0.3 ± 0.1* | 0.3 ± 0.1$^{b}$* |
| 5N1P | 414.9 ± 7.0 | 14.3 ± 0.9$^{bA}$ | 1.1 ± 0.0$^{abC}$ | 3.4 ± 0.5$^{a}$ | 0.4 ± 0.2* | 0.2 ± 0.0$^{ab}$* |
| 10N1P | 431.3 ± 8.1 | 20.5 ± 0.8$^{cC}$* | 1.2 ± 0.0$^{bC}$ | 3.2 ± 0.3$^{a}$ | 0.5 ± 0.1* | 0.2 ± 0.0$^{b}$* |

Different lowercase letters represent significant differences among N treatments under the same P addition rate. Different uppercase letters represent significant differences among P treatments under the same N addition rate. Asterisks represent significant differences between the short- and long-term fertilization at the same N or P addition rate.

TABLE 2 Porewater chemical properties under different treatments in the short- and long-term fertilizations.

| Treatment | DOC (mg C $L^{-1}$) | $NH_4^+$-N × 10 (mg N $L^{-1}$) | $NO_3$-N × 10 (mg N $L^{-1}$) | DON (mg N $L^{-1}$) | DIP × 10 (mg P $L^{-1}$) | DOP × 10 (mg P $L^{-1}$) |
|---|---|---|---|---|---|---|
| **Short-term fertilization** | | | | | | |
| 0N0P | 51.9 ± 3.0 | 0.4 ± 0.1$^{a}$ | 0.7 ± 0.1 | 0.3 ± 0.0$^{a}$ | 0.6 ± 0.1 | 0.3 ± 0.2 |
| 5N0P | 62.0 ± 4.8* | 0.8 ± 0.7$^{a}$ | 0.3 ± 0.7 | 0.4 ± 0.0$^{ab}$* | 0.6 ± 0.1 | 0.3 ± 0.1 |
| 10N0P | 59.0 ± 4.4 | 2.0 ± 0.5$^{b}$ | 0.5 ± 1.0 | 0.5 ± 0.2$^{b}$* | 0.7 ± 0.1 | 0.5 ± 0.2 |
| 0N0.5P | 66.8 ± 3.4 | 0.7 ± 0.1$^{a}$ | 0.4 ± 0.1 | 0.4 ± 0.0$^{a}$* | 0.7 ± 0.1 | 0.5 ± 0.1 |
| 0N1P | 60.0 ± 7.6 | 0.6 ± 0.1$^{a}$ | 0.2 ± 0.1 | 0.3 ± 0.0$^{a}$* | 0.6 ± 0.1 | 0.3 ± 0.1 |
| 5N0.5P | 51.4 ± 5.6 | 0.9 ± 0.5$^{a}$ | 0.2 ± 0.5 | 0.8 ± 0.0$^{ab}$* | 0.6 ± 0.1 | 0.3 ± 0.1 |
| 10N0.5P | 54.7 ± 0.5 | 4.9 ± 2.0$^{b}$ | 0.9 ± 1.1 | 0.3 ± 0.0$^{b}$* | 0.9 ± 0.1 | 0.2 ± 0.1 |
| 5N1P | 54.8 ± 7.4 | 0.7 ± 0.1$^{a}$ | 0.5 ± 0.1 | 0.4 ± 0.0$^{ab}$* | 0.9 ± 0.1 | 0.1 ± 0.2 |
| 10N1P | 70.4 ± 0.1 | 2.7 ± 0.9$^{b}$ | 0.4 ± 0.2 | 0.5 ± 0.0$^{b}$* | 0.7 ± 0.1 | 0.4 ± 0.1 |
| **Long-term fertilization** | | | | | | |
| 0N0P | 70.6 ± 12.3 | 1.0 ± 1.0$^{a}$ | 0.3 ± 0.3 | 0.5 ± 0.0$^{a}$* | 0.3 ± 0.1 | 0.3 ± 0.3 |
| 5N0P | 75.8 ± 9.6* | 6.5 ± 1.5$^{b}$ | 0.7 ± 0.05 | 1.4 ± 0.2$^{b}$* | 0.3 ± 0.1 | 0.2 ± 0.2 |
| 10N0P | 73.3 ± 28.7 | 6.4 ± 2.1$^{b}$ | 0.9 ± 1.0 | 2.1 ± 0.5$^{c}$* | 0.3 ± 0.3 | 0.2 ± 0.4 |
| 0N0.5P | 56.7 ± 4.9 | 1.2 ± 0.4$^{a}$ | 0.7 ± 0.2 | 0.8 ± 0.0$^{a}$* | 0.3 ± 0.1 | 0.1 ± 0.3 |
| 0N1P | 62.8 ± 4.0 | 0.9 ± 0.1$^{a}$ | 0.1 ± 0.1 | 0.7 ± 0.0$^{a}$* | 0.4 ± 0.3 | 0.4 ± 0.3 |
| 5N0.5P | 58.8 ± 12.1 | 5.7 ± 2.9$^{b}$ | 0.3 ± 0.4 | 1.0 ± 0.4$^{b}$* | 0.4 ± 0.2 | 0.1 ± 0.1 |
| 10N0.5P | 67.7 ± 3.8 | 5.9 ± 0.8$^{b}$ | 0.7 ± 0.4 | 1.7 ± 0.3$^{c}$* | 0.4 ± 0.3 | 0.4 ± 0.5 |
| 5N1P | 61.8 ± 10.6 | 8.8 ± 1.2$^{b}$ | 1.0 ± 0.6 | 1.2 ± 0.1$^{b}$* | 0.5 ± 0.3 | 0.2 ± 0.3 |
| 10N1P | 73.0 ± 9.5 | 5.8 ± 0.7$^{b}$ | 1.1 ± 0.6 | 1.8 ± 0.3$^{c}$* | 0.6 ± 0.1 | 0.1 ± 0.1 |

Different lowercase letters represent significant differences among N treatments under the same P addition rate. Different uppercase letters represent significant differences among P treatments under the same N addition rate. Asterisks represent significant differences between the short- and long-term fertilization under the same N or P addition rate.

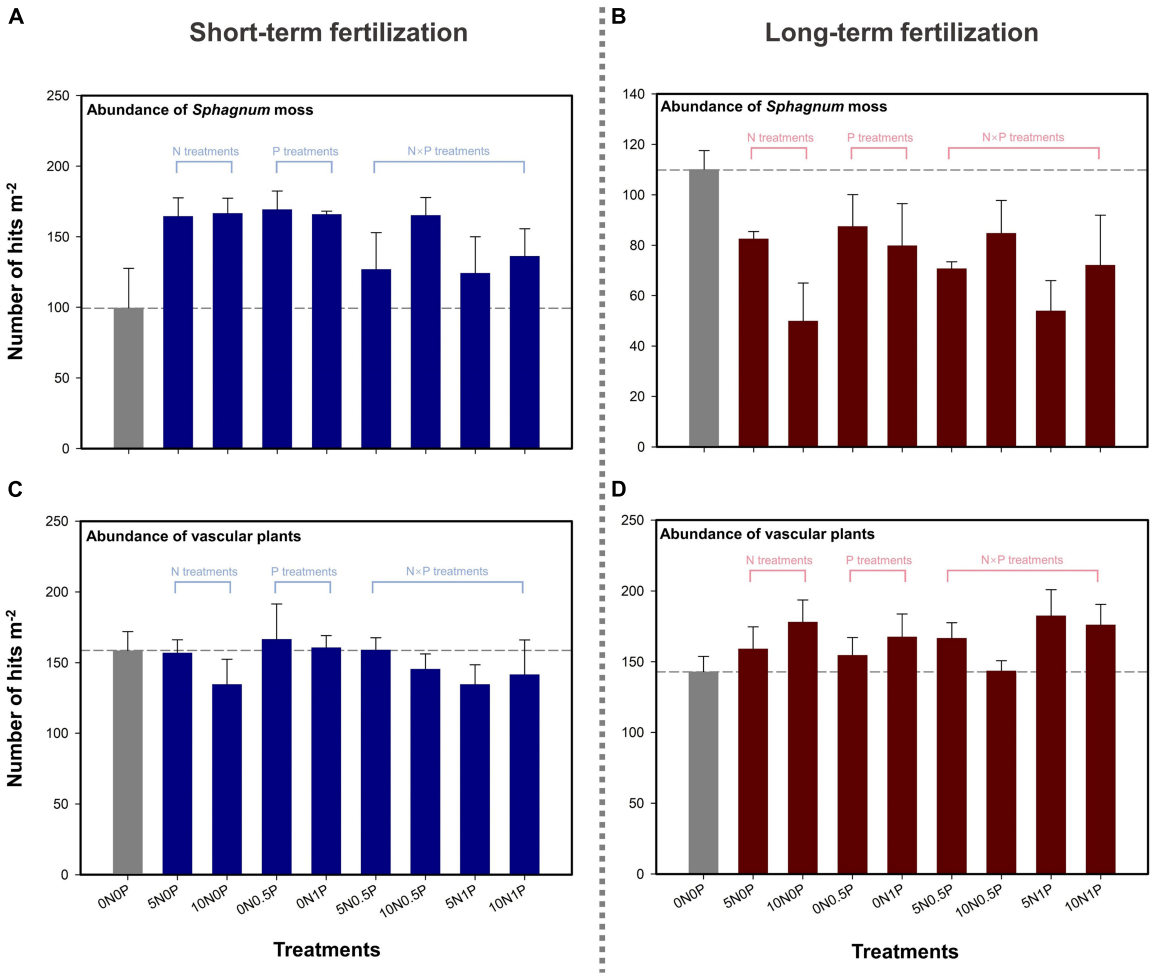


FIGURE 1
Abundance of *Sphagnum* moss **(A,C)** and vascular plants **(B,D)** in response to the short- and long-term fertilizations.

by the humification indices (Figure 3). For the short-term fertilization, N and P additions weakly increased the absorbances of refractory components of the organic compounds (i.e., carboxylates and humic acids at 1,420 $cm^{-1}$; lignin and phenolics at 1,510 $cm^{-1}$; aromatics at 1,630 $cm^{-1}$; carboxylates–acids at 1,720 $cm^{-1}$) and labile polysaccharide moieties (1,090 $cm^{-1}$; Figure 3A). The humification indices did not change significantly after N and/or P additions (Figures 3B–E). For the long-term fertilization, N and/or P additions, especially the combination of N and P additions, increased the absorbances of refractory components of organic compounds relative to the control (Figure 3F). Two of the humification indices (i.e., 1,510/1,090 and 1,630/1,090) were significantly increased in the long-term fertilized plots (Figures 3H,I). Specifically, N addition increased the ratio of 1,510/1,090 under the same rate of P addition, and this ratio also increased with P addition under the same rate of N addition (Figure 3H). However, the effect of N addition on the ratio of 1,630/1,090 depended on P addition rates (i.e., interactive effect). That is, the ratio of 1,630/1,090 was significantly increased by N addition only under the largest rate of P addition (i.e., 1 g P $m^{-2}$ $year^{-1}$). In combination with 5N treatment, the largest rate of P addition significantly increased the ratio of 1,630/1,090 (Figure 3I).

Results of hierarchical partitioning analysis indicated that TP concentration was the most important factor influencing the variations in humification indices both under the short- and long-term fertilizations (Figures 2B,D). For the short-term fertilization, the full model $R^2$ of environmental variables was 0.09, indicating that peat and porewater chemical properties only had weak relationships with humification indices (Figure 2B). Specifically, TP concentration explained the largest proportion of variations in humification indices ($R^2$ = 0.07), followed by DOC ($R^2$ = 0.03) and TN concentrations ($R^2$ = 0.02). For the long-term fertilization, the full model $R^2$ of environmental variables was 0.42. TP concentration was the most important factor in explaining the

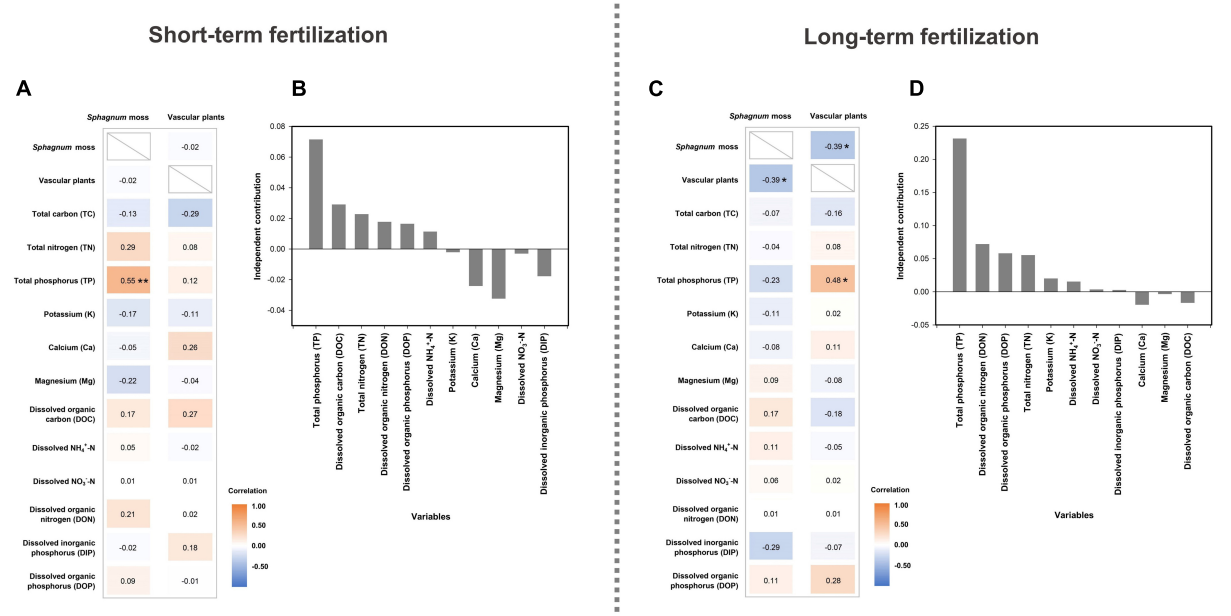


FIGURE 2
Spearman's correlations between plant species abundance and physicochemical properties of peat and porewater under the short- **(A)** and long-term fertilizations **(C)**, and the hierarchical partitioning between physicochemical properties of peat and porewater and the humification indices under the short- **(B)** and long-term fertilizations **(D)**. Asterisks represent significant correlations.

variations in humification indices ($R^2 = 0.23$), followed by DON ($R^2 = 0.07$) and DOP concentrations ($R^2 = 0.06$; **Figure 2D**).

# Discussion

## Changes in plant abundance and environmental variables

We found divergent results with regard to the responses of plant abundance to the short- and long-term fertilizations (**Figure 1**). During the short-term fertilization, the abundance of *Sphagnum* moss was increased by 25–70% after N and/or P additions (**Figure 1A**). It is not surprising to observe a positive effect of inorganic N and/or P inputs on the growth of *Sphagnum* moss at a low cumulative amount, considering that plant growth in peatlands is often constrained by limited N and/or P availabilities (Leon et al., 2019; Dash et al., 2020). This increase of *Sphagnum* moss abundance under short-term fertilization has been observed in many previous studies (e.g., Limpens et al., 2004; Bubier et al., 2007; Leon et al., 2019). Meanwhile, the positive correlations between *Sphagnum* moss abundance and TN and TP concentrations (**Figure 2A**) may indicate N and P co-limitation as observed in other peatlands (e.g., Cusell et al., 2014; Wang et al., 2016).

Long-term fertilization has shifted the dominant plant functional type from being *Sphagnum* moss to vascular plants (**Figures 1C,D**). Specifically, the increase in vascular plant abundance and decline in *Sphagnum* moss abundance were observed after the additions of N, P and their combinations (**Figures 1C,D**). Namely, the effects of nutrient addition on plant growth and community composition were dependent on the cumulative amount (i.e., rate and duration) of N and P additions (Larmola et al., 2013). Wieder et al. (2019) has documented that 5-year N addition (25 kg N $ha^{-1}$ $year^{-1}$) inhibited the growth of *Sphagnum fuscum*, while increased the net primary productivity of shrubs and a tree species (*Picea mariana*). Li et al. (2018) observed that the productivity of *S. palustre* was the largest when the rate of P addition reached 2 kg P $ha^{-1}$ $year^{-1}$, whereas any further increase in the addition rate inhibited its growth. Overall, the expansion of vascular plants owing to long-term nutrient enrichment has become a more commonly observed phenomenon in northern peatlands (e.g., Kool and Heijmans, 2009; Wang et al., 2016; Moore et al., 2019).

This shift in plant community composition may be induced by a variety of factors, including nutrient toxicity, shading effect, and microtopography disturbance (Heijmans et al., 2001; Pouliot et al., 2011; Larmola et al., 2013). In the early stage of fertilization, N and/or P additions stimulated *Sphagnum* moss growth by improving nutrient-poor condition (Leon et al., 2019). Subsequently, with cumulative nutrient input, *Sphagnum* moss began to lose the filtering capacity and suffered from the competition of vascular plants which had access to enriched N and P availabilities in peat (Bragazza et al., 2005; Larmola et al., 2013). This possible toxic effect owing to nutrient

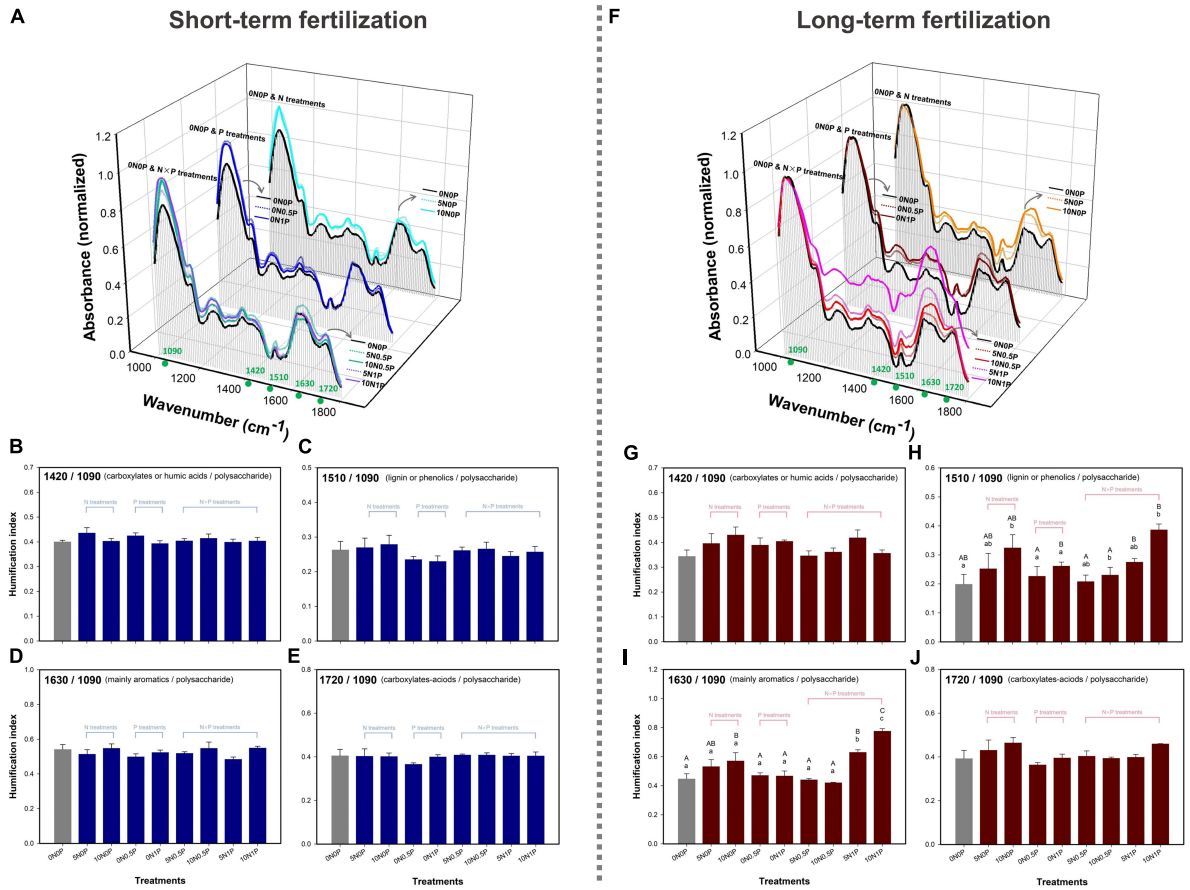


FIGURE 3
Fourier-transform infrared (FTIR) spectra under the short- **(A)** and long-term fertilizations **(F)**, and the humification indices under the short- **(B–E)** and long-term fertilizations **(G–J)**. Different lowercase letters represent significant differences among N treatments under the same P addition rate in the long-term fertilization. Different uppercase letters represent significant differences among P treatments under the same N addition rate in the long-term fertilization.

addition drove plant species change with loss of *Sphagnum* moss, and increased the abundance of vascular plants (Larmola et al., 2013). Furthermore, during the long-term fertilization, the increased vascular plant biomass and litter accumulation would further inhibit *Sphagnum* moss growth *via* shading effect (Heijmans et al., 2001; Nordbakken et al., 2003). As observed by Limpens and Berendse (2003), about 53% shading was close to the tolerance limit of *Sphagnum* moss. As the height and root biomass of vascular plants increased after long-term fertilization, the difference in microtopography were enhanced by physically reinforced "hummockification" (Pouliot et al., 2011). This change of microtopography further resulted in a lowering of water table by augmenting evapotranspiration (Diamond et al., 2020). Aside from the water stress, the increasing abundance of vascular plants would also reduce the accessibility of *Sphagnum* moss to light and nutrient, which further retarded its growth (Pouliot et al., 2011; Wieder et al., 2019). This competition between *Sphagnum* moss and vascular plants was confirmed by the significantly negative relationship between their abundances under the long-term fertilization (**Figure 2C**).

The changes of peat properties were owing to the combined effects of nutrient addition and plant growth (Moore et al., 2019). It was not surprising to observe the increase of TN and TP concentrations after N and P additions (**Table 1**). We did not find significant interaction between N and P after 3-year fertilization, likely because of limited duration of nutrient addition (Kellera et al., 2005). Interestingly, TP concentration was positively correlated with the abundance of *Sphagnum* moss under the short-term fertilization and the abundance of vascular plants under the long-term fertilization, indicating that P may play a more important role than N in controlling plant growth at Hani peatland (Li et al., 2019). Compared to the short-term fertilization, K concentration significantly increased and that of Ca and Mg significantly decreased after the long-term fertilization (**Table 1**). The much smaller concentrations of Ca and Mg in the long-term fertilized plots relative to the short-term ones might be caused by the larger plant uptake

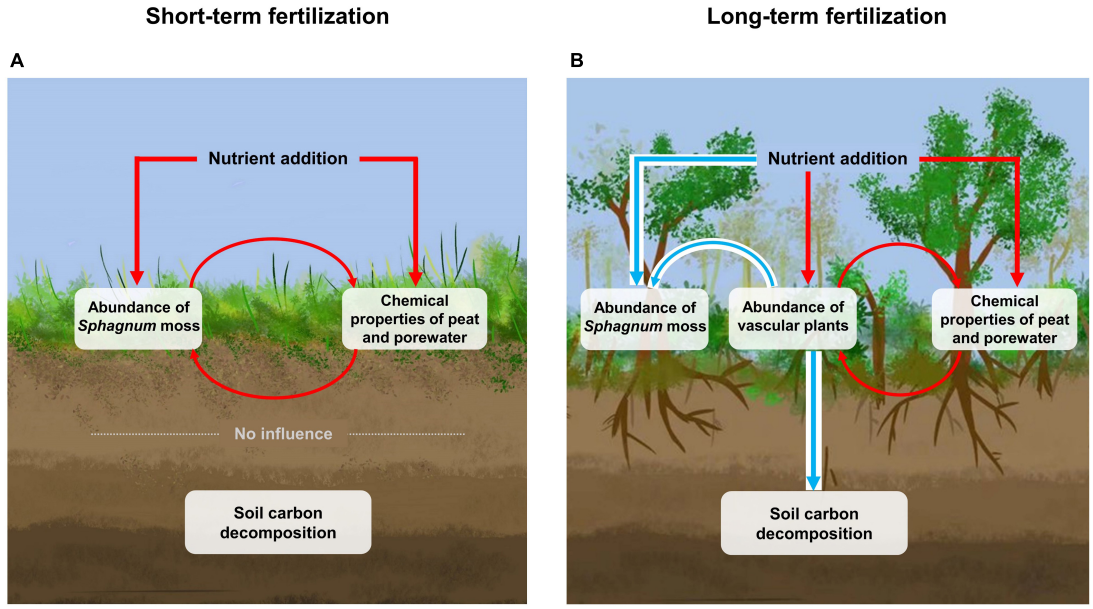


FIGURE 4
Schematic diagrams of the mechanisms of soil C protection in the short- **(A)** and long-term fertilizations **(B)**. Red arrows indicate positive influences and blue arrows indicate negative influences.

owing to favored growth of vascular plants under the long-term fertilization (Moore et al., 2019). The increase in K concentration could be mainly attributed to high leaching velocity with litter decomposition of vascular plants under the long-term fertilization (Bragazza et al., 2007).

Porewater chemistry was not only associated with external nutrient input, but also regulated by the metabolism of soil microorganisms and plants (Moore et al., 2019). Our results disclosed that DON was the dominant dissolved N form, followed by $NH_4^+$-N and $NO_3^-$-N (**Table 2**), which was in line with many previous studies (e.g., Chiwa et al., 2016; Moore et al., 2019). In particular, we found that N addition significantly led to the build-up of DON and $NH_4^+$-N under both the short- and long-term fertilizations. It is possible that large rate or long-term N addition can enhance microbial activity and plant growth, and stimulate the secretion of secondary metabolites (e.g., amino acids; Bragazza and Limpens, 2004). Moreover, we observed a slight increase in DIN concentration after the long-term fertilization, which may be related to the decline in the capacity of *Sphagnum* moss as a natural N "filter" owing to the decrease in abundance. However, dissolved P concentration did not change significantly (**Table 2**). The dissolved nutrients in porewater could be easily assimilated by microorganisms or plants in the form of monomers (Dugan et al., 2011). If a certain type of nutrient limitation in peatlands was deteriorated, the corresponding dissolved nutrients in porewater should be preferentially assimilated by microorganisms and plants (Dugan et al., 2011; Schlesinger and Bernhardt, 2020). Consequently, considering that P might be more limited than N in northern peatlands (e.g., Dimitrov et al., 2014; Hill et al., 2014), the dissolved P in porewater was rapidly assimilated, and thus no significant change in its concentration was observed after nutrient addition.

## Weak response of soil carbon

Overall, based on the results of peat and porewater chemistry, TC and DOC concentrations and organic matter composition did not vary considerably neither in our short-term fertilized plots on *Sphagnum* moss-dominated hummocks, nor on the hummocks where vascular plants expanded after long-term N and/or P enrichment. These results contrasted with our first hypothesis that N and P additions would significantly change the composition of soil chemical moieties and compromise soil C storage during the short-term fertilization (**Tables 1**, **2**). However, they partly supported our second hypothesis that the flourish of vascular plants at the expense of *Sphagnum* moss eventually protected soil C from being lost during the long-term fertilization.

Specifically, as for the short-term fertilization, we observed that TC and DOC concentrations did not change remarkably with N and P additions (**Tables 1**, **2**). Similarly, changes in FTIR spectra were minimal, and we did not observe a significant effect of the short-term nutrient addition on peat organo-chemical composition as indicated by the humification indices (**Figures 3A–E**). The short-term nutrient addition did

not dramatically change the acidic, waterlogged, and nutrient-deficient conditions, and thus the preserved C in peatlands remained relatively stable (Clymo and Hayward, 1982; Fritz et al., 2011). And this finding was also supported by the extremely low contribution of environmental variables to the humification indices. In addition, the balance between litterfall and decomposition controls soil C dynamics (Berg and Laskowski, 2006). In our study, the FTIR bands indicative of polysaccharide increased in the fertilized plots (**Figure 3A**), likely due to larger organic matter input instead of greater litter production of predominant *Sphagnum* moss in the fertilized plots relative to the control. Thus, *Sphagnum* moss growth may partly compensate for the positive effects of short-term nutrient enrichment on soil C release.

The shift in plant community composition could change the accumulation of high molecular weight compounds *via* litterfall under long-term fertilization (Moore et al., 2019). The results of FTIR spectra showed that the absorptions of refractory phenolic compounds, carboxylates, and humic acids were enhanced in the fertilized plots, accompanied by a tendency of increasing abundance of vascular plants. Such effects of nutrient addition on FTIR spectra by driving change of plant community composition have also been noted by other studies (e.g., Artz et al., 2008; Chen et al., 2018; Moore et al., 2019). However, for the long-term fertilization, we still did not observe any significant change in the concentrations of TC and DOC, and the humification indices had only slightly changed after being fertilized for 10 years. A possible explanation for this phenomenon might be that vascular plants inhibit the activity of microbial decomposers *via* the increase of high-phenolic litter production (Keuskamp et al., 2015; Fenner and Freeman, 2020). FTIR spectroscopic analysis demonstrated that the long-term nutrient addition increased the concentrations of aromatic compounds in peat, especially after the combination of N and P additions, as indicated by increasing peak ratios of 1510/1090 and 1630/1090 (i.e., lignin and phenolics/polysaccharide, and aromatics/polysaccharide, respectively; **Figures 3H,I**). The phenolics (e.g., tannin) and other aromatic components of plant litter were strongly correlated with microbial decomposition, considering that they could bind protein and retard nutrient mobilization *via* oxidative degradation and biotoxicity (Wang et al., 2015; Fenner and Freeman, 2020). Meanwhile, phenolics have been found to inhibit key hydrolase activities (e.g., β-1,4-glucosidase, invertase, and cellobiohydrolase) and impede nutrient cycling and decomposition (Freeman et al., 2001, 2004). This "enzymatic latch" mechanism is expected to play a key role in peatlands dominated by vascular plants (Wang et al., 2015).

Other processes associated with vascular plant expansion may also retard soil C decomposition. First, the phenolics not only directly impede microbial activity (Freeman et al., 2001; Fenner and Freeman, 2020), but could also shift the fungal community to a slow-growing strategy (Wang et al., 2021). For example, Wang et al. (2021) found that nearly 85% of fungi were fast-growing in *Sphagnum*-dominated habitat, while shrub-dominated habitat was dominated by slow-growing fungi (75%). The different composition of fungal community with different growing strategies led to the variation in decomposition rate, which was faster in *Sphagnum*-dominated peatlands than that in peatlands dominated by vascular plants (Koch, 2001; Wang et al., 2021). Second, the extensive root system helps shrub efficiently capture available N and P in soils (Lambers et al., 2006), and compared to soil microorganisms, vascular plants may have advantages of nutrient acquisition (Smith et al., 2011). The competition for nutrients between vascular plants and soil microorganisms might indirectly reduce the sensitivity of soil microorganisms to external nutrient enrichment.

In this study, we formulated a hypothetical logic frame, i.e., C storage involved complex interrelation among peat, porewater, and vegetation processes, and assessed the divergent effects of the short- and long-term fertilizations on organic matter decomposition as indicated by the humification indices. Interestingly, the physicochemical properties of peat and porewater had little effect on the humification indices in the short-term fertilization plots where *Sphagnum* moss-dominated. Besides, the harsh conditions for microbial decomposers, combined with the increased C return from litterfall of *Sphagnum* moss, likely resulted in the lack of significant changes in soil C concentrations and organo-chemical composition during the short-term fertilization (**Figure 4A**). For the long-term fertilization, although the contribution of environmental variables to organic matter decomposition has increased, the input of high-phenolic litters owing to the shift in plant community composition from being *Sphagnum* moss- to vascular plant-dominated, may ultimately inhibit microbial activity and soil C release (**Figure 4B**).

## Data availability statement

The raw data supporting the conclusions of this article will be made available by the authors upon request.

## Author contributions

TL and MW: conceptualization. TL, XY, LG, CC, YS, ZL, SL, and MW: field sampling and laboratory analyses. All authors contributed to manuscript preparation.

## Funding

This study was funded by the National Natural Science Foundation of China (41971118).

## Acknowledgments

We are grateful to Jingjing Huang, Lin Zhu, Liying Lin, and Xuying Pei for their assistance in the laboratory, and Li Zhao for the assistance of sampling in a pilot study.

## Conflict of interest

The authors declare that the research was conducted in the absence of any commercial or financial relationships that could be construed as a potential conflict of interest.

## Publisher's note

All claims expressed in this article are solely those of the authors and do not necessarily represent those of their affiliated organizations, or those of the publisher, the editors and the reviewers. Any product that may be evaluated in this article, or claim that may be made by its manufacturer, is not guaranteed or endorsed by the publisher.

## References

Ackerman, D., Millet, D. B., and Chen, X. (2019). Global estimates of inorganic nitrogen deposition across four decades. *Glob. Biogeochem. Cycles* 33, 100–107. doi: 10.1029/2018GB005990

Artz, R. R., Chapman, S. J., Robertson, A. J., Potts, J. M., Laggoun-Défarge, F., Gogo, S., et al. (2008). FTIR spectroscopy can be used as a screening tool for organic matter quality in regenerating cutover peatlands. *Soil Biol. Biochem.* 40, 515–527. doi: 10.1016/j.soilbio.2007.09.019

Berg, B., and Laskowski, R. (2006). *Litter Decomposition: A Guide to Carbon and Nutrient Turnover*. Amsterdam: Elservier Academic Press.

Biester, H., Knorr, K. H., Schellekens, J., Basler, A., and Hermanns, Y. M. (2014). Comparison of different methods to determine the degree of peat decomposition in peat bogs. *Biogeosciences* 11, 2691–2707. doi: 10.5194/bg-11-2691-2014

Bragazza, L., and Limpens, J. (2004). Dissolved organic nitrogen dominates in European bogs under increasing atmospheric N deposition. *Glob. Biogeochem. Cycles* 18:GH4018. doi: 10.1029/2004GB002267

Bragazza, L., Limpens, J., Gerdol, R., Grosvernier, P., Hajek, M., Hajek, T., et al. (2005). Nitrogen concentration and delta 15N signature of ombrotrophic *Sphagnum mosses* at different N deposition levels in Europe. *Glob. Change Biol.* 11, 106–114. doi: 10.1111/j.1365-2486.2004.00886.x

Bragazza, L., Siffi, C., Iacumin, P., and Gerdol, R. (2007). Mass loss and nutrient release during litter decay in peatland: the role of microbial adaptability to litter chemistry. *Soil Biol. Biochem.* 39, 257–267. doi: 10.1016/j.soilbio.2006.07.014

Broder, T., Blodau, C., Biester, H., and Knorr, K. H. (2012). Peat decomposition records in three pristine ombrotrophic bogs in southern Patagonia. *Biogeosciences* 9, 1479–1491. doi: 10.5194/bg-9-1479-2012

Bu, Z. J., Rydin, H., and Chen, X. (2011). Direct and interaction-mediated effects of environmental changes on peatland bryophytes. *Oecologia* 166, 555–563. doi: 10.1007/s00442-010-1880-1

Bubier, J. L., Moore, T. R., and Bledzki, L. A. (2007). Effects of nutrient addition on vegetation and carbon cycling in an ombrotrophic bog. *Glob. Change Biol.* 13, 1168–1186. doi: 10.1111/j.1365-2486.2007.01346.x

Chen, X., Jin, M. C., Zhang, Y. J., Hu, J. W., Gao, H. J., Chu, W. Y., et al. (2018). Nitrogen application increases abundance of recalcitrant compounds of soil organic matter: a 6-year case study. *Soil Sci.* 183, 169–178. doi: 10.1097/SS.0000000000000243

Chiwa, M., Sheppard, L. J., Leith, I. D., Leeson, S. R., Tang, Y. S., and Cape, J. N. (2016). Sphagnum can 'flter' N deposition, but effects on the plant and pore water depend on the N form. *Sci. Total Environ.* 559, 113–120. doi: 10.1016/j.scitotenv.2016.03.130

Clymo, R. S., and Hayward, P. M. (1982). "The ecology of *Sphagnum*," in *Bryophyte Ecology*, ed. A. J. E. Smith (Dordrecht: Springer), 229–289.

Cocozza, C., D'Orazio, V., Miano, T. M., and Shotyk, W. (2003). Characterization of solid and aqueous phases of a peat bog profle using molecular fluorescence spectroscopy, ESR and FT-IR, and comparison with physical properties. *Org. Geochem.* 34, 49–60. doi: 10.1016/S0146-6380(02)00208-5

Cusell, C., Kooijman, A., and Lamers, L. P. M. (2014). Nitrogen or phosphorus limitation in rich fens? – Edaphic differences explain contrasting results in vegetation development after fertilization. *Plant Soil* 384, 153–168. doi: 10.1007/s11104-014-2193-7

Dash, S., Borah, S. S., and Kalamdhad, A. S. (2020). Study of the limnology of wetlands through a one-dimensional model for assessing the eutrophication levels induced by various pollution sources. *Ecol. Modell.* 416:108907. doi: 10.1016/j.ecolmodel.2019.108907

Diamond, J. S., McLaughlin, D. L., Slesak, R. A., and Stovall, A. (2020). Microtopography is a fundamental organizing structure of vegetation and soil chemistry in black ash wetlands. *Biogeosciences* 17, 901–915. doi: 10.5194/bg-17-901-2020

Dimitrov, D. D., Bhatti, J. S., and Grant, R. F. (2014). The transition zones (ecotone) between boreal forests and peatlands: ecological controls on ecosystem productivity along a transition zone between upland black spruce forest and a poor forested fen in central Saskatchewan. *Ecol. Modell.* 291, 96–108. doi: 10.1016/j.ecolmodel.2014.07.020

Drollinger, S., Knorr, K. H., Knierzinger, W., and Glatzel, S. (2020). Peat decomposition proxies of Alpine bogs along a degradation gradient. *Geoderma* 369, 114331. doi: 10.1016/j.geoderma.2020.114331

Dugan, J. E., Hubbard, D. M., Page, H. M., and Schimel, J. P. (2011). Marine macrophyte wrack inputs and dissolved nutrients in Beach Sands. *Estuar. Coasts* 34, 839–850. doi: 10.1007/s12237-011-9375-9

Fenner, N., and Freeman, C. (2020). Woody litter protects peat carbon stocks during drought. *Nat. Climate Chang.* 10, 363–369. doi: 10.1038/s41558-020-0727-y

Freeman, C., Ostle, N. J., Fenner, N., and Kang, H. (2004). A regulatory role for phenol oxidase during decomposition in peatlands. *Soil Biol. Biochem.* 36, 1663–1667. doi: 10.1016/j.soilbio.2004.07.012

Freeman, C., Ostle, N., and Kang, H. (2001). An enzymic 'latch' on a global carbon store. *Nature* 409:149. doi: 10.1038/35051650

Fritz, C., van Dijk, G., Smolders, A. J. P., Pancotto, V. A., and Elzenga, T. J. T. M. (2011). Nutrient additions in pristine Patagonian Sphagnum bog vegetation: can phosphorus addition alleviate (the effects of) increased nitrogen loads. *Plant Biol.* 14, 491–499. doi: 10.1111/j.1438-8677.2011.00527.x

Gorham, E. (1991). Northern peatlands: role in the carbon cycle and probable responses to climatic warming. *Ecol. Appl.* 1, 182–195. doi: 10.2307/1941811

Heijmans, M. P. D., Berendase, F., Arp, W. J., Masselink, A. K., Kless, H., de Visser, W., et al. (2001). Effects of elevated carbon dioxide and increased nitrogen deposition on bog vegetation in the Netherlands. *J. Ecol.* 89, 268–279. doi: 10.1046/j.1365-2745.2001.00547.x

Hill, B. H., Elonen, C. M., Jicha, T. M., Kolka, R. K., Lehto, L. L. P., Sebestyen, S. D., et al. (2014). Ecoenzymatic stoichiometry and microbial processing of organic matter in northern bogs and fens reveals a common P-limitation between peatland types. *Biogeochemistry* 120, 203–224. doi: 10.1007/s10533-014-9991-0

Kellera, J. K., Bridghamb, S. D., Chapin, C. T., and Iversend, C. M. (2005). Limited effects of six years of fertilization on carbon mineralization dynamics in a Minnesota fen. *Soil Biol. Biochem.* 37, 1197–1204. doi: 10.1016/j.soilbio.2004.11.018

Keuskamp, J. A., Feller, I. C., Laanbroek, H. J., Verhoeven, J. T. A., and Hefting, M. M. (2015). Short- and long-term effects of nutrient enrichment on microbial exoenzyme activity in mangrove peat. *Soil Biol. Biochem.* 81, 38–47. doi: 10.1016/j.soilbio.2014.11.003

Koch, A. L. (2001). Oligotrophs versus copiotrophs. *Bioessays* 23, 657–661. doi: 10.1002/bies.1091

Kool, A., and Heijmans, M. M. P. D. (2009). Dwarf shrubs are stronger competitors than graminoid species at high nutrient supply in peat bogs. *Plant Ecol.* 204, 125–134. doi: 10.1007/s11258-009-9574-7

Lai, J. S., Zhou, Y., Zhang, J. L., and Peres-neto, P. R. (2022). Generalizing hierarchical and variation partitioning in multiple regression and canonical analyses using the rdacca.hp R package. *Methods Ecol. Evol.* 13, 782–788. doi: 10.1111/2041-210X.13800

Lambers, H., Shane, M. W., Cramer, M. D., Pearse, S. J., and Veneklaas, E. J. (2006). Root structure and functioning for efficient acquisition of phosphorus: matching morphological and physiological traits. *Ann. Bot.* 98, 693–713. doi: 10.1093/aob/mcl114

Larmola, T., Bubier, J. L., Kobyljanec, C., Basiliko, N., Juutinen, S., Humphreys, E., et al. (2013). Vegetation feedbacks of nutrient addition lead to a weaker carbon sink in an ombrotrophic bog. *Glob Change Biol.* 19, 3729–3739. doi: 10.1111/gcb.12328

Leon, C. A., Neila-Pivet, M., Benitez-Mora, A., and Lara, L. (2019). Effect of phosphorus and nitrogen on *Sphagnum* regeneration and growth: an experience from Patagonia. *Wetl. Escol. Manag.* 27, 257–266. doi: 10.1007/s11273-019-09657-4

Li, T. T., Lei, Y., Dai, C., Yang, L. F., Li, Z. Q., and Wang, Z. X. (2018). Effects of both substrate and nitrogen and phosphorus fertilizer on *Sphagnum palustre* growth in subtropical high-mountain regions and implications for peatland recovery. *Wetl. Ecol. Manag.* 26, 651–663. doi: 10.1007/s11273-018-9598-7

Li, T., Bu, Z. J., Liu, W. Y., Zhang, M. Y., Peng, C. H., Zhu, Q. A., et al. (2019). Weakening of the 'enzymatic latch' mechanism following long-term fertilization in a minerotrophic peatland. *Soil Biol. Biochem.* 136:107528. doi: 10.1016/j.soilbio.2019.107528

Li, T., Ge, L. M., Huang, J. J., Yuan, X., Peng, C. H., Wang, S. Z., et al. (2020). Contrasting responses of soil exoenzymatic interactions and the dissociated carbon transformation to short- and long-term drainage in a minerotrophic peatland. *Geoderma* 377:114585. doi: 10.1016/j.geoderma.2020.114585

Limpens, J., and Berendse, F. (2003). Growth reduction of Sphagnum magellanicum subjected to high nitrogen deposition: the role of amino acid nitrogen concentration. *Oecologia* 135, 339–345. doi: 10.1007/s00442-003-1224-5

Limpens, J., Berendse, F., and Klees, H. (2004). How phosphorus availability affects the impact of nitrogen deposition on *Sphagnum* and vascular plants in bogs. *Ecosystems* 7, 793–804. doi: 10.1007/s10021-004-0274-9

Moore, T. R., Bubier, J. L., Frolking, S. E., Lafleur, P. M., and Roulet, N. T. (2002). Plant biomass and production and CO2 exchange in an ombrotrophic bog. *J. Ecol.* 90, 25–36. doi: 10.1046/j.0022-0477.2001.00633.x

Moore, T. R., Knorr, K. H., Thompson, L., Roy, C., and Bubier, J. L. (2019). The effect of long-term fertilization on peat in an ombrotrophic bog. *Geoderma* 343, 176–186. doi: 10.1016/j.geoderma.2019.02.034

Murphy, J., and Riley, J. P. (1962). A modified single solution method for the determination of phosphate in natural waters. *Anal. Chim. Acta* 26, 31–36. doi: 10.1021/ja038277x

Niemeyer, J., Chen, Y., and Bollag, J. M. (1992). Characterization of humic acids, composts, and peat by diffuse reflectance Fourier-transform infrared spectroscopy. *Soil Sci. Soc. Am. J.* 56, 135–140. doi: 10.2136/sssaj1992.03615995005600010021x

Nordbakken, J. F., Ohlson, M., and Hogbeng, P. (2003). Boreal bog plants: nitrogen sources and uptake of recently deposited nitrogen. *Environ. Poll.* 126, 191–200. doi: 10.1016/S0269-7491(03)00194-5

Ohno, T., and Zibilske, L. M. (1991). Determination of low concentrations of phosphorus in soil extracts using malachite green. *Soil Sci. Soc. Am. J.* 55:3. doi: 10.2136/sssaj1991.03615995005500030046x

Parkinson, J. A., and Allen, S. E. (2008). A wet oxidation procedure suitable for the determination of nitrogen and mineral nutrients in biological material. *Commun. Soil Sci. Plant Anal.* 6, 1–11. doi: 10.1080/00103627509366539

Peñuelas, J., Poulter, B., Sardans, J., Ciais, P., van der Velde, M., Bopp, L., et al. (2013). Human-induced nitrogen-phosphorus imbalances alter natural and managed ecosystems across the globe. *Nat. Commun.* 4:2934. doi: 10.1038/ncomms3934

Pouliot, R., Rochefort, L., Karofeld, E., and Mercier, C. (2011). Initiation of *Sphagnum moss* hummocks in bogs and the presence of vascular plants: is there a link? *Acta Oecol.* 37, 346–354. doi: 10.1016/j.actao.2011.04.001

Qiao, S. (1993). A preliminary study on Hani peat mire in the west part of the Changbai Mountain (in Chinese). *Sci. Geogr. Sin.* 13, 279–286. doi: 10.13249/j.cnki.sgs.1993.03.279

R Core Team (2021). *R: A Language and Environment for Statistical Computing*. Vienna: R Foundation for Statistical Computing. Available online at: https://www.R-project.org/

Rice, K. C., and Herman, J. S. (2012). Acidification of Earth: an assessment across mechanisms and scales. *Appl. Geochem.* 27, 1–14. doi: 10.1016/j.apgeochem.2011.09.001

Rousk, J., Smith, A. R., and Jones, D. L. (2013). Investigating the long-term legacy of drought and warming on the soil microbial community across five European shrubland ecosystems. *Glob. Change Biol.* 19, 3872–3884. doi: 10.1111/gcb.12338

Rydin, H., and Jeglum, J. K. (2013). *The Biology of Peatlands*. New York, NY: Oxford University Press.

Schlesinger, W. H., and Bernhardt, E. S. (2020). "Wetland ecosystem," in *Biogeochemistry: An Analysis of Global Change, Fourth edition*, ed. A. Shapiro (Salt Lake City, UT: American Academic Press), 249–291.

Schothorst, C. J. (1977). Subsidence of low moor peat soils in the western Netherlands. *Geoderma* 17, 265–291. doi: 10.1016/0016-7061(77)90089-1

Smith, S. E., Jakobsen, I., Gronlund, M., and Smith, F. A. (2011). Roles of arbuscular mycorrhizas in plant phosphorus nutrition: interactions between pathways of phosphorus uptake in arbuscular mycorrhizal roots have important implications for understanding and manipulating plant phosphorus acquisition. *Plant Physiol.* 156, 1050–1057. doi: 10.1104/pp.111.174581

Teickner, H. (2022). *ir: Functions to Handle and Preprocess Infrared Spectra*. Available online at: https://zenodo.org/record/5747170 (assessed July 5, 2022).

Teickner, H., and Hodgkins, S. B. (2022). *irpeat: Functions to Analyze Mid Infrared Spectra of Peat Samples*. Available online at: https://github.com/henningte/irpeat (accessed July 5, 2022).

Tipping, E., Benham, S., Boyle, J., Crow, P., Davies, J., Fischer, U., et al. (2014). Atmospheric deposition of phosphorus to land and freshwater. *Environ. Sci. Process. Impacts* 16, 1608–1617. doi: 10.1039/c3em00641g

van Breemen, N. (1995). How *Sphagnum bogs* down other plants. *Trends Ecol. Evol.* 10, 270–275. doi: 10.1016/0169-5347(95)90007-1

Wang, H. J., Richardson, C. J., and Ho, M. C. (2015). Dual controls on carbon loss during drought in peatlands. *Nat. Clim. Change* 5, 584–587. doi: 10.1038/nclimate2643

Wang, H. J., Tian, J. Q., Chen, H., Ho, M. C., Vilgalys, R., Bu, Z. J., et al. (2021). Vegetation and microbes interact to preserve carbon in many wooded peatlands. *Commun. Earth Environ.* 2:67. doi: 10.1038/s43247-021-00136-4

Wang, M., Larmola, T., Murphy, M. T., Moore, T. R., and Bubier, J. L. (2016). Stoichiometric response of shrubs and mosses to long-term nutrient (N, P and K) addition in an ombrotrophic peatland. *Plant Soil* 400, 403–416. doi: 10.1007/s11104-015-2744-6

Wieder, R. K., Vitt, D. H., Vile, M. A., Graham, J. A., Hartsock, J. A., Fillingim, H., et al. (2019). Experimental nitrogen addition alters structure and function of a boreal bog: critical load and thresholds revealed. *Ecol. Monogr.* 89:e01371. doi: 10.1002/ecm.1371

Yu, Z., Loisel, J., Brosseau, D. P., Beilman, D. W., and Hunt, S. J. (2010). Global peatland dynamics since the last glacial maximum. *Geophys. Res. Lett.* 37, 69–73. doi: 10.1029/2010GL043584

frontiers | Frontiers in Ecology and Evolution

ORIGINAL RESEARCH
published: 01 August 2022
doi: 10.3389/fevo.2022.950605

# Soil Bacterial Community Structure in Different Micro-Habitats on the Tidal Creek Section in the Yellow River Estuary

*Zhikang Wang[1], Kaixin Yang[1], Junbao Yu[1]*, Di Zhou[1], Yunzhao Li[1], Bo Guan[1], Yang Yu[1], Xuehong Wang[1], Zhonghua Ren[1], Wei Wang[1], Xin Chen[2] and Jisong Yang[1,3]**

*[1] Key Laboratory of Ecological Restoration and Conservation of Coastal Wetlands in Universities of Shandong, The Institute for Advanced Study of Coastal Ecology, Ludong University, Yantai, China, [2] Key Laboratory of Pollution Ecology and Environment Engineering, Institute of Applied Ecology, Chinese Academy of Sciences, Shenyang, China, [3] Dongying Academy of Agricultural Sciences, Dongying, China*

Tidal creeks have attracted considerable attention in estuary wetland conservation and restoration with diverse micro-habitats and high hydrological connectivity. Bacterial communities act effectively as invisible engines to regulate nutrient element biogeochemical processes. However, few studies have unveiled the bacterial community structures and diversities of micro-habitats soils on the tidal creek section. Our study selected three sections cross a tidal creek with obviously belt-like habitats "pluff mudflat – bare mudflat – *Tamarix chinensis* community – *T. chinensis-Suaeda salsa* community– *S. salsa* community" in the Yellow River estuarine wetland. Based on soil samples, we dissected and untangled the bacterial community structures and special bacterial taxa of different habitats on the tidal creek section. The results showed that bacterial community structures and dominant bacterial taxa were significantly different in the five habitats. The bacterial community diversities significantly decreased with distance away from tidal creeks, as well as the dominant bacteria Flavobacteriia and δ-Proteobacteria, but in reverse to Bacteroidetes and Gemmatimonadetes. Moreover, the important biomarkers sulfate-reducing bacteria and photosynthetic bacteria were different distributions within the five habitats, which were closely associated with the sulfur and carbon cycles. We found that the bacterial communities were heterogeneous in different micro-habitats on the tidal creek section, which was related to soil salinity, moisture, and nutrients as well as tidal action. The study would provide fundamental insights into understanding the ecological functions of bacterial diversities and biogeochemical processes influenced by tidal creeks.

**Keywords: tidal creek, micro-habitats, bacterial community, sulfate-reducing bacteria, ecological functions**

OPEN ACCESS

***Edited by:***
*Chuanyu Gao,*
*Northeast Institute of Geography and Agroecology (CAS), China*

***Reviewed by:***
*Lei Qin,*
*Northeast Institute of Geography and Agroecology (CAS), China*
*Xiaofei Lv,*
*China Jiliang University, China*

****Correspondence:***
*Junbao Yu*
*junbao.yu@gmail.com*
*Jisong Yang*
*yangjisong@ldu.edu.cn*

***Specialty section:***
*This article was submitted to Conservation and Restoration Ecology, a section of the journal Frontiers in Ecology and Evolution*

***Received:*** *23 May 2022*
***Accepted:*** *22 June 2022*
***Published:*** *01 August 2022*

***Citation:***
*Wang Z, Yang K, Yu J, Zhou D, Li Y, Guan B, Yu Y, Wang X, Ren Z, Wang W, Chen X and Yang J (2022) Soil Bacterial Community Structure in Different Micro-Habitats on the Tidal Creek Section in the Yellow River Estuary. Front. Ecol. Evol. 10:950605. doi: 10.3389/fevo.2022.950605*

## INTRODUCTION

Estuary wetlands, between ocean and terrestrial ecosystems, play important ecological functions in climate change regulation, biodiversity preservation, and environmental remediation (Fennessy, 2014; Murray et al., 2019; Xiao et al., 2019). In the front estuary wetlands by field investigation and aerial photography, there are a variety of small and different micro-habitats around tidal creeks,

which compose the tidal creek salt marshes. Tidal creek salt marshes are active and critical to biogeochemical processes and biological diversities with high hydrological connectivity (Mallin and Lewitus, 2004; Vandenbruwaene et al., 2012; Cui et al., 2016). Along with the frequent and long-time tidal alternation, the tidal creek salt marshes comprise many different micro-habitats and have orderly occurred in habitat successions with unvegetated mudflat initiation, vegetation colonization, organic and inorganic sediment deposition, and upper marsh elevation (Wilson et al., 2014; Chirol et al., 2018; Wu et al., 2020). For example, the micro-habitats are bare lands and/or the *Spartina alterniflora* community near tidal creeks due to long-time flooding and in the upper lands away from tidal reeks colonized by more plant communities like *Suaeda glauca*, *Salicornia europaea*, and *Phragmites communis* (Kim, 2018; Liu et al., 2020). It should be notable that the diverse micro-habitats on the tidal creek section are to advantage to maintain the eco-functions, including biogeochemical processes, matter exchanges, environmental resilience, and so on (Arriola and Cable, 2017; Tan et al., 2020; Trifunovic et al., 2020; Wu et al., 2020).

It is extensively focused on that bacterial communities that are indispensable to understanding and untangling the estuary wetland eco-functions, because engines act as a driver for soil carbon and nitrogen turnover processes, environment resistance, resilience, and so on (Huang et al., 2020; Zou et al., 2020; Coban et al., 2022). Previous studies have demonstrated that bacterial communities are greatly affected by many environmental factors, such as pH, organic matter, nutrient availability, soil salinity, and moisture (Fierer, 2017). In coastal wetland, soil salinity and nutrients were regarded as the important environmental filters (An et al., 2019). As well, soil bacterial community structures and functions, like sulfate-reducing and nitrifying bacteria, were significantly different, ranging from oligohaline to hypersaline habitats (Li et al., 2019; Zhang et al., 2020). Thus, it is important to unveil the relationships between bacterial communities and habitats in tidal creek salt marshes to better understand eco-functions of estuary wetlands.

The Yellow River estuary wetland is focused by previous studies on micro-habitat types, biogeochemical processes, and eco-functions of wetlands (Zhao et al., 2010; Yu et al., 2018; Gong et al., 2021). Several recent studies have found that bacteria communities have existed in great variations, which were relevant to geographic patterns, season variations, plant types, and soil salinities (Lv et al., 2016; Zhang et al., 2017; Zhang et al., 2020; Li et al., 2021). However, it is poorly to announce bacterial community structures in the micro-habitat soils on the tidal creek section, which would limit our understanding of the biogeochemical processes and eco-functions in estuary wetland ecosystem. Herein, the present study has selected a tidal creek to investigate the bacterial community structures and unveil the keystone bacteria in response to the soil biogeochemical processes of different micro-habitats. Our hypotheses are that (1) dominant bacteria and bacterial biomarkers should be different across the five micro-habitats on the section of the tidal creek, (2) the differences may be related to the effects of tidal action and soil properties together.

# MATERIALS AND METHODS

## Soil Sampling and Soil Physicochemical Properties Analysis

We selected a tidal creek (37°46′−37°49′N, 119°5′−119°6′E), approximately 6,430-m length and 110–190-m width in the Yellow River estuarine wetland, located at Dongying City, Shandong Province, Eastern China (**Figure 1A**). Along the tidal creek, three sections, 200 m away from each other, were set, and each section was divided into five micro-habitats according to hydrologic conditions and the vegetation community, including pluff mudflat (PM), bare mudflat (BM), *Tamarix chinensis* community (TC), *T. chinensis-Suaeda salsa* community (TSC), *S. salsa* community (SC) (**Figure 1B**). In detail, PM was closest to the tidal creek with long-time flooding and no plant coverage. BM suffered medium-time flooding and uncovered vegetation, but more fiddler carb bioturbation. Compared with the lower micro-habitats of PM and BM, the upper micro-habitats of TC, TSC, and SC were short-time flooding by spring tidal current and colonized with two dominant halophytes of *T. chinensis* and *S. salsa*.

The soil samples (2–10 cm) in every habitat were collected with three repetitions in July 2018. All of the soil subsamples were quickly sealed in sterile Eppendorf tubes and stored in liquid nitrogen for 16S rRNA analysis, and the others were air dried for soil physicochemical analyses in the laboratory.

Soil physicochemical properties consisting of soil moisture content (SMC), pH value, electrical conductivity (EC), soil organic carbon (SOC), total nitrogen (TN), and total phosphorus (TP) were measured using standard soil test methods as described by the agriculture protocols for China (Lu, 2000). In brief, SMC was determined by weight loss after drying 20 g of wet soil at 105°C for 24 h. Soil pH and EC were determined by a pH meter and an electronic probe (the soil-to-water ratio was 1:5). The SOC, TN, and TP were determined by the potassium dichromate heating oxidation-volumetric method, Kjeldahl nitrogen method, Mo-Sb anti spectrophotometric method, respectively.

## Soil Bacterial DNA Extraction and PCR Amplification

Our study used the E.Z.N.A.® soil DNA Kit (Omega Bio-Tek, Norcross, GA, U.S.) to extract microbial DNA from soil samples. The final DNA concentration and purification were determined by a NanoDrop 2000 UV-vis spectrophotometer, and DNA quality was checked by 1% agarose gel electrophoresis. The V3-V4 hypervariable regions of 16S rRNA were selected to identify bacteria species (Yang et al., 2018), and amplified using the barcoded primers 338F/806R (5'-ACTCCTACGGGAGGCAGCAG-3'/5'-GGACTACHVGGGTWTCTAAT-3') from the qualified DNA templates. Briefly, the PCR reactions were amplified using the following program: 3 min of initial denaturation at 95°C, followed by 27 cycles of denaturation at 95°C for 30 s, primer annealing at 55°C for 30 s, elongation at 72°C for 45 s, and a final extension of 10 min at 72°C. The resulted PCR products were extracted from a 2% agarose gel and purified using the AxyPrep DNA Gel Extraction Kit. All of the purified PCR products were quantified using QuantiFluor™-ST (Promega, USA).

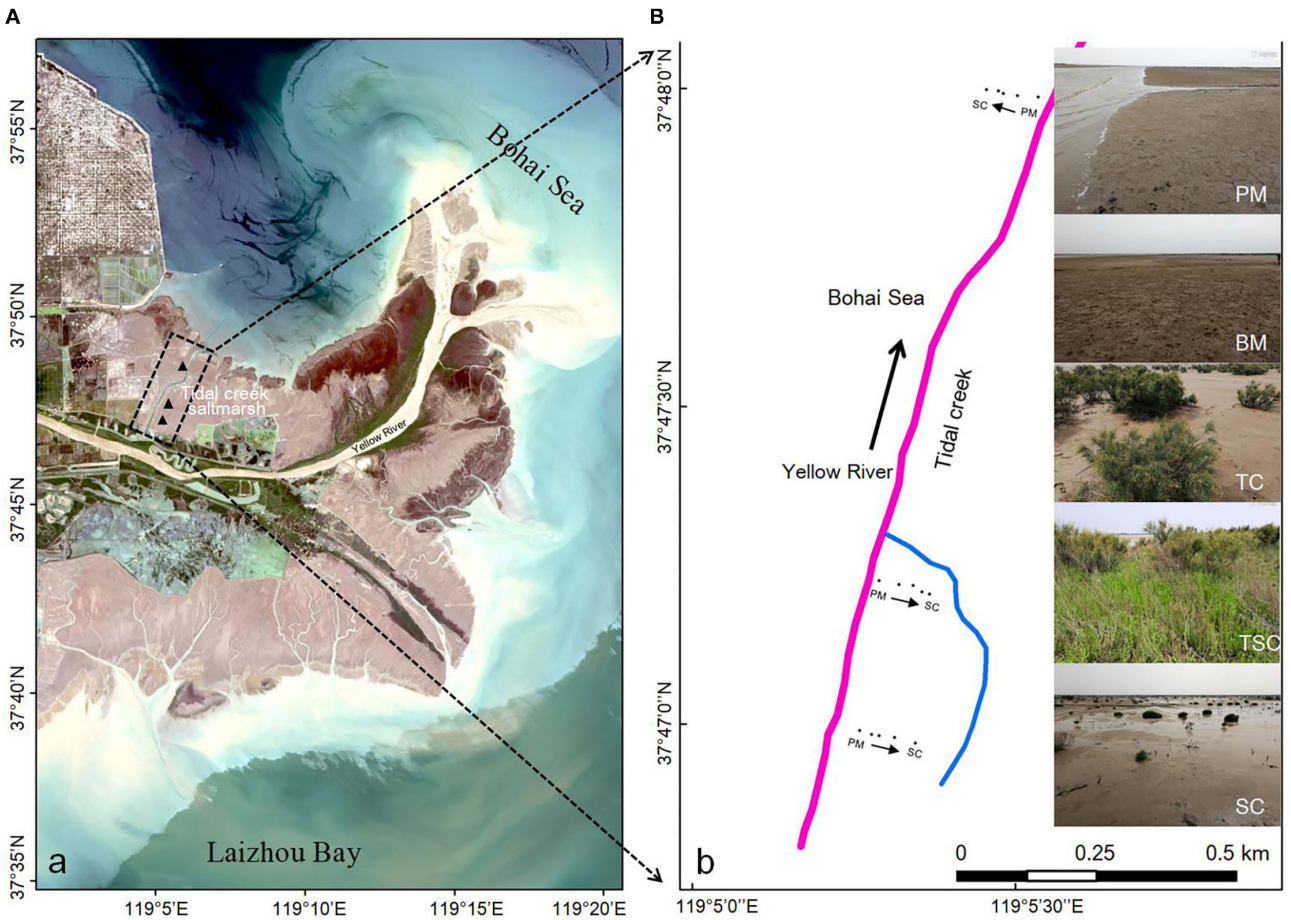


**FIGURE 1 | (A)** Location of the micro-habitats around the tidal creek in the Yellow River estuary wetland. **(B)** Landforms of the micro-habitats around the tidal creek, namely PM (pluff mudflat), BM (bare mudflat), TC (*Tamarix chinensis* community), TSC (*T. chinensis* and *Suaeda salsa* community), and SC (*S. salsa* community).

## Illumina MiSeq16S rRNA High-Throughput Sequencing and Data Processing

Purified amplicons were pooled in equimolar and paired-end sequenced (2 × 300) on an Illumina MiSeq platform (Illumina, San Diego, USA) according to the standard protocols by Majorbio Bio-Pharm Technology Co. Ltd. (Shanghai, China). Raw fastq files were quality-filtered by Trimmomatic and merged by FLASH with the following criteria: (1) The reads were truncated at any site receiving an average quality score < 20 over a 50-bp sliding window. (2) Sequences of overlap being longer than 10 bp were merged according to their overlap with mismatch no more than 2 bp. (3) Sequences of each sample were separated according to barcodes (exactly matching) and Primers (allowing 2 nucleotide mismatching), and reads containing ambiguous bases were removed.

Operational taxonomic units (OTUs) were clustered with a 97% identity cutoff using UPARSE (version7.0.1090, http://drive5.com/uparse/), with a novel "greedy" algorithm that performs chimera filtering and OTU clustering simultaneously. The taxonomy of each 16S rRNA gene sequence was analyzed by RDP Classifier algorithm (https://sourceforge.net/projects/rdp-classifier/) against the Silva project's version 138 release (https://www.arb-silva.de/) using a confidence threshold of 70%. Mothur1.30.2 and Qiime 1.9.1 have calculated the bacterial α-diversity and β-diversity, respectively.

## Statistical Analysis

The differences in soil physicochemical properties, bacterial α-diversity, and species were estimated by one-way ANOVA analysis in SPSS 22. Bacterial β-diversity analysis was displayed with principal coordinate analysis (PCoA) based on the weighted normalized unifrac (WNU) metric. Heatmap analysis and redundancy analysis (RDA) were used to find the differential OTUs, and the relationships between bacteria and soil physicochemical properties in the five habitats, respectively. All biomarkers of the five bacterial communities have been identified by linear discriminant analysis (LDA) effect size (LDA > 3, $p$ <0.05) on the Galaxy (https://huttenhower.sph.harvard.edu/galaxy/root) to mine special biomarkers and explain the differences in different bacterial communities (Segata et al., 2011).

# RESULTS

## Soil Physicochemical Properties

As shown in **Table 1**, the values of SOC, TN, EC, and SMC were significantly different among micro-habitats ($p < 0.05$). In detail, the SOC content was highest in SC and followed in TSC, TC, BM, and PM, with means of 7,368.23 ± 10, 6,508.12 ± 83, 5,960.18 ± 76, 5,844.81 ± 56, 4,659.71 ± 49 mg·kg$^{-1}$, respectively. The TN contents in upper micro-habitats (TC, TSC, and SC) were higher than in lower micro-habitats (PM and BM), with the range from 298.77 to 328.42 mg·kg$^{-1}$ vs. 164.84 to 240.07 mg·kg$^{-1}$. As well, the soil EC in vegetation micro-habitats was higher than in the two bare mudflats, with a range from 3.11 to 5.85 ms·cm$^{-1}$ vs. 66 to 1.47 ms·cm$^{-1}$. The SMC was 34 ± 0.02% in PM, which was highest among all the micro-habitats. However, there were no significant differences in pH values ($p = 0.208$) and TP contents ($p = 0.38$) among the five micro-habitats.

## Overview of 16S rRNA High-Throughput Sequencing and Bacterial OTU Diversity

The study has got 702,472 high-quality amplicons with an average length of 440 bp in 15 soil samples, and 99.81% of them were even distributed into the ranges from 401 to 460 bp in length (**Figure 2A**). After picking out the chimeras and single sequences, it generalized 534,284 valid reads and clustered into a total of 4,657 valid OTUs in the five micro-habitats (**Table 2**). With Good's coverage scores ranging from 98.42 to 99.41% as a result, there were most OTUs in BM (2,155), and followed by TC (1,947), PM (1,915), SC (1,384), and TSC (1,048). The bacterial α-diversity analysis showed that community richness estimators ACE, Chao1, and diversity index Shannon were significantly different in the five micro-habitat soils (all $p < 0.01$), except for Simpson index ($p = 0.107$). ACE, Chao1, and Shannon index of PM, BM, and TC were significantly higher than that of the TSC and SC. With the increase of sample sequences, the rarefaction curves of bacterial OTUs and Shannon-Wiener index have approached the plateaus (**Figures 2B,C**), which indicated that our subsampling analysis can reflected the bacteria diversity in each sample. Furthermore, the bacterial β-diversity explained the OTUs separation with PCoA ($R^2 = 0.558$, $p = 0.001$), which showed a significant variance among the five micro-habitats. The first axis PC1 and second axis PC2 explained 55.16% of the total variance with PCoA (**Figure 2D**). Together, the bacterial α- and β-diversity implied that bacterial community structures were different between the lower micro-habitats vs. the upper micro-habitats.

## Bacterial Community Structures in Different Micro-Habitats

At the bacterial OTU level, there were 573 shared bacterial OTUs in five micro-habitats, accounting for 22.31% (PM), 18.56% (BM), 19.29% (TC), 31.04% (TSC), and 23.86% (SC), respectively (**Figure 3A**). On the contrary, 170 OTUs were individual in PM (6.62%), BM (5.05%), TC (4.91%), TSC (11.38%), and SC (8.03%), respectively. Moreover, 67 bacterial classes were shared and accounted for 59.82% (PM), 56.78% (BM), 55.83% (TC), 79.76% (TSC), and 66.34% (SC) (**Figure 3B**). However, only a few bacteria were uniquely or commonly observed in the other combinations with 1 to 16 overlapped classes, even no shared, which implied that bacterial taxa were relatively stable at the class level vs. at the OTU level across the five micro-habitats.

The dominant bacterial classes of the five habitats were γ-Proteobacteria (15.76%), α-Proteobacteria (10.89%), Bacteroidetes IncertaeSedis (9.04%), Gemmatimonadetes (8.3%), Flavobacteriia (8.94%), Actinobacteria (7.31%), δ-Proteobacteria (7.22%), Anaerolineae (4.2%), Acidobacteria (3.8%), Sphingobacteriia (3.41%), and so on (**Figure 3C**). Of them, Bacteroidetes IncertaeSedis and Gemmatimonadetesin upper micro-habitats (SC, TSC, and TC) were obviously higher than them in lower micro-habitats (PM and BM), with 16.04–0.8% ($p = 0.02$) and 11.74–2.09% ($p = 0.02$), while Flavobacteriia and δ-Proteobacteria were decreased from PM to SC with 14.16–3.25% ($p = 0.04$) and 12.58–4.96% ($p = 0.02$). In addition, Acidobacteria ($p = 0.03$) and Sphingobacteriia ($p = 0.04$) were significantly different in the five micro-habitats.

The top 50 bacterial OTUs were selected to compare the OTU abundances and taxa to characterize the variations of bacterial community structures (**Figure 4**). Fourteen OTUs were significantly enriched in PM, BM, and TC ($p < 0.05$), which belonged to eight bacterial families of *JTB255*, *Flavobacteriaceae*, *Unknown γ-Proteobacteria*, *Sva1033*, *Rhodobacteraceae*, *Rhodobiaceae*, *Rhodospirillaceae*, and *OM1 clade*. Meanwhile, about 20 OTUs were abundant in TC, TSC, and SC, widely mapped into *Flavobacteriaceae*, *Rhodobacteraceae*, *Trueperaceae*, unclassified *Chloroflexi*, *OM1 clade*, etc.

**TABLE 1 |** The heterogeneous soil properties in the tidal creek salt marsh.

| Site | SMC (%)* | pH | EC (ms/cm)* | SOC (mg/kg)* | TN (mg/kg)* | TP (mg/kg) |
|---|---|---|---|---|---|---|
| PM | 0.24 ± 0.02 | 8.07 ± 0.42 | 0.66 ± 0.07 | 4,659.71 ± 49 | 273.4 ± 22.44 | 43.91 ± 8.38 |
| BM | 0.25 ± 0.05 | 7.97 ± 0.30 | 1.47 ± 0.52 | 5,844.81 ± 56 | 154.84 ± 14.18 | 38.96 ± 1.44 |
| TC | 0.24 ± 0.04 | 7.62 ± 0.62 | 3.11 ± 1.06 | 5,960.18 ± 76 | 288.4 ± 20.69 | 40.02 ± 21.49 |
| TSC | 0.22 ± 0.01 | 7.79 ± 0.27 | 5.85 ± 0.79 | 6,508.12 ± 83 | 298.77 ± 23.55 | 42.29 ± 11.55 |
| SC | 0.24 ± 0.01 | 7.24 ± 0.39 | 5.29 ± 1.1 | 7,368.23 ± 10 | 305.09 ± 9.22 | 30.63 ± 7.28 |

*The asterisks (*) indicate the soil properties are significantly different, and the $p < 0.05$.*

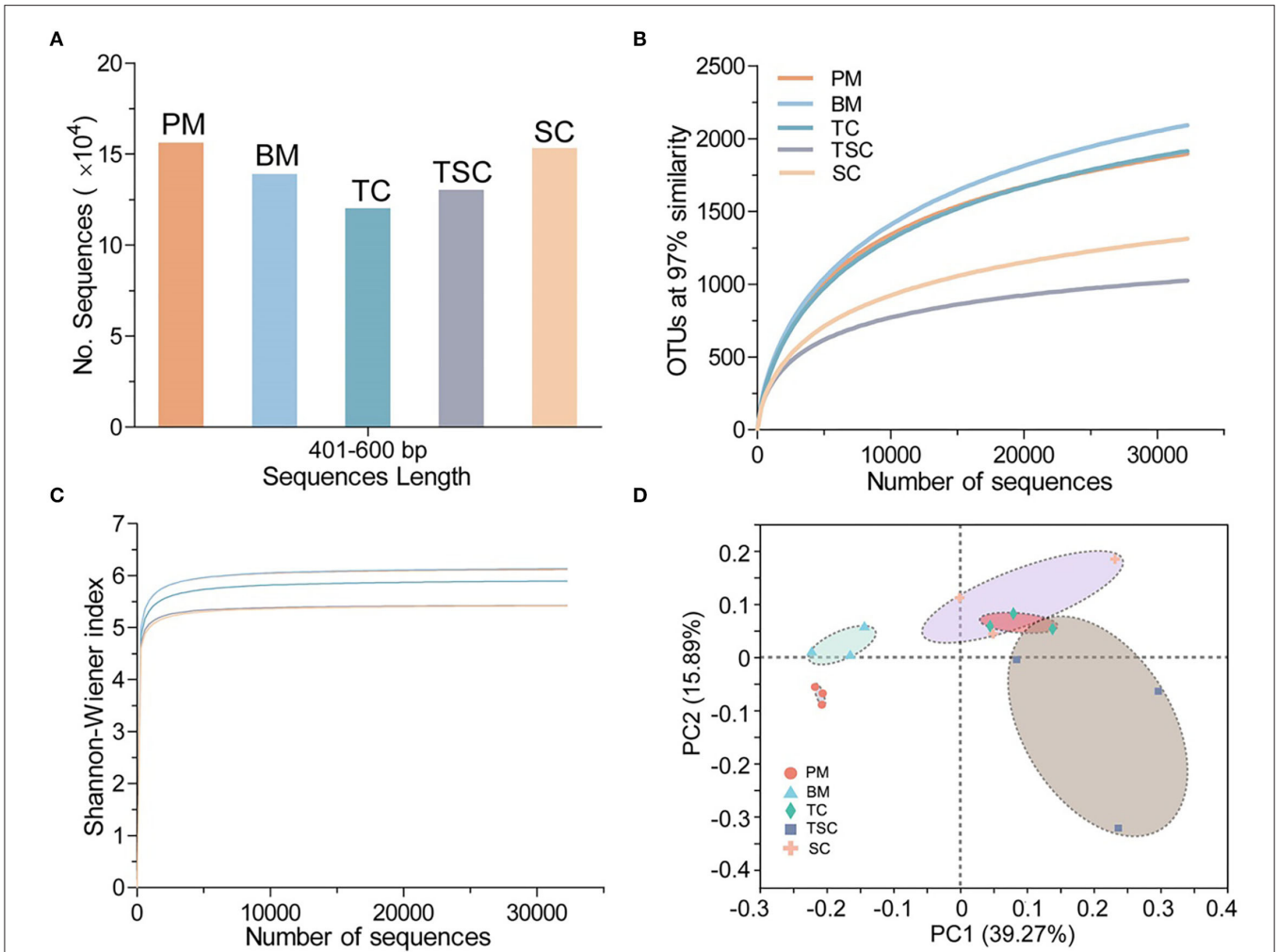


**FIGURE 2 | (A)** 16S rRNA V3-V4 amplicons ranged from 401 to 460 bp in the five habitats. **(B)** Rarefaction curves of 97% similar OTUs. **(C)** Shannon-Wiener curves in the five habitats. **(D)** β-diversity of the bacterial community in the five habitats.

**TABLE 2 |** The bacterial communities in valid sequence reads, 97% OTUs, Good's Coverage, and bacterial α-diversity indices.

| Site | Reads | OTUs | Good's coverage | ACE | Chao1 | Shannon index | Simpson index |
|---|---|---|---|---|---|---|---|
| PM | 33,680 | 2,568 | 98.57% | 2,268 | 2,310 | 6.12 | 0.0062 |
| BM | 35,768 | 3,088 | 98.22% | 2,598 | 2,581 | 6.14 | 0.0063 |
| TC | 34,356 | 2,971 | 98.42% | 2,354 | 2,375 | 5.89 | 0.0106 |
| TSC | 3,5607 | 1,846 | 99.35% | 1,198 | 1,217 | 5.43 | 0.0107 |
| SC | 38,684 | 2,402 | 98.96% | 1,611 | 1,635 | 5.42 | 0.0157 |

## Bacterial Biomarkers in Different Micro-Habitats

A total of 129 bacterial biomarkers were identified in the five micro-habitats, with 63 biomarkers (12 bacterial classes) in PM, 16 (5 classes) in BM, 9 (4 classes) in TC, 33 (2 phyla and 8 classes) in TSC, and 8 (2 classes) in SC, respectively (**Supplementary Table S1**). The bacterial communities of PM and TSC had more biomarkers, which mainly clustered into the classes of α-, δ-, γ-Proteobacteria, Flavobacteriia, Acidobacteria, Actinobacteria, etc. At the bacterial genus level, these biomarkers belonged to 60 genera, and most enriched in PM with 29 bacterial genera, followed by in BM (12), TSC (10), TC (5), and SC (4) (**Figure 5**). For example, the result found that 10 genera (*Desulfococcus*, *Desulfosarcina*, the *Sva0081* sediment group, no-rank *Desulfobulbaceae*, unclassified *Desulfobulbaceae*, *Desulfobulbus*, *Syntrophobacteraceae*, *Desulfuromonadales*,

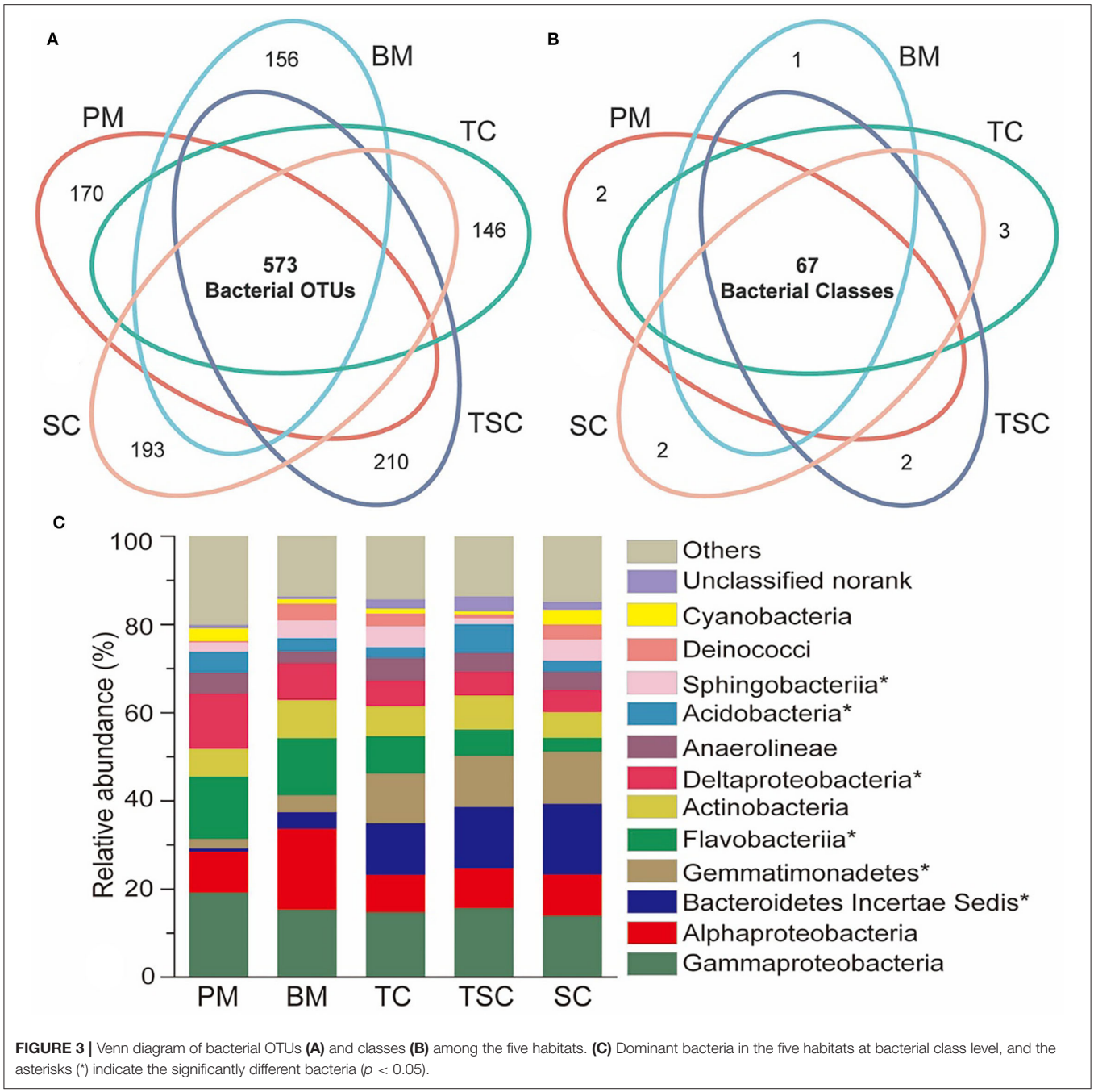


**FIGURE 3 |** Venn diagram of bacterial OTUs **(A)** and classes **(B)** among the five habitats. **(C)** Dominant bacteria in the five habitats at bacterial class level, and the asterisks (*) indicate the significantly different bacteria ($p < 0.05$).

unclassified *Desulfuromonadales*, and *Geothermobacter*) of sulfate-reducing bacteria (SRB) were the biomarkers in PM and BM. In addition, aerobic anoxygenic phototrophic bacteria (AAPB) were also significantly different and diverse in the five micro-habitats with 14 bacterial genera, such as *Rhodobacteraceae*, *Rhodospirillaceae*, and *Roseovarius*. It would be noted that several AAPBs were abundant in *Rhodobacteraceae* (5.42%), *Rhodospirillaceae* (1.68%), *Ectothiorhodospiraceae* (1.05%), *Subsection III* (0.56%), *Rhodobiaceae* (0.48%).

## The Relationship Between Bacterial Community Structures and Soil Physicochemical Properties

At the bacterial class level, the first axis RDA1 and second axis RDA2 have explained 47.56% variances between bacterial community structures and soil physicochemical properties (**Figure 6A**). The RDA result showed that bacterial community structures of TC, TSC, and SC were positively related to SOC, TN, and EC but negatively related to SMC, pH,

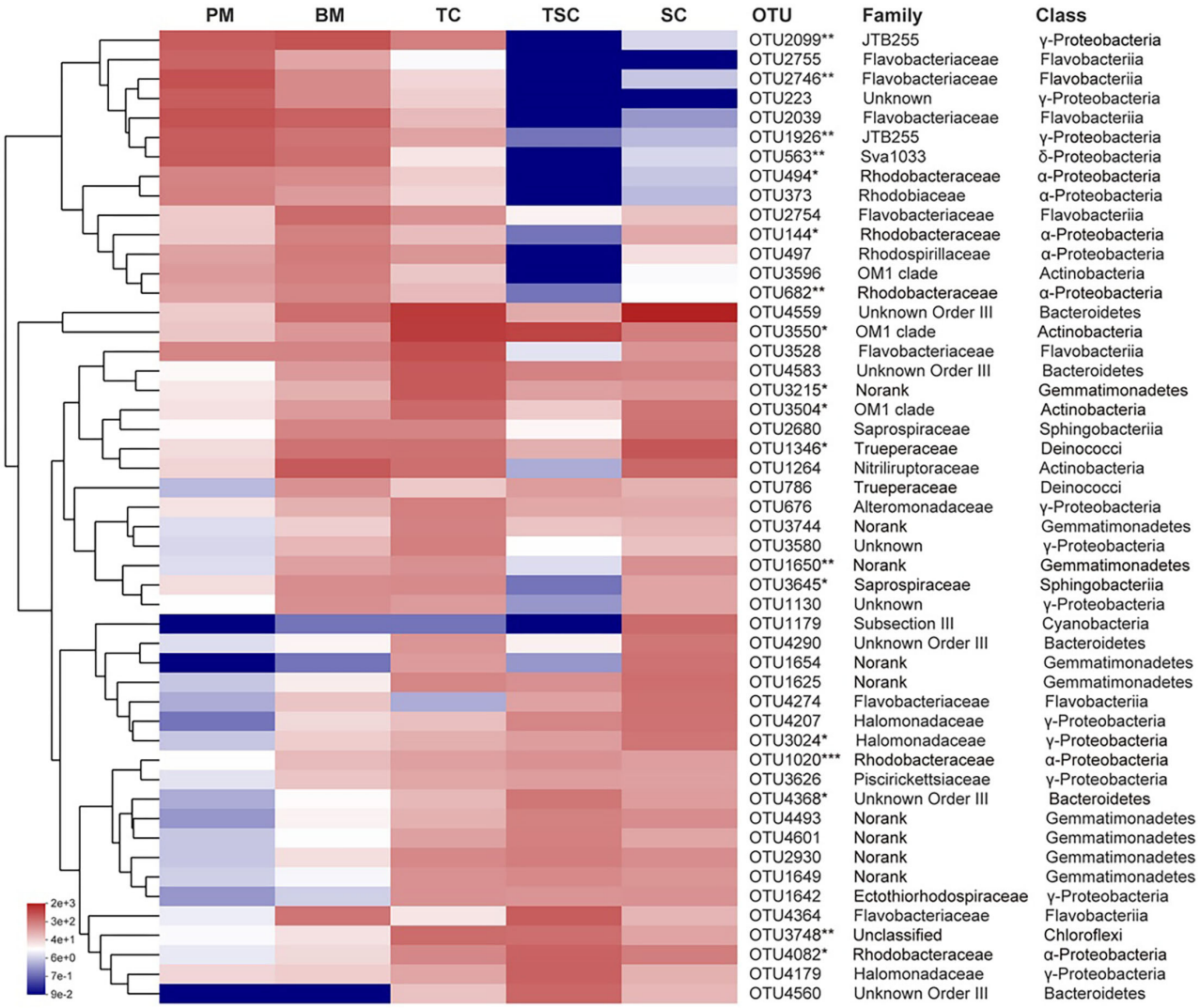


**FIGURE 4 |** The relative abundances of top 50 OTUs at the family and class levels in the five habitats. The symbol (*) indicates the significantly different bacteria. The * symbol indicates the value of $p < 0.05$, the ** symbol indicates the value of $p < 0.01$, and the *** symbol indicates the value of $p < 0.001$.

and TP, that of PM and BM in reverse. Furthermore, our study selected the top 20 bacterial classes and 50 bacterial families to unveil the relationship with soil properties. In detail, heatmap analysis showed that the classes Bacteroidetes, Phycisphaerae, Gemmatimonadetes, and unclassified Chloroflexi were positively related to SOC, TN, and EC, in contrast to α-, δ-Proteobacteria, and Flavobacteriia (**Figure 6B**). Moreover, the bacterial classes (e.g., Flavobacteriia, Verrucomicrobiae, Phycisphaerae) were significantly affected by SMC and pH. At the family level, the result showed that 26 bacteria were closely related to SOC, TN, EC, and SMC (**Figure 6C**). The majority of them were the dominant class α-, δ-, γ-Proteobacteria, Gemmatimonadetes, Bacteroidetes, and Flavobacteriia, suggesting that the soil properties of SOC, TN, EC, and SMC were the important environmental factors to alter the bacterial community structures in the five micro-habitats.

## DISCUSSION

Tidal creek salt marshes have characterized as frequently tidal flooding and strongly hydrological connectivity, and shape active and uneven ecosystems with several small and diverse micro-habitats (Mooraki et al., 2009; Cabezas et al., 2017; Wang et al., 2021). Some studies have shown that these micro-habitats were important to maintain health estuary wetland eco-functions, such as carbon capture and storage, wetland restoration and buffering disturbances (Wu et al., 2020; Glaser et al., 2021). In field investigation, there were five micro-habitats of pluff mudflat, bare mudflat, *T. chinensis*, *T. chinensis-S. salsa*, and *S. salsa* around the tidal creek. This may be due to that tidal creek greatly altered microtopography, soil seed colonization, and vegetation succession *via* tidal fluctuation in the estuary wetland (Chang et al., 2010; Zhu et al., 2021). These micro-habitats around tidal creeks generated significantly different soil properties of soil

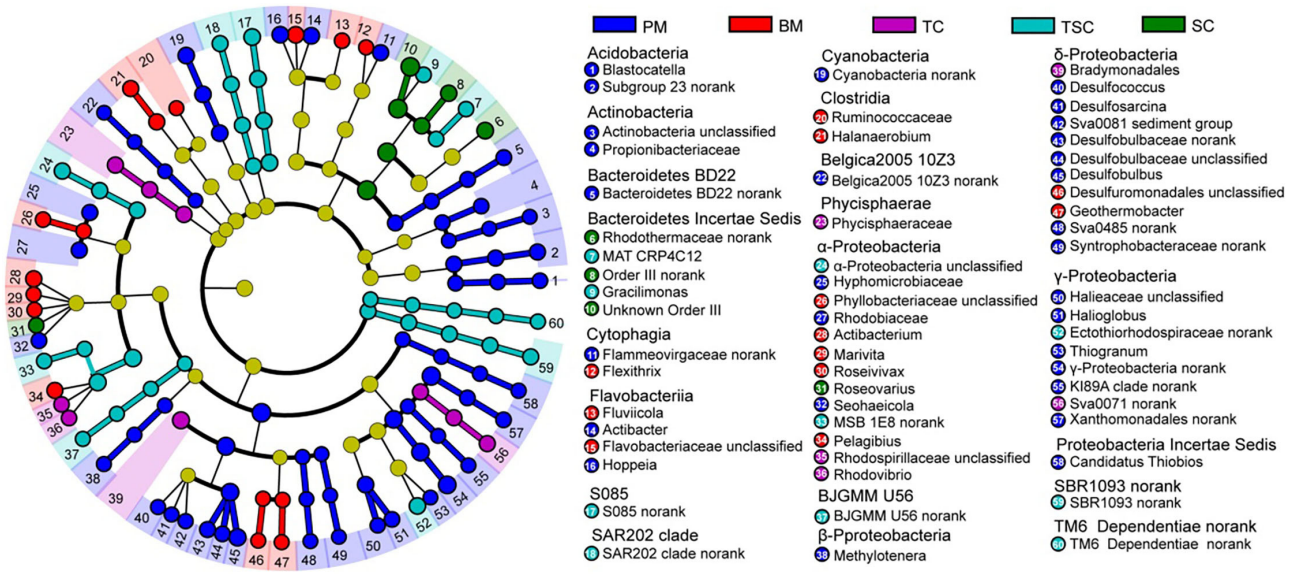


**FIGURE 5 |** Linear discriminant analysis effect size (LefSe) of bacterial biomarkers in the five habitats.

moisture, salinity, and nutrients (**Table 1**). Because of near tidal creeks and frequent tidal flooding, SMC of the lower micro-habitats (pluff and bare mudflats) was higher. However, the upper micro-habitats (*T. chinensis*, *T. chinensis-S. salsa*, and *S. salsa* communities) were suffered by short-time flooding and strong evaporation, which should be the major reasons and thus to aggregate the higher EC and lower SMC in these surface soils (Kearney and Fagherazzi, 2016; Zhou et al., 2020). Moreover, soil nutrients of the lower micro-habitats were taken away by tidal fluctuation, meanwhile accumulated in the upper micro-habitats due to litter decompositions (Chomel et al., 2016; Koceja et al., 2021; Yang et al., 2021).

The present study found the bacterial community structures were significantly different in the five micro-habitats on the tidal creek sections, and these differences may be greatly affected by the tidal action and soil properties together. On one hand, the bacterial community structures of lower micro-habitats (PM and BM) had more diversities than these of upper micro-habitats (TC, TSC, and SC). This may be due to that more frequent tidal action contributed to the passive dispersal of bacterial taxa *via* the marine bacteria. It has been confirmed that several marine bacteria were enrichment in PM and BM, including the dominant bacterial families *JTB 255* (γ-Proteobacteria) (Dyksma et al., 2015), *Flavobacteriaceae* (Flavobacteriia) (Cho and Giovannoni, 2004), and *OM1 clade* (Actinobacteria) (Morris et al., 2012). In addition, the soil properties may contribute main influence to the differences in bacterial community structures (**Figure 6A**). Although pH was regarded as the most important environmental factor to affect soil bacterial communities (Fierer, 2017; Xun et al., 2019), the soil nutrient, salinity, and moisture were more important to the bacterial community structures in our study. Many pieces of evidence have supported our result that the soil nutrient availability and salinity were the predominant reasons for bacterial communities in estuary wetland (An et al., 2019; Li et al., 2019; Rath et al., 2019; Zhang et al., 2020). On the other hand, the differences in bacterial community structures were also exhibited in dominant bacterial taxa, in particular with a high variable in the α-, δ-, γ-Proteobacteria, Bacteroidetes, Gemmatimonadetes, Flavobacteriia, Acidobacteria, and Sphingobacteriia, accounting for about 70% (**Figure 3C**). Indeed, the study found EC, SMC, SOC, and TN may be greatly responsible for them between the lower and upper micro-habitats (**Figures 6B,C**).

Recent years, SRB and AAPB have got many attentions on sulfur cycling, carbon mineralization, and sequestration in the coastal wetland (Stegman et al., 2014; Jørgensen et al., 2019; Rolando et al., 2022). The present study found SRB and AAPB were characterized as the bacterial biomarkers in tidal creek salt marsh, and may partly result in the differences of structures and functions. SRB were widely distributed in anoxic environments, and the lower micro-habitats (PM and BM) were suffered by long-time seawater flooding and abundance $SO_4^{2-}$, which were suitable for the SRB groups (Zeleke et al., 2013). Our study found that SRB of 10 genera were great enrichment, which suggests that they may be the potential indicators of the sulfur cycle in lower micro-habitats. Moreover, AAPB were genetically diverse in Proteobacteria (Bryant and Frigaard, 2006; Ritchie and Johnson, 2012), in agreement with our results across α-, β-, and γ-Proteobacteria (**Figure 5**). Some studies reported that *Rhodobacteraceae* were high in abundance up to 25% of the total bacterial community in seawater (Buchan et al., 2005; Lenk et al., 2012). In the present study, the *Rhodobacteraceae* (*Actibacterium*, *Marivita*, *Roseivivax*, *Roseovarius*, and *Seohaeicola*) were greatly

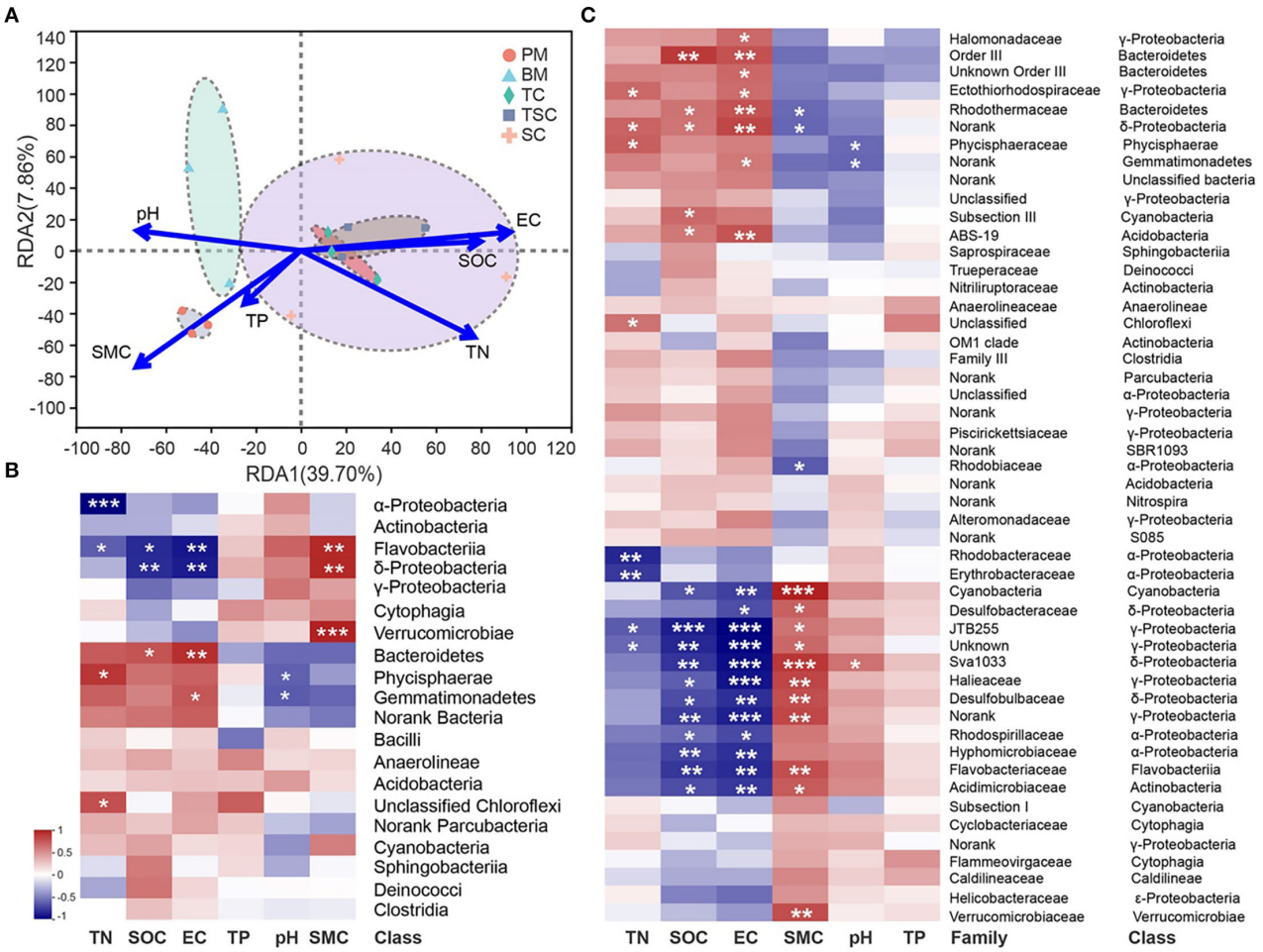


**FIGURE 6 | (A)** Redundancy analysis (RDA) between soil properties and bacterial community structures at class level. The correlation heatmaps of soil properties and dominant bacteria at class **(B)** and family **(C)** level. The symbol (*) indicates the significantly different bacteria. The * symbol indicates the value of $p < 0.05$, the ** symbol indicates the value of $p < 0.01$, and the *** symbol indicates the value of $p < 0.001$.

enriched in the lower micro-habitats (PM and BM), which may be associated with dispersal between the lower micro-habitats and seawater. In addition, the *Rhodospirillaceae* was abundant in upper micro-habitats (TC, TSC, and SC). Several studies have reported that *Rhodospirillaceae* was ability to $N_2$ fixation and positive relation of soil nutrient contents and plant successions (Madigan et al., 1984; Ding et al., 2017).

## CONCLUSION

Our study found that the bacterial communities were greatly diverse and heterogeneous in the tidal creek salt marsh, and the diversities were greatly altered by the effects of tidal action, soil salinity, moisture, and nutrients. In particular, the important biomarker taxa of SRB and AAPB groups were close correspondence in different micro-habitats. These results provide fundamental insights into unveiling bacterial community diversities and important bacterial biomarkers of different micro-habitats.

## DATA AVAILABILITY STATEMENT

The original contributions presented in the study are publicly available. This data can be found at NCBI: http://www.ncbi.nlm.nih.gov/bioproject/851955, or with the accession number: PRJNA851955.

## AUTHOR CONTRIBUTIONS

ZW: conceptualization, writing—original draft, and editing. KY: resources and formal analysis. DZ, YL, BG, YY, XW, ZR, WW, and XC: investigation and data curation. JYa: visualization. JYu: supervision and review. All authors contributed to the article and approved the submitted version.

## FUNDING

This work was supported by the National Natural Science Foundation of China (U1806218, 41871087, 31800011,

and U2106214). Moreover, the Coastal Resources and Environment Team for Blue-Yellow Area as follow: The Project of the Cultivation Plan of Superior Discipline Talent Teams of Universities in Shandong Province-The Coastal Resources and Environment Team for Blue-Yellow Area.

## SUPPLEMENTARY MATERIAL

The Supplementary Material for this article can be found online at: https://www.frontiersin.org/articles/10.3389/fevo.2022.950605/full#supplementary-material

## REFERENCES


An, J. X., Liu, C., Wang, Q., Yao, M. J., Rui, J. P., Zhang, S. H., et al. (2019). Soil bacterial community structure in Chinese wetlands. *Geoderma.* 15, 290–299. doi: 10.1016/j.geoderma.2018.09.035

Arriola, J. M., and Cable, J. E. (2017). Variations in carbon burial and sediment accretion along a tidal creek in a florida salt marsh. *Limnol. Oceanogr.*62, S15–S28. doi: 10.1002/lno.10652

Bryant, D. A., and Frigaard, N. U. (2006). Prokaryotic photosynthesis and phototrophy illuminated. *Trends Microbiol.* 14, 488–496. doi: 10.1016/j.tim.2006.09.001

Buchan, A., González, J. M., and Moran, M. A. (2005). Overview of the marine *Roseobacter* lineage. *Appl. Environ. Microbiol.* 71, 5665–5677. doi: 10.1128/AEM.71.10.5665-5677.2005

Cabezas, A., Mitsch, W. J., Macdonnell, C., Zhang, L., Bydatek, F., and Lasso, A. (2017). Methane emissions from mangrove soils in hydrologically disturbed and reference mangrove tidal creeks in southwest Florida. *Ecol. Eng.* 114, 57–65. doi: 10.1016/j.ecoleng.2017.08.041

Chang, E. R., Veeneklaas, R. M., and Bakker, J. P. (2010). Seed dynamics linked to variability in movement of tidal water. *J. Veg. Sci.* 18, 253–262. doi: 10.1111/j.1654-1103.2007.tb02536.x

Chirol, C., Haigh, I. D., Pontee, N., and Thompson, C. E. L. (2018). Parametrizing tidal creek morphology in mature saltmarshes using semi automated extraction from lidar. *Remote Sens. Environ.* 209, 291–311. doi: 10.1016/j.rse.2017.11.012

Cho, J. C., and Giovannoni, S. J. (2004). Robiginitaleabiformata gen. nov., sp. nov., a novel marine bacterium in the family Flavobacteriaceae with a higher G+C content. *Int. J. Syst. Evol.* 54, 1101–1106. doi: 10.1099/ijs.0.03023-0

Chomel, M., Guittonny-Larchevêque, M., Fernandez, C., Gallet, C., DesRochers, A., Par,é D., et al. (2016). Plant secondary metabolites: a key driver of litter decomposition and soil nutrient cycling. *J. Ecol.* 104, 1527–1541. doi: 10.1111/1365-2745.12644

Coban, O., De Deyn, G. B., and van der Ploeg, M. (2022). Soil microbiota as game-changers in restoration of degraded lands. *Science.* 375. doi: 10.1126/science.abe0725

Cui, B. S., Cai, Y. Z., Xie, T., Ning, Z. H., and Hua, Y. Y. (2016). Ecological effects of wetland hydrological connectivity: problems and prospects. *J. Beijing Normal Univ.* 52, 738–746. doi: 10.16360/j.cnki.jbnuns.2016.06.011

Ding, L., j., Su, J. Q., Li, H., Zhu, Y. G., and Cao, Z. H. (2017). Bacterial succession along a long-term chronosequence of paddy soil in the Yangtze River Delta, China. *Soil Biol. Biochem.* 104, 59–67. doi: 10.1016/j.soilbio.2016.10.013

Dyksma, S., Bischof, K., Fuchs, B. M., Hoffmann, K., Meier, D., Meyerdierks, A., et al. (2015). Ubiquitous Gammaproteobacteria dominate dark carbon fixation in coastal sediments. *ISME J.* 10, 1939–1953. doi: 10.1038/ismej.2015.257

Fennessy, S. (2014). Wetland ecosystems and global change. *Global Environm. Chan.* 255–261. doi: 10.1007/978-94-007-5784-4_129

Fierer, N. (2017). Embracing the unknown: disentangling the complexities of the soil microbiome. *Nat. Rev. Microbiol.* 15, 579–590. doi: 10.1038/nrmicro.2017.87

Glaser, C., Frei, S., Massmann, G., and Gilfedder, B. S. (2021). Tidal creeks as hot-spots for hydrological exchange in a coastal landscape. *J. Hydrol.* 597, 126158. doi: 10.1016/j.jhydrol.2021.126158

Gong, Z. H., Mou, K. N., Wang, Q. W., Qiu, H. C., Zhang, C., and Zhou, D. M. (2021). Parameterizing the Yellow River Delta tidal creek morphology using automated extraction from remote sensing images. *Sci. Total Environ.* 769, 144–572. doi: 10.1016/j.scitotenv.2020.144572

Huang, L. B., Bai, J. H., Wen, X. J., Zhang, G. L., Zhang, C. D., Cui, B. S., et al. (2020). Microbial resistance and resilience in response to environmental changes under the higher intensity of human activities than global average level. *Global Change Biol.* 26, 2377–2389. doi: 10.1111/gcb.14995

Jørgensen, B. B., Findlay, A. J., and Pellerin, A. (2019). The biogeochemical sulfur cycle of marine sediments. *Front. Microbiol.* 10, 849. doi: 10.3389/fmicb.2019.00849

Kearney, W., and Fagherazzi, S. (2016). Salt marsh vegetation promotes efficient tidal channel networks. *Nat. Commun.* 7, 12287. doi: 10.1038/ncomms12287

Kim, D. (2018). Modeling spatial and temporal dynamics of plant species richness across tidal creeks in a temperate salt marsh. *Ecol. Indic.* 93, 188–195. doi: 10.1016/j.ecolind.2018.04.080

Koceja, M. E., Bledsoe, R. B., Goodwillie, C., and Peralta, A. L. (2021). Distinct microbial communities alter litter decomposition rates in a fertilized coastal plain wetland. *Ecosphere.* 12, 1–18. doi: 10.1002/ecs2.3619

Lenk, S., Moraru, C., Hahnke, S., Arnds, J., Richter, M., Kube, M., et al. (2012). *Roseobacter* clade bacteria are abundant in coastal sediments and encode a novel combination of sulfur oxidation genes. *ISME J.* 6, 2178–2187. doi: 10.1038/ismej.2012.66

Li, H., Chi, Z. F., Li, J. L., Wu, H. T., and Yan, B. X. (2019). Bacterial community structure and function in soils from tidal freshwater wetlands in a Chinese delta: Potential impacts of salinity and nutrient. *Sci. Total Environ.* 696, 134029. doi: 10.1016/j.scitotenv.2019.134029

Li, J. Y., Chen, Q. F., Li, Q., Zhao, C. S., and Feng, Y. (2021). Influence of plants and environmental variables on the diversity of soil microbial communities in the Yellow River Delta wetland, China. *Chemosphere.* 274, 129967. doi: 10.1016/j.chemosphere.2021.129967

Liu, L. Y., Qu, F. Z., Li, Y. Z., Yu, J. B., Yang, J. S., and An, C. B. (2020). Correlation between creek tidal distribution and vegetation coverage in the Yellow River Delta coastal wetland. *Chinese J. Ecol.* 39, 1830–1837. doi: 10.13292/j.1000-4890.202006.006

Lu, R. K. (2000). Soil Agro-chemistrical Analysis. *China Agriculture Scientech Press.* p. 72–77.

Lv, X. F., Ma, B., Yu, J. B., Chang, S. X., Xu, J. M., Li, Y. Z., et al. (2016). Bacterial community structure and function shift along a successional series of tidal flats in the Yellow River Delta. *Sci. Rep.* 6, 36550. doi: 10.1038/srep36550

Madigan, M., Cox, S. S., and Stegeman, R. A. (1984). Nitrogen fixation and nitrogenase activities in members of the family *Rhodospirillaceae*. *J. Bacteriol.* 157, 73–78. doi: 10.1128/jb.157.1.73-78.1984

Mallin, M. A., and Lewitus, A. J., (2004). The importance of tidal creek ecosystems. *J. Exp. Mar. Biol. Ecol.* 298, 145–149. doi: 10.1016/S0022-0981(03)00356-3

Mooraki, N., Sari, E. A., Soltani, M., and Valinassab, T. (2009). Spatial distribution and assemblage structure of macrobenthos in a tidal creek in relation to industrial activities. *Int. J. Environm. Sci. Technol.* 6, 651–662. doi: 10.1007/BF03326106

Morris, R. M., Frazar, C. D., and Carlson, C. A., (2012). Basin-scale patterns in the abundance of SAR11 subclades, marine *Actinobacteria* (OM1), members of the *Roseobacter* clade and OCS116 in the South Atlantic. *Environ. Microbiol.* 14, 1133–1144. doi: 10.1111/j.1462-2920.2011.02694.x

Murray, N. J., Phinn, S. R., DeWitt, M., Ferrari, R., Johnston, R., Lyons, M. B., Clinton, N., Thau, D., and Fuller, R. A., (2019). The global distribution and trajectory of tidal flats. *Nature.* 565, 222–225. doi: 10.1038/s41586-018-0805-8

Rath, K. M., Fierer, N., Murphy, D. V., and Rousk, J. (2019). Linking bacterial community composition to soil salinity along environmental gradients. *ISME J.* 13, 836–846. doi: 10.1038/s41396-018-0313-8

Ritchie, A. E., and Johnson, Z. I. (2012). Abundance and genetic diversity of aerobic anoxygenic phototrophic bacteria of coastal regions of the Pacific ocean. *Appl. Environ. Microbiol.* 78, 2858–2866. doi: 10.1128/AEM.06268-11

Rolando, J. L., Kolton, M., Song, T., and Kostka, J. E. (2022). The core root microbiome of *Spartina alterniflora* is predominated by sulfur-oxidizing and sulfate-reducing bacteria in Georgia salt marshes, USA. *Microbiome.* 10, 37. doi: 10.1186/s40168-021-01187-7

Segata, N., Izard, J., Waldron, L., Gevers, D., Miropolsky, L., Garrett, W. S., et al. (2011). Metagenomic biomarker discovery and explanation. *Genome Biol.* 12, R60. doi: 10.1186/gb-2011-12-6-r60

Stegman, M. R., Cottrell, M. T., and Kirchman, D. L. (2014). Leucine incorporation by aerobic anoxygenic phototrophic bacteria in the Delaware estuary. *ISME J.* 8, 2339–2348. doi: 10.1038/ismej.2014.75

Tan, L. S., Ge, Z. M., Fei, B. L., Xie, L. N., Li, Y. L., Li, S. H., et al. (2020). The roles of vegetation, tide and sediment in the variability of carbon in the salt marsh dominated tidal creeks. *Estuar. Coast. Shelf Sci.* 239, 106752. doi: 10.1016/j.ecss.2020.106752

Trifunovic, B., Vázquez-Lule, A., Capooci, M., Seyfferth, A. L., Moffat, C., and Vargas, R. (2020). Carbon dioxide and methane emissions from temperate salt marsh tidal creek. *Journal of Geophysical Research: Biogeosciences.* 125, 1–16. doi: 10.1029/2019JG005558

Vandenbruwaene, W., Meire, P., and Temmerman, S. (2012). Formation and evolution of a tidal channelnetwork within a constructed tidal marsh. *Geomorphology*, 151-152:–*No match found*–114–125. doi: 10.1016/j.geomorph.2012.01.022

Wang, Q., Xie, T., Ning, Z. H., Chen, C., Man, Y., and Cui, B. S. (2021). Enhancement of lateral connectivity promotes the establishment of plants in saltmarshes. *Sci. Total Environ.* 767, 145484. doi: 10.1016/j.scitotenv.2021.145484

Wilson, C. A., Hughesb, Z. J., FitzGeraldb, D. M., Hopkinsonc, C. S., Valentined, V., and Kolkere, A. S. (2014). Saltmarsh pool and tidal creek morphodynamics: dynamic equilibrium of northern latitude saltmarshes? *Geomorphology.* 213, 99–115. doi: 10.1016/j.geomorph.2014.01.002

Wu, Y. N., Liu, J. K., Yan, G. X., Zhai, J. X., Cong, L., Dai, L. Y., Zhang, Z. M., and Zhang, M. X. (2020). The size and distribution of tidal creeks affects salt marsh restoration. *J. Environ. Manage.* 259, 110070. doi: 10.1016/j.jenvman.2020.110070

Xiao, D. R., Deng, L., Kim, D. G., Hang, C. B., and Tian, K. (2019). Carbon budgets of wetland ecosystems in china. *Global Change Biology.* 25. doi: 10.1111/gcb.14621

Xun, W. B., Li, W., Xiong, W., Ren, Y., Liu, Y. P., Miao, Y. Z., et al. (2019). Diversity-triggered deterministic bacterial assembly constrains community functions. *Nature Communicat.* 10, 3833. doi: 10.1038/s41467-019-11787-5

Yang, J. S., Zhan, C., Li, Y. Z., Zhou, D., Yu, Y., and Yu, J. B. (2018). Effect of salinity on soil respiration in relation to dissolved organic carbon and microbial characteristics of a wetland in the Liaohe River estuary, Northeast China. *Sci. Total Environ.* 642, 946–953. doi: 10.1016/j.scitotenv.2018.06.121

Yang, X. L., Wang, X. T., Xiao, S., Liu, Z. Y., Zhou, X. H., Du, G. Z., et al. (2021). Dominant plants affect litter decomposition mainly through modifications of the soil microbial community. *Soil Biol. Biochem.* 161, 108399. doi: 10.1016/j.soilbio.2021.108399

Yu, X. J., Zhang, Z. S., Xue, Z. S., Song, X. L., Zhang, H. R., and Wu, H. T. (2018). Morphological characteristics and connectivity of tidal channels in the yellow river delta for 7 periods since 1989. *Wetland Sci.* 16, 517–523. doi: 10.13248/j.cnki.wetlandsci.2018.04.010

Zeleke, J., Sheng, Q., Wang, J. G., Huang, M. Y., Xia, F., Wu, J. H., et al. (2013). Effects of Spartina alterniflora invasion on the communities of methanogens and sulfate-reducing bacteria in estuarine marsh sediments. *Front. Microbiol.* 4, 243. doi: 10.3389/fmicb.2013.00243

Zhang, G. L., Bai, J. H., Tebbe, C. C., Zhao, Q. Q., Jia, J., Wang, W., et al. (2020). Salinity controls soil microbial community structure and function in coastal estuarine wetlands. *Environ. Microbiol.* 23, 1020–1037. doi: 10.1111/1462-2920.15281

Zhang, H. X., Zheng, S., Ding, J. W., Wang, O. M., and Liu, F. H. (2017). Spatial variation in bacterial community in natural wetland-river-sea ecosystems. *J. Basic Microbiol.* 57, 536–546. doi: 10.1002/jobm.201700041

Zhao, X. S., Cui, B. S., Sun, T., and He, Q. (2010). The relationship between the spatial distribution of vegetation and soil environmental factors in the tidal creek areas of the Yellow River Delta. *Ecol. Environm. Sci.* 19, 1855–1861. doi: 10.16258/j.cnki.1674-5906.2010.08.009

Zhou, T. Z., Xin, P., Li, L., and Barry, D. A., Šimunekb, J. (2020). Effects of large macropores on soil evaporation in salt marshes. *J. Hydrol.* 584, 124754. doi: 10.1016/j.jhydrol.2020.124754

Zhu, Z. C., Bouma, T. J., Zhu, Q., Cai, Y. P., and Yang, Z. F. (2021). Effects of waves and sediment disturbance on seed bank persistence at tidal flats. *Front. Mar. Sci.* 8, 728065. doi: 10.3389/fmars.2021.728065

Zou, Y. X., Yan, J. G., Hou, S. W., Yi, Y. J., and Cui, B. S. (2020). Intensive land uses modify assembly process and potential metabolic function of edap hic bacterial communities in the Yellow River Delta, China. *Sci. Total Environ.* 720, 137713. doi: 10.1016/j.scitotenv.2020.137713

**Conflict of Interest:** The authors declare that the research was conducted in the absence of any commercial or financial relationships that could be construed as a potential conflict of interest.

**Publisher's Note:** All claims expressed in this article are solely those of the authors and do not necessarily represent those of their affiliated organizations, or those of the publisher, the editors and the reviewers. Any product that may be evaluated in this article, or claim that may be made by its manufacturer, is not guaranteed or endorsed by the publisher.

frontiers | Frontiers in Ecology and Evolution

TYPE Brief Research Report
PUBLISHED 03 August 2022
DOI 10.3389/fevo.2022.964198



OPEN ACCESS

EDITED BY
He Yixin,
Key Laboratory of Mountain Ecological Rehabilitation and Biological Resource Utilization, Chengdu Institute of Biology (CAS), China

REVIEWED BY
Meng Li,
Chinese Academy of Forestry, China
Huan Meng,
Shenyang Agricultural University, China

*CORRESPONDENCE
Zhu Weihong
whzhu@ybu.edu.cn
Qin Lei
qinlei@iga.ac.cn

SPECIALTY SECTION
This article was submitted to Conservation and Restoration Ecology, a section of the journal Frontiers in Ecology and Evolution

RECEIVED 08 June 2022
ACCEPTED 18 July 2022
PUBLISHED 03 August 2022

CITATION
Wei T, Dongjie Z, Guanglan C, Wanling X, Weihong Z and Lei Q (2022) Effect of agricultural intervention on nutrient stoichiometry from root to leaf in the helophyte species *Glyceria spiculosa*. *Front. Ecol. Evol.* 10:964198. doi: 10.3389/fevo.2022.964198



# Effect of agricultural intervention on nutrient stoichiometry from root to leaf in the helophyte species *Glyceria spiculosa*

Tian Wei[1,2], Zhang Dongjie[3], Cao Guanglan[2], Xu Wanling[2], Zhu Weihong[2]* and Qin Lei[4]*

[1]Key Laboratory of Vegetation Ecology of the Ministry of Education, Institute of Grassland Science, Jilin Songnen Grassland Ecosystem National Observation and Research Station, Northeast Normal University, Changchun, China, [2]College of Geography and Ocean Sciences, Yanbian University, Yanji, China, [3]Shandong Key Laboratory of Eco-Environmental Science for Yellow River Delta, Binzhou University, Binzhou, China, [4]Key Laboratory of Wetland Ecology and Environment, Heilongjiang Xingkai Lake Wetland Ecosystem National Observation and Research Station, Northeast Institute of Geography and Agroecology, Chinese Academy of Sciences, Changchun, China

Plant nutrient stoichiometry indicates the balance of plant internal nutrients and its nutrient-use strategies in response to environmental changes. However, the responses of nutrient stoichiometry in different wetland plant organs under agricultural intervention are poorly understood. Here, we compared the nitrogen (N), phosphorus (P), and the ratio of N:P in the plant organs (leaves, stems, roots, and root hair) of a typical helophyte plant (*Glyceria spiculosa*) in reference, drained, nutrient-rich, and cultivated wetlands (CW) located downstream of the Tumen River in Northeast China. Compared with that in reference wetlands (RW), the results indicate that the average N content in plant leaves, stems, roots, and root hair in nutrient-rich wetlands (NW) was significantly higher by 76, 61, 56, and 39%, respectively ($p < 0.05$), whereas the N content of roots and root hair in drained wetlands (DW) was significantly higher by 17 and 32%, respectively ($p < 0.05$). It was found that plant root P increased only in nutrient-rich and DW ($p < 0.05$). Interestingly, the agricultural interventions significantly affected soil N and P availability, resulting in positive effects on plant leaves, stems, roots, and root hair. Nutrient stoichiometry analysis showed the highest increase in plant leaf N:P ratio in NW, followed by that in drained and CW, but its ratio in root and root hair showed no significant changes under different agricultural interventions, which suggests that *G. spiculosa* allocates nutrients differently in different organs under agricultural interventions. These results imply that plant nutrient stoichiometry should incorporate various plant organs for an in-depth understanding of plant strategies against environmental changes.

KEYWORDS

**wetland, stoichiometry, plant organs, nutrient, drainage, agricultural intervention**

## Introduction

The concept of ecological stoichiometry refers to the balance between multiple chemical elements in ecological interactions (Sterner and Elser, 2003). Nitrogen (N) and phosphorus (P) are the most important nutrients for proper plant growth and functioning (Li et al., 2018). Plant stoichiometry of N and P in plant organs indicates the limitation of plant nutrients as well as the plant homeostasis under the influence of environmental changes (Alvarez-Clare and Mack, 2015; Zhang et al., 2021), and this concept has been widely used to identify plant strategies that control population stability, competition, and succession (Yu et al., 2015; Guiz et al., 2016).

Wetlands are land areas that are inundated or saturated by water frequently, resulting in low nutrient availability (Bedford et al., 1999). To overcome the limitation of insufficient nutrients, wetland plants have evolved strategies for survival, including forming aerenchyma, and altering nutrient and biomass allocation (Aerts and Chapin, 1999; Moor et al., 2017). During the past decades, anthropogenic activities of wetland cultivation have significantly caused over 50% of degradation or loss of wetlands (Zedler and Kercher, 2005), consequently increasing wetland fragmentation and altering the hydrological conditions as well as soil nutrient conditions due to drainage and fertilization (Zedler and Kercher, 2005; Zheng et al., 2017; Qin et al., 2021). Further, these variations in hydrology and soil nutrients have been found to affect plant growth, reproduction, and community structures in wetlands (Li et al., 2018; Bai et al., 2021).

The response of nutrient levels and nutrient stoichiometry have been widely studied under the conditions of water level and nutrient addition in wetlands (Güsewell, 2004; Mao et al., 2016; Li et al., 2018; Zhang et al., 2021). However, these studies tend to focus on the plant leaf or stem and neglect the belowground plant organs as plant growth and reproduction depend upon the roots to absorb and fix nutrients (Kramer-Walter et al., 2016). Given the tendency of plants to allocate nutrients among different organs to maximize soil nutrient availability (Yu et al., 2015; Di Palo and Fornara, 2017; Bai et al., 2021), the study of plant nutrient stoichiometries above- and below-ground could lead to a better understanding of wetland plant responses to agricultural interventions.

*Glyceria spiculosa* (Schmidt) Roshev. (Gramineae) is an emergent macrophyte commonly found in freshwater marshes and is widely distributed in China, East Russia, and North Korea (Bai et al., 2021). Related studies have shown that both N and P fertilizers can contribute to the dominance of *G. spiculosa* (Mao et al., 2014, 2016). The responses of biomass allocation and root clonal structures of *G. spiculosa* under nutrient input and flooding show that it has high plasticity under environmental changes (Luo et al., 2010; Bai et al., 2021). Nevertheless, little is known about the nutrient stoichiometries of roots, stems, and leaf organs of the species, and this limits the understanding of the responses of *G. spiculosa* and its community succession in different agricultural interventions.

To address this knowledge gap, we conducted a field investigation in different wetlands located downstream of the Tumen River, where *G. spiculosa* dominates the wetland community. In this region, agricultural practices have caused a drastic reduction in water levels and increased nutrient levels within the wetlands (Zheng et al., 2017). Here, we investigated the stoichiometry of N and P in *G. spiculosa* organs (from roots to stems to leaves) among reference (natural), drained, nutrient-enriched, and drained wetlands (DW), as well as the boundary of agriculture [paddy fields converted from wetlands, hereafter referred to as cultivated wetlands (CW)]. We hypothesized that agricultural intervention would weakly alter nutrient concentrations in different organs of plants, but nutrient stoichiometry would remain relatively constant.

## Materials and methods

### Study site

The study site is located downstream of the Tumen River Basin (129°52′00″E–131°18′30″E, 42°25′20″N–43°30′18″N), which is the boundary area of China, Russia, and North Korea. This area is characterized by the temperate-zone monsoon climate with mean annual precipitation of around 400–650 mm and average temperature of 2°C–6°C (Zheng et al., 2017). In this area, the wetlands are widely distributed and they include marshes, riverine habitats, and lakeshore habitats and the dominant plants include *G. spiculosa*, *Carex appendiculata*, and *Phragmites australis*. Many wetlands have been converted into paddy fields due to the growing population and food demand. By the application of fertilizers and building of a drainage ditch near natural wetlands, agricultural development has not only resulted in the loss of wetlands but also altered their hydrology and nutrient conditions (Zheng et al., 2017).

### Field sampling and measurement

We conducted field investigations near Jintang village, where natural wetlands have been converted into disturbed wetlands and paddy fields. Four agricultural impacted wetlands were selected (**Figure 1**): (1) a nutrient-rich wetland (NW), which is adjacent to a paddy field, (2) a DW, which was drained for agriculture in 2010 due to wetland protection policy, and tillage is forbidden but the drainage ditch is still present; there is no obvious surface runoff throughout the year in this wetland; (3) a CW, which is an agricultural land (paddy field) and the species *G. spiculosa* is distributed at the boundary of the field; and (4) a reference wetland (RW), which is a natural wetland.

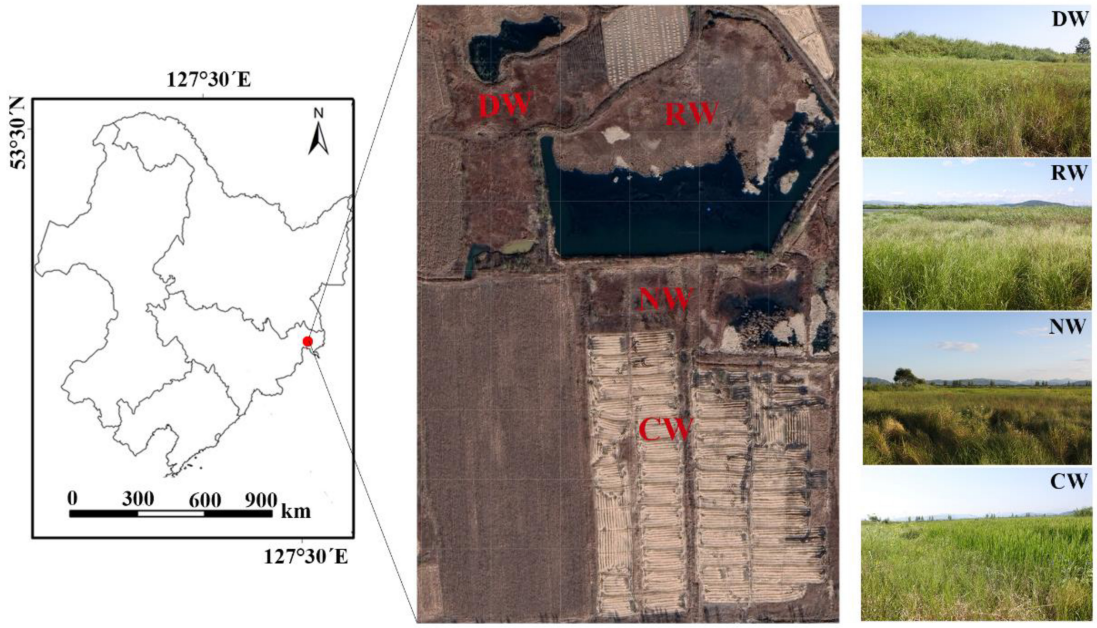


FIGURE 1
Map of the wetland study sites downstream of the Tumen River. RW, reference wetlands; DW, drained wetlands; NW, nutrient-rich wetlands; CW, cultivated wetlands.

Sampling was conducted in early August 2016. In reference, nutrient-rich, and DW, samples were collected along two transects at equidistant intervals. The length of the transects depended on the diameters of the sites, and three sampling plots were set on each transect, with six replicates for each type of wetland. Soil samples and plants were collected from 1 m × 1 m plots. The soil samples were combined into a composite sample; for the plant samples, five replicates were randomly selected and the plants were divided into leaves, stems, roots, and root hair, and the same plant organ was combined as a composite plant sample within each 1 m × 1 m plot. Since *G. spiculosa* grows only along the boundary of paddy fields, we randomly collected six soil and plant samples along the paddy fields as described above. Both soil and plant samples were frozen in ice and transported for analysis to the laboratory of Yanbian University.

Following air-drying and grinding of soil samples, soil samples (0.4 g) were digested with catalysts (1.8 g, potassium sulfate: copper sulfate pentahydrate: selenium = 100:10:1) and 4 ml sulfuric acid (400°C, 2–3 h) and the digests were diluted with distilled water (100 ml) and measured using a continuous flow analyzer (SAN + + , Skalar, Breda, Netherlands) (Wang et al., 2019). The soil N and P were extracted by 2 M potassium chloride and 0.5 M sodium bicarbonate (pH = 8), respectively. The soil N and P concentrations in all extractions were determined using a continuous flow analyzer (SAN + + , Skalar, Breda, Netherlands). The plant organs were oven-dried at 65°C for 48 h and subsequently ground to measure the N and P concentrations. Subsamples of organ samples (0.1 g) were digested with hydrogen peroxide and sulfuric acid. The extracted solutions were used for the measurement of plant N and P concentrations using a continuous flow analyzer (SAN + + , Skalar, The Netherlands).

## Statistical analysis

One-way analysis of variance (ANOVA) was used to test the effects of the agricultural intervention on the N and P content of the soil and plant, coupled with Duncan's test for significance ($p < 0.05$). Similarly, we compared the percentages of N and P in each organ under different agricultural interventions. A linear regression model was carried out to determine the effects of soil N and P on plant organ N and P content values. All statistical analyses were performed using R 4.1.2 (R Core Team, 2019).

# Results

## Soil properties between wetland types

The average soil total nitrogen (TN) content in the RW was 4.05 mg/g, which was similar to the value in DW, but was significantly lower than the value of 6.56 mg/g observed in NW ($p < 0.05$, **Figure 2A**). The soil total phosphorus content (TP) was similar between reference and DW, which were both significantly lower than the average content values

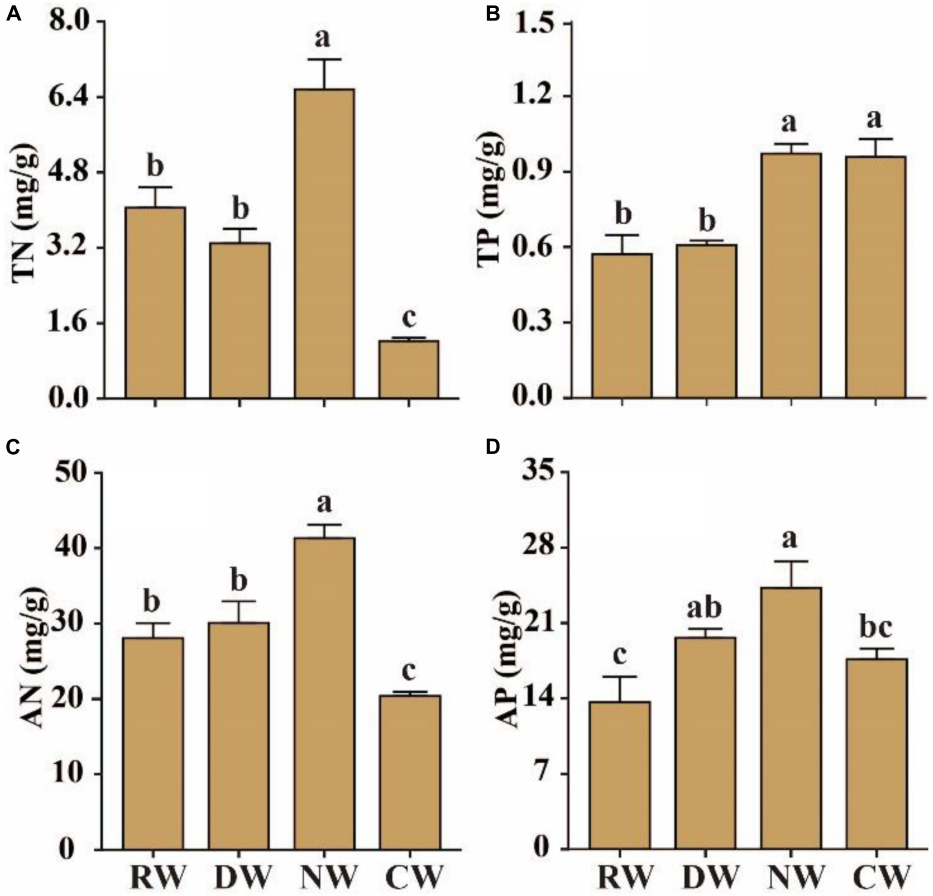


FIGURE 2
Effects of agricultural intervention on soil properties. **(A)** Soil total nitrogen (TN); **(B)** soil total phosphorus (TP); **(C)** soil available nitrogen (AN); **(D)** soil available phosphorus (AP). RW, reference wetlands; DW, drained wetlands; NW, nutrient-rich wetlands; CW, cultivated wetlands. Error bars represent ± SE. Different letters indicate significant differences ($p < 0.05$).

of 0.96 mg/g and 0.97 mg/g in nutrient-rich and cultivated wetlands, respectively ($p < 0.05$, Figure 2B). The average soil available nitrogen content was 28.07 mg/kg, with the maximum value of 41.32 mg/kg recorded in NW and a value of 30.07 mg/kg recorded in DW (Figure 2C). Similarly, the soil available P in RW was 13.64 mg/kg, which was significantly lower than the values in drained and NW ($p < 0.05$, Figure 2D).

## Nitrogen and phosphorus levels in plant organs

In RW, N values in plant leaves, stems, roots, and root hair averaged 12.19, 6.65, 5.41, and 4.87 mg/kg, respectively, and were higher by 76, 61, 56, and 39% in NW, respectively ($p < 0.05$, Figures 3A–D). While the average N content values of root and root hair in DW were 9.07 and 7.12 mg/kg, these values were also significantly higher than those in RW ($p < 0.05$, Figures 3A–D). Plant leaves, stems, roots, and root hair in RW had average P content values of 1.50, 1.05, 1.29, and 1.63 mg/kg, respectively. The P content of plant roots in cultivated wetlands and plant stems in DW differed significantly only from the values in RW by 58 and 33%, respectively ($p < 0.05$, Figures 3E–H).

## Nitrogen and phosphorus stoichiometry in plant organs

The average leaf N:P ratio in RW was 8.12, while the maximum value of 13.42 was observed in NW, followed by similar ratios of 10.34 and 10.27 in cultivated and DW, respectively (Figure 3I). In the DW, the average stem N:P ratio was 6.02, similar to the average ratio of 6.41 in the RW, while that in cultivated wetlands was significantly lower, but was higher by 46% in the NW ($p < 0.05$, Figure 3J). The root and root hair N:P ratio remained constant under different intervention conditions (Figures 3K,L).

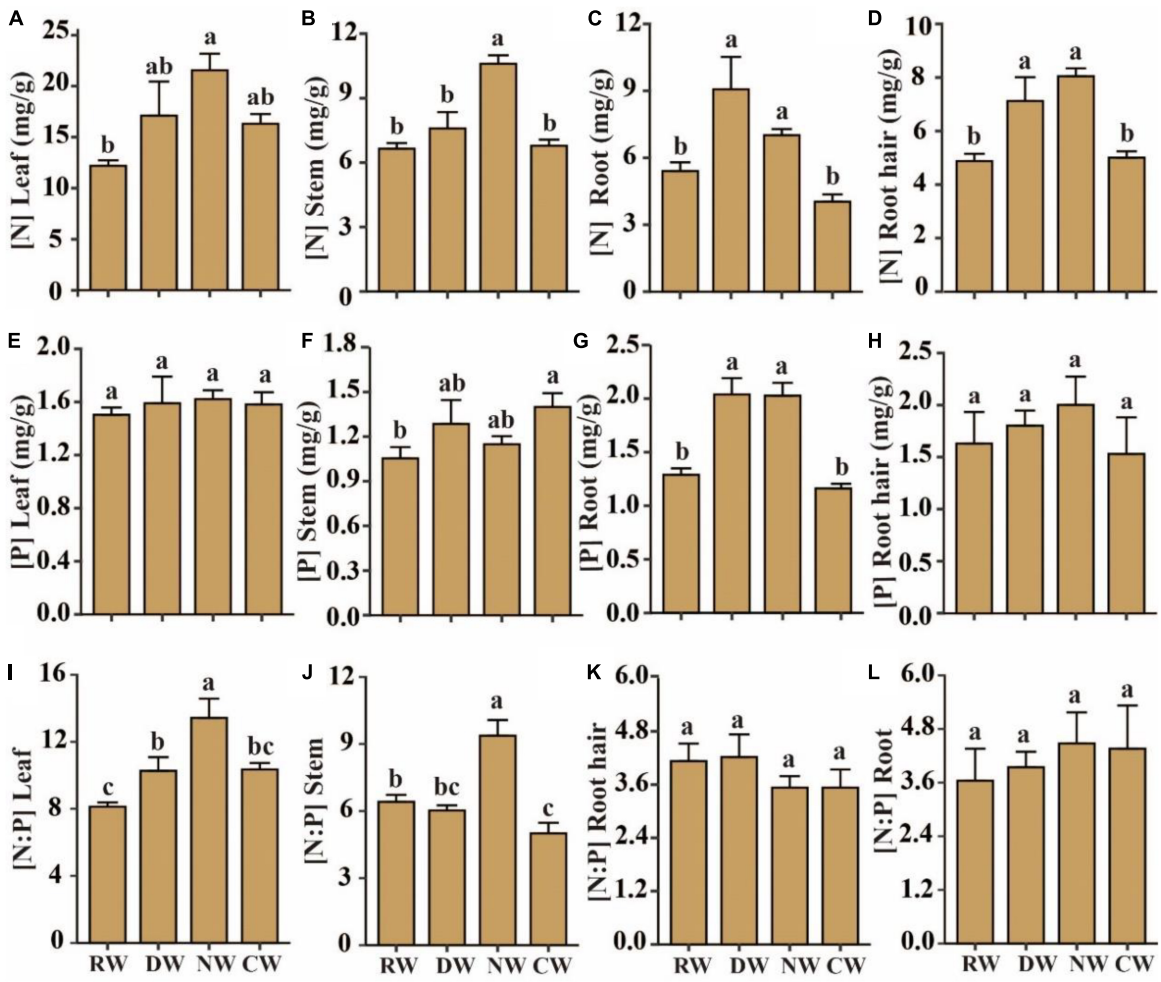


FIGURE 3
Effects of agricultural intervention on N and P stoichiometry of plant tissues. **(A–D)** Plant tissue N content; **(E–H)** plant tissue P content; **(I–L)** plant tissue N and P stoichiometry. RW, reference wetlands; DW, drained wetlands; NW, nutrient-rich wetlands; CW, cultivated wetlands. Error bars represent ± SE. Different letters indicate significant differences between sites ($p < 0.05$).

## The relationship between soil nutrients and plant organ nitrogen or phosphorus content

Soil available N and P positively influenced N content values in plant root hair, roots, stems, and leaves, with the maximum effects observed on leaf N, which showed the highest correlation with leaf N ($p < 0.05$, **Figures 4A–H**). Soil available N and P were found to positively influence root P content and had no influence on the other organs ($p < 0.05$, **Figures 4I–P**).

# Discussion

While the nutrient content of natural wetlands is determined by groundwater and rainfall, chemical fertilizers used during agricultural development possibly influenced the nutrient composition (Craft and Richardson, 1993). The nutrient loading not only enhances nutrient availability but also facilitates the accumulation of nutrients (Li et al., 2019). The findings of these studies are consistent with our results that TN, TP, and available N and P in the wetlands which exchange flow frequently with paddy (NW) were significantly higher than that in natural wetlands (**Figures 2A,B**). Although the content values of TN and TP in DW were similar to those in natural wetlands, available P significantly increased (**Figure 2D**). This is mainly because drainage increases soil oxygen availability, potentially accelerating soil nutrient cycling and influencing nutrient availability (Laiho et al., 1999). In cultivated wetlands, TN decreased significantly, while TP increased significantly (**Figures 2A–D**). Previously, it has been shown that changes in soil physical factors, water conditions, and nutrient levels contribute to N mineralization (Laiho et al., 1999; Raiesi, 2006;

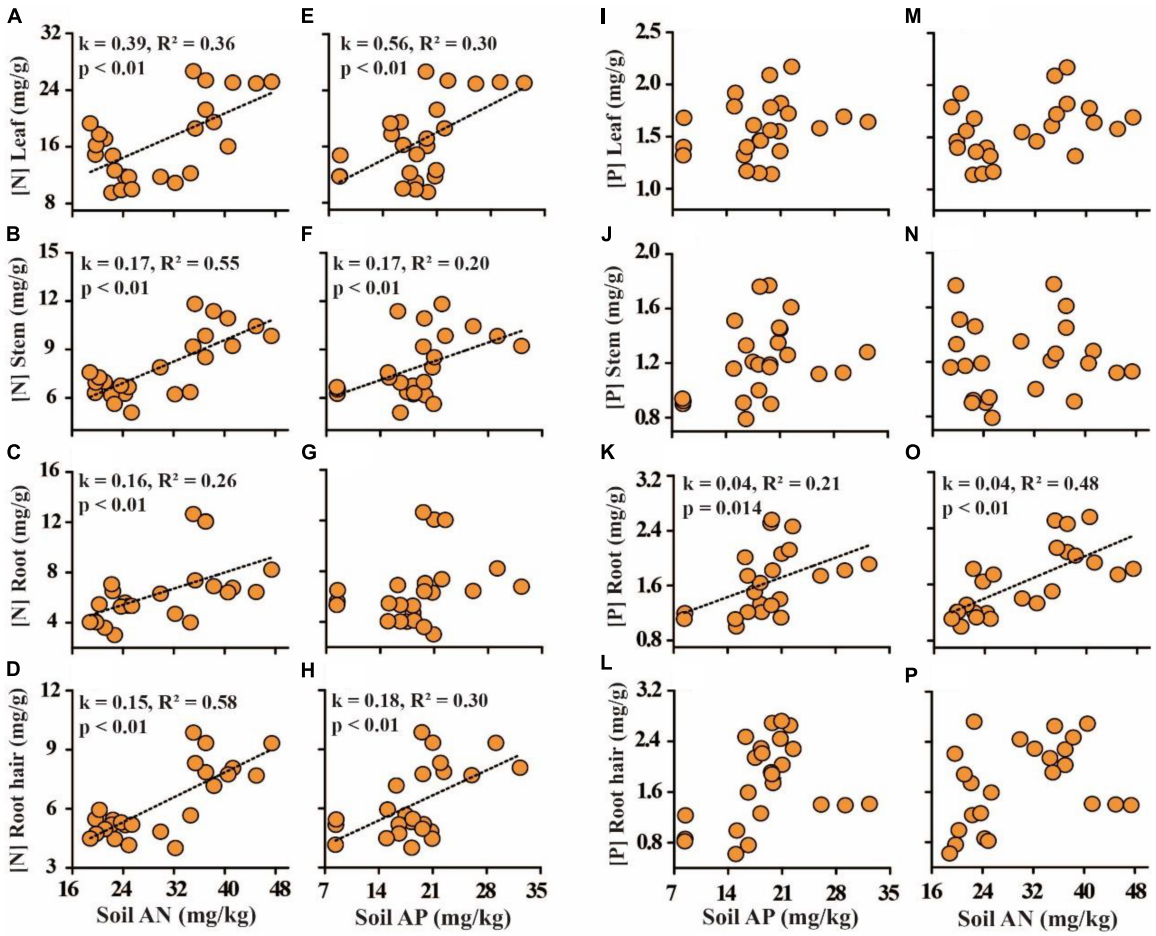


FIGURE 4
The relationship between soil nutrient availability on the N and P of plant tissues. **(A–D)** Soil available nitrogen (AN) and plant tissue N; **(E–H)** soil available phosphorus (AP) and plant tissue P; **(I–L)** soil AP and plant tissue P; **(M–P)** soil AN and plant tissue P.

Wang et al., 2017). On the other hand, P cycling differs from N cycling since it does not involve atmospheric recharge, therefore soil P stocks are determined by P input and export with the flow (Nesme et al., 2018). Furthermore, soil minerals including Fe and Al oxidases have a strong adsorption capacity for orthophosphate ions (Negassa and Leinweber, 2009), which could possibly increase P retention in cultivated wetlands.

Plants often trade off nutrient allocation and environmental changes for growth and reproduction (Zhang et al., 2021). Our results showed that the N content values in plant leaves, stems, roots, and root hair in NW were significantly higher than those in the RW (**Figures 3A–D**). Interestingly, the N content values in leaves, roots, and root hair were similar to those in nutrient-rich and DW. This may be explained by the complementarity of environmental elements (nutrients vs. hydrology). Lower water levels reduce plant above- and below-ground biomass and inhibit plant height, leaf area, and root length (Bai et al., 2021). Declining biomass production and accumulation increase the relative content values of organ nutrients based on a fundamental trade-off in plant functioning between the rapid production of biomass and efficient conservation of nutrients (Garnier et al., 2001). In DW, microbial biomass and activity increased the coupling of nutrient mineralization. This is consistent with the findings of Brown et al. (2017) that draining significantly increased nitrification and P mineralization. In the cultivated wetlands, the leaf N content was similar to that in the RW, but the N content values in the stem, root, and root hair were significantly lower (**Figures 3A–D**). N and P availability in the study wetlands were lower than those in the RW (**Figure 2**), however, long-term agricultural fertilizer application possibly compensates for the plant's nutrient requirements. Furthermore, long-term cultivation also reduces soil organic matter, thereby affecting plant nutrient uptake and utilization (Seiter and Horwath, 2004). Soil N and P availability showed strong positive effects on plant organ N, especially on plant leaf N in this study (**Figures 4A–H**). N is essential for photosynthetic C fixation and biomass accumulation in plants (Staswick, 1994), and adding N

increases plant nitrate concentration (Güsewell, 2004; Esmeijer-Liu et al., 2009; Mao et al., 2014). The addition of P to plants also improves their capacity to absorb dissolved organic nitrogen in cold and nutrient-limited conditions (Feller et al., 2003; Mao et al., 2016).

Phosphorus is the second most essential element after nitrogen for the synthesis of nucleic acids and is a component of the adenosine phosphates, which play a key role in the transfer of energy (Elser et al., 1996). Despite different agricultural interventions, P levels in leaves, stems, and root hair remained similar (**Figures 3E–H**). The amount of root P in nutrient-rich and DW was significantly higher than that in agricultural and RW. As roots are the primary organs responsible for nutrient storage, they may have a strong capacity to retain phosphorus. In addition, our results showed a positive relationship between N and P availability and root P concentration in plants (**Figures 4I–P**). Plants have evolved a P economy when nutrient availability is limited, and they conserve nutrients through the resorption of nutrients from senescing to new leaves or storage in the roots (Rejmánková and Snyder, 2008). Plant P resorption efficiency can reach approximately 52% (Aerts, 1996; Huang et al., 2021). On the other hand, plants can acquire P by secreting hydrolytic enzymes such as phosphates, which could promote organic P mineralization (Rejmánková and Snyder, 2008). Plants can also reduce phosphate secretion when soil P availability increases (Olander and Vitousek, 2000).

N:P ratios reflect plant nutrient demand, which is a critical indicator to determine population size, stability, and organization (Koerselman and Meuleman, 1996). We found that the responses of the N:P ratios in plant organs varied significantly from roots to leaves (**Figures 3I–L**), which did not support the hypothesis that agricultural disturbance may have weak effects on the N:P ratios in plant organs. Both the root and root hair showed little variation in the N:P ratio under agricultural intervention, however, the N:P ratios of leaves and stems were higher in NW than that in the other sites (**Figures 3I–L**). Roots are important sources of energy storage, so they typically maintain a constant variation ratio in their functionality (Rejmánková and Snyder, 2008). Despite the fact that the aboveground biomass is often reduced in DW, the N:P ratio in the leaf is maintained to meet its photosynthesis requirements for growth and reproduction (Staswick, 1994). A mass N:P ratio of less than 14 or greater than 16 indicates N or P limitation, respectively, and a value between 14 and 16 indicates N and P co-limitation (Koerselman and Meuleman, 1996). In this study, the N:P ratio was less than 14 in all wetlands, indicating that N had a determinant effect on *G. spiculosa*, and high nutrient levels also increased its requirement for nutrients. Interestingly, cultivation and drainage had similar effects on plant leaf N:P ratios, which were higher than those of the RW (**Figures 3I–L**). These findings indicate that plants exhibit high plasticity and subsequent self-regulation strategies under agricultural disturbances (Weiner, 2004).

Overall, the results of this study show that agricultural interventions significantly altered the N levels and nutrient stoichiometry of *G. spiculosa*, particularly in the leaves. Soil N and P availability co-influenced plant N levels, and *G. spiculosa* showed relatively high plasticity in mediating its nutrient stoichiometry in the plant organs under different agricultural interventions. In addition, roots are the most important organs for nutrient acquisition, storage, and transformation. Although their nutrient levels fluctuate with soil nutrient levels, they maintain a constant N to P ratio throughout, highlighting the plasticity of the roots as well as the importance of nutrient stoichiometry from root to leaf.

## Data availability statement

The raw data supporting the conclusions of this article will be made available by the authors, without undue reservation.

## Author contributions

TW, QL, and ZW contributed to the conception and design of the study. TW and QL performed the statistical analysis and wrote the first draft of the manuscript. ZD, CG, and XW contributed to manuscript revision. All authors contributed to the article and read and approved the submitted version.

## Acknowledgments

We acknowledge the funders of this study; the National Natural Science Foundation of China (41830643 and 42101114) and the China Postdoctoral Science Foundation (2021M703199). We thank two reviewers, Abel B. Ahungu, and Wang Guodong for their valuable suggestions.

## Conflict of interest

The authors declare that the research was conducted in the absence of any commercial or financial relationships that could be construed as a potential conflict of interest.

## Publisher's note

# References


Aerts, R. (1996). Nutrient resorption from senescing leaves of perennials: Are there general patterns? *J. Ecol.* 84, 597–608. doi: 10.2307/2261481

Aerts, R., and Chapin, F. S. (1999). The mineral nutrition of wild plants revisited: A re-evaluation of processes and patterns. *Adv. Ecol. Res.* 30, 1–67. doi: 10.1016/S0065-2504(08)60016-1

Alvarez-Clare, S., and Mack, M. C. (2015). Do foliar, litter, and root nitrogen and phosphorus concentrations reflect nutrient limitation in a lowland tropical wet forest? *PLoS One* 10:e0123796. doi: 10.1371/journal.pone.0123796

Bai, J. S., Tang, H. R., Chen, F. Y., and Lou, Y. J. (2021). Functional traits response to flooding depth and nitrogen supply in the helophyte *Glyceria spiculosa* (Gramineae). *Aquat. Bot.* 175:103449.

Bedford, B. L., Walbridge, M. R., and Aldous, A. (1999). Patterns in nutrient availability and plant diversity of temperate North American wetlands. *Ecology* 80, 2151–2169. doi: 10.2307/176900

Brown, R. L., Hangs, R., Schoenau, J., and Bedard-Haughn, A. (2017). Soil nitrogen and phosphorus dynamics and uptake by wheat grown in drained prairie soils under three moisture scenarios. *Soil Sci. Soc. Am. J.* 81, 1496–1504. doi: 10.2136/sssaj2017.01.0036

Craft, C. B., and Richardson, C. J. (1993). Peat accretion and N, P, and organic C accumulation in nutrient-enriched and unenriched everglades peatlands. *Ecol. Appl.* 3, 446–458. doi: 10.2307/1941914

Di Palo, F., and Fornara, D. A. (2017). Plant and soil nutrient stoichiometry along primary ecological successions: Is there any link? *PLoS One* 12:e0182569. doi: 10.1371/journal.pone.0182569

Elser, J. J., Dobberfuhl, D. R., MacKay, N. A., and Schampel, J. H. (1996). Organism size, life history, and N:P stoichiometry. *Bioscience* 46, 674–684. doi: 10.2307/1312897

Esmeijer-Liu, A. J., Aerts, R., Kurschner, W. M., Bobbink, R., Lotter, A. F., and Verhoeven, J. T. A. (2009). Nitrogen enrichment lowers *Betula pendula* green and yellow leaf stoichiometry irrespective of effects of elevated carbon dioxide. *Plant Soil* 316, 311–322. doi: 10.1007/s11104-008-9783-1

Feller, I. C., McKee, K. L., Whigham, D. F., and O'Neill, J. P. (2003). Nitrogen vs. phosphorus limitation across an ecotonal gradient in a mangrove forest. *Biogeochemistry* 62, 145–175. doi: 10.1023/A:1021166010892

Garnier, E., Laurent, G., Bellmann, A., Debain, S., Berthelier, P., Ducout, B., et al. (2001). Consistency of species ranking based on functional leaf traits. *New Phytol.* 152, 69–83. doi: 10.1046/j.0028-646x.2001.00239.x

Guiz, J., Hillebrand, H., Borer, E. T., Abbas, M., Ebeling, A., Weigelt, A., et al. (2016). Long-term effects of plant diversity and composition on plant stoichiometry. *Oikos* 125, 613–621. doi: 10.1111/oik.02504

Güsewell, S. (2004). N:P ratios in terrestrial plants: Variation and functional significance. *New Phytol.* 164, 243–266. doi: 10.1111/j.1469-8137.2004.01192.x

Huang, Y., Lou, C., Luo, L., and Wang, X. C. (2021). Insight into nitrogen and phosphorus coupling effects on mixotrophic *Chlorella vulgaris* growth under stably controlled nutrient conditions. *Sci. Total Environ.* 752:141747. doi: 10.1016/j.scitotenv.2020.141747

Koerselman, W., and Meuleman, A. F. M. (1996). The vegetation N:P ratio: A new tool to detect the nature of nutrient limitation. *J. Appl. Ecol.* 33, 1441–1450. doi: 10.2307/2404783

Kramer-Walter, K. R., Bellingham, P. J., Millar, T. R., Smissen, R. D., Richardson, S. J., Laughlin, D. C., et al. (2016). Root traits are multidimensional: Specific root length is independent from root tissue density and the plant economic spectrum. *J. Ecol.* 104, 1299–1310. doi: 10.1111/1365-2745.12562

Laiho, R., Sallantaus, T., and Laine, J. (1999). The effect of forestry drainage on vertical distributions of major plant nutrients in peat soils. *Plant Soil* 207, 169–181. doi: 10.1023/A:1026470212735

Li, F., Hu, J. Y., Xie, Y. H., Yang, G. S., Hu, C., Chen, X. S., et al. (2018). Foliar stoichiometry of carbon, nitrogen, and phosphorus in wetland sedge *Carex brevicuspis* along a small-scale elevation gradient. *Ecol. Indic.* 92, 322–329. doi: 10.1016/j.ecolind.2017.04.059

Li, T., Bu, Z. J., Liu, W. Y., Zhang, M. Y., Peng, C. H., Zhu, Q. A., et al. (2019). Weakening of the 'enzymatic latch' mechanism following long-term fertilization in a minerotrophic peatland. *Soil Biol. Biochem.* 136:107528.

Luo, W. B., Xie, Y. H., Chen, X. S., Li, F., and Qin, X. Y. (2010). Competition and facilitation in three marsh plants in response to a water-level gradient. *Wetlands* 30, 525–530. doi: 10.1007/s13157-010-0064-4

Mao, R., Chen, H. M., Zhang, X. H., Shi, F. X., and Song, C. C. (2016). Effects of P addition on plant C:N:P stoichiometry in an N-limited temperate wetland of Northeast China. *Sci. Total Environ.* 559, 1–6. doi: 10.1016/j.scitotenv.2016.03.158

Mao, R., Zhang, X. H., and Song, C. C. (2014). Effects of nitrogen addition on plant functional traits in freshwater wetland of Sanjiang Plain, Northeast China. *Chin. Geogr. Sci.* 24, 674–681. doi: 10.1007/s11769-014-0691-4

Moor, H., Rydin, H., Hylander, K., Nilsson, M. B., Lindborg, R., and Norberg, J. (2017). Towards a trait-based ecology of wetland vegetation. *J. Ecol.* 105, 1623–1635. doi: 10.1111/1365-2745.12734

Negassa, W., and Leinweber, P. (2009). How does the Hedley sequential phosphorus fractionation reflect impacts of land use and management on soil phosphorus: A review. *J. Plant Nutr. Soil Sci.* 172, 305–325. doi: 10.1002/jpln.200800223

Nesme, T., Metson, G. S., and Bennett, E. M. (2018). Global phosphorus flows through agricultural trade. *Glob. Environ. Chang.* 50, 133–141. doi: 10.1016/j.gloenvcha.2018.04.004

Olander, L. P., and Vitousek, P. M. (2000). Regulation of soil phosphatase and chitinase activity by N and P availability. *Biogeochemistry* 49, 175–191. doi: 10.1023/a:1006316117817

Qin, L., Freeman, C., Jia, X. Y., Zhang, Z. S., Liu, B., Zhang, S. Q., et al. (2021). Microbial enzyme activity and stoichiometry signal the effects of agricultural intervention on nutrient cycling in peatlands. *Ecol. Indic.* 122:107242.

R Core Team (2019). *R: A language and environment for statistical computing*. Vienna: R Foundation for Statistical Computing.

Raiesi, F. (2006). Carbon and N mineralization as affected by soil cultivation and crop residue in a calcareous wetland ecosystem in Central Iran. *Agric. Ecosyst. Environ.* 112, 13–20. doi: 10.1016/j.agee.2005.07.002

Rejmánková, E., and Snyder, J. M. (2008). Emergent macrophytes in phosphorus limited marshes: Do phosphorus usage strategies change after nutrient addition? *Plant Soil* 313, 141–153. doi: 10.1007/s11104-008-9687-0

Seiter, S., and Horwath, W. R. (2004). "Strategies for managing soil organic matter to supply plant nutrients,"in *Soil organic matter in sustainable agriculture*, eds F. Magdoff and R. Weil (Boca Raton, FL: CRC Press), 269–293. doi: 10.1201/9780203496374.ch9

Staswick, P. E. (1994). Storage proteins of vegetative plant tissues. *Annu. Rev. Plant Physiol. Plant Mol. Biol.* 45, 303–322. doi: 10.1146/annurev.pp.45.060194.001511

Sterner, R. W., and Elser, J. J. (2003). *Ecological stoichiometry: The biology of elements from molecules to the biosphere*. Princeton, NJ: Princeton University Press. doi: 10.1515/9781400885695

Wang, G., Otte, M. L., Jiang, M., Wang, M., Yuan, Y., and Xue, Z. (2019). Does the element composition of soils of restored wetlands resemble natural wetlands? *Geoderma* 351, 174–179. doi: 10.1016/j.geoderma.2019.05.032

Wang, Z. C., Liu, S. S., Huang, C., Liu, Y. Y., and Bu, Z. J. (2017). Impact of land use change on profile distributions of organic carbon fractions in peat and mineral soils in Northeast China. *Catena* 152, 1–8. doi: 10.1016/j.catena.2016.12.022

Weiner, J. (2004). Allocation, plasticity and allometry in plants. *Perspect. Plant Ecol.* 6, 207–215. doi: 10.1078/1433-8319-00083

Yu, Q., Wilcox, K., La Pierre, K., Knapp, A. K., Han, X., and Smith, M. D. (2015). Stoichiometric homeostasis predicts plant species dominance, temporal stability, and responses to global change. *Ecology* 96, 2328–2335. doi: 10.1890/14-1897.1

Zedler, J. B., and Kercher, S. (2005). Wetland resources: Status, trends, ecosystem services, and restorability. *Annu. Rev. Environ. Resour.* 30, 39–74. doi: 10.1146/annurev.energy.30.050504.144248

Zhang, D. J., Qi, Q., Tong, S. Z., Wang, J., Zhang, M. Y., Zhu, G. L., et al. (2021). Effect of hydrological fluctuation on nutrient stoichiometry and trade-offs of *Carex schmidtii*. *Ecol. Indic.* 120:106924.

Zheng, X. J., Sun, P., Zhu, W. H., Xu, Z., Fu, J., Man, W. D., et al. (2017). Landscape dynamics and driving forces of wetlands in the Tumen River Basin of China over the past 50 years. *Landsc. Ecol. Eng.* 13, 237–250. doi: 10.1007/s11355-016-0304-8

frontiers | Frontiers in Ecology and Evolution

TYPE Original Research
PUBLISHED 10 August 2022
DOI 10.3389/fevo.2022.979194



OPEN ACCESS

EDITED BY
Chuanyu Gao,
Northeast Institute of Geography and Agroecology (CAS), China

REVIEWED BY
Yonghong Xie,
Key Laboratory of Agro-Ecological Processes in Subtropical Region, Institute of Subtropical Agriculture (CAS), China
Junhong Bai,
Beijing Normal University, China

*CORRESPONDENCE
Jisong Yang
yangjisong@ldu.edu.cn
Junbao Yu
yu.junbao@gmail.com

SPECIALTY SECTION
This article was submitted to Conservation and Restoration Ecology, a section of the journal Frontiers in Ecology and Evolution

RECEIVED 27 June 2022
ACCEPTED 08 July 2022
PUBLISHED 10 August 2022

CITATION
Liu X, Sun D, Qin J, Zhang J, Yang Y, Yang J, Wang Z, Zhou D, Li Y, Wang X, Ning K and Yu J (2022) Spatial distribution of soil iron across different plant communities along a hydrological gradient in the Yellow River Estuary wetland. *Front. Ecol. Evol.* 10:979194. doi: 10.3389/fevo.2022.979194



# Spatial distribution of soil iron across different plant communities along a hydrological gradient in the Yellow River Estuary wetland

Xue Liu[1], Dandan Sun[1], Jifa Qin[1], Jiapeng Zhang[1], Yunfei Yang[1], Jisong Yang[1,2]*, Zhikang Wang[1], Di Zhou[1], Yunzhao Li[1], Xuehong Wang[1], Kai Ning[2] and Junbao Yu[1]*

[1]The Institute for Advanced Study of Coastal Ecology, Ludong University, Yantai, China, [2]Dongying Academy of Agricultural Sciences, Dongying, China

Iron is an important element and its biogeochemical processes are vital to the matter and energy cycles of wetland ecosystems. Hydrology greatly controls characteristics of soil property and plant community in wetlands, which can regulate the behavior of iron and its oxides. However, it remains unclear how the spatial distribution of iron and its forms in estuarine wetlands responses to hydrological conditions. Five typical plant communities along a naturally hydrological gradient in the Yellow River Estuary wetland, including *Phragmites australis* in freshwater marsh (FPA), *Phragmites australis* in salt marsh (SPA), *Tamarix chinensis* in salt marsh (TC), *Suaeda salsa* in salt marsh (SS) and *Spartina alterniflora* in salt marsh (SA), as sites to collect soil samples. The total iron ($Fe_T$) and three iron oxides (complexed iron, $Fe_p$; amorphous iron, $Fe_o$; free iron, $Fe_d$) in samples were determined to clarify the spatial distribution of iron and explore its impact factors. The mean contents of $Fe_T$, $Fe_p$, $Fe_o$ and $Fe_d$ were 28079.4, 152.0, 617.2 and 8285.3 $mg{\cdot}kg^{-1}$ of soil at 0–40 cm depth in the different sites, respectively. The means were significantly different across communities along the hydrological gradient, with the higher values for SA on the upper intertidal zone and for SPA on the lower intertidal zone, respectively. Iron and its forms were positively correlated with the total organic carbon (TOC), dissolved organic carbon (DOC), total nitrogen (TN) and clay, and negatively correlated with electrical conductivity (EC). The indexes of iron oxides ($Fe_p/Fe_d$, $Fe_o/Fe_d$ and $Fe_d/Fe_T$) were also different across communities, with a higher value for SA, which were positively correlated with soil water content (WC) and TOC. The results indicate that a variety of plant community and soil property derived from the difference of hydrology might result in a spatial heterogeneity of iron in estuarine wetlands.

KEYWORDS

**iron oxide, spatial distribution, community type, impact factor, estuarine wetland**

## Introduction

Estuarine wetlands are located in the interaction between water and land ecosystems (Jiang et al., 2006), which are generated by the deposition of sediment carried by rivers into the sea. They play a vital role in maintaining biodiversity, protecting estuarine coastline and regulating climate (Barbier et al., 2011; Jiang et al., 2020). Estuarine wetlands are also one of the important carriers for biogeochemical processes of iron (Fe), sulfur (S), carbon (C), nitrogen (N), phosphorus (P) and so on (Telfeyan et al., 2017; Luo et al., 2019; Lu et al., 2020a). As the fourth abundant element in the earth crust, iron is one of the major redox materials in soil, which is widely distributed in the forms of iron oxide (Weaver and Tarney, 1984). Iron (hydr-)oxides, the main existing forms in soil, are a part of soil colloid, which play an important role in the formation of soil aggregates. The quantities of iron oxides reflect the process and environment of soil-developing (Molina et al., 2001), regulating the nutrient cycles in soil. The redox reaction of iron can affect the decomposition of soil organic matter and the adsorption or transformation of heavy metals in wetland soils (Fimmen et al., 2008; Zhang et al., 2009). Thus, the oxidation/reduction of iron is vital to matter and energy cycles of wetland ecosystems. It's necessary to better understand the importance of iron behaviors for the biogeochemical processes of relevant elements.

Iron oxides in soil consist of the four forms: exchangeable iron, complexed iron ($Fe_p$), amorphous iron ($Fe_o$), free iron ($Fe_d$). Exchangeable iron oxide is abundant in acid soil, while the content in alkaline and neutral soil is less than 1mg $kg^{-1}$, which is difficult to determine (Zhou and Shen, 2013). $Fe_d$ has a high activity of migration and transformation, and the percentage of $Fe_d$ in $Fe_T$ is called the free degree of iron ($Fe_d/Fe_T \times 100\%$), which can reflect the weathering degree of soil (He and Chen, 1983). $Fe_o$ represents amorphous or weakly crystalline iron oxides, which is one of the most easily utilized forms by plant. As an electron acceptor for iron-reducing microorganisms, it can promote the oxidative decomposition of organic matter (Hori et al., 2010; Yu et al., 2021). The percentage of $Fe_o$ in $Fe_d$ (activation degree: $Fe_o/Fe_d \times 100\%$) can determine the genesis characteristics of soil, reflecting the influence of environment on soil developing. $Fe_p$ belongs to amorphous iron oxides, and its formation process is important for iron ion migration in soil, which is important for the soil fertility (He and Chen, 1983; Tipping et al., 2002). The percentage of $Fe_p$ in $Fe_d$ (complexation degree: $Fe_p/Fe_d \times 100\%$) is important for immobility of soil organic matter. Compared with $Fe_p$ and $Fe_d$, $Fe_o$ has a large specific surface area, high adsorption and low crystallinity, which is easily utilized by iron-reducing microorganisms and can be reduced quickly (Hyacinthe et al., 2006).

Iron and its oxides in wetland soils can be influenced by biotic and abiotic factors, e.g., hydrological condition, soil property, microbes and vegetation type (Kappler et al., 2004; Zou et al., 2011; Karimian et al., 2018). The redox status in wetland soil depends on hydrological condition, which regulates the oxidation/reduction reaction of iron (Zhang and Furman, 2021). Under reduction conditions, iron exists as dissolved $Fe^{2+}$ and has a strong mobility, while the protection of organic matter can promote the stability of iron complexes; under oxidation conditions, iron can exist as $Fe^{3+}$ and is easily formed to insoluble iron (hydr-)oxides, which would decrease iron migration and transformation in sediments (Melton et al., 2014; Jiang et al., 2019). The pH can affect the redox status, microbial activity and soil adsorption capacity, regulating the transformation and availability of iron in wetland soils (Johnston et al., 2014; Ye et al., 2022). Soil organic matter dynamics is closely related to the biogeochemical cycles of iron, and the reduction rate of Fe(III) will be greatly improved in tidal flat sediments rich in organic matter (Santos-Echeandia et al., 2010; Lalonde et al., 2012). Soil salinity level determines the ionic strength to some extends, which may affect the transformation of iron oxides in salt marshes by regulating the turnover of soil organic carbon and exchange capacity of cations (Williams et al., 1994; Laing et al., 2007; Qu et al., 2018). Due to a high activity of roots, rhizosphere as an important micro-zone in soil is different from the surrounding soil in physical, chemical and biological characteristics, consequently resulting in an acceleration of iron cycles (Adejumo et al., 2018; Zhai et al., 2018).

The Yellow River Estuary wetland is the most complete, broadest and youngest wetland ecosystem in the warm temperate zone of China. There is a naturally hydrological gradient from the riverside to the coast, where various plant communities and soil properties develop on the different micro-topographies. Thus, it is expected to be heterogeneous for soil iron and its forms in the Yellow River Estuary wetland (Zhang et al., 2017). However, it remains unclear how the spatial distribution of iron and its forms in estuarine wetlands responses to hydrological conditions. In the present study, we selected five communities along a hydrological gradient in the Yellow River Estuary wetland to clarify the spatial distribution of iron and explore its impact factors. Our hypotheses are 1) there would be a significantly spatial heterogeneity of iron and its oxides along a hydrological gradient, and 2) the iron distribution could be related to soil property under different hydrological conditions.

## Materials and methods

### Study area

The Yellow River Estuary wetland (37°40′–38°10′N, 118°41′–119°16′E) is located in the western bank of Bohai Sea. It is an important migration transfer station and winter habitat for birds. The wetland is a flat and wide marine sedimentary plain. The soil is mainly meadow soil and salt marsh soil. The area belongs a warm temperate continental monsoon

and has the climatic characteristics of the same rain-heat season and dry-cold season. The annual average temperature is 12.1°C, and the annual average precipitation is 552.6 mm, most of which is concentrated in summer. The annual average evapotranspiration is 1928.2 mm, which is more threefold than the annual precipitation (Cui et al., 2009). The dominant vegetation types are *P. australis*, *T. chinensis*, *S. salsa*, and *S. alterniflora*, in which *P. australis*, *S. salsa* and *S. alterniflora* are widely distributed.

## Study sites and soil sampling

Along a naturally hydrological gradient from the northern side of the Yellow River to the coast, five typical plant communities were selected as sampling sites in turn (**Figure 1**), including *P. australis* in freshwater marsh (FPA), *P. australis* in salt marsh (SPA), *T. chinensis* in salt marsh (TC), *S. salsa* in salt marsh (SS) and *S. alterniflora* in salt marsh (SA), with three repeated samples in each site. The five sites have obviously different hydrological conditions (**Figure 2**). FPA site is located on the riverside of the supratidal zone and is almost unaffected by tides, with sources of river water or/and rainfall and seasonal flooding; SPA site is located on the upper edge of the intertidal zone near the supratidal zone, with a similar hydrological characteristic as FPA, but influenced by extreme tide events; TC site is located on the upper intertidal zone and the surface is occasionally flooded; SS and SA sites are on the middle intertidal zone and the lower intertidal zone, respectively, and the surface is periodic flooded.

In September 2020, soil samples at the depths of 0–10, 10–20, 20–30, and 30–40 cm were collected from the sites using a drill of stainless steel. The subsamples were immediately sealed in an icebox filled $N_2$ to determine iron oxides. The other subsamples were dried in air to determine soil physicochemical properties, including water content (WC), pH, electrical conductivity (EC), total organic carbon (TOC), dissolved organic carbon (DOC), total nitrogen (TN) and total sulfur (TS). Soil properties were shown in **Table 1**.

## Sample measurement

The contents of $Fe_T$ in soil samples were determined using a mothed of phenanthroline - spectrophotometry. Briefly, 0.25 g of dried soil samples were placed in 30 mL polytetrafluoroethylene crucibles and 2–3 drops of water were added to wet samples, followed by addition of 4 mL hydrofluoric acid, 5 mL nitric acid and 0.5 mL perchloric acid. The samples were heated at 300°C until perchlorate acid fumes were thoroughly exhausted. The residues in the crucibles were dissolved with 1 mL hydrochloric acid (1:1), moved into 50 mL colorimetric tubes, colored for 2 h by phenanthroline reagents, and determined the concentrations of $Fe_T$ at 510 nm using the spectrophotometry (TU-1810DS, China).

The $Fe_p$, $Fe_o$ and $Fe_d$ in the soils were continuously extracted with alkaline sodium pyrophosphate, acid ammonium oxalate and sodium dithionite - sodium citrate - sodium bicarbonate (DCB), respectively (Weiss et al., 2004). Briefly, 1.0 g of wet soil samples and 20 mL 0.1 M sodium pyrophosphate were placed in 50 mL centrifuge tubes under the $N_2$ condition. After suspension solutions were shocked for 2 h and centrifugated for 10 min, the supernatants were transferred into 50 mL colorimetric tubes, added 5 drops of sulfuric acid (1:1) and 2 drops of 5% potassium permanganate, and kept for a night. The residues were added 40 mL acid ammonium oxalate (0.14 M oxalate acid and 0.2 M ammonium oxalate), shaken in dark for 4 h and centrifugated for 10 min, followed by extracting 5 mL of supernatants. The residues were added 20 mL 1 M sodium citrate and 2.5 mL 1 M sodium bicarbonate, heated for 15 min in water bath at 80°C, and oscillated with addition of 0.5 g sodium hydrosulfite. Then, the suspension solutions were shocked for 2 h and centrifugated for 10 min again, and the supernatants of 5 mL were taken into 50 mL colorimetrical tubes. The extracted solutions of $Fe_p$, $Fe_o$, and $Fe_d$ were colored for 24, 12 and 2 h by phenanthroline reagents, respectively, and determined iron concentrations at 510 nm using spectrophotometry.

Iron is calculated as below:

$$Fe_T = \frac{x \times V \times a}{m} \quad (1)$$

$$Fe_y = \frac{x_y \times V \times a \times 1.43}{m} \quad (2)$$

Where $Fe_T$ and $Fe_y$ are content of iron and oxides in the soil ($mg{\cdot}kg^{-1}$), $x$ and $x_y$ are concentrations of iron and oxides in the solution ($mg{\cdot}L^{-1}$), $V$ is volume of the solution (L), $a$ is dilution multiple of the solution, $m$ is weight of dried soil sample (kg) and *1.43* is the coefficient of conversion.

The content of TOC was determined by high-temperature external thermal potassium dichromate oxidation method. The content of DOC was determined by TOC analyzer (Elementar, Germany). The content of TN was determined by continuous flow analyzer (Futura, France). The content of TS was determined by magnesium nitrate oxidation - barium sulfate turbidimetric method. Soil pH (water:soil = 5:1) was determined by pH meter. Soil EC (water:soil = 5:1) was determined by conductivity meter. Soil particle (clay: < 4 μm; silt: 4–63 μm; sand: 64–2,000 μm) was determined by laser particle size analyzer (Mastersizer 3000, England) after pretreatment with hydrogen peroxide and hydrochloric acid.

## Statistical analysis

General linear model (GLM) was used to test the effect of community and soil depth on the contents of iron ($p < 0.05$).

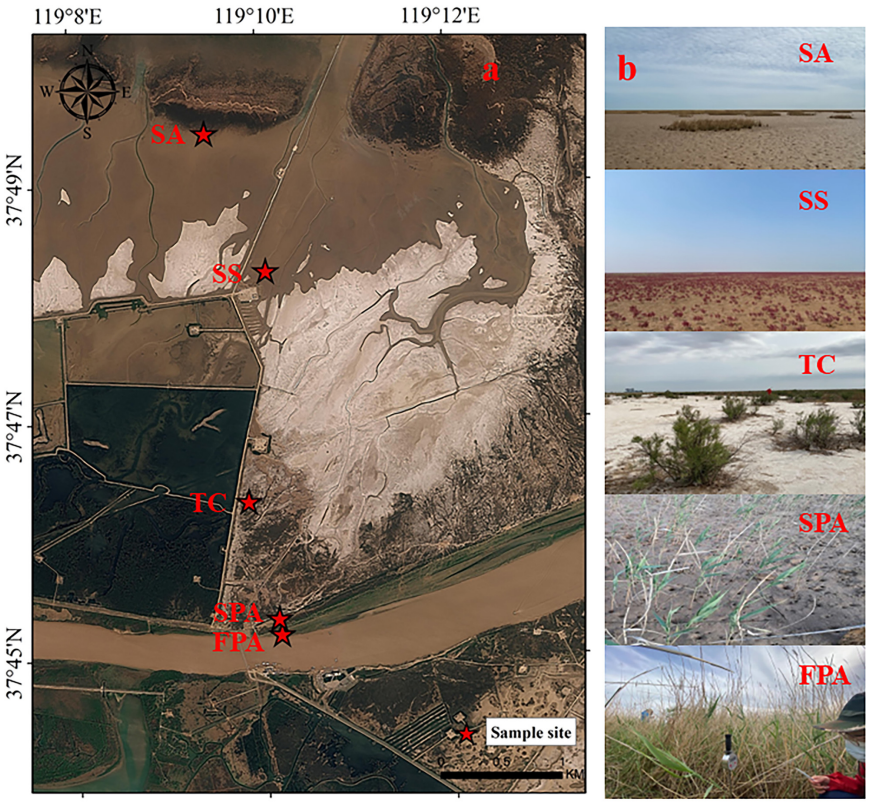


FIGURE 1
The sample sites **(a)** and plant communities **(b)** in the study area. FPA, *P. australis* in freshwater marsh; SPA, *P. australis* in salt marsh; TC, *T. chinensis* in salt marsh; SS, *S. salsa* in salt marsh; SA, *S. alterniflora* in salt marsh.

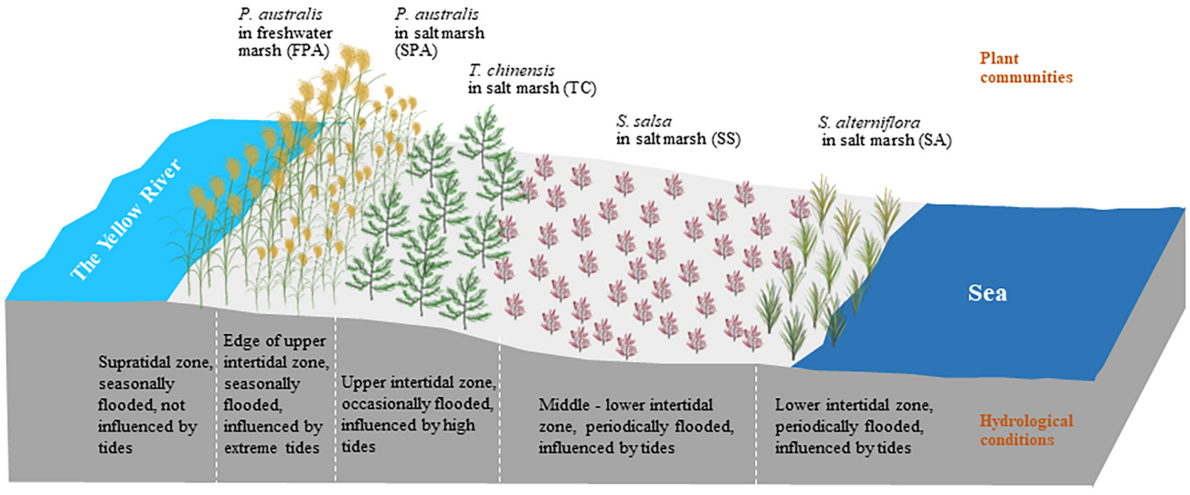


FIGURE 2
Schematic diagram of the hydrological conditions for different plant communities.

TABLE 1 Soil properties in the different communities.

| Community type | Soil depth | EC mS·cm$^{-1}$ | WC % | pH | TOC g·kg$^{-1}$ | DOC mg·kg$^{-1}$ | TN g·kg$^{-1}$ | TS mg·kg$^{-1}$ | Clay % |
|---|---|---|---|---|---|---|---|---|---|
| FPA | 0–10 cm | 0.15 ± 0.021 | 40.38 ± 0.15 | 6.41 ± 0.12 | 3.54 ± 0.21 | 77.00 ± 24.00 | 0.32 ± 0.001 | 79.18 ± 2.91 | 5.92 ± 0.34 |
| | 10–20 cm | 0.14 ± 0.042 | 40.00 ± 1.21 | 6.60 ± 0.06 | 3.56 ± 0.13 | 116.15 ± 1.80 | 0.32 ± 0.006 | 91.54 ± 2.91 | 4.14 ± 0.17 |
| | 20–30 cm | 0.17 ± 0.007 | 28.17 ± 3.15 | 6.73 ± 0.17 | 3.96 ± 0.11 | 118.76 ± 27.70 | 0.32 ± 0.007 | 93.60 ± 2.91 | 5.03 ± 0.00 |
| | 30–40 cm | 0.22 ± 0.014 | 45.45 ± 3.01 | 6.73 ± 0.14 | 3.28 ± 0.07 | 181.41 ± 9.20 | 0.38 ± 0.143 | 212.05 ± 18.94 | 8.72 ± 0.56 |
| SPA | 0–10 cm | 1.18 ± 0.050 | 25.93 ± 0.52 | 7.24 ± 0.23 | 10.41 ± 0.39 | 203.59 ± 7.30 | 0.44 ± 0.014 | 679.67 ± 77.20 | 13.66 ± 044 |
| | 10–20 cm | 1.30 ± 0.085 | 26.83 ± 0.63 | 7.60 ± 0.10 | 19.58 ± 0.29 | 366.73 ± 9.20 | 0.97 ± 0.004 | 527.23 ± 27.68 | 16.88 ± 1.08 |
| | 20–30 cm | 1.77 ± 0.021 | 48.48 ± 5.12 | 7.80 ± 0.01 | 7.53 ± 0.28 | 170.97 ± 9.20 | 0.30 ± 0.010 | 434.53 ± 13.11 | 13.29 ± 2.14 |
| | 30–40 cm | 2.00 ± 0.001 | 37.84 ± 0.78 | 7.88 ± 0.00 | 9.45 ± 0.39 | 198.37 ± 7.40 | 0.45 ± 0.133 | 429.38 ± 87.40 | 25.33 ± 2.35 |
| TC | 0–10 cm | 9.67 ± 0.849 | 20.34 ± 1.11 | 7.80 ± 0.16 | 5.71 ± 0.04 | 160.53 ± 5.50 | 0.28 ± 0.001 | 853.74 ± 58.27 | 7.63 ± 0.27 |
| | 10–20 cm | 6.50 ± 0.092 | 27.91 ± 0.03 | 7.85 ± 0.15 | 5.02 ± 0.11 | 154.00 ± 11.10 | 0.29 ± 0.001 | 476.76 ± 34.96 | 6.12 ± 0.01 |
| | 20–30 cm | 3.48 ± 0.001 | 23.26 ± 0.18 | 7.77 ± 0.21 | 3.77 ± 0.11 | 113.54 ± 1.80 | 0.30 ± 0.001 | 405.69 ± 30.59 | 7.70 ± 0.57 |
| | 30–40 cm | 3.87 ± 0.001 | 31.37 ± 0.99 | 7.93 ± 0.26 | 5.17 ± 0.14 | 151.39 ± 7.40 | 0.29 ± 0.001 | 541.65 ± 85.94 | 12.63 ± 0.34 |
| SS | 0–10 cm | 3.79 ± 0.247 | 36.96 ± 4.21 | 8.08 ± 0.01 | 4.78 ± 0.23 | 118.76 ± 5.50 | 0.34 ± 0.069 | 773.40 ± 40.79 | 14.71 ± 1.39 |
| | 10–20 cm | 2.22 ± 0.001 | 34.21 ± 0.89 | 8.42 ± 0.13 | 4.67 ± 0.34 | 130.51 ± 9.50 | 0.29 ± 0.002 | 485.00 ± 2.91 | 15.41 ± 0.99 |
| | 20–30 cm | 2.71 ± 0.021 | 30.43 ± 1.54 | 8.35 ± 0.13 | 4.15 ± 0.04 | 118.76 ± 16.60 | 0.29 ± 0.005 | 556.07 ± 85.94 | 17.29 ± 2.12 |
| | 30–40 cm | 3.78 ± 0.001 | 36.84 ± 1.99 | 8.28 ± 0.14 | 4.53 ± 0.25 | 134.42 ± 42.50 | 0.28 ± 0.002 | 720.87 ± 129.64 | 17.12 ± 0.75 |
| SA | 0–10 cm | 2.99 ± 0.007 | 48.08 ± 0.68 | 8.40 ± 0.11 | 15.19 ± 0.14 | 191.85 ± 20.30 | 0.54 ± 0.272 | 794.00 ± 2.91 | 20.01 ± 0.01 |
| | 10–20 cm | 2.35 ± 0.113 | 39.47 ± 3.65 | 8.44 ± 0.00 | 14.01 ± 0.09 | 168.36 ± 1.80 | 0.36 ± 0.162 | 700.27 ± 18.94 | 17.56 ± 0.33 |
| | 20–30 cm | 3.47 ± 0.184 | 48.84 ± 3.10 | 8.28 ± 0.16 | 8.18 ± 0.10 | 151.39 ± 3.70 | 0.32 ± 0.004 | 671.43 ± 16.02 | 23.28 ± 3.01 |
| | 30–40 cm | 2.97 ± 0.587 | 51.28 ± 4.01 | 8.25 ± 0.06 | 9.83 ± 0.28 | 261.02 ± 7.40 | 0.31 ± 0.002 | 623.02 ± 34.96 | 19.64 ± 0.95 |
| Differences across communities (0–40 cm) | | FPA $^{a}$ | FPA $^{ab}$ | FPA $^{a}$ | FPA $^{a}$ | FPA $^{a}$ | FPA $^{ab}$ | FPA $^{a}$ | FPA $^{a}$ |
| | | SPA $^{ab}$ | SPA $^{bc}$ | SPA $^{b}$ | SPA $^{b}$ | SPA $^{b}$ | SPA $^{a}$ | SPA $^{b}$ | SPA $^{b}$ |
| | | TC $^{c}$ | TC $^{c}$ | TC $^{b}$ | TC $^{a}$ | TC $^{a}$ | TC $^{b}$ | TC $^{b}$ | TC $^{a}$ |
| | | SS $^{b}$ | SS $^{bc}$ | SS $^{c}$ | SS $^{a}$ | SS $^{a}$ | SS $^{b}$ | SS $^{b}$ | SS $^{b}$ |
| | | SA $^{b}$ | SA $^{ad}$ | SA $^{c}$ | SA $^{b}$ | SA $^{ab}$ | SA $^{ab}$ | SA $^{b}$ | SA $^{b}$ |
| *p* | | <0.001 | 0.008 | <0.001 | 0.002 | 0.027 | 0.130 | <0.001 | <0.001 |

EC, electrical conductivity; WC, water content; TOC, total organic carbon; DOC, dissolved organic carbon; TN, total nitrogen; TS, total sulfur, respectively. The different lower case letters represent a significant difference ($p < 0.05$).





10.3389/fevo.2022.979194

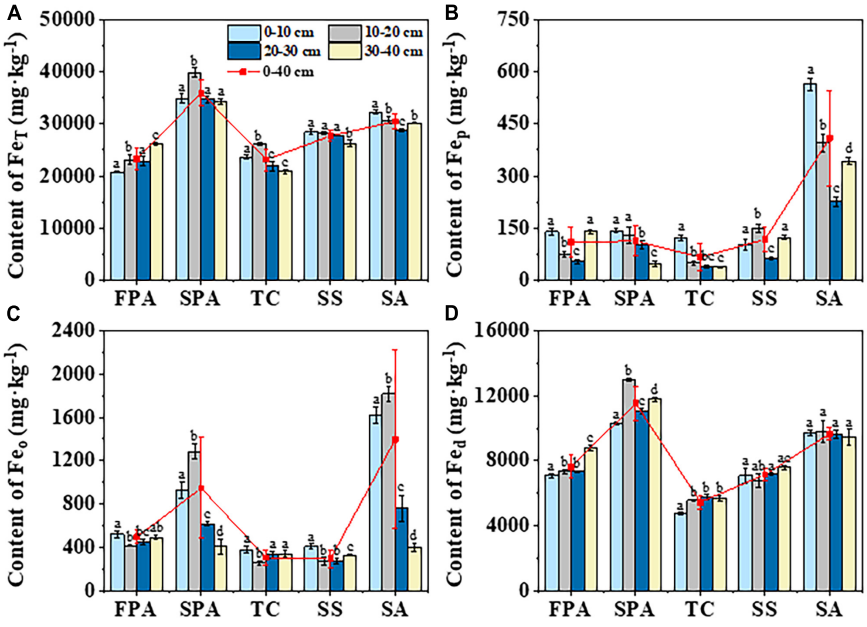


FIGURE 3
Distribution characteristics of $Fe_T$ **(A)**, $Fe_p$ **(B)**, $Fe_o$ **(C)** and $Fe_d$ **(D)** in soils of different communities. $Fe_T$, total iron; $Fe_p$, complexed iron; $Fe_o$, amorphous iron; $Fe_d$, free iron. Lower letters represent significant differences across depths of the same site ($p < 0.05$).

TABLE 2 Effects of community, soil depth as well as the interaction effects on iron based on general linear model (GLM) at $\alpha = 0.05$.

| Item | df | | $Fe_T$ | $Fe^{2+}$ | $Fe_p$ | $Fe_o$ | $Fe_d$ | $Fe_p/Fe_d$ | $Fe_o/Fe_d$ | $Fe_d/Fe_T$ |
|---|---|---|---|---|---|---|---|---|---|---|
| $R^2$ | | | 0.99 | 0.99 | 0.99 | 0.99 | 0.99 | 0.99 | 0.98 | 0.93 |
| Community type(CT) | 4 | *F* | 1018.9 | 6882.1 | 1404.9 | 617.6 | 951.2 | 793.8 | 317.2 | 151.4 |
| | | *p* | <0.001 | <0.001 | <0.001 | <0.001 | <0.001 | <0.001 | <0.001 | <0.001 |
| Soil depth(SD) | 3 | *F* | 48.1 | 915.2 | 247.6 | 255.6 | 31.7 | 264.5 | 247.1 | 25.7 |
| | | *p* | <0.001 | <0.001 | <0.001 | <0.001 | <0.001 | <0.001 | <0.001 | <0.001 |
| CT × SD | 12 | *F* | 32.4 | 331.1 | 75.7 | 121.8 | 16.4 | 52.8 | 92.0 | 7.1 |
| | | *p* | <0.001 | <0.001 | <0.001 | <0.001 | <0.001 | <0.001 | <0.001 | <0.001 |

$Fe_p$, complexed iron; $Fe_o$, amorphous iron; $Fe_d$, free iron; $Fe_T$, total iron, respectively.

The one-way ANOVA with LSD ($p < 0.05$) was used to test the differences in the content of iron and soil depth among the different community types. Origin 2019b was used to determine correlations between the contents of iron and soil properties ($p < 0.05$).

# Results

## Distribution characteristics of $Fe_T$ in the different communities

The mean contents of $Fe_T$ in soils at 0–40 cm depth across the different communities of FPA, SPA, TC, SS and SA were 23212.0, 35926.4, 23113.4, 27682.3 and 30462.7 mg·kg$^{-1}$, respectively, with a higher value in SPA and a lower in TC (Figure 3A). There was an increasing trend with soil depth in FPA, a decreasing trend in SS and SA, and a higher value at the 10–20 cm depth in SPA and TC. Overall, the $Fe_T$ contents were significantly different across the different communities ($p$<0.001) and soil depths ($p$<0.001) (Table 2).

## Distribution characteristics of iron oxides in the different communities

The mean contents of $Fe_p$, $Fe_o$ and $Fe_d$ ranged from 37.2 to 563.9, from 277.1 to 1814.9 and from 4768.2 to 12986.2 mg·kg$^{-1}$ in soils at 0–40 cm depth across the different communities, respectively (Figures 3B–D). The values were higher in SA or SPA and lower in TC. At the soil depth, the higher values of $Fe_p$ and $Fe_o$ were determined in the upper soil layers (0–10 cm

and 10–20 cm), and the higher value of $Fe_d$ was determined in the lower soil layers (30–40 cm). Overall, there were significant differences across communities ($p < 0.001$) and soil depths ($p<0.001$) (Table 2).

The complexation degree of iron oxide ($Fe_p/Fe_d$) in soils at 0–40 cm depth across the five communities were 1.3, 0.9, 1.2, 1.5, and 4.0%, respectively, with a higher value in SA and a lower in SS (Figure 4A). The corresponding values for activity degree of iron oxide ($Fe_o/Fe_d$) were 6.2, 7.0, 6.1, 4.5, and 11.8%, respectively, with a higher value in SA and a lower in SPA (Figure 4B). On the whole, the complexation degree and activity degree of the upper soil layers was higher than that of the lower soil layers. The free degree of iron oxide ($Fe_d/Fe_T$) were 32.9, 32.1, 23.9, 25.9, and 31.8%, respectively, with a higher value in FPA and a lower in TC (Figure 4C), and the values were higher in the lower soil layers than those in the upper soil layers. Overall, there were significant differences across communities ($p < 0.001$) and soil depths ($p < 0.001$) (Table 2).

## Correlations between the contents of iron and soil properties

The mean contents of pH, EC, TOC, DOC, TN, and TS of soil at 0–40 cm depth were 7.74, 2.67 $mS{\cdot}cm^{-1}$, 7.48 $g{\cdot}kg^{-1}$, 167.38 $mg{\cdot}kg^{-1}$, 0.37 $g{\cdot}kg^{-1}$, and 273.66 $mg{\cdot}kg^{-1}$ in FPA, SPA, TC, SS, and SA, respectively (Table 1). The values of pH, EC, TOC, DOC and TS were significantly different across communities ($p < 0.05$). The clay in soils accounted for 4.14–25.33%, which were significantly different across communities ($p < 0.05$).

$Fe_T$ was positively correlated with TOC, DOC, TN, TS, and clay (Figure 5); $Fe_p$ was positively correlated with TOC, WC and clay; $Fe_o$ was positively correlated with TOC, TN, and DOC; $Fe_d$ was positively correlated with TOC, DOC, TN and clay, and negatively correlated with EC. Overall, the contents of iron and its oxides were closely related to organic carbon, nitrogen and soil texture. $Fe_p/Fe_d$ was positively correlated with WC and TOC; $Fe_o/Fe_d$ was positively correlated with TOC; $Fe_d/Fe_T$ was positively correlated with WC, and negatively correlated with EC.

# Discussion

Iron and its oxides in wetland soil would be different in regions due to variously environmental and climate conditions (Jiang et al., 2011). The contents of $Fe_T$ in some wetland soils have reported in the previous studies, e.g., 22018.5–27551.9 $mg{\cdot}kg^{-1}$ in mangrove sediment of Manukau Harbour, New Zealand (Bastakoti et al., 2019); 27780–29700 $mg{\cdot}kg^{-1}$ in Jiaozhou Bay coastal wetland, China (Yan et al., 2020); approximately 13067.0 $mg{\cdot}kg^{-1}$ in Sanjiang Plain wetland, China (Huo et al., 2011). In the present study, the means of $Fe_T$ were 20732.3–39879.3 $mg{\cdot}kg^{-1}$ in the Yellow River Estuary wetland soil, with a higher value compared with those in other wetlands. The possible explanation is that the alluvial deposition of sediment carried by the Yellow River leads to the accumulation of abundant iron-bearing minerals in the delta. In the last 70 years, the annual amount of sediment transported from the Yellow River to the Bohai Sea is approximately $6.62 \times 10^8$ t (Wang et al., 2021a), and the mean concentration of iron in suspended sediments is 41.3 $mg{\cdot}kg^{-1}$, approximately accounting for $2.7 \times 10^4$ t iron transported to sea annually (Yao et al., 2015). Additionally, the Yellow River Delta is a new-born wetland and soil has a lower degree of soil weathering ($Fe_d/Fe_T$: 20.2–34.3%), which can be beneficial to the enrichment of mineral elements (Liu et al., 2019).

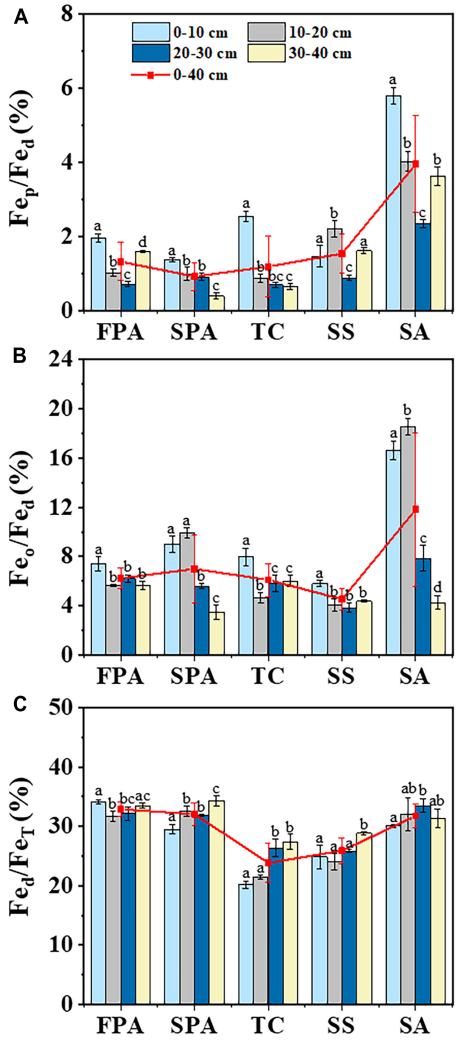


FIGURE 4
Distribution characteristics of iron oxide complexation degree **(A)**, activity degree **(B)** and free degree **(C)** in soils of different communities.

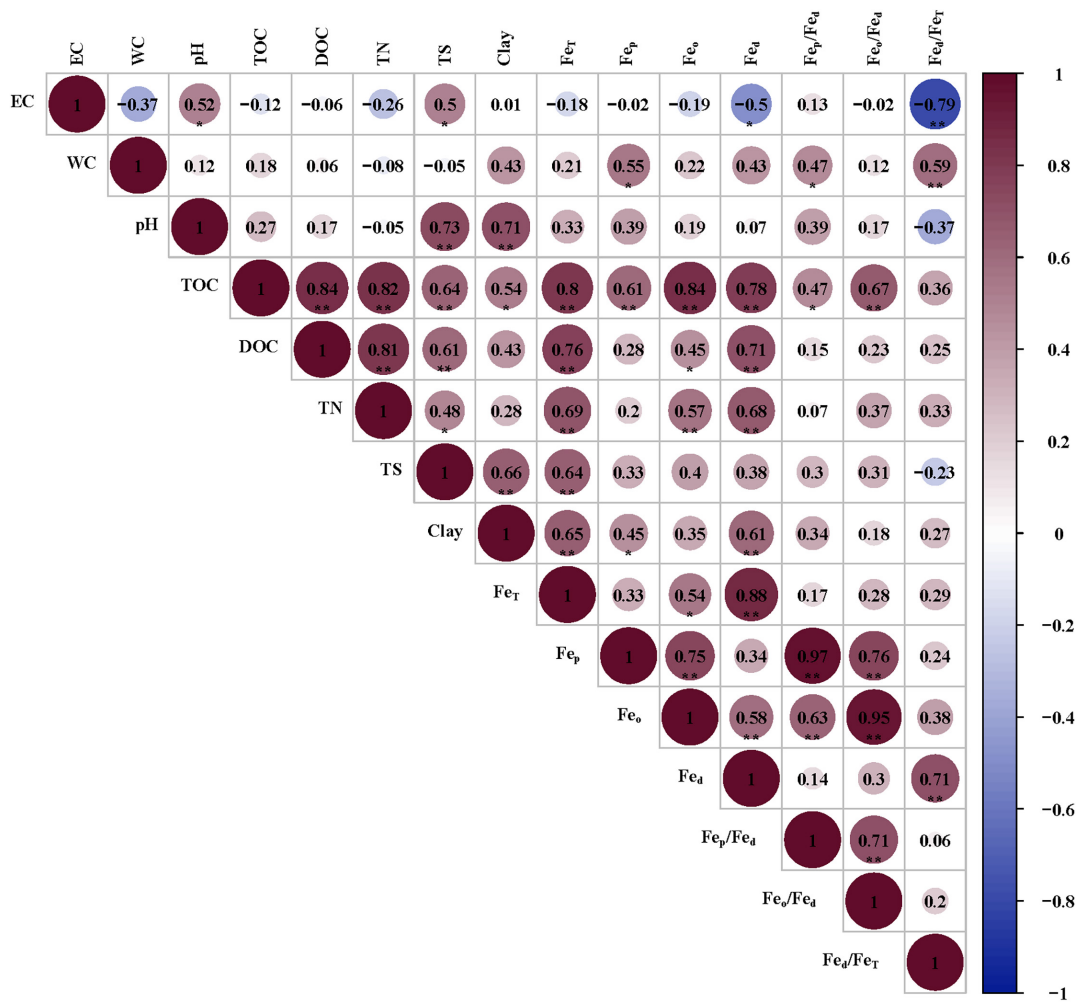


FIGURE 5
Correlations between iron and factors in soils of different communities. EC, WC, TOC, DOC, TN, and TS represent electrical conductivity, water content, total organic carbon, dissolved organic carbon, total nitrogen, total sulfur, respectively. * and ** represent a significant difference at the level of 0.05 and 0.01, respectively.

The distribution of iron and its oxides in wetland soil are controlled by biotic and abiotic factors, such as hydrologic condition, soil properties, vegetation, microbial community and so on (Hoang et al., 2018; Richir et al., 2020; Sui et al., 2021). In the present study, there were significant differences in iron and its oxides across communities. The contents of $Fe_T$, $Fe_o$, and $Fe_d$ were higher in SA and SPA, and $Fe_p$ was higher in SA (**Figure 3**), indicating that iron distribution can be controlled by vegetation with different hydrologic conditions. Previous studies demonstrated that hydrologic condition can regulate processes of deposition and transformation in wetlands through changing hydrodynamic and aerobic/anoxic conditions, which would control the stability of organic matter and the immobility of iron ions and oxides in soil (Calabrese and Porporato, 2019; Calabrese et al., 2020). SA is on the lower intertidal zoon and *S. alterniflora* is an invasive plant in the coastal wetland of the Yellow River Estuary, with a total area of 4406.95 $hm^2$ (Li Y. R. et al., 2021). It develops quickly and has well developed roots (Wan et al., 2014), which can reduce wave erosion and increase sediment accumulation (Wang et al., 2022), resulting in a high input and deposition of iron in the soil. FPA is on the riverside where the sediment carried by floods of the Yellow River deposits, leading to a large amount of iron accumulation. SPA is on the edge of the intertidal zone near the supratidal zone, and the hydrologic condition is only controlled by extreme tide events and river floods, resulting in less frequent and depth of flooding compared with other sites. Iron in soil of SPA might be inclined to form iron (hydr-)oxides (e.g., α-FeOOH, α-$Fe_2O_3$, γ-FeOOH and γ-$Fe_2O_3$) and aggravate the enrichment of iron under the weakly anoxic or aerobic environment (Rezapour et al., 2015). Furthermore, plant may be ascribed to the distribution of iron because plant absorption and litter

decomposition can affect iron migration and return into soil (Lu et al., 2020b). The plants of *S. alterniflora* and *P. australis* have a higher biomass (52.59–247.73 $g{\cdot}m^{-2}$ and 5.92–224.46 $g{\cdot}m^{-2}$) (Xie et al., 2021), meaning more iron absorbed by plant and returned into soil as litter decomposition (Costa et al., 2020). In addition, the iron oxides in the rhizosphere can also be regulated by oxygen transported through the plant stress-resistant tissues (Li C. et al., 2021). The well ventilation tissue and root system of *S. alterniflora* and *P. australis* can function as a great ability of radial oxygen loss, which makes iron oxidized to form iron spots in the rhizosphere (Zhang et al., 2019). The spots are mainly composed of amorphous iron and crystalline iron oxides, which can reduce the mobility of iron and promote the enrichment of iron in wetland soil (Wang and Peverly, 1999).

Estuarine wetlands have a stronger carbon sequestration capacity, which is critical for iron immobility and deposition through iron oxides bound on organic carbon (Yu et al., 2019). Dynamics of soil organic carbon is closely related to biogeochemical cycles of iron in wetlands (Lalonde et al., 2012; Wang et al., 2021b). In the present study, total iron and its oxides in soil were positively correlated with TOC and DOC (**Figure 5**), which is consistent to the results reported by some studies in the estuarine wetlands and paddy field (Wang et al., 2012; Sun et al., 2013; Huang et al., 2020). Previous studies have shown that iron oxides can promote the retention of organic carbon in soil through adsorption, chelation or co-precipitation (Duan et al., 2020; Bai et al., 2021). Weak crystalline and amorphous iron oxides have strong adsorption capacity for organic matter, consequently composing stable organic metal complexes (Rezapour et al., 2010). In the study, the contents of $Fe_o$ in SPA and SA were significantly higher than those in the other vegetation types (**Figure 3C**), which corresponded to higher values of TOC and DOC in the sites. Additionally, microbial-mediated iron reduction can significantly affect organic carbon mineralization and thus carbon cycling (Hussain et al., 2019). In the process, organic carbon can provide energy for iron-reducing bacteria, leading to drive the reduction of Fe(III) and promote the migration of iron ions (Lovley, 1997; Xiao et al., 2019).

The biogeochemical processes of iron in coastal wetland soil can be coupled with nitrogen cycles through surface adsorption of iron oxides and Fe(III) reduction (Zhao et al., 2019). In the present study, $Fe_o$, $Fe_d$ and $Fe_T$ were positively correlated with TN (**Figure 5**). In the Yellow River Estuary wetland, inorganic nitrogen accounted for less than 20% of the total nitrogen (Mu et al., 2012). Iron oxides can promote the stability of organic nitrogen and inhibit the nitrogen mineralization by adsorbing organic matter on the surface (Heng et al., 2010; Liu et al., 2020). However, the microbial reduction of Fe(III) plays an important regulation in the transformation nitrogen. Guan et al. (2018) found that adding Fe(III) oxide has increased $N_2$ production of sediments in the mangrove wetland, suggesting that Fe(III) reduction could promote anaerobic ammonia oxidation and increase nitrogen loss. The result about the positive correlation between iron oxides and TN in our study indicates that surface adsorption of iron oxides but Fe(III) reduction may contribute nitrogen fixation. Moreover, the biogeochemical processes of iron are also closely related with sulfur cycles in coastal wetlands (Burton et al., 2011). In the present study, we found that $Fe_T$ was significantly positively correlated with TS (**Figure 5**). In the coastal wetlands, $H_2S$ can act as a reducing agent for Fe(III) oxides in sulfide-rich environments (Johnston et al., 2014; Sheng et al., 2015; Karimian et al., 2018), and sulfide ($S^{2-}$) reacts with $Fe^{2+}$ to form FeS or $FeS_2$ in the process of sulfate reduction, which could promote iron immobility in the sediment (Schoepfer et al., 2014; Hu et al., 2022). *S. alterniflora* is on the lower tide zone with a higher sulfur content in soil (**Table 1**), possibly ascribed to a higher content of iron oxides due to more iron combining with sulfur to form pyrite. However, FPA is in the freshwater environment with a lower content of sulfur in soil, which may cause less iron combined by sulfur, possibly resulting in more iron loss in the form of dissolved $Fe^{2+}$ and more iron oxides remained in soil.

Soil texture is one of the important factors affecting iron forms, and especially clay can promote the enrichment of iron (Finck, 2020). We found that the contents of soil clay in the Yellow River Estuary wetland ranged from 4.14 to 25.33% (**Table 1**), which were positively correlated with $Fe_T$, $Fe_d$ and $Fe_p$ (**Figure 5**). Clay minerals can be wrapped by Fe/Al oxides to form stable aggregate structure to improve water retention capacity and physical quality of soil (AL-Shamare and Essa, 2021; Bai et al., 2021; Mendes et al., 2022). Moreover, clay minerals can also be combined with soil organic matter to form organic-inorganic complex, leading to a stronger immobility of iron (Zhang et al., 2001; Angst et al., 2021). The salinity reflects the ionic strength in soil and has an important impact on soil properties and the distribution of iron and its oxides (Celik et al., 2021; Ury et al., 2022). Previous studies showed that iron from boreal rivers display a higher resistance toward salinity-induced aggregation, e.g., iron (hydr-)oxides are selectively removed by aggregation processes, and organic iron complexes are less affected by increasing salinity (Herzog et al., 2019). In the present study, iron contents were negatively correlated with EC to some extents (**Figure 5**). Besides FPA, the other four communities were influenced by tides in different intensity (**Figure 2**), and the hydrologic conditions varied with the depth and frequency of tidal flood. Therefore, soil EC in the communities showed a great variety, which may contribute the differentiation of iron oxides in soils. For example, the soil surface in TC was always exposed and submerged only at high tides, which leads to the salt accumulation in soil due to an intense evaporation/transpiration. Consequently, the iron oxides are relatively low under the action of salinity aggregation. However, there was no obviously negative effect of salinity on iron content in FPA, which indicated that the distribution of iron and its oxides in the coastal wetland

soils could be controlled by the interaction of factors. In addition, salinity of coastal wetland soil has an important effect on microbial community and activity by regulating soil extracellular osmotic potential, which can directly or indirectly regulate the transformation and bioavailability of iron (Richard and Frances, 2001; Laing et al., 2007).

The values of $Fe_d/Fe_T$, $Fe_o/Fe_d$ and $Fe_p/Fe_d$ are important indexes which can indicate the degree of soil weathering, which is controlled by environmental conditions (He and Chen, 1983). We found that all the three degrees were different across the communities, with a higher value in the *S. alterniflora* and *P. australis* communities (**Figure 4** and **Table 2**), indicating a well weathering for the soils. In the present study, the values of $Fe_d/Fe_T$ in different communities were negatively correlated with EC and positively correlated with WC, which possibly ascribed to the negatively effects of EC and the positively effects of WC on iron oxides, respectively (**Figure 5**). The values of $Fe_p/Fe_d$ and $Fe_o/Fe_d$ were positively correlated with TOC (**Figure 5**). Organic matter is rich in fulvic acid which can inhibit iron oxides deposition, and thus increases the activation degree of iron oxides (Fan et al., 2016). Free iron oxides are effective adsorbents for multivalence superoxide anions; of them, amorphous iron has a higher affinity for multivalence superoxide anions due to a large specific surface area and a high reactivity of surface functional groups, which has a stronger ability to combined soil organic matter (Zhao et al., 2018). Moreover, free iron oxides are also an important mineral cement in soil, and their decrease may lead to the deterioration of soil structure and aggravate the degradation of soil (Duiker et al., 2003; Zhang et al., 2016). Therefore, free iron oxides can regulate carbon sequestration because they can be combined with organic matter through adsorption/coprecipitation to form a stable Fe-OC complex (Zhang et al., 2012; Zhao et al., 2017). Given that hydrological conditions in the estuarine wetlands would alter with climate change, the iron and its forms could shift accordingly. The result suggests that the carbon sequestration in estuarine wetlands could change with hydrological alteration under climate change.

## Conclusion

In the study, we found that iron and its forms in estuarine wetland soils varied with communities along a hydrological gradient. The contents of iron and its oxides were higher in the *S. alterniflora* and *P. australis* (in the salt marsh) communities, which was positively correlated with soil organic carbon, nitrogen and clay, and negatively correlated with salinity. The weathering indicators were also different across plant communities with a higher free degree in *S. alterniflora* and *P. australis* communities, which was correlated with soil water content, organic matter and salinity. The results indicate that iron and its forms in estuarine wetland soils depends on hydrological conditions, suggesting that high strength of hydrological effects (e.g., frequency and depth of tides or floods) may benefit the iron immobility. The results would be helpful to understand the mechanisms of iron biogeochemistry and explore the coupled cycles of iron with other elements in estuarine wetlands.

## Data availability statement

The original contributions presented in this study are included in the article/supplementary material, further inquiries can be directed to the corresponding authors.

## Author contributions

XL: methodology, validation, and writing – original draft. DS, JQ, JZ, YY, YL, and XW: resources and investigation. JSY: conceptualization, supervision, and writing – review and editing. ZW, DZ, and KN: software and data curation. JBY: formal analysis and validation. All authors contributed to the article and approved the submitted version.

## Funding

This work was supported by the National Natural Science Foundation of China (41871087, U1806218, and 42171111), Yellow River Delta Scholar Talent Project, and the Project of the Cultivation Plan of Superior Discipline Talent Teams of Universities in Shandong Province "The Coastal Resources and Environment Team for Blue-Yellow Area".

## Conflict of interest

The authors declare that the research was conducted in the absence of any commercial or financial relationships that could be construed as a potential conflict of interest.

## Publisher's note

# References

Adejumo, S. A., Tiwari, S., Shinde, V., and Sarangi, B. K. (2018). Heavy metal (Pb) accumulation in metallophytes as influenced by the variations in rhizospheric and non-rhizospheric soils physico-chemical characteristics. *Int. J. Phytoremediation* 20, 237–248. doi: 10.1080/15226514.2017.1374333

AL-Shamare, A. H., and Essa, S. K. (2021). Contribution of clay, silt, organic matter, free iron oxides and active calcium carbonate in cation wxchange capacity in Wasit and Maysan Soils. *Indian J. Ecol.* 48, 61–65.

Angst, G., Pokorn, J., Mueller, C. W., Prater, I., Preusser, S., Kandeler, E., et al. (2021). Soil texture affects the coupling of litter decomposition and soil organic matter formation. *Soil Biol. Biochem.* 159:108302. doi: 10.1016/j.soilbio.2021.108302

Bai, J., Luo, M., Yang, Y., Xiao, S. Y., Zhai, Z. F., and Huang, J. F. (2021). Iron-bound carbon increases along a freshwater-oligohaline gradient in a subtropical tidal wetland. *Soil Biol. Biochem.* 154:108128. doi: 10.1016/j.soilbio.2020.108128

Barbier, E. B., Hacker, S. D., Koch, E. W., Stier, A. C., and Silliman, B. R. (2011). "Estuarine and coastal ecosystems and their services". *Treatise on Estuarine and Coastal Science*, eds E. Wolanski and D. McLusky (Amsterdam: Elsevier Science) 12, 109–127. doi: 10.1016/B978-0-12-374711-2.01206-7

Bastakoti, U., Bourgeois, C., Marchand, C., and Alfaro, A. C. (2019). Urban-rural gradients in the distribution of trace metals in sediments within temperate mangroves (New Zealand). *Mar. Pollut. Bull.* 149:110614. doi: 10.1016/j.marpolbul.2019.110614

Burton, E. D., Bush, R. T., Johnston, S. G., Sullivan, L. A., and Keene, A. F. (2011). Sulfur biogeochemical cycling and novel Fe-S mineralization pathways in a tidally re-flooded wetland. *Geochim. Cosmochim. Acta.* 75, 3434–3451. doi: 10.1016/j.gca.2011.03.020

Calabrese, S., and Porporato, A. (2019). Impact of ecohydrological fluctuations on iron-redox cycling. *Soil Biol. Biochem.* 133, 188–195. doi: 10.1016/j.soilbio.2019.03.013

Calabrese, S., Barcellos, D., Thompson, A. A., and Porporato, A. (2020). Theoretical constraints on Fe reduction rates in upland soils as a function of hydroclimatic conditions. *J. Geophys. Res.* 125, e2020JG005894 doi: 10.1029/2020JG005894

Celik, S., Anderson, C. J., Kalin, L., and Rezaeianzadeh, M. (2021). Long-term salinity, hydrology, and forested wetlands along a tidal freshwater gradient. *Estuaries Coast.* 44, 1816–1830. doi: 10.1007/s12237-021-00911-8

Costa, L., Mirlean, N., Quintana, G., Adebayo, S., and Johannesson, K. (2020). Effects of bioirrigation and salinity on arsenic distributions in ferruginous concretions from salt marsh dediment cores (Southern Brazil). *Aquat. Geochem.* 27, 79–103. doi: 10.1007/s10498-020-09387-7

Cui, B. S., Yang, Q. C., Yang, Z. F., and Zhang, K. J. (2009). Evaluating the ecological performance of wetland restoration in the Yellow River Delta. China. *Ecol. Eng.* 35, 1090–1103. doi: 10.1016/j.ecoleng.2009.03.022

Duan, X., Yu, X. F., Li, Z., Wang, Q. G., Liu, Z. P., and Zou, Y. C. (2020). Iron-bound organic carbon is conserved in the rhizosphere soil of freshwater wetlands. *Soil Biol. Biochem.* 149:107949. doi: 10.1016/j.soilbio.2020.107949

Duiker, S. W., Rhoton, F. E., Torrent, J., Smeck, N. E., and Lal, R. (2003). Iron (hydr) oxide crystallinity effects on soil aggregation. *Soil Sci. Soc. Am. J.* 67, 606–611. doi: 10.2136/sssaj2003.6060

Fan, S. S., Chang, F. H., Hsueh, H. T., and Ko, T. H. (2016). Measurement of total free iron in soils by $H_2S$ chemisorption and comparison with the citrate bicarbonate dithionite method. *J. Anal. Methods Chem.* 2016:7213542. doi: 10.1155/2016/7213542

Fimmen, R. L., Richter, D. D., Vasudevan, D., Williams, M. A., and West, L. T. (2008). Rhizogenic Fe-C redox cycling: a hypothetical biogeochemical mechanism that drives crustal weathering in upland soils. *Biogeochemistry* 87, 127–141. doi: 10.1007/s10533-007-9172-5

Finck, N. (2020). Iron speciation in Opalinus clay minerals. *Appl. Clay Sci.* 193:105679. doi: 10.1016/j.clay.2020.105679

Guan, Q. S., Cao, W. Z., Wang, M., Wu, G. J., Wang, F. F., Jiang, C., et al. (2018). Nitrogen loss through anaerobic ammonium oxidation coupled with iron reduction in a mangrove wetland. *Eur. J. Soil Sci.* 69, 732–741. doi: 10.1111/ejss.12552

He, Q., and Chen, J. F. (1983). Determination of free and complexed iron in soil. *Soil* 15, 242–245. doi: 10.13758/j.cnki.tr.1998.01.001

Heng, L. S., Wang, D. C., Jiang, X., Rao, W., Zhang, W. H., Guo, C. Y., et al. (2010). Relationship between Fe. Al oxides and stable organic carbon, nitrogen in the Yellow-Brown Soils. *Environ. Sci.* 31, 2748–55. doi: 10.13227/j.hjkx.2010.11.040

Herzog, S. D., Conrad, S., Ingri, J., Persson, P., and Kritzberg, E. S. (2019). Spring flood induced shifts in Fe speciation and fate at increased salinity. *Appl. Geochem.* 109:104385. doi: 10.1016/j.apgeochem.2019.104385

Hoang, T. K., Probst, A., Orange, D., Gilbert, F., Elger, A., Kallerhoff, J., et al. (2018). Bioturbation effects on bioaccumulation of cadmium in the wetland plant Typha latifolia: a nature-based experiment. *Sci. Total Environ.* 618, 1284–1297. doi: 10.1016/j.scitotenv.2017.09.237

Hori, T., Müller, A., Igarashi, Y., Conrad, R., and Friedrich, M. W. (2010). Identification of iron-reducing microorganisms in anoxic rice paddy soil by $^{13}$C-acetate probing. *ISME J.* 4, 267–278. doi: 10.1038/ismej.2009.100

Hu, M. J., Sardans, J., Le, Y. X., Yan, R. B., Zhong, Y., and Peñuelas, J. (2022). Effects of wetland types on dynamics and couplings of labile phosphorus, iron and sulfur in coastal wetlands during growing season. *Sci. Total Environ.* 830:154460. doi: 10.1016/j.scitotenv.2022.154460

Huang, X. L., Kang, W. J., Wang, L., Yu, G. H., Ran, W., Hong, J. P., et al. (2020). Preservation of organic carbon promoted by iron redox transformation in a rice-wheat cropping system. *Appl. Soil Ecol.* 147:103425. doi: 10.1016/j.apsoil.2019.103425

Huo, L. L., Lv, X. G., and Zou, Y. C. (2011). Changes of iron in top soil of paddies as affected by reclamation ages in Sanjiang Plain. *Bull. Soil Water Conserv.* 31:5. doi: 10.1016/S1671-2927(11)60313-1

Hussain, S., Zhang, M., Zhu, X. X., Khan, M. H., Li, L. F., and Cao, H. (2019). Significance of Fe(II) and environmental factors on carbon-fixing bacterial community in two paddy soils. *Ecotoxicol. Environ. Saf.* 182:109456. doi: 10.1016/j.ecoenv.2019.109456

Hyacinthe, C., Bonneville, S., and Cappellen, P. V. (2006). Reactive iron(III) in sediments: chemical versus microbial extractions. *Geochim. Cosmochim. Acta* 70, 4166–4180. doi: 10.1016/j.gca.2006.05.018

Jiang, M., Lu, X. G., Wang, H. Q., Zou, Y. C., and Wu, H. T. (2011). Transfer and transformation of soil iron and implications for hydrogeomorpholocial changes in Naoli River catchment. Sanjiang Plain, northeast China. *Chin. Geogr. Sci.* 21, 149–158. doi: 10.1007/s11769-011-0454-4

Jiang, M., Lv, X. G., Yang, Q., and Tong, S. Z. (2006). Iron biogeochemical cycle and its environmental effect in wetlands. *Acta Pedologica Sinica* 3, 493–499. doi: 10.11766/trxb200412270320

Jiang, X., Zhu, L., Xu, S. G., and Xie, Z. G. (2019). Institute of water and environmental research, faculty of infra effects of seasonal stratification and suspended sediment behaviors on the mobilization of manganese and iron in a drinking water reservoir-a case of Biliuhe reservoir, Liaoning province. *Lake Sci.* 375–385. doi: 10.18307/2019.0207

Jiang, Y. X., Wang, Y. Z., Zhou, D. M., Ke, Y. H., Bai, J. H., Li, W. W., et al. (2020). The impact assessment of hydro-biological connectivity changes on the estuary wetland through the ecological restoration project in the Yellow River Delta. China. *Sci. Total Environ.* 758:143706. doi: 10.1016/j.scitotenv.2020.143706

Johnston, S. G., Burton, E. D., Aaso, T., and Tuckerman, G. (2014). Sulfur, iron and carbon cycling following hydrological restoration of acidic freshwater wetlands. *Chem. Geol.* 371, 9–26. doi: 10.1016/j.chemgeo.2014.02.001

Kappler, A., Benz, M., Schink, B., and Brune, A. (2004). Electron shuttling via humic acids in microbial iron(III) reduction in a freshwater sediment. *FEMS Microbiol. Ecol.* 47, 85–92. doi: 10.1016/S0168-6496(03)00245-9

Karimian, N., Johnston, S. G., and Burton, E. D. (2018). Iron and sulfur cycling in acid sulfate soil wetlands under dynamic redox conditions: a review. *Chemosphere* 197, 803–816. doi: 10.1016/j.chemosphere.2018.01.096

Laing, G. D., Vandecasteele, B., Grauwe, P. D., Moors, W., Lesage, E., Meers, E., et al. (2007). Factors affecting metal concentrations in the upper sediment layer of intertidal reedbeds along the river Scheldt. *J. Environ. Monitor.* 9, 449–455. doi: 10.1039/b618772b

Lalonde, K., Mucci, A., Ouellet, A., and Gélinas, Y. (2012). Preservation of organic matter in sediments promoted by iron. *Nature* 483, 198–200. doi: 10.1038/nature10855

Li, C., Ding, S. M., Ma, X., Chen, M. S., Zhong, Z. L., Zhang, Y., et al. (2021). $O_2$ distribution and dynamics in the rhizosphere of *Phragmites australis*, and implications for nutrient removal in sediments. *Environ. Poll.* 287:117193. doi: 10.1016/j.envpol.2021.117193

Li, Y. R., Wu, H. T., Zhang, S., Lu, X., and Lu, K. L. (2021). Morphological characteristics and changes of tidal creeks in coastal wetlands of the Yellow River Delta under *spartina alterniflora* invasion and continuous expansion. *Wetl. Sci.* 19, 88–97. doi: 10.13248/j.cnki.wetlandsci.2021.01.009

Liu, C. F., Wang, W. X., and Ma, H. L. (2020). Role of Fe and Al oxides in soil nitrogen transformation under nitrogen addition condition. *Res. Environ. Sci.* 1946–1953. doi: 10.13198/j.issn.1001-6929.2019.12.03

Liu, F. D., Zheng, B. W., Zheng, Y., Mo, X., and Li, D. (2019). Accumulation risk and sources of heavy metals in supratidal wetlands along the west coast of the Bohai Sea. *RSC Adv.* 9, 30615–30627. doi: 10.1039/C9RA05332H

Lovley, D. R. M. (1997). Microbial Fe(III) reduction in subsurface environments. *FEMS Microbiol. Rev.* 20, 305–313.

Lu, Q. Q., Bai, J. H., Yan, D. H., Cui, B. S., and Wu, J. J. (2020a). Sulfur forms in wetland soils with different flooding periods before and after flow-sediment regulation in the Yellow River Delta. China. *J. Clean. Prod.* 276:122969. doi: 10.1016/j.jclepro.2020.122969

Lu, Q. Y., Pei, L. X., Ye, S. Y., Laws, E. A., and Brix, H. (2020b). Negative feedback by vegetation on soil organic matter decomposition in a coastal wetland. *Wetlands* 40, 2785–2797. doi: 10.1007/s13157-020-01350-0

Luo, M., Zhu, W. F., Huang, J. F., Liu, Y. X., Duan, X., Wu, J., et al. (2019). Anaerobic organic carbon mineralization in tidal wetlands along a low-level salinity gradient of a subtropical estuary: rates, pathways, and controls. *Geoderma* 33, 1245–1257. doi: 10.1016/j.geoderma.2018.07.030

Melton, E. D., Swanner, E. D., Behrens, S., Schmidt, C., and Kappler, K. A. (2014). The interplay of microbially mediated and abiotic reactions in the biogeochemical Fe cycle. *Nat. Rev. Microbiol.* 12, 797–808. doi: 10.1038/nrmicro3347

Mendes, W. D. S., Demattê, J. A. M., Minasny, B., Silvero, N. E. Q., Bonfatti, B. R., and Safanelli, J. L. (2022). Free iron oxide content in tropical soils predicted by integrative digital mapping. *Soil Tillage Res.* 219:105346. doi: 10.1016/j.still.2022.105346

Molina, N. C., Caceres, M. R., and Pietroboni, A. M. (2001). Factors affecting aggregate stability and water dispersible clay of recently cultivated semiarid soils of Argentina. *Arid Land Res. Manag.* 15, 77–87. doi: 10.1080/153249801300000833

Mu, X. J., Sun, Z. G., and Liu, X. T. (2012). Spatial distribution patterns of nitrate nitrogen and ammonia nitrogen in typical tidal marsh soils of Yellow River Delta. *Bull. Soil Water Conserv.* 32, 256–261. doi: 10.13961/j.cnki.stbctb.2012.06.005

Qu, W. D., Li, J. Y., Han, G. X., Wu, H. T., Song, W. M., and Zhang, X. S. (2018). Effect of salinity on the decomposition of soil organic carbon in a tidal wetland. *J. Soils Sediments* 19, 609–617. doi: 10.1007/s11368-018-2096-y

Rezapour, S., Azhah, H., Momtaz, H., and Ghaemian, N. (2015). Changes in forms and distribution pattern of soil iron oxides due to long-term cropping in the Northwest of Iran. *Environ. Earth Sci.* 73, 7275–7286.

Rezapour, S., Jafarzadeh, A. A., Samadi, A., and Oustan, S. (2010). Distribution of iron oxides forms on a transect of calcareous soils, north-west of Iran. *Arch. Agron. Soil Sci.* 56, 165–182. doi: 10.1038/ismej.2014.77

Richard, R. G., and Frances, R. P. (2001). Changes in dissolved and total Fe and Mn in a young constructed wetland: implications for retention performance. *Ecol. Eng.* 17, 373–384. doi: 10.1016/j.biocon.2015.11.019

Richir, J., Bouillon, S., Gobert, S., Skov, M. W., and Borges, A. V. (2020). Editorial: structure, functioning and conservation of coastal vegetated wetlands. *Front. Ecol. Evol.* 8:134. doi: 10.3389/fevo.2020.00134

Santos-Echeandia, J., Vale, C., Caetano, M., Pereira, P., and Prego, R. (2010). Effect of tidal flooding on metal distribution in pore waters of marsh sediments and its transport to water column (Tagus estuary. Portugal). *Mar. Environ. Res.* 70, 358–367. doi: 10.1016/j.marenvres.2010.07.003

Schoepfer, V. A., Bernhardt, E. S., and Burgin, A. J. (2014). Iron clad wetlands: soil iron-sulfur buffering determines coastal wetland response to salt water incursion. *Biogeosciences* 119, 2209–2219. doi: 10.1002/2014JG002739

Sheng, Y. G., Sun, Q. Y., Shi, W. J., Bottrell, S., and Mortimer, R. (2015). Geochemistry of reduced inorganic sulfur, reactive iron, and organic carbon in fluvial and marine surface sediment in the Laizhou Bay region. China. *Environ. Earth Sci.* 74, 1151–1160. doi: 10.1007/s12665-015-4101-8

Sui, X., Zhang, R. G., Frey, B., Yang, L. B., Liu, Y. N., Ni, H. W., et al. (2021). Soil physicochemical properties drive the variation in soil microbial communities along a forest successional series in a degraded wetland in northeastern China. *Ecol. Evol.* 11, 2194–2208. doi: 10.1002/ece3.7184

Sun, W. G., Gan, Z. T., Sun, Z. G., Li, L. L., Sun, J. K., Sun, W. L., et al. (2013). Spatial distribution characteristics of Fe and Mn contents in the new-born coastal marshes in the Yellow River Estuary. *Environ. Sci.* 34, 4411–4419. doi: 10.13227/j.hjkx.2013.11.045

Telfeyan, K., Breaux, A., Kim, J., Cable, J. E., Kolker, A. S., Grimm, D. A., et al. (2017). Arsenic, vanadium, iron, and manganese biogeochemistry in a deltaic wetland, southern Louisiana. USA. *Mar. Chem.* 192, 32–48. doi: 10.1016/j.marchem.2017.03.010

Tipping, E., Rey-Castro, C., Bryan, S. E., and Hamilton-Taylor, J. (2002). Al(III) and Fe(III) binding by humic substances in freshwaters, and implications for trace metal speciation. *Geochim. Cosmochim. Acta* 66, 3211–3224. doi: 10.1016/S0016-7037(02)00930-4

Ury, E. A., Wright, J. P., Ardón, M., and Bernhardt, E. S. (2022). Saltwater intrusion in context: soil factors regulate impacts of salinity on soil carbon cycling. *Biogeochemistry* 157, 215–226. doi: 10.1007/s10533-021-00869-6

Wan, H. W., Qiao, W., Jiang, D., Fu, J. Y., Yang, Y. P., and Liu, X. M. (2014). Monitoring the invasion of *Spartina Alterniflora* using very high resolution unmanned aerial vehicle imagery in Beihai. Guangxi (China). *Sci. World J.* 2014:638296. doi: 10.1155/2014/638296

Wang, B., Zhang, K., Liu, Q. X., He, Q., van de Koppel, J., Teng, S. N., et al. (2022). Long-distance facilitation of coastal ecosystem structure and resilience. *PNAS* 119:e2123274119. doi: 10.1073/pnas.2123274119

Wang, J. J., Bing, S., and Hu, Y. Z. (2021a). Prediction of sediment transport from the Yellow River to the Bohai Sea based on the CEEMDAN-WNN coupled model. *Trans. Oceanol. Limnol.* 43, 34–41. doi: 10.13984/j.cnki.cn27-1141.2021.05.005

Wang, S. M., Jia, Y. F., Liu, T., Wang, Y. Y., Liu, Z. G., and Feng, X. J. (2021b). Delineating the role of calcium in the large-scale distribution of metal-bound organic carbon in soils. *Geophys. Res. Lett.* 48:e2021GL092391. doi: 10.1029/2021GL092391

Wang, T. G., and Peverly, J. H. (1999). Iron oxidation states on root surfaces of a wetland plant (*phragmites australis*). *Soil Sci. Soc. Am. J.* 63, 247–252. doi: 10.2136/sssaj1999.03615995006300010036x

Wang, W. Q., Wang, C., Zeng, C. S., and Tong, C. (2012). Soil carbon, nitrogen and phosphorus ecological stoichiometry of *Phragmites australis* wetlands in different reaches in Minjiang River estuary. *Acta Ecol. Sinica* 32, 4087–4093. doi: 10.5846/stxb201106160817

Weaver, B. L., and Tarney, J. (1984). Empirical approach to estimating the composition of the continental crust. *Nature* 310, 575–577. doi: 10.1038/310575a0

Weiss, J. V., Emerson, D., and Megonigal, J. P. (2004). Geochemical control of microbial Fe(III) reduction potential in wetlands: comparison of the rhizosphere to non-rhizosphere soil. *FEMS Microbiol. Ecol.* 48, 89–100. doi: 10.1016/j.femsec.2003.12.014

Williams, T. P., Bubb, J. M., and Lester, J. N. (1994). Metal accumulation within salt marsh environments: a review. *Mar Pollut. Bull.* 28, 277–290. doi: 10.1016/0025-326X(94)90152-X

Xiao, D. R., Lei, D., Kim, D. G., Huang, C. B., and Tian, K. (2019). Carbon budgets of wetland ecosystems in China. *Glob. Change Biol.* 25, 2061–2076. doi: 10.1111/gcb.14621

Xie, X., Li, X. W., Bai, J. H., and Zhi, L. H. (2021). Variations of aboveground biomass of 4 kinds of Typical Plants with surface elevation of wetlands in the Yellow River Delta. *Wetl. Sci.* 19, 226–231. doi: 10.13248/j.cnki.wetlandsci.2021.02.010

Yan, Q., Xie, W. X., Sha, M. Q., and Li, P. (2020). Effects of *spartina alterniflora* invasion on soil total iron distribution in estuary wetland of Jiaozhou Bay. *Acta Ecol. Sinica* 40, 3991–3999. doi: 10.5846/stxb201903120466

Yao, Q. Z., Wang, X. J., Jian, H. M., Chen, H. T., and Yu, Z. G. (2015). Characterization of the particle size fraction associated with heavy metals in suspended sediments of the Yellow River. *Int. J. Environ. Res. Public Health* 12, 6725–6744. doi: 10.3390/ijerph120606725

Ye, C. L., Huang, W. J., Hall, S. J., and Hu, S. J. (2022). Association of organic carbon with reactive iron oxides driven by soil pH at the global scale. *Glob. Biogeochem. Cycles* 36:e2021GB007128. doi: 10.1029/2021GB007128

Yu, C. X., Xie, S. R., Song, Z. L., Xia, S. P., and Strm, M. E. (2021). Biogeochemical cycling of iron (hydr-)oxides and its impact on organic carbon turnover in coastal wetlands: a global synthesis and perspective. *Earth Sci. Rev.* 218:103658. doi: 10.1016/j.earscirev.2021.103658

Yu, L., Zhuang, T., Bai, J. H., Wang, J. J., Yua, Z. B., Wanga, X., et al. (2019). Effects of water and salinity on soil labile organic carbon in estuarine wetlands of the Yellow River Delta. China. *Ecohydrol. Hydrobiol.* 20, 556–569. doi: 10.1016/j.ecohyd.2019.12.002

Zhai, Y. M., Hou, M. M., and Nie, S. A. (2018). Variance of microbial composition and structure and relation with soil properties in rhizospheric and non-rhizospheric soil of a flooded paddy. *Paddy Water Environ.* 16, 163–172. doi: 10.1007/s10333-017-0627-6

Zhang, G. S., Liu, H. J., Liu, R. P., and Qu, J. H. (2009). Removal of phosphate from water by a Fe-Mn binary oxide adsorbent. *J. Colloid Interface Sci.* 335, 168–174. doi: 10.1016/j.jcis.2009.03.019

Zhang, H. X., Zheng, S. L., Ding, J. W., Wang, O. M., and Liu, F. H. (2017). Spatial variation in bacterial community in natural wetland-river-sea ecosystems. *J. Basic Microbiol.* 57, 536–546. doi: 10.1002/jobm.201700041

Zhang, X. W., Kong, L. W., Cui, X. L., and Yin, S. (2016). Occurrence characteristics of free iron oxides in soil microstructure: evidence from XRD. SEM and EDS. *Bull. Eng. Geol. Environ.* 75, 1493–1503. doi: 10.1007/s10064-015-0781-2

Zhang, Y., Liu, X. L., Fu, C. Y., Li, X. H., Yan, B. X., and Shi, T. H. (2019). Effect of $Fe^{2+}$ addition on chemical oxygen demand and nitrogen removal in horizontal subsurface flow constructed wetlands. *Chemosphere* 220, 259–265. doi: 10.1016/j.chemosphere.2018.12.144

Zhang, Z. W., Zhu, Z. X., Fu, W. L., and Wen, Z. L. (2012). Morphology of soil iron oxides and its correlation with soil-forming process and forming conditions in a karst mountain. *Environ. Sci.* 33, 2013–2020. doi: 10.13227/j.hjkx.2012.06.014

Zhang, Z. X., Yang, K. Y., Wang, P., and Gao, Y. (2001). A study on the availability of Fe in the dry farming yellow moist soil. *Soil Fertilizer* 2001, 27–30.

Zhang, Z. Y., and Furman, A. (2021). Soil redox dynamics under dynamic hydrologic regimes - a review. *Sci. Total Environ.* 763:143026. doi: 10.1016/j.scitotenv.2020.143026

Zhao, Q., Adhikari, D., Huang, R. X., Patel, A., Wang, X. L., Tang, Y. Z., et al. (2017). Coupled dynamics of iron and iron-bound organic carbon in forest soils during anaerobic reduction. *Chem. Geol.* 464, 118–126. doi: 10.1016/j.chemgeo.2016.12.014

Zhao, Z. J., Jin, R., Fang, D., Wang, H., Dong, Y., Xu, R. K., et al. (2018). Paddy cultivation significantly alters the forms and contents of Fe oxides in an Oxisol and increases phosphate mobility. *Soil Tillage Res.* 184, 176–180. doi: 10.1016/j.still.2018.07.012

Zhao, Z. M., Zhang, X., Cheng, M. Q., Song, X. S., Zhang, Y. J., and Zhong, X. M. (2019). Influences of iron compounds on microbial diversity and improvements in organic C. N, and P removal performances in constructed wetlands. *Microbial Ecol.* 78, 792–803. doi: 10.1007/s00248-019-01379-7

Zhou, J. M., and Shen, R. F. (2013). *Dictionary of Soil Science*. Beijing: Science Press.

Zou, Y. C., Jiang, M., Yu, X. F., Lu, X. G., David, J. L., and Wu, H. T. (2011). Distribution and biological cycle of iron in freshwater peatlands of Sanjiang Plain. Northeast China. *Geoderma* 164, 238–248. doi: 10.1016/j.geoderma.2011.06.017

frontiers | Frontiers in Ecology and Evolution

TYPE Original Research
PUBLISHED 12 August 2022
DOI 10.3389/fevo.2022.956903



OPEN ACCESS

EDITED BY
He Yixin,
Key Laboratory of Mountain Ecological Rehabilitation and Biological Resource Utilization, Chengdu Institute of Biology (CAS), China

REVIEWED BY
Feng Li,
Institute of Subtropical Agriculture (CAS), China
Xiaoming Kang,
Institute of Wetland Research, China

*CORRESPONDENCE
Xiaoyan Zhu
zhuxy0613@126.com

SPECIALTY SECTION
This article was submitted to Conservation and Restoration Ecology, a section of the journal Frontiers in Ecology and Evolution

RECEIVED 30 May 2022
ACCEPTED 26 July 2022
PUBLISHED 12 August 2022

CITATION
Yuan Y, Wang Q, Dong X, Zhu Y, Wu Z, Yang Q, Zuo Y, Liang S, Wang C and Zhu X (2022) *In situ*, high-resolution evidence of metals at the sediment-water interface under ice cover in a seasonal freezing lake. *Front. Ecol. Evol.* 10:956903. doi: 10.3389/fevo.2022.956903



# *In situ*, high-resolution evidence of metals at the sediment-water interface under ice cover in a seasonal freezing lake

Yuxiang Yuan[1], Qichen Wang[2], Xiangqian Dong[2], Yinze Zhu[2], Zhong Wu[2], Qian Yang[3], Yunjiang Zuo[1], Shuang Liang[2], Chunqing Wang[4] and Xiaoyan Zhu[2]*

[1]Key Laboratory of Wetland Ecology and Environment, Northeast Institute of Geography and Agroecology, Chinese Academy of Sciences, Changchun, China, [2]Key Laboratory of Songliao Aquatic Environment, Ministry of Education, Jilin Jianzhu University, Changchun, China, [3]School of Geomatics and Prospecting Engineering, Jilin Jianzhu University, Changchun, China, [4]Key Laboratory for Comprehensive Energy Saving of Cold Regions Architecture of Ministry of Education, Jilin Jianzhu University, Changchun, China

The ice cover in winter as a physical barrier and duration would profoundly impact on changes in endogenous metal loading, migration, and transformation. Although a gradual reduction in duration and occurrence of lake ice cover in boreal lake ecosystems has been confirmed, little attention to the ice-covered period is received compared to open water studies. In this study, novel-developed diffusive gradients in thin films (DGT, ZrO-Chelex) probes were deployed to obtain the *in-situ* and high-resolution information on metals (Cu, Zn, Pb, Mn, Cd, Cr, and As) at the sediment-water interface (SWI) in a seasonal ice-covered lake, Chagan Lake. In addition, "source-sink" characteristics of each metal related to their endogenous release were determined based on Fick's first law. Concentrations of labile metals at the SWI demonstrated significant spatial heterogeneity, peaking exactly below the SWI. Compared with other similar studies, concentrations of Pb (0.55 μg/L), Cr (0.58 μg/L), and As (2.4 μg/L) were a little higher even under-ice than that in other freshwater rivers and lakes, indicating potential pollution due to the agricultural intensification and petroleum extraction. The apparent diffusive fluxes suggested that sediments acted as a sink for Pb (−0.01 mg $m^{-2}$ $day^{-1}$), Cr (−2.37 mg $m^{-2}$ $day^{-1}$), and Cd (−0.1 mg $m^{-2}$ $day^{-1}$), diffusing from the overlying water into the sediment, while Cu (0.12 mg $m^{-2}$ $day^{-1}$), Zn (0.75 mg $m^{-2}$ $day^{-1}$), Mn (15.89 mg $m^{-2}$ $day^{-1}$), and As (2.12 mg $m^{-2}$ $day^{-1}$) as a source from sediments into the overlying water. Dissolved oxygen was the principal factor (79.5%, $P$ = 0.032), determining the variation of the available metals at the SWI. As the urgent need for research focused on under-ice ecosystem dynamics, this study addressed the previously unknown behavior

of the labile metals at the SWI and provided a unique perspective for the lake management during the ice-cover periods when external nutrient input was cut off.

KEYWORDS

Chagan Lake, *in-situ* high resolution, diffusive fluxes, winter, sediment-water interface

## Introduction

More than half of the world's lakes (>50 million) are periodically frozen, and partially or fully covered with ice (Hampton et al., 2017). During the ice period, the ice cover significantly impacts the concentrations, migration, and transformation of metals due to the transportation differences between ice and water, and the elimination of wave action, which mixes the oxygen and contaminant (Ozersky et al., 2021). Besides, when the aqueous solutions are frozen, hydrophobic and hydrophilic compounds are known to become spontaneously segregated at grain boundaries of ice during the phase transition, leading to relatively higher concentrations of ions and metals in the water beneath the ice (Heger et al., 2006). Due to global warming, the duration and extent of lake ice cover in winter are predicted to decrease in many temperate lakes (Kamari et al., 2018). Therefore, it is vital to understand the biogeochemical dynamics of nutrients and contaminants underneath the ice (Hampton et al., 2017; Ozersky et al., 2021).

The accumulation of heavy metals in lake sediments poses a severe risk to benthic and aquatic biota and ecosystem function, ultimately, affecting human health through the food chain (Gall et al., 2015; Green and Planchart, 2018). The sediment-water interface (SWI) is one of the most important interfaces in the critical zone, and the micro-reactions and environmental changes of physical, chemical, and biological reactions dominate with a complex impact on the state and migration-transformation behavior of metals near the interface (Harper et al., 1998; Gall et al., 2015; Fan, 2019). Almost all the pollution and ecological problems are associated with aquatic environments at the SWI (Fan, 2019). Traditional sediment chemistry studies were mainly based on ex-situ measurements, which cannot reflect the actual information on heavy metals' physical and chemical characteristics (Ding et al., 2010; Ren et al., 2015). It has been verified that the diffusive gradients in thin films (DGT) is an ideal tool for the *in situ* evaluation of metal bioavailability in sediments (Menegario et al., 2017). Previous studies indicated that under anaerobic conditions, the concentrations of liable metals by DGT perform considerable apparent diffusion from sediment on the low dissolved oxygen (DO) condition (Ren et al., 2015; Yuan et al., 2020). Their surface binding characteristics with different solid phases (i.e., Fe/Mn oxides and organic matter) and metal binding regulation are influenced by the pH, redox potentials, and pore water composition.

The Chagan Lake (CL) is the representative lake in the cold regions of northeast China, which acts as an essential ecological barrier against desertification (Bu et al., 2009; Liu et al., 2021). Research suggests that aquacultural development has dynamically increased the metal concentrations in the CL (Xie, 2021). However, most studies on metals currently focus on open water season, while studies in the ice-covered period have often been neglected or assumed to be less important (Hampton et al., 2017; Kamari et al., 2018). There is still a significant research gap in the understanding and estimation of stocks and fluxes of metals under ice cover. In this study, the ZrO-Chelex DGT technique was employed for the first time to obtain accurate information regarding the spatial distributions of labile Cu, Zn, Pd, Mn, Cd, Cr, and As at the SWI of CL during the ice-covered period. Due to redox conditions under ice cover, we hypothesized that considerable concentrations and release of labile metal would be found at the SWI due to redox conditions under ice cover, even though the cold temperature would significantly affect water quality in the following spring. This study would provide a brand-new insight into the control of internal metal loading during ice-covered periods when external input was cut off.

## Materials and methods

### Study area and sampling collection

As the largest inland lake in Jilin Province, the CL is located west of Songnen Plain, Northeast China. It covers an area of 372 $km^2$, holding 5.98 $\times$ $10^8$ $m^3$ of water. The average and maximum depths of the CL are 1.52 and 6 m. The CL is located in a semi-arid and sub-humid region with a long-term annual average temperature of 5.5°C. The duration of the ice cover is approximately 4 months, from late November to next March. The CL plays a vital role in the regional economic and cultural heritage and is well-known for winter fishing. The CL receives the discharge from Daan and Qianguo irrigation districts. Therefore, a substantial amount of N, P, and heavy metals flow into the lake with irrigation discharge.

An ice drill was used to prepare holes with a diameter of 50 cm on the surface of the CL on December 20th, 2020, when the winds over the lake were light. Six cores (Table 1) with 20 cm overlying water were collected using a gravity corer (φ90 mm × 500 mm) and then covered with a rubber plug on both ends. Water temperature, DO, pH, conductivity, and *chlorophyll* a were measured by a portable multi-probe (YSI 650 MDS, United States). The concentrations of DOC were determined by Xpert-TOC/TN. Surface sediment samples were collected using a grab sampler and then placed in acid-washed plastic bags. Then the samples were transported carefully to the laboratory and stored at −18°C for further analysis.

## Preparation of diffusive gradients in thin films devices

The sediment cores were stabilized for 12 h to ensure the equilibrium at the interface between the sediment and the water. The DGT device involves a device consisting of four components: a ZrO-Chelex binding gel, a diffusive gel, a membrane filter, and a fixed shell (2.5 cm × 18 cm). The ZrO-Chelex binding gel was prepared using the method described by Xu D. et al. (2012). The diffusive gel was prepared from polyacrylamide using the method published by Zhang and Davison (2002). Specifically, the ZrO-Chelex binding gel is on the top, and the diffusive gel is sandwiched between a Whatman membrane filter with a pore size of 0.45 μm, and the three layers were stacked on the base of the fixed shell. The assembled device was immersed in a 0.01 mol $L^{-1}$ NaCl solution, to which $N_2$ was added continuously for 16 h before use.

## Application of the diffusive gradients in thin films device

The ZrO-Chelex DGT devices would simultaneously measure multiple labile cations and oxyanions, and were provided by EasySensor Ltd (Nanjing, China)[1] . During the application, the ZrO-Chelex DGT device was slowly inserted into the sediment cores for 72 h. Water temperature was simultaneously measured three times at each site during the deployment. The SWI was marked after being withdrawn and then washed with deionized water to remove the sediment particles. A ceramic cutter was then used to cut the binding gel at 2 mm intervals. The gel samples were transferred to a 1.5 mL PE bottle with 1.8 mL 1 mol $L^{-1}$ $HNO_3$ for 24 h. Quality control was ensured by analyzing duplicate samples with a precision of three replicates of 15% (relative standard deviation). All the concentrations of metals and solutions were analyzed using an Agilent 7700 inductively coupled plasma mass spectrometer.

## Statistical analysis

### Determination of labile metal concentrations

The concentrations of ($C_{DGT}$) of each metal (μg/L) are calculated using:

$$C_{\mathrm{DGT}} = \frac{M \times \Delta g}{D \times A \times T} \quad (1)$$

where $M$ is the amount of the target analyte accumulated in the DGT device (μg); $\Delta g$ is the total thickness of the diffusive gel and the membrane filter (cm); $D$ is the diffusion coefficient of the target metal in the diffusive gel ($cm^2\ s^{-1}$); $A$ is the area of the window of the DGT device ($cm^2$); $T$ is the time that the system was allowed to stand still (s).

### Estimation of the diffusive fluxes at the sediment-water interface

The net exchange flux $F$ of each metal at the SWI can be estimated based on Fick's first law:

$$F = F_{\mathrm{s}} + F_{\mathrm{w}} = \left(-\phi D s \frac{\partial c_{\mathrm{s}}}{\partial x_{\mathrm{s}}}\right) + \left(-\phi D_{\mathrm{w}} \frac{\partial c_{\mathrm{w}}}{\partial x_{\mathrm{w}}}\right), \quad (2)$$

1 http://www.easysensor.net

TABLE 1 Sampling site information.

| Sites | Latitude | Longitude | Air temperature °C | | Water temperature °C | | Wind speed m/s | Ice thickness mm | Water depth m |
|---|---|---|---|---|---|---|---|---|---|
| | | | Max | Min | Max | Min | | | |
| CG1 | 45.117667 | 124.270637 | −10.3 | −10.5 | 1.9 | 0.8 | – | 469.5 | 1.6 |
| CG2 | 45.225368 | 124.104844 | −11.8 | −12.1 | 2.4 | 2.1 | 3.06 | 465.65 | 0.6 |
| CG3 | 45.176735 | 124.167416 | −10.1 | −11 | 2 | 1.3 | 3.42 | 453.89 | 2 |
| CG4 | 45.143761 | 124.214428 | −9 | −9.4 | 1.8 | 0.9 | 4.65 | 470.5 | 1.9 |
| CG5 | 45.1158841 | 124.214273 | −7.8 | −8.8 | 1.5 | 1.1 | 5.36 | 503.8 | 2.45 |
| CG6 | 45.108007 | 124.138007 | 0.5 | 0.4 | −8.1 | −8.4 | 5.36 | 557.87 | 3.2 |

where $F$ is the diffusive flux at the SWI (mg $m^{-2}$ $day^{-1}$); $F_s$ is the diffusive flux from the sediment; $F_w$ is the diffusive flux from the overlying water; $\partial c_s/\partial x_s$ is the concentration gradient in the sediment; $\partial c_w/\partial x_w$ is the concentration gradient in the overlying water; $x$ is the depth of the sediment (cm); $c$ is the ion concentration (mg $L^{-1}$); $D_s$ is the diffusion coefficient of each metal in the sediment, which can be calculated based on the molecular diffusion coefficient in water $D_w$ and the surface sediment porosity $\varphi$ .

### Data processing and analysis

In this study, the diffusive flux patterns were produced using Microsoft Excel. SPSS Statistics 23.0 was used to analyze variance (ANOVA) and independent-samples $t$-tests. RStudio 6.5 was used to analyze correlation analysis. In addition, the RStudio 6.5 and Canoco 5 were used to perform redundancy analysis (RDA) to determine the factors influencing the metal profiles during the ice-covered period.

## Results

### Spatial profiles of labile metals during the ice-covered period

The DOC of the CL under ice in winter ranged from 10.29 to 27.42 mg/L (mean: 13.23 ± 7.06 mg/ L); DO from 10.15 to 11.96 mg/ L (mean: 11.41 ± 0.67 mg/ L); ORP from 8.4 to 35.5 mV (mean: 27.55 ± 10.82 mV); Sal from 0.61 to 0.92 psu (mean: 0.70 ± 0.11 psu); TDS from 797 to 1,178 mg/L (mean: 910.17 ± 138.76 mg/L); Turbidity from 853.54 to 1,307.04 FNU (mean: 1,198.75 ± 177 FNU); and pH from 6.75 to 7.42 (mean: 6.96 ± 0.25). The mean values of DO and pH of CG2 were slightly lower than other sites (Table 2).

Concentrations of liable Cu ranged from 0.0005 to 1.99 μg/L (mean: 0.18 μg/ L); Zn from 4.43 to 18.81 μg/L (mean: 8.06 μg/L); Pb from 0.28 to 23.61 μg/L (mean: 0.55 μg/L); Cd from 0.06 to 0.29 μg/L (mean: 0.09 μg/L); Cr from 0.11 to 16.18 μg/L (mean: 0.58 μg/L); and As from 0.14 to 7.13 μg/L (mean: 2.4 μg/L). The Mn concentration ranged from 0.46 to 72.51 μg/L, the highest compared to the other metals (Figure 1). In the profile, the concentrations of all metals initially increased and then decreased with increasing depth peaking exactly below the water-sediment interface. The concentrations of Mn and Pb were considerably higher at site CG2 than at any other sampling site.

There were significant differences between different sampling sites in the concentrations of Mn ($P < 0.001$), Cu ($P < 0.001$), Zn ($P < 0.001$), and Pb ($P < 0.001$) by ANONA analysis, as well as insignificant differences between the concentrations of Cd, Cr, and As at the SWI (from −20 mm to 20 mm) of CL during the ice-covered period.

Correlation analysis revealed that the $C_{DGT}$ value for labile Cu was extremely significantly positively correlated with that of labile Zn ($R = 0.78$, $P < 0.001$) and Pb ($R = 0.75$, $P < 0.001$; Figure 2). The $C_{DGT}$ value for Zn was significantly positively correlated with Pb ($R = 0.77$, $P < 0.001$). The $C_{DGT}$ for Mn was significantly negatively correlated with Cu, Zn, and Pb values. There were no significant correlations between the $C_{DGT}$ values for Cr and As and that of any other metals (Figure 2).

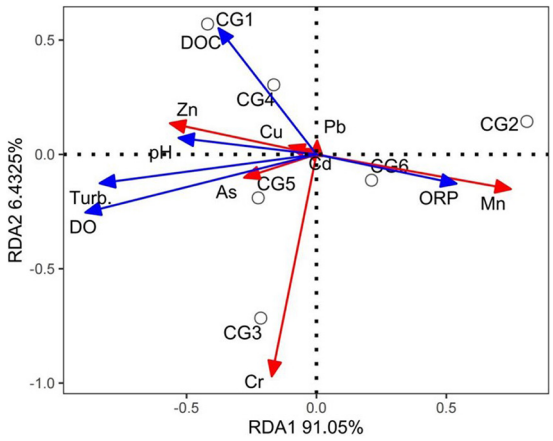


FIGURE 1
RDA analysis of influencing factors of metals during the ice-covered period.

TABLE 2 Physicochemical properties in Chagan Lake.

| | DOC (mg/L) | DO (mg/L) | ORP (mV) | Sal (psu) | TDS (mg/L) | Turbidity (FNU) | pH |
|---|---|---|---|---|---|---|---|
| CG1 | 27.42 | 11.92 | 25 | 0.72 | 932 | 1,292 | 6.98 |
| CG2 | 11.7 | 10.15 | 35.5 | 0.92 | 1,178 | 853.54 | 6.75 |
| CG3 | 10.92 | 11.96 | 33.8 | 0.64 | 836 | 1,307.04 | 6.81 |
| CG4 | 8.073 | 11.27 | 24.9 | 0.61 | 797 | 1,289.03 | 7.02 |
| CG5 | 10.95 | 11.58 | 8.4 | 0.68 | 875 | 1,164.3 | 7.42 |
| CG6 | 10.29 | 11.59 | 37.7 | 0.65 | 843 | 1,286.61 | 6.77 |
| Mean ± sd | 13.23 ± 7.06 | 11.41 ± 0.67 | 27.55 ± 10.82 | 0.70 ± 0.11 | 910.1 ± 138.7 | 1,198.7 ± 177 | 6.96 ± 0.25 |

DO, dissolved oxygen; DOC, dissolved organic carbon; ORP, oxidation-reduction potential; Sal, salinity; and TDS, total dissolved solids.

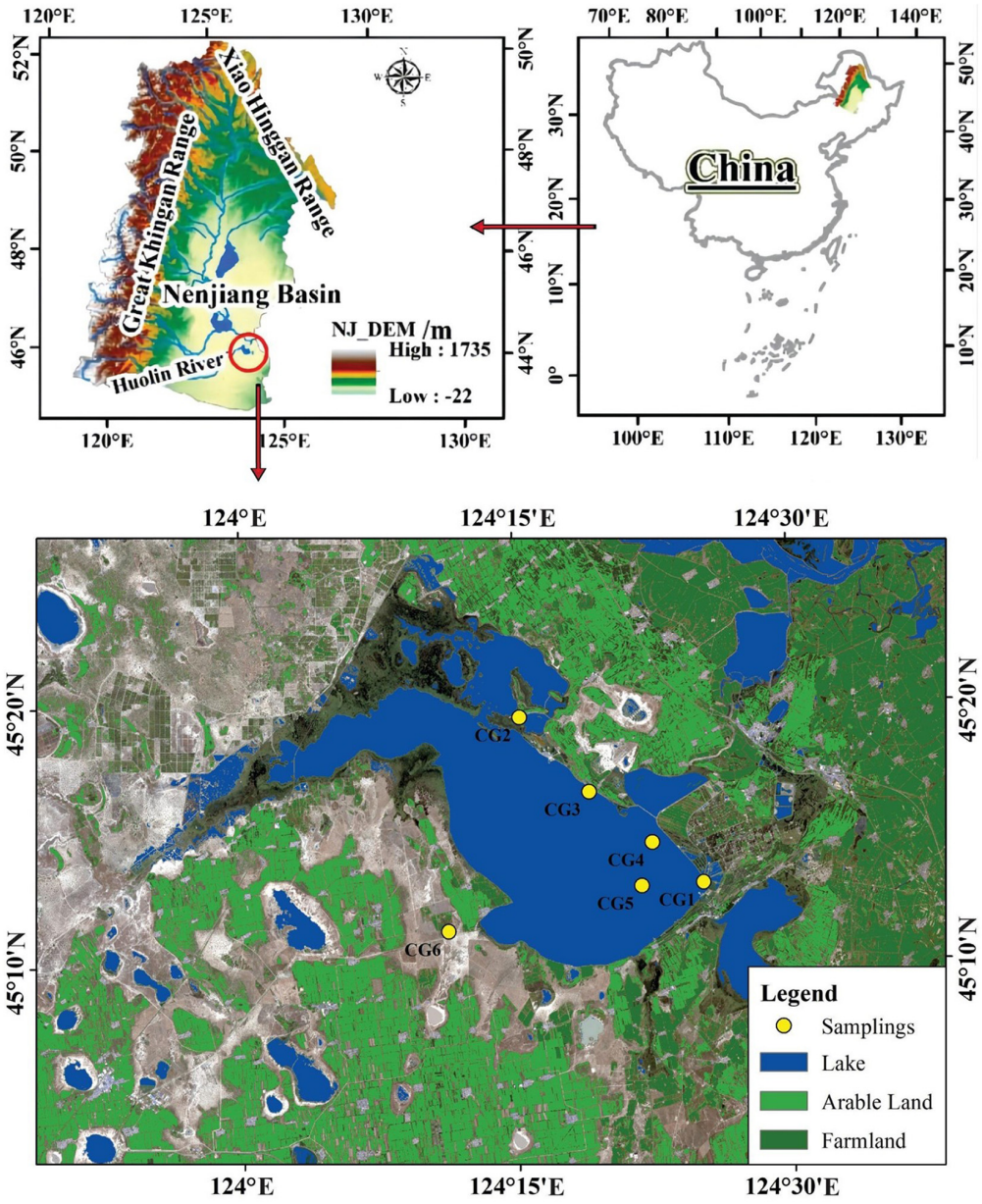


FIGURE 2
Location of Chagan Lake and sampling sites.

## The apparent fluxes of metals across the sediment-water interface

The apparent diffusive fluxes of liable Cu ranged from −0.12 to 0.26 mg $m^{-2}$ $day^{-1}$ (mean: 0.12 mg $m^{-2}$ $day^{-1}$); Zn from −4.53 to 6.76 mg $m^{-2}$ $day^{-1}$ (mean: 0.51 mg $m^{-2}$ $day^{-1}$); Pb from −0.11 to 0.11 mg $m^{-2}$ $day^{-1}$ (mean: −0.01 mg $m^{-2}$ $day^{-1}$); Cd from −0.34 to 0.02 mg $m^{-2}$ $day^{-1}$ (mean: −0.10 mg $m^{-2}$ $day^{-1}$); Cr from −18.51 to 3.85 mg $m^{-2}$ $day^{-1}$ (mean: −2.37 mg $m^{-2}$ $day^{-1}$) and As from −3.47 to 5.14 mg $m^{-2}$ $day^{-1}$ (mean: 2.13 mg $m^{-2}$ $day^{-1}$; Figure 3). Concentrations of liable Mn ranged from 0.32 to 50.1 mg $m^{-2}$ $day^{-1}$, the highest among the other metals. Positive apparent diffusive fluxes were observed at most sampling sites for Cu, Mn, and As, indicating the upward movement from the sediment to the overlying water. Negative apparent diffusive fluxes were observed at most sampling sites for Zn, Pb, Cr, and Cd, with sediment as a sink.

The RDA analysis indicates that the DO explains 79.5% ($P$ = 0.032) of the variation in the whole profile, and the RDA1 axis explains 91.05% of the variation in the SWI (Figure 4).

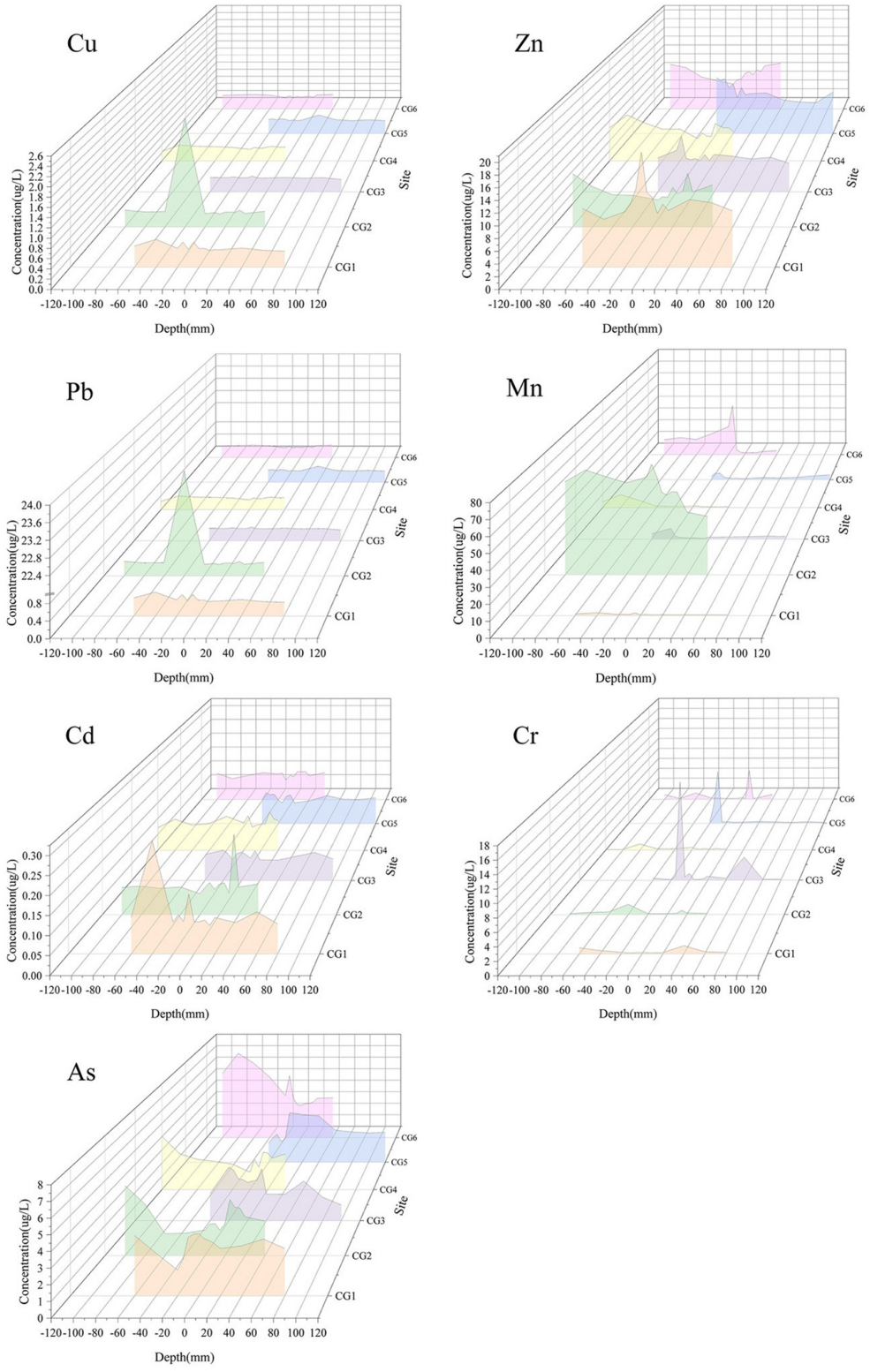


FIGURE 3
The vertical distributions of labile Cu, Zn, Pb, Mn, Cd, Cr, and As at the sediment-water interface during the ice-covered period of Chagan Lake.

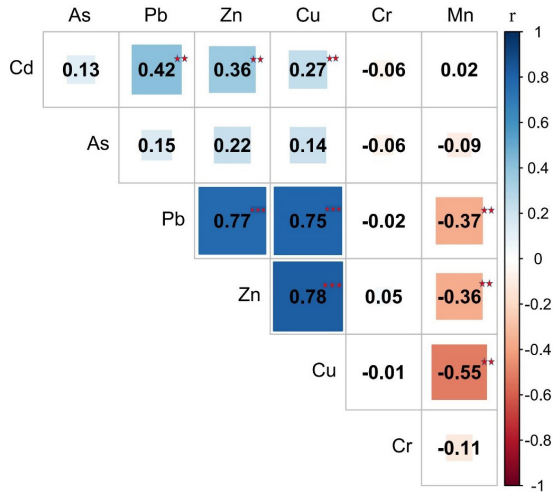


FIGURE 4
.Correlation analysis between metals at the sediment-water interface of Chagan Lake during the ice-covered period. **Represents $P < 0.01$, ***represents $P < 0.001$.

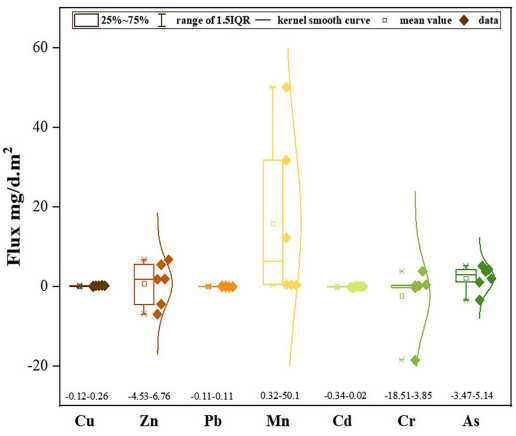


FIGURE 5
Diffusion fluxes of metals at the sediment-water interface during the ice-covered period.

# Discussion

## Spatial profiles of labile metals during the ice-covered period

The SWI is the boundary between the overlying water column and sediments, and this zone is easily affected by physical disturbance (e.g., temperature, currents caused by resuspension), biological processes (e.g., bioturbation generating mounds and trenches), and chemical process (Wu et al., 2014, 2016; Fan, 2019). These processes affect the migration and transformation of metals around the SWI in complex ways (e.g., oxidation, reduction, adsorption, desorption, and degradation; Voermans et al., 2017; Fan, 2019). In this study, peak concentrations of labile metals also appeared just below the SWI during the ice-covered period (**Figure 5**). The vertical variation of labile metals on the sediment profiles generally shows a decreasing trend with depth. Most metals in the surface sediment were reported in an active or incompletely degraded state, therefore they have a high tendency to participate in the biogeochemical process at the SWI (Ren et al., 2015; Wu et al., 2015; Liu et al., 2016). The behavior of labile metals near the SWI is significant because the dynamic chemical and biochemical processes occurring in surface sediment cause major transformations in the speciation/mobility of metals due to remobilization or sequestration from minerals/organisms (Wu et al., 2014). These processes can result in an increase in the CDGT values of the metals at the SWI. Moreover, the biological and physical disturbances increase the sediment's porosity and resuspended sediment particles, consequently inducing the release of contaminations from the sediment to the pore water. This results in increases in the concentrations of labile metals in the pore water at the SWI (Song et al., 2005; Fan, 2019). A substantially higher average concentration was found at sampling site CG2 than at any other site ($P < 0.001$), indicating notable spatial heterogeneity (**Figure 5**).

Few studies were reported on labile metals by DGT technique during the ice-covered period in lakes in China, and it is only possible to compare our findings with the former research in Lake Xingkai (In press). Compared with the Lake Xingkai Basin, the CL had a considerably higher concentration of labile Cr (0.58 vs 0.06 μg/L), Pb (0.55 vs 0.26 μg/L), Cd (0.09 vs 0.04 μg/L), and As (2.4 vs 1.06 μg/L; **Table 3**). Different from Lake Xingkai Basin, located far away in the border area, the CL was extensively affected by human activity, such as petroleum extraction, the use of pesticides and fertilizers, and famous winter fishing, contributing to the accumulation of heavy metals (Zhang et al., 2008; Xie et al., 2010). Besides, there were fewer inflow rivers to the CL, thus intensifying the accumulation of metals with low flow. A much lower concentration of labile Mn (12.5 vs 366.27 μg/L) was found compared to the Lake Xingkai basin but similar to the background value of soil in Jilin Province (452.65 ppm), which might be caused by the diagenetic process (Zhao et al., 1987). Compared with world average freshwater, concentrations of most metals in CL were a little higher even in a cold season, while much lower than in the developed warm area (Lake Xuanwu), indicating potential pollution in the CL.

Similar to previous studies (Yuan et al., 2011, 2014), strong correlations were found between Cu, Zn, and Pb concentrations, while there was a significantly negative correlation between Mn and Cu, Zn and Pb (**Figure 2**). This might cause by Mn oxides in sediments mainly origin from natural geochemical processes (Yuan et al., 2014; Maina et al., 2019). Besides, Mn/Fe oxides have a strong capacity to adsorb metals due to the large specific surface areas and regular porous structures (Xu L. et al., 2012;

TABLE 3 The Cdgt of labile metals (μg/L) in Chagan Lake and other areas.

| | Cu | Zn | Pb | Mn | Cd | Cr | As | References |
|---|---|---|---|---|---|---|---|---|
| Chagan Lake | 0.18 | 8.06 | 0.55 | 12.5 | 0.09 | 0.58 | 2.4 | This study |
| Lake Xiaoxingkai | 0.05 | 8.91 | 0.26 | 366.27 | 0.04 | 0.04 | 1.64 | Unpublished data |
| Lake Xingkai | 0.11 | 10.83 | 0.26 | 302.9 | 0.04 | 0.06 | 1.06 | Unpublished data |
| Sava River, Croatia | 0.166 | 1.86 | 0.02 | 8.24 | 0.0016 | 0.033 | | Dragun et al., 2008 |
| Xizhi River | 2.03 | 31.12 | 1.55 | | | | | Gao et al., 2021 |
| Lake Xuanwu | 1.32 | 4.43 | l.47 | 0.68 | 0.3 | 5.87 | 5.85 | Wang, 2018 |
| Aha Lake | 0.54 | 2.17 | 0.06 | 28.34 | 0.02 | 0.11 | 0.71 | Fei et al., 2021 |
| World average freshwater | 2 | 10 | 0.2 | 5 | 0.07 | 0.5 | 2 | Foerstner and Wittmann, 1980 |

Xia et al., 2020). Therefore, the reductive dissolution of iron and manganese oxides would release labile metals (e.g., Cu, Zn, and Pb), resulting in higher concentrations (Yuan et al., 2011). Moreover, previous research has shown that Mn oxides in sediment are essential oxidants for the degradation of OM (Luo et al., 2000). The notable release of dissolved Mn at the SWI of Aha Lake was a result of the participation of $MnO_2$ in OM degradation as an oxidant (Liu, 2019). The flux estimates obtained in this study similarly revealed a marked release of dissolved Mn at the SWI of CL. This may be an essential factor leading to the significant negative correlations between the concentration of Mn and Cu, Zn and Pb.

## Source-sink characteristic of internal metal loading under the ice

Lake sediment can function either as an internal metal load or sink. Therefore, studies on the source-sink characteristics at the SWI are becoming a hotspot (Templeton et al., 2000; Wang et al., 2015). It is found that the diffusive fluxes of Zn, Pb, Cr, and Cd were negative, suggesting that the sediment acted as a sink for these metals. In contrast, the diffusive fluxes of Cu, Mn, and As were positive, indicating sediments as a source. During the initial stage of the ice-covered period in winter, the DO concentration in the CL's water was still relatively high, and the SWI might still be in a continuously oxidative environment. Under these conditions, as micro- and nanoparticles, Fe/Mn oxides known for their high activity and large surface areas were important geological adsorbents for metals such as Zn, Pb, Cr, and Cd (Banks et al., 2012; Wang, 2018; Liu, 2019). The OM-bound metals are another major form of these metals in sediment (Zoumis et al., 2001; Fan et al., 2002, 2019). The OM bound with metal degradation was to be reported released into the overlying water. In lake sediment, sulfides, after sulfate reduction, also have a strong ability to bind to metal ions. This produces insoluble metal sulfides, one of the major forms of metals in sediment (Burdige, 1993; Toro et al., 2002).

Biological disturbances resuspend sediment particles and metal sulfides were exposed to water containing active aerobic organisms (Caille et al., 2003). In the presence of sulfur-oxidizing bacteria, metal sulfides were oxidized into sulfates, releasing metals bound to the sulfides (Vera et al., 2013). The oxidation of sulfides produces $H^+$ and therefore reduces the pH at the SWI (Miao et al., 2006). The relatively high DO content and the low water pH of 6.75 during the ice-covered period indicated a weak release of Cu and As.

## Mechanisms behind the metal distributions

DO was found as the primary factor (79.5%, $P = 0.032$) affecting the vertical distribution of the labile metals at the SWI. In sediments, metals combine with Fe/Mn oxides and sulfides, forming insoluble oxidizable states. As the DO concentration increased, the Fe (II) and Mn (II) released due to oxidation rapidly form colloidal Fe and Mn oxides or hydroxides, which have a strong ability to adsorb metal ions and are highly susceptible to co-precipitating with metals. During the freezing period, ice cover and continuous mineralization of organic aggregates would lead to conditions of hypoxia and anoxia at the SWI. This created favorable conditions for endogenous metal release from bounded to Fe/Mn/S oxides into the pore water (Toro et al., 2002; Shao et al., 2012; Xia et al., 2020). Therefore, changes in DO concentration control the release and precipitation of metals. Moreover, metals bound to OM were a major form in sediments (Zoumis et al., 2001; Fan et al., 2002). When OM bound to metals was degraded by microorganisms, these metals were released into the water. As a principal factor affecting microorganism-induced degradation (Canfield et al., 1993), DO also substantially impacts the concentrations of metals in the water. DO dynamics with a high spatiotemporal resolution by planar optode should be obtained in further study.

# Conclusion

Diffusive gradients in thin films technique was firstly employed to acquire high-resolution millimeter-scale *in situ*

information regarding the labile Cu, Zn, Pb, Mn, Cd, Cr, and As at the SWI in the CL during the ice-covered period. The labile metals at the SWI of CL displayed markedly different spatial and vertical distribution patterns. Specifically, the concentration of each metal peaked exactly below the interface. Based on Fick's first law, the diffusive fluxes revealed that the sediment acted as a sink for Zn, Pb, Cr, and Cd, while a source for Cu, Mn, and As in winter. Compared with other studies, Pb, Cr, and As concentrations under-ice were even slightly higher, indicating potentially ecological risk. *In situ* passive sampling techniques could help inform potential ecological or human health risks associated with metal contamination without disturbing aquatic biota. DO was identified as the primary factor affecting the vertical distribution of the labile metals at the SWI. It may be worth considering actions to take into account redox processes and control the $O_2$ dynamics when management decision-making during remediation planning. Our results quantified the endogenous metal concentrations and diffusion fluxes across the SWI during the ice-cover period, giving insight into lake water quality management in temperate seasonal frozen lakes.

## Data availability statement

The original contributions presented in this study are included in the article/supplementary material, further inquiries can be directed to the corresponding author.

## Author contributions

XZ and YY proposed and structured the study. QW, ZW, YzZ, QY, and SL were involved in the experiments. XZ, QW, XD, and ZW wrote the manuscript. QW, XD, and YjZ made the figure. XZ, QW, and YY reviewed and improved the English of the manuscript and made a funding acquisition. All authors participated in discussion of the research.

## Funding

This research was financially supported by the Jilin Province Education Department Science and Technology Research Project (No. JJKH20210289KJ); National Natural Science Foundation of China (No. 42101071); Natural Science Foundation of Jilin Province (YDZJ202201ZYTS480); and Scientific and Technological Innovation and Entrepreneurship Project for Overseas Researchers in Jilin Province in 2021.

## Acknowledgments

We would like to thank M. Y. Sang for his help in the field work; Y. R. Wang, Z. X. Liu, Q. Y. Zhu, and D. Zhang for their preparation for the data.

## Conflict of interest

The authors declare that the research was conducted in the absence of any commercial or financial relationships that could be construed as a potential conflict of interest.

## Publisher's note



## References

Banks, J., Ross, D. J., and Keough, M. J. (2012). Short-term (24 h) effects of mild and severe hypoxia (20% and 5% dissolved oxygen) on metal partitioning in highly contaminated estuarine sediments. *Estuarine Coastal Shelf Sci.* 99, 121–131. doi: 10.1016/j.ecss.2011.12.025

Bu, X. J., Chai, S. L., Zhang, Q. W., and Xu, X. C. (2009). The spatial distributions of elements in sediments of lake Chagan in west Jilin Province. *J. Arid Land Resour. Environ.* 23, 179–184.

Burdige, D. J. (1993). The biogeochemistry of manganese and iron reduction in marine sediments. *Earth-Science Rev.* 35, 249–284. doi: 10.1016/0012-8252(93)90040-E

Caille, N., Tiffreau, C., Leyval, C., and Morel, J. L. (2003). Solubility of metals in an anoxic sediment during prolonged aeration. *Sci. Total Environ.* 301, 239–250. doi: 10.1016/s0048-9697(02)00289-9

Canfield, D. E., Jørgensen, B. B., Fossing, H., Glud, R., Gundersen, J., Ramsing, N. B., et al. (1993). Pathways of organic carbon oxidation in three continental margin sediments. *Mar. Geol.* 113, 27–40. doi: 10.1016/0025-3227(93)90147-N

Ding, S., Xu, D., Sun, Q., Yin, H., and Zhang, C. (2010). Measurement of dissolved reactive phosphorus using the diffusive gradients in thin films technique with a high-capacity binding phase. *Environ. Sci. Technol.* 44, 8169–8174. doi: 10.1021/es1020873

Dragun, Z., Raspor, B., and Roje, V. (2008). The labile metal concentrations in Sava River water assessed by diffusive gradients in thin films. *Chem. Speciation Bioavail.* 20, 33–46. doi: 10.3184/095422908X299164

Fan, C. X. (2019). Research progress and Prospect of lake sediment water interface. *Lake Sci.* 31, 1191–1218.

Fan, W., Wang, W.-X., Chen, J., Li, X., and Yen, Y.-F. (2002). Cu, Ni, and Pb speciation in surface sediments from a contaminated bay of northern China. *Mar. Pollut. Bull.* 44, 820–826. doi: 10.1016/s0025-326x(02)00069-3

Fan, X., Ding, S., Chen, M., Gao, S., Fu, Z., Gong, M., et al. (2019). Peak chromium pollution in summer and winter caused by high mobility of chromium in sediment of a eutrophic lake: in situ evidence from high spatiotemporal sampling. *Environ. Sci. Technol.* 53, 4755–4764. doi: 10.1021/acs.est.8b07060

Fei, Z., Wang, Z., and Tang, Y. (2021). Characteristics and source analysis of heavy metals in Aha Lake during wet and dry periods. *Earth Environ.* 49, 42–50.

Foerstner, U., and Wittmann, G. T. W. (1980). *Metal Pollution in the Aquatic Environment*. Berlin: Springer.

Gall, J. E., Boyd, R. S., and Rajakaruna, N. (2015). Transfer of heavy metals through terrestrial food webs: a review. *Environ. Monit. Assess* 187:201. doi: 10.1007/s10661-015-4436-4433

Gao, L., Li, R., Liang, Z., Wu, Q., Yang, Z., Li, M., et al. (2021). Mobilization mechanisms and toxicity risk of sediment trace metals (Cu, Zn, Ni, and Pb) based on diffusive gradients in thin films: a case study in the Xizhi River basin, South China. *J. Hazard. Mater.* 410:124590. doi: 10.1016/j.jhazmat.2020.124590

Green, A. J., and Planchart, A. (2018). The neurological toxicity of heavy metals: a fish perspective. *Comp. Biochem. Physiol. Part C Toxicol. Pharmacol.* 208, 12–19. doi: 10.1016/j.cbpc.2017.11.008

Hampton, S. E., Galloway, A. W. E., Powers, S. M., Ozersky, T., Whiteford, E. J., and Xenopoulos, M. A. (2017). Ecology under lake ice. *Ecol. Lett.* 20, 98–111.

Harper, M. P., Davison, W., Zhang, H., and Tych, W. (1998). Kinetics of metal exchange between solids and solutions in sediments and soils interpreted from DGT measured fluxes. *Geochim. Cosmochim. Acta* 62, 2757–2770. doi: 10.1016/S0016-7037(98)00186-180

Heger, D., Klánová, J., and Klán, P. (2006). Enhanced protonation of cresol red in acidic aqueous solutions caused by freezing. *J. Phys. Chem. B* 110, 1277–1287. doi: 10.1021/jp0553683

Kamari, M., Tattari, S., Lotsari, E., Koskiaho, J., and Lloyd, C. E. M. (2018). High-frequency monitoring reveals seasonal and event-scale water quality variation in a temporally frozen river. *J. Hydrol.* 564, 619–639. doi: 10.1016/j.jhydrol.2018.07.037

Liu, C., Fan, C., Shen, Q., Shao, S., Zhang, L., and Zhou, Q. (2016). Effects of riverine suspended particulate matter on post-dredging metal re-contamination across the sediment-water interface. *Chemosphere* 144, 2329–2335. doi: 10.1016/j.chemosphere.2015.11.010

Liu, J. (2019). *Adsorption, Oxidation / Reduction and Crystal Growth of Metal Ions on Typical Iron Oxide Surfaces*. Doctor thesis, China: University of Chinese Academy of Sciences.

Liu, P., Zheng, C., Wen, M., Luo, X., Wu, Z., Liu, Y., et al. (2021). Ecological risk assessment and contamination history of heavy metals in the sediments of Chagan lake. Northeast China. *Water* 13:894. doi: 10.3390/w13070894

Luo, S. S., Wan, G. J., and Huang, R. G. (2000). Distribution and migration characteristics of iron and manganese at the sediment water interface of Erhai Lake, Yunnan. *Chongqing Environ. Sci.* 6, 19–21.

Maina, C. W., Sang, J. K., Raude, J. M., and Mutua, B. M. (2019). Geochronological and spatial distribution of heavy metal contamination in sediment from Lake Naivasha. Kenya. *J. Radiation Res. Appl. Sci.* 12, 37–54. doi: 10.1080/16878507.2019.1593718

Menegario, A. A., Yabuki, L. N. M., Luko, K. S., Williams, P. N., and Blackburn, D. M. (2017). Use of diffusive gradient in thin films for in situ measurements: a review on the progress in chemical fractionation, speciation and bioavailability of metals in waters. *Anal. Chim. Acta* 983, 54–66. doi: 10.1016/j.aca.2017.06.041

Miao, S., DeLaune, R. D., and Jugsujinda, A. (2006). Influence of sediment redox conditions on release/solubility of metals and nutrients in a Louisiana Mississippi River deltaic plain freshwater lake. *Sci. Total Environ.* 371, 334–343. doi: 10.1016/j.scitotenv.2006.07.027

Ozersky, T., Bramburger, A. J., Elgin, A. K., Vanderploeg, H. A., Wang, J., Austin, J. A., et al. (2021). The changing face of winter: lessons and questions from the laurentian Great Lakes. *J. Geophys. Res. Biogeosci.* 126:e2021JG006247. doi: 10.1029/2021JG006247

Ren, J., Williams, P. N., Luo, J., Ma, H., and Wang, X. (2015). Sediment metal bioavailability in Lake Taihu, China: evaluation of sequential extraction, DGT, and PBET techniques. *Environ. Sci. Pollution Res.* 22, 12919–12928. doi: 10.1007/s11356-015-4565-4569

Shao, L., Xiao, H. Y., Wu, D. S., and Tang, C. G. (2012). Research progress of metals pollution from traffic sources. *Earth Environ.* 40, 445–459. doi: 10.14050/j.cnki.1672-9250.2012.03.016

Song, C. L., Cao, X. Y., Li, J. Q., Li, Q. M., Chen, G. Y., and Zhou, Y. Y. (2005). Contribution of phosphatase and microbial activity to endogenous load of phosphorus in lakes and its relation to eutrophication. *Sci. China Series* S2, 90–100.

Templeton, D. M., Ariese, F., Cornelis, R., Danielsson, L.-G., Muntau, H., van Leeuwen, H. P., et al. (2000). Guidelines for terms related to chemical speciation and fractionation of elements. definitions, structural aspects, and methodological approaches (IUPAC Recommendations 2000). *Pure Appl. Chem.* 72, 1453–1470. doi: 10.1351/pac200072081453

Toro, D. M. D., Mahony, J. D., Hansen, D. J., Scott, K. J., Carlson, A. R., and Ankley, G. T. (2002). *Acid Volatile Sulfide Predicts the Acute Toxicity of Cadmium and Nickel in Sediments*. Washington, DC: ACS Publications.

Vera, M., Schippers, A., and Sand, W. (2013). Progress in bioleaching: fundamentals and mechanisms of bacterial metal sulfide oxidation–part A. *Appl. Microbiol. Biotechnol.* 97, 7529–7541. doi: 10.1007/s00253-013-4954-2

Voermans, J. J., Ghisalberti, M., and Ivey, G. N. (2017). The variation of flow and turbulence across the sediment-water interface. *J. Fluid Mechan.* 824, 413–437. doi: 10.1017/jfm.2017.345

Wang, Y. (2018). *High Resolution Simultaneous Acquisition and Microscale Migration Mechanism of Metalss at Sediment Interface*. Doctor thesis, China: University of Chinese Academy of Sciences.

Wang, Y. P., Guan, Q. W., Li, C., Xu, D., and Ding, S. M. (2015). DGT in situ simultaneous analysis of available phosphorus and sulfur in sediments of Chaohu Lake. *J. Environ. Sci.* 35, 2512–2518. doi: 10.13671/j.hjkxxb.2014.0996

Wu, Z., Jiao, L., and Wang, S. (2016). The measurement of phosphorus, sulfide and metals in sediment of Dianchi Lake by DGT (diffusive gradients in thin films) probes. *Environ. Earth Sci.* 75:193. doi: 10.1007/s12665-015-4978-4972

Wu, Z., Wang, S., He, M., and Wu, F. (2015). The measurement of metals by diffusive gradients in thin films (DGT) at sediment/water interface (SWI) of bay and remobilization assessment. *Environ. Earth Sci.* 73, 6283–6295. doi: 10.1007/s12665-014-3851-z

Wu, Z., Wang, S., Jiao, L., and Wu, F. (2014). The simultaneous measurement of phosphorus, sulfide, and trace metals by Ferrihydrite/AgI/Chelex-100 DGT (Diffusive Gradients in Thin Films) probe at sediment/water interface (SWI) and remobilization assessment. *Water Air Soil Pollution* 225:2188. doi: 10.1007/s11270-014-2188-2182

Xia, J. D., Long, J. Y., Gao, Y. P., Chen, Y., Meng, J., Zhou, Y. Q., et al. (2020). Ecological risk assessment and source analysis of metals pollution in sediments of Chaohu Lake. *Earth Environ.* 48, 220–227. doi: 10.14050/j.cnki.1672-9250.2020.01.020

Xie, R. F. (2021). *Metals Deposition Characteristics, Pollution Sources and Trend Prediction of Typical Lakes in Northern China*. Doctor thesis, China: Harbin Normal University.

Xie, X. J., Kang, J. C., Li, W. L., Wang, G. D., Yan, G. D., and Zhang, J. P. (2010). Distribution and source analysis of metalss in agricultural soil in Baoshan District of Shanghai. *Environ. Sci.* 31, 768–774. doi: 10.13227/j.hjkx.2010.03.010

Xu, D., Ding, S., Sun, Q., Zhong, J., Wu, W., and Jia, F. (2012). Evaluation of in situ capping with clean soils to control phosphate release from sediments. *Sci. Total Environ.* 438, 334–341. doi: 10.1016/j.scitotenv.2012.08.053

Xu, L., Zhang, L., Hou, X., and Xu, K. (2012). Adsorption of metals ions on two types of manganese oxides analyzed by AAS and AFS. *Spectroscopy Spectral Anal.* 32, 2842–2846. doi: 10.3964/j.issn.1000-0593201210-2842-2845

Yuan, H., Shen, J., Liu, E., Wang, J., and Meng, X. (2011). Assessment of nutrients and heavy metals enrichment in surface sediments from Taihu Lake, a eutrophic shallow lake in China. *Environ. Geochem. Health* 33, 67–81. doi: 10.1007/s10653-010-9323-9329

Yuan, H., Yin, H., Yang, Z., Yu, J., Liu, E., Li, Q., et al. (2020). Diffusion kinetic process of heavy metals in lacustrine sediment assessed under different redox conditions by DGT and DIFS model. *Sci. Total Environ.* 741:140418. doi: 10.1016/j.scitotenv.2020.140418

Yuan, Z., Taoran, S., Yan, Z., and Tao, Y. (2014). Spatial distribution and risk assessment of heavy metals in sediments from a hypertrophic plateau lake Dianchi. China. *Environ. Monit. Assess* 186, 1219–1234. doi: 10.1007/s10661-013-3451-3455

Zhang, H., and Davison, W. (2002). *Performance Characteristics of Diffusion Gradients in Thin Films for the in Situ Measurement of Trace Metals in Aqueous Solution*. Washington, DC: ACS Publications.

Zhang, M. K., Wang, H., and Zhang, H. M. (2008). Source identification of metalss in farmland soil of marine plain in eastern Zhejiang. *J. Environ. Sci.* 10, 1946–1954. doi: 10.13671/j.hjkxxb.2008.10.003

Zhao, Z. L., Dong, G. F., Li, Z. X., Zhang, H. T., Yu, S. Q., and Yu, B. (1987). Study on background values of nine heavy metals in natural soils in Jilin Province. *Soil* 6, 315–317.

Zoumis, T., Schmidt, A., Grigorova, L., and Calmano, W. (2001). Contaminants in sediments: remobilisation and demobilisation. *Sci. Total Environ.* 266, 195–202. doi: 10.1016/s0048-9697(00)00740-3

frontiers | Frontiers in Ecology and Evolution

TYPE Original Research
PUBLISHED 12 August 2022
DOI 10.3389/fevo.2022.977899



OPEN ACCESS

EDITED BY
Chuanyu Gao,
Northeast Institute of Geography and Agroecology (CAS), China

REVIEWED BY
Junhong Bai,
Beijing Normal University, China
Wenguang Sun,
University of Nebraska-Lincoln, United States
Jia Jia,
Yellow River Institute of Hydraulic Research, China

*CORRESPONDENCE
Junbao Yu
junbao.yu@gmail.com
Baoquan Li
bqli@yic.ac.cn

†These authors have contributed equally to this work

SPECIALTY SECTION
This article was submitted to Conservation and Restoration Ecology, a section of the journal Frontiers in Ecology and Evolution

RECEIVED 25 June 2022
ACCEPTED 15 July 2022
PUBLISHED 12 August 2022

CITATION
Sun D, Li Y, Yu J, Li B, Guan B, Zhou D, Wang X, Yang J, Ma Y, Zhang X, Li X, Ling Y, Zou Y, Jia S and Shen F (2022) Spatial distribution of soil quality under different vegetation types in the Yellow River Delta wetland. *Front. Ecol. Evol.* 10:977899. doi: 10.3389/fevo.2022.977899



# Spatial distribution of soil quality under different vegetation types in the Yellow River Delta wetland

Debin Sun[1,2,3,4†], Yunzhao Li[1,2†], Junbao Yu[1,2*], Baoquan Li[3*], Bo Guan[1,2], Di Zhou[1,2], Xuehong Wang[1,2], Jisong Yang[1,2], Yuanqing Ma[5], Xin Zhang[1,2], Xue Li[1,2], Yue Ling[1,2], Yuhan Zou[1,2], Shaoning Jia[1,2] and Fa Shen[1,2]

[1]Key Laboratory of Ecological Restoration and Conservation of Coastal Wetlands in Universities of Shandong (Ludong University), Yantai, China, [2]The Institute for Advanced Study of Coastal Ecology, Ludong University, Yantai, China, [3]Yantai Institute of Coastal Zone Research, Chinese Academy of Sciences, Yantai, China, [4]University of Chinese Academy of Sciences, Beijing, China, [5]Shandong Marine Resources and Environment Research Institute, Yantai, China

The soils from four typical natural wetlands, namely, *Phragmites australis*, *Tamarix chinensis*, *Suaeda salsa*, and tidal flat, as well as reclaimed wetland, were selected to evaluate the soil quality in the Yellow River Delta. Fourteen soil physicochemical property indexes were employed to build a minimum data set (MDS). Combined with vegetation type and soil depth, the soil quality index (SQI) was conducted. A fuzzy logic model was applied for data normalization. The contrast test was conducted to verify the accuracy of the MDS. The results showed that the MDS consists of TOC, $NO_3^-$-N, soil salinity, TS, TP, Mg, C/N and pH. The soil quality decreased from the inland to the coastline and from reclaimed wetland to tidal flat with the change of vegetation type. The soil quality of 0–10 cm soil depth was better than that of 20–30 cm soil depth. The soil qualities of reclaimed land were significantly better than those of natural wetlands at the same soil depth. Correlation analysis results showed that agricultural reclamation has become an important factor of soil quality change in the study area. Comparative results of two methods of MDS and the total data set (TDS) testified that the method of MDS was credible and accurate for soil quality assessment of the study area. Our results indicated that wetland protection and agricultural reclamation in coastal areas should keep a rational balance.

KEYWORDS

**soil quality, coastal wetland, vegetation type, the Yellow River Delta, minimum data set**

## Introduction

As a natural ecotone between the marine ecosystem and the terrestrial ecosystem, the coastal wetland is a vulnerable ecosystem with various ecological functions (Yu et al., 2016). As the dominant substrate in coastal wetland ecosystems, soil plays an important role in plant growth and system stability (Zhang et al., 2013; Huang and Yuan, 2021).

Soil quality, which is sensitive to the dynamic change of soil condition and soil management, can be used as a comprehensive index to evaluate soil function (Chaer et al., 2009; Adebo et al., 2020; Raiesi and Beheshti, 2022). To assess the effects of heavy metals on water and soil, the concept of soil quality was first put forward in the 1970's (Sultana et al., 1970; Peters, 1973). Since then, the connotation of soil quality has been continuously enriched (Shokr et al., 2021). Currently, due to the concept covering a range of synthetical aspects, a widely accepted definition has not been established. According to the existing standpoints, three main elements for soil quality include the abilities of maintaining ecosystem productivity, sustaining environmental quality, and promoting biotic health (Wander et al., 2002; Abdel-Fattah et al., 2021; Mazzon et al., 2021; Rathore et al., 2022). Soil quality assessment is a decision-making method for quantitative reflection of soil quality by selecting suitable evaluation indexes in a certain area (Chen et al., 2021; Yuan et al., 2022).

The accuracy of soil quality assessment is decided by the method and index selection (Armenise et al., 2013; Wang et al., 2018). A number of methods, such as soil quality index (SQI) (Granatstein and Bezdicek, 1992; Andrews et al., 2002, 2003), dynamic soil quality models (Karlen et al., 2003; Nyeck et al., 2018; Fathizad et al., 2020), soil quality cards and test kits (Purakayastha et al., 2019; Kasno, 2021), soil management assessment framework (Cherubin et al., 2017; Jimenez et al., 2022), and fuzzy association rules (Burrough, 1989; Burrough et al., 1992; Wu et al., 2019), have been applied to assess soil quality in various ecosystems of the cropland, forest, grassland, and wetland, etc. SQI has been widely used in numerous ecosystems due to its simplicity, flexibility, and applicability (Andrews et al., 2002; Wang et al., 2018). The SQI includes three essential steps: (1) selecting appropriate indexes to establish datasets; (2) normalizing the index data; and (3) combining index scores to produce the comprehensive SQI (Chaer et al., 2009; Zhang et al., 2016; Wang et al., 2018). Normally, in order to make the assessment results more comprehensive and accurate, a dataset needs to contain abundant indexes, leading to a lot of redundant information being contained in the total data set (TDS) (Wu et al., 2019; Shao et al., 2020). Therefore, the Minimum Data Set (MDS) needs to be established (Raiesi, 2017; Jiang et al., 2020; Guo et al., 2021). The MDS contains a series of representative indexes which are screened from TDS. The MDS is considered a set of sensitive and comprehensive methods to remove redundancy with less information loss (Wang et al., 2018). Several studies showed that the assessment-based MDS was better than TDS in cropland, forest, grassland, and coastal areas (Rahmanipour et al., 2014; Volchko et al., 2014; Wu et al., 2019). The methods of multiple linear regression, factor analysis, discriminant analysis, and scoring functions are employed for index screening (Rezaei et al., 2006; Yao et al., 2013). Factor analysis has been widely used in MDS as the method that can efficiently reduce redundant information (Raiesi, 2017; Shao et al., 2020).

The Yellow River Delta wetland is one of the largest nascent coastal wetland ecosystems in the world (Yu et al., 2016). Due to the serious erosion of soil and water in the middle reaches of the Yellow River, a mass of sediment is carried to the estuary from the Loess Plateau. The typical coastal wetlands in deltas along the Pacific Coast are formed by sediment accumulation over years (Yu et al., 2015; Ji et al., 2022). *Phragmites australis*, *Tamarix chinensis*, and *Suaeda salsa* are dominant vegetation types in the natural wetland of the Yellow River Delta (Jiao et al., 2014). The tidal flat is widely distributed with low vegetation coverage. Most communities are dominated by one plant species with few concomitant species. The natural wetlands with a simple structure, such as *Phragmites australis*, *Tamarix chinensis*, *Suaeda salsa*, and tidal flat, which is the main body of shrub wetland, herbaceous wetland, salt marsh, and tidal flat wetland, are formed (Jiao et al., 2014; Chi et al., 2020). Influenced by land-sea-river interaction, all types of natural wetlands are distributed with a zonal sequence from land to sea (Cao et al., 2015). In addition, a large area of cropland which is reclaimed from natural wetlands over years covers this region (Yu et al., 2016). Due to the biological characteristics of saline-alkali-tolerant, *Gossypium spp*. has been widely planted and has become the dominant crop type. The wetland reclamation could alter vegetation type and soil physicochemical properties dramatically (Jiao et al., 2019). Therefore, the spatial heterogeneity of soil conditions in the Yellow River Delta wetland is influenced by natural and human factors such as hydrological processes, vegetation types, and land reclamation, which lead to a soil quality with high complexity. At present, only a few references related to the soil quality in the Yellow River Delta are found. Zhang et al. (2016) evaluated the effects of flooding conditions and seasonal variations on soil quality in natural wetlands in five selected natural wetland types over three seasons (Zhang et al., 2016). The results showed that soil salinity might be a characteristic indicator of soil quality assessment in coastal regions. Xia et al. (2019) studied the relationship between soil quality and forest-grass composite patterns in this region using the membership function method (Xia et al., 2019). Wu et al. (2019) found that the soil quality was higher in inland areas than in coastal areas by evaluating the soil quality of the crop land (Wu et al., 2019). Employing the method of SQI, Zhao et al. (2019) assessed the effects of freshwater inputs on soil quality in natural wetlands (Zhao et al., 2019). Yang et al. (2021) used principal component analysis to evaluate the effects of different *Tamarix chinensis*-grass patterns on the soil quality of coastal saline soil and found that certain community patterns could significantly decrease the salt contents and increase the available nutrient contents in the coastal saline-alkali soil (Yang et al., 2021).

Several problems related to soil quality in the study region still remain. Due to sampling sites and limited participating

assessment indexes, the assessment results were insufficient to reflect upon the distribution law and overall situation of regional soil quality. There was no comparative study under a unified assessment framework for the SQI of current studies confined to natural wetlands or cropland. The impact of wetland reclamation on soil quality in this region is not clear. Therefore, the present study assessed the soil qualities under different vegetation types of the natural wetland and reclaimed wetland in the Yellow River Delta applying the MDS based on 14 soil property indexes. The purposes of the study were to (1) reveal the spatial distribution characteristics of the soil quality in the Yellow River Delta, (2) clarify the function of wetland reclamation on soil quality change in a coastal wetland, and (3) verify the suitability of an MDS on coastal wetland soil quality assessment. The result could provide a scientific reference for maintaining the ecological balance of wetland protection and agricultural reclamation in coastal areas.

# Materials and methods

## Study area

The study was conducted in the Yellow River Delta (37°34′-38°09′N, 118°31′-119°18′E) (Figure 1). The study area has a warm-temperate and continental monsoon climate with distinct seasons. The average annual temperature, precipitation, and evaporation are 12.8°C, 537.3 mm, and 1,928.2 mm, respectively (He and Cui, 2015). The precipitation mainly concentrates in summer and autumn. The main water supplement is atmospheric precipitation, river, and tidal water. Due to the interactive effects of land-sea-river, the soil conditions are complex and changeable. Affected by tidal action and soil evapotranspiration, *Phragmites australis* wetland (Pa), *Tamarix chinensis* wetland (Tc), *Suaeda salsa* wetland (Ss), and tidal flat wetland (Td) showed a regular ribbon distribution from land to sea along different degrees of soil salinity (Figure 1). Reclaimed wetlands (Cp), mainly distributed in the interior region of deltas which are far from the sea, are mostly reclaimed from natural wetlands.

## Sample collection and analysis

The Landsat Thematic Mapper (TM) of 2018 digital images (spatial resolution of 30 ×30 m) were used to interpret the land use and land cover in the study area. The land use classification map of the Yellow River Delta was produced after calibration by the field investigation. According to the grid distribution point method, the sampling points were set up in four selected natural wetlands, of *Phragmites australis* wetland (Pa) (40 sites), *Tamarix chinensis* wetland (Tc) (18 sites), *Suaeda salsa* wetland (Ss) (19 sites) and tidal flat wetland (Td) (21 sites), as well as reclaimed wetland (Cp) (20 sites), in mid-August 2019. A total of 118 soil sampling sites were implemented with three parallel treatments at each site (Figure 1). Soil samples of 0–10, 10–20, and 20–30 cm in depth were collected from bottom to top in soil profiles by a core sampler. Three duplicate soil samples were collected and mixed homogeneity *in situ* after removing plant residues, roots, and debris. The samples were air dried after removing plant debris and stones. The air-dried soil samples were sieved with a 0.149-mm diameter nylon sieve after grinding using a mortar to determine soil properties.

Soil total organic carbon (TOC) was determined by TOC Analyzer (vario TOC cube, Elementar, Germany) after inorganic carbon was eliminated using 1M HCl. Soil total nitrogen (TN) and total phosphorus (TP) were determined by a continuous flow analyzer (Futura A16786, Alliance, France) after digestion and filtration. Soil total sulfur (TS) was measured using the barium sulfate turbidimetric method. Soil total (TK), Na, and Mg were determined by atomic absorption spectrometer (iCE 3300 AAS, Thermo, America) after digestion and filtration. Soil $NH_4^+$-N and $NO_3^-$-N in supernatant liquor, which were filtrated by a 0.45-μm membrane, were determined by a continuous flow analyzer after extraction with 2 M KCl from sieved dry soil samples. Soil pH (water: soil = 2.5:1) and electrical conductivity (EC) (water: soil = 5:1) were determined by a pH meter (FE28-Standard, Mettler Toledo, Switzerland) and an electrical conductivity meter (FE38, Mettler Toledo, Switzerland), respectively. The stoichiometric ratios of C/N, C/P, and N/P were calculated as the ratio of the amount of TOC to TN, TN to TP, and TN to TP, respectively.

## Assessment of soil quality index

To calculate the SQI which can represent the comprehensive characteristics of soil quality, the Minimum Data Set (MDS) was screened by the principal component analysis (PCA) of the total data set (TDS). The MDS was screened following these five steps. (1) The results of correlations between different soil property indexes and coefficient of variation (CV) incorporated determine the necessity to screen indexes from TDS. (2) The PCA was used to screen indexes for MDS. Only the components with eigenvalues ≥1 were retained. The soil property indexes with loading ≥0.5 in each component were divided into one group. (3) The vector norm value (Equation 1) was employed to reflect the influence degree of internal factors (i.e., 14 soil properties) on soil quality. A large norm value indicates that the index has a large comprehensive load on all principal components. (4) The improvement methods by Pulido et al. (2017) and Wu et al. (2019) were referenced to select the external factors. The soils under different vegetation types (i.e., Pa, Tc, Ss, Td, and Cp) and soil depth (i.e., 0–10 cm, 10–20 cm, and 20–30 cm) were selected as external factors in the study. Multivariate analysis and normal linear transformation were used to reflect

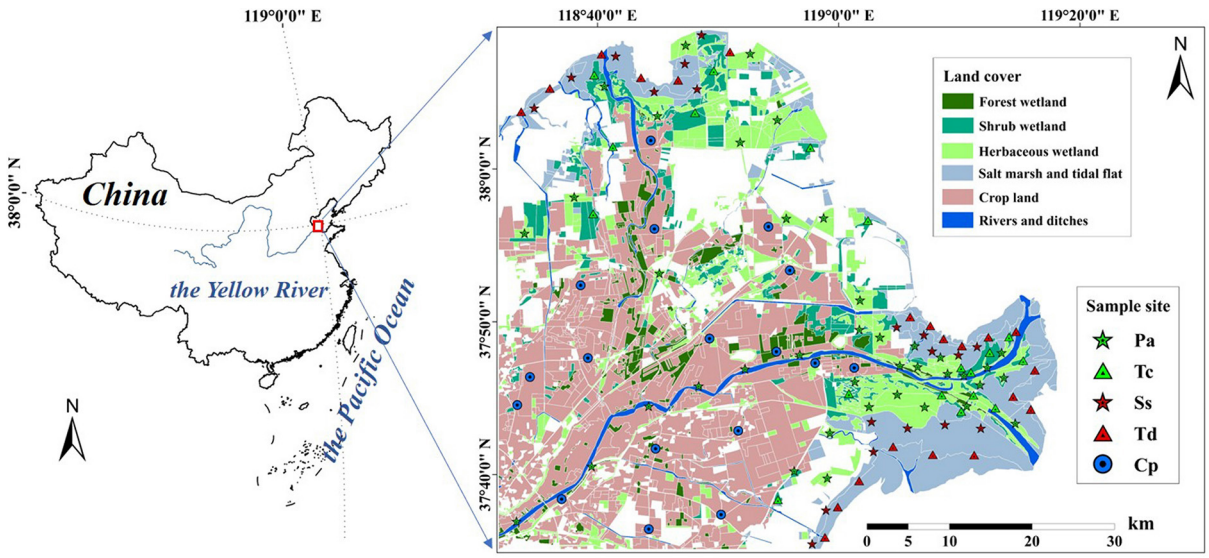


FIGURE 1
Map of study area and sample sites.

the influence degree of soil type and soil depth on soil quality. The accumulated values of internal and external factors were used to screen indexes of MDS. (5) The soil properties with the highest accumulated value were screened for preliminary indexes in each group. Soil properties within 90% of the highest value were also selected. If the correlation value of any two preliminary indexes were higher than 0.5 in one group, the indicator with a higher value was screened for MDS (Zhang et al., 2016). The weighting of each index was the proportion of its accumulated value to the sum of total values in MDS.

$$\mathbf{N_{ik}} = \sqrt{\sum_{\mathbf{i=1}}^{\mathbf{k}} (\mathbf{U_{ik}^2} \cdot \lambda_{\mathbf{k}})} \tag{1}$$

where $N_{ik}$ is the comprehensive loading of soil property $i$ in the first $k$ principal components with eigenvalues≥1, $\lambda k$ is the eigenvalue of PC$k$, and U$ik$ is the variable loading of soil property. N$ik$ of the indexes within 10% of the highest norm values was selected for the MDS.

The indexes of MDS were normalized by fuzzy set methodology to determine the membership degree. Fuzzy function with a bell-shaped curve was used to calculate the memberships of different indexes (Burrough, 1989; Burrough et al., 1992). The method produced contiguous value distribution of membership value and rejected low information during the analysis process, which was much better than linear transformation for membership calculation (Yang et al., 2021). Three steps were operated in this method. (1) The suitable range of each index in MDS was selected. In order to make an analysis normalization, the 5–95% interval of the normal distribution as the threshold value of each index was used in this study. (2) The bell-shaped curve was employed as the fuzzy logic membership function because the nutrient contents and soil salinity were the predominant soil property indexes in the study (Equation 2). (3) The fuzzy logic model was established after the coefficients $b$ and $d$ of Equation 2 were calculated by the suitable range of each index. If the index value is within the suitable range, the membership value could be determined by Equation 2. Otherwise, it could be chosen 0 or 1 based on the effect of the index. Finally, the membership value and weighting of each index were combined to generate the comprehensive soil quality index (SQI) of each sample using Equation 3.

$$\mathbf{MF_{xi}} = [\mathbf{1}/(\mathbf{1}+\{(\mathbf{x_i}-\mathbf{b})/\mathbf{d}\}^{\mathbf{2}})] \tag{2}$$

where $MF_{xi}$ is the individual membership value for $i$th soil index of $x$ ($0 \leq MF_{xi} \leq 1$), $d$ is the width of the transition zone, which is the difference between the index values where the membership values range from 0.5 to 1, and $b$ is the value of soil index at the ideal point or standard index where the membership value is 1.

$$\mathbf{SQI} = \sum_{\mathbf{i=1}}^{\mathbf{n}} \mathbf{W_i} \cdot \mathbf{MF_{xi}} \tag{3}$$

where SQI is the joint membership for all indexes within MDS of $x$ (i.e., the comprehensive soil quality index), W$i$ is the weighting of $i$th soil index in MDS, $MF_{xi}$ is the individual membership value for $i$th soil index of $x$, and $n$ is the number of the index in MDS.

## Data analysis

IBM SPSS 24.0 was used for data analysis. The data satisfied the homogeneity of variance and normal distribution assumptions by Shapiro-Wilk's and Levene's tests ($p > 0.05$). The mean value, standard deviation (SD), and CV of each soil property were calculated, respectively. The differences were tested by a one-way analysis of variance (one-way ANOVA) with LSD ($p < 0.05$) and linear mixed effects models ($p < 0.05$). Pearson correlation analysis was performed to reveal the relationships among soil indexes. The significant effects of vegetation type and soil depth on soil properties were assessed by multifactor analysis of variance (multi-way-ANOVA). ArcGIS 10.8 was used to test normal distribution, reject abnormal values, select interpolation method, analyze trend effect, and map spatial distribution. All datasets were projected to WGS84-based Transverse Mercator orthographic projection coordinate system. Space interpolation analyses of SQI were conducted by the Empirical Bayes Kriging method (EBK). The spatial distribution of the rivers, salt pan, culture pond, residence zone, industrial, and mining district were eliminated from interpolation ultimately. Origin 9.8 software was used to draw.

# Results

## Statistical analysis of soil properties

The averaged contents of soil TOC, TN, TP, TS, TK, Mg, $NH_4^+$-N, and $NO_3^-$-N were 3.94, 0.36, 0.58, 0.86, 20.96, 13.54, 8.00, and 6.02 mg·kg$^{-1}$ in study area, respectively (Supplementary Table 1). The averaged values of C/N, C/P, and N/P were 12.85, 17.29, and 1.37 by the substance amount. In order to adequately analyze the soil quality of saline-alkali soil, the soil Na, soil salinity (Sa), and pH were selected as characteristic indexes in the study. The mean values of soil Na, Sa, and pH in the study area were 16.97 g·kg$^{-1}$, 5.82‰, and 8.33. The CV values of $NO_3^-$-N (198.17%), $NH_4^+$-N (77.44%), Sa (60.26%), TN (56.10%), TOC (56.46%), N/P (50.51%), and C/P (51.90%) were higher than 50%, illustrating that these soil indexes have strong spatial variability. Except for TK and pH, the other indexes showed moderate or above moderate variability (CV >10%).

## MDS establishment and normalization

The considerably significant correlations ($p < 0.01$) were observed among 68.13% of soil indexes in TDS by Pearson analysis (Table 1). Therefore, the redundancy existing in TDS and an MDS should be established.

The cumulative variance of the first five components reached 80.70% (Supplementary Table 2), indicating that the first five

TABLE 1 Pearson analysis of soil properties.

| Property | TOC | TN | TP | TS | TK | Mg | Na | $NH_4^+$-N | $NO_3^-$-N | C/N | C/P | N/P | Sa | pH |
|---|---|---|---|---|---|---|---|---|---|---|---|---|---|---|
| TOC | 1.00 | | | | | | | | | | | | | |
| TN | 0.91** | 1.00 | | | | | | | | | | | | |
| TP | 0.39** | 0.40** | 1.00 | | | | | | | | | | | |
| TS | 0.18** | 0.12* | 0.08 | 1.00 | | | | | | | | | | |
| TK | 0.39** | 0.47** | 0.29** | 0.13* | 1.00 | | | | | | | | | |
| Mg | 0.54** | 0.58** | 0.37** | 0.24** | 0.85** | 1.00 | | | | | | | | |
| Na | −0.60** | −0.68** | −0.18** | 0.01 | −0.25** | −0.47** | 1.00 | | | | | | | |
| $NH_4^+$-N | 0.62** | 0.70** | 0.27** | −0.02 | 0.40** | 0.50** | −0.69** | 1.00 | | | | | | |
| $NO_3^-$-N | 0.22** | 0.35** | 0.30** | −0.19** | 0.16** | 0.21** | −0.26** | 0.36** | 1.00 | | | | | |
| C/N | 0.25** | −0.13* | 0.02 | 0.09 | −0.13* | −0.04 | 0.13* | −0.13* | −0.19** | 1.00 | | | | |
| C/P | 0.97** | 0.86** | 0.19** | 0.17** | 0.36** | 0.51** | −0.59** | 0.58** | 0.16** | 0.28** | 1.00 | | | |
| N/P | 0.88** | 0.97** | 0.21** | 0.11* | 0.45** | 0.56** | −0.69** | 0.68** | 0.29** | −0.15** | 0.89** | 1.00 | | |
| Sa | −0.21** | −0.24** | −0.05 | 0.39** | −0.09 | −0.07 | 0.22** | −0.28** | −0.26** | 0.03 | −0.22** | −0.25** | 1.00 | |
| pH | −0.11 | −0.13* | 0.01 | 0.10 | −0.31** | −0.23** | −0.01 | −0.16** | −0.11* | 0.05 | −0.10 | −0.12* | 0.24** | 1.00 |

* and ** denote the correlation is significant at the 0.05 and 0.01 level, respectively.

components could represent the principal characteristics of total data. The communalities for soil properties showed that the first five components could explain more than 90% of the variance of TOC, TN, C/N, C/P, and N/P and more than 80% of TP, TK, and Mg, which indicates that the most variances of soil properties could be explained by principal components (Table 2).

Based on the screening regulations for MDS establishment (The soil properties with loadings ≥0.5 in each component were divided into one group. If the loading of one soil property ≥0.5 was observed in more than one component, that should be divided into one group in which the correlation of soil properties was relatively low), five groups were established (Table 2): TOC, TN, TK, Na, $NH_4^+$-N, C/P, and N/P were in group 1, TS, $NO_3^-$-N, and Sa in group 2, Mg in group 3, C/N and pH in group 4, and TP in group 5.

According to Equation 1, the norm value of each index was calculated (Table 2). The adjusted coefficients of all soil properties with soil type ($R^2_{(St)}$) and soil depth ($R^2_{(Sd)}$) were calculated by multivariate analysis. Then, the norm value, $R^2_{(St),}$ and $R^2_{(Sd)}$ of each soil property were transformed by normal transformation. At last, the MDS was established using accumulated values and the Pearson analysis results (Table 1). The six indexes including TOC, TS, $NO_3^-$-N, Sa, Mg, C/N, pH, and TP were grouped in MDS ultimately (Table 2).

Indexes related to soil nutrient elements (i.e., TOC, TS, $NO_3^-$-N, Mg, C/N, and TP) were considered as "more is better" so that the asymmetric left variant of the bell-shaped curve was employed, while the Sa and pH were considered as "less is better" due to the characteristics of barren saline-alkali soil in the study area so that the asymmetric right variant was employed. The coefficients *b* and *d* were determined in Table 3. When the index value is within the suitable range, the membership value could be determined by Equation 2, and without the range, the membership value could choose 0 or 1 based on the effect of the index (Table 3). The membership values of each index were calculated ultimately.

## Weighting assessment and soil quality calculation

The weighting of each index was the proportion of its accumulated value to the sum of total values in MDS. The weighting assessment results showed that TOC accounted for the highest weight of 20.88% in the group of "more is better" and that Sa accounted for the highest weight of 15.13% in the group of "less is better" (Tables 2, 3).

According to Equation 3, the mean SQI values of the Yellow River Delta under different vegetation types varied from 0.42 (Ss, 20–30 cm) to 0.70 (Cp, 0–10 cm) (Figure 2A). The mean SQI values in natural wetlands followed the order of Pa (0.56)

TABLE 2 The weighting of each soil index in MDS.

| TDS | Group | Norm | $R^2_{(St)}$ | $R^2_{(Sd)}$ | $T_{(Norm)}$ | $T_{(St)}$ | $T_{(Sd)}$ | A-Value | MDS | W (%) |
|---|---|---|---|---|---|---|---|---|---|---|
| TOC | 1 | 2.26 | 0.10 | 0.13 | 0.98 | 0.20 | 1.00 | 2.18 | Yes | 20.88 |
| TN | 1 | 2.31 | 0.16 | 0.09 | 1.00 | 0.32 | 0.70 | 2.03 | No | - |
| TP | 5 | 1.30 | 0.03 | 0.01 | 0.72 | 0.05 | 0.04 | 0.81 | No | 10.25 |
| TS | 2 | 1.09 | 0.14 | 0.01 | 0.80 | 0.28 | 0.05 | 1.13 | No | 14.27 |
| TK | 1 | 1.67 | 0.14 | 0.01 | 0.84 | 0.29 | 0.05 | 1.18 | No | - |
| Mg | 3 | 1.91 | 0.10 | 0.10 | 0.94 | 0.19 | 0.81 | 1.95 | No | 8.72 |
| Na | 1 | 1.85 | 0.15 | 0.07 | 0.98 | 0.30 | 0.53 | 1.81 | No | - |
| $NH_4^+$-N | 1 | 1.94 | 0.26 | 0.06 | 0.47 | 0.53 | 0.49 | 1.49 | Yes | - |
| $NO_3^-$-N | 2 | 1.25 | 0.48 | 0.01 | 0.54 | 0.98 | 0.10 | 1.61 | Yes | 15.42 |
| C/N | 4 | 1.10 | 0.49 | 0.01 | 0.52 | 1.00 | 0.06 | 1.58 | Yes | 7.66 |
| C/P | 1 | 2.18 | 0.04 | 0.00 | 0.83 | 0.09 | 0.00 | 0.91 | Yes | - |
| N/P | 1 | 2.27 | 0.09 | 0.02 | 0.48 | 0.18 | 0.14 | 0.80 | Yes | - |
| Sa | 2 | 1.21 | 0.05 | 0.03 | 0.46 | 0.09 | 0.25 | 0.80 | Yes | 15.13 |
| pH | 4 | 1.06 | 0.06 | 0.05 | 0.56 | 0.11 | 0.39 | 1.07 | Yes | 7.66 |

$R^2_{(St)}$ and $R^2_{(Sd)}$ denote the adjusted coefficient of all soil properties with soil type and soil depth by multivariate analysis, respectively. $T_{(Norm)}$, $T_{(St)}$ and $T_{(Sd)}$ denote the normal linear transformation results of Norm, $R^2_{(St)}$ and $R^2_{(Sd)}$ values, respectively. A-Value is accumulated value. W denote the weighting of each soil index in MDS.

TABLE 3 The optimal ranges of MDS indexes.

| Index | Suitable range | *b* | *d* | Effect |
|---|---|---|---|---|
| TOC | 1.35–9.03 | 9.03 | 5.53 | More is better |
| TS | 0.55–1.28 | 1.28 | 0.43 | More is better |
| $NO_3^-$-N | 1.15–32.34 | 32.34 | 30.02 | More is better |
| Sa | 1.28–12.21 | 1.28 | 4.25 | Less is better |
| Mg | 9.90–18.10 | 18.10 | 4.89 | More is better |
| C/N | 7.93–18.83 | 18.83 | 6.22 | More is better |
| pH | 7.67–9.06 | 7.67 | 0.61 | Less is better |
| TP | 0.48–0.71 | 0.71 | 0.14 | More is better |

> Tc (0.52) > Ss (0.47) and Td (0.47). The SQI value of reclaimed wetland (0.64) was considerably higher than that of natural wetlands ($p < 0.05$). The SQI values in soil profiles showed a decreasing trend with a soil depth increase. The SQI value of 0–10 cm soil layer of all the vegetation types but Tc were significantly higher than those in 20–30 cm soil layer ($p < 0.05$).

The influence degree of each index for SQI changed with vegetation type by the analysis of contribution rate (Figures 2B,C). In the study area, the greatest positive contribution of SQI was TOC, followed TS and $NO_3^-$-N. The contribution proportion of TOC was stable (about 20%) among different vegetation types. The proportion of TS in natural wetlands (11–22%) was more than the proportion in the reclaimed wetlands (7%). The $NO_3^-$-N proportion in natural wetlands (13–15%) was lower than the proportion in the reclaimed wetlands (20%). The contribution proportion of TP, Mg, and C/N was relatively low, and there was little difference among different vegetation types except for C/N. The contribution proportion of C/N in natural wetlands was about 1.4–1.8 times that of reclaimed wetlands. The negative effect was mainly mediated by Sa. The tendency of Sa contribution followed Pa (20%) > Tc (12%) > Ss (9%) and Td (9%) in natural wetlands, and the proportion of reclaimed wetlands (21%) was higher than those of natural wetlands. The contribution of TOC decreased with the increase of soil depth, while the changing trend of Sa was the opposite.

The multi-way-ANOVA results showed that SQI was significantly correlated with vegetation type ($p < 0.05$) and soil depth ($p < 0.05$) (Supplementary Table 3). A significantly positive correlation was observed between SQI and soil nutrient elements in a 0–30-cm soil layer of natural wetlands ($p < 0.05$) and reclaimed wetlands ($p < 0.05$, Table 4). A significant negative correlation between SQI with soil Sa and pH was observed in a 0–30-cm soil layer of natural wetlands ($p < 0.05$), but this significant correlation was not observed in the reclaimed wetlands ($p > 0.05$).

## The spatial distribution of SQI

The SQI values of 0–10 cm and 10–20 cm soil layer increased and distributed in a ribbon shape from coastline to inland, while the spatial change gradient of SQI values in a 20–30-cm soil layer was not obvious (Figures 3A–C). The linear fitting analysis results of SQI and the logarithmic function of the distance on vertical distance from the coastline in each sampling point showed that SQI increased with the increase of distance to the coastline (Figures 3A–C). The slope of fitting equation followed the order of 0–10 cm (0.07) > 10–20 cm (0.06) > 20–30 cm (0.05), indicating the spatial heterogeneity of soil quality in horizontal direction decreased with soil depth in 0–30 cm.

The highest SQI value of 0–30 cm soil layer is concentratedly distributed in the central region of the delta where there was a reclaimed area that is far away from the sea (Figure 4A). The lowest SQI value is mainly distributed near the coastline of a Td area. To be consistent with the vertical distance to the coastline, the mean values of SQI in 0–30 cm followed: Cp > Pa > Tc > Ss and Td (Figure 4B). The results indicated that the soil quality in the study area decreased gradually from upper soil to lower soil (0–30 cm), from inland to coastline, from reclaimed wetlands to tidal flat.

## The contrast test of $SQI_{MDS}$ and $SQI_{TDS}$

To test the accuracy of MDS for soil quality assessment in the Yellow River Delta, we compared the SQI results of the MDS ($SQI_{MDS}$) with the total data set ($SQI_{TDS}$). There was a strong linear relationship between $SQI_{MDS}$ values and $SQI_{TDS}$ values under different vegetation types and soil depth (Figure 5). The coefficient of determination ($r^2$) of linear regression in Pa, Tc, Ss, Td, and Cp were 0.83, 0.79, 0.81, 0.79, and 0.86, respectively. The $r^2$ in 0–10 cm, 10–20 cm, and 20–30 cm were 0.81, 0.86, and 0.86, respectively. The results of the contrast test demonstrated that the MDS with high accuracy and credibility was suitable for assessing the soil quality of the Yellow River Delta.

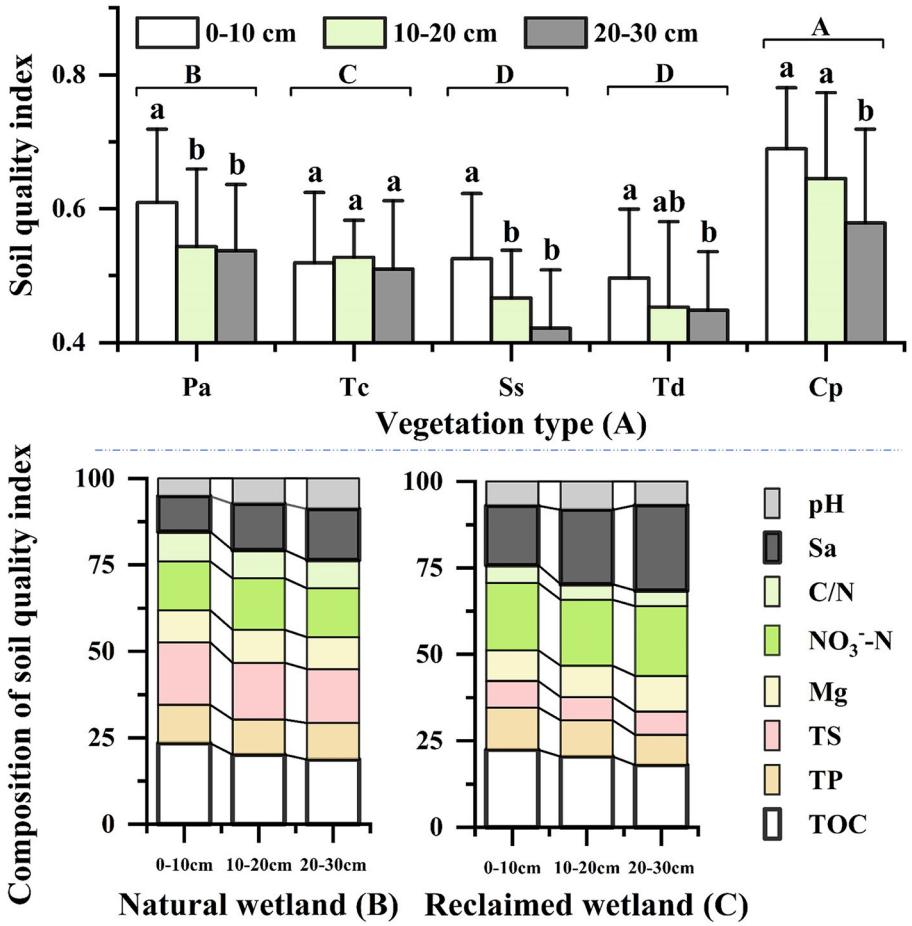


FIGURE 2
The SQI values in soil profiles under different vegetation types **(A)** and the composition of SQI in natural wetland **(B)** and reclaimed wetland **(C)**. The vertical bar is standard deviation; different lower letter denotes the significant differences among soil depth for the same vegetation type ($p < 0.05$); different upper letter denotes the significant differences among vegetation types in 0–30 cm ($p < 0.05$).

## Discussion

The main influencing factors of soil quality spatial distribution in the study area were soil nutrients and soil salinity (Table 2), which was the comprehensive results of soil formation process, vegetation type, and anthropological activities. The soil parent material of the Yellow River Delta was originated from the Loess Plateau (Yu et al., 2016; Ji et al., 2022). A large amount of sediment was carried by the Yellow River and deposited in the estuarine area, and the typical estuarine delta wetlands were formed over years by the accumulation of sediment (Zhao et al., 2003; Yu et al., 2014). Along with the succession, tidal flat, Suaeda salsa, Tamarix chinensis, and Phragmites australis developed zonal with the distance from the sea (Figure 1). And the soil qualities of natural wetlands were decided by soil maturation degree (Liu et al., 2010; Guo et al., 2018). Previous studies showed that the soil nutrient elements such as carbon, nitrogen, phosphorus, and sulfur in the study area had obvious spatial distribution differences (Lu et al., 2016), which were affected by land cover and land formation age (Jiao et al., 2014; Yu et al., 2016). The regulation of SQI that increased with the increase of the distance to the coastline (ordered Cp > Pa > Tc > Ss and Td) was observed in the study (Figure 3). Yu and Wang found that soil salinity decreased from east to west in the study area, i.e., the farther away the coastline, the lower the soil salinity (Yu et al., 2014; Wang et al., 2017). Our results of SQI spatial distribution regulation in natural wetlands were opposite to those of soil salinity because Sa was one of the significant negative factors for SQI of natural wetlands (Table 4). Under the influence of tidal action, the spatial distribution of soil salinity showed a ribbon shape with different distance ranges to the coastline (Yu et al., 2014; Wang et al., 2017). Referring to the map of land use classification (Figure 1) in natural wetlands, Pa is mainly located along the Yellow River or in the supratidal

TABLE 4 Pearson relations of SQI with the soil indexes in MDS.

| SQI | Soil depth | TOC | TP | TS | Mg | $NO_3^-$-N | C/N | Sa | pH |
|---|---|---|---|---|---|---|---|---|---|
| Natural wetland | 0–10 cm | 0.77** | 0.50** | 0.27** | 0.60** | 0.43** | 0.17 | −0.56** | −0.46** |
| | 10–20 cm | 0.76** | 0.51** | 0.25* | 0.68** | 0.43** | 0.47** | −0.46** | −0.30** |
| | 20–30 cm | 0.74** | 0.16 | 0.18 | 0.71** | 0.45** | 0.28** | −0.49** | −0.31** |
| | 0–30 cm | 0.76** | 0.42** | 0.29** | 0.66** | 0.47** | 0.34** | −0.47** | −0.28** |
| Reclaimed wetland | 0–10 cm | 0.77** | 0.53** | 0.60** | 0.86** | 0.06 | 0.01 | −0.05 | −0.12 |
| | 10–20 cm | 0.89** | 0.73** | 0.86** | 0.81** | 0.35* | 0.26 | 0.06 | −0.08 |
| | 20–30 cm | 0.95** | 0.20 | 0.85** | 0.78** | 0.48* | 0.48* | −0.23 | −0.39* |
| | 0–30 cm | 0.88** | 0.54** | 0.76** | 0.75** | 0.33* | 0.31* | 0.09 | −0.13 |

* and ** denote the significant correlation at $p < 0.05$ and $p < 0.01$, respectively.

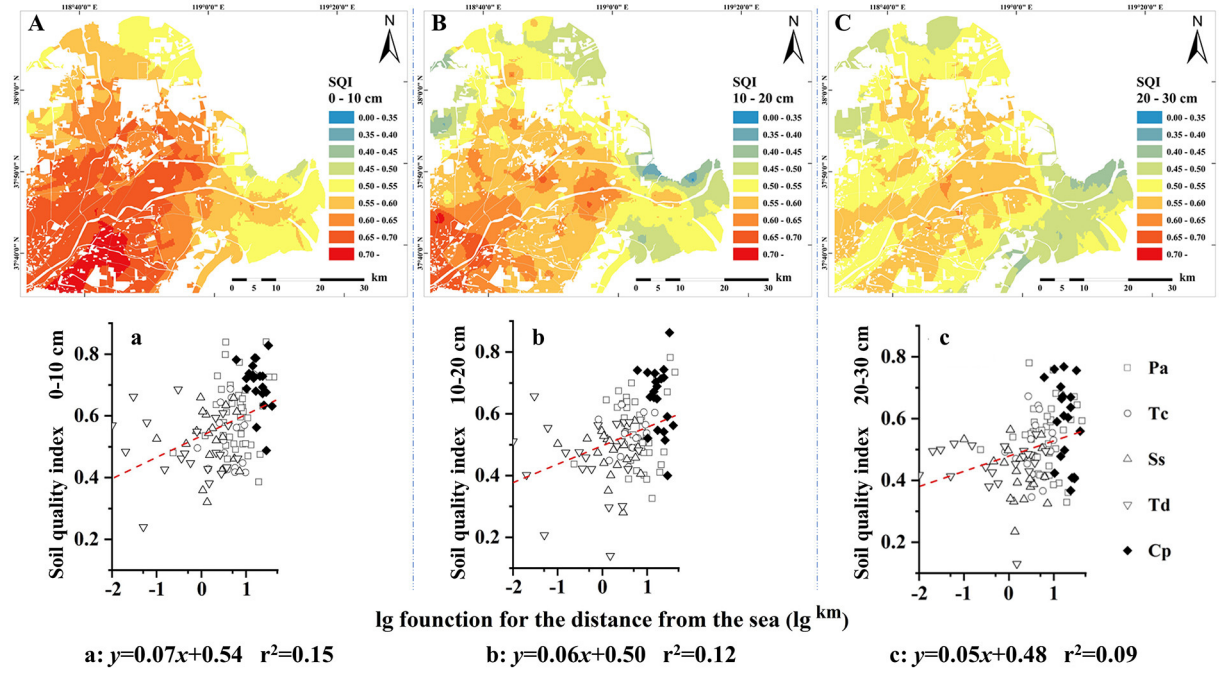


FIGURE 3
The spatial distribution of SQI in soil profiles of 0–10 cm **(A)**, 10–20 cm **(B)** and 20–30 cm **(C)** in the Yellow River Delta.

zone, Tc is mainly distributed in the supratidal zone and was submerged by seawater at high tide, Ss and Td are distributed in the intertidal zone, where were submerged by seawater periodically. Various plant communities occupied different ecological niches according to their adaptability for soil salinity-alkali property. The multi-way ANOVA result showed that the values of SQI were significantly correlated with vegetation type and soil depth ($p < 0.05$) (Supplementary Table 3). The abilities of soil nutrients absorption, utilization, fixation, and return of plants (Jiao et al., 2014) led to the SQI of 0–10 cm soil layer being significantly higher than 20–30 cm of soil layer ($p < 0.05$) (Figures 2A, 3).

The crucial factor that changed soil quality in the study area was human reclamation activities, which led the SQI of reclaimed wetlands to be significantly higher than those of natural wetlands (Figure 2) ($p < 0.05$). Similar results were also found in the previous study (Zhang et al., 2015). Different from most freshwater wetlands, the soil types in the study area were mostly saline-alkali soil with low nutrients content and poor original soil fertility (Verhoeven and Setter, 2010; Ouyang et al., 2013; Xu et al., 2019). The soil salinity was reduced greatly and quickly during cultivation under the measures of drainage salinity and freshwater replenishment (Li et al., 2014; Xiao et al., 2022). Meanwhile, the agricultural process could

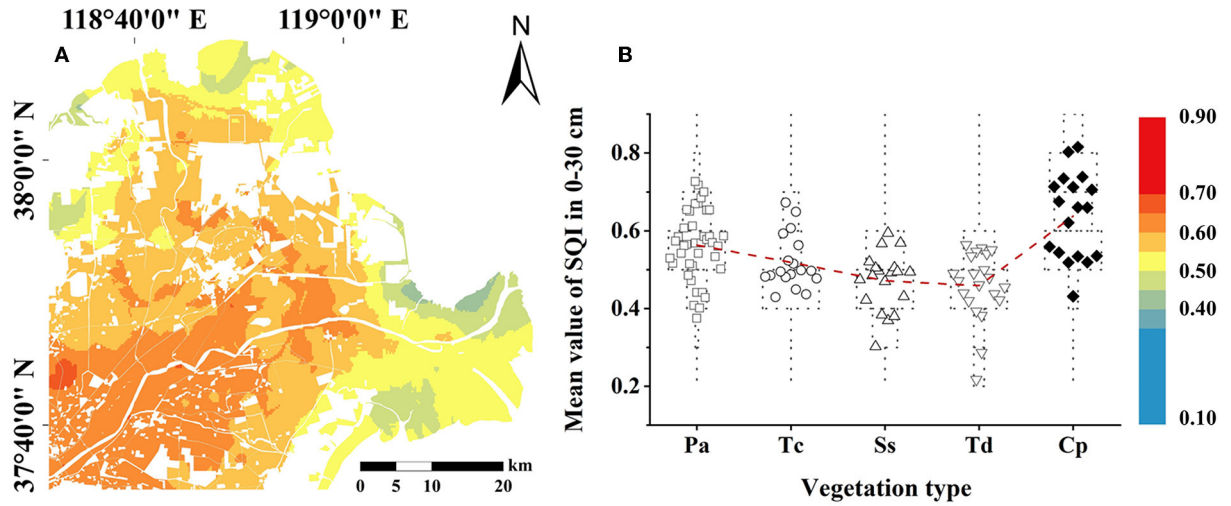


FIGURE 4
The mean SQI value of 0–30 cm **(A)** and different vegetation **(B)** in the Yellow River Delta.

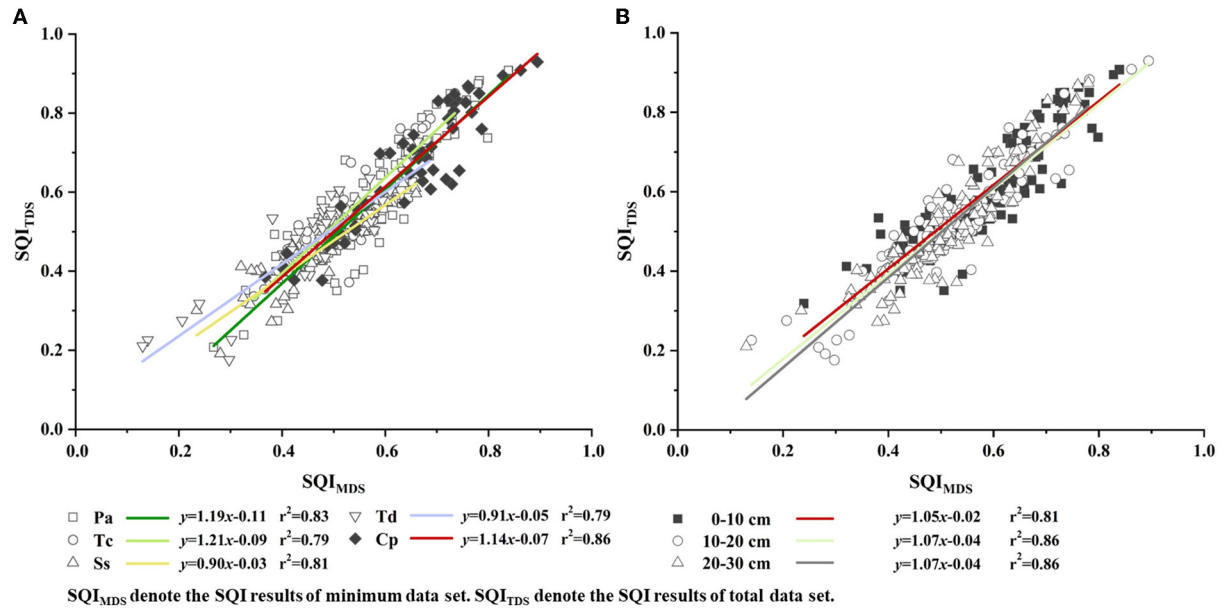


FIGURE 5
The linear regression and determination coefficient ($r^2$) of $SQI_{MDS}$ and $SQI_{TDS}$ under different vegetation types **(A)** and soil depth **(B)**.

help to loosen surface soil to alleviate the salt enrichment in the topsoil layer (Cheng-Song et al., 2010). The soil TOC, $NO_3^-$-N, and TP increased considerably because of a large amount of fertilizer application in reclaimed wetlands under the agricultural planting mode of high-input and high-yield (Jiao et al., 2019; Wang et al., 2021). Therefore, on the one hand, the reclamation of coastal wetland changed the distribution characteristics of soil nutrients in the study area, which led to the increase in soil fertility in the reclaimed wetland. On the other hand, the process of reclamation could reduce soil salinity and have an obvious improvement effect on saline-alkali land. The above factors contributed to the significant difference in the soil quality between natural wetlands and reclaimed wetlands ($p < 0.05$). While high intensity fertilization may also

lead to high soil nutrient residues and water eutrophication and then lead to a series of ecological problems. This is also an issue that needs further comprehensive consideration in the future study. The anthropological activities in reclaimed wetlands that resulted in the significantly negative correlation between SQI with Sa and pH were not observed in reclaimed wetlands, which was different with that in natural wetlands (Table 4). These differences in SQI between reclaimed wetlands and natural wetlands (Figure 4) indicated that agricultural reclamation could alter natural influence and become an important impact factor on soil quality in the coastal wetlands to a great extent.

Moreover, to test the accuracy of MDS, $SQI_{TDS}$ and $SQI_{MDS}$ were compared in our study. The results showed the coefficient of determination ($r^2$) of linear regression in Pa, Tc, Ss, Td, and Cp were 0.83, 0.79, 0.81, 0.79, and 0.86, respectively (Figure 5A). Therefore, the method of MDS with less data redundancy could replace $SQI_{TDS}$ for soil quality evaluation in the study area because it could well-explain the soil quality characteristics.

## Conclusion

An MDS based on 14 soil property indexes and a fuzzy logic model were employed to execute soil quality assessment in the Yellow River Delta. The contrast test of TDS and MDS was conducted to test the accuracy of SQI results. The results showed that (1) the soil quality of the Yellow River Delta decreased from the inland to the coastline with the change of vegetation type and from topsoil layer to subsoil layer in each soil type; (2) the soil qualities of reclaimed wetlands were significantly higher than those of natural wetlands, indicating that the agricultural reclamation could greatly alter natural influence and become an important factor of soil quality to a great extent; and (3) the method of MDS with less data redundancy could well-explain the soil quality characteristics of the Yellow River Delta.

## Data availability statement

The original contributions presented in the study are included in the article/Supplementary material, further inquiries can be directed to the corresponding authors.

## Author contributions

DS and YLi wrote the main manuscript text. JYu and BL are supervisors of DS and provided the idea of the manuscript. BG, DZ, XW, and JYa sampled the soils in field and analyzed statistical data related the manuscript. YM and XZ interpreted the remote sensing images and prepared the figures. XL, YLin, YZ, SJ, and FS did the field land cover survey and designed the filed monitoring sites. All authors reviewed the manuscript. All authors contributed to the article and approved the submitted version.

## Funding

This work was funded by the Key Program from the National Natural Science Foundation of China (U1806218 and U2006215), the National Natural Science Foundation of China (41871087 and 42171111), the Project of the Cultivation Plan of Superior Discipline Talent Teams of Universities in Shandong Province: the Coastal Resources and Environment team for Blue-Yellow Area.

## Conflict of interest

The authors declare that the research was conducted in the absence of any commercial or financial relationships that could be construed as a potential conflict of interest.

## Publisher's note



## Supplementary material

The Supplementary Material for this article can be found online at: https://www.frontiersin.org/articles/10.3389/fevo.2022.977899/full#supplementary-material

## References

Abdel-Fattah, M. K., Mohamed, E. S., Wagdi, E. M., Shahin, S. A., Aldosari, A. A., Lasaponara, R., et al. (2021). Quantitative evaluation of soil quality using principal component analysis: the case study of El-Fayoum depression Egypt. *Sustainability*. 13, 1824. doi: 10.3390/su13041824

Adebo, B. O., Aweto, A. O., and Ogedengbe, K. (2020). Assessment of soil quality under different agricultural land use systems: a case study of the ibadan farm settlement. *Int. J. Plant Soil Sci.* 32, 89–104. doi: 10.9734/ijpss/2020/v32i430275

Andrews, S. S., Flora, C. B., Mitchell, J. P., and Karlen, D. L. (2003). Growers' perceptions and acceptance of soil quality indices. *Geoderma*. 114, 187–213. doi: 10.1016/S0016-7061(03)00041-7

Andrews, S. S., Karlen, D. L., and Mitchell, J. P. (2002). A comparison of soil quality indexing methods for vegetable production systems in Northern California. *Agric. Ecosyst. Environ*. 90, 25–45. doi: 10.1016/S0167-8809(01)00174-8

Armenise, E., Redmile-Gordon, M. A., Stellacci, A. M., Ciccarese, A., and Rubino, P. (2013). Developing a soil quality index to compare soil fitness for agricultural use under different managements in the Mediterranean environment. *Soil Tillage Res*. 130, 91–98. doi: 10.1016/j.still.2013.02.013

Burrough, P. A. (1989). Fuzzy mathematical methods for soil survey and land evaluation. *J. Soil Sci*. 40, 477–492. doi: 10.1111/j.1365-2389.1989.tb01290.x

Burrough, P. A., MacMillan, R. A., and Van Deursen, W. (1992). Fuzzy classification methods for determining land suitability from soil profile observations and topography. *J. Soil Sci*. 43, 193–210. doi: 10.1111/j.1365-2389.1992.tb00129.x

Cao, L., Song, J., Li, X., Yuan, H., Li, N., Duan, L., et al. (2015). Geochemical characteristics of soil C, N, P, and their stoichiometrical significance in the coastal wetlands of Laizhou Bay, Bohai Sea. *Clean Soil Air Water*. 43, 260–270. doi: 10.1002/clen.201300752

Chaer, G. M., Myrold, D. D., and Bottomley, P. J. (2009). A soil quality index based on the equilibrium between soil organic matter and biochemical properties of undisturbed coniferous forest soils of the Pacific Northwest. *Soil Biol. Biochem*. 41, 822–830. doi: 10.1016/j.soilbio.2009.02.005

Chen, S., Jin, Z., Zhang, J., and Yang, S. (2021). Soil quality assessment in different dammed-valley farmlands in the hilly-gully mountain areas of the Northern Loess Plateau, China. *J. Arid Land*. 13, 777–789. doi: 10.1007/s40333-021-0014-4

Cheng-Song, X. I., He-Zhong, D. O., Zhen, L. U., Wei, T. A., Zhang, D. M., Wei-Jiang, L. I., et al. (2010). Effects of N, P, and K fertilizer application on cotton growing in saline soil in Yellow River Delta. *Acta Agronomica Sinica*. 36, 1698–1706. doi: 10.1016/S1875-2780(09)60078-X

Cherubin, M. R., Tormena, C. A., and Karlen, D. L. (2017). Soil quality evaluation using the soil management assessment framework (SMAF) in Brazilian Oxisols with contrasting texture. *Revista Brasileira de Ciência do Solo*. 41, e0160148. doi: 10.1590/18069657rbcs20160148

Chi, Y., Sun, J., Sun, Y., Liu, S., and Fu, Z. (2020). Multi-temporal characterization of land surface temperature and its relationships with normalized difference vegetation index and soil moisture content in the Yellow River Delta, China. *Glob. Ecol. Conserv*. 23, e01092. doi: 10.1016/j.gecco.2020.e01092

Fathizad, H., Ardakani, M. A., Heung, B., Sodaiezadeh, H., Rahmani, A., Fathabadi, A., et al. (2020). Spatio-temporal dynamic of soil quality in the central Iranian desert modeled with machine learning and digital soil assessment techniques. *Ecol. Indic*. 118, 106736. doi: 10.1016/j.ecolind.2020.106736

Granatstein, D., and Bezdicek, D. F. (1992). The need for a soil quality index: local and regional perspectives. *Am. J. Alternative Agric*. 7, 12–16. doi: 10.1017/S0889189300004380

Guo, J., Luo, Z., Tao, J., Zhang, J., Gan, Z., Lin, F., et al. (2021). Soil chemical quality assessment and spatial distribution of pomelo orchards in acidic red soil hilly regions of China. *J. Sci. Food Agric*. 102, 2613–2622. doi: 10.1002/jsfa.11603

Guo, S., Han, X., Li, H., Wang, T., Tong, X., Ren, G., et al. (2018). Evaluation of soil quality along two revegetation chronosequences on the Loess Hilly Region of China. *Sci. Total Environ*. 633, 808–815. doi: 10.1016/j.scitotenv.2018.03.210

He, Q., and Cui, B. (2015). Multiple mechanisms sustain a plant-animal facilitation on a coastal ecotone. *Sci. Rep*. 5, 8612. doi: 10.1038/srep08612

Huang, J., and Yuan, Z. (2021). Ecological stoichiometric characteristics of Soil SOC, TN, and TP under different restoration methods in qixing river wetland. *J. King Saud Univ. Sci*. 33, 101407. doi: 10.1016/j.jksus.2021.101407

Ji, H., Chen, S., Pan, S., Xu, C., Tian, Y., Li, P., et al. (2022). Fluvial sediment source to sink transfer at the Yellow River Delta: quantifications, causes, and environmental impacts. *J. Hydrol*. 608, 127622. doi: 10.1016/j.jhydrol.2022.127622

Jiang, M., Xu, L., Chen, X., Zhu, H., and Fan, H. (2020). Soil quality assessment based on a minimum data set: a case study of a county in the typical river delta wetlands. *Sustainability*. 12, 9033. doi: 10.3390/su12219033

Jiao, S., Li, J., Li, Y., Jia, J., and Xu, Z. (2019). Soil C, N, and P distribution as affected by plant communities in the Yellow River Delta, China. *PLoS ONE*. 14, e0226887. doi: 10.1371/journal.pone.0226887

Jiao, S., Zhang, M., Wang, Y., Liu, J., and Li, Y. (2014). Variation of soil nutrients and particle size under different vegetation types in the Yellow River Delta. *Acta Ecol. Sin*. 34, 148–153. doi: 10.1016/j.chnaes.2014.03.003

Jimenez, L. C., Queiroz, H. M., Cherubin, M. R., and Ferreira, T. O. (2022). Applying the soil management assessment framework (SMAF) to assess mangrove soil quality. *Sustainability*. 14, 3085. doi: 10.3390/su14053085

Karlen, D. L., Ditzler, C. A., and Andrews, S. S. (2003). Soil quality: why and how. *Geoderma*. 114, 145–156. doi: 10.1016/S0016-7061(03)00039-9

Kasno, A. (2021). Financial benefits of using soil test kit of PUTS for determining dosage of lowland rice fertilizer. *IOP Conf. Ser. Earth Environ. Sci*. 648, 012039. doi: 10.1088/1755-1315/648/1/012039

Li, J., Pu, L., Zhu, M., Zhang, J., Li, P., Dai, X., et al. (2014). Evolution of soil properties following reclamation in coastal areas: a review. *Geoderma*. 226–227, 130–139. doi: 10.1016/j.geoderma.2014.02.003

Liu, P., Wang, Q., Bai, J., Gao, H., Huang, L., and Xiao, R. (2010). Decomposition and return of C and N of plant litters of *Phragmites australis* and *Suaeda salsa* in typical wetlands of the Yellow River Delta, China. *Procedia Environ. Sci*. 2, 1717–1726. doi: 10.1016/j.proenv.2010.10.183

Lu, Q., Bai, J., Zhang, G., Zhao, Q., and Wu, J. (2016). Spatial and seasonal distribution of carbon, nitrogen, phosphorus, and sulfur and their ecological stoichiometry in wetland soils along a water and salt gradient in the Yellow River Delta, China. *Phys. Chem. Earth*. 104, 9–17. doi: 10.1016/j.pce.2018.04.001

Mazzon, M., Cavani, L., Ciavatta, C., Campanelli, G., Burgio, G., and Marzadori, C. (2021). Conventional versus organic management: application of simple and complex indexes to assess soil quality. *Agric. Ecosyst. Environ*. 322, 107673. doi: 10.1016/j.agee.2021.107673

Nyeck, B., Mbogba, M. N., Njilah, I. K., Yemefack, M., and Bilong, P. (2018). Contributions of soil chemical and physical properties in the dynamics of soil quality in the southern Cameroon plateau shifting agricultural landscape. *Int. J. Biol. Chem. Sci*. 12, 1042. doi: 10.4314/ijbcs.v12i2.32

Ouyang, W., Xu, Y., Hao, F., Wang, X., Siyang, C., and Lin, C. (2013). Effect of long-term agricultural cultivation and land use conversion on soil nutrient contents in the Sanjiang plain. *Catena*. 104, 243–250. doi: 10.1016/j.catena.2012.12.002

Peters, B. C. (1973). Changing ideas about the use of vegetation as an indicator of soil quality: example of New York and Michigan. *J. Geogr* 72, 18–28. doi: 10.1080/00221347308981021

Pulido, M., Schnabel, S., Contador, J. F., Lozano-Parra, J., Gómez-Gutiérrez, Á. (2017). Selecting indicators for assessing soil quality and degradation in rangelands of Extremadura (SW Spain). *Ecol. Indic*. 74, 49–61. doi: 10.1016/j.ecolind.2016.11.016

Purakayastha, T. J., Pathak, H., Kumari, S., Biswas, S., Chakrabarty, B., Padaria, R. N., et al. (2019). Soil health card development for efficient soil management in Haryana, India. *Soil Tillage Res*. 191, 294–305. doi: 10.1016/j.still.2018.12.024

Rahmanipour, F., Marzaioli, R., Bahrami, H. A., Fereidouni, Z., and Bandarabadi, S. R. (2014). Assessment of soil quality indices in agricultural lands of Qazvin Province, Iran. *Ecol. Indic*. 40, 19–26. doi: 10.1016/j.ecolind.2013.12.003

Raiesi, F. (2017). A minimum data set and soil quality index to quantify the effect of land use conversion on soil quality and degradation in native rangelands of upland arid and semiarid regions. *Ecol. Indic*. 75, 307–320. doi: 10.1016/j.ecolind.2016.12.049

Raiesi, F., and Beheshti, A. (2022). Evaluating forest soil quality after deforestation and loss of ecosystem services using network analysis and factor analysis techniques. *Catena*. 208, 105778. doi: 10.1016/j.catena.2021.105778

Rathore, A. P., Chaudhary, D. R., and Jha, B. (2022). Assessing the effects of *Salicornia brachiata* Roxb. growth on coastal saline soil quality over temporal and spatial scales. *Appl. Soil Ecol*. 169, 104196. doi: 10.1016/j.apsoil.2021.104196

Rezaei, S. A., Gilkes, R. J., and Andrews, S. S. (2006). A minimum data set for assessing soil quality in rangelands. *Geoderma*. 136, 229–234. doi: 10.1016/j.geoderma.2006.03.021

Shao, G., Ai, J., Sun, Q., Hou, L., and Dong, Y. (2020). Soil quality assessment under different forest types in the Mount Tai, central Eastern China. *Ecol. Indic*. 115, 106439. doi: 10.1016/j.ecolind.2020.106439

Shokr, M. S., Abdellatif, M. A., El Baroudy, A. A., Elnashar, A., Ali, E. F., Belal, A. A., et al. (2021). Development of a spatial model for soil quality assessment under arid and semi-arid conditions. *Sustainability*. 13, 2893. doi: 10.3390/su13052893

Sultana, M. S., Islam, M. S., Rahman, S., and Al-Mansur, M. A. (1970). Study of surface water and soil quality affected by heavy metals of Pabna Sadar. *Bangladesh J. Sci. Ind. Res*. 46, 133–140. doi: 10.3329/bjsir.v46i1.8117

Verhoeven, J. T., and Setter, T. L. (2010). Agricultural use of wetlands: opportunities and limitations. *Ann. Bot*. 105, 155–163. doi: 10.1093/aob/mcp172

Volchko, Y., Norrman, J., Rosèn, L., and Norberg, T. (2014). A minimum data set for evaluating the ecological soil functions in remediation projects. *J. Soils Sediments*. 14, 1850–1860. doi: 10.1007/s11368-014-0939-8

Wander, M. M., Walter, G. L., Nissen, T. M., Bollero, G. A., Andrews, S. S., and Cavanaugh-Grant, D. A. (2002). Soil quality. *Agron. J.* 94, 23–32. doi: 10.2134/agronj2002.2300

Wang, D., Bai, J., Wang, W., Zhang, G., Cui, B., Liu, X., et al. (2018). Comprehensive assessment of soil quality for different wetlands in a Chinese delta. *Land Degrad. Dev*. 29, 3783–3795. doi: 10.1002/ldr.3086

Wang, Y., Liu, G., and Zhao, Z. (2021). Spatial heterogeneity of soil fertility in coastal zones: a case study of the Yellow River Delta, China. *J. Soils Sediments*. 21, 1826–1839. doi: 10.1007/s11368-021-02891-5

Wang, Z., Zhao, G., Gao, M., and Chang, C. (2017). Spatial variability of soil salinity in coastal saline soil at different scales in the Yellow River Delta, China. *Environ. Monit. Assess*. 189, 80. doi: 10.1007/s10661-017-5777-x

Wu, C., Liu, G., Huang, C., and Liu, Q. (2019). Soil quality assessment in Yellow River Delta: establishing a minimum data set and fuzzy logic model. *Geoderma*. 334, 82–89. doi: 10.1016/j.geoderma.2018.07.045

Xia, J., Ren, J., Zhang, S., Wang, Y., and Fang, Y. (2019). Forest and grass composite patterns improve the soil quality in the coastal saline-alkali land of the Yellow River Delta, China. *Geoderma*. 349, 25–35. doi: 10.1016/j.geoderma.2019.04.032

Xiao, L., Yuan, G., Feng, L., Shah, G. M., and Wei, J. (2022). Biochar to reduce fertilizer use and soil salinity for crop production in the Yellow River Delta. *J. Soil Sci. Plant Nutr*. 22, 1478–1489. doi: 10.1007/s42729-021-00747-y

Xu, C., Pu, L., Li, J., and Zhu, M. (2019). Effect of reclamation on C, N, and P stoichiometry in soil and soil aggregates of a coastal wetland in eastern China. *J. Soils Sediments*. 19, 1215–1225. doi: 10.1007/s11368-018-2131-z

Yang, H., Xia, J., Cui, Q., Liu, J., Wei, S., Feng, L., et al. (2021). Effects of different *Tamarix chinensis*-grass patterns on the soil quality of coastal saline soil in the Yellow River Delta, China. *Sci. Total Environ*. 772, 145501. doi: 10.1016/j.scitotenv.2021.145501

Yao, R., Yang, J., Gao, P., Zhang, J., and Jin, W. (2013). Determining minimum data set for soil quality assessment of typical salt-affected farmland in the coastal reclamation area. *Soil Tillage Res*. 128, 137–148. doi: 10.1016/j.still.2012.11.007

Yu, J., Li, Y., Han, G., Zhou, D., Fu, Y., Guan, B., et al. (2014). The spatial distribution characteristics of soil salinity in coastal zone of the Yellow River Delta. *Environ. Earth Sci.* 72, 589–599. doi: 10.1007/s12665-013-2980-0

Yu, J., Lv, X., Bin, M., Wu, H., Du, S., Zhou, M., et al. (2015). Fractal features of soil particle size distribution in newly formed wetlands in the Yellow River Delta. *Sci. Rep*. 5, 10540. doi: 10.1038/srep10540

Yu, J., Zhan, C., Li, Y., Zhou, D., Fu, Y., Chu, X., et al. (2016). Distribution of carbon, nitrogen and phosphorus in coastal wetland soil related land use in the Modern Yellow River Delta. *Sci. Rep*. 6, 37940. doi: 10.1038/srep37940

Yuan, P., Wang, J., Li, C., Xiao, Q., Liu, Q., Sun, Z., et al. (2022). Soil quality indicators of integrated rice-crayfish farming in the Jianghan Plain, China using a minimum data set. *Soil Tillage Res*. 204, 104732. doi: 10.1016/j.still.2020.104732

Zhang, G., Bai, J., Xi, M., Gao M., Zhao, Q., Lu, Q., et al. (2015). Comprehensive assessment of soil quality of wetlands in the Yellow River Delta. *Wetland Sci*. 13, 744–751. doi: 10.13248/j.cnki.wetlandsci.2015.06.014

Zhang, G., Bai, J., Xi, M., Zhao, Q., Lu, Q., and Jia, J. (2016). Soil quality assessment of coastal wetlands in the Yellow River Delta of China based on the minimum data set. *Ecol. Indic*. 66, 458–466. doi: 10.1016/j.ecolind.2016.01.046

Zhang, Z. S., Song, X. L., Lu, X. G., and Xue, Z. S. (2013). Ecological stoichiometry of carbon, nitrogen, and phosphorus in estuarine wetland soils: influences of vegetation coverage, plant communities, geomorphology, and seawalls. *J. Soils Sediments* 13, 1043–1052. doi: 10.1007/s11368-013-0693-3

Zhao, G., Shi, Y., Chen, W., Li, J., Ann, S. W., Kim, Y. C., et al. (2003). Dynamic changes of newly formed wetlands in the Yellow River mouth based on GIS and remote sensing. *J. Environ. Sci. Int*. 12, 133–137. doi: 10.5322/JES.2003.12.2.133

Zhao, Q., Bai, J., Gao, Y., Zhao, H., Huang, Y., Zhang, W., et al. (2019). Effects of freshwater inputs on soil quality in the Yellow River Delta, China. *Ecol. Indic*. 98, 619–626. doi: 10.1016/j.ecolind.2018.11.041

frontiers | Frontiers in Environmental Science

SYSTEMATIC REVIEW
published: 15 August 2022
doi: 10.3389/fenvs.2022.947783

# Vegetated Steel Slag Substrate Constructed Wetlands can Achieve High Efficiency Simultaneous Nitrogen and Phosphorus Removal

*Jingyao Zhang*[1], *Yuanchun Zou*[2], *Xiaofei Yu*[1,2]*, *Shanshan Ding*[1], *Jiawen Yan*[1] and *Yongen Min*[1]

[1]State Environmental Protection Key Laboratory for Wetland Conservation and Vegetation Restoration & Jilin Provincial Key Laboratory of Ecological Restoration and Ecosystem Management & Key Laboratory of Vegetation Ecology of Ministry of Education, School of Environment, Northeast Normal University, Changchun, China, [2]Key Laboratory of Wetland Ecology and Environment & Jilin Provincial Joint Key Laboratory of Changbai Mountain Wetland and Ecology, Northeast Institute of Geography and Agroecology, Chinese Academy of Sciences, Changchun, China

OPEN ACCESS

**Edited by:**
He Yixin,
Chengdu Institute of Biology (CAS), China

**Reviewed by:**
Weiqi Wang,
Fujian Normal University, China
Junfeng Chen,
Qufu Normal University, China

***Correspondence:**
Xiaofei Yu
yuxf888@nenu.edu.cn

**Specialty section:**
This article was submitted to Conservation and Restoration Ecology, a section of the journal Frontiers in Environmental Science

**Received:** 19 May 2022
**Accepted:** 16 June 2022
**Published:** 15 August 2022

**Citation:**
Zhang J, Zou Y, Yu X, Ding S, Yan J and Min Y (2022) Vegetated Steel Slag Substrate Constructed Wetlands can Achieve High Efficiency Simultaneous Nitrogen and Phosphorus Removal. Front. Environ. Sci. 10:947783. doi: 10.3389/fenvs.2022.947783

Steel slag substrate constructed wetlands (SSCWs) can effectively remove phosphorus (P) from sewage through Ca-P precipitation and adsorption. Nonetheless, the disadvantages of a high pH value of the effluent and low nitrogen (N) removal efficiency limit the practical application of SSCWs. To improve these shortcomings, plant cultivation and combining steel slag with other substrate materials have been applied in SSCWs. However, related studies have not obtained a unanimous consensus elucidating such improvements. To accurately evaluate improvements, we statistically analyzed the experimental data reported in 27 related papers and found that combining steel slag with other substrate materials in SSCWs significantly increased the removal amount of total nitrogen (TN) (51.58 mg TN/L) and ammonium nitrogen ($NH_4^+$-N) (74.15 mg $NH_4^+$-N/L) but reduced the removal amount of total phosphorus (TP) (7.76 mg TP/L). In these combined substrate SSCWs, plant cultivation could compensate for the decline in TP removal amount and improve upon the simultaneous removal of N and P (6.02 mg TP/L, 62.18 mg TN/L, and 69.16 mg $NH_4^+$-N/L). Moreover, compared with vertical flow SSCWs, horizontal flow enables plant-cultivated and combined substrate SSCWs to achieve a higher TP removal capacity (6.38 mg TP/L). In addition, operational parameters, including temperature, hydraulic retention time (HRT), pH value, and influent concentration, significantly affected the N and P removal capacity of SSCWs. Our research results provide a theoretical reference for the design and operation of SSCWs for efficient N and P removal.

**Keywords: steel slag, planting, constructed wetlands, nitrogen removal, phosphorus removal**

## INTRODUCTION

As early as the 1980s, research on the application of steel slag to remove phosphorus (P) began (Yamada et al., 1986). The use of steel slag, a by-product of the iron and steel industry, as a substrate in constructed wetlands (CWs) to treat nitrogen (N) and P in sewage (Park et al., 2016) provides broad prospects for the recycling of steel slag waste. Steel slag substrate CWs (SSCWs) remove pollutants through physical, chemical, and biological processes mediated by substrate, plants, and microorganisms. Among these components, the steel slag substrate plays a particularly prominent role in P removal, and the main mechanism is Ca-P precipitation and adsorption (Pratt et al., 2007). On the one hand, CaO in steel slag is hydrolyzed to form Ca-P precipitates with $PO_4^{3-}$ in sewage (Baker et al., 1998; Kim et al., 2006). On the other hand, active sites such as metal oxide and hydroxyl oxide (Mo (OH)) sites adsorb P onto the surface of steel slag and gradually form hydroxyapatite (HAP) crystals (Drizo et al., 2006; Chazarenc et al., 2007). In column experiments of basic oxygen furnace steel slag, the $PO_4^{3-}$ removal efficiency was higher than 99%, and the removal capacity reached 3.1 mg P/g (Blanco et al., 2016). The TP removal rate from urban sewage by vertical flow SSCWs can reach 76% (Ge et al., 2016). Vertical and horizontal flow SSCWs can be connected in series, and the total phosphorus (TP) removal rate from construction sewage can reach 62% (Barca et al., 2013).

However, the strong alkalinity of steel slag is not conducive to plant growth and microbial survival, and it leads to a high pH of the effluent, which is attributed to the low efficiency of N removal by plants and microbes. Although ion exchange adsorption between $NH_4^+$ and metal ions (such as $Al^{3+}$, $Fe^{2+}$, and $Mn^{4+}$) in steel slag can remove some ammonium nitrogen ($NH_4^+$-N) (Xu et al., 2019), when compared with microbial nitrogen removal, the nitrogen removed by adsorption is limited. This makes simultaneously removing N and P efficiently in SSCWs difficult. Combing steel slag with other materials, mixed or layered filling, might address these difficulties by relieving the strong alkalinity in SSCWs, whereas the reduced proportion of steel slag in the substrate could decrease P removal (Shen et al., 2020).

Due to the ability of plant roots to absorb N and P (Cui et al., 2015; Yun et al., 2015; Yuan et al., 2017; Saeed et al., 2020), as well as the active microbial metabolism of roots, plant cultivation in combined substrate SSCWs might be an effective way to compensate for the reduced P removal capacity of a combined substrate. The plants cultivated in these SSCWs are mainly common wetland plants, such as *Vetiveria zizanioides*, *Canna indica*, *Acorus calamus*, and *Phragmites australis*, which demonstrate high nutrient levels absorption rates and tolerance to saline and alkaline conditions. However, the role of plants in SSCWs has been controversial. Some studies showed that the death and decay of plants under excessively alkaline conditions can cause the release of P and reduce the removal amount of P (Lu et al., 2021; Zheng et al., 2021). In addition, the influence of operation parameters on the capacity of SSCWs to remove N and P also lacks a summative general mechanism. Based on these aspects, we systematically analyzed existing research results on SSCWs to clarify the following questions: 1) Can vegetated SSCWs improve the capacity to simultaneously remove N and P?, and 2) What is the general rule whereby operation parameters affect the capacity to remove N and P?

## DATA COLLECTION AND STATISTICAL METHODS

### Dataset Formation

In this study, a comprehensive literature search was conducted to collect research data on SSCWs. The databases considered mainly included the Web of Science, Scopus, and Springer Link. The main keywords used included CWs, steel slag, nitrogen removal and phosphorus removal. This search contained almost all studies on SSCWs. These studies are described in **Section 3**, and the results are summarized and discussed. Next, not all articles could be employed for further analysis because they were review articles, and certain articles did not contain data on N and P removal amounts. By reading the title, abstract, and text of the articles during screening, 27 articles (Huang and He, 2011; Wu et al., 2011; Xiong et al., 2011; Barca et al., 2013; Shilton et al., 2013; Barca et al., 2014; Ren et al., 2014; Shi et al., 2014; Cui et al., 2015; Ge et al., 2015; Hussain et al., 2015; Yun et al., 2015; Zhang et al., 2015; Blanco et al., 2016; Ge et al., 2016; Lu et al., 2016; Mohamed et al., 2016; Ahmad et al., 2017; Shi P. et al., 2017; Park et al., 2017; Yuan et al., 2017; Adera et al., 2018; Xu et al., 2019; Chen et al., 2020; Hamdan et al., 2020; Saeed et al., 2020; Wan et al., 2020) met our requirement and were finally selected for data analysis, which provided a highly uniform dataset and reliable results. Datasets of the substrate filling mode, plant cultivation, flow direction of CW, steel slag particle size (SSPS), temperature (T), hydraulic retention time (HRT), hydraulic loading rate (HLR), pH value (pH), influent concentration ($C_{in}$), total nitrogen (TN), $NH_4^+$-N, and TP removal amounts ($\Delta C = C_{in} - C_{out}$) were extracted from these articles, and some original data were modified.

### Statistical Analysis

To reveal the influence of substrate filling mode, plant cultivation and flow direction on TP, TN, and $NH_4^+$-N removal, a single-factor analysis of variance was carried out of the TP, TN, and $NH_4^+$-N removal amounts achieved by CWs with steel slag substrate filling, layered steel slag and other substrate filling, mixed steel slag and other substrate filling, non-planted and planted CWs, and horizontal flow and vertical flow. Before analysis, the sample data must conform to a normal distribution, and the variance must be homogeneous. Otherwise, the data were converted until the above conditions were met, and variance analysis was subsequently performed. For the sample data that still did not meet the above conditions after conversion, a Kruskal–Wallis nonparametric analysis was performed. For example, during the grouping of the substrate filling modes, the $NH_4^+$-N removal data still did not conform to a normal distribution after conversion, so Kruskal–Wallis

**TABLE 1 |** Summary of steel slag substrate constructed wetlands studies carried out at different areas with various experiment scale treatment of scale, sewage type, plant, substrate, and removal rates.

| Study | Scale | Sewage Type | Plant | Substrate | Removal rates (%) | Study Area |
|---|---|---|---|---|---|---|
| Baker et al. (1998) | Batch | Stock phosphate solution | No plants | 50 wt% silica sand, 45 wt% limestone and 5 wt% BOF steel slag | $PO_4^{3-}$-P: 99 | Canada |
| Drizo et al. (2006) | Batch | Stock phosphate solution | No plants | 100 wt% EAF steel slag<br>79 wt% EAF steel slag and 21 wt % limestone | $PO_4^{3-}$-P: 100<br>$PO_4^{3-}$-P: 100 | Canada |
| Kim et al. (2006) | Batch | Stock phosphate solution | No plants | Converter slag | $PO_4^{3-}$-P: 70–98 | South Korea |
| Huang and He, (2011) | Laboratory | Septic tank sewage | *Canna indica* L | 30 cm washed sand and soil mixture, 30 cm limestone and 10 cm steel slag from the top to the bottom | COD: 77<br>$NH_4^+$-N: 85<br>$PO_4^{3-}$-P: 96 | China |
| Wu et al. (2011) | Laboratory | Low concentration domestic sewage | No plants | Steel slag<br>30 cm anthracite, 30 cm vermiculite and 30 cm steel slag from the top to the bottom | TP: 90.26<br>TP: 82.45 | China |
| Xiong et al. (2011) | Integrated constructed treatment system | Secondary effluents | *Vetiver zizanioides* (L.) Nash | 40 cm peat, 60 cm steel slag and 20 cm coarse sand from the top to the bottom | COD: 61.36<br>TP: 76.58 (removal rates for the vertical flow constructed wetland) | China |
| Barca et al. (2013) | Field experiments | Municipal wastewater | No plants | EAF steel slag<br>BOF steel slag | TP: 44.71<br>TP: 58.82 | France |
| Shilton et al. (2013) | Mesocosm | Real pond effluent | No plants | Steel slag | TP: 90 | New Zealand |
| Barca et al. (2014) | Laboratory | Synthetic solution | No plants | EAF steel slag<br>BOF steel slag | TP: 98<br>TP: 99 | France |
| Shi et al. (2014) | Microcosm | Slightly polluted river water | No plants | 1:2 mixture of zeolite and steel slag | COD: 57.55<br>$NH_4^+$-N: 62.77<br>$NO_3^-$-N: 34.79<br>TP: 96.31 | China |
| Yun et al. (2015) | Pilot | Domestic wastewater with a low phosphorus concentration | *Phragmites australis* | 50 cm steel slag and 20 cm coarse gravel from the top to the bottom<br>50 cm modified steel slag and 20 cm coarse gravel from the top to the bottom | TP: 84<br>TP: 88 | China |
| Ge et al. (2015) | Large scale demonstration | Polluted river water | *Phragmites australis* | Steel slag and gravel | COD: 73.5<br>TN: 23.2<br>TP: 53.5 | China |
| Hussain et al. (2015) | Pilot | Septic tank sewage | No plants | 10 cm washed limestone gravel, 57 cm BOF steel slag and gravel mixture and 10 cm basal sand from the top to the bottom | $PO_4^{3-}$-P: 98.6–99.8 | Canada |
| Ren et al. (2014) | Laboratory | Synthetic wastewater | No plants | 2.5 cm zeolite, 2.5 cm steel slag and 2.5 cm gravel from the top to the bottom | COD: 75.90<br>$NH_4^+$-N: 68.39<br>TN: 45.16<br>TP: 74.55 | China |
| Zhang et al. (2015) | Laboratory | Secondary effluent from a municipal sewage treatment plant | *Phragmites australis* | 10 cm cobble and rice husk, 25 cm steel slag and 20 cm limestone from the top to the bottom | COD: 66–83<br>$NH_4^+$-N: 100<br>TN: 100; TP: 81–90<br>(removal rates for the two-stage vertical flow constructed wetland) | China |
| Blanco et al. (2016) | Batch | Stock phosphate solution | No plants | BOF steel slag | $PO_4^{3-}$-P: 84–99 | Spain |
| Lu et al. (2016) | Mesocosm | Rural household sewage | Aquatic plants | Soil, steel slag, gravel stone from the top to the bottom | COD: 79.7<br>$NH_4^+$-N: 80.0<br>TN: 74.4<br>TP: 83.5 | China |
| Mohamed et al. (2016) | Pilot | Household graywater | No plants | 12.7 cm clamshells, 12.7 cm steel slag and limestone mixture and | COD: 74 | Malaysia |

(Continued on following page)

**TABLE 1 |** (*Continued*) Summary of steel slag substrate constructed wetlands studies carried out at different areas with various experiment scale treatment of scale, sewage type, plant, substrate, and removal rates.

| Study | Scale | Sewage Type | Plant | Substrate | Removal rates (%) | Study Area |
|---|---|---|---|---|---|---|
| | | | | 12.7 cm sand from the top to the bottom | | |
| Ge et al. (2016) | Laboratory | Polluted urban river water | *Phragmites australis* | BOF steel slag | TP: 76 | China |
| Park et al. (2017) | Microcosm | Hydroponic wastewater | *Iris pseudoacorus* | Rapid cooled BOF steel slag (RC-BOFS) | $PO_4^{3-}$-P: 94.2 | South Korea |
| | | | | 75% coarse sand and 25% RC-BOFS | $PO_4^{3-}$-P: 89.3 | |
| Shi et al. (2017a) | Microcosm | Synthetic wastewater | No plants | 20 cm zeolites and 10 cm steel slag from the top to the bottom | TP: 80–90 | China |
| Yuan et al. (2017) | Pilot | Domestic and agricultural wastewaters | No plants | 50 wt% coarse sand, 30 wt% pebble aggregate, 10 wt% $TiO_2$ processing residue, 4 wt% wood chip, 3 wt% blast furnace slag, 3 wt% blast furnace slag | TN: 55<br>TP: 81 | China |
| Ahmad et al. (2017) | Laboratory | Synthetic wastewater | No plants | High calcium EAF steel slag | $PO_4^{3-}$-P: 76–98 | Malaysia |
| Adera et al. (2018) | Mesocosm | Dairy farm wastewater | No plants | EAF steel slag | DRP: 99 | United States of America |
| Chen et al. (2020) | Pilot | Wastewater treatment plant secondary effluent | No plants | Ceramsite and steel slag | COD: 81.3<br>TN: 31.3<br>TP: 85.0 | China |
| Xu et al. (2019) | Mesocosm | Simulated wastewater | *Acorus calamus* | 10 cm sand and 30 cm Ti-bearing blast furnace slag from the top to the bottom | $NH_4^+$-N: 77.54<br>TN: 71.07<br>TP: 98.00 | China |
| | | | | 10 cm sand and 30 cm converter steelmaking slag from the top to the bottom | $NH_4^+$-N: 59.23<br>TN: 53.02<br>TP: 96.00 | |
| Hamdan et al. (2020) | Pilot | Domestic wastewater | No plants | Steel slag | $NH_4^+$-N: 91 | Malaysia |
| Saeed et al. (2020) | Mesocosm | Leachate | *Vetiver* | 5 cm stone,1 m steel slag, 1 m concrete block and 5 cm stone from the top to the bottom | COD: 40.4<br>$NH_4^+$-N: 91.3<br>TN: 30.3<br>TP: 91.6 | Bangladesh |

nonparametric analysis was performed. Then, samples with insufficient data were finally removed.

Next, the Pearson correlation coefficient is widely adopted to measure the degree of correlation between two variables. This value varies between −1 and 1. A negative value suggests a negative correlation, and a positive value indicates a positive correlation. To quantify the relationship between the TP, TN, and $NH_4^+$-N removal amounts and SSPS, T, HRT, HLR, pH, and $C_{in}$, a Pearson correlation coefficient matrix was established. In addition, to describe the interaction between the TP, TN, and $NH_4^+$-N removal amounts and the abovementioned operation parameters, redundancy analysis (RDA) was conducted.

To quantitatively describe the relationship between the TP, TN, and $NH_4^+$-N removal amounts and the operation parameters, a regression analysis method was applied. In a multiple linear regression model, the dependent variable is a linear function of the independent variables $X_i$, as follows:

$$Y = a + b_1X_1 + b_2X_2 + ... + b_nX_n \quad (1)$$

where Y is the predicted value of the dependent variable, and $X_1$, $X_2$, ... $X_n$ are the independent variables. The dependent variables included the TP, TN, and $NH_4^+$-N removal amounts $\Delta C = C_{in} - C_{out}$ (mg/L), and the independent variables were the SSPS (mm), T (°C), HRT (d), HLR (m/d), pH, and $C_{in}$ (mg/L). All variables inserted in the model were considered significant at $p < 0.05$.

We employed SPSS 26 software (IBM, United States) for variance analysis, the Kruskal–Wallis test for nonparametric analysis, and set the condition for statistical significance at $p < 0.05$. An RDA was conducted by Canoco 5. Also, R 4.0.3 was used for illustrations.

# EVALUATION OF STEEL SLAG SUBSTRATE CONSTRUCTED WETLANDS

## Applications of Steel Slag Substrate Constructed Wetlands

In the initial application stage, SSCWs stuffed with single steel slag as substrate were used to remove P from sewage with different P concentrations. Following that, SSCWs with a combined and modified substrate were used to comprehensively improve the quality of septic tank sewage (Huang and He, 2011; Hussain et al., 2015), domestic sewage (Wu et al., 2011; Yun et al., 2015; Mohamed et al., 2016; Hamdan et al., 2020), urban sewage (Barca et al., 2013), pond sewage

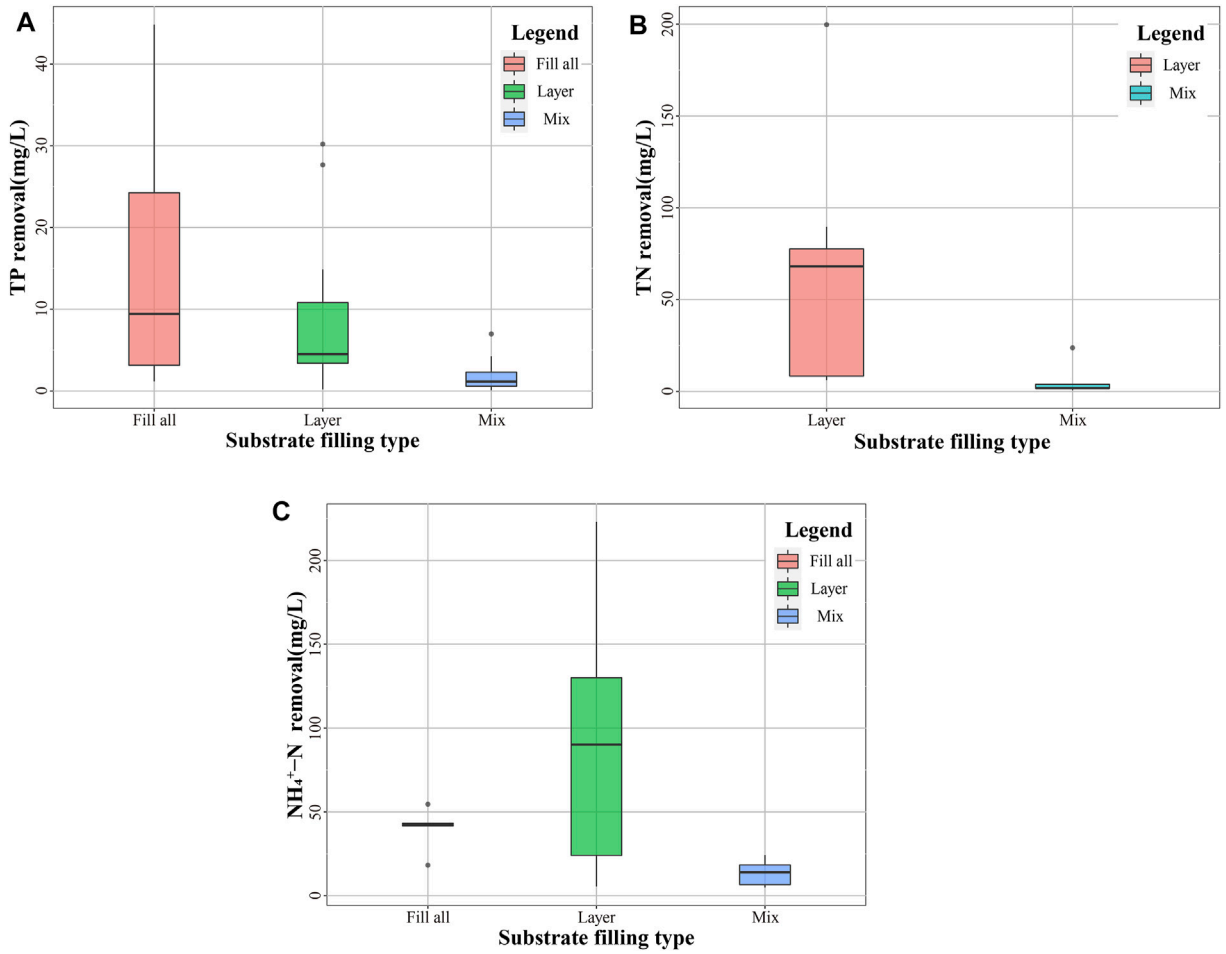


**FIGURE 1 |** Influence of the substrate filling mode on pollutant removal by steel slag substrate constructed wetlands (SSCWs). **(A)** total phosphorus (TP) **(B)** total nitrogen (TN) **(C)** ammonium nitrogen ($NH_4^+$-N) (the pictures are all original data plots, and data conversion is performed during data analysis).

(Shilton et al., 2013), secondary effluent of sewage treatment plants (Xiong et al., 2011; Zhang et al., 2015; Chen et al., 2020), polluted river waters (Shi et al., 2014; Ge et al., 2015; Ge et al., 2016), hydroponic sewage (Park et al., 2017), agricultural sewage (Lu et al., 2016; Yuan et al., 2017), dairy farm sewage (Adera et al., 2018), leachate (Saeed et al., 2020), and other sewage. Besides, SSCWs demonstrate high P recovery potential. **Table 1** summarizes the latest crucial scientific research on SSCWs, most of which were carried out on the scale of batch experiments (Baker et al., 1998; Kim et al., 2006; Blanco et al., 2016) in laboratories (Huang and He, 2011; Wu et al., 2011; Barca et al., 2014; Ren et al., 2014; Zhang et al., 2015; Ge et al., 2016; Ahmad et al., 2017). Some of the studies were conducted on a pilot scale (Hussain et al., 2015; Yun et al., 2015; Mohamed et al., 2016; Yuan et al., 2017; Chen et al., 2020; Hamdan et al., 2020), nothing in which full-scale field applications are not yet available.

Steel slag substrates stuffed in SSCWs mainly include BOF steel slag (Baker et al., 1998; Hussain et al., 2015; Blanco et al., 2016; Ge et al., 2016), electric arc furnace (EAF) steel slag (Drizo et al., 2006; Barca et al., 2013; Barca et al., 2014; Adera et al., 2018), and modified steel slag (Ahmad et al., 2017; Park et al., 2017). Due to the addition of limestone in the steelmaking process, BOF steel slag contains high concentrations of CaO and exhibits high P removal capacity (Barca et al., 2013). Therefore, in some studies, when BOF slag is rapidly cooled, the content of unstable crystalline-free CaO and the alkalinity of SSCWs will be significantly reduced (Park et al., 2016). Regarding P removal capacity, BOF steel slag performs better than EAF steel slag. However, with a low pH value and many adsorption sites, the latter can remove P not only by precipitation but also by adsorption (Ge et al., 2016).

Subsurface SSCWs are most widely used according to the flow direction and are divided into unsaturated vertical flow (Huang and He, 2011; Wu et al., 2011; Xiong et al., 2011; Shilton et al., 2013; Ren et al., 2014; Shi et al., 2014; Cui et al., 2015; Hussain et al., 2015; Zhang et al., 2015; Blanco et al., 2016; Ge et al., 2016; Lu et al., 2016; Mohamed et al., 2016; Ahmad et al., 2017; Yuan et al., 2017; Adera et al., 2018; Hamdan et al., 2020; Saeed et al., 2020) and saturated horizontal flow (Barca et al., 2013; Barca et al., 2014; Ren et al., 2014; Cui et al., 2015; Ge et al., 2015; Park et al., 2017; Yuan et al., 2017; Adera et al., 2018; Xu et al., 2019; Chen et al., 2020) SSCWs. Next, vertical flow SSCWs require only

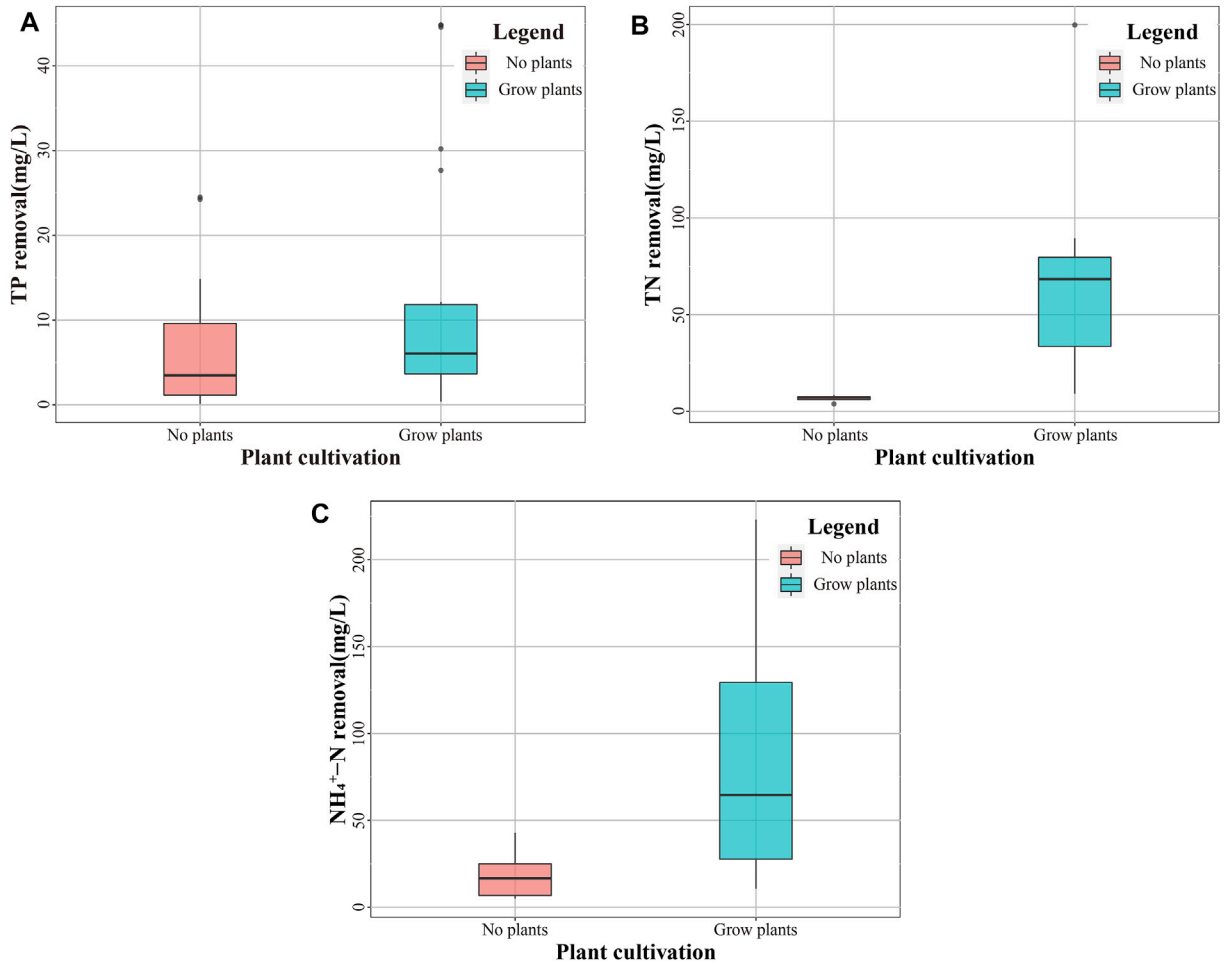


**FIGURE 2 |** Influence of plant cultivation on pollutant removal in SSCWs. **(A)** TP **(B)** TN **(C)** $NH_4^+$-N (the pictures are all original data plots, and data conversion is performed during data analysis).

a small amount of ground to operate but provide appropriate contact time and anaerobic time between water and substrate to ensure a better nitrogen and phosphorus removal performance (Yun et al., 2015). The intermittent water inflow and aeration condition (Shi X. et al., 2017) can promote the nitrification process and P transformation process. Like vertical flow SSCWs, horizontal flow SSCWs also demonstrate enough contact time to remove P in the sewage, but they require a larger amount of ground. Besides, $CO_2$ interference is avoided for saturated operation, and little $CaCO_3$ blockage is generated in the horizontal flow SSCWs. In addition, the alkalinity of effluent can be neutralized by spraying $CO_2$ on the effluent. With low cost and minimal technical requirements, horizontal flow SSCWs exhibit enough contact time to remove P in the sewage. No air entering $CO_2$ avoids interference, and almost no $CaCO_3$ will be generated, thereby reducing the blockage (Ren et al., 2014). However, in the light of the alkalinity of the effluent, the pH value of the sewage can be neutralized by spraying $CO_2$ in later stages (Park et al., 2017).

In addition, contentious issues exist regarding the pollutant removal efficiency of SSCWs. For example, one study proposed that EAF steel slag would release P when removing low P concentration sewage (Drizo et al., 2006) and believed that steel slag was not suitable for removing low P concentration sewage, which is in contrast to the results of other studies. Moreover, contradictions are found on the issue of whether the main P removal mechanism is adsorption or precipitation (Barca et al., 2014; Ge et al., 2016). In fact, the acid–base condition determines the main mechanism of P removal. Under alkaline conditions, precipitation, depending on the content of CaO in the substrate, is the main removal mechanism; thus, P can be quickly removed. In contrast, under acidic conditions, P is removed mainly by adsorption, and the removal process is slow and lasting (Ahmad et al., 2017; Xu et al., 2019). Moreover, HRT is a significant factor influencing removal efficiency. Too short HRT would result in incomplete removal of N and P, while a longer than the optimal time would lead to an unstable release of adsorbed P (Shilton et al., 2013), limited microbial growth, and

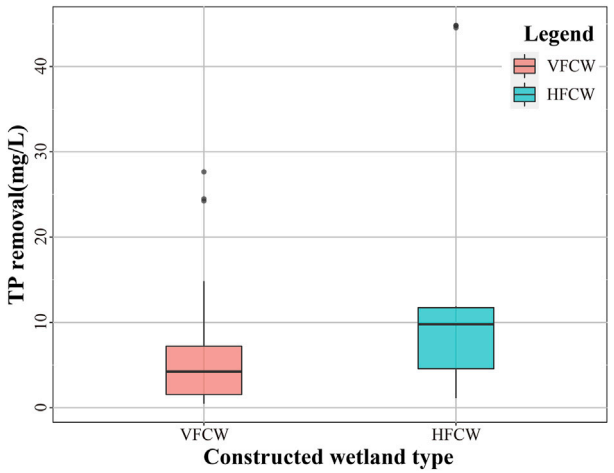


**FIGURE 3 |** TP removal in horizontal and vertical flow SSCWs with plant cultivation (the pictures are all original data plots, and data conversion is performed during data analysis).

increased pH value of effluent. In recent years, some studies focused on the issue of whether other pollutants in the sewage would influence P removal efficiency. On the one hand, researchers revealed that organic acids and organic colloids can block active surface sites of substrates and reduce P adsorption. On the other hand, some laboratory experiments showed that the inhibitory effect mentioned above can be mitigated over time, and eventually, P adsorption can be promoted, such as in iron oxide compounds, cations, and algae (Barca et al., 2013; Ge et al., 2016).

## Significant Influence of the Substrate Filling Mode on the Nitrogen and Phosphorus Removal Capacity

The substrate filling method imposed a significant influence on the removal of TP ($p = 0.001$), TN ($p = 0.002$), and $NH_4^+$-N ($p = 0.009$) (**Figure 1**). The degree of TP removal in SSCWs with different filling modes was ordered as follows: single steel slag substrate filling (14.95 mg TP/L) > layered combined substrate filling (7.19 mg TP/L) > mixed combined substrate filling (1.95 mg TP/L) (**Figure 1A**). The main reason why the TP removal amount of combined substrate filling is significantly lower than that of single steel slag filling is that in a limited-volume CW, the introduction of other substrates can reduce the steel slag amount, resulting in a decrease in the P removal amount during the adsorption and co-precipitation process. The main reason why the TP removal amount of mixed combined substrate filling is significantly lower than that of layered combined substrate filling is that mixed combined substrates can cause the steel slag surface to be partially covered, thus reducing the number of adsorption sites, or they can impede the release of calcium ions (Shi X. et al., 2017).

Next, the pH of SSCWs filled with single steel slag can reach as high as 12.4 (Gomes et al., 2018), which is not conducive to plant growth and microbial survival. These systems lack plant root adsorption and microbial metabolic activities and only achieve a small amount of physical adsorption. Compared to single steel slag, a combined substrate composed of steel slag and other substrate materials improved N removal due to the relatively suitable environment for microorganisms and plants (Shen et al., 2020). The TN removal of SSCWs with different combined substrate filling modes was as follows: layered combined substrate filling (14.75 mg TN/L) > mixed combined substrate filling (4.38 mg TN/L) (**Figure 1B**). The $NH_4^+$-N removal of SSCWs with different substrate filling modes was as follows: layered combined substrate filling (87.59 mg $NH_4^+$-N/L) > single steel slag substrate filling (40.46 mg $NH_4^+$-N/L) > mixed combined substrate filling (13.44 mg $NH_4^+$-N/L) (**Figure 1C**). These results indicate that the different substrate filling modes exert a profound impact on the removal amounts of N and P, and layered combined substrate SSCWs exhibit a better N removal capacity. Compared to layered combined substrate filling, mixed combined substrate filling causes other substrate materials to cover the adsorption sites of the steel slag substrate, thereby reducing the adsorption capacity of the steel slag substrate (Shi P. et al., 2017). Moreover, in the layered combined SSCWs, plants are usually cultivated in the non-steel slag materials layer with a milder acid–base condition (Cui et al., 2015; Yuan et al., 2017; Zheng et al., 2021), which better promotes the de-N effect of plants and microorganisms (Lan et al., 2018).

## Plant Cultivation can Improve the Simultaneous Nitrogen and Phosphorus Removal Capacity of Steel Slag Substrate Constructed Wetlands

The strong alkalinity of single steel slag is not conducive to plant survival, so plants are usually cultivated in the combined substrate SSCWs. Plant cultivation in SSCWs significantly increased the removal amounts of TP by 6.02 mg TP/L ($p = 0.026$), TN by 62.18 mg TN/L ($p = 0.000$), and $NH_4^+$-N by 69.16 mg $NH_4^+$-N/L ($p = 0.000$) (**Figure 2**), indicating plant cultivation can improve the simultaneous N and P removal capacity of SSCWs. The adsorption of P by plant roots helps to remove P. However, the high pH can lead to plant death and the release of P through decaying plants (Lu et al., 2021; Zheng et al., 2021); thus, generating two opposing views on whether plant cultivation can improve the simultaneous removal of N and P. Our results suggest that the P adsorbed by plant roots offsets the P released by plant death. In this way, plant cultivation can enable the SSCWs to simultaneously remove N and P with high efficiency.

## Horizontal Flow (Vs. Vertical Flow) Steel Slag Substrate Constructed Wetlands Have a Higher Removal Capacity of P

The average TP removal amount in horizontal flow SSCWs was 6.38 mg TP/L larger than that in vertical flow SSCWs (**Figure 3**). In SSCWs, Ca-P deposits cover the surface of steel slag, resulting in decreased P removal. The phenomenon is more serious in

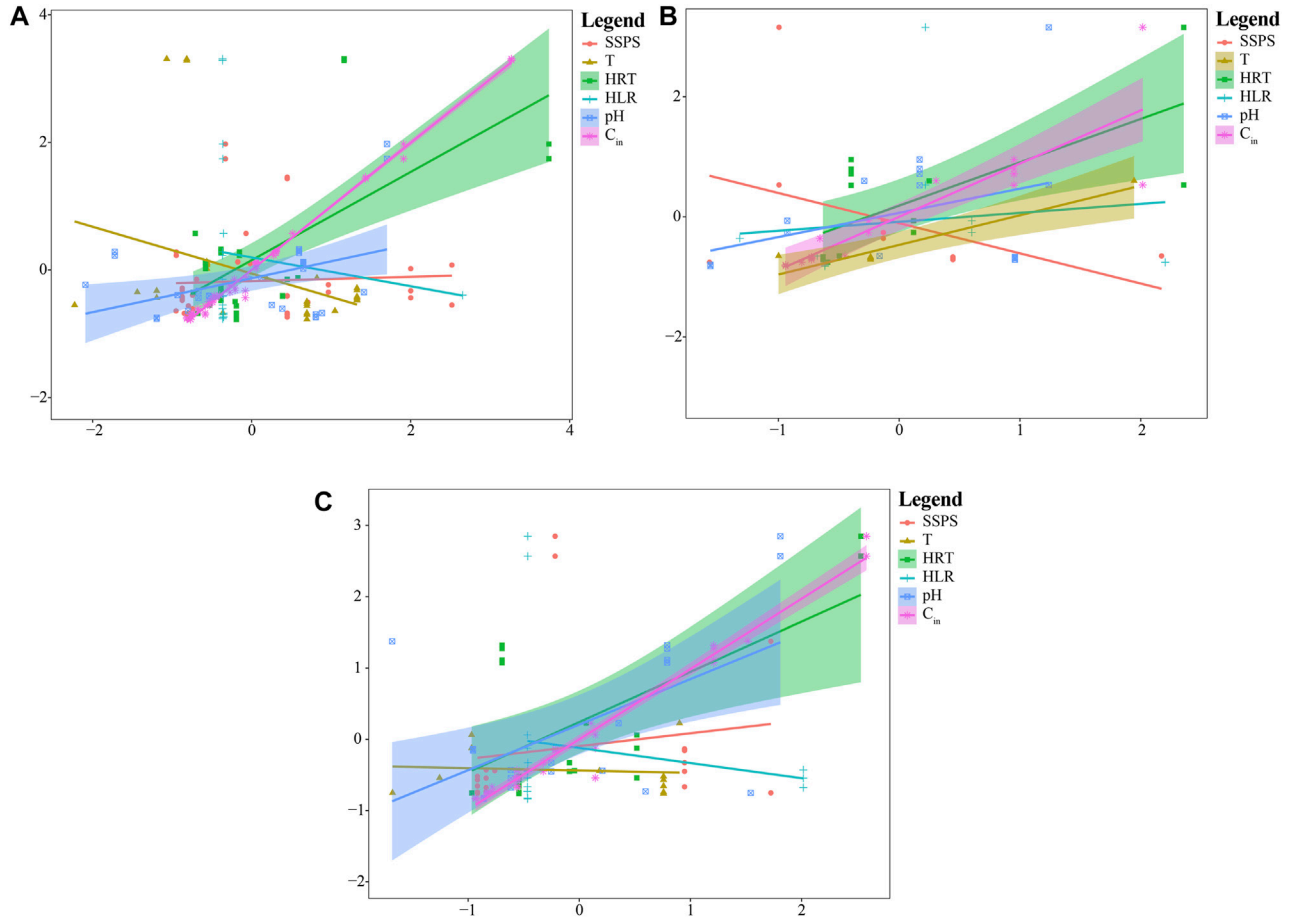


**FIGURE 4 |** Pearson correlation analysis scatter plot and fitting line of the pollutant removal amount and experimental parameters. The error range of the experimental parameters with $p < 0.05$ is shown in figure. **(A)** TP **(B)** TN **(C)** $NH_4^+$-N.

vertical SSCWs due to the frequent intermittent vertical flow transporting the deposits to the deeper substrates, then reducing the P adsorption. In contrast, the water flow remains horizontal and stable in horizontal flow SSCWs, enabling the sewage to be in full contact with steel slag, thus resulting in increased removal of P. In addition, strictly controlling the hydraulic residence time is necessary to reduce the pH while ensuring pollutant removal in horizontal flow SSCWs.

## Operation Parameters of Steel Slag Substrate Constructed Wetlands Affected N and P Removal Capacity

The TP removal amount of SSCWs was positively correlated with the HRT (r = 0.643; $p$ = 0.000), pH (r = 0.430; $p$ = 0.010), and $C_{in}$ (r = 0.997; $p$ = 0.000) (**Figure 4A**). With increasing HRT, the contact time between steel slag and sewage increased, consequently increasing the reaction time, thereby improving the TP removal amount. However, an excessively long HRT could increase the pH value of the effluent. In practical applications, the HRT should be reasonably controlled. Alkaline conditions are conducive to forming Ca-P, while acidic conditions are conducive to forming Fe-P and Al-P, each less stable than Ca-P. In addition, excessively high alkalinity could lead to the release of P (Shen et al., 2020). Considering the sewage discharge standards in most countries (pH 6–9), the pH of the effluent should be stabilized below 9. The positive correlation between TP removal and $C_{in}$ suggests that in most experiments, steel slag can release enough $Ca^{2+}$ to form precipitation with the high concentration of $PO_4^{3-}$ in sewage.

The TN removal amount was positively correlated with T (r = 0.943; $p$ = 0.005), HRT (r = 0.689; $p$ = 0.004) and $C_{in}$ (r = 0.887; $p$ = 0.000) (**Figure 4B**). The $NH_4^+$-N removal amount was positively correlated with the HRT (r = 0.624; $p$ = 0.004), pH (r = 0.573; $p$ = 0.005) and $C_{in}$ (r = 0.914; $p$ = 0.000) (**Figure 4C**). With increasing temperature, the nitrification–denitrification rate was improved, and the TN removal amount increased.

Among these operation parameters, $C_{in}$ was the most important factor influencing N and P removal amount ($p$ = 0.002) (**Figure 5**), followed by HRT ($p$ = 0.002), and then, T ($p$ = 0.004) and pH ($p$ = 0.008) decreased sequentially and positively correlated with N and P removal amount.

In addition, based on regression analysis, we quantitatively described the relationships between the TP, TN, $NH_4^+$-N removal amount and the operation parameters in SSCWs.

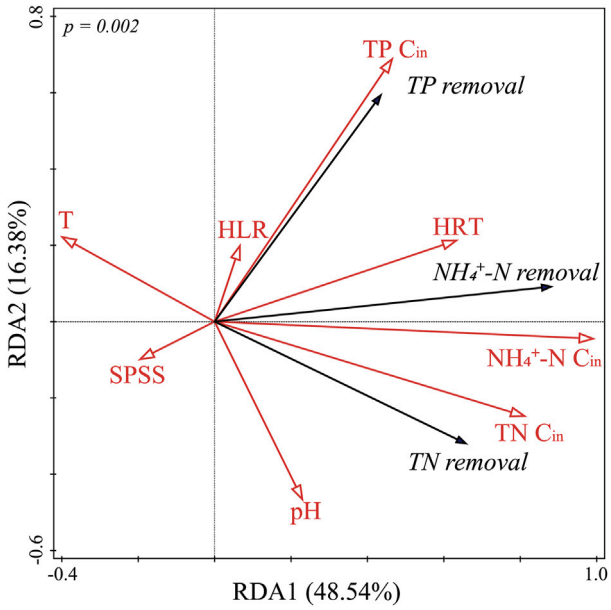


**FIGURE 5 |** Redundancy analysis of the influence of the operation parameters on pollutant removal.

**Eqs 2–4** described the above relationships in non-plant cultivation SSCWs.

$$\Delta C_{TP} = -0.017\,SSPS + 0.998\,C_{in} \quad (r^2 = 0.995; n = 57; p = 0.000; F = 1511.000) \tag{2}$$

$$\Delta C_{TN} = 0.540\,C_{in} \quad (r^2 = 0.800; n = 19; p = 0.000; F = 8.021) \tag{3}$$

$$\Delta C_{NH_4^+-N} = -221.562 + 1.112\,SSPS + 3.832\,T + 16.121\,pH + 0.866\,C_{in} \quad (r^2 = 0.983; n = 31; p = 0.000; F = 235.000) \tag{4}$$

where $\Delta C = C_{in} - C_{out}$ denotes the TP, TN, and $NH_4^+$-N removal amounts (mg/L); $C_{in}$ and $C_{out}$ are the influent and effluent concentrations (mg/L), respectively; SSPS is the steel slag particle size (mm); T is the temperature (°C); and pH denotes the acidity or alkalinity.

**Eqs 5–7** described the above relationships in plant cultivation SSCWs:

$$\Delta C_{TP} = 8.681 - 0.287\,T + 0.963\,C_{in} \quad (r^2 = 0.999; n = 27; p = 0.000; F = 2506.000) \tag{5}$$

$$\Delta C_{TN} = -391.380 + 56.980\,pH + 0.226\,C_{in} \quad (r^2 = 0.695; n = 27; p = 0.000; F = 7.585) \tag{6}$$

$$\Delta C_{NH_4^+-N} = -174.065 + 3.912\,T + 0.871\,C_{in} \quad (r_2 = 0.983; n = 27; p = 0.000; F = 190.400) \tag{7}$$

where $\Delta C = C_{in} - C_{out}$ denotes the TP, TN, and $NH_4^+$-N removal amounts (mg/L); $C_{in}$ and $C_{out}$ are the influent and effluent concentrations (mg/L), respectively; T is the temperature (°C); and pH denotes the acidity or alkalinity.

**Eqs 2** and **4**, **5**, and **7** indicate that plant cultivation weakens the dependence of SSCWs on SSPS for P and $NH_4^+$-N removal. Compared to non-plant cultivation SSCWS, temperature is one of the determinants of P removal in plant cultivation SSCWs.

## CONCLUSION

Our results indicate that layered combined substrates can significantly increase the TN and $NH_4^+$-N removal amounts in SSCWs but reduce the TP removal amount. Plant cultivation in combined substrate SSCWs can compensate for the decline in TP removal. Compared with vertical flow, horizontal flow SSCWs demonstrate a higher removal capacity of P. Next, T, HRT, pH, and $C_{in}$ significantly affected the N and P removal capacity of SSCWs. To conclude, plant cultivation and combined substrates can improve the simultaneous removal of N and P in SSCWs. This study can serve as a reference to solve certain problems encountered in SSCWs.

## DATA AVAILABILITY STATEMENT

The original contributions presented in the study are included in the article/Supplementary material, and further inquiries can be directed to the corresponding author.

## AUTHOR CONTRIBUTIONS

JZ: Data curation and analysis, writing—original draft. YZ: Aided in interpreting the results and worked on the manuscript. XY: Worked on the technical details, supervised the findings of the work and helped in the development of manuscript. SD: Writing—review and editing. JY: Data curation. YM: Data curation.

## FUNDING

This work was supported by the National Natural Science Foundation of China (41871100), the National Natural Science Foundation of China (41971136), and the National Natural Science Foundation of China (42171107).

## REFERENCES

Adera, S., Drizo, A., Twohig, E., Jagannathan, K., and Benoit, G. (2018). Improving Performance of Treatment Wetlands: Evaluation of Supplemental Aeration, Varying Flow Direction, and Phosphorus Removing Filters. *Water Air Soil Pollut.* 229, 100. doi:10.1007/s11270-018-3723-3

Ahmad, S. Z. N., Hamdan, R., Wan Mohamed, W. A., Othman, N., Mohd Zin, N. S., and Musa, S. (2017). Comparisons Study of Phosphate Removal in Unaerated and Aerated High Calcium Steel Slag Filter System of Different pH Feed. *MATEC Web Conf.* 103, 06018. doi:10.1051/matecconf/201710306018

Baker, M. J., Blowes, D. W., and Ptacek, C. J. (1998). Laboratory Development of Permeable Reactive Mixtures for the Removal of Phosphorus from Onsite

Wastewater Disposal Systems. *Environ. Sci. Technol.* 32 (15), 2308–2316. doi:10.1021/es970934w

Barca, C., Meyer, D., Liira, M., Drissen, P., Comeau, Y., Andrès, Y., et al. (2014). Steel Slag Filters to Upgrade Phosphorus Removal in Small Wastewater Treatment Plants: Removal Mechanisms and Performance. *Ecol. Eng.* 68, 214–222. doi:10.1016/j.ecoleng.2014.03.065

Barca, C., Troesch, S., Meyer, D., Drissen, P., Andrès, Y., and Chazarenc, F. (2013). Steel Slag Filters to Upgrade Phosphorus Removal in Constructed Wetlands: Two Years of Field Experiments. *Environ. Sci. Technol.* 47 (1), 549–556. doi:10.1021/es303778t

Blanco, I., Molle, P., Sáenz de Miera, L. E., and Ansola, G. (2016). Basic Oxygen Furnace Steel Slag Aggregates for Phosphorus Treatment. Evaluation of its Potential Use as a Substrate in Constructed Wetlands. *Water Res.* 89, 355–365. doi:10.1016/j.watres.2015.11.064

Chazarenc, F., Brisson, J., and Comeau, Y. (2007). Slag Columns for Upgrading Phosphorus Removal from Constructed Wetland Effluents. *Water Sci. Technol.* 56 (3), 109–115. doi:10.2166/wst.2007.499

Chen, X., Sun, X., Xu, P., Wang, S., Zhou, T., Wang, X., et al. (2020). Optimal Regulation of N/P in Horizontal Sub-surface Flow Constructed Wetland through Quantitative Phosphorus Removal by Steel Slag Fed. *Environ. Sci. Pollut. Res.* 27 (6), 5779–5787. doi:10.1007/s11356-019-06696-5

Cui, L., Ouyang, Y., Yang, W., Huang, Z., Xu, Q., and Yu, G. (2015). Removal of Nutrients from Septic Tank Effluent with Baffle Subsurface-Flow Constructed Wetlands. *J. Environ. Manag.* 153, 33–39. doi:10.1016/j.jenvman.2015.01.035

Drizo, A., Forget, C., Chapuis, R. P., and Comeau, Y. (2006). Phosphorus Removal by Electric Arc Furnace Steel Slag and Serpentinite. *Water Res.* 40 (8), 1547–1554. doi:10.1016/j.watres.2006.02.001

Ge, Y., Wang, X. C., Dzakpasu, M., Zheng, Y., Zhao, Y., and Xiong, J. (2016). Characterizing Phosphorus Removal from Polluted Urban River Water by Steel Slags in a Vertical Flow Constructed Wetland. *Water Sci. Technol.* 73 (11), 2644–2653. doi:10.2166/wst.2016.118

Ge, Y., Wang, X., Zheng, Y., Dzakpasu, M., Zhao, Y., and Xiong, J. (2015). Functions of Slags and Gravels as Substrates in Large-Scale Demonstration Constructed Wetland Systems for Polluted River Water Treatment. *Environ. Sci. Pollut. Res.* 22, 12982–12991. doi:10.1007/s11356-015-4573-9

Gomes, H. I., Mayes, W. M., Baxter, H. A., Jarvis, A. P., Burke, I. T., Stewart, D. I., et al. (2018). Options for Managing Alkaline Steel Slag Leachate: A Life Cycle Assessment. *J. Clean. Prod.* 202, 401–412. doi:10.1016/j.jclepro.2018.08.163

Hamdan, R., Ibrahim, I. I., Wan Mohamed, W. A., Al-Gheethi, A., Othman, N., and Mohamed, R. (2020). Optimizing Vertical Flow Aerated Steel Slag Filter System with Nitrifiers Bacteria for Nutrients' Removal from Domestic Wastewater: a Pilot Study. *J. Chem. Technol. Biotechnol.* 96 (4), 1067–1079. doi:10.1002/jctb.6618

Huang, L., and He, X. (2011). Construction of Steel Slag-Limestone Wetland with Mixed Progressively-Sized and Anti-sized Bed for Living Sewage Treatment. *Environ. Pollut. Control* 33 (9), 25–28. doi:10.15985/j.cnki.1001-3865.2011.09.011

Hussain, S. I., Blowes, D. W., Ptacek, C. J., Jamieson-Hanes, J. H., Wootton, B., Balch, G., et al. (2015). Mechanisms of Phosphorus Removal in a Pilot-Scale Constructed Wetland/BOF Slag Wastewater Treatment System. *Environ. Eng. Sci.* 32 (4), 340–352. doi:10.1089/ees.2014.0376

Kim, E.-H., Lee, D.-W., Hwang, H.-K., and Yim, S. (2006). Recovery of Phosphates from Wastewater Using Converter Slag: Kinetics Analysis of a Completely Mixed Phosphorus Crystallization Process. *Chemosphere* 63 (2), 192–201. doi:10.1016/j.chemosphere.2005.08.029

Lan, W., Zhang, J., Hu, Z., Ji, M., Zhang, X., Zhang, J., et al. (2018). Phosphorus Removal Enhancement of Magnesium Modified Constructed Wetland Microcosm and its Mechanism Study. *Chem. Eng. J.* 335, 209–214. doi:10.1016/j.cej.2017.10.150

Lu, H., Xiao, L., Wang, T., Lu, S., Wang, H., Guo, X., et al. (2021). The Application of Steel Slag in a Multistage Pond Constructed Wetland to Purify Low-Phosphorus Polluted River Water. *J. Environ. Manag.* 292, 112578. doi:10.1016/j.jenvman.2021.112578

Lu, S., Zhang, X., Wang, J., and Pei, L. (2016). Impacts of Different Media on Constructed Wetlands for Rural Household Sewage Treatment. *J. Clean. Prod.* 127, 325–330. doi:10.1016/j.jclepro.2016.03.166

Mohamed, R. M. S. R., Al-Gheethi, A. A., Miau, J. A., and Kassim, A. H. M. (2016). Multi-component Filters for Domestic Graywater Treatment in Village Houses. *jawwa* 108 (7), E405–E415. doi:10.5942/jawwa.2016.108.0103

Park, J.-H., Kim, S.-H., Delaune, R. D., Kang, B.-H., Kang, S.-W., Cho, J.-S., et al. (2016). Enhancement of Phosphorus Removal with Near-Neutral pH Utilizing Steel and Ferronickel Slags for Application of Constructed Wetlands. *Ecol. Eng.* 95, 612–621. doi:10.1016/j.ecoleng.2016.06.052

Park, J.-H., Wang, J. J., Kim, S.-H., Cho, J.-S., Kang, S.-W., Delaune, R. D., et al. (2017). Phosphate Removal in Constructed Wetland with Rapid Cooled Basic Oxygen Furnace Slag. *Chem. Eng. J.* 327, 713–724. doi:10.1016/j.cej.2017.06.155

Pratt, C., Shilton, A., Pratt, S., Haverkamp, R. G., and Bolan, N. S. (2007). Phosphorus Removal Mechanisms in Active Slag Filters Treating Waste Stabilization Pond Effluent. *Environ. Sci. Technol.* 41 (9), 3296–3301. doi:10.1021/es062496b

Ren, L.-J., Xu, L.-L., Zhang, Y.-Y., Pan, W., Yin, S.-L., Zhou, Y., et al. (2014). Effects of Connection Mode and Hydraulic Retention Time on Wastewater Pollutants Removal in Constructed Wetland Microcosms. *Clean. Soil Air Water* 43 (12), 1574–1581. doi:10.1002/clen.201300842

Saeed, T., Miah, M. J., Majed, N., Hasan, M., and Khan, T. (2020). Pollutant Removal from Landfill Leachate Employing Two-Stage Constructed Wetland Mesocosms: Co-treatment with Municipal Sewage. *Environ. Sci. Pollut. Res.* 27, 28316–28332. doi:10.1007/s11356-020-09208-y

Shen, S., Li, X., Cheng, F., Zha, X., and Lu, X. (2020). Review: Recent Developments of Substrates for Nitrogen and Phosphorus Removal in CWs Treating Municipal Wastewater. *Environ. Sci. Pollut. Res.* 27, 29837–29855. doi:10.1007/s11356-020-08808-y

Shi, P., Jiang, Y., Zhu, H., and Sun, D. (2017a). Impact of Steel Slag on the Ammonium Adsorption by Zeolite and a New Configuration of Zeolite-Steel Slag Substrate for Constructed Wetlands. *Water Sci. Technol.* 76 (3), 584–593. doi:10.2166/wst.2017.232

Shi, P., Zhu, H., and Sun, D. (2014). Removal Efficiency of Typical Pollutants by Different Substrate Combinations for Constructed Wetlands. *Huanjing Kexue Xuebao/Acta Sci. Circumstantiae* 34 (3), 704–711. doi:10.13671/j.hjkxxb.2014.0122.html

Shi, X., Fan, J., Zhang, J., and Shen, Y. (2017b). Enhanced Phosphorus Removal in Intermittently Aerated Constructed Wetlands Filled with Various Construction Wastes. *Environ. Sci. Pollut. Res.* 24, 22524–22534. doi:10.1007/s11356-017-9870-z

Shilton, A., Chen, L., Elemetri, I., Pratt, C., and Pratt, S. (2013). Active Slag Filters: Rapid Assessment of Phosphorus Removal Efficiency from Effluent as a Function of Retention Time. *Environ. Technol.* 34 (2), 195–200. doi:10.1080/09593330.2012.689365

Wan, Z., Zhang, Y., Lu, S., Zhang, X., Liu, X., and Yang, Y. (2020). Effect of Packing Substrates on the Purification of Municipal Wastewater Treatment Plant Effluent. *Environ. Sci. Pollut. Res.* 27, 15259–15266. doi:10.1007/s11356-020-08068-w

Wu, J., He, F., Xu, D., Wang, R., Zhang, X., Xiao, E., et al. (2011). Phosphorus Removal by Laboratory-Scale Unvegetated Vertical-Flow Constructed Wetland Systems Using Anthracite, Steel Slag and Related Blends as Substrate. *Water Sci. Technol.* 63 (11), 2719–2724. doi:10.2166/wst.2011.573

Xiong, J., Qin, Y., Mahmood, Q., Liu, H., and Yang, D. (2011). Phosphorus Removal from Secondary Effluents through Integrated Constructed Treatment System. *Mar. Pollut. Bull.* 63 (5-12), 98–101. doi:10.1016/j.marpolbul.2011.04.020

Xu, R., Zhang, Y., Liu, R., Cao, Y., Wang, G., Ji, L., et al. (2019). Effects of Different Substrates on Nitrogen and Phosphorus Removal in Horizontal Subsurface Flow Constructed Wetlands. *Environ. Sci. Pollut. Res.* 26, 16229–16238. doi:10.1007/s11356-019-04945-1

Yamada, H., Kayama, M., Saito, K., and Hara, M. (1986). A Fundamental Research on Phosphate Removal by Using Slag. *Water Res.* 20 (5), 547–557. doi:10.1016/0043-1354(86)90018-7

Yuan, Z., Fu, S., Xu, X., and Wendling, L. A. (2017). Mineral Processing Residue Use as Substrate in a Modular Engineered Wetland for Wastewater Treatment. *Environ. Process.* 4, 523–547. doi:10.1007/s40710-017-0247-6

Yun, Y., Zhou, X., Li, Z., Uddin, S. M. N., and Bai, X. (2015). Comparative Research on Phosphorus Removal by Pilot-Scale Vertical Flow Constructed Wetlands Using Steel Slag and Modified Steel Slag as Substrates. *Water Sci. Technol.* 71 (7), 996–1003. doi:10.2166/wst.2015.059

Zhang, C., Tan, S., Li, J., and Peng, C. (2015). Polishing of Secondary Effluent by a Two-Stage Vertical-Flow Constructed Wetland. *Pol. J. Environ. Stud.* 24 (2), 923–928. doi:10.15244/pjoes/23868

Zheng, Y., Cao, T., Zhang, Y., Xiong, J., Dzakpasu, M., Yang, D., et al. (2021). Characterization of Dissolved Organic Matter and Carbon Release from Wetland Plants for Enhanced Nitrogen Removal in Constructed Wetlands for Low C-N Wastewater Treatment. *Chemosphere* 273, 129630. doi:10.1016/j.chemosphere.2021.129630

**Conflict of Interest:** The authors declare that the research was conducted in the absence of any commercial or financial relationships that could be construed as a potential conflict of interest.

frontiers | Frontiers in Ecology and Evolution

TYPE Original Research
PUBLISHED 16 August 2022
DOI 10.3389/fevo.2022.980441



OPEN ACCESS

EDITED BY
Chuanyu Gao,
Northeast Institute of Geography and Agroecology (CAS), China

REVIEWED BY
Xingliang Xu,
Institute of Geographic Sciences and Natural Resources Research (CAS), China
Jinshu Chi,
Hong Kong University of Science and Technology, Hong Kong SAR, China

*CORRESPONDENCE
Liang Yan
yanliang@caf.ac.cn

†These authors have contributed equally to this work and share first authorship

SPECIALTY SECTION
This article was submitted to Conservation and Restoration Ecology, a section of the journal Frontiers in Ecology and Evolution

RECEIVED 28 June 2022
ACCEPTED 26 July 2022
PUBLISHED 16 August 2022

CITATION
Yang A, Kang X, Li Y, Zhang X, Zhang K, Kang E, Yan Z, Li M, Wang X, Niu Y and Yan L (2022) Alpine wetland degradation reduces carbon sequestration in the Zoige Plateau, China.
*Front. Ecol. Evol.* 10:980441.
doi: 10.3389/fevo.2022.980441



# Alpine wetland degradation reduces carbon sequestration in the Zoige Plateau, China

Ao Yang[1,2,3†], Xiaoming Kang[1,2,3†], Yong Li[1,2,3], Xiaodong Zhang[1,2,3], Kerou Zhang[1,2,3], Enze Kang[4,5], Zhongqing Yan[1,2,3], Meng Li[1,2,3], Xiaodong Wang[1,2,3], Yuechuan Niu[6] and Liang Yan[1,2,3*]

[1]Wetland Research Center, Institute of Ecological Conservation and Restoration, Chinese Academy of Forestry, Beijing, China, [2]Beijing Key Laboratory of Wetland Services and Restoration, Beijing, China, [3]Sichuan Zoige Wetland Ecosystem Research Station, Tibetan Autonomous Prefecture of Aba, Sichuan, China, [4]University of Chinese Academy of Sciences, Beijing, China, [5]State Key Laboratory of Vegetation and Environmental Change, Institute of Botany, Chinese Academy of Sciences (CAS), Beijing, China, [6]College of Life Sciences, University of Chinese Academy of Sciences, Beijing, China

Alpine wetland plays an important role in the global carbon balance but are experiencing severe degradation under climate change and human activities. With the aim to clarify the effect of alpine wetland degradation on carbon fluxes (including net ecosystem $CO_2$ exchange, NEE; ecosystem respiration, ER; gross ecosystem productivity, GEP, and $CH_4$ flux), we investigated 12 sites and measured carbon fluxes using the static chamber method in the Zoige alpine wetland during August 2018, including undegraded wetland (UD), lightly degraded wetland (LD), moderately degraded wetland (MD), and severely degraded wetland (SD). The results showed that carbon sink strengths differ among the Zoige wetlands with different degradation stages during the growing season. From UD to LD, the rate of carbon sequestration (mean value of NEE) increased by 25.70%; however, from LD to SD, it decreased by 81.67%. Wetland degradation significantly reduced soil water content (SWC), soil organic carbon (SOC), microbial biomass carbon (MBC), and microbial biomass nitrogen (MBN). NEE was significantly correlated with MBC and MBN, while ER was positively correlated with ST but negatively correlated with SOC ($P < 0.01$). Among all measured environmental factors, GEP was positively correlated with pH ($P < 0.01$), while $CH_4$ flux was most closely correlated with SOC, SWC, MBC, MBN, and ST ($P < 0.001$), and was also affected by pH and $NO_3^-$ content ($P < 0.01$). These results suggest that the capacity of carbon sequestration in the Zoige wetlands reduced with intensification of the degradation. This study provides a reference for sustainably managing and utilizing degraded wetlands under climate change.

KEYWORDS

**degradation, carbon sequestration, $CH_4$ flux, environmental factors, alpine wetland**

## Introduction

Wetlands are one of the most important natural ecosystems on earth and are formed from the interaction between terrestrial and aquatic ecosystems (Li Y. et al., 2021). Wetlands account for only 5–8% of the land surface area but store 25–30% of soil organic carbon (SOC) in the terrestrial ecosystem (Mitsch and Gosselink, 2011). Wetlands are sensitive to climate change and human activities (Yan et al., 2022), and play pivotal roles in flood prevention, runoff regulation, pollution control, climate regulation, and sustaining ecosystems and global carbon balance (Spieles, 2022). Located on the Qinghai-Tibet Plateau, alpine wetland accumulates a large amount of herbaceous litter with a slow decomposition rate, resulting in higher soil carbon density than other ecosystems (Yarwood, 2018). Meanwhile, these alpine wetlands also contain large amounts of SOC (Wang et al., 2002). However, the increase in temperature, drainage, and overgrazing in recent years has led to the degradation of alpine wetland (Zhu et al., 2022), which have become alpine meadows (Li et al., 2018). Therefore, the carbon cycle changed with the degradation of the alpine wetland (Rui et al., 2011). Degradation changes the hydrothermal conditions in alpine wetland, which directly affects the complex physical, chemical, and biological factors of wetland soil, thereby changing the physiological characteristics of wetland plants. The contents of SOC, nitrogen, phosphorus, and water decrease with intensification of the alpine wetland's degradation. The distribution of plant functional groups is more sensitive to variations in soil water content (SWC), total nitrogen (TN) content, and other factors. Vegetation cover and richness are also affected by the degradation of alpine wetland (Wang et al., 2015; Yuan et al., 2020), which leads to variations in root exudates and soil litter, and affects the carbon and nitrogen conversion rate by soil microorganisms.

Many studies have investigated the changes in carbon fluxes in alpine wetland during different seasons, and most studies have shown that alpine wetland are significant carbon sinks in summer (Zhao et al., 2005; Shi et al., 2006). However, flux observations in the Luanhaizi and Haibei alpine wetlands showed that alpine wetlands are $CO_2$ sources (Zhao et al., 2010; Zhu et al., 2020). Moreover, atmospheric methane ($CH_4$) also plays a key role in climate change and the carbon cycle. Natural $CH_4$ emissions from wetlands are the largest single source in the global $CH_4$ budget (Ringeval et al., 2010), whereas wetland $CH_4$ emissions dominate the interannual variability in the global $CH_4$ source (Walter et al., 2001; Bousquet et al., 2006). Some researchers have reported that degradation of the Zoige peatland due to drainage has greatly reduced $CH_4$ emissions (Zhang et al., 2019). Degradation not only affects net ecosystem $CO_2$ exchange (NEE) but also affects ecosystem respiration (ER) (Chen et al., 2013). Furthermore, previous studies have reported that gross ecosystem productivity (GEP) is significantly higher in slightly degraded than in severely degraded land (Peng et al., 2015). The rates of NEE are significantly lower in degenerated wetlands than in non-degraded wetlands (Xia et al., 2019). Xu et al. (2022) reported that extremely land degradation significantly decreases NEE and ER by 60.61% and 67.53%, respectively. However, another study showed that the average ER flux of degrading vegetation (218.04 ± 95.08 mg C $m^{-2}$ $h^{-1}$ in 2013 and 219.03 ± 140.96 mg C $m^{-2}$ $h^{-1}$ in 2014) is considerably larger than that of healthy vegetation (163.78 ± 87.51 mg C $m^{-2}$ $h^{-1}$ in 2013 and 143.91 ± 84.44 mg C $m^{-2}$ $h^{-1}$ in 2014) (Ma et al., 2020). Thus, degradation has a variable effect on carbon fluxes. Studies have shown that although degradation affects carbon sequestration in alpine wetland, the degree of the impact varies with the intensity of degradation (Pei et al., 2022). Therefore, it is important to explore the impact of degradation on carbon cycle variables (including $CH_4$) in the Zoige alpine wetland along four different degradation gradients.

The Zoige alpine wetland are the largest plateau peat swamp in the world, located in the upper reaches of the Yellow River in the northeastern Qinghai-Tibet Plateau (Jiang et al., 2017). The unique climatic, geological and geographical conditions of the Zoige alpine wetland provide the environmental conditions for the survival of a large number of wetland wild animals and plants and make it one of the huge SOC pools in China (Huo et al., 2013). However, frequent extreme climate events and overgrazing since the 1970s have caused serious degradation of the Zoige alpine wetland (Qiu et al., 2009). Drainage and ditching have aggravated the degradation of the Zoige wetlands to varying degrees (Mei et al., 2012). Degradation leads to a reduction in the area of alpine wetland and a drop in water table, which in turn leads to accelerated peat decomposition and carbon release (Moorcroft et al., 2008), thereby exacerbating the global greenhouse effect (Rey et al., 2011). The aims of the present study were to (1) measure the variation of NEE, ER, GEP, and $CH_4$ flux and determined the environmental factors along different wetland degradation gradients; (2) analyze the relationship between environmental factors and carbon fluxes; and (3) clarify the effect of alpine wetland degradation on carbon fluxes. This study will improve our understanding of the degradation impacts on alpine wetland, and provide data to support the theoretical basis for scientifically evaluating the system carbon budget of degraded alpine wetland.

## Materials and methods

### Study site

The Zoige wetlands (33° 55′ 42″ N, 102° 52′ 14″ E) are located in the northeastern Qinghai-Tibet Plateau with an average altitude of 3,600 m above sea level (**Figure 1**). The wetlands are in Zoige County, Aba Prefecture, Sichuan Province, and represent the largest plateau peatland in the world (Chen et al., 2009). The wetland area is 6,180 $km^2$, accounting for 31.5% of the total area of the Zoige Plateau (Hao et al., 2011).

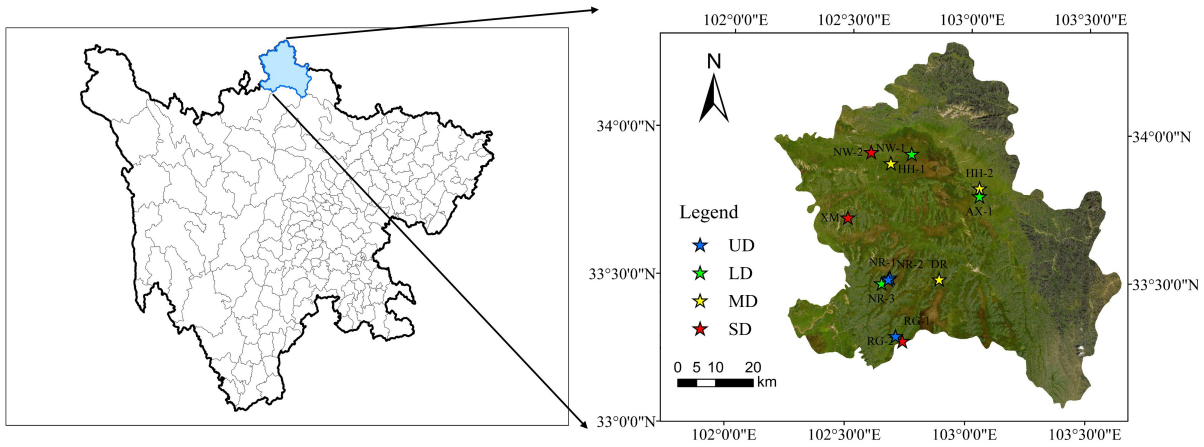


FIGURE 1
Locations of the sampling sites in the Zoige Plateau. The left panel is the location of Zoige in Sichuan Province, and the right panel is the location of the sampling point in Zoige. UD, undegraded wetland; LD, lightly degraded wetland; MD, moderately degraded wetland; SD, severely degraded wetland.

Due to the high altitude, the air pressure is low at about 668.8 hPa. The region is in the humid climate of the plateau cold temperate zone, with a short spring and autumn, and annual average temperatures of about −1.7–3.3°C (Kang et al., 2018). The annual average rainfall is 650–750 mm, and the rainy season is warm and humid (May to September), whereas the dry season is cold and dry (October–April) (Liu et al., 2020a; Kang et al., 2022). The dominant species are *Kobresia tibetica*, *Carex lasiocarpa*, *Stipa capillata*, and other marsh plants (Liu et al., 2020b). The soil type in the study area was mainly meadow soil, and the vegetation type was mainly alpine meadow vegetation. The depth of the peat in the vertical profile of the Zoige alpine wetland is 2–5 m (Gao et al., 2011) with dry weight of 2.9 Pg and pH of 6.8–7.2 (Chen et al., 2014; Yan et al., 2021). Since the 1960s, the peatland has experienced artificial drainage and expanded pasture (Xiang et al., 2009), which has drained nearly 41% of the total area of the Zoige peatland and has changed the plant community, vegetation cover, and soil properties (Wu et al., 2017).

## Experimental design

We investigated 12 sites including four degradation grades, i.e., undegraded wetlands (UD), lightly degraded wetlands (LD), moderately degraded wetlands (MD), and severely degraded wetlands (SD) in the Zoige Plateau during August 2018. Three sites were selected for each degradation gradient, and three 0.5 m × 0.5 m quadrats representing replicates were randomly selected within each site. We investigated the VC in the quadrats, collected soil samples, and measured $CO_2$ and $CH_4$ fluxes *in situ* during the growing season. The degradation gradients of the alpine wetland were determined according to the vegetation cover (VC) referred from the classification of alpine wetland degradation grade by Ma et al. (2002). The basic information of each degradation gradient is shown in **Table 1**.

## Measurement of carbon fluxes

The carbon fluxes included NEE, ER, GEP, and $CH_4$. The NEE, ER, and $CH_4$ fluxes were measured using the static chamber method (Niu et al., 2010) carried out between 9:00 and 16:00 on a clear and cloudless day. Acrylic materials with light transmittance > 95% were used to make the cubic chamber (size = 0.5 m × 0.5 m × 0.5 m). Two fans were installed on the inner side of the chamber to ensure the uniform mixing of gases in the chamber, and the chamber had an air pipe connected with an LGR-ICOS groove portable greenhouse gas analyzer (UGGA-30p, LGR, United States) to measure the net exchange rate of the $CO_2$ and $CH_4$ at the different degraded sampling sites (**Supplementary Figure 1**). The base of the cubic chamber was an aluminum alloy bottom groove of 0.5 m × 0.5 m, which vertically hit the ground at 5 cm and maintained the base level. A water seal was used to ensure air tightness inside the cubic chamber during measurements. The cubic chamber was

TABLE 1 Evaluation grade standard for degraded alpine wetlands.

| Degradation degree | Vegetation cover (%) |
|---|---|
| UD | 80∼100 |
| LD | 70∼80 |
| MD | 50∼70 |
| SD | < 50 |

UD, undegraded wetland; LD, lightly degraded wetland; MD, moderately degraded wetland; SD, severely degraded wetland.

buckled on the bottom of an aluminum alloy tank, and counting began after the system stabilized. The instrument recorded the concentrations of $CO_2$ and $CH_4$ with the frequency of 1 Hz for 120 s continuously. According to the variations in the $CO_2$ and $CH_4$ concentrations during the measurement period (5–118 s), the change in the slopes of $CO_2$ and $CH_4$ with time was calculated, and the $CO_2$ and $CH_4$ fluxes in the cubic chamber per unit time were determined by combining the slope with air temperature, water pressure, and air pressure during the measurement period (**Equation 1**). The NEE (a positive value is $CO_2$ emissions, a negative value is net $CO_2$ uptake by the ecosystem, and the following methods for measuring ER and $CH_4$ fluxes were the same) and $CH_4$ was determined under the lighting conditions. The ER fluxes were measured with the cubic chamber covered with a dark opaque cloth. The NEE, ER, and $CH_4$ fluxes were calculated from Equation 1. GEP was the difference between ER and NEE.

$$F_c = \frac{d_c}{d_t} \times \frac{M}{V_0} \times \frac{P}{P_0} \times \frac{T_0}{T} \times H \quad (1)$$

Where $F_c$ is the gas flux (mg·m$^{-2}$·h$^{-1}$). where $dc/dt$ is the slope of the linear regression for gas concentration gradient through time; where $M$ and $V_0$ are the molar mass of the gas (g mol$^{-1}$) and the standard molar volume is 22.4 L mol$^{-1}$, respectively; $P$ and $P_0$ are the measured atmospheric pressure and the standard atmospheric pressure, respectively; $T$ and $T_0$ (°C) represent the average value and the absolute temperature of the air temperature in the chamber, respectively; and $H$ (cm) is the height of the static chamber.

## Environmental factors

Soil temperature (ST) at a depth of 5 cm was measured in each sample plot with a portable digital thermometer (JM624, Jinming Institute Co., Tianjing, China), and SWC at a depth of 5 cm was determined with a TDR300 moisture meter (Spectrum Technologies, Inc., Aurora, IL, United States). Three soil samples at a depth of 5 cm were randomly collected from each sample plot and stored at 4°C until the soil properties were determined. The soil samples were passed through a 2 mm sieve to divide the soil into two parts. Ammonia ($NH_4^+$), nitrate ($NO_3^-$), microbial biomass carbon (MBC), microbial biomass nitrogen (MBN), and dissolved organic carbon (DOC) were determined in fresh soil samples. Soil pH, SOC, and TN were determined in air-dried samples. Soil pH was measured with a pH electrode in a slurry solution with a ratio of soil to water of 1:2.5 (PHS 29, China). SOC and TN were analyzed by a C/N

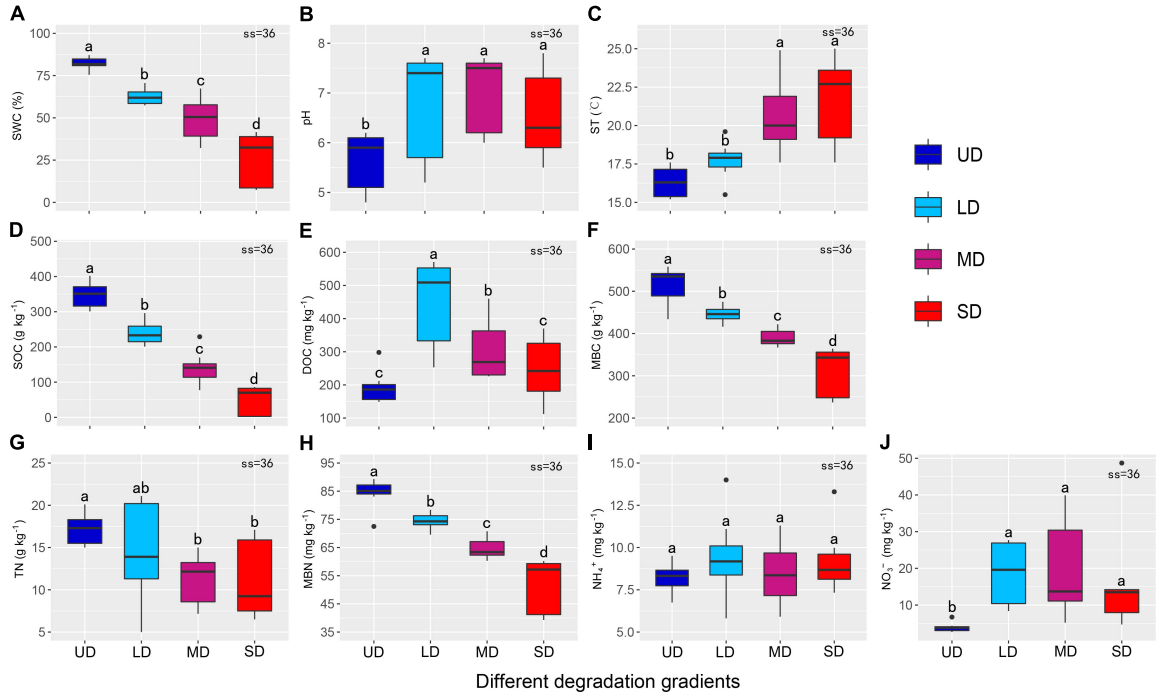


FIGURE 2
Environmental factors at the different degradation gradient sites. **(A–J)** Represent the trends of SWC, pH, ST, SOC, DOC, MBC, TN, MBN, $NH_4^+$, and $NO_3^-$ content with degradation gradient, respectively. Different lowercase letters indicate significant differences at the $P < 0.05$ level (error bars indicate standard errors). UD, undegraded wetland; LD, lightly degraded wetland; MD, moderately degraded wetland; SD, severely degraded wetland; SWC, soil water content; ST, soil temperature at the 5 cm depth; SOC, soil organic carbon; MBN, microbial biomass nitrogen; MBC, microbial biomass carbon; DOC, dissolved organic carbon; $NO_3^-$, nitrate; $NH_4^+$, ammonia; TN, total nitrogen.

analyzer (multi-N/C 3100, Analytik Jena AG, Jena, Germany). Soil $NH_4^+$ content was analyzed using the salicylic acid-sodium nitroprusside method with a spectrophotometer (PharmaSpec UV1700, Shimadzu, Tokyo, Japan), and soil $NO_3^-$ was analyzed using a Technicon automated analyzer and by the cadmium reduction method with a 2 M KCl solution. Soil MBC and soil MBN were measured by the chloroform fumigation extraction technique with a fumigation time of 20 h and a 25 mM $K_2SO_4$ extract. Soil DOC was extracted by adding 50 mL of 0.5 M $K_2SO_4$ to 12.5 g of a homogenized subsample followed by stirring on a 120 rpm orbital shaker for 1 h. The filtrate was subjected to a total organic carbon analyzer (multi-55 N/C 3100, Analytik Jena). After digestion with perchloric acid, soil TN was determined by the Kjeldahl method.

## Statistical analysis

The effects of the degradation gradient on the NEE, ER, GEP, and $CH_4$ fluxes were tested by one-way analysis of variance. The LSD (least significant difference) post-test was applied to test for differences among the degradation gradients. Additionally, redundancy analysis (RDA) was used to explore the relationships between the different degradation gradients

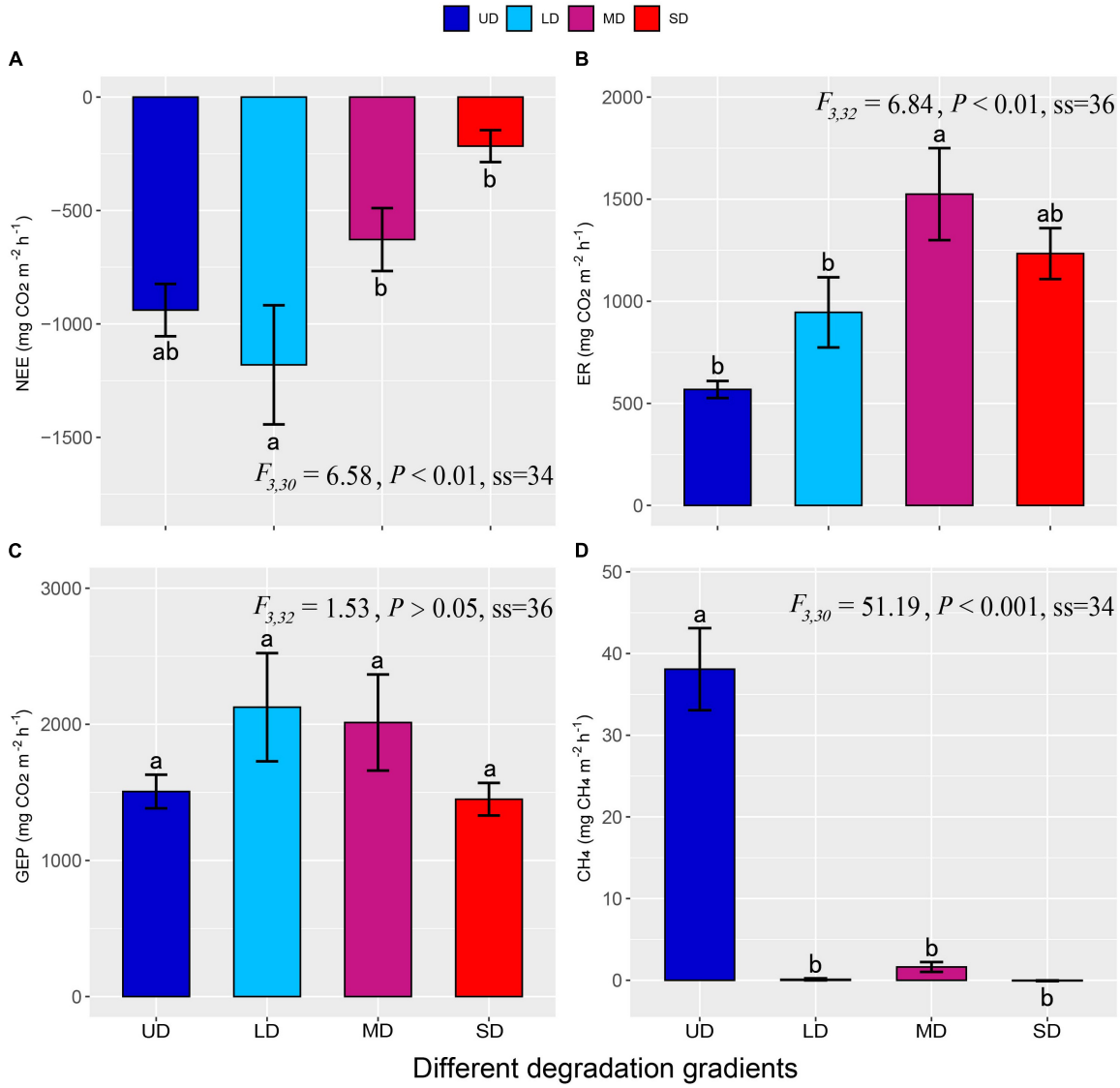


FIGURE 3
The NEE **(A)**, ER **(B)**, GEP **(C)**, and $CH_4$ **(D)** fluxes in the alpine wetlands degraded to different degrees. Different lowercase letters indicate a significant difference at the $P < 0.05$ level (error bars indicate the standard errors). UD, undegraded wetland; LD, lightly degraded wetland; MD, moderately degraded wetland; SD, severely degraded wetland; NEE, net ecosystem $CO_2$ exchange; ER, ecosystem respiration; GEP, gross ecosystem productivity; $CH_4$ flux, methane flux.

and environmental factors in the Zoige alpine wetland. The heatmap was prepared to show the relationships between the carbon fluxes and environmental factors. All analyses were conducted in R v4.2.0 software (R Core Team, 2020).

# Results

## Environmental factors

The environmental factors were classified into soil physical properties (including SWC, pH, and ST; Figures 2A–C), soil carbon content (including SOC, DOC, and MBC; Figures 2D–F), and soil nitrogen content (including TN, MBN, $NH_4^+$, and $NO_3^-$; Figures 2G–J). Degradation significantly altered SWC, ST, SOC, MBC, and MBN in the alpine wetland (Figure 2). SWC decreased with degradation severity, from 82.35% in UD to 26.59% in SD (Figure 2A). The pH at the UD sites was significantly lower than that at the other three degradation gradient sites (Figure 2B). In contrast, ST was significantly higher at the MD and SD sites than that at the UD and LD sites, with the highest value of 20.53°C in the SD and the lowest value of 16.16°C in the UD (Figure 2C). SOC, MBC, and MBN were in ranges of 49.43–348.33 g·kg$^{-1}$, 314.53–513.10 mg·kg$^{-1}$, and 52.20–84.49 mg·kg$^{-1}$, respectively, and all decreased significantly with

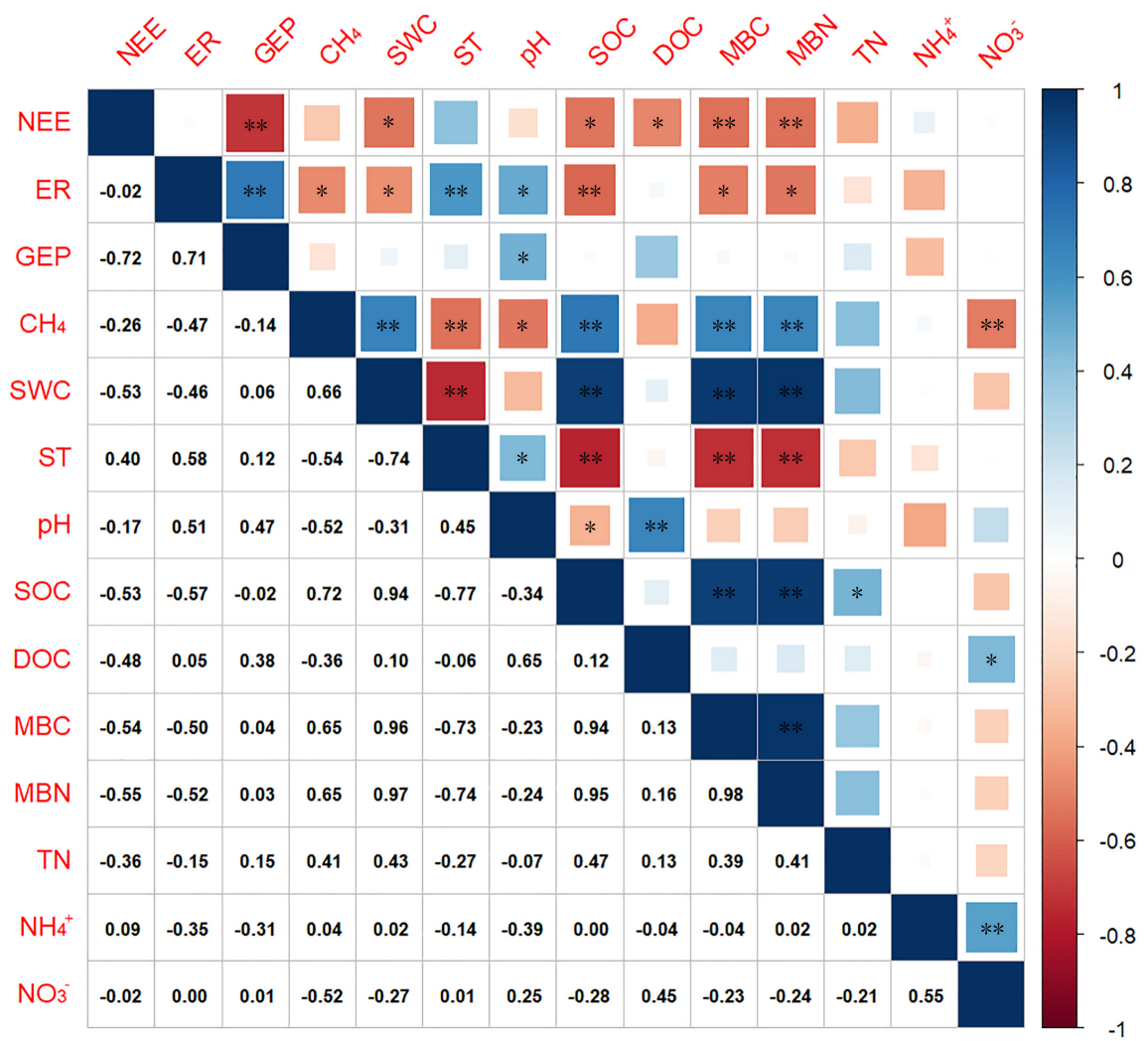


FIGURE 4
Heatmap of the correlations between NEE, ER, GEP, and $CH_4$ and the environmental factors. A blue square indicates that the correlation coefficient is positive, and a red circle indicates that the correlation coefficient is negative. The correlation coefficient decreased as the color became lighter and the size became smaller. NEE, net ecosystem $CO_2$ exchange; ER, ecosystem respiration; $CH_4$ flux, methane flux; SWC, soil water content; ST, soil temperature at the 5 cm depth; SOC, soil organic carbon; DOC, dissolved organic carbon; MBC, microbial biomass carbon; MBN, microbial biomass nitrogen; TN, total nitrogen; $NH_4^+$, ammonia; $NO_3^-$, nitrate; "*" and "**" represent significant differences at the 0.01 and 0.001 levels, respectively.

the degradation gradient (Figures 2D,F,H). SOC at the LD, MD, and SD sites decreased by 31.53%, 59.34%, and 85.81%, compared with that at the UD sites, respectively. The MBC and MBN decreased by 38.70% and 38.22%, respectively, from UD to SD with the degradation of the wetlands. DOC content was the highest in LD, with a value of 448.58 mg·kg$^{-1}$, but it decreased significantly from LD to SD (Figure 2E). TN decreased from UD to MD and increased from MD to SD (Figure 2G), and ranged from 10.47 to 17.20 g·kg$^{-1}$. $NH_4^+$content was not significantly different among the four degradation gradients (Figure 2I). $NO_3^-$ content was lowest in UD, while it was much higher at the sites where degradation occurred (Figure 2J).

## Variations in the ecosystem carbon fluxes

The NEE of the Zoige alpine wetland ranged from –216.31 to –1,180.24 mg $CO_2$ m$^{-2}$·h$^{-1}$, with an average of –747.53 ± 102.24 mg $CO_2$ m$^{-2}$·h$^{-1}$, indicating a carbon sink (Figure 3A). NEE weakened from LD to SD with increased wetland degradation. ER increased with degradation severity, the increase in alpine wetland degradation, ranging from 567.96 in UD to 1,524.60 mg $CO_2$ m$^{-2}$·h$^{-1}$ in MD, with an average value of 1,067.90 ± 95.70 mg $CO_2$ m$^{-2}$·h$^{-1}$. The ER values of LD, MD, and SD increased by 66.50%, 168.44%, and 117.17% compared with the UD, respectively (Figure 3B). GEP ranged from 1,449.73 to 2,125.86 mg $CO_2$ m$^{-2}$·h$^{-1}$ and reaching the maximum value in LD, although the difference among the four degrees of degradation was not significant (Figure 3C). The alpine wetland acted as a strong $CH_4$ source in UD (Figure 3D). The UD had a strong $CH_4$ source (38.09 ± 5.02 mg $CH_4$ m$^{-2}$·h$^{-1}$). However, $CH_4$ flux at the LD, MD, and SD sites were only 0.37, 1.62, and –0.06 mg $CH_4$ m$^{-2}$·h$^{-1}$, respectively, and no significant differences were observed among the LD, MD, or SD sites.

## Correlations between the environmental variables and carbon fluxes

The heatmap shows that NEE was significantly correlated with MBC and MBN, respectively (Figure 4). ER was positively correlated with ST ($r^2$ = 0.58), and negatively correlated with SOC ($r^2$ = –0.57, $P$ < 0.001). However, no correlation was detected between GEP and the measured environmental factors in this study, except pH ($r^2$ = 0.47, $P$ < 0.01). $CH_4$ flux has significantly positive relationships with SOC, SWC, MBC, and MBN ($P$ < 0.001). A negative correlation was observed between $CH_4$ and ST with $NO_3^-$ ($P$ < 0.001). A negative correlation was detected between $CH_4$ and ST and pH with correlation coefficients of –0.54 and –0.52, respectively. In addition to $CH_4$, the carbon flux components of the Zoige alpine wetland under different degradation succession gradients sites were not correlated with TN, $NH_4^+$, or $NO_3^-$ ($P$ > 0.05, Figure 4).

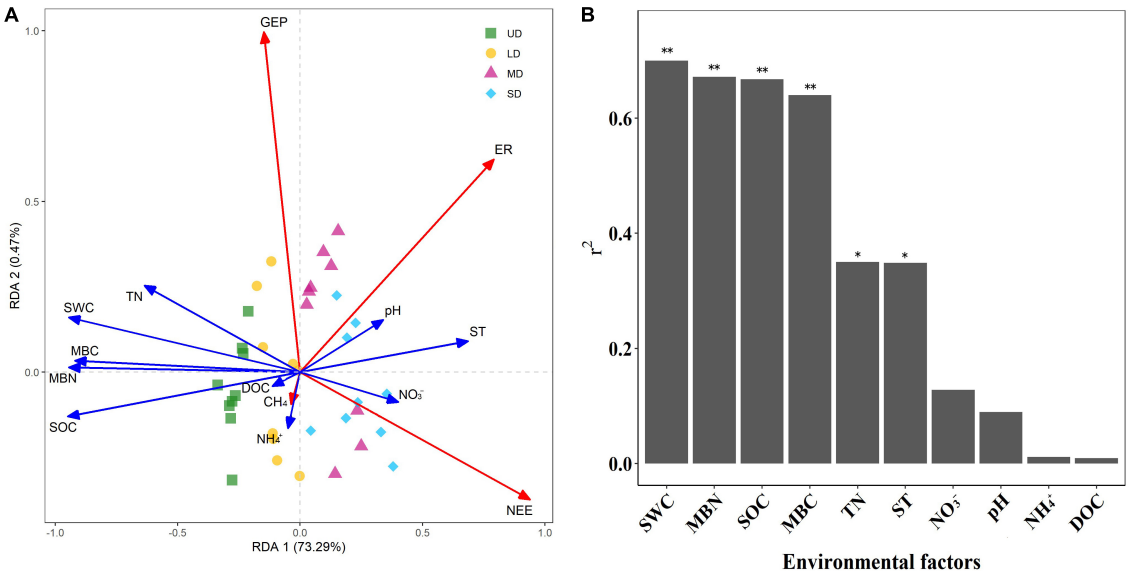


FIGURE 5
**(A)** Ordination plots of the redundancy analysis (RDA) for all plots and environmental factors across all sites and **(B)** a histogram of the explanatory rates of the different environmental factors for carbon fluxes. UD, undegraded wetland; LD, lightly degraded wetland; MD, moderately degraded wetland; SD, severely degraded wetland; SWC, soil water content; ST, soil temperature at a depth of 5 cm; SOC, soil organic carbon; DOC, dissolved organic carbon; MBC, microbial biomass carbon; MBN, microbial biomass nitrogen; TN, total nitrogen; $NH_4^+$, ammonia; $NO_3^-$, nitrate; "*" and "**" represent significant differences at $P$ < 0.01 and $P$ < 0.001, respectively.

The RDA results showed that the ten environmental factors explained 73.76% of the variation in the carbon fluxes (**Figure 5A**). SOC, MBN, MBC, and SWC were the main factors affecting the change in gas fluxes in the different degradation succession gradients, and they were highly correlated. The correlation coefficients between the four soil properties and the carbon fluxes under the different degradation succession gradients were 0.67, 0.67, 0.64, and 0.70, respectively (**Figure 5B**). ST and TN were correlated with the carbon fluxes of the four degradation gradients in the Zoige alpine wetland ($P < 0.01$).

# Discussion

## Effects of degradation on the environmental factors

The environmental factors were different under the different degradation gradients. As the degree of degradation intensified, the water table level in the Zoige alpine wetland decreased, and SWC decreased significantly (**Figure 2A**). The lack of water inhibits plant growth and affects nutrient absorption by the plants (Vargas et al., 2020). Therefore, the lower SWC resulted in inadequate growth conditions, which further degraded the alpine wetland. As an indicator of soil properties, SOC is a mixture of plant, animal, and microbial remains, excreta, secretions, their partial decomposition products, and soil humus (Piñeiro et al., 2010). Here, wetland degradation significantly reduced SOC content (**Figure 2D**). Some studies (Tang et al., 2010) have shown that simple vegetation composition and low diversity reduce the number of aboveground vegetation residues entering the soil; thus, resulting in lower SOC content. We found the same pattern for MBC and MBN (**Figures 2F**, H). Soil MBC and MBN contents increase in areas where plants grow well and decrease in areas where plants do not grow (Yan et al., 2012). When alpine wetland degrades to the severe degradation stage, the soil organic matter, MBC, and MBN are lost in large quantities.

Temperature is a key factor promoting the changes in root distribution and stock (Shen et al., 2016). The soil surface temperature of the Zoige alpine wetland increased gradually as degradation of the wetlands increased. Previous studies have shown that soil surface temperature, bulk density, and other properties increase with increasing alpine wetland degradation gradients (Li C. Y. et al., 2021). The reason may be that the high-altitude Zoige alpine wetland have stronger solar radiation, which makes the temperature of the soil with low water content increase rapidly, so the more severe the degradation, the higher the surface temperature (5 cm). Meanwhile, another reason for the increase of soil surface temperature may be the reduction of vegetation coverage caused by degradation, which increases the bare soil area and water loss through evaporation (Cui et al., 2005). Due to less vegetation cover and the "heat island" effect of bare land, the soil surface

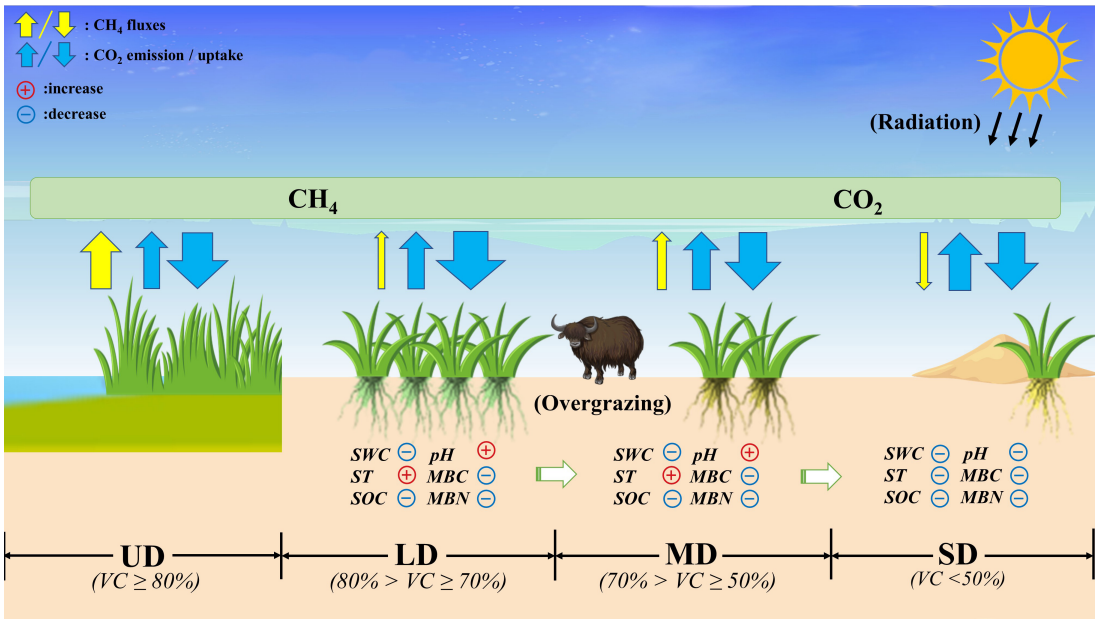


FIGURE 6
Carbon budget and environmental factors in the Zoige alpine wetlands under different degradation gradients. UD, undegraded wetland; LD, lightly degraded wetland; MD, moderately degraded wetland; SD, severely degraded wetland; SWC, soil water content; ST, soil temperature at the 5 cm depth; SOC, soil organic carbon; MBN, microbial biomass nitrogen; MBC, microbial biomass carbon; VC, vegetation cover.

temperature (5 cm) increases with the degradation gradient (Cao et al., 2004).

Soil pH affects the absorption of soil nutrients by plants (Ma et al., 2017), and plant growth and physiological and biological characteristics affect soil pH in turn. In this study, soil pH did not change significantly with the degradation gradient. However, the pH values in the LD, MD, and SD degraded areas were higher than those in the UD area, indicating that wetland degradation reduces soil acidity. The more serious the degradation, the less the vegetation cover (Li C. Y. et al., 2021), and the less vegetation cover interferes with the soil pH (Li et al., 2008), so the soil becomes neutral. However, the specific effects of soil pH and the different degradation gradients in the Zoige alpine wetland remain unclear; thus, further research is necessary on the specific mechanism.

## Effects of degradation on carbon fluxes

Significant differences in $CO_2$ fluxes were observed in the Zoige alpine wetland with different degrees of degradation, except GEP ($P > 0.05$), and NEE and GEP reached their maximum values at the LD sites (**Figure 3A**). The water table level at the UD sites was high and flooded, which led to low coverage and low photosynthetic capacity. However, a drop in the water table level reduced the flooding stress for plants at the LD sites and increased biomass and photosynthetic capacity. Therefore, the NEE and GEP values at the LD sites were higher than those at the UD sites, suggesting that the carbon sequestration capacity in the wetlands improved under the non-flooded LD condition (**Supplementary Figure 2**). However, the NEE and GEP rates decreased gradually with the increase in the degradation gradient (**Figures 3A,C**). The rate of carbon sequestration increased by 25.70% from UD to LD but decreased by 81.67% from LD to SD. The reason was attributed to the factors affecting photosynthesis. The photosynthetic ability of an ecosystem is closely related to environmental factors, such as light intensity, soil moisture, air humidity, air temperature, and atmospheric $CO_2$ concentration (Moore et al., 2006). Photosynthetic ability is also affected by the vegetation type, coverage, and leaf area index (Feng et al., 2008). When the alpine wetland is transformed into an extreme degradation stage, the plant community becomes smaller and sparse, the compositional structure changes, the coverage decreases, grass yield decreases, and the number of species and the amount of fine forage grass decrease (Zhou et al., 2005). The environmental conditions deteriorated rapidly, which made the photosynthetic rate of the community decrease rapidly, and the NEE and GEP also decreased. ER showed a trend of increasing first and then decreasing (**Figure 3B**) and was positively related to the degree of degradation. As the soil surface temperature of the degraded alpine wetland is high, the higher surface temperature led to an increase in microbial activity, which enhanced ER. As a result, ER was stronger and NEE was weaker and the more severe the degradation of the alpine wetland, the lower the GEP of its ecosystem.

$CH_4$ flux is closely associated with soil moisture (Yu et al., 2013). The SWC at the UD sites was sufficient and the water table level was high; thus, the $CH_4$ flux was very significant and the UD sites were an extremely important source of $CH_4$. In contrast, at the LD, MD, and SD sites, the decline in the water table level resulted in a significant decrease in $CH_4$ flux. Soil organic matter (crop straw of previous crop and photosynthetic products of the current season) is decomposed into methane by methanogenic bacteria (Conrad, 2007), and the high-water table level at the UD sites in this study created the conditions for generating methane. The Zoige alpine wetland exhibited a transformation from a $CH_4$ source to a $CH_4$ sink at the sites with a low MD to SD water table level, but the rate was extremely low. The $CO_2$-eq net flux of $CH_4$ was shown in **Supplementary Figure 3**. The Zoige alpine wetland had carbon absorption potential in the different degradation stages, and its carbon sink capacity varied with the degree of degradation (**Figure 6**), which was consistent with previous studies. Our study shows that the carbon sink function gradually weakened with the increase in the degradation gradient.

## Effects of the environmental factors on the carbon fluxes

Carbon fluxes in the Zoige alpine wetland were regulated by a variety of factors. Temperature was the primary factor controlling the ecosystem carbon fluxes (**Figure 4**). Previous studies have shown that temperature is one of the main factors affecting the respiratory rates of different soil use types (Hursh et al., 2016), as variations in temperature control carbon flux to a certain extent. Higher soil surface temperature stimulates the activity of microorganisms, enhances soil enzyme activities, and accelerates litter decomposition (Updegraff et al., 2001) so ST was the dominant ER controlling factor. Notably, NEE had a strong relationship with MBN, MBC, SOC, and SWC (**Figure 4**). MBC and MBN represent microbial activity, which was directly affected by soil fertility, water holding capacity, soil erosion resistance, and soil bulk density. The variations in MBC and MBN indirectly indicate the degree of wetland degradation, and they have an important effect on soil respiration and carbon balance in an alpine ecosystem. Therefore, MBC and MBN were strongly correlated with the carbon flux (**Figure 4**), and the carbon flux were high when MBC and MBN contents were high. Moreover, vegetation degradation and soil degradation are interrelated (Tang et al., 2015). One of the main reasons for vegetation degradation in the Zoige alpine wetland was the increase in grazing intensity and the increased rate of activities on the plateau (Liu et al., 2020b). Grazing decreases vegetation coverage and increases the amount of bare soil exposed to the

air (Sun et al., 2011), which aggravates the weathering of surface soil. At the same time, a large number of rodents invaded the plateau. Soil quality continued to decline as the rodents gnawed on the roots of plants and increased the number of underground caves, which shifted the Zoige alpine wetland to a severe degree of degradation. Ecosystem respiration decreases when the vegetation becomes severely damaged. Therefore, the carbon exchange rate of the ecosystem was lowest at the SD sites (**Figures 3A,D**). Therefore, further research on the degradation of the Zoige alpine wetland vegetation caused by grazing and rodent activities should be conducted.

Emissions of the greenhouse gas $CH_4$ account for 15% of the total greenhouse effect (Soebandiono et al., 2021). Here, our results show that $CH_4$ emissions at the UD sites were much higher than those at the LD, MD, or SD sites, and $CH_4$ flux was significantly correlated with SWC, ST, SOC, MBC, and MBN (**Figure 4**). Studies have shown that nitrates, sulfates, and others act as electron acceptors in wetland sediments, where they promote the anaerobic oxidation of $CH_4$ and reduce $CH_4$ emissions (Zhu et al., 2010). Moreover, soil microorganisms, such as methane-oxidizing bacteria, play an important role in inhibiting methane emissions. pH is an important environmental factor affecting microbial growth. Previous studies have reported that neutral and weak alkaline environments are more conducive to growing such microorganisms (Conrad, 2007). The pH of the soil in this study was 5.7–7.1, which was slightly acidic at the UD sites and was not beneficial for the survival of methane-oxidizing bacteria, suggesting why the $CH_4$ flux at this site was higher than the other three sites.

However, carbon fluxes in alpine wetland are influenced by many factors, such as climate conditions, vegetation type, and soil conditions (Luo and Zhou, 2006). Single-factor analyses of some main soil physical and chemical factors in this study only explained part of the question. Therefore, other factors such as climate conditions and vegetation types, should be considered more in follow-up research, and their effects on carbon fluxes in the alpine wetland should be comprehensively analyzed by multiple factors.

## Conclusion

In this study, we comprehensively investigated the carbon fluxes and environmental factors under 12 sites including four degradation grades in Zoige alpine wetland. Our finding indicated that the carbon fluxes of the Zoige alpine wetland during the growing season were closely related to the successional degradation gradients, and Zoige alpine wetland acted as a carbon sink under the four degradation gradients. Meanwhile, we found that degradation changed the environmental factors of alpine wetland, which weakened Zoige alpine wetland carbon sequestration capacity. Considering the complexity of the alpine wetland and the uncertainty of global climate change, further studies on the mechanisms of degradation on carbon sequestration in alpine wetland are needed in the future.

## Data availability statement

The original contributions presented in this study are included in the article/**Supplementary material**, further inquiries can be directed to the corresponding author.

## Author contributions

LY and XK conceived and designed the experiments. AY, XZ, XK, YL, ZY, ML, EK, XW, and YN conducted the experiments. AY analyzed the data. AY and XK wrote the manuscript. KZ, LY, XK, and YL revised the manuscript. All authors have read and agreed to the published version of the manuscript.

## Funding

This study was supported by the Fundamental Research Funds of CAF (CAFYBB2019QB009), the National Natural Science Foundation of China (32171597, 32171598, and 42041005), the Second Tibetan Plateau Scientific Expedition and Research Program (STEP) (2019 QZKK0304).

## Conflict of interest

The authors declare that the research was conducted in the absence of any commercial or financial relationships that could be construed as a potential conflict of interest.

## Publisher's note



## Supplementary material

The Supplementary Material for this article can be found online at: https://www.frontiersin.org/articles/10.3389/fevo.2022.980441/full#supplementary-material

# References


Bousquet, P., Ciais, P., Miller, J. B., Dlugokencky, E. J., Hauglustaine, D. A., Prigent, C., et al. (2006). Contribution of anthropogenic and natural sources to atmospheric methane variability. *Nature* 443, 439–443. doi: 10.1038/nature05132

Cao, G. M., Tang, Y. H., Mo, W. H., Wang, Y. S., Li, Y. N., and Zhao, X. Q. (2004). Grazing intensity alters soil respiration in an alpine meadow on the Tibetan plateau. *Soil Biol. Biochem.* 36, 237–243. doi: 10.1016/j.soilbio.2003.09.010

Chen, H., Wu, N., Gao, Y. H., Wang, Y. F., Luo, P., and Tian, J. Q. (2009). Spatial variations on methane emissions from Zoige alpine wetlands of Southwest China. *Sci. Total Environ.* 407, 1097–1104. doi: 10.1016/j.scitotenv.2008.10.038

Chen, H., Yang, G., Peng, C. H., Zhang, Y., Zhu, D., Zhu, Q. Y., et al. (2014). The carbon stock of alpine peatlands on the Qinghai–Tibetan Plateau during the Holocene and their future fate. *Quat. Sci. Rev.* 95, 151–158. doi: 10.1016/j.quascirev.2014.05.003

Chen, W. W., Zheng, X. H., Chen, Q., Wolf, B., Butterbach-Bahl, K., Brüggemann, N., et al. (2013). Effects of increasing precipitation and nitrogen deposition on CH4 and N2O fluxes and ecosystem respiration in a degraded steppe in Inner Mongolia. *China. Geoderma.* 192, 335–340. doi: 10.1016/j.geoderma.2012.08.018

Conrad, R. (2007). Microbial ecology of methanogens and methanotrophs. *Adv. Agron.* 96, 1–63. doi: 10.1016/S0065-2113(07)96005-8

Cui, X., Wang, Y., Niu, H., Wu, J., Wang, S., Schnug, E., et al. (2005). Effect of long-term grazing on soil organic carbon content in semiarid steppes in Inner Mongolia. *Ecol. Res.* 20, 519–527. doi: 10.1007/s11284-005-0063-8

Feng, Y. L., Fu, G. L., and Zheng, Y. L. (2008). Specific leaf area relates to the differences in leaf construction cost, photosynthesis, nitrogen allocation, and use efficiencies between invasive and noninvasive alien congeners. *Planta* 228, 383–390. doi: 10.1007/s00425-008-0732-2

Gao, J. Q., OuYang, H., Lei, G. C., Xu, X. L., and Zhang, M. X. (2011). Effects of temperature, soil moisture, soil type and their interactions on soil carbon mineralization in Zoigê alpine wetland. Qinghai-Tibet Plateau. *Chin. Geogr. Sci.* 21, 27–35. doi: 10.1007/s11769-011-0439-3

Hao, Y. B., Cui, X. Y., and Kang, X. M. (2011). Predominance of precipitation and temperature controls on ecosystem CO2 exchange in Zoige alpine Wetlands of Southwest China. *Wetlands* 31, 413–422. doi: 10.1007/s13157-011-0151-1

Huo, L. L., Chen, Z. K., Zou, Y. C., Lu, X. G., Guo, J. W., and Tang, X. G. (2013). Effect of Zoige alpine wetland degradation on the density and fractions of soil organic carbon. *Ecol. Eng.* 51, 287–295. doi: 10.1016/j.ecoleng.2012.12.020

Hursh, A., Ballantyne, A., Cooper, L., Maneta, M., Kimball, J., and Watts, J. (2016). The sensitivity of soil respiration to soil temperature, moisture, and carbon supply at the global scale. *Glob. Chang. Biol.* 23, 2090–2103. doi: 10.1111/gcb.13489

Jiang, W., Lv, J., Wang, C., Chen, Z., and Liu, Y. (2017). Marsh wetland degradation risk assessment and change analysis: A case study in the Zoige Plateau. *China. Ecol. Indic.* 82, 316–326. doi: 10.1016/j.ecolind.2017.06.059

Kang, E. Z., Li, Y., Zhang, X. D., Yan, Z. Q., Zhang, W. T., Zhang, K. R., et al. (2022). Extreme drought decreases soil heterotrophic respiration but not methane flux by modifying the abundance of soil microbial functional groups in alpine peatland. *Catena* 212:106043. doi: 10.1016/j.catena.2022.106043

Kang, X. M., Yan, L., Cui, L. J., Zhang, X. D., Hao, Y. B., Wu, H. D., et al. (2018). Reduced carbon dioxide sink and methane source under extreme drought condition in an alpine peatland. *Sustainability* 10:4285. doi: 10.3390/su10114285

Li, C. Y., Peng, F., Xue, X., Lai, C. M., Zhang, W. J., You, Q. G., et al. (2021). Degradation stage effects on vegetation and soil properties interactions in alpine steppe. *J. Mt. Sci.* 18, 646–657. doi: 10.1007/s11629-020-6192-2

Li, C., Hao, X., Zhao, M., Han, G., and Willms, W. D. (2008). Influence of historic sheep grazing on vegetation and soil properties of a Desert Steppe in Inner Mongolia. *Agr. Ecosyst. Environ.* 128, 109–116. doi: 10.1016/j.agee.2008.05.008

Li, F., Liu, Z., Jia, T., Li, S., Bai, Y., Guo, C., et al. (2018). Functional diversity of soil microbial community carbon metabolism with the degradation and restoration of alpine wetlands and meadows. *Acta Ecol. Sin.* 38, 6006–6015. doi: 10.5846/stxb201706161096

Li, Y., Ma, J., Gao, C., Li, Y., Shen, X., Zhang, S., et al. (2021). Anaerobic ammonium oxidation (anammox) is the main microbial N loss pathway in alpine wetland soils of the Qinghai-Tibet Plateau. *Sci. Total Environ.* 787:147714. doi: 10.1016/j.scitotenv.2021.147714

Liu, M., Zhang, Z. C., Sun, J., Ming, X. U., BaiBing, M. A., Baba, T. S., et al. (2020a). The response of vegetation biomass to soil properties along degradation gradients of alpine meadow at Zoige Plateau. *Chin. Geogr. Sci.* 30, 446–455. doi: 10.1007/s11769-020-1116-1

Liu, M., Zhang, Z. C., Sun, J., Wang, Y., Wang, J. N., Tsunekawa, A., et al. (2020b). One-year grazing exclusion remarkably restores degraded alpine meadow at Zoige, eastern Tibetan Plateau. *Glob. Ecol. Conserv.* 22:e00951. doi: 10.1016/j.gecco.2020.e00951

Luo, Y. Q., and Zhou, X. H. (2006). *Soil respiration and the environment*. Amsterdam: Elsevier, 257–305. doi: 10.1016/b978-0-12-088782-8.x5000-1

Ma, M. J., Baskin, C. C., Yu, K. L., Ma, Z., and Du, G. Z. (2017). Wetland drying indirectly influences plant community and seed bank diversity through soil pH. *Ecol. Indic.* 80, 186–195. doi: 10.1016/j.ecolind.2017.05.027

Ma, W. W., Li, G., Wu, J. H., Xu, G. R., and Wu, J. Q. (2020). Respiration and CH4 fluxes in Tibetan peatlands are influenced by vegetation degradation. *Catena* 195:104789. doi: 10.1016/j.catena.2020.104789

Ma, Y. S., Lang, B. N., Li, Q. Y., Shi, J. J., and Dong, Q. M. (2002). Study on rehabilitating and rebuilding technologies for degenerated alpine meadow in the Changjiang and Yellow river source region. *Pratacultural Sci.* 19, 1–5. doi: 10.3969/j.issn.1001-0629.2002.09.001

Mei, L., Li, L., Liao, H., Huang, Z., and Huang, W. (2012). The influence of drainage on wetland degradation in Zoige Plateau. *Dis. Adv.* 5, 659–666.

Mitsch, W. J., and Gosselink, J. G. (2011). *Wetlands*, 5th Edn. Hoboken, NJ: John Wiley & Sons, Inc.

Moorcroft, P. R., Wofsy, S. C., Dunn, A. L., and Ise, T. (2008). High sensitiviy of peat decomposition to climate change through water-table feedback. *Nat. Geosci.* 1, 763–766. doi: 10.1038/ngeo331

Moore, T. R., Lafleur, P. M., Poon, D. M., Heumann, B. W., Seaquist, J. W., and Roulet, N. T. (2006). Spring photosynthesis in a cool temperate bog. *Glob. Chang. Biol.* 12, 2323–2335. doi: 10.1111/j.1365-2486.2006.01247.x

Niu, S., Wu, M. Y., Han, Y. I., Xia, J., Zhe, Z., Yang, H., et al. (2010). Nitrogen effects on net ecosystem carbon exchange in a temperate steppe. *Glob. Chang. Biol.* 16, 144–155. doi: 10.1111/j.1365-2486.2009.01894.x

Pei, J. M., Yan, D., Li, J. Q., Qiong, L., Yang, Y. W., Fang, C. M., et al. (2022). Alpine meadow degradation enhances the temperature sensitivity of soil carbon decomposition on the Qinghai-Tibetan plateau. *Appl. Soil Ecol.* 170:104290. doi: 10.1016/j.apsoil.2021.104290

Peng, F., Quangang, Y., Xue, X., Guo, J., and Wang, T. (2015). Effects of rodent-induced land degradation on ecosystem carbon fluxes in an alpine meadow in the Qinghai–Tibet Plateau. *China Solid Earth* 6, 303–310. doi: 10.5194/se-6-303-2015

Piñeiro, G., Paruelo, J. M., Oesterheld, M., and Jobbágy, E. G. (2010). Pathways of Grazing Effects on Soil Organic Carbon and Nitrogen. *Rangeland Ecol. Manag.* 63, 109–119. doi: 10.2111/08-255.1

Qiu, P. F., Wu, N., Luo, P., Wang, Z. Y., and Li, M. H. (2009). Analysis of dynamics and driving factors of wetland landscape in Zoige. Eastern Qinghai-Tibetan Plateau. *J. Mt. Sci.* 6, 42–55. doi: 10.1007/s11629-009-0230-4

R Core Team (2020). *A language and environment for statistical computing*. Vienna, Austria: R Foundation for Statistical Computing.

Rey, A., Pegoraro, E., Oyonarte, C., Were, A., Escribano, P., and Raimundo, J. (2011). Impact of land degradation on soil respiration in a steppe (*Stipa tenacissima* L.) semi-arid ecosystem in the SE of Spain. *Soil Biol. Biochem.* 43, 393–403. doi: 10.1016/j.soilbio.2010.11.007

Ringeval, B., de Noblet-Ducoudré, N., Ciais, P., Bousquet, P., Prigent, C., Papa, F., et al. (2010). An attempt to quantify the impact of changes in wetland extent on methane emissions on the seasonal and interannual time scales. *Glob. Biogeochem. Cy.* 24. doi: 10.1029/2008gb003354

Rui, Y. C., Wang, S. P., Xu, Z. H., Wang, Y. F., Chen, C. R., Zhou, X. Q., et al. (2011). Warming and grazing affect soil labile carbon and nitrogen pools differently in an alpine meadow of the Qinghai–Tibet Plateau in China. *J. Soil. Sediment.* 11, 903. doi: 10.1007/s11368-011-0388-6

Shen, Z. X., Wang, J. W., Sun, W., Li, S. W., Fu, G., Zhang, X. Z., et al. (2016). The soil drying along the increase of warming masks the relation between temperature and soil respiration in an alpine meadow of Northern Tibet. *Pol. J. Eco.* 64, 125–129. doi: 10.3161/15052249pje2016.64.1.011

Shi, P. L., Sun, X. M., Xu, L. L., Zhang, X. Z., He, Y. T., Zhang, D. Q., et al. (2006). Net ecosystem CO2 exchange and controlling factors in a steppe—Kobresia meadow on the Tibetan Plateau. *Sci. China Ser. D Earth Sci.* 49, 207–218. doi: 10.1007/s11430-006-8207-4

Soebandiono, S., Muhibuddin, A., Purwanto, E., and Purnomo, D. (2021). The effect of indigenous organic fertilizer on paddy field methane emissions. *Org. Agr.* 11, 393–407. doi: 10.1007/s13165-020-00345-9

Spieles, D. J. (2022). Wetland construction, restoration, and integration: A comparative review. *Land* 11:554. doi: 10.3390/land11040554

Sun, D. S., Wesche, K., Chen, D. D., Zhang, G. L., Wu, G. Z., Du, N. B., et al. (2011). Grazing depresses soil carbon storage through changing plant biomass and composition in a Tibetan alpine meadow. *Plant. Soil. Environ.* 57, 271–278. doi: 10.17221/7/2011-pse

Tang, H. J., Qiu, J. J., Wang, L. G., Li, H., Li, C.-S., and Ranst, E. V. (2010). Modeling soil organic carbon storage and its dynamics in croplands of China. *Agr. Sci. China* 9, 704–712. doi: 10.1016/s1671-2927(09)60146-2

Tang, L., Dong, S. K., Sherman, R., Liu, S. L., Liu, Q. R., Wang, X. X., et al. (2015). Changes in vegetation composition and plant diversity with rangeland degradation in the alpine region of Qinghai-Tibet Plateau. *Rangeland J.* 37, 107–115. doi: 10.1071/rj14077

Updegraff, K., Bridgham, S. D., Pastor, J., Weishampel, P., and Harth, C. (2001). Response of CO2 and CH4 emissions from peatlands to warming and water table manipulation. *Ecol. Appl.* 11, 311–326. doi: 10.1111/gcb.12041

Vargas, A. I., Schaffer, B., and Sternberg, L. (2020). Plant water uptake from soil through a vapor pathway. *Phys. Plant.* 170, 433–439. doi: 10.1111/ppl.13173

Walter, B. P., Heimann, M., and Matthews, E. (2001). Modeling modern methane emissions from natural wetlands: 2. Interannual variations 1982–1993. *J. Geophys. Res.* 106, 34207–34219. doi: 10.1029/2001jd900164

Wang, G., Qian, J., Cheng, G., and Lai, Y. (2002). Soil organic carbon pool of grassland soils on the Qinghai-Tibetan Plateau and its global implication. *Sci. Total Environ.* 291, 207–217. doi: 10.1016/S0048-9697(01)01100-7

Wang, X. X., Sherman, R., Liu, Q. R., Liu, S. L., Li, Y. Y., and Wu, Y. (2015). A comparison of biodiversity–ecosystem function relationships in alpine grasslands across a degradation gradient on the Qinghai–Tibetan Plateau. *Rangeland J.* 37:45. doi: 10.1071/rj14081

Wu, X. W., Cao, R., Wei, X., Xi, X. Q., Shi, P. L., Eisenhauer, N., et al. (2017). Soil drainage facilitates earthworm invasion and subsequent carbon loss from peatland soil. *J. Appl. Ecol.* 54, 1291–1300. doi: 10.1111/1365-2664.12894

Xia, X., Jiang, H. L., Tian, X. Y., Guan, M. X., and Wang, L. F. (2019). Response of the plant and soil features to degradation grades in semi-arid grassland of the inner Mongolia. *China. IOP Conf. Ser. Mater. Sci. Eng.* 484:012039. doi: 10.1088/1757-899X/484/1/012039

Xiang, S., Guo, R. Q., Wu, N., and Sun, S. C. (2009). Current status and future prospects of Zoige Marsh in Eastern Qinghai-Tibet Plateau. *Ecol. Eng.* 35, 553–562. doi: 10.1016/j.ecoleng.2008.02.016

Xu, D., Mou, W., Wang, X., Zhang, R., Gao, T., Ai, D., et al. (2022). Consistent responses of ecosystem CO2 exchange to grassland degradation in alpine meadow of the Qinghai-Tibetan Plateau. *Ecol. Indic.* 141:109036. doi: 10.1016/j.ecolind.2022.109036

Yan, M. C., Xu, T. T., Song, P. H., and Dai, J. J. (2012). Effects of different cropping patterns of soybean and maize seedlings on soil enzyme activities and MBC and MBN. *J. Northeast Agri. Univ.* 19, 42–47. doi: 10.1016/s1006-8104(13)60049-5

Yan, W. C., Wang, Y. Y., Chaudhary, P., Ju, P. J., Zhu, Q. A., Kang, X. M., et al. (2022). Effects of climate change and human activities on net primary production of wetlands on the Zoige Plateau from 1990 to 2015. *Glob. Ecol. Conserv.* 35:e02052. doi: 10.1016/j.gecco.2022.e02052

Yan, Z. Q., Kang, E. Z., Zhang, K. R., Li, Y., Hao, Y. B., Wu, H. D., et al. (2021). Plant and soil enzyme activities regulate CO2 efflux in alpine peatlands after 5 years of simulated extreme drought. *Front. Plant Sci.* 12:756956. doi: 10.3389/fpls.2021.756956

Yarwood, S. A. (2018). The role of wetland microorganisms in plant-litter decomposition and soil organic matter formation: A critical review. *FEMS Microbiol. Ecol.* 94:fiy175. doi: 10.1093/femsec/fiy175

Yu, L., Tang, J., Zhang, R., Wu, Q., and Gong, M. (2013). Effects of biochar application on soil methane emission at different soil moisture levels. *Biol. Fert. Soils* 49, 119–128. doi: 10.1007/s00374-012-0703-4

Yuan, Z. Q., Wu, Q. B., Song, X., Jiang, X. J., Gao, S. R., Wang, Q. F., et al. (2020). Pasture degradation impact on soil carbon and nitrogen fractions of alpine meadow in a Tibetan permafrost region. *J. Soil. Sediment.* 20, 2330–2342. doi: 10.1007/s11368-020-02596-1

Zhang, H., Yao, Z., Ma, L., Zheng, X., Wang, R., Wang, K., et al. (2019). Annual methane emissions from degraded alpine wetlands in the eastern Tibetan Plateau. *Sci. Total Environ.* 657, 1323–1333. doi: 10.1016/j.scitotenv.2018.11.443

Zhao, L., Li, J., Xu, S., Zhou, H., Li, Y., Gu, S., et al. (2010). Seasonal variations in carbon dioxide exchange in an alpine wetland meadow on the Qinghai-Tibetan Plateau. *Biogeosciences* 7, 1207–1221. doi: 10.5194/bg-7-1207-2010

Zhao, L., Li, Y. N., Zhao, X. Q., Xu, S. X., Tang, Y. H., Yu, G. R., et al. (2005). Comparative study of the net exchange of CO2 in 3 types of vegetation ecosystems on the Qinghai-Tibetan Plateau. *Chin. Sci. Bull.* 50, 1767–1774. doi: 10.1360/04wd0316

Zhou, H., Zhao, X., Tang, Y., Song, G., and Li, Z. (2005). Alpine grassland degradation and its control in the source region of the Yangtze and Yellow Rivers, China. *Grassl. Sci.* 51, 191–203. doi: 10.1111/j.1744-697X.2005.00028.x

Zhu, G. B., Jetten, M. S. M., Kuschk, P., Ettwig, K. F., and Yin, C. Q. (2010). Potential roles of anaerobic ammonium and methane oxidation in the nitrogen cycle of wetland ecosystems. *Appl. Microbiol. Biot.* 86, 1043–1055. doi: 10.1007/s00253-010-2451-4

Zhu, J. B., Zhang, F. W., Li, H. Q., He, H., Li, Y. N., Yang, Y. S., et al. (2020). Seasonal and inter-annual variations of CO2 fluxes over 10 years in an alpine wetland on the Qinghai-Tibetan Plateau. *Authorea* doi: 10.22541/au.159714934.45073192

Zhu, L., Ke, Y., Hong, J., Zhang, Y., and Pan, Y. (2022). Assessing degradation of lake wetlands in Bashang Plateau, China based on long-term time series Landsat images using wetland degradation index. *Ecol. Indic.* 139:108903. doi: 10.1016/j.ecolind.2022.108903

frontiers | Frontiers in Ecology and Evolution

TYPE Original Research
PUBLISHED 07 September 2022
DOI 10.3389/fevo.2022.993849



OPEN ACCESS

EDITED BY
He Yixin,
Key Laboratory of Mountain Ecological Rehabilitation and Biological Resource Utilization, Chengdu Institute of Biology (CAS), China

REVIEWED BY
Qitao Xiao,
Nanjing Institute of Geography and Limnology (CAS), China
Guan Bo,
Ludong University, China

*CORRESPONDENCE
Yan Liu
liuyan@iga.ac.cn

SPECIALTY SECTION
This article was submitted to Conservation and Restoration Ecology, a section of the journal Frontiers in Ecology and Evolution

RECEIVED 14 July 2022
ACCEPTED 22 August 2022
PUBLISHED 07 September 2022

CITATION
Cui G, Liu Y and Tong S (2022) Hydrogeochemical processes controlling the salinity of surface water and groundwater in an inland saline-alkali wetland in western Jilin, China.
*Front. Ecol. Evol.* 10:993849.
doi: 10.3389/fevo.2022.993849



# Hydrogeochemical processes controlling the salinity of surface water and groundwater in an inland saline-alkali wetland in western Jilin, China

Geng Cui[1], Yan Liu[1,2]* and Shouzheng Tong[1]

[1]Northeast Institute of Geography and Agroecology, Chinese Academy of Sciences, Changchun, China, [2]School of Geographical Sciences, Changchun Normal University, Changchun, China

Understanding the hydrochemical evolutionary mechanisms of surface water and groundwater in saline-alkali wetlands in arid and semi-arid regions is necessary for assessing how wetland water resource utilization and restoration processes may affect the natural interface between wetland salinity and water. The Momoge National Nature Reserve (MNNR) is an inland wetland in northeastern China that is mainly fed by irrigation water and floods from the Nenjiang River. The purpose of the present study is to describe the spatial distribution characteristics of surface water and groundwater hydrochemistry and salinity in the MNNR and analyze the main processes controlling these parameters. The composition of stable isotopes ($\delta^2H$ and $\delta^{18}O$) and water chemistry, including the levels of Na, K, Ca, Mg, $HCO_3$, $SO_4$, and Cl, of 156 water samples were analyzed. The results show that the lake water in the MNNR is at a risk of salinization owing to a high degree of evaporation. The analysis of the ion ratio and mineral saturation index showed that the ions in water are primarily derived from aquifer leaching, and the precipitation of $Ca^{2+}$ and $Mg^{2+}$ resulted in lower $Ca^{2+}$ and $Mg^{2+}$ levels in lake water than in groundwater. Hydrogen and oxygen stable isotope and deuterium excess analyses show that evaporation is the dominant factor controlling the hydrochemistry and salinity of lake water in the MNNR. Long-term effective monitoring of lake water and groundwater must be developed to provide an early warning for the salinization of lake water and a scientific basis for the protection and restoration of wetland ecosystem functions within the MNNR.

KEYWORDS

**hydrogeochemical processes, inland wetland, salinity, hydrochemistry, stable isotope**

# Introduction

Wetland ecosystems have a variety of unique functions and structures between terrestrial and aquatic ecosystems. Inland saline-alkali wetlands are an important type of wetlands. They are mostly distributed in arid, semi-arid, and sub-humid transition areas and characterized by inundation or shallow-surface water environments, where saline-alkali soils and halobiotic communities develop and constitute a unique geographical complex of inland saline-alkali land ecosystems (Sun et al., 2000; Zhao et al., 2021). Multiple threats from climate change, population growth, land use, and hydraulic engineering have resulted in inland wetlands being exposed to the risk of increased saline inflows (Fowler et al., 2014; Herbert et al., 2015). Salinization is an important factor that affects and drives the ecological characteristics of the water environment in saline-alkali wetlands. The salinization of wetland water bodies in arid and semi-arid regions has attracted attention worldwide (Lyons et al., 2007; Nachshon et al., 2014; Liu et al., 2018a; Chamberlain et al., 2020). Owing to the stress of wetland water salinization, the metabolism and carbon sequestration of wetland aquatic plants have been seriously affected, resulting in a gradual weakening in the functionality of wetlands as carbon pools (Wen et al., 2017).

Climate, topography, water-rock interactions, and surface water-groundwater (SW-GW) interactions play important roles in the variation in salinity and hydrochemistry of wetlands. Owing to the influence of these factors, the increase in water salinity may be a slow process, lasting thousands to tens of thousands of years (Skrzypek et al., 2013). High evapotranspiration directly affects the salinity of wetland water and contributes to the formation of soluble salts, which are incorporated into wetland water by groundwater or tidal flow (Alvarez Mdel et al., 2015). Wetlands are often located at lower elevations, which exposes them to the risk of secondary salinization because of rising water table levels. Furthermore, highly dynamic surface-groundwater interactions in wetlands drive the salinity, which can have positive or negative impacts on wetland ecology (Jolly et al., 2008; Xin et al., 2022). Stable isotopes and major ions in water are important tracers for understanding the process of salinity change, and they can be used to analyze the causes of water salinity in coastal or inland wetlands (Galliari et al., 2021).

The saline-alkali soil region in western Jilin Province, China, is a plain surrounded by mountains and watersheds. The source of soil salinity is the accumulation of soluble salts in the parent rock where groundwater flows from the surrounding uplands to the depressions. The Momoge National Nature Reserve (MNNR) is located in northwest Jilin, where groundwater from the surrounding uplands converges. In 2013, it was included in the list of wetlands of international importance under the Ramsar Convention. The main geochemical processes that control the salinity and hydrochemical characteristics of the MNNR surface water and groundwater need to be explored. The objectives of this study are to (1) explore the salinity and hydrochemical distribution characteristics of surface water and groundwater in the MNNR and (2) determine the main geochemical processes that drive water chemistry and salinity in water bodies within the MNNR.

# Materials and methods

## Study area

The MNNR is located in the western region of Jilin Province, China, with an area of approximately 1,440 $km^2$ and a geographic range between 45°42′25″–46°180″ N and 123°27′0″–124°4′33.7″ E (**Figure 1**). The MNNR is a typical reserve established to protect inland wetlands and aquatic ecosystems in northeastern China. It is an important migratory stop for the endangered species *Grus leucogeranus* and was included in the list of wetlands of international importance in 2013. The altitude of the reserve is between 100 and 171 m, which is high in the northwest and low in the southeast. The uplands in the western MNNR surround many small and large lakes, while the eastern region is relatively flat with an elevation difference of 2–5 m.

## Lake distribution

MNNR is located on the western edge of the Songnen Plain in the northern region of the Songliao subsidence belt. Due to the Mesozoic rifted basin and the combined action of paleogeography and paleoenvironment, alluvial, lacustrine plains, and scattered lakes were formed. At the beginning of the Quaternary Period, the Songnen Plain sank slowly, and erosion was strengthened, causing transported gray-white sand and gravel to be deposited at the bottom of the Quaternary loose layer of the Songnen Plain. In the Early Pleistocene, the western part of the Songnen Plain continued to sink and formed a large ancient lake. In the Late Pleistocene, due to the slow uplift of the watershed, the subsidence center of the Songnen Plain continued to shrink and migrate westward. As a result of the Wurm glacial stage, the cold climate spread to the Songnen Plain, and the resulting cold and dry state caused the ancient lake to gradually decline. The lake area shrank, and it was divided into scattered small lakes. The rivers that entered the plain became unconfined, and the paleohydrological network underwent major changes, forming inland river systems and lakes, accompanied by extensive saline-alkali flatlands. Driven by severe cold and high pressure, the anticyclonic winds were strong, and wind erosion formed ancient sand dunes, sand ridges, and wind-eroded depressions, which became the present day saline-alkali lake bubbles. Since

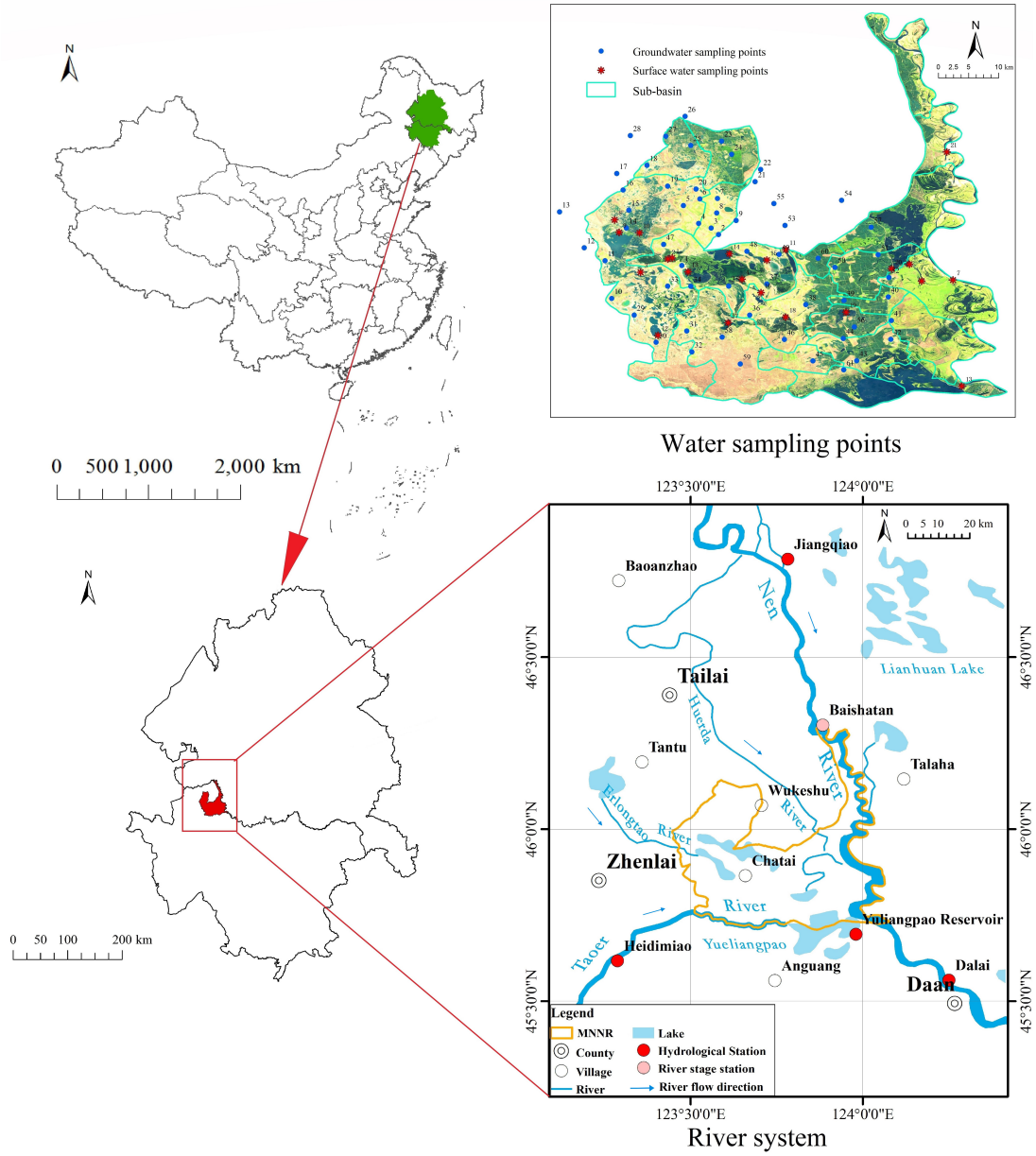


FIGURE 1
Location of the study area and distribution of sampling points.

the Late Pleistocene, the lake area has gradually decreased and been divided into smaller lakes. Therefore, MNNR is a lacustrine alluvial plain formed by the combined action of lakes and rivers. The continuous development and multiple river diversions have resulted in numerous lakes.

## Meteorology and hydrology

MNNR is located in a semi-arid region and has a temperate continental monsoon climate with an average annual temperature of 4.2°C. The highest temperature occurs in July, with an average of 23.5°C, and the lowest temperature occurs in January, with an average of −17.4°C. The average annual precipitation is 391.8 mm. Generally, precipitation is concentrated from June to September, reaching 300 mm and accounting for 76.6% of the annual precipitation. The average annual evaporation is 1585.1 mm, with the highest evaporation in May.

The MNNR is bounded by two natural rivers to the south and east. The Nenjiang River, to the east, flows through the reserve for 111.50 km, with a drainage area of more than 300

km$^2$. The Taoer River, to the south, flows through the reserve for 60 km and then joins the Yueliangpao Reservoir. There are two seasonal rivers that flow through the reserve: the Erlongtao and Huerda rivers (**Figure 1**). Many lakes have developed within this reserve under the combined influence of topography and surface runoff. The west is dominated by brackish lakes dammed by piedmont fan-edge depressions, the east is dominated by floodplain freshwater lakes affected by floods, the middle is dominated by low plains, and the lower reaches of the river form a number of water passages from north to south, developing a series of beaded freshwater lakes. The Qianhang Drainage Station on the northern boundary of the reserve begins to discharge farmland water into the reserve annually in May and continues to discharge downstream through the sluice gate of Baihe Lake.

## Sample collection and field monitoring

Groundwater and surface water in the reserve were sampled three times during one hydrological year in 2019 (**Figure 1**). The samples included (1) groundwater from 43 wells, (2) surface water from 18 lakes, and (3) water from major rivers flowing into the reserve. The samples were collected before the wet period (June), during the wet period (September), and during the dry period (November). All groundwater samples were collected after pumping three times the volume of water in the pipe. Groundwater sampling was concentrated in the central and western parts of the reserve as there are few boreholes in the eastern floodplain of the MNNR. Twenty-one sub-basins were divided based on the topography to ensure that groundwater sampling points were evenly distributed in each sub-basin in these areas. During the sampling campaign, the groundwater table was measured at each sampling point. These results provided a basis for assessing the effects of precipitation and hydrodynamic conditions on the isotopic and chemical compositions of lake and alluvial aquifer groundwater.

A total of 156 water samples were analyzed for stable isotope ($\delta^2$H and $\delta^{18}$O) and hydrochemical characteristics. The pH, dissolved oxygen (DO), electrical conductivity (EC), and total dissolved solids (TDS) were tested and recorded on-site using multi-parameter water quality analyzers (HANNA HI98121 and HI98129, Italy). Laboratory analysis was completed at the Northeast Institute of Geography and Agroecology, Chinese Academy of Sciences. The $\delta^2$H and $\delta^{18}$O values of the water samples were measured using a stable isotope mass spectrometer (MAT253, United States), and the measurement results were corrected with Vienna Standard Mean Ocean Water (VSMOW). The accuracies of $\delta^2$H and $\delta^{18}$O were found to be 0.3‰ and 0.1‰, respectively. The $K^+$, $Na^+$, $Ca^{2+}$, and $Mg^{2+}$ concentrations of the water samples were determined using inductively coupled plasma spectrometry (ICP-OES735E, United States), and $HCO_3^-$, $Cl^-$, and $SO_4^{2-}$ were determined using ion chromatography (ICS-2100, United States).

## Data analysis

The varying trends of precipitation, temperature, and evaporation in the MNNR from 1960 to 2019 were analyzed. The local deuterium excess was calculated using the equation proposed by Dansgaard (1964). Using the weighted linear regression model in SPSS software, a correlation analysis of the main ions and environmental parameters in surface water and groundwater in MNNR was conducted, based on which the causes of water salinity were inferred. The possible hydrogeochemical processes and the causes of surface water and groundwater chemistry were determined using a Piper diagram, main ion relationship analysis, and mineral saturation index calculation.

# Results

## Hydrochemical characteristics

Alkaline water occupied most of the depression wetlands in the MNNR, and the pH varied from 7.17 to 9.44. The groundwater was practically neutral, with a pH ranging from 6.93 to 7.88. The groundwater and surface water varied from freshwater (0.11 g/L) to brackish (3.97 g/L). The TDS of the Nenjiang River water were between 0.10 and 0.15 g/L, while the TDS of groundwater and lake water (including reservoirs) was considerably higher than that of river water. The average TDS of the sampling points in November was 0.80 g/L, which was nearly 0.20 g/L higher than that in September (0.61 g/L). In addition, the groundwater TDS at each sampling point did not change significantly during the three sampling campaigns. Water in the Nenjiang River was dominated by $HCO_3^-$, $Ca^+$, $Mg^{2+}$, and $Na^+$, and the types of cations varied seasonally. The lake water was dominated by $HCO_3^-$ and $Na^+$, which accounted for approximately 80% of the main ions in the lake water. $HCO_3$-Na●-Ca type water occurred continuously in the reservoir water. Finally, most of the groundwater was dominated by $HCO_3^-$, $Na^+$, and $Ca^+$, and the cations in a small fraction of the groundwater were dominated by $Mg^{2+}$ (**Table 1** and **Figure 2**).

## Distribution of H and O stable isotopes

The local meteoric water line (LMWL) was determined to be $\delta^2H = 5.75\delta^{18}O\text{-}16.85$ by fitting the annual stable isotopes for precipitation measured data from 2019. The slope of the LMWL was smaller than that of the global meteoric water line (GMWL), reflecting the semi-arid characteristics of the area. Evaporation

TABLE 1 Average concentration of chemical components in water (mg/L).

| Time | Water type | $HCO_3^- + CO_3^{2-}$ | $Cl^-$ | $SO_4^{2-}$ | $Na^+ + K^+$ | $Mg^{2+}$ | $Ca^{2+}$ | TDS | Hydrochemical type |
|---|---|---|---|---|---|---|---|---|---|
| Jun. | Lake | 537.68 | 47.3 | 51.22 | 201.7 | 15.26 | 22.81 | 735.8 | $HCO_3$-Na |
| | Reservoir | 219.54 | 30.71 | 30.88 | 44.31 | 12.32 | 36.66 | 371.31 | $HCO_3$-Na·Ca |
| | Groundwater | 512.01 | 42.21 | 22.69 | 85.66 | 26.41 | 72.23 | 505.2 | $HCO_3$-Na·Ca |
| | River | 65.88 | 17.75 | 6.13 | 7.57 | 5.03 | 18.02 | 120.88 | $HCO_3$-Mg·Ca |
| Sep. | Lake | 699.26 | 71.55 | 43.37 | 266.47 | 16.46 | 20.6 | 749.59 | $HCO_3$-Na |
| | Reservoir | 222.33 | 31.24 | 21.66 | 48.71 | 112.33 | 33.4 | 258.06 | $HCO_3$-Na·Ca |
| | Groundwater | 508.74 | 55.07 | 30.5 | 94.5 | 27.97 | 55.63 | 518.04 | $HCO_3$-Na·Ca |
| | River | 89.3 | 17.04 | 5.32 | 11.39 | 5.07 | 20.01 | 107.85 | $HCO_3$-Ca |
| Nov. | Lake | 840.7 | 87.61 | 79.04 | 345.67 | 18.73 | 24.39 | 975.79 | $HCO_3$-Na |
| | Reservoir | 240.1 | 32.84 | 20.13 | 51.96 | 13.23 | 37.18 | 275.4 | $HCO_3$-Na·Ca |
| | Groundwater | 481.16 | 73.62 | 44.93 | 122.42 | 30.06 | 74.47 | 586.074 | $HCO_3$-Na·Ca |
| | River | 124.44 | 22.01 | 9.34 | 22.7 | 7.28 | 23.09 | 146.65 | $HCO_3$-Na-Ca |

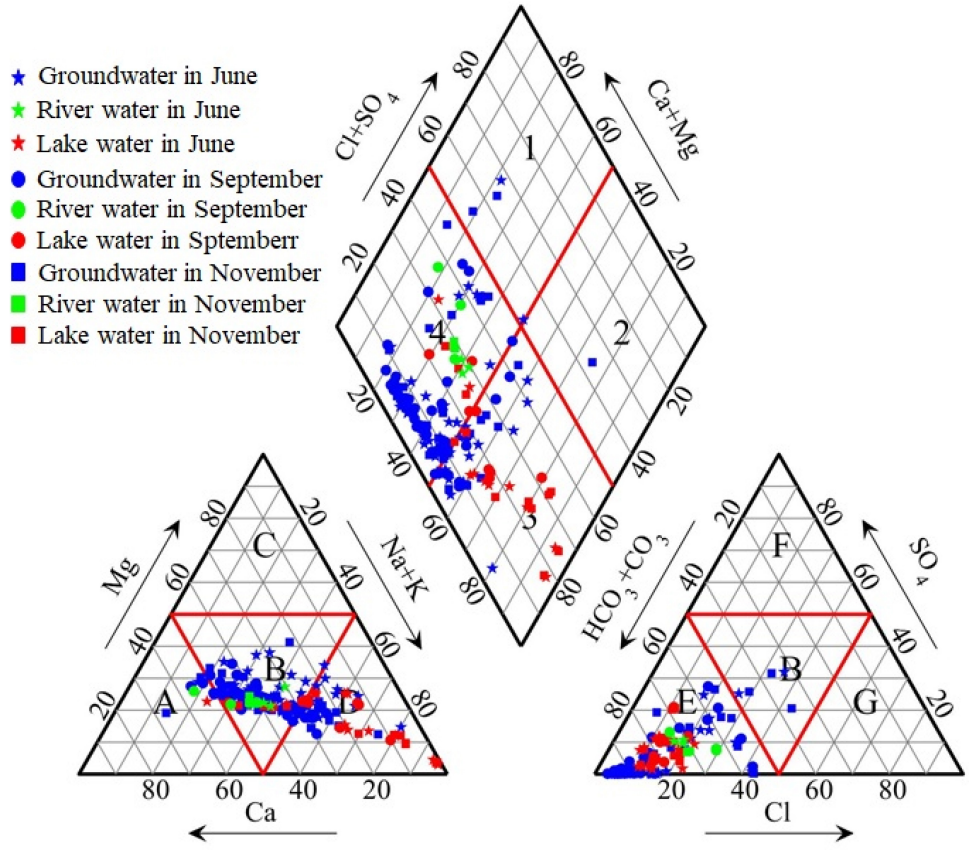


FIGURE 2
Piper diagram of different water bodies in the study area.

of precipitation from the surface accounts for a large proportion of the local water vapor source. The average values of $\delta^2H$ and $\delta^{18}O$ in the groundwater, lake water, and river water were −76.3, −9.1, and −50.8% and −4.7, −55.5, and −5.3%, respectively (Figure 3). The isotope values of groundwater, lake water, and river water in the MNNR were distributed along the LMWL, indicating the interaction between different water bodies was driven by precipitation recharge. The large water surface and arid climate contributed to the strong surface evaporation that occurred in the lake and the tail of the Erlongtao River, resulting in strong $\delta^2H$ and $\delta^{18}O$ enrichment, while the stable isotopes of groundwater and Nenjiang River water were relatively depleted.

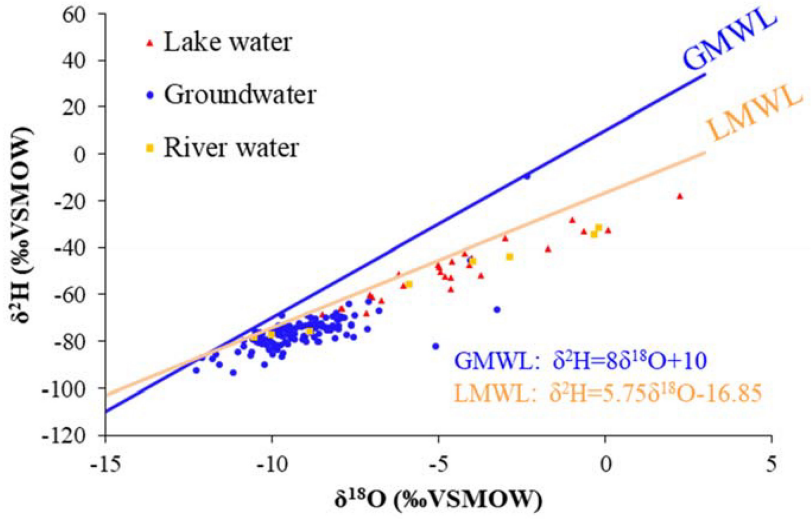


FIGURE 3
Relationship between $\delta^{18}O$ and $\delta^{2}H$ in different water bodies within MNNR.

## Source of water solute

Driven by topography, groundwater flows from the northwest to southeast in the study area. During this process, water and rock interactions are dominated by leaching from fresh groundwater, with a TDS of approximately 0.5 g/L. Owing to the fine particle size of wetland sediments, the effect of groundwater recharge was weaker than that of the concentration caused by evaporation. This led to a significant increase in the TDS of the isolated wetland to 2.3 g/L. However, for Baihe Lake and other lakes fed by irrigation drainage, the effect of water mixing was stronger than that of the concentration, and the TDS of the lake water became stable at approximately 150 mg/L due to the large amount of freshwater input from the irrigation channel. The TDS concentrations correlated with that of $Cl^-$ and $Na^+$ in groundwater ($R > 0.90$) (**Figure 4**), indicating the dissolution of halite in the aquifer. However, the TDS concentrations were primarily correlated with that of $HCO_3^-$ and $Na^+$ in the lake water ($R = 0.99$), which was different from groundwater. This indicated that groundwater is not the only recharge source of lake water and that river water may be a larger potential source. $HCO_3^-$ is continuously input into the lake water from the river water and gradually accumulates under strong evaporation. In addition, pH was an important factor affecting the water chemistry of lake water, and it significantly correlated with the concentrations of $HCO_3^-$ and $Na^+$, and the pH range of lake water, resulting in $HCO_3^-$ dominating the carbonate balance.

The results of the relationship between the main ions (**Figure 5**) show that the groundwater points of $HCO_3^-$ and $SO_4^{2-}$ against $Ca^{2+}$ and $Mg^{2+}$ were distributed around the 1:1 line, indicating the dissolution of calcite, gypsum, and other carbonate and sulfate minerals. However, the $Ca^{2+}$ and $Mg^{2+}$ concentrations in the lake water were considerably lower than those in the groundwater, and the proportion of $Na^+$ in the lake water markedly increased. This was due to the precipitation of $Ca^{2+}$ and $Mg^{2+}$ in the lake water during repeated evaporation processes, which is the main process forming the saline-alkali soil in the MNNR.

# Discussion

## Mineral dissolution and precipitation

The saturation index (SI) of minerals in water is helpful in determining the dissolution and precipitation state of minerals to describe the hydrochemical origin and salinization process of the water body. The absence of $Ca^{2+}$ and $Mg^{2+}$ in the surface water (**Figure 5**) was due to the precipitation of calcite and dolomite (**Figures 6A,B**), as they were oversaturated in the surface water because of high evaporation. The $Ca^{2+}$ produced by the dissolution of anhydrite and gypsum could not resist the precipitation of calcite and dolomite (**Figures 6C,D**). The SI values of halite in the groundwater and lake water were negative and similar, indicating that halite still had the potential to dissolve further and produce more $Na^+$ and $Cl^-$ (**Figure 6E**).

## Indication of d-excess characteristics

Studies have shown that evaporation leads to the fractional enrichment of $^2H$ and $^{18}O$ in water bodies, which is accompanied by an increase in TDS (Jin et al., 2018;

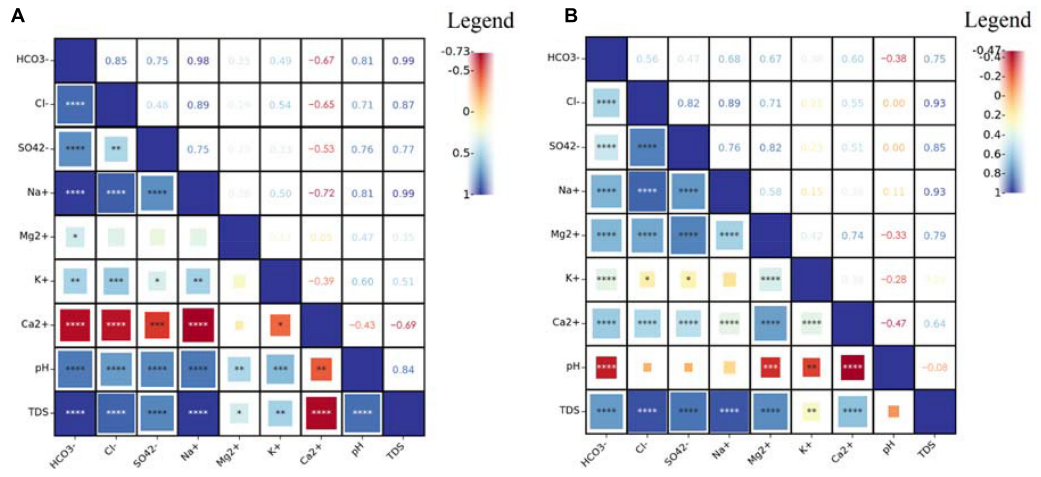


FIGURE 4
Correlation matrices of hydrochemistry and environmental parameters (**A**: lake water; **B**: groundwater; the number of * from 1 to 4 indicate the significance levels less than 0.05, 0.01, 0.001, and 0.0001 respectively).

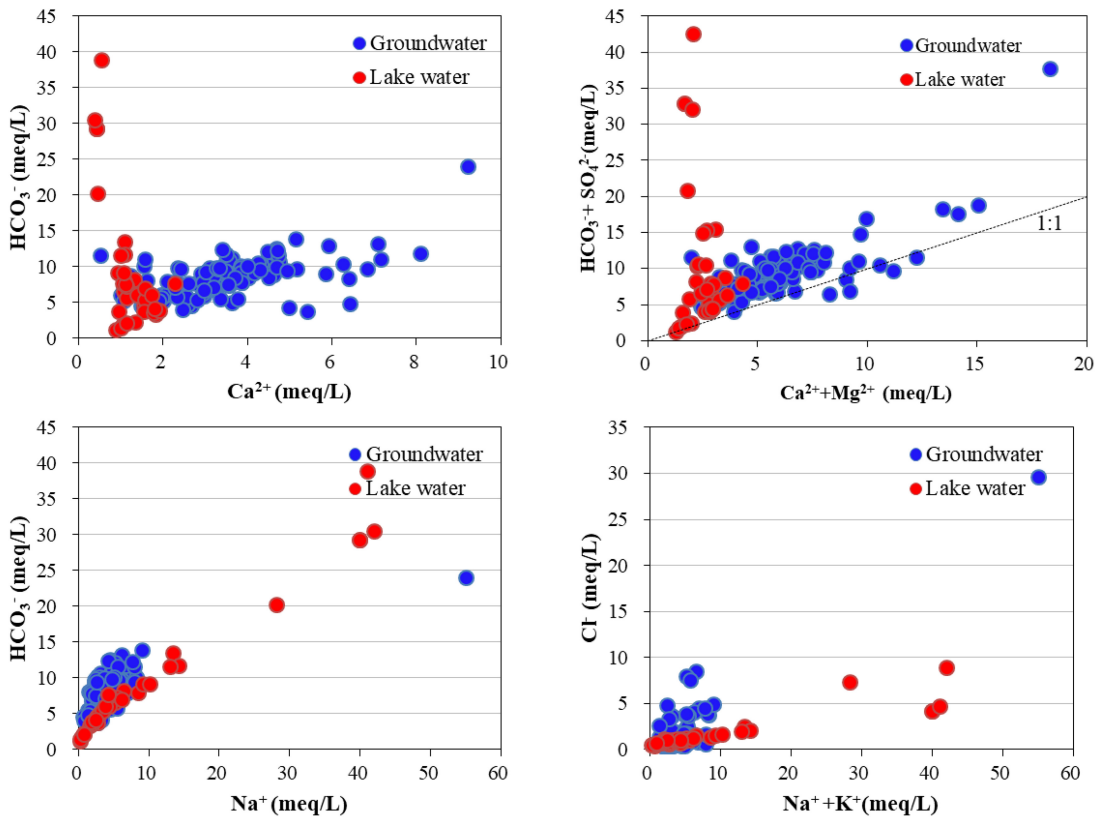


FIGURE 5
Scatter plot of the relationship between main ions in groundwater and lake water.

Chen et al., 2020). The positive correlation between TDS and $\delta^{18}O$ in the MNNR lake water ($R^2$ = 0.4031) was not evident in the groundwater (Figure 7A). As the degree of evaporation increased, the $\delta^{18}O$ in the lake water reached 2.26‰, and the TDS reached 2,499 mg/L. In contrast to the d-excess proposed by Dansgaard (1964), the LMWL equation was used to calculate the local d-excess. The local d-excess and TDS of lake water were negatively correlated ($R^2$ = 0.2197),

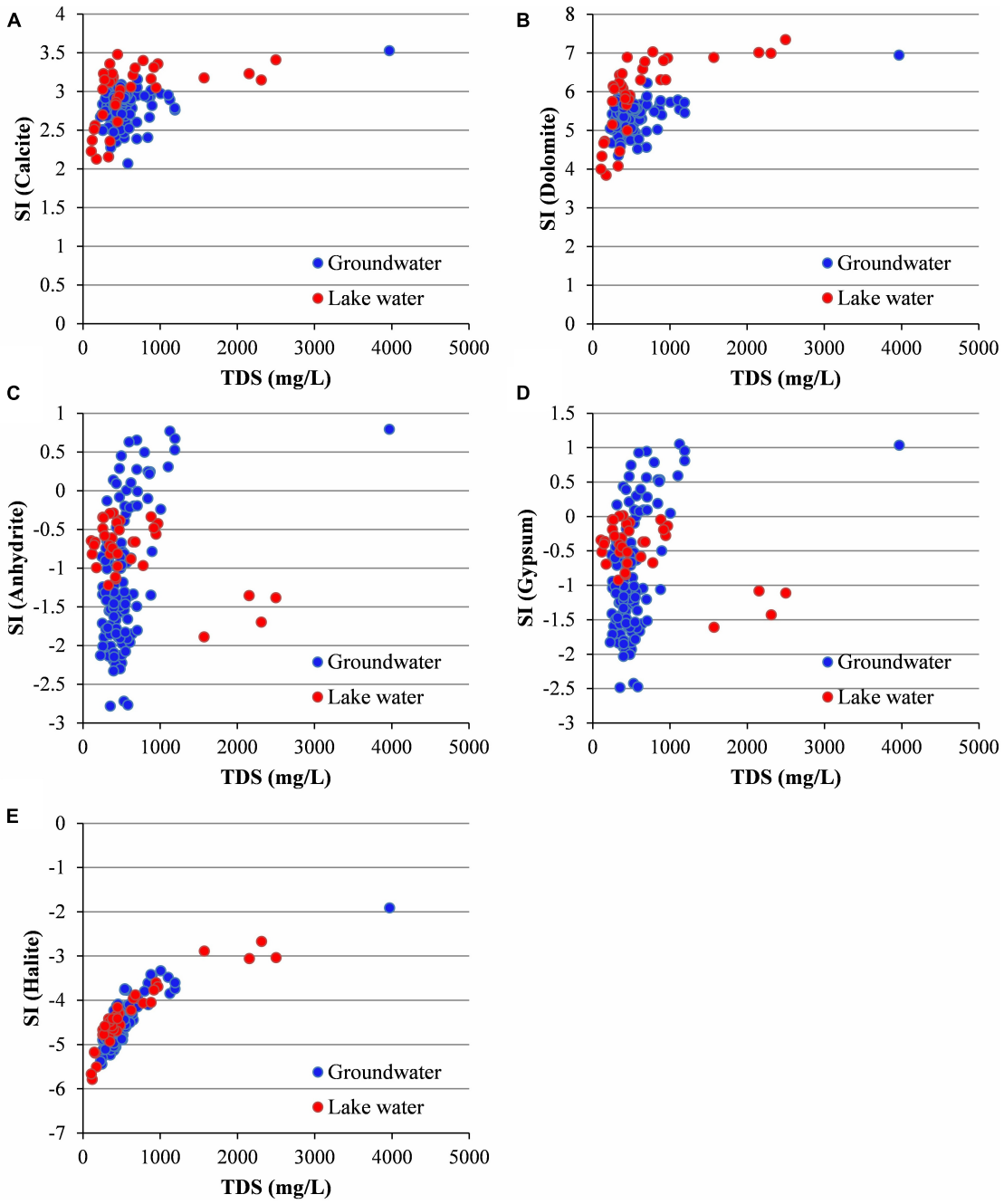


FIGURE 6
Saturation indices (SI) of water samples for selected minerals. **(A)** Calcite; **(B)** dolomite; **(C)** anhydrite; **(D)** gypsum; **(E)** halite.

whereas the d-excess and TDS of groundwater were not significantly correlated (Figure 7B). The d-excess is important for identifying the mechanism of water salinization. After seawater evaporates, underground and surface runoff form through the hydrological cycle, and depression lake wetlands form in the discharge area. After the lake water evaporates again, the d-excess continues to decrease, and the salinity increases owing to continuous accumulation. This negative correlation between d-excess and TDS can explain the effect of evaporation on the stable isotopes, salinity, and the on-going salinization of the water body. The lake water in the MNNR undergoes salinization due to evaporation, and the groundwater salinity is mainly affected by aquifer leaching in the water flow path.

The precipitation, evaporation, and temperature data from Baicheng Station, a meteorological station near the study area,

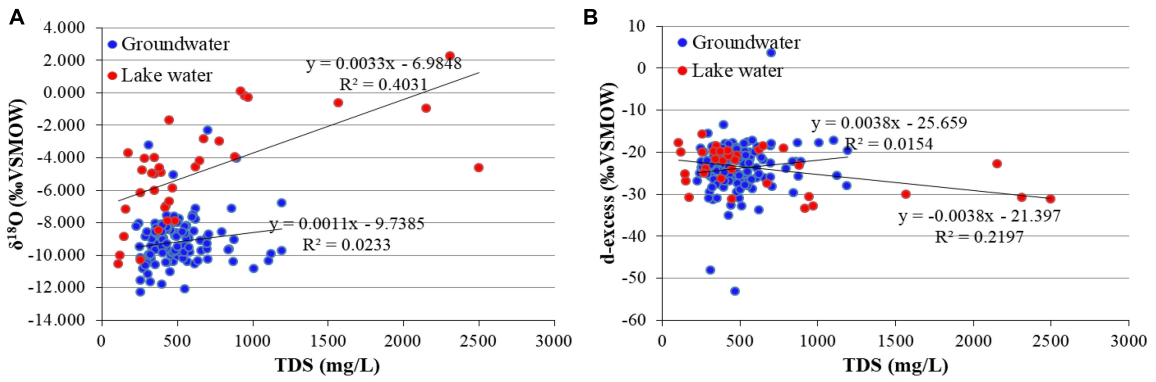


FIGURE 7
Relationships between TDS and H and O stable isotope parameters. **(A)** TDS and $\delta^{18}O$; **(B)** TDS and d-excess.

showed that from 1960 to 2019, the annual precipitation was in the range of 123–726 mm, with a gradual trend of decline. The annual evaporation was in the range of 1,137–2,240 mm. The 60-year average annual evaporation is nearly 4.4 times the average annual precipitation, which confirms the semi-arid climatic conditions and strong evaporation in the region. As evidence of global warming in the MNNR, the annual average temperature in the study area has gradually increased at an average rate of 0.053°C per year, but the annual evaporation in the study area has exhibited a decreasing trend (**Figure 8**). This is due to a decrease in the amount of solar radiation due to a decrease in the number of sunshine hours globally.

## Ecological consequences of wetland salinization

Salinization poses a significant threat to the structure and ecological functions of inland and coastal wetlands. Climate change, human modification, or destruction of the natural hydrological cycle has changed the balance of water and salinity, resulting in increased soil and water salinity in a number of wetlands at a higher rate than natural levels (Skrzypek et al., 2013). Natural changes in wetland salinity may occur over time scales of 10,000 years, whereas secondary salinization caused by anthropogenic factors may only occur over several decades. By analyzing the hydrochemical and isotopic characteristics of groundwater and surface water in the Manas River Basin, Liu et al. (2018b) concluded that mineral dissolution, transpiration, and agricultural irrigation activities are the main causes of groundwater salinization, which is consistent with the findings of this study. Elevated soil salinity during secondary salinization has the potential to increase the link between soil respiration and moisture content (Drake et al., 2014). Through laboratory-controlled experiments on peat deposits in coastal wetlands, van Dijk et al. (2015) found that soil and water salinization have an important impact on soil biogeochemical processes, and sediment cation exchange and brackish water supply can alter nitrogen and phosphorus availability and methane production rate Albecker et al. (2019) found that changes in water salinity affect frog skin microbial communities, thereby increasing the survival and health of the host frog These and other studies have displayed the causes of wetland salinization and the possible consequences for wetland ecology. From macro-to micro-perspectives, salinization plays an important role in the wetland carbon cycle, biological community distribution, and biogeochemical processes. Thus, the importance of freshwater wetlands should be clearly recognized. The effective monitoring and assessment of the sali process of freshwater wetlands are two important steps in protecting their ecological environment.

## Protect wetlands from salinization

As freshwater demand increases, the control and remediation of freshwater salinization becomes increasingly important (Vörösmarty et al., 2010). Moreover, once salinization or secondary salinization occurs in freshwater wetlands, the original plant community is irreversibly degraded (Wang et al., 2019), causing the wetland to gradually change from an oasis to a desert. Researchers have attempted to use a variety of methods to slow the process of wetland salinization, providing several good case studies (Zalidis, 1998; Litalien and Zeeb, 2020; Wang et al., 2021). However, as each anthropogenic source of freshwater salinization is associated with a specific set of ions, there is currently no global standard for evaluating the salinization of freshwater wetlands (Schuler et al., 2018; Hintz et al., 2022). In the future, establishing standards and legislation for wetland salinization may be an effective way to slow the process of wetland salinization, as they play an important positive role in wetland salinization assessment and the reduction of anthropogenic impacts.

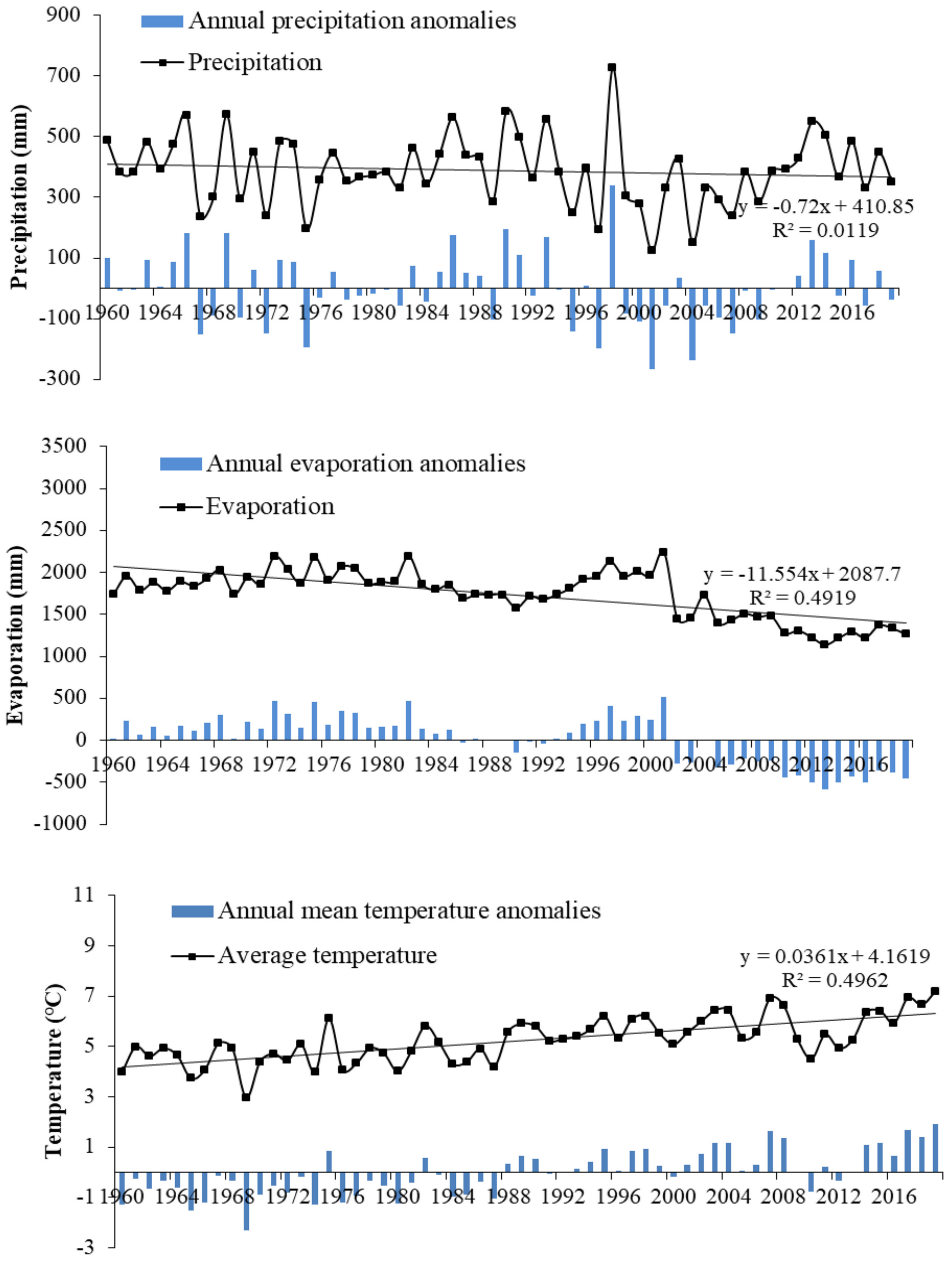


FIGURE 8
Variation of precipitation, evaporation, and temperature in the study area from 1960 to 2019.

## Conclusion

A portion of the lake water in the MNNR has been converted to brackish water or is near the threshold range for fresh and brackish water. In addition, the location and climatic conditions of the MNNR place it at risk for lake salinization. Groundwater brings salinity into depression lakes through aquifer leaching along the flow path, and semi-arid climatic conditions and high evaporation lead to the precipitation of $Ca^{2+}$ and $Mg^{2+}$ in lake waters. Although the discharge of irrigation water dilutes the water and forms drainage channels in certain downstream lakes, reducing the risk of lake salinity, it may increase the downstream nitrogen and phosphorus loads. Lakes lacking recharge water sources and drainage channels have now become brackish. Long-term effective monitoring of lake water and groundwater should be suggested to provide early warning of salinization of lake water within the MNNR, and active measures such as formulating relevant evaluation standards and regulations should be taken to avoid further salinization, which has a large impact on wetland ecosystems.

## Data availability statement

The original contributions presented in this study are included in the article/supplementary material, further inquiries can be directed to the corresponding author.

## Author contributions

YL: investigation, data curation, writing—original draft preparation, and funding acquisition. GC: software, visualization, validation, and writing—review and editing. ST: conceptualization, supervision, and methodology. All authors contributed to the manuscript and approved the submitted version.

## Funding

This research was funded by the Chinese Academy of Sciences (XDA23060402), China Postdoctoral Science Foundation (2021M693154), and the Jilin Association of Science and Technology (QT202029). The authors express their deep gratitude to the funders for supporting this research.

## Conflict of interest

The authors declare that the research was conducted in the absence of any commercial or financial relationships that could be construed as a potential conflict of interest.

## Publisher's note

All claims expressed in this article are solely those of the authors and do not necessarily represent those of their affiliated organizations, or those of the publisher, the editors and the reviewers. Any product that may be evaluated in this article, or claim that may be made by its manufacturer, is not guaranteed or endorsed by the publisher.

## References

Albecker, M. A., Belden, L. K., and McCoy, M. W. (2019). Comparative analysis of anuran amphibian skin microbiomes across Inland and Coastal Wetlands. *Microb. Ecol.* 78, 348–360. doi: 10.1007/s00248-018-1295-9

Alvarez Mdel, P., Carol, E., and Dapena, C. (2015). The role of evapotranspiration in the groundwater hydrochemistry of an arid coastal wetland (Peninsula Valdes, Argentina). *Sci. Total Environ.* 50, 299–307. doi: 10.1016/j.scitotenv.2014.11.028

Chamberlain, S. D., Hemes, K. S., Eichelmann, E., Szutu, D. J., Verfaillie, J. G., and Baldocchi, D. D. (2020). Effect of drought-induced salinization on wetland methane emissions, gross ecosystem productivity, and their interactions. *Ecosystems* 23, 675–688.

Chen, J., Qian, H., Gao, Y., Wang, H., and Zhang, M. (2020). Insights into hydrological and hydrochemical processes in response to water replenishment for lakes in arid regions. *J. Hydrol.* 581:124386.

Dansgaard, W. (1964). Stable isotopes in precipitation. *Tellus* 16, 436–446.

Drake, P. L., McCormick, C. A., and Smith, M. J. (2014). Controls of soil respiration in a salinity-affected ephemeral wetland. *Geoderma* 22, 96–102. doi: 10.1016/j.geoderma.2014.01.010

Fowler, D. N., King, S. L., and Weindorf, D. C. (2014). Evaluating abiotic influences on soil salinity of inland managed wetlands and agricultural croplands in a semi-arid environment. *Wetlands* 34, 1229–1239.

Galliari, J., Santucci, L., Misseri, L., Carol, E., and Alvarez, M. D. P. (2021). Processes controlling groundwater salinity in coastal wetlands of the southern edge of South America. *Sci. Total Environ.* 754:141951. doi: 10.1016/j.scitotenv.2020.141951

Herbert, E. R., Boon, P., Burgin, A. J., Neubauer, S. C., Franklin, R. B., Ardón, M., et al. (2015). A global perspective on wetland salinization: Ecological consequences of a growing threat to freshwater wetlands. *Ecosphere* 6, 1–43.

Hintz, W. D., Arnott, S. E., Symons, C. C., Greco, D. A., McClymont, A., Brentrup, J. A., et al. (2022). Current water quality guidelines across North America and Europe do not protect lakes from salinization. *Proc. Natl. Acad. Sci. U.S.A.* 119:e2115033119. doi: 10.1073/pnas.2115033119

Jin, K., Rao, W., Tan, H., Song, Y., Yong, B., Zheng, F., et al. (2018). HO isotopic and chemical characteristics of a precipitation-lake water-groundwater system in a desert area. *J. Hydrol.* 559, 848–860.

Jolly, I. D., McEwan, K. L., and Holland, K. L. (2008). A review of groundwater-surface water interactions in arid/semi-arid wetlands and the consequences of salinity for wetland ecology. *Ecohydrology* 1, 43–58. doi: 10.1002/eco.6

Litalien, A., and Zeeb, B. (2020). Curing the earth: A review of anthropogenic soil salinization and plant-based strategies for sustainable mitigation. *Sci. Total Environ.* 698:134235. doi: 10.1016/j.scitotenv.2019.134235

Liu, Y., Ding, Z., Bachofen, C., Lou, Y., Jiang, M., Tang, X., et al. (2018a). The effect of saline-alkaline and water stresses on water use efficiency and standing biomass of *Phragmites australis* and *Bolboschoenus planiculmis*. *Sci. Total Environ.* 644, 207–216. doi: 10.1016/j.scitotenv.2018.05.321

Liu, Y., Jin, M., and Wang, J. (2018b). Insights into groundwater salinization from hydrogeochemical and isotopic evidence in an arid inland basin. *Hydrol. Process.* 32, 3108–3127. doi: 10.1002/hyp.13243

Lyons, M. N., Halse, S. A., Gibson, N., Cale, D. J., Lane, J. A. K., Walker, C. D., et al. (2007). Monitoring wetlands in a salinizing landscape: Case studies from the Wheatbelt region of Western Australia. *Hydrobiologia* 591, 147–164. doi: 10.1007/s10750-007-0805-4

Nachshon, U., Ireson, A., Van Der Kamp, G., Davies, S., and Wheater, H. J. H. (2014). Impacts of climate variability on wetland salinization in the North American prairies. *Hydrol. Earth Syst. Sci.* 18, 1251–1263.

Schuler, M. S., Canedo-Arguelles, M., Hintz, W. D., Dyack, B., Birk, S., and Relyea, R. A. (2018). Regulations are needed to protect freshwater ecosystems from salinization. *Philos. Trans. R. Soc. B Biol. Sci.* 374:20180019. doi: 10.1098/rstb.2018.0019

Skrzypek, G., Dogramaci, S., and Grierson, P. F. (2013). Geochemical and hydrological processes controlling groundwater salinity of a large inland wetland of northwest Australia. *Chem. Geol.* 357, 164–177. doi: 10.1016/j.chemgeo.2013.08.035

Sun, G.-y, Luo, X.-z, Yi, F.-k, and Zhang, X.-p (2000). Concept, distribution law and formation machanism of inland saline-alkaline wetland. *Chin. Geogr. Sci.* 10, 254–260.

van Dijk, G., Smolders, A. J. P., Loeb, R., Bout, A., Roelofs, J. G. M., and Lamers, L. P. M. (2015). Salinization of coastal freshwater wetlands; effects of constant versus fluctuating salinity on sediment biogeochemistry. *Biogeochemistry* 126, 71–84. doi: 10.1007/s10533-015-0140-1

Vörösmarty, C. J., McIntyre, P. B., Gessner, M. O., Dudgeon, D., Prusevich, A., Green, P., et al. (2010). Global threats to human water security and river biodiversity. *Nature* 467, 555–561.

Wang, X., Zhang, D., Qi, Q., Tong, S., An, Y., Lu, X., et al. (2019). The restoration feasibility of degraded Carex Tussock in soda-salinization area in arid region. *Ecol. Indic.* 98, 131–136. doi: 10.1016/j.ecolind.2018.08.066

Wang, Z., Tan, W., Yang, D., Zhang, K., Zhao, L., Xie, Z., et al. (2021). Mitigation of soil salinization and alkalization by bacterium-induced inhibition of evaporation and salt crystallization. *Sci. Total Environ.* 755(Pt 1):142511. doi: 10.1016/j.scitotenv.2020.142511

Wen, B., Li, X., Yang, F., Lu, X., Li, X., and Yang, F. (2017). Growth and physiology responses of *Phragmites australis* to combined drought-flooding condition in inland saline-alkaline marsh. *Northeast China*. *Ecol. Eng.* 108, 234–239.

Xin, P., Wilson, A., Shen, C., Ge, Z., Moffett, K. B., Santos, I. R., et al. (2022). Surface water and groundwater interactions in salt marshes and their impact on plant ecology and coastal biogeochemistry. *Rev. Geophys.* 60, e2021RG00 0740.

Zalidis, G. (1998). Management of river water for irrigation to mitigate soil salinization on a coastal wetland. *J. Environ. Manag.* 54, 161–167.

Zhao, Y., Wang, G., Zhao, M., Wang, M., Xue, Z., Liu, B., et al. (2021). Seed limitation and saline-alkaline stress restrict wetland restoration potential in the Songnen Plain, northeastern China. *Ecol. Indic.* 129:107998. doi: 10.1016/j.ecolind. 2021.107998

frontiers | Frontiers in Ecology and Evolution

TYPE Original Research
PUBLISHED 14 September 2022
DOI 10.3389/fevo.2022.1005194



OPEN ACCESS

EDITED BY
He Yixin,
Chengdu Institute of Biology (CAS), China

REVIEWED BY
Jiusheng Ren,
East China University of Technology, China
Chengxue Ma,
Northeast Forestry University, China

*CORRESPONDENCE
Yuxiang Yuan
yuanyuxiang@iga.ac.cn

†These authors have contributed equally to this work and share first authorship

SPECIALTY SECTION
This article was submitted to Conservation and Restoration Ecology, a section of the journal Frontiers in Ecology and Evolution

RECEIVED 28 July 2022
ACCEPTED 26 August 2022
PUBLISHED 14 September 2022

CITATION
Jiang M, Wang Q, Tian X, Zhu X, Dong X, Wu Z and Yuan Y (2022) Spatiotemporal variation and ecological risk assessment of sediment heavy metals in two hydrologically connected lakes. *Front. Ecol. Evol.* 10:1005194. doi: 10.3389/fevo.2022.1005194



# Spatiotemporal variation and ecological risk assessment of sediment heavy metals in two hydrologically connected lakes

Mengyu Jiang[1,2†], Qichen Wang[1,3†], Xue Tian[1], Xiaoyan Zhu[3], Xiangqian Dong[1,3], Zhong Wu[1,3] and Yuxiang Yuan[1*]

[1]Key Laboratory of Wetland Ecology and Environment & Heilongjiang Xingkai Lake Wetland Ecosystem National Observation and Research Station, Northeast Institute of Geography and Agroecology, Chinese Academy of Sciences, Changchun, China, [2]College of Geographical Sciences, Changchun Normal University, Changchun, China, [3]Key Laboratory of Songliao Aquatic Environment, Ministry of Education, Jilin Jianzhu University, Changchun, China

Excessive accumulation of heavy metals in global lake sediments poses a serious threat to lake water quality and ecosystem security. However, there is still a knowledge gap in comparison of heavy metal variation and pollution in hydrologically connected lakes. In this study, concentrations of As, Cd, Cr, Cu, Hg, Pb, and Zn in sediments of two hydrologically connected lakes, Xingkai Lake and Xiaoxingkai Lake, were determined during the hydrologically connected periods (May and September) and disconnected period (January and July) in 2021. We found the range of As was 2.58~14.35 mg/kg, Cd was 0.050~0.21 mg/kg, Cr was 28.58~262.3 mg/kg, Cu was 3.12~28.05 mg/kg, Hg was 0.0030~0.14 mg/kg, Pb was 10.87~58.86 mg/kg, and Zn was 18.21~90.73 mg/kg. Heavy metal concentrations were lower than grade I level in Chinese soil quality standards with significant spatial and temporal differences in the basin. Overall, most of the sampling sites in Xingkai Lake and Xiaoxingkai Lake were at the uncontaminated level and moderate ecological risk during the sampling period. Two lakes showed different heavy metal compositions, accompanied by higher contamination level and higher potential ecological risk in the small lake than those in the large lake based on analysis of the geo-accumulation index and potential ecological risk index. Besides, the contamination level and potential ecological risk in May and September were higher than those in January and July, mainly due to human activities and hydrological connectivity. The ecological risks were moderate for Cd and Hg, and low for As, Cr, Cu, Pb, and Zn. Correlation and PCA analyses showed that Cd mainly originated from anthropogenic sources, while other metals mainly came from natural sources. These findings elucidate the effects of agriculture and hydrological connectivity on heavy metals in sediments, and provide scientific basis for the reasonable management of lake ecosystem.

KEYWORDS

**heavy metals, ecological risk, Xingkai Lake, hydrological connectivity, agriculture**

## Introduction

Heavy metal pollution is one of the most concerning issues globally, and is considered as typical pollutant in the environment due to their high toxicity, environmental persistence, bioaccumulation, carcinogenicity, and complex mechanisms with multiple sources and pathways (Yu et al., 2021; Miranda et al., 2022). Heavy metals are discharged into lakes through multiple natural and anthropogenic pathways such as atmospheric deposition, rain wash, and surface runoff, and then deposit in the sediments (Yu et al., 2021), resulting in increasing heavy metal concentrations in global lakes from 1970s to 2010s (Zhou et al., 2020). Although many studies on heavy metal pollution in lakes have been carried out (e.g., Veeranam Lake in India, Suresh et al., 2012; Poyang Lake in China, Feng et al., 2019), it is still necessary to conduct relevant studies on individual lakes due to their differences in local economic development, pollution sources, and geographical conditions, particular for hydrologically connected lakes that characterized by complex hydrodynamics and landscape heterogeneity (Teng et al., 2020).

Lake sediment shows strong adsorption capacity for heavy metals and thus reduces the pollution level of overlying water (Xu et al., 2017). However, heavy metals are released into water under changing environmental conditions, including pH (Zhang Y. et al., 2018), dissolved oxygen, salinity, nitrogen, and phosphorus (Liu M. et al., 2019; Wang et al., 2021), and in turn cause secondary pollution to the water environment (Liu M. et al., 2019), influencing the structure and function of lake ecosystem (Xu et al., 2017). Moreover, heavy metal pollution in lakes has changed from single metal pollution to mixed metal pollution (Zhou et al., 2020), associated with complex interactions with clay, Fe-Mn oxides, and organic matter by means of ion exchange, complexation and chemical adsorption (Yuan et al., 2014; Yu et al., 2021). Sediment adsorption and desorption capacity play a key role in regulating the bioavailability and bioaccumulation of heavy metals along the food chain in lakes that ultimately endangers human health (Coelho et al., 2018). Therefore, it is crucial to understand heavy metal pollution and ecological risk and their interactions with environmental variables in sediments for the scientific management of lakes.

China is increasingly concerned about heavy metal risks and impacts, due to the rapid development of urbanization, industrialization, and agriculture that are considered as main sources of heavy metals in lakes (Xu et al., 2017; Han et al., 2020; Zhou et al., 2020). In particular, long-term irrational use of chemical fertilizer, pesticide, herbicide, and mulching film in agricultural activities can lead to severe heavy metal pollution in lake sediments (Li et al., 2017; Peng et al., 2020). Cd, Hg, As, Cu, Pb, Cr, and Zn show high pollution levels and potential ecological risk in 71% of provinces in China, and thus are considered as key management targets for relevant administrative agencies (Xu et al., 2017). Understanding the temporal and spatial variation of heavy metals and differentiating the source of the metal accumulation in surface sediment are critical for sediment quality assessment and lake ecosystem protection.

Xingkai (Khanka) Lake, a shallow transboundary lake shared by China and Russia, is the largest freshwater lake in northeast China. Lots of large farms have been built concomitant with rapid shrinkage and fragmentation of wetlands (Song et al., 2012; Yuan et al., 2018). Moreover, continuous use of fertilizer, pesticide, and herbicide in agriculture activities contributed to increased concentrations of nutrients and heavy metals and decreased water quality in the entire basin (Yuan et al., 2021). As a consequence, the water quality of Xingkai Lake and its hydrologically connected lake (Xiaoxingkai Lake) has changed from oligotrophic to eutrophic which may affect water quality in the Russian part of this lake (Piao and Wang, 2011). Nevertheless, little is known about the heavy metal pollution and ecological risk in Xingkai Lake and Xiaoxingkai Lake. Understanding the temporal and spatial variation, pollution and ecological risk of heavy metals in sediments of these two lakes is helpful to provide a scientific basis for ecological assessment of water quality and effective basin management.

The principal goal of our study was to investigate the temporal and spatial variation of different heavy metals in the surface sediment and to evaluate their potential ecological risks in two hydrologically connected lakes. We also examined the interactions between heavy metals and environmental variables to identify the primary driving factors. Our hypotheses were that: (1) heavy metals show significant temporal and spatial differences in sediments; and (2) different potential ecological risks of heavy metals in two lakes although they are hydrologically connected.

## Materials and methods

### Study area

Xingkai Lake basin (44° 30' – 45° 30' N, 132° 00' – 132° 50' E) (**Figure 1**) is an important breeding area and migration habitat for waterfowl, including *Grus japonensis*, *Grus vipio*, and *Ciconia boyciana* (Jin and Zhai, 2006), with an open water area of 4,190 $km^2$ and a catchment area of 16,890 $km^2$ (Sun et al., 2018). Xingkai Lake is a typical semi-enclosed shallow lake (mean water depth 3.5 m) and is characterized by frequent strong winds and low water transparency (Yuan et al., 2021). Xiaoxingkai Lake is an inland shallow lake (mean water depth 1.8 m) with a volume of $3.3 \times 10^8$ $m^3$ water. These two lakes are formed in a Cenozoic tectonic depression and divided by a nature sandy ridge, and their hydrological connectivity is controlled by floodgates. Large amounts of natural silt minerals

were brought into the lakes by inflow rivers, leading to the dominance of silt with a content ranging from 61.9 to 93.8% in sediments (Sun et al., 2018). The climate is characterized by a temperate continental monsoon, with below-freezing temperatures from October to April. The annual precipitation is 574 mm, up to 80% of which takes place from May to September (Song et al., 2012). The annual water inflow into the entire catchment is 55.68 × $10^8$ $m^3$, and the annual outflow is 17.2 × $10^8$ $m^3$. The main inflow coming from the Muling River contributes more than 70% of the total inflows of Xiaoxingkai Lake. The Song'acha River is the single outflow channel through which the water of Xingkai Lake flows into the Ussuri River (Jin and Zhai, 2006).

## Sample collection and processing

According to the technical manual of lake ecology survey (Huang, 2000), combined with the characteristics of geography and surrounding environment in the study area, a total of 15 sampling sites were set up. Of all sampling sites, there were nine sites (XCZH, X25L, XXKL, XHX, XDH, XYZ, XKK, XEZ, and X31L) in Xiaoxingkai Lake and six sites (DBPZ, DLWZ, DXKL, DBYT, DYZ, and DEZ) in Xingkai Lake, as shown in **Figure 1**. Of these sites, X25L, X31L, XCZH, XDH, and XKK were at irrigation channels that connected with Xiaoxingkai Lake, XXKL was a tourism site with shipping activity, XYZ, XEZ, DLWZ, DYZ, DXKL, and DEZ were near flooding gates between Xingkai Lake and Xiaoxingkai Lake, DBPZ, and DBYT were fishing sites, while XHX was at the center of Xiaoxingkai Lake.

Surface sediment (0–10 cm) samples were collected using a grab sampler from each sampling site during the hydrologically connected periods (May and September) and disconnected period (January and July) in 2021 in Xingkai Lake and Xiaoxingkai Lake, and then stored in sealed bags at -18°C for subsequent analysis. The collected sediment samples were dried at 60°C, and then crushed and homogenized using a ceramic mortar and pestle. The ground samples were sieved through a 2-mm-mesh screen for soil organic matter (OM) content by loss-on-ignition method (Zhu et al., 2021) and through a 63-μm-mesh screen for determination of heavy metals, including Chromium (Cr), Copper (Cu), Zinc (Zn), Cadmium (Cd), Arsenic (As), Mercury (Hg), and Lead (Pb).

All sediment samples were analyzed in the Analysis and Measurement Center of Northeast Institute of Geography and Agroecology, Chinese Academy of Sciences. Cd and Pb were measured using an Inductively Coupled Plasma Mass Spectrometer (ICP-MS, ICAP Qc, Thermo Fisher, Germany). Concentrations of Cr, Cu, and Zn were determined by Inductively Coupled Plasma Atomic Emission Spectroscopy (ICP-AES, Perkin-Elmer Corp., Norwalk, United States). As and Hg were measured using Atomic Fluorescence Spectrometry (AFS, AFS-9750, Haiguang Instrument Co., China). Soil total nitrogen (TN) was determined using the modified Kjeldahl method (Kjeltec Auto Analyzer, Behr Labor Technik, Germany), and soil total phosphorus (TP) was measured by alkali fusion–Mo-Sb Anti spectrophotometric method with a UV–Vis spectrophotometer (Lambda750, PerkinElmer, United States).

TABLE 1 The values of *GI* and their indicated pollution levels.

| Class | Value | Pollution level |
|---|---|---|
| 0 | $GI \leq 0$ | Practically uncontaminated |
| 1 | $0 < GI \leq 1$ | Uncontaminated to moderately contaminated |
| 2 | $1 < GI \leq 2$ | Moderately contaminated |
| 3 | $2 < GI \leq 3$ | Moderately to heavily contaminated |
| 4 | $3 < GI \leq 4$ | Heavily contaminated |
| 5 | $4 < GI \leq 5$ | Heavily to extremely contaminated |
| 6 | $5 < GI$ | Extremely contaminated |

## Assessment and homology analysis of heavy metal pollution

The ecological risk and detected heavy metal contamination were quantified in this study. The Geo-accumulation index (*GI*) and Hakanson's potential ecological risk index (*PERI*) were used to spatially quantify the pollution status and potential threats caused by heavy metal concentrations. Pearson correlation coefficient and principal component analysis were used to deduce the statistical relation of heavy metal homology.

### Geo-accumulation index

Geo-accumulation index was proposed by Muller (1969), which has been widely used to assess the pollution degree of heavy metals in sediments and to determine the impact of human activities on the environment. Therefore, it is considered to be an important parameter to distinguish the concentration level of heavy metals induced by human influence and nature (Zhang P. et al., 2018; Liu et al., 2022). The index expression is shown as Equation 1:

$$GI = \log_2\left(\frac{C_i}{1.5B_i}\right) \quad (1)$$

In the equation, *GI* is the Geo-accumulation index of heavy metals, *Ci* is the measured concentrations of heavy metals in sediments, in $mg \cdot kg^{-1}$. *Bi* is the geochemical background value measured in the deposition of heavy metals, and the background values of soil heavy metals in Heilongjiang Province are adopted. 1.5 is a constant that allows for variations in background values possibly caused by diagenesis and weathering (Loska et al., 2004). According to the *GI* value, heavy metal pollution is divided into seven levels, ranging from practically uncontaminated to extremely contaminated, as shown in **Table 1**.

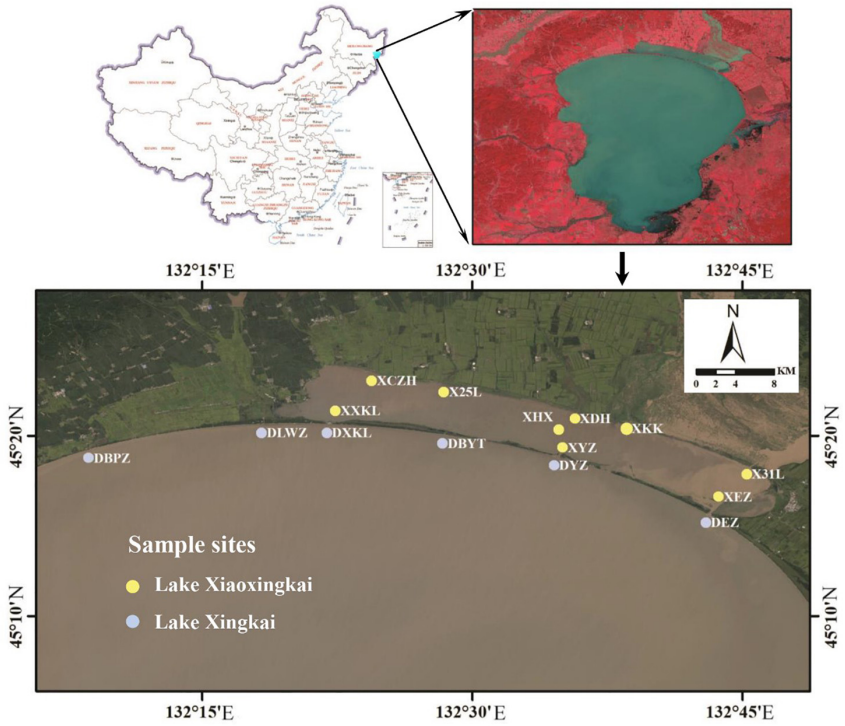


FIGURE 1
Location of sampling sites in Xingkai Lake and Xiaoxingkai Lake.

## Potential ecological risk index

The index of potential ecological risk is proposed by Hakanson (1980), which simultaneously regards the heavy metal concentrations in sediments, type of pollutant, level of toxicity, and sensitivity of water bodies to heavy metal pollution (Zhang P. et al., 2018), and thus is usually used to comprehensively assess the potential impact of heavy metals on lake ecosystems. Equation 2 is used to calculate the ecological risk value of individual heavy metals in sediments:

$$E_i = T_i \times (C_i/B_i) \quad (2)$$

Equation 3 calculates the comprehensive ecological risk of heavy metals in sediments:

$$\mathrm{RI} = \sum_{i=1}^{n} E_i \quad (3)$$

where *RI* is the comprehensive potential ecological risk index, $E_i$ is the individual potential ecological risk index of heavy metal *i*. *Ti* is the toxicity coefficient of heavy metal *i* (Cr = 2, Cu = 5, Zn = 1, As = 10, Cd = 30, Hg = 40, Pb = 5) (Yi et al., 2011). *Ci* is the measured value of heavy metal *i* in the sediment. *Bi* is the background value of heavy metal *i* in study area. Potential ecological risk of heavy metals in sediments are divided into five levels, and the specific classification is shown in **Table 2**.

## Inverse distance weighted

Inverse distance weighted (IDW) method was applied to simulate and predict heavy metal content based on the clear spatial distribution of heavy metals in the surface sediment as an exact interpolator, according to the consideration of data characteristics, sampling site setting and literature data (Chen et al., 2018). IDW interpolation uses a linearly weighted combination of a set of sampling points to determine pixel values for unsampled points (Haldar et al., 2020). Moreover, IDW is a deterministic method for multivariate interpolation of a known scattered set of points (Song et al., 2015), and can process extreme values (outliers) in a data set to make a comprehensive prediction of values in an unknown region (Wu et al., 2021). The general IDW interpolation formula is shown in Equations 4, 5:

$$Z(x) = \sum_{i=1}^{n} w_i z_i / \sum_{i=1}^{n} w_i \quad (4)$$

$$w_i = d_i^{-u} \quad (5)$$

where *Z(x)* is the predicted value at an interpolated point *x*, $Z_i$ is a known point, *n* is the total number of known points used in interpolation, $d_i$ is the distance between point *i* and the prediction point, and $w_i$ is the weight assigned to point *i*. Greater weighting values are assigned to values closer to the interpolated point. Considering the distance increases with decreasing the

TABLE 2 Classification of potential ecological risks according to *Ei* and *RI* values (Hakanson, 1980; Yi et al., 2011; Liu et al., 2021).

| *Ei* | Potential ecological risk for single regulator | *RI* | Ecological risk for all factors |
|---|---|---|---|
| $Ei < 40$ | Low | $RI < 95$ | Low |
| $40 \leq Ei < 80$ | Moderate | $95 \leq RI < 190$ | Moderate |
| $80 \leq Ei < 160$ | Considerable | $190 \leq RI < 380$ | Considerable |
| $160 \leq Ei < 320$ | High | $RI \geq 380$ | Very high |
| $Ei \geq 320$ | Very high | | |

weight (Shepard, 1968; Chen et al., 2018), $u$ is the weighting power that determines how the weight decreases as the distance increases.

## Statistical analysis

The patterns of heavy metal composition in sediments are visualized using non-metric multidimensional scaling (NMDS) based on Bray-Curtis distance. Similar metal compositions were grouped together on a two-dimensional NMDS diagram. Stress values are used to determine the number of dimensions. A stress value less than 0.1 is considered a good ordination of the data (Stauffer et al., 2014; Yuan et al., 2018).

Principal component analysis (PCA) is widely applied to identify the underlying factors and further explain their structure and internal relationships through transforming and rearranging correlated variables into a reduced set of new independent, orthogonal components, which are called principal components (PCs) (Gao et al., 2016). In this study, PCA of all metals with the varimax rotation of the standardized component loadings was conducted to distinguish the sources of possible pollutions. The Kaiser–Meyer–Olkin test and Bartlett's test were performed to evaluate the validity of PCA, which required that the Kaiser–Meyer–Olkin (KMO) values should be more than 0.5 and Bartlett's test be significant (<0.001). The loadings in PCA illustrated the extent to which each original variable contributes to the PCs. The association coefficients between variables and factors reflect the degree of proximity between them. Such proximity increases with the absolute value (loading) of a coefficient.

Data-processing software Excel 2016, SPSS 26, and R 4.1.0 were used to conduct statistical analysis of data. IDW interpolation method in Arcgis 10.2 was used to analyze spatial differences of heavy metals across the study area. Pearson correlation analysis was used to explore the relationships between the physicochemical properties and heavy metals, and one-way ANOVA and two-way ANOVA were applied to identify significant spatial and seasonal differences of heavy metals in sediments. Means ± standard errors of heavy metal concentrations and environmental variables are reported further. Significant results are reported at the 95% confidence level ($p < 0.05$).

# Results

## Characteristics of heavy metals in the sediment

The characteristics of heavy metals, TN, TP, and OM in the sediment of Xingkai Lake and Xiaoxingkai Lake were shown in Table 3. Average concentrations of metals in the surface sediments were ranked by Cr > Zn > Pb > Cu > As > Cd > Hg. Regarding to the coefficient of variation, the dispersion degree of Zn was the smallest with a low CV value of 0.26, while Hg showed the largest dispersion degree with a high CV value of 0.73. By contrast, the dispersion degrees of TN, TP, and OM were relatively higher (one-way ANOVA, $p < 0.05$) compared with those of heavy metals.

Cd, Cu, OM and TN showed significant spatial differences (two-way ANOVA, $p < 0.05$) at all sampling sites, and the significant temporal differences (two-way ANOVA, $p < 0.01$) were observed in As, Cd, Cr, Hg, and TP from January to September. However, the interaction of site and sampling time had no effects on heavy metals and nutrients.

IDW spatial interpolation model was used to predict the spatial distribution of heavy metals in sediments (Figure 2). Taking the spatial distribution of metals as a whole, we found that there were two different distribution trends of seven heavy metals in two lakes. The spatial distribution trends of As, Cr, Cu, and Pb were similar, showing low-high-low concentrations distribution pattern from the western region to the eastern region. By contrast, heavy metals of Cd, Hg, and Zn showed higher concentrations in the western region compared to those in the eastern region (one-way ANOVA, $p < 0.05$), especially Cd (one-way ANOVA, $p < 0.01$). Besides, heavy metals in Xingkai Lake showed significant difference compared with those in Xiaoxingkai Lake (one-way ANOVA, $p < 0.01$), except Cu and Zn.

## Heavy metal compositions in the sediment

The compositions of heavy metals in two lakes were further explored using NMDS (Figure 3). In Xingkai Lake, heavy metals in different months were mainly distributed

TABLE 3 Characteristics of heavy metals (mg/kg), TN (mg/kg), TP (mg/kg), and OM (%) in sediments of Xingkai Lake and Xiaoxingkai Lake.

| | | Cr | Cu | Zn | As | Cd | Hg | Pb | OM | TN | TP |
|---|---|---|---|---|---|---|---|---|---|---|---|
| Min | | 28.58 | 3.12 | 18.21 | 2.58 | 0.050 | 0.0030 | 10.87 | 0.26 | 256.5 | 142.9 |
| Max | | 262.3 | 28.05 | 90.73 | 14.35 | 0.21 | 0.14 | 58.86 | 31.93 | 12361 | 1989 |
| Mean | | 60.31 | 11.80 | 47.17 | 9.21 | 0.13 | 0.040 | 19.09 | 3.26 | 1474 | 563.3 |
| SD | | 36.34 | 5.35 | 12.19 | 2.66 | 0.040 | 0.030 | 6.72 | 5.67 | 2124 | 404.8 |
| CV | | 0.60 | 0.45 | 0.26 | 0.29 | 0.30 | 0.73 | 0.35 | 1.74 | 1.44 | 0.72 |
| Two-way ANOVA | Site | 0.092 | **0.031** | 0.10 | 0.39 | **0.00044** | 0.75 | 0.17 | **0.012** | **0.018** | 0.49 |
| | Time | **0.00096** | 0.35 | 0.12 | **0.0011** | **0.0045** | **0.00010** | 0.067 | 0.39 | 0.33 | **0.00010** |
| | Time × Site | 0.53 | 0.82 | 0.59 | 0.78 | 0.44 | 0.79 | 0.99 | 0.41 | 0.37 | 0.21 |

Two-way ANOVA was applied to examine the spatial and temporal differences of heavy metals, and the significant differences were represented by bold *p* value.

in the left lower quadrant. In contrast, heavy metals in Xiaoxingkai Lake were mainly distributed in the right upper quadrant. Thus, heavy metal compositions were divided into two groups with low similarity between two lakes. Furthermore, total heavy metal concentration in XXKL was relatively higher than that in other sites (one-way ANOVA, $p < 0.01$, Figure 4).

Meanwhile, heavy metal compositions were similar in May, July, and September, whereas heavy metal composition in January showed low similarity with other three months. Comparing total heavy metal concentrations in four months (Figure 4), we found that the total heavy metal concentration was lower in July than that in other months (one-way ANOVA, $p < 0.05$). Among the four months, the standard deviation of total heavy metal concentration was higher in January (one-way ANOVA, $p < 0.05$), and the CV value further calculated in January was about twice that of other months (CV value of January was 0.41, May 0.20, July 0.24, and September 0.27, respectively), indicating high spatial variation of heavy metals in January.

## Pollution and risk assessment of heavy metals in sediments

### Geo-accumulation index

The *GI* values of heavy metals in the sediment of each sampling site are shown in Table 4. According to the spatial variation of *GI* value, only the heavy metal Cr in XXKL was in uncontaminated to moderately contaminated level. By contrast, other sites were subject to uncontaminated levels. Overall, the contamination level of heavy metals in Xiaoxingkai was higher than that in Xingkai Lake ($p < 0.05$), except Pb. From the perspective of temporal variation of *GI* value, the *GI* values of Cr in January (0.059), Cd in May (0.004) and September (0.208), and Hg in September (0.483) were determined to be uncontaminated to moderately contaminated level, whereas other heavy metals As, Cu, Pb, and Zn were at uncontaminated level during the sampling time. In total, the contamination level of heavy metals in September was higher than that in other months ($p < 0.05$).

### Potential ecological risk index

The PERIs of heavy metals showed significant spatial (one-way ANOVA, $p < 0.05$) and temporal differences (one-way ANOVA, $p < 0.05$) in the sediment of the study area (Table 5). The temporal variation of individual potential ecological risk and comprehensive potential ecological risk of Cd and Hg showed that they were at moderate to considerable ecological risk levels in May and September, and low ecological risk level in January and July. While other metals were at low ecological risk level during the sampling period. According to the variation of $E_i$ value, Cd and Hg were considered at moderate ecological risk in most of the sampling sites, whereas other heavy metals As, Cr, Cu, Pb, and Zn showed low ecological risks in all sampling sites. In terms of *RI* value, most of the sampling sites were considered at moderate risk (Table 5). The *RI* value was particularly higher in XXKL with considerable ecological risk (one-way ANOVA, $p < 0.01$), while DEZ, XDH, and XKK showed lower *RI* values with low ecological risk in sediments compared to other sites (one-way ANOVA, $p < 0.01$).

When taking all sampling sites apart into two lakes, Xiaoxingkai Lake faced higher ecological risks compared with Xingkai Lake in September (one-way ANOVA, $p < 0.05$). In addition, the overall ecological risk in Xingkai Lake and Xiaoxingkai Lake was lower in January and July than that in May and September (one-way ANOVA, $p < 0.05$).

## Pollution source identification

### Correlations between metals and nutrition elements

The correlations between heavy metals and nutrition elements in sediments were visually expressed in Figure 5. Most of heavy metals showed positive relationships with each other. Cr showed strongly positive correlations with As ($r = 0.578$, $p < 0.05$), Cu ($r = 0.779$, $p < 0.001$), Hg ($r = 0.607$, $p < 0.05$), Pb ($r = 0.772$, $p < 0.001$), and Zn ($r = 0.818$, $p < 0.001$). Cu

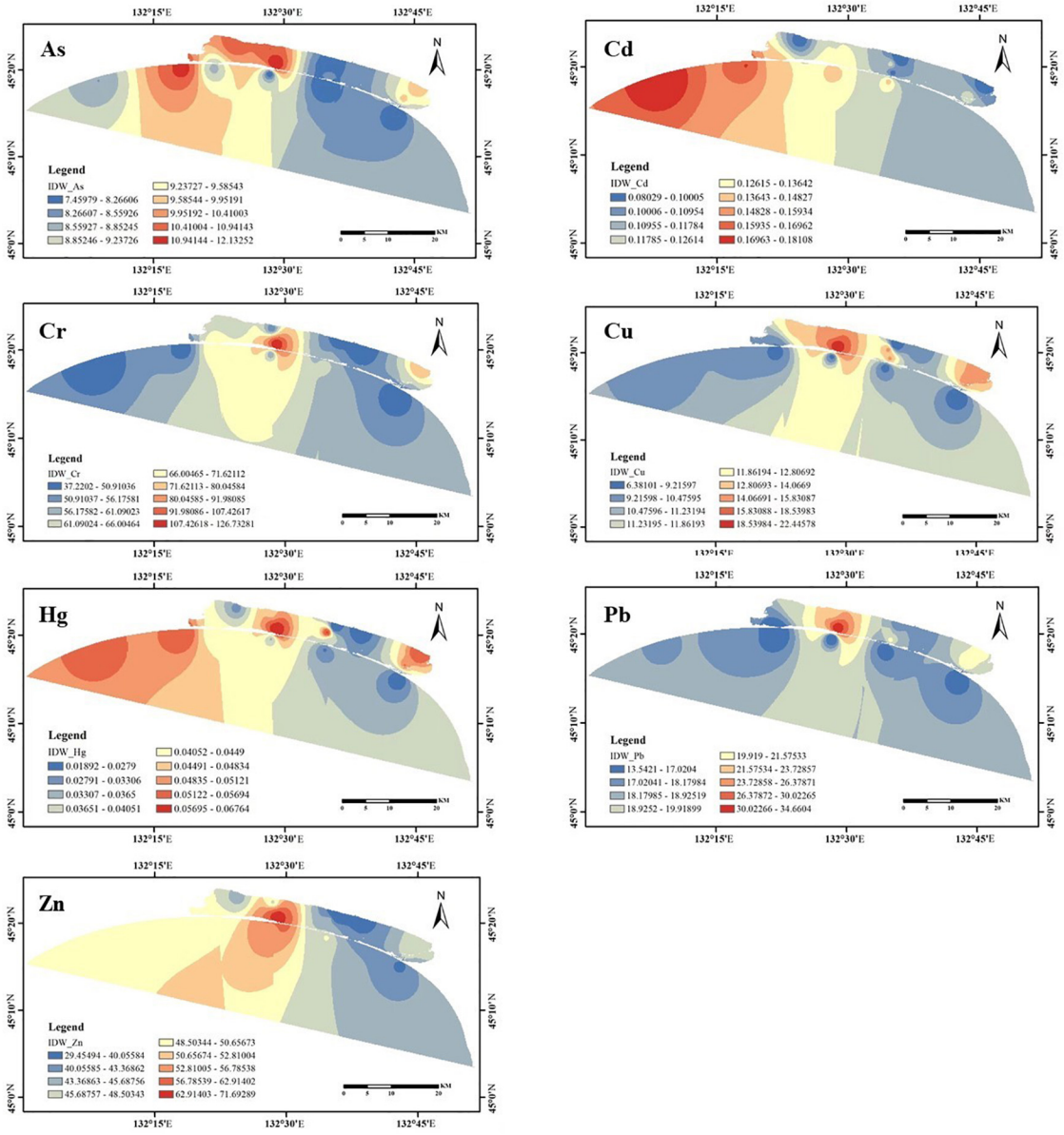


FIGURE 2
Spatial distribution of heavy metals in sediments in two lakes using IDW spatial interpolation model.

was strong positively correlated with As ($r$ = 0.699, $p < 0.01$), Hg ($r$ = 0.724, $p < 0.01$), Pb ($r$ = 0.901, $p < 0.001$), and Zn ($r$ = 0.658, $p < 0.01$). As was positively correlated with Hg ($r$ = 0.606, $p < 0.05$) and Pb ($r$ = 0.736, $p < 0.01$). Zn showed positive relationships with As ($r$ = 0.585, $p < 0.05$), Hg ($r$ = 0.748, $p < 0.01$), and Pb ($r$ = 0.624, $p < 0.05$). Meanwhile, Hg and Pb had a strong positive correlation ($r$ = 0.601, $p < 0.05$). However, Cd showed no significant relationship with other metals or nutrients.

Of all nutrition elements, OM was only strong positively correlated with TN ($r$ = 0.997, $p < 0.001$), whereas OM and TN were not significantly correlated with any metals. By contrast, TP showed strong positive correlations with heavy metals, including Cr ($r$ = 0.538, $p < 0.05$), Cu ($r$ = 0.767, $p < 0.001$), Hg ($r$ = 0.755, $p < 0.001$), and Pb ($r$ = 0.624, $p < 0.05$).

## Principal component analysis of heavy metals

The results of PCA of heavy metal contents in sediments are listed in Table 6. Firstly, the applicability of PCA was tested by Kaiser-Meyer-Olkin (KMO) to verify the adequacy of the sample and Barlett tests to examine the independence of each variable, with the results that KMO of 0.611 (>0.5) and Barlett test value of 0 (<0.05), indicating that the data is suitable for PCA.

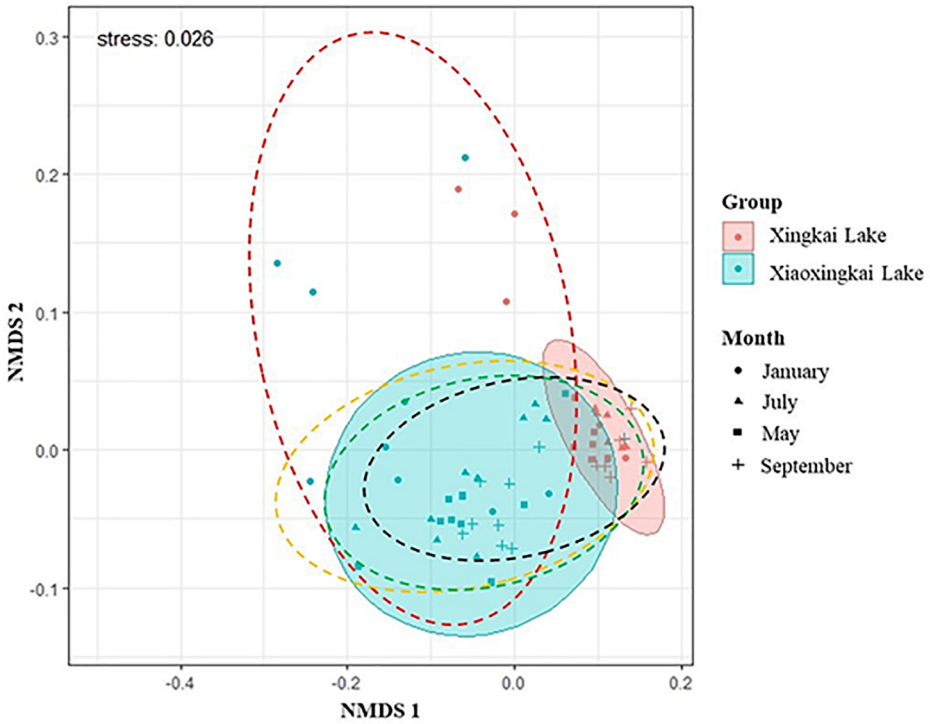


FIGURE 3
Ordination diagrams for non-metric multidimensional scaling of heavy metals in Xingkai Lake and Xiaoxingkai Lake in 4 months. The distance between points represents the similarity degree in heavy metal composition. Metals in January, May, July, and September are enclosed by red, orange, green, and black dotted lines. Metals in Xingkai Lake and Xiaoxingkai Lake are enclosed by pink and cyan circles. Stress = 0.026.

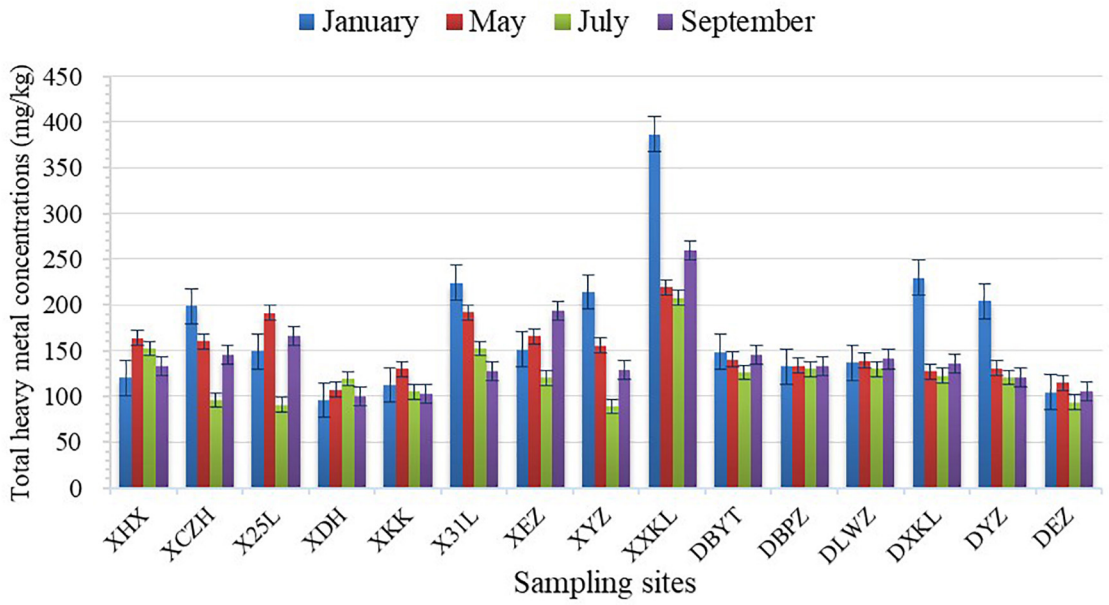


FIGURE 4
Total heavy metal concentrations in all sampling sites in January, May, July, and September.

10.3389/fevo.2022.1005194

TABLE 4 The spatial and temporal variations of Geo-accumulation index (*GI*) value for heavy metals in sediments.

| | *GI* value | | | | | | |
|---|---|---|---|---|---|---|---|
| | **Cr** | **Cu** | **Zn** | **As** | **Cd** | **Hg** | **Pb** |
| XHX | −0.665 | −2.607 | −0.963 | −3.465 | −9.509 | −10.580 | −2.202 |
| XCZH | −0.522 | −2.705 | −0.990 | −3.012 | −9.881 | −11.420 | −2.155 |
| X25L | −0.732 | −2.624 | −0.865 | −3.006 | −9.448 | −10.849 | −1.961 |
| XDH | −1.001 | −3.742 | −1.580 | −3.465 | −10.099 | −12.189 | −2.327 |
| XKK | −1.144 | −3.205 | −1.251 | −3.375 | −9.567 | −11.984 | −2.336 |
| X31L | −0.138 | −2.490 | −0.866 | −3.158 | −9.900 | −10.613 | −2.124 |
| XEZ | −0.471 | −2.528 | −0.884 | −3.176 | −9.498 | −10.740 | −2.043 |
| XYZ | −0.596 | −2.607 | −0.956 | −3.372 | −9.847 | −11.184 | −2.113 |
| XXKL | **0.530** | −1.967 | −0.293 | −2.856 | −9.392 | −10.342 | −1.340 |
| DBYT | −0.639 | −3.351 | −0.716 | −3.466 | −9.255 | −11.252 | −2.699 |
| DBPZ | −0.932 | −3.210 | −0.819 | −3.360 | −8.923 | −10.693 | −2.280 |
| DLWZ | −0.881 | −3.183 | −0.808 | −2.975 | −9.016 | −10.633 | −2.338 |
| DXKL | −0.296 | −3.353 | −0.826 | −3.330 | −9.228 | −11.019 | −2.564 |
| DYZ | −0.458 | −3.436 | −0.844 | −3.499 | −9.293 | −11.657 | −2.576 |
| DEZ | −1.241 | −3.786 | −1.187 | −3.559 | −9.573 | −12.134 | −2.572 |
| January | **0.059** | −1.304 | −1.182 | −0.625 | −0.215 | −0.494 | −1.171 |
| May | −0.698 | −1.213 | −1.053 | −0.100 | **0.004** | −0.153 | −0.681 |
| July | −0.964 | −1.629 | −1.365 | −0.279 | −0.233 | −1.489 | −0.976 |
| September | −0.801 | −1.275 | −1.095 | −0.062 | **0.208** | **0.483** | −0.925 |

The *GI* values were marked in bold if considered to be second (uncontaminated to moderately contaminated) or higher pollution degree.

TABLE 5 Potential ecological risk index (PERI) of heavy metals in sediments at different sampling months and sites.

| | *Ei* value | | | | | | | *RI* value |
|---|---|---|---|---|---|---|---|---|
| | **Cr** | **Cu** | **Zn** | **As** | **Cd** | **Hg** | **Pb** | |
| XHX | 1.892 | 3.606 | 0.638 | 10.904 | **42.096** | **69.628** | 3.948 | **132.712** |
| XCZH | 2.089 | 3.369 | 0.626 | 14.927 | 32.511 | 38.895 | 4.077 | **96.494** |
| X25L | 1.806 | 3.566 | 0.683 | 14.990 | **43.913** | **57.756** | 4.664 | **127.379** |
| XDH | 1.499 | 1.642 | 0.416 | 10.903 | 27.965 | 22.815 | 3.620 | 68.861 |
| XKK | 1.358 | 2.383 | 0.522 | 11.607 | **40.422** | 26.302 | 3.597 | 86.192 |
| X31L | 2.727 | 3.911 | 0.682 | 13.487 | 32.096 | **68.023** | 4.167 | **125.094** |
| XEZ | 2.164 | 3.809 | 0.674 | 13.326 | **42.402** | **62.297** | 4.406 | **129.078** |
| XYZ | 1.985 | 3.606 | 0.641 | 11.629 | 33.305 | **45.783** | 4.197 | **101.148** |
| XXKL | 4.333 | 5.620 | 1.015 | 16.633 | **45.644** | **82.098** | 7.172 | **162.515** |
| DBYT | 1.926 | 2.153 | 0.757 | 10.895 | **50.200** | **43.699** | 2.797 | **112.427** |
| DBPZ | 1.572 | 2.374 | 0.705 | 11.724 | **63.169** | **64.363** | 3.739 | **147.646** |
| DLWZ | 1.629 | 2.419 | 0.710 | 15.312 | **59.239** | **67.087** | 3.593 | **149.989** |
| DXKL | 2.444 | 2.150 | 0.701 | 11.977 | **51.130** | **51.328** | 3.072 | **122.802** |
| DYZ | 2.184 | 2.030 | 0.693 | 10.651 | **48.894** | 32.995 | 3.046 | **100.493** |
| DEZ | 1.269 | 1.593 | 0.546 | 10.216 | **40.262** | 23.713 | 3.054 | 80.652 |
| January | 3.925 | 3.323 | 0.675 | 8.202 | 33.464 | 39.985 | 3.130 | 92.704 |
| May | 1.843 | 3.312 | 0.721 | 14.213 | **44.772** | **54.712** | 4.814 | **124.387** |
| July | 1.537 | 2.425 | 0.582 | 12.362 | 38.293 | 21.381 | 3.812 | 80.392 |
| September | 1.722 | 3.099 | 0.702 | 14.370 | **51.997** | **83.846** | 3.951 | **159.687** |

The values of the comprehensive potential ecological risk index (*RI*) and the individual potential ecological risk index (*Ei*) of heavy metals were presented and were marked in bold if considered to be moderate or a higher ecological risk.

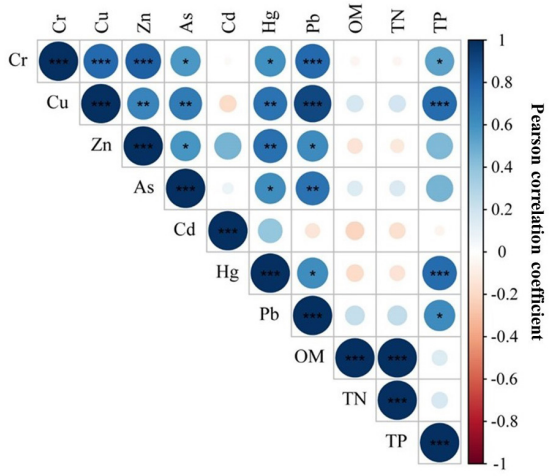


FIGURE 5
Pearson correlations between heavy metals and nutrition elements in sediments. The color and size of all circles indicate the strength of the correlations. The significant differences were represented by *$p < 0.05$, **$p < 0.01$, and ***$p < 0.001$.

Based on the PCA result, the concentrations of As, Cd, Cr, Cu, Hg, Pb, and Zn could be divided into a two-component model, which accounted for 83.94% of all of the data variation. The initial component matrix (F1) showed that As, Cr, Cu, Hg, Pb, and Zn had strong positive loads and their values were greater than 0.80 with a cumulative contribution rate of 64.21%, suggesting these metals were possibly derived from similar sources. In the second component (F2, a contribution rate of 21.35%), Cd showed much higher values than other heavy metals ($p < 0.05$), indicating a notably different source for Cd compared with other metals.

# Discussion

## Spatial and temporal distribution of heavy metals

Consistent with a previous study in Taihu Lake (Rajeshkumar et al., 2018), the significant seasonal difference was observed in most of heavy metals, including As, Cd, Cr, and Hg, which were selected as the priority control heavy metals, due to their prevalently high concentrations in lake sediments (Xu et al., 2017). On the one hand, the distinct hydrodynamics in different seasons causes great difference in sediment resuspension process, thus transforming metal speciation from stable to labile fractions and changing the content of heavy metals in sediments (Huang et al., 2012; Tang et al., 2020). In fact, Xingkai Lake basin is freezing with weak water fluidity under the ice in January, whereas Xingkai Lake and Xiaoxingkai Lake showed strong hydrological connectivity with high water flow velocity in May, July, and September. On the other hand, consistent with Sun et al. (2019) that the highest mean concentration of total heavy metals occurred in the freezing period, resulting from the contribution of ice cover to the accumulation of chemical substances in sediments, such as anoxic condition and less bioturbation at the water-sediment interface (Jansen et al., 2021). Moreover, the NMDS result of heavy metal composition visibly distinguished January from other months, which further confirmed the accumulation characteristics of heavy metals in sediments in January.

As expected, heavy metals in Xingkai Lake showed significant difference compared with those in Xiaoxingkai Lake, with low similarity between two lakes. This may be caused by their different sources of heavy metals, Xingkai Lake is a transboundary lake receiving metal source from both China and Russia, whereas Xiaoxingkai Lake is separated from Xingkai Lake by a natural sandy ridge with main metal source coming from surrounding farmland. Based on the IDW spatial interpolation model, heavy metals showed noticeably different variations in eastern, central, and western regions in two lakes. Compared with the central and western regions, heavy metal concentrations in the eastern region were relatively lower, attributing to a large area of natural lacustrine marsh around the eastern region with respect to pollutant retention function compared to the great contribution of pollutant source from large area of farmland in the western region. Particularly, total heavy metal concentrations at a unique tourism site (XXKL) were significantly higher (one-way ANOVA, $p < 0.05$) than those in other sites in the Xingkai Lake basin, mainly due to heavy fuel oil burning in the ship emissions during navigation process (Wen et al., 2018).

Concentrations of As, Cr, and Zn were higher in lakes compared with marsh, dry farmland and paddy in the Xingkai Lake basin (Shi and Tian, 2020), indicating an enrichment effect of these three metals via surface runoff. In comparison, Cu showed lower concentrations in lakes, which may due to bio-utilization and complex physicochemical processes along the transmission pathway. Besides, Cd and Pb were relatively stable in different land use types in the Xingkai Lake basin.

The chemical forms and mobility of heavy metals are controlled by environmental variables, such as pH, redox potential and nutrients (Kang et al., 2017). We found positive correlations between most metals and TP, suggesting that the sediment nutrients had a great influence on the metal concentrations in the Xingkai Lake basin, which was consistent with studies in other lakes (Zhang H. et al., 2018), may due to high TP in the sediment in Xingkai Lake basin can reduce the mobility of metals by forming new materials such as low-solubility phosphates (Li et al., 2015). However, consistent with previous studies (Li et al., 2015), the concentrations of most metals showed weak correlations with OM and TN, indicating that the variations in OM and TN did not play significant roles in metal enrichment. Moreover, due to the dominance of silt with

TABLE 6 Principal component analysis to distinguish the sources of possible pollutions with total variance explanation and component matrices of heavy metal concentrations in the sediment of Xingkai Lake and Xiaoxingkai Lake.

| Component | Initial eigenvalues | | | Extraction sums of squared loadings | | | Rotation sums of squared loadings | | |
|---|---|---|---|---|---|---|---|---|---|
| | Total | % of variance | Cumulative% | Total | % of variance | Cumulative% | Total | % of variance | Cumulative% |
| 1 | 4.49 | 64.20 | 64.2 | 4.49 | 64.21 | 64.21 | 4.38 | 62.60 | 62.60 |
| 2 | 1.38 | 19.7 | 83.9 | 1.38 | 19.74 | 83.94 | 1.49 | 21.35 | 83.94 |
| 3 | 0.49 | 7.04 | 91.0 | | | | | | |
| 4 | 0.35 | 4.96 | 95.9 | | | | | | |
| 5 | 0.19 | 2.66 | 98.6 | | | | | | |
| 6 | 0.074 | 1.06 | 99.7 | | | | | | |
| 7 | 0.024 | 0.35 | 100 | | | | | | |

| | Component matrix | | Rotated component matrix[a] | | Component score coefficient matrix | |
|---|---|---|---|---|---|---|
| | F1 | F2 | F1 | F2 | F1 | F2 |
| Cr | 0.88 | -0.11 | 0.88 | 0.06 | 0.21 | -0.041 |
| Cu | **0.92** | -0.30 | 0.96 | -0.12 | 0.24 | -0.17 |
| Zn | **0.86** | 0.39 | 0.77 | 0.55 | 0.13 | 0.31 |
| As | **0.81** | -0.058 | 0.80 | 0.097 | 0.18 | -0.007 |
| Cd | 0.094 | **0.98** | -0.094 | 0.98 | -0.11 | 0.70 |
| Hg | **0.83** | 0.30 | 0.76 | 0.45 | 0.14 | 0.25 |
| Pb | **0.89** | -0.29 | 0.93 | -0.12 | 0.24 | -0.17 |

Rotation method: varimax with Kaiser normalization. The "a" marked in the upper right represents rotation converged in three iterations. The bold values represent that the correlations between the extracted principal components and the original variables are significant and > 0.8.



10.3389/fevo.2022.1005194

low OM content in Xingkai Lake and Xiaoxingkai Lake, heavy metals are less likely to be combined by coarse-grained particles in the sediment (Maslennikova et al., 2012; Kang et al., 2017).

## Heavy metals pollution and potential risk assessment

Compared with most lacustrine sediments, such as Dianchi Lake in southwest, Taihu Lake in eastern, and Jingbo Lake in northeast China (Guo et al., 2015; Xu et al., 2017; Li et al., 2022), heavy metal concentrations in Xingkai Lake and Xiaoxingkai Lake were relatively lower, even lower than grade I level in Chinese soil quality standards. In recent years, the implementation of protection project along the lakeshore, for instance, surrounding wetlands restoration and sewage interception construction, can effectively intercept pollutants from the process of migration and reduce the risk of metal dispersal (Xu et al., 2017), and thus leading to considerable heavy metal removal from exogenous inflows in the Xingkai Lake basin. According to the *GI* and *PERI* analysis, sampling sites in the Xingkai Lake basin were at uncontaminated level and moderate ecological risk, except for XXKL with a notably high *GI* value of Cr and the highest *RI* value, indicating a considerable ecological risk in this tourism site because of human tourism behavior.

The overall heavy metal contamination level and ecological risk in Xiaoxingkai were higher than those in Xingkai Lake based on their *GI* and *PERI* values, mainly caused by the direct discharge of domestic sewage from nearby villages and agricultural wastewater from surrounding farmland to Xiaoxingkai Lake, and then flow into Xingkai Lake after reduction of heavy metal concentrations through adsorption, precipitation and other processes. Furthermore, the PERI value notably decreased with increasing lake surface area (Li et al., 2022), indicating a relatively low ecological risk level in Xingkai Lake which had a large area.

In terms of the temporal variations of *GI* and *RI*, the contamination level and ecological risk of heavy metals in both Xingkai Lake and Xiaoxingkai Lake in May and September were higher than those in other months, because the intensive agricultural activities and strong hydrological connectivity throughout the whole basin carrying a large amount of mud and sand in these two months that could elevate heavy metals via sediment deposition. Hydrological connectivity coupled with transport and transfer of heavy metals lead to distinctly spatial differences of heavy metal distribution. Previous study has found that Cd and Cr concentrations are higher in lakes connected to the Yangtze River, whereas concentrations of Cu, Zn, Pb, and As are higher in lakes disconnected with the Yangtze River, resulting in enriched metal pollutants in connected lakes, downstream and multi-branch (Luo et al., 2021). In addition to the direct transfer of heavy metals, hydrological connectivity also has indirect effects on heavy metals. For instance, hypoxic effect and high concentrations of nitrogen and phosphorus caused by hydrological connectivity can improve the bioavailability and accelerate the biogeochemical cycling of Cd and Zn (Liu M. et al., 2019; Niu et al., 2021). Particularly, Cd and Hg concentrations in the sediment were generally high with relatively high ecological risk levels due to agricultural exploration and farmland irrigation system construction in May and September, indicating an increase of the Cd and Hg input flux into water in agricultural seasons and may in turn leading a serious issue for human health by bioaccumulation and biomagnification via the food chain (Wang et al., 2016).

## Source apportionment of heavy metals

High correlations between specific heavy metals in the sediment may reflect similar levels of contamination and/or release from the same sources of pollution (Yi et al., 2011). According to PCA result, the elements, As, Cr, Cu, Hg, Pb, and Zn were grouped together with strong positive loads indicating that the anthropogenic sources of these heavy metals were closely related in the sediment in the Xingkai Lake basin. By contrast, Cd was separated from other heavy metals, indicating a notably different source for Cd. Moreover, compared with previous study in Xingkai Lake (Guo et al., 2015), concentrations of Cr, Cu, Pb, and Zn synchronously decreased in sediments associated with low ecological risk level, but Cd concentration was remained at a high level associated with relatively high *GI* value, indicating a high potential eco-risk and high contaminated level of Cd now and in the future that strongly correlated with the long-term fertilizer application in this area (Shi and Tian, 2020), and further confirmed the distinct sources for Cd and other metals.

Heavy metals in sediments mainly come from natural sources (for example, soil erosion and rock weathering) and anthropogenic sources (for instance, industry, agriculture, transportation and domestic sewage) (Xu et al., 2017; Zhou et al., 2020). Metals of As, Cd, Cu, Pb, and Zn have been widely used in phosphate fertilizer, pesticides, or fungicides to control pests and diseases and promote agricultural production in China (Yu et al., 2021; Liu et al., 2022). Cr belongs to the iron group elements, which are easily combined with soil oxides and is closely related to soil parent materials (Sun et al., 2019). More than 80% of Hg originates from industrial activities such as coal burning and petrochemical production in China (Li et al., 2022). Cd is always considered as the marker of unreasonable agricultural management, and can be fixed and deposited into the sediment in the form of carbonate or hydroxide complex at an alkaline condition

(Liu et al., 2022; Miranda et al., 2022). Meanwhile, tourism may increase heavy metal accumulation in sediments via heavy fuel oil burning during the ship navigation process, particularly in Cd (Wen et al., 2018). Notably, the study area is located in an economically undeveloped region characterized by tourism and agriculture but simple road networks. The industry in the Xingkai Lake basin is dominated by coal mining, which is mainly distributed in distant cities and their surroundings, contributing negligibly to sediment metal accumulation via atmospheric dust loading in the Xingkai Lake basin (Sun et al., 2018). In addition, the measured concentrations of Cd in this study were slightly higher than the background values in soil in Heilongjiang Province, probably attributing to the total emissions of Cd from anthropogenic sources. On the contrary, other metals were comparable to or lower than the background values in soil in Heilongjiang Province, which could be derived from natural sources. Therefore, the mixed sources of agricultural and shipping activities had a great influence on the accumulation of Cd, while As, Cr, Cu, Hg, Pb and Zn mainly came from natural sources.

## Conclusion

Our study presented an explicit analysis of spatial distribution and temporal variation of heavy metals (As, Cd, Cr, Cu, Hg, Pb, and Zn) in sediments of two hydrologically connected lakes in the Xingkai Lake basin. Nutritional components of TN, TP, and OM were also measured to examine the influencing variables on heavy metals. Pollution and ecological risk level and sources of metals were determined based on multiple analysis methods. We found significant spatial and temporal variations of heavy metals in relation to human activities and hydrological connectivity in the basin. Xingkai Lake and Xiaoxingkai Lake showed different heavy metal compositions, and the distribution of each metal varied from eastern to western regions in two lakes. Overall, the contamination level and potential ecological risk of heavy metals in two lakes were low, but relatively higher in the small lake than those in the large lake based on the geo-accumulation index and potential ecological risk index, mainly caused by agricultural activities. In particular, the only tourism site showed relatively a higher pollution level than other sites, mainly due to heavy fuel oil burning in the ship emissions during the navigation process. Besides, the contamination level and potential ecological risk in May and September were higher than those in January and July. Most of metals showed strong relationships with TP in sediments, but not TN and OM. Of all metals, Cd exhibited a high potential eco-risk and high contaminated level, mainly coming from agricultural and shipping activities. By contrast, other metals with low concentrations mainly came from natural sources. These findings are in accordance with our hypotheses, and provide a clearer understanding of heavy metal variation and pollution in hydrologically connected lakes. Therefore, government regulators should make efforts to reduce the use of heavy metal products (e.g., phosphate fertilizer, pesticides, and fungicides) and regulate ship voyage to maintain lake ecosystem sustainability.

## Data availability statement

The original contributions presented in this study are included in the article/supplementary material, further inquiries can be directed to the corresponding author.

## Author contributions

YY and XZ designed the study. MJ, QW, XT, XD, ZW, and YY performed field investigation and preliminary sample treatment. MJ and QW contributed to quality control of samples testing. YY, XZ, XT, and MJ conducted data collection, analysis, interpretation, and drafted of the manuscript. All authors worked together to interpret results, provided feedback on the manuscript, and approved its final version.

## Funding

This research was financially supported by the National Natural Science Foundation of China (Nos. 42101071 and 42171107); Strategic Priority Research Program of the Chinese Academy of Sciences (Nos. XDA28100304 and XDA28100103); Young Scientist Group Project of Northeast Institute of Geography and Agroecology, Chinese Academy of Sciences (2022QNXZ01); Jilin Province Education Department Science and Technology Research Project (No. JJKH20210289KJ); and Natural Science Foundation of Jilin Province (YDZJ202201ZYTS480).

## Acknowledgments

The authors thank Yongzheng Lu for his help in the field work.

## Conflict of interest

The authors declare that the research was conducted in the absence of any commercial or financial relationships that could be construed as a potential conflict of interest.

## Publisher's note



## References

Chen, Y., Jiang, X., Wang, Y., and Zhuang, D. (2018). Spatial characteristics of heavy metal pollution and the potential ecological risk of a typical mining area: a case study in China. Process Saf. Environ. Prot. 113, 204–219. doi: 10.1016/j.psep.2017.10.008

Coelho, C., Foret, C., Bazin, C., Leduc, L., Hammada, M., Inácio, M., and Bedell, J. P. (2018). Bioavailability and bioaccumulation of heavy metals of several soils and sediments (from industrialized urban areas) for Eisenia fetida. *Sci. Total Environ.* 635, 1317–1330. doi: 10.1016/j.scitotenv.2018.04.213

Feng, Y., Chenglin, L., and Bowen, W. (2019). Evaluation of heavy metal pollution in the sediment of Poyang Lake based on stochastic geo-accumulation model (SGM). *Sci. Total Environ.* 659, 1–6. doi: 10.1016/j.scitotenv.2018.12.311

Gao, Q., Li, Y., Cheng, Q., Yu, M., Hu, B., Wang, Z., et al. (2016). Analysis and assessment of the nutrients, biochemical indexes and heavy metals in the Three Gorges Reservoir, China, from 2008 to 2013. *Water Res.* 92, 262–274. doi: 10.1016/j.watres.2015.12.055

Guo, W., Huo, S., Xi, B., Zhang, J., and Wu, F. (2015). Heavy metal contamination in sediments from typical lakes in the five geographic regions of China: Distribution, bioavailability, and risk. *Ecol. Engineer.* 81, 243–255. doi: 10.1016/j.ecoleng.2015.04.047

Hakanson, L. (1980). An ecological risk index for aquatic pollution control.a sedimentological approach. *Water Res.* 14, 975–1001. doi: 10.1016/0043-1354(80)90143-8

Haldar, K., Kujawa-Roeleveld, K., Dey, P., Bosu, S., Datta, D. K., and Rijnaarts, H. H. M. (2020). Spatio-temporal variations in chemical-physical water quality parameters influencing water reuse for irrigated agriculture in tropical urbanized deltas. *Sci. Total Environ.* 708:134559. doi: 10.1016/j.scitotenv.2019.134559

Han, R., Zhou, B., Huang, Y., Lu, X., Li, S., and Li, N. (2020). Bibliometric overview of research trends on heavy metal health risks and impacts in 1989-2018. *J. Clean. Product.* 276:123249. doi: 10.1016/j.jclepro.2020.123249

Huang, J., Ge, X., and Wang, D. (2012). Distribution of heavy metals in the water column, suspended particulate matters and the sediment under hydrodynamic conditions using an annular flume. *J. Environ. Sci.* 24, 2051–2059. doi: 10.1016/S1001-0742(11)61042-5

Huang, X. (2000). *Survey, observation and analysis of lake ecology*. Beijing: Standards press of China.

Jansen, J., MacIntyre, S., Barrett, D. C., Chin, Y. P., Cortés, A., Forrest, A. L., et al. (2021). Winter limnology: How do hydrodynamics and biogeochemistry shape ecosystems under ice? *J. Geophys. Res.* 126:e2020JG006237. doi: 10.1029/2020JG006237

Jin, X., and Zhai, P. (2006). *Lake Xingkai/Khanka. Experience and Lessons Learned Brief*. San Francisco, CA: Scopus.

Kang, X., Song, J., Yuan, H., Duan, L., Li, X., Li, N., et al. (2017). Speciation of heavy metals in different grain sizes of Jiaozhou Bay sediments: bioavailability, ecological risk assessment and source analysis on a centennial timescale. *Ecotoxicol. Environ. Saf.* 143, 296–306. doi: 10.1016/j.ecoenv.2017.05.036

Li, D., Yu, R., Chen, J., Leng, X., Zhao, D., Jia, H., et al. (2022). Ecological risk of heavy metals in lake sediments of China: a national-scale integrated analysis. *J. Clean. Product.* 334:130206. doi: 10.1016/j.jclepro.2021.130206

Li, J., Pu, L., Liao, Q., Zhu, M., Dai, X., Xu, Y., et al. (2015). How anthropogenic activities affect soil heavy metal concentration on a broad scale: a geochemistry survey in Yangtze River Delta, Eastern China. *Environ. Earth Sci.* 73, 1823–1835. doi: 10.1007/s12665-014-3536-7

Li, N., Tian, Y., Zhang, J., Zuo, W., Zhan, W., and Zhang, J. (2017). Heavy metal contamination status and source apportionment in sediments of Songhua River Harbin region, Northeast China. *Environ. Sci. Pollut. Res.* 24, 3214–3225. doi: 10.1007/s11356-016-7132-0

Liu, B., Dong, D., Hua, X., Dong, W., and Li, M. (2021). Spatial distribution and ecological risk assessment of heavy metals in surface sediment of Songhua River, Northeast China. *Chin. Geogr. Sci.* 31, 223–233. doi: 10.1007/s11769-021-1186-8

Liu, J. J., Diao, Z. H., Xu, X. R., and Xie, Q. (2019). Effects of dissolved oxygen, salinity, nitrogen and phosphorus on the release of heavy metals from coastal sediments. *Sci. Total Environ.* 666, 894–901. doi: 10.1016/j.scitotenv.2019.02.288

Liu, M., Chen, J., Sun, X., Hu, Z., and Fan, D. (2019). Accumulation and transformation of heavy metals in surface sediments from the Yangtze River estuary to the East China Sea shelf. *Environ. Pollut.* 245, 111–121. doi: 10.1016/j.envpol.2018.10.128

Liu, P., Wu, Q., Wang, X., Hu, W., Liu, X., Tian, K., et al. (2022). Spatiotemporal variation and sources of soil heavy metals along the lower reaches of Yangtze River, China. *Chemosphere* 291:132768. doi: 10.1016/j.chemosphere.2021.132768

Loska, K., Wiechuła, D., and Korus, I. (2004). Metal contamination of farming soils affected by industry. *Environ. Int.* 30, 159–165. doi: 10.1016/S0160-4120(03)00157-0

Luo, M., Yu, H., Liu, Q., Lan, W., Ye, Q., Niu, Y., et al. (2021). Effect of river-lake connectivity on heavy metal diffusion and source identification of heavy metals in the middle and lower reaches of the Yangtze River. *J. Hazard. Mater.* 416:125818. doi: 10.1016/j.jhazmat.2021.125818

Maslennikova, S., Larina, N., and Larin, S. (2012). The effect of sediment grain size on heavy metal content. *Lakes Reserv. Ponds* 6, 43–54.

Miranda, L. S., Ayoko, G. A., Egodawatta, P., and Goonetilleke, A. (2022). Adsorption-desorption behavior of heavy metals in aquatic environments: influence of sediment, water and metal ionic properties. *J. Hazard. Mater.* 421:126743. doi: 10.1016/j.jhazmat.2021.126743

Muller, G. (1969). Index of geoaccumulation in sediments of the Rhine River. *Geojournal* 2, 109–118. doi: 10.1016/j.envint.2020.106032

Niu, L., Cai, H., Jia, L., Luo, X., Tao, W., Dong, Y., et al. (2021). Metal pollution in the pearl river estuary and implications for estuary management: the influence of hydrological connectivity associated with estuarine mixing. *Ecotoxicol. Environ. Saf.* 225:112747. doi: 10.1016/j.ecoenv.2021.112747

Peng, M., Zhao, C., Ma, H., Yang, Z., Yang, K., Liu, F., et al. (2020). Heavy metal and Pb isotopic compositions of soil and maize from a major agricultural area in Northeast China: contamination assessment and source apportionment. *J. Geochem. Explor.* 208:106403. doi: 10.1016/j.gexplo.2019.106403

Piao, D., and Wang, F. (2011). Environmental conditions and the protection countermeasures for waters of Xingkai Lake (in Chinese). *J. Lake Sci.* 23, 196–202.

Rajeshkumar, S., Liu, Y., Zhang, X., Ravikumar, B., Bai, G., and Li, X. (2018). Studies on seasonal pollution of heavy metals in water, sediment, fish and oyster from the Meiliang Bay of Taihu Lake in China. *Chemosphere* 191, 626–638. doi: 10.1016/j.chemosphere.2017.10.078

Shepard, D. (1968). "A two-dimensional interpolation function for irregularly-spaced data," in *Proceedings of the 1968 23rd ACM National Conference*, New York, NY, doi: 10.1145/800186.810616

Shi, L., and Tian, X. (2020). Pollution and ecological risk assessment of heavy metals in soils under different land use patterns in Xingkai Lake, Heilongjiang Province (in Chinese). *Jiangsu Agric. Sci.* 48, 282–286. doi: 10.15889/j.issn.1002-1302.2020.09.053

Song, K., Wang, Z., Li, L., Tedesco, L., Li, F., Jin, C., et al. (2012). Wetlands shrinkage, fragmentation and their links to agriculture in the Muleng-Xingkai Plain, China. *J. Environ. Manage.* 111, 120–132. doi: 10.1016/j.jenvman.2012.06.038

Song, L., Jian, J., Tan, D.-J., Xie, H.-B., Luo, Z.-F., and Gao, B. (2015). Estimate of heavy metals in soil and streams using combined geochemistry and field spectroscopy in Wan-sheng mining area, Chongqing, China. *Int. J. Appl. Earth Observ. Geoinf.* 34, 1–9. doi: 10.1016/j.jag.2014.06.013

Stauffer, B. A., Goes, J. I., McKee, K. T., do Rosario Gomes, H., and Stabeno, P. J. (2014). Comparison of spring-time phytoplankton community composition in two cold years from the western Gulf of Alaska into the southeastern Bering Sea. *Deep Sea Res. II* 109, 57–70. doi: 10.1016/j.dsr2.2014.03.007

Sun, C., Zhang, Z., Cao, H., Xu, M., and Xu, L. (2019). Concentrations, speciation, and ecological risk of heavy metals in the sediment of the Songhua River in an urban area with petrochemical industries. *Chemosphere* 219, 538–545. doi: 10.1016/j.chemosphere.2018.12.040

Sun, W., Zhang, E., Liu, E., Chang, J., and Shen, J. (2018). Linkage between Lake Xingkai sediment geochemistry and Asian summer monsoon since the last interglacial period. *Palaeogeogr. Palaeoclimatol. Palaeoecol.* 512, 71–79. doi: 10.1016/j.palaeo.2018.06.026

Suresh, G., Sutharsan, P., Ramasamy, V., and Venkatachalapathy, R. (2012). Assessment of spatial distribution and potential ecological risk of the heavy metals in relation to granulometric contents of Veeranam lake sediments, India. *Ecotoxicol. Environ. Saf.* 84, 117–124. doi: 10.1016/j.ecoenv.2012.06.027

Tang, C., Li, Y., He, C., and Acharya, K. (2020). Dynamic behavior of sediment resuspension and nutrients release in the shallow and wind-exposed Meiliang Bay of Lake Taihu. *Sci. Total Environ.* 708:135131. doi: 10.1016/j.scitotenv.2019.135131

Teng, J., Xia, S., Liu, Y., Cui, P., Chen, J., Si, W., et al. (2020). Differences of regulative flexibility between hydrological isolated and connected lakes in a large floodplain: insight from inundation dynamics and landscape heterogeneity. *Water* 12:991. doi: 10.3390/w12040991

Wang, F., Ouyang, W., Hao, F., Jiao, W., Shan, Y., and Lin, C. (2016). Role of freeze-thaw cycles and chlorpyrifos insecticide use on diffuse Cd loss and sediment accumulation. *Sci. Rep.* 6:27302. doi: 10.1038/srep27302

Wang, Y., Ouyang, W., Wang, A., Liu, L., Lin, C., and He, M. (2021). Synergetic loss of heavy metal and phosphorus: evidence from geochemical fraction and estuary sedimentation. *J. Hazard. Mater.* 416:125710. doi: 10.1016/j.jhazmat.2021.125710

Wen, J., Wang, X., Zhang, Y., Zhu, H., Chen, Q., Tian, Y., et al. (2018). PM2. 5 source profiles and relative heavy metal risk of ship emissions: source samples from diverse ships, engines, and navigation processes. *Atmosph. Environ.* 191, 55–63. doi: 10.1016/j.atmosenv.2018.07.038

Wu, H., Xu, C., Wang, J., Xiang, Y., Ren, M., Qie, H., et al. (2021). Health risk assessment based on source identification of heavy metals: a case study of Beiyun River, China. *Ecotoxicol. Environ. Saf.* 213:112046. doi: 10.1016/j.ecoenv.2021.112046

Xu, Y., Wu, Y., Han, J., and Li, P. (2017). The current status of heavy metal in lake sediments from China: pollution and ecological risk assessment. *Ecol. Evol.* 7, 5454–5466. doi: 10.1002/ece3.3124

Yi, Y., Yang, Z., and Zhang, S. (2011). Ecological risk assessment of heavy metals in sediment and human health risk assessment of heavy metals in fishes in the middle and lower reaches of the Yangtze River basin. *Environ. Pollut.* 159, 2575–2585. doi: 10.1016/j.envpol.2011.06.011

Yu, Z., Liu, E., Lin, Q., Zhang, E., Yang, F., Wei, C., et al. (2021). Comprehensive assessment of heavy metal pollution and ecological risk in lake sediment by combining total concentration and chemical partitioning. *Environ. Pollut.* 269:116212. doi: 10.1016/j.envpol.2020.116212

Yuan, X., Zhang, L., Li, J., Wang, C., and Ji, J. (2014). Sediment properties and heavy metal pollution assessment in the river, estuary and lake environments of a fluvial plain, China. *Catena* 119, 52–60. doi: 10.1016/j.catena.2014.03.008

Yuan, Y., Jiang, M., Liu, X., Yu, H., Otte, M. L., Ma, C., et al. (2018). Environmental variables influencing phytoplankton communities in hydrologically connected aquatic habitats in the Lake Xingkai basin. *Ecol. Indic.* 91, 1–12. doi: 10.1016/j.ecolind.2018.03.085

Yuan, Y., Jiang, M., Zhu, X., Yu, H., and Otte, M. L. (2021). Interactions between Fe and light strongly affect phytoplankton communities in a eutrophic lake. *Ecol. Indic.* 126:107664. doi: 10.1016/j.ecolind.2021.107664

Zhang, H., Huo, S., Yeager, K. M., Xi, B., Zhang, J., He, Z., et al. (2018). Accumulation of arsenic, mercury and heavy metals in lacustrine sediment in relation to eutrophication: impacts of sources and climate change. *Ecol. Indic.* 93, 771–780. doi: 10.1016/j.ecolind.2018.05.059

Zhang, P., Qin, C., Hong, X., Kang, G., Qin, M., Yang, D., et al. (2018). Risk assessment and source analysis of soil heavy metal pollution from lower reaches of Yellow River irrigation in China. *Sci. Total Environ.* 633, 1136–1147. doi: 10.1016/j.scitotenv.2018.03.228

Zhang, Y., Zhang, H., Zhang, Z., Liu, C., Sun, C., Zhang, W., et al. (2018). pH effect on heavy metal release from a polluted sediment. *J. Chem.* 2018:7597640. doi: 10.1155/2018/7597640

Zhou, Q., Yang, N., Li, Y., Ren, B., Ding, X., Bian, H., et al. (2020). Total concentrations and sources of heavy metal pollution in global river and lake water bodies from 1972 to 2017. *Glob. Ecol. Conserv.* 22:e00925. doi: 10.1016/j.gecco.2020.e00925

Zhu, X., Yuan, Y., Jiang, M., Song, C., Li, Y., Wang, G., et al. (2021). Multi-element fingerprinting of soils can reveal conversion of wetlands to croplands. *Sci. Total Environ.* 752:141997. doi: 10.1016/j.scitotenv.2020.141997

frontiers | Frontiers in Environmental Science

TYPE Original Research
PUBLISHED 15 September 2022
DOI 10.3389/fenvs.2022.1007662



OPEN ACCESS

EDITED BY
Chuanyu Gao,
Northeast Institute of Geography and Agroecology, (CAS), China

REVIEWED BY
Guodong Wang,
Northeast Institute of Geography and Agroecology, (CAS), China
Chunguang He,
Northeast Normal University, China

*CORRESPONDENCE
Guanglan Cao,
guanglancao@ybu.edu.cn

SPECIALTY SECTION
This article was submitted to Conservation and Restoration Ecology, a section of the journal Frontiers in Environmental Science

RECEIVED 30 July 2022
ACCEPTED 01 September 2022
PUBLISHED 15 September 2022

CITATION
Zong J, Cao G, Jin X, Jin R and Zhu W (2022), Potential distribution prediction of Deyeuxia angustifolia in the Tumen River Basin and analysis of major impact factors.
*Front. Environ. Sci.* 10:1007662.
doi: 10.3389/fenvs.2022.1007662



# Potential distribution prediction of *Deyeuxia angustifolia* in the Tumen River Basin and analysis of major impact factors

Jin Zong[1,2], Guanglan Cao[1,2]*, Xuemei Jin[3], Ri Jin[1,2] and Weihong Zhu[1,2,4,5,6]

[1]College of Geography and Ocean Sciences, Yanbian University, Hunchun, China, [2]Jilin Provincial Joint Key Laboratory of Changbai Mountain Wetland and Ecology, Changchun, China, [3]Wangqing County No. 1 Secondary School, Wangqing, China, [4]Jilin Province Key Laboratory of Changbai Mountain Wetland Ecosystem Function and Ecological Security, Hunchun, China, [5]Tumen River Basin Wetland and Ecology International Joint Research Center of Jilin Province, Hunchun, China, [6]Wetland Research Center of Yanbian University, Yanbian University, Hunchun, China

*Deyeuxia angustifolia* acts as an indicator of the changes in wetland ecosystems and plays an important ecological role in their functions. Previous studies have shown that the Tumen River Basin is of wide global interest as a transboundary basin area with abundant wetland ecological resources. Despite the implementation of wetland conservation measures in recent years, the distribution area of *D. angustifolia* in this basin has been reduced due to climate change and anthropogenic activities. Therefore, we used MaxEnt and geographic information system to model a suitable habitat for this species, simulated changes in the habitat, and applied Jackknife to assess the influencing environmental variables. The Jackknife tests showed that slope orientation, solar radiation in September, and total nitrogen were the dominant environmental factors affecting the potential distribution of *D. angustifolia*. Compared to the current distribution, the total area of land highly and moderately suitable for this species will decrease in the 2050's and 2070's, respectively, under two representative concentration paths (RCPs), shifting the centroid of its suitable area and direction of wetland degradation to the northeast. Our study of the projected potential distribution of *D. angustifolia* in the basin under future climate change could provide important information for its conservation, management, sustainable use, and early warning to prevent its extinction.

KEYWORDS

**Deyeuxia angustifolia, Wetlands, suitability zones, maxent model, Tumen River Basin**

**Abbreviations:** TRB, Tumen River Basin; AUC, Area under the curve; RCP, Representative concentration pathway.

## Introduction

*D. angustifolia* is a perennial saprophytic herb of the grass family Wild Cycads, with a cold-temperate habitat (Mark et al., 1993), growing mainly in mountain hinterland grasslands, forest grasslands, and roadside and ditch-side wetlands at elevations of 680–2,300 m. It easily forms pure stands in seasonally flooded swamps and wet grasslands (Zhang et al., 2014), and is a wet mesophytic, clump-forming plant typical of meadows, and a dominant species in wet meadow and swamp communities (Hongwei et al., 1998). As *D. angustifolia* likes moist environments, it grows well in wetland protruding towers and highly humid locations, and has a wide range of moisture adaptation, high drought tolerance, and a well-developed root system, and can grow well in dry environments. It is mainly distributed in the northeast of China, with the highest concentration in the Sanjiang Plain (Zhou et al., 1992). *D. angustifolia* is rich in nutrition, has high edible value, and can provide high-quality forage for livestock (Lupo et al., 1991).

*D. angustifolia* grows easily in wet environments, which gradually reduces the moisture of the wetland, further enhancing the suitability of the environment for its growth. The reduction of wetland moisture has been found to lead to wetland degradation (Zhao et al., 2021), and previous studies have suggested that IndVal values ≥0.5 indicate a degraded wetland and that *D. angustifolia* can be an indicator of such conditions (Xuemei 2019). The IndVal value of wetland vegetation in the Tumen River Basin (TRB) is 0.628, indicating that wetlands with high growth of *D. angustifolia* may have a degradation risk. The degradation rate of wetlands is mainly manifested in the change of the fitness zone of *D. angustifolia* and also reflects the change in wetland health, which plays an important role in wetland ecology. Therefore, the changes in the growth status and fitness zone of *D. angustifolia* are of great significance in predicting wetland degradation.

The TRB is an important support area for the national implementation of the "The Belt and Road[1]" strategy, with diverse wetland types and rich species in the region (Jin 2019). In recent years, the TRB has been subject to climate change and human interference, resulting in the gradual degradation of wetlands in the basin and a significant decrease (22.39%) in wetland area from 1,161.80 $km^2$ in 1976 to 901.62 $km^2$ in 2016, exhibiting an average annual decrease of 6.50 $km^2$ (Zhang H. et al., 2020). These changes primarily occurred due to the rapid conversion of wetlands to drylands and construction land, which poses a serious threat to the ecological security of wetlands (Liu et al., 2021). This has led to major issues, such as the decline in functional services of wetland ecosystems and the loss of water-holding capacity. Therefore, this study examines the changes in the habitat area of *D. angustifolia*, which are useful for monitoring the status and rate of wetland degradation in the region (Yang et al., 2020). In addition, it provides a scientific and theoretical basis for the future conservation of wetland species and the stable development of wetland ecosystems in the TRB.

In this study, data from 42 sampling sites, soil data from the same sites, and environmental data under the current and future BCC-CSM1-1 models (Simulation of RCP2.6, 8.5 scenarios) combined with the MaxEnt model were used to investigate and predict the distribution of suitable areas for *D. angustifolia*. The specific objectives of this study are to 1) observe the current distribution of *D. angustifolia* habitats in the TRB and predict the future distribution of their habitats in the basin in the 2050's and 2070's using the RCP2.6 and RCP8.5 models; 2) determine the overall changes in their habitat area in the TRB by predicting these changes from the present to 2050–2070; 3) determine the direction and distance of *D. angustifolia* habitat development by shifting the center of mass of their habitat; and 4) determine the main environmental factors affecting the distribution of *D. angustifolia* habitat, and provide a reasonable basis for predicting the degradation of wetlands in the TRB to achieve healthy and sustainable development of these wetland ecosystems.

## Materials and methods

### Study area

The TRB is located in the cross-border area of China, North Korea, and Russia, bordering Russia to the east and North Korea to the south, with geographic coordinates of 41°59′N–44°30′N, 127°27′E–131°18′ E. The basin and wetland areas are 22616.14 and 191.20 $km^2$, respectively (Zhang Y. et al., 2020). This area is in the middle temperate humid monsoon climate, with an average annual temperature of 5.9°C, maximum and minimum average temperatures of 36°C and −32°C, respectively, and average precipitation of 551.7 mm (Zhu et al., 2014). The TRB has various types of wetland ecosystems with rich wetland resources and high biodiversity, as well as a transient habitat for endangered migratory birds and various rare plants and animals, making it one of the most important territories for maintaining biodiversity in Northeast Asia (Zheng et al., 2017).

### Data source

Distribution data for July–September 2017 were obtained from 42 *D. angustifolia* sample sites within the TRB wetland patches (Figure 1), including 14 forested swamp, 13 herbaceous swamp, 7 riverine, 6 scrub swamp, and 2 artificial wetlands. Soil factor data were obtained from wetland soil samples collected in the field during the same period at a depth of 0–20 cm. The samples were placed in vinyl

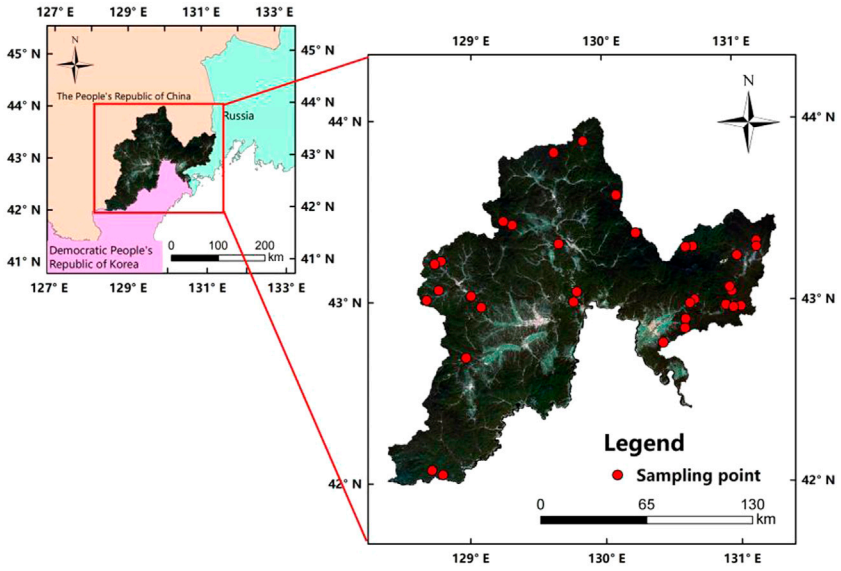


FIGURE 1
Study area and distribution points of *Deyeuxia angustifolia*.

TABLE 1 Principal component analysis of 19 climate factors and eigen values of each variable.

| Variables | Eigen vectors | |
|---|---|---|
| | PC1 | PC2 |
| BIO1 (Annual mean temperature) | −0.012 | −0.006 |
| BIO2 (Mean diurnal range) | 0.002 | 0.011 |
| BIO3 (Isothermality) | 0.006 | 0.004 |
| BIO4 (Temperature seasonality) | −0.273 | 0.924 |
| BIO5 (Max. temperature of the warmest month) | −0.012 | 0.009 |
| BIO6 (Min. temperature of the coldest month) | −0.007 | −0.027 |
| BIO7 (Temperature of annual range) | −0.005 | 0.036 |
| BIO8 (Mean temperature of the wettest quarter) | −0.013 | 0.006 |
| BIO9 (Mean temperature of the driest quarter) | −0.007 | −0.018 |
| BIO10 (Mean temperature of the warmest quarter) | −0.013 | 0.006 |
| BIO11 (Mean temperature of the coldest quarter) | −0.007 | −0.018 |
| BIO12 (Annual precipitation) | 0.663 | −0.013 |
| BIO13 (Precipitation of the wettest month) | 0.190 | 0.088 |
| BIO14 (Precipitation of the driest month) | 0.007 | 0.001 |
| BIO15 (Precipitation seasonality) | 0.012 | 0.059 |
| BIO16 (Precipitation of the wettest quarter) | 0.473 | 0.250 |
| BIO17 (Precipitation of the driest quarter) | 0.030 | 0.003 |
| BIO18 (Precipitation of the warmest quarter) | 0.473 | 0.264 |
| BIO19 (Precipitation of the coldest quarter) | 0.030 | 0.003 |
| Contribution rate (%) | 60.99 | 36.04 |
| Cumulative contribution rate (%) | 60.99 | 97.03 |

self-sealing bags and recorded with numbers (numbers were consistent with the vegetation collection numbers). The water content was measured through the drying method, the pH was measured using an acidity meter, the soil total nitrogen was determined through the sulfuric acid-perchloric acid digestion-semi-micro Kjeldahl method, the soil total phosphorus was determined through the sodium hydroxide fusion-molybdenum antimony anti-colorimetric method, and the soil total potassium was determined through sodium hydroxide fusion. The measured surface soil data were screened and the abnormal values were rejected in SPSS.

The topographic factors studied included the elevation, slope, and slope direction, and the elevation data were the actual measured (GPS) data of the sample site at that time. Both the slope and slope orientation were obtained from Digital Elevation Model (DEM) data by spatial extraction and analysis (http://www.gscloud.cn/), and the resolution of the DEM data was 30 m × 30 m. The climate database for current and future scenarios was downloaded from the WorldClim database (http://world clim.org/) and included 19 bioclimatic variables (numbered in order bio1-bio19) and 30 monthly meteorological factors (Qingliang et al., 2017), with the downloaded climate data at a resolution of 30′ × 30′. To reduce covariance, principal component analysis (Table 1) was performed on the 19 biometeorological factors and a Pearson correlation test was performed with the 30 monthly meteorological factors (Xiao-Ge et al., 2013). According to the correlation results (Figure 2),

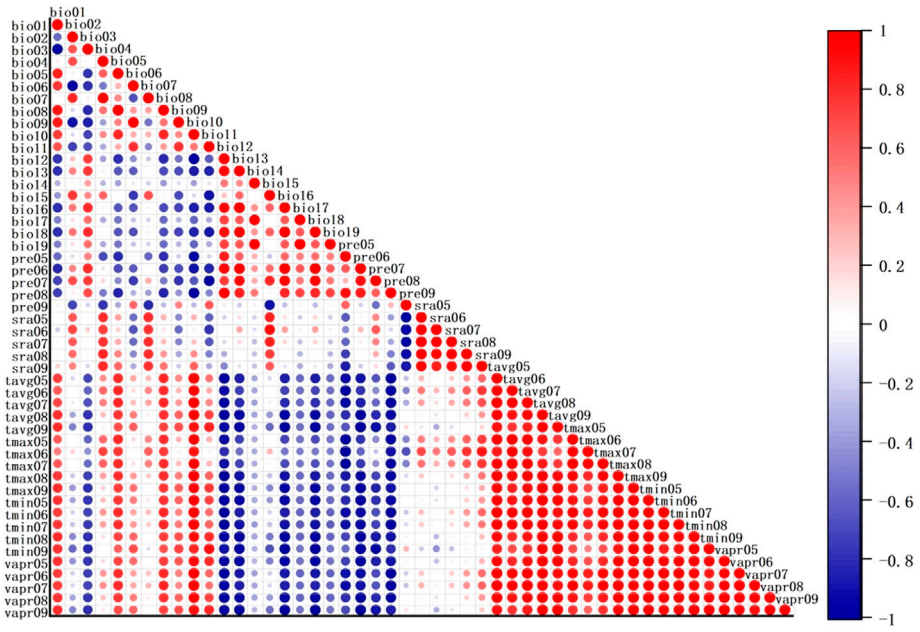


FIGURE 2
Results of correlation analysis of 49 environmental factors.

environmental variables with correlation coefficients of >0.8 were excluded, and the final selection of 16 environmental variables, which were identified as the final modeling data, are listed in Supplementary Table S1.

## MaxEnt model prediction and result evaluation methods

The distribution data of *D. angustifolia* in the TRB with topographic, climatic, and soil data were input into the MaxEnt model to predict the potential distribution areas of the leaflet chapter; 75% of the data were randomly selected as training data to train the model, and the remaining 25% of the data were used as the evaluation subset (testing data) to validate the model (Ye et al., 2019). The evaluation of the model-related performance was conducted using the area under the receiver operating characteristic curve (AUC), and the average training AUC value was automatically calculated when the MaxEnt model was repeatedly run 10 times. The AUC value of the training data was generally between 0 and 1, and the prediction results converged to 1 infinitely, indicating better prediction results (Luo-rong et al., 2007). The AUC evaluation criteria were: 0.5–0.7, low accuracy; 0.7–0.8, average accuracy; 0.8–0.9, good accuracy; and >0.9, very good accuracy (Jessica et al., 2014). Ten iterations were performed for the MaxEnt model and the logical output format.

## Jackknife analyses to validate the influence of environmental variables

Jackknife validation built the model by sequentially using and excluding one environmental variable until all environmental variables were used. The importance of the environmental variables was expressed as the regularized training gain, test gain, and AUC value results. The Jackknife test used bioclimatic variables sequentially to exclude certain ones while building the model and provided three checks: regularized training gain, test gain, and AUC value (Wang et al., 2021). The results were used to measure the importance of the environmental variables (Zhang H. et al., 2020). The knife-cut method was chosen to assess the contribution of environmental variables and thresholds to the potentially suitable areas for *D. angustifolia* within the TRB.

## Species suitability division

The suitability index of *D. angustifolia* was classified using the manual grading method in the reclassification tool in ArcGIS 10.8 software (Yixin 2021). In the statistical principle, when $p < 0.05$, the probability of *D. angustifolia* distribution is small and the occupied area is not suitable for its growth; the closer the value to 1, the greater the probability of *D. angustifolia* existence and the more suitable the occupied area is for its growth. The

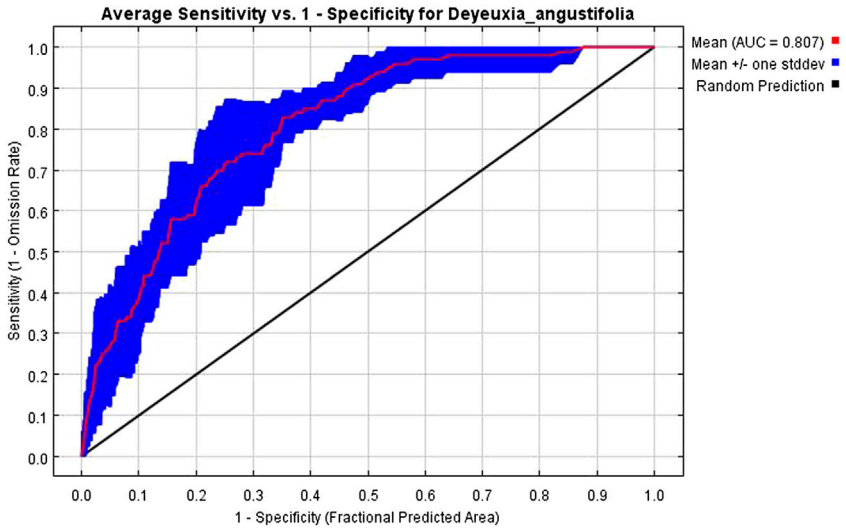


FIGURE 3
Receiver operating characteristic curve and area under the curve value of potential distribution prediction results of *Deyeuxia angustifolia*.

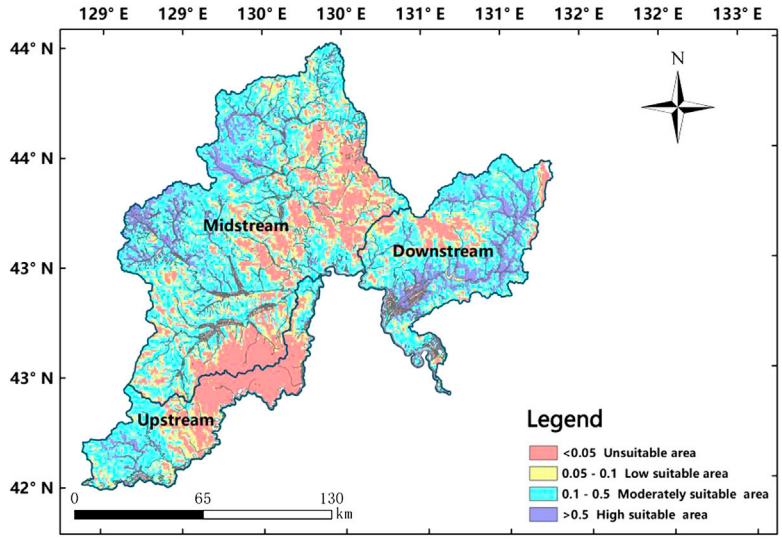


FIGURE 4
Distribution map of current ecological suitability of *Deyeuxia angustifolia*.

remaining possibilities were classified as: 0.05–0.1, low suitability; 0.1–0.5, medium suitability; and >0.5, high suitability (Guojun et al., 2012). Different suitability classes were calculated in the ArcGIS 10.8 spatial analysis module (SDM toolbox) (Brown 2014; Che et al., 2014). In addition, the changes in the area of *D. angustifolia* fitness zones between the present and 2050's or 2070's were compared in ArcGIS 10.8, as well as the changes in the area conversion of fitness zones under different climate change scenarios in the future.

# Results

## MaxEnt model prediction result accuracy evaluation

In this study, the accuracy of the results predicted by the MaxEnt model was tested using the receiver operating characteristic curves, and the working characteristic curves of the simulation results based on 10 iterations of objects are shown

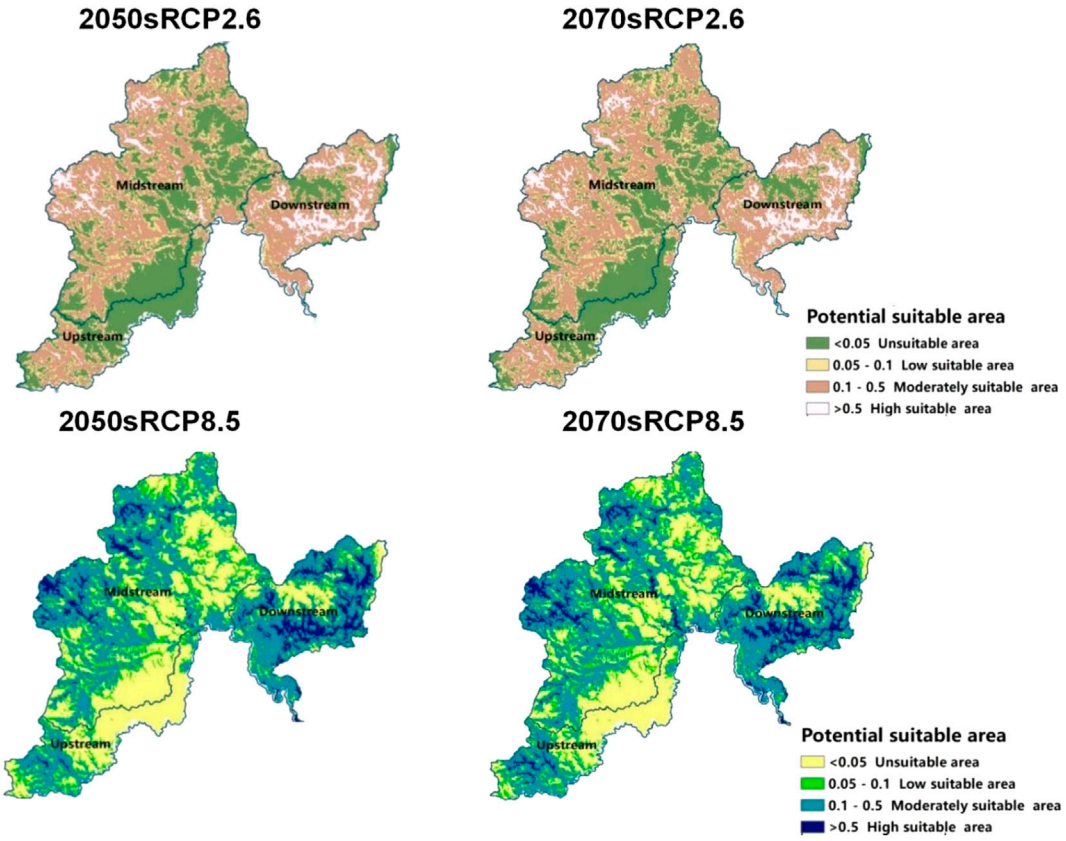


FIGURE 5
Distribution map of future ecological suitability of *Deyeuxia angustifolia*.

in Figure 3. The AUC value of the MaxEnt prediction results was 0.807, which was significantly larger than that of the random prediction distribution model. This indicates that the MaxEnt model prediction results were "very good" and reliable in simulating the *D. angustifolia* distribution area of TRB.

## Present and future changes in the suitable area of *Deyeuxia angustifolia* in Tumen River Basin

The predicted potential distribution of *D. angustifolia* is shown in Figure 4; the larger the value shown in the result, the more suitable the area is for the survival of *D. angustifolia*. In increasing order of suitability, the high-suitability areas of *D. angustifolia* are mainly located in the northwestern part of the upper Tumen River, the western part of the middle Tumen River, and the eastern part of the lower Tumen River. *D. angustifolia* serves as an indicator for degraded wetlands, so the degradation rate of wetlands in the lower reaches of the TRB is much greater than that in the upper and middle reaches of the Tumen River, and is mainly concentrated in the eastern and western parts of TRB. The high-fitness zone of *D. angustifolia* is mainly located at the intersection of rivers and forest swamps, and near paddy fields in the eastern and western areas of the TRB, where the rate of wetland degradation is faster. The area and proportion of suitable areas in the TRB are as follows: high suitability—2,268.40 $km^2$ (10.03%); medium suitability—12,027.26 $km^2$ (53.18%); low suitability—3,485.15 $km^2$ (15.41%); non-suitable—4,835.33 $km^2$ (21.38%).

## Future suitable area of *D. angustifolia*

Compared with the current climate, the distribution and area of the fitness zone of *D. angustifolia* in the 2050's and 2070's under the future climate change scenarios are different, according to the MaxEnt model simulation (Figure 5), area change (Table 2), and ArcGIS calculation results. The results show that the predicted future distribution in the 2050's will be as follows: the non-suitable zone in the TRB will be 8,059.66 $km^2$ (35.64%), the low-suitability zone will be 3,651.75 $km^2$ (16.15%), the medium-suitability zone will be 9,306.55 $km^2$ (41.15%), and

10.3389/fenvs.2022.1007662

TABLE 2 Area and proportion of the distribution of *Deyeuxia angustifolia*.

| | 2050 RCP2.6 ($km^2$) | Proportion (%) | 2050 RCP8.5 (km2) | Proportion (%) | 2070 RCP2.6 (km2) | Proportion (%) | 2070 RCP8.5 (km2) | Proportion (%) |
|---|---|---|---|---|---|---|---|---|
| Unsuitable area | 8,059.66 | 35.64 | 7,759.82 | 34.31 | 7,711.92 | 34.10 | 7,697.22 | 34.03 |
| Low-suitability area | 3,651.75 | 16.15 | 3,705.58 | 16.38 | 3,704.44 | 16.38 | 3,685.37 | 16.30 |
| Moderately suitable area | 9,306.55 | 41.15 | 9,663.08 | 42.73 | 9,559.28 | 42.27 | 9,599.45 | 42.45 |
| Highly suitable area | 1,598.17 | 7.07 | 1,487.67 | 6.58 | 1,640.51 | 7.25 | 1,634.09 | 7.23 |

the high-suitability zone will be 1,598.17 $km^2$ (7.07%). In the case of high concentration using the RCP8.5 model, the non-suitable zone in the TRB will be 7,759.8 2 $km^2$ (34.31%), the low-suitability zone will be 3,705.58 $km^2$ (16.38%), the medium-suitability zone will be 9,663.0 8 $km^2$ (42.73%), and the high-suitability zone will be 1,487.67 $km^2$ (6.58%).

The results for the predicted future distribution in the 2070s are as follows: the non-suitable area in the TRB will be 7,711.92 $km^2$ (34.10%), the low-suitability area will be 3,704.44 $km^2$ (16.38%), the medium-suitability area will be 9,559.28 $km^2$ (42.27%), and the high-suitability area will be 1,640.51 $km^2$ (7.25%). At the high concentration using the RCP8.5 model, the non-suitable zone in the TRB will be 7,697.22 $km^2$ (34.31%), the low-suitability zone will be 3,685.37 $km^2$ (16.38%), the medium-suitability zone will be 9,599.45 $km^2$ (42.73%), and the high-suitability zone will be 1,634.09 $km^2$ (6.58%). Compared to the current fitness zone, the area of the future fitness zone will also mainly be concentrated in the medium-fitness zone, and the area of the high-fitness zone will slightly decrease, reducing the degree of fragmentation and indirectly leading to a reduced risk of wetland degradation.

## Future predicted area change and center of mass shift of *Deyeuxia angustifolia* in Tumen River Basin

The model simulations (Figure 6 and Table 3) showed that the area of the suitable zone of *D. angustifolia* in the TRB in the future under both RCP2.6 and RCP8.5 scenarios showed a decreasing trend, and the rate of decrease in the suitable area was greater than the rate of increase. Compared to the original area, using the RCP2.6-RCP8.5 scenario in the 2050s, the unsuitable area showed the same decreasing trend, and was 29.45 $km^2$ (0.13%), and the continuously decreasing area and the same unchanged increasing area were 271.39 $km^2$ (1.2%). In the 2070's, from RCP2.6 to RCP8.5, the non-tolerant area showed the same decreasing trend and the same continuously increasing area of 88.2 $km^2$ (0.39%), and the same continuous decreasing area and the same unchanged increasing area of 508.86 $km^2$ (1.2%).

Under the RCP2.6 scenario, the unsuitable area showed a decreasing trend from the 2050's to the 2070's of 61.12 $km^2$ (0.27%); the continuous decrease was 287.22 $km^2$ (1.27%). Under the RCP8.5 scenario, the unsuitable area showed the same decreasing trend of 119.87 $km^2$ (0.53%); the continuous decrease was 524.69 $km^2$ (2.32%). Changing RCP2.6-RCP8.5 for different scenarios, the unsuitable area for *D. angustifolia* showed a decrease and the area of tolerable zones increased. Thus, the increase in temperature will accelerate the growth and spread of *D. angustifolia*, to some extent. However, the reduction in the area of the tolerant zone was much greater than the increase;

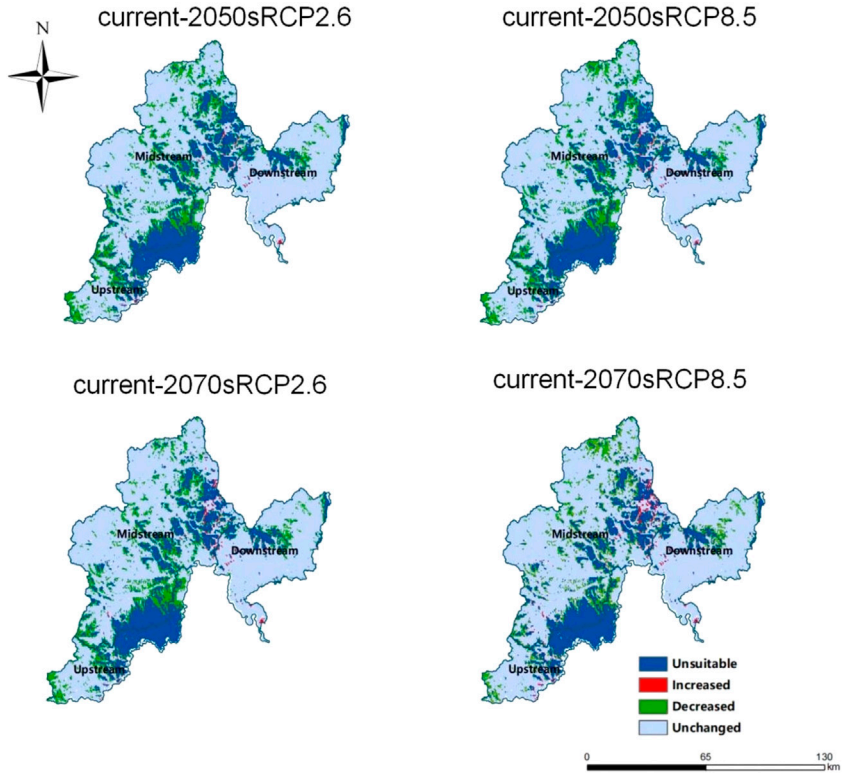


FIGURE 6
Changes of *Deyeuxia angustifolia* in the suitable area of the Tumen River Basin under different climate change scenarios.

therefore, the overall change in the area of the tolerant zone of *D. angustifolia* was negative.

In the climate change scenarios, the fitness zone of *D. angustifolia* in the TRB shifted to the east. In the 2050's, the center of mass moved 4.68 km to the northeast in the future RCP2.6 scenario and 3.99 km to the northeast in the RCP8.5 scenario. In the 2070's it moved 4.19 km to the northeast in the RCP2.6 scenario, 5.93 km to the northeast in the RCP8.5 scenario, and 5.93 km to the northwest in the RCP2.6 scenario. From 2050 to 2070, the center of mass of the fitness zone is predicted to shift 0.83 km in the northwest direction in the RCP2.6 scenario and 2.49 km in the northeast direction in RCP8.5 scenario (Figure 7; Supplementary Table S2).

## Analysis of environmental impact factors in *Deyeuxia angustifolia* suitable area

Based on contemporary environmental data, total nitrogen, slope direction, and elevation were found to have a significant influence on the habitat of *D. angustifolia*, with contribution rates of 23.7%, 20.1%, and 13.1%, respectively. Jackknife analysis was used to determine the importance of the environmental factors in predicting the results. The three variables with the highest regularized training gain, test gain, and AUC values were the slope direction, elevation, and total nitrogen when simulated with individual variables only. The results of the Jackknife analysis showed (Figure 8) that these environmental factors contained valid information that other variables did not have, and had important effects on the current distribution of potentially suitable areas for *D. angustifolia*. When combining the effects of the model simulations and Jackknife tests, soil factors accounted for 36.0%, climate factors for 16.1%, and topography factors for 47.9% (Supplementary Table S3). Overall, soil and topographic factors were the dominant factors influencing the potential distribution of *D. angustifolia*.

# Discussion

## Current distribution of suitable habitats for *D. angustifolia*

The study results showed that the high-suitability area for the growth of *D. angustifolia* was distributed in the eastern and western areas of the TRB near the intersection of rivers, forest

TABLE 3 Variation in the area of *Deyeuxia angustifolia* distribution.

| | 2050 RCP2.6 (km2) | Proportion (%) | 2050 RCP8.5 (km2) | Proportion (%) | 2070 RCP2.6 (km2) | Proportion (%) | 2070 RCP8.5 (km2) | Proportion (%) |
|---|---|---|---|---|---|---|---|---|
| Unsuitable | 4,720.04 | 20.87 | 4,690.59 | 20.74 | 4,658.92 | 20.6 | 4,570.72 | 20.21 |
| Increased | 115.34 | 0.51 | 144.74 | 0.64 | 176.41 | 0.78 | 264.61 | 1.17 |
| Decreased | 3,340.4 | 14.77 | 3,069.01 | 13.57 | 3,053.18 | 13.50 | 2,544.32 | 11.25 |
| Unchanged | 14,440.41 | 63.85 | 14,711.80 | 65.05 | 14,729.89 | 65.13 | 15,236.49 | 67.37 |

swamps, and paddy fields. Such areas are more seriously degraded; combined with the spatial changes of wetlands in the TRB between 1976 and 2016, wetlands show an overall trend of shrinkage, with the most serious shrinkage seen in rivers and swamp wetlands, of which swamp wetlands are more degraded. The degradation rate of paddy fields has also increased significantly (Hua 2019), which is consistent with the findings of this study that indicate that wetland degradation will appear first in the high-suitability area of *D. angustifolia*, such as rivers and forest swamps. Paddy fields are generally subject to greater amounts of human activity due to their proximity to residential areas and rivers, and the rate of degradation is closely related to it (Chen 2008). The high-suitability area of *D. angustifolia* is greater downstream and decreases upstream because the topography of the TRB is high in the west and low in the east. The west is more prone to soil erosion, which will accelerate the reduction of wetland moisture and intensify degradation (van Lent et al., 2019). The eastern area of the Tumen River is mainly located in Hunchun City in the Yanbian Korean Autonomous Prefecture. The wetland area in this region is extensive, the downstream and midstream show mild degradation, and the upper reaches are subhealthy, which is consistent with the study results (Jin et al., 2019).

## Future area change and plastid shift in *D. angustifolia*

In all future climate scenarios, global climate change greatly affects the distribution of species, leading to the expansion, shifting, and contraction of the fitness zone of populations (Sales et al., 2019). *D. angustifolia* is more sensitive to the effects of $CO_2$, with high-fitness zones decreasing with increasing $CO_2$ concentrations, indicating that overall, high $CO_2$ concentrations inhibit the growth of *D. angustifolia*. Mingyi (2015) found that high $CO_2$ concentrations caused a decrease in the internal index of *D. angustifolia*, which had a significant impact on its ability to carry out photosynthesis and reduced its normal growth rate, which is consistent with the results of this study. The reduction in the area of *D. angustifolia* over the next 20 years resulted in an increasing trend in wetland area. An improvement in wetland ecosystems may be due to the decline in small-leaved camphor. Conversely, degradation of wetlands may lead to increased infestation of this camphor species. Therefore, changes in small-leaved camphor and wetland development are closely linked and may have a constraining effect on the *D. angustifolia* species. The increase in wetland area of 1780.83 ha found by Zhang Y. et al. (2020) slowed down the rate of degradation in the area and mitigated the current situation of wetland degradation to some extent. According to different emission scenarios from 2050 to 2070, the overall migration route of the center of mass gradually shifted towards the northeast, which is consistent with the trend of migration of species fitness zones

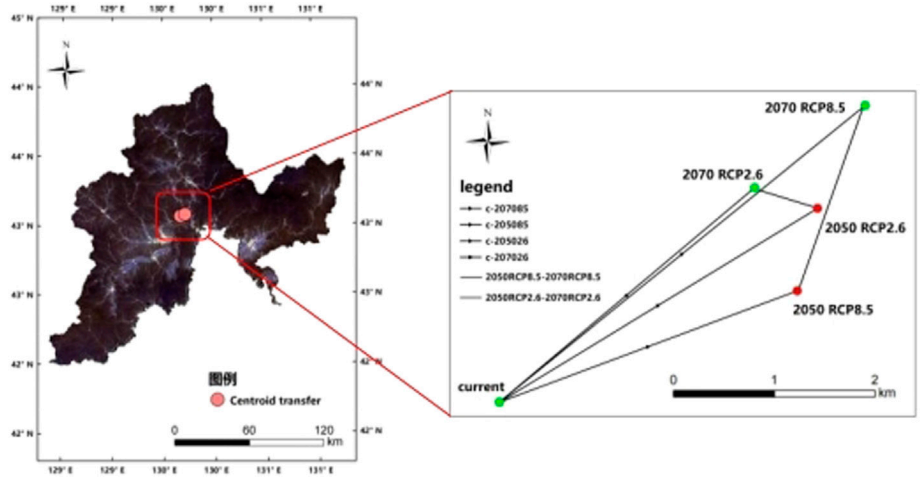


FIGURE 7
Variation in suitable areas of *Deyeuxia angustifolia* in the Tumen River Basin.

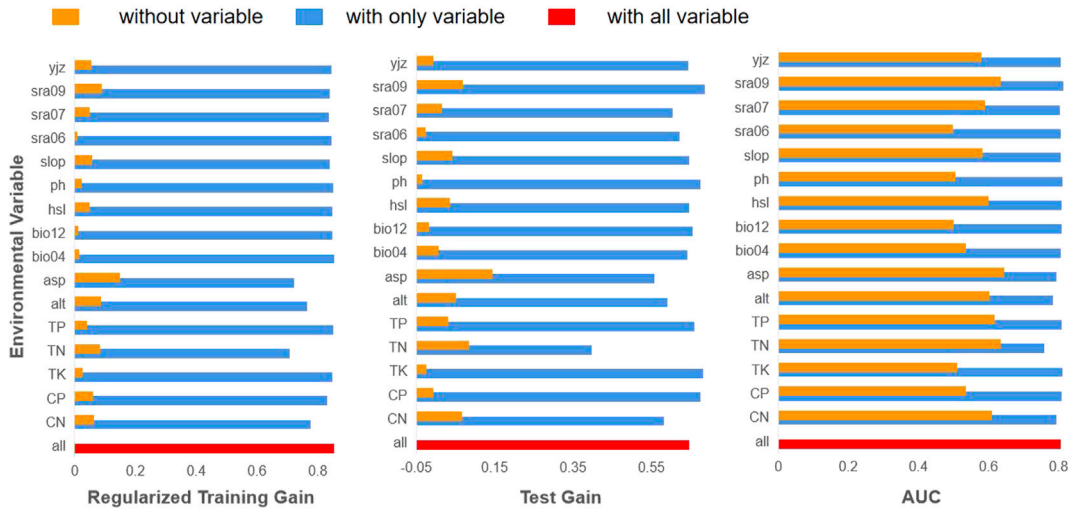


FIGURE 8
Contribution rate diagram of environmental factors based on Jackknife.

to higher latitudes in the context of global climate change outcomes (Zhang et al., 2018).

## Influencing factors affecting the change of suitable habitat in *Deyeuxia angustifolia*

According to the environmental factors predicted by the model, the most important factor affecting *D. angustifolia* is total nitrogen, which is one of the factors affecting the species composition, diversity, and nutritional conditions, as the enrichment of nitrogen changes the content of soil nutrients (Fu et al., 2014). Numerous studies have found that the increase in nitrogen promotes the growth of *D. angustifolia*, increases its productivity, and enhances its competitiveness (Jin et al., 2016), making it a dominant species in the environment, which is consistent with the results obtained in this study. The second dominant factor affecting the growth of *D. angustifolia* is the

slope direction. Found that the disturbance of the slope affects the distribution of vegetation (Shengwei 2014). The third factor is altitude, and *D. angustifolia* is prone to growing at high altitudes, but is less prevalent at low altitudes, which is consistent with the observations of Luo et al. (2008).

This result is highly consistent with the expectations of this study, after considering anthropogenic improvements as well as restoration of the natural state of the wetland ecosystem. The improvement of the wetlands in the future can also demonstrate the effects of implementing wetland conservation measures and the extremely important role of public intervention. However, the Jackknife analysis showed that, in addition to the great influence of total nitrogen and slope direction on leaflets, the solar radiation in September also had a high rate of influence on the distribution of *D. angustifolia,* albeit not as high as that of the slope direction. These results indicated that soil warming promoted the growth of *D. angustifolia*, and, under the same environmental conditions, the higher the heat, the more lush the plant. However, the response of *D. angustifolia* physiology to soil temperature was more obvious under flooded conditions than under unflooded conditions (Dou et al., 2009). Furthermore, the increase in temperature and decrease in water increased the growth of *D. angustifolia* and accelerate the degradation of wetlands (Hou et al., 2013). Therefore, *D. angustifolia,* as a representative plant of wetlands, can provide a basis for research on wetland conservation and utilization, as well as wetland restoration.

## Future prospects

In this study, the prediction of the potential distribution of *D. angustifolia* depends mainly on the data of its distribution points and of the surrounding environmental factors in the TRB. The evaluation of habitat suitability based on these data provides valuable information and theoretical reference for the determination of suitable areas for *D. angustifolia* in the TRB in the future (Soilhi et al., 2022). The distribution data of *D. angustifolia* were obtained from actual field vegetation community surveys; however, some distribution points were difficult to reach due to various reasons, which can affect the distribution and number of sampling points. Other environmental factors, such as soil characteristics, topography, land use, and biotic interactions, also impact the potential geographic distribution of the species (Abolmaali et al., 2018) and require multiple validations. This also significantly impacts the improvement of model accuracy owing to the lack of specific requirements on the number of factors and the selection and quantification of human interference factors, such as fast-acting nutrients, enzyme activity, microbial activity, etc. Future studies should consider actual measurement data and other local adaptation and microclimate factors (Ngarega et al., 2021) to improve the accuracy of the model and facilitate better prediction of species distribution models. In addition, RCP of climate change scenarios have low spatial resolution with no standard scale of analysis. Therefore, later stages of these scenarios should be analyzed with more accurate resolution to increase the simulation accuracy. RCPs have been proposed globally by the IPCC and they can represent future climate change under different conditions and scenarios. However, the TRB in this study is located along the borders of China, North Korea, and Russia; thus, future studies should consider reducing the scale of RCP to improve accuracy.

# Conclusion

The main objective of this study was to investigate the influence of environmental factors and climate change on the habitat area of *D. angustifolia* in the TRB, and to provide scientific reference for the degradation range of wetlands and reasonable wetland construction in the TRB. In this study, the MaxEnt model was used to determine the current distribution of the habitat of *D. angustifolia* and the key environmental factors affecting its distribution, predict the distribution and area changes of the habitat range in future years, accompanied by different future scenarios, and derive the process of the movement of the heart of the habitat range in the TRB. The main findings of the study are as follows:

1) Approximately 2,268.40 $km^2$ (10.03%) of the high-fitness area of *D. angustifolia* in the TRB is mainly located in the northwestern part of the upper Tumen River, followed by the western part of the middle Tumen River, and the eastern part of the lower Tumen River. These areas are mainly in the eastern and western parts of the TRB, near the intersection of rivers, forest swamps, and paddy fields.
2) The moderately suitable area of *D. angustifolia* accounted for the main distribution area of the whole TRB area, and the high-suitability area showed an increasing trend with decreasing fragmentation. In the future, the habitat area of *D. angustifolia* in the TRB under both RCP2.6 and RCP8.5 scenarios will tend to decrease, and the center of mass of the habitat as a whole will move to the east.
3) Soil and topographic factors are the dominant factors influencing the potential distribution of *D. angustifolia*, among which slope direction, solar radiation in September, and total nitrogen are the three environmental factors that have the greatest influence.

In recent years, owing to the implementation of relevant management measures, the wetland ecological environment has improved, and the degradation area as well as rate have decreased. However, wetland degradation continues to occur every year. Based on the findings of this study, future studies should undertake strict monitoring of the area identify the

relevant negative changes in a timely manner, and implement measures to reduce the degradation rate and area, to the maximum possible extent. This is necessary to protect the wetland ecological environment of the TRB and reduce the negative impacts of the increase in species.

## Data availability statement

The datasets presented in this article are not readily available because In research. Requests to access the datasets should be directed to Guanglan Cao, guanglancao@ybu.edu.cn.

## Author contributions

JZ conducted the investigation, resources, visualization, formal analysis and writing; XJ conducted Investigation, Resources; GC conducted Supervision, Writing review; WZ and RJ conducted Supervision. All authors have read and approved the submitted version

## Funding

This work was supported by the National Natural Science Foundation of China under the Key Project (41830643) and the National Science and Technology Basic Resources Survey Project (2019FY101703), as well as the Jilin Provincial Science and Technology Development Program Project (YDZJ202203CGZH023) and the Yanbian University Doctoral Initiation Fund Yanbian University [(2020) No. 36].

## Acknowledgments

Thanks to Jilin Provincial Key Laboratory of wetland ecosystem function and ecological security in Changbai Mountain, thanks to GC for her guidance, encouragement and suggestions on this article, WZ for her comments and suggestions on this article, thanks to RJ for his guidance on data processing, and thanks to XJ for her discussion on data.

## Conflict of interest

The authors declare that the research was conducted in the absence of any commercial or financial relationships that could be construed as a potential conflict of interest.

## Publisher's note

All claims expressed in this article are solely those of the authors and do not necessarily represent those of their affiliated organizations, or those of the publisher, the editors and the reviewers. Any product that may be evaluated in this article, or claim that may be made by its manufacturer, is not guaranteed or endorsed by the publisher.

## Supplementary material

The Supplementary Material for this article can be found online at: https://www.frontiersin.org/articles/10.3389/fenvs.2022.1007662/full#supplementary-material

## References

Abolmaali, S. M. R., Tarkesh, M., and Bashari, H. (2018). MaxEnt modeling for predicting suitable habitats and identifying the effects of climate change on a threatened species, Daphne mucronata, in central Iran. *Ecol. Inf.* 43, 116–123. doi:10.1016/j.ecoinf.2017.10.002

Brown, J. L. (2014). SDM toolbox: A python-based GIS toolkit for landscape genetic, biogeographic and species distribution model analyses. *Methods Ecol. Evol.* 5, 694–700. doi:10.1111/2041-210X.12200

Che, L., Cao, B., Bai, C. K., Wang, J., Zhang, L., et al. (2014). Potential distribution prediction and suitability evaluation of Taibai rice based on MaxEnt and ArcGIS. *Bull. Bot. Res.* 34 (5), 642–649.

Chen, J. (2008). "Study on the degradation mechanism of paddy ecosystem caused by unreasonable fertilizer application and its restoration effect of fertilizer application [dissertation]," (Changsha, Hunan: Hunan Agricultural University).

Dou, J. X., Liu, J. S., Wang, Y., and Zhao, G. Y. (2009). Effects of simulated soil warming on the growth and physiological characters of Deyeuxia angustifolia. *Ying yong sheng tai xue bao* 20, 1845–1851.

Fu, X. L., Ma, F., Ni, H. W., and Wang, J. B. (2014) Effects of nitrogen deposition on soil nutrient content of Deyeuxia angustifolia. *Adv. Mater. Res.*, 955. 3655–3660.

Guojun, Q. I., Yan, G. A. O., and Dechao, H. (2012). Invasive dispersal dynamics and fitness analysis of rice weevil in China based on Maxent. *J. Plant Prot.* 39, 129–136.

Hongwei, N. I., Xing, Z., and Li, J. (1998). Above-ground biomass dynamics of typical meadow populations of little leaf, in the Sanjiang Plain. *J. Plant Res.* 03, 72–79.

Hou, C., Song, C., Li, Y., Wang, J., Song, Y., and Wang, X. (2013). Effects of water table changes on soil $CO_2$, $CH_4$ and $N_2O$ fluxes during the growing season in freshwater marsh of Northeast China. *Environ. Earth Sci.* 69, 1963–1971. doi:10.1007/s12665-012-2031-2

Hua, C. (2019). "Study on spatial and temporal distribution characteristics and driving forces of wetland degradation in Tumen River Basin [dissertation]," (Yanbian University).

Jessica, B. S., Christine, R. W., and Karen, V. R. (2014). Developing macro habitat models for bats in parks using maxent and testing them with data collected by citizen scientists. *Int. J. Biodivers. Conserv.* 6, 171–183. doi:10.5897/IJBC2013.0647

Jin, Y., Xu, J., Wang, Y., Wang, S., Chen, Z., Huang, X., et al. (2016). Effects of nitrogen deposition on tundra vegetation undergoing invasion by Deyeuxia angustifolia in Changbai Mountains. *Chin. Geogr. Sci.* 26, 99–108. doi:10.1007/s11769-015-0746-1

Jin, Z. (2019). "Comprehensive assessment of the water-holding function of wetland ecosystems in the Tumen River basin [dissertation]," (Yanbian University).

Jin, Z., Weihong, Z., and Ri, J. (2019). Study on wetland ecosystem health evaluation in Tumen River basin, China. *Wetl. Sci.* 17, 344–351.

Liu, Y., Jin, R., and Zhu, W. (2021). Conversion of natural wetland to farmland in the Tumen River basin: Human and environmental factors. *Remote Sens. (Basel).* 13, 3498. doi:10.3390/rs13173498

Luo, W., Song, F., and Xie, Y. (2008). Trade-off between tolerance to drought and tolerance to flooding in three wetland plants. *Wetlands* 28, 866–873. doi:10.1672/07-225.1

Luo-rong, W. A. N. G., LÜ-yi, M. A., Xi-qun, W. A. N. G., and Sui-chao, H. E. (2007). Seedling techniques of Magnolia wufengensis and M. wufengensis var. multitepala. *J. Zhejiang Agric. For. Univ.* 24 (2), 242–246.

Lupo, Z., Yuemin, P., Jianling, X., and Youbin, Z. (1991). Calamagrostis angustifolia development and utilization research. *Mod. Agric.* 04, 10–12.

Mark, P., Zhou, R. C., and Zhang, Y. (1993). Study on aboveground biomass composition and seasonal dynamics of Calamagrostis angustifolia Grassland in Sanjiang Plain. *China Grassl.* 02, 27–31.

Mingyi, X. (2015). "Simulation of the effect of elevated atmospheric CO2 on photosynthetic properties and molecular mechanisms in Chaparral [dissertation]," (Northeastern Agricultural University).

Ngarega, B. K., Masocha, V. F., and Schneider, H. (2021). Forecasting the effects of bioclimatic characteristics and climate change on the potential distribution of Colophospermum mopane in southern Africa using Maximum Entropy (Maxent). *Ecol. Inf.* 65, 101419. doi:10.1016/j.ecoinf.2021.101419

Qingliang, L., Yao, L., and Shengzuo, F. (2017). PPrediction of potential suitable cultivation area based on MaxEnt model. *J. Nanjing For. Univ. (Nat. Sci. Ed.).* 41, 25–29.

Sales, L. P., Ribeiro, B. R., Pires, M. M., Chapman, C. A., and Loyola, R. (2019). Recalculating route: Dispersal constraints will drive the redistribution of amazon primates in the anthropocene. *Ecography* 42, 1789–1801. doi:10.1111/ecog.04499

Shengwei, Z. (2014). "Vegetation changes and mechanisms in the subalpine tundra zone of Changbai Mountain [dissertation]," (Northeast Normal University).

Soilhi, Z., Sayari, N., Benalouache, N., and Mekki, M. (2022). Predicting current and future distributions of Mentha pulegium L. in Tunisia under climate change conditions, using the MaxEnt model. *Ecol. Inf.* 68, 101533. doi:10.1016/j.ecoinf.2021.101533

van Lent, J., Hergoualc'h, K., Verchot, L., Oenema, O., and van Groenigen, J. W. (2019). Greenhouse gas emissions along a peat swamp forest degradation gradient in the Peruvian amazon: Soil moisture and palm roots effects. *Mitig. Adapt. Strateg. Glob. Chang.* 24, 625–643. doi:10.1007/s11027-018-9796-x

Wang, R., Jiang, C., Liu, L., Shen, Z., Yang, J., Wang, Y., et al. (2021). Prediction of the potential distribution of the predatory mite Neoseiulus californicus McGregor in China using MaxEnt. *Glob. Ecol. Conserv.* 29, e01733. doi:10.1016/j.gecco.2021.e01733

Xiao-Ge, X., Tong-Wen, W., and Jie, Z. (2013). Introduction of CMIP5 experiments carried out with the climate system models of Beijing Climate Center. *Adv. Clim. Change Res.* 4, 41–49. doi:10.3724/SP.J.1248.2013.041

Xuemei, J. (2019). "A study on the potential distribution of plant diversity and small-leaved chapter in wetlands of Yanbian Prefecture [dissertation]," (Yanbian University).

Yang, C. H. P., Zhao, X., and Wang, J. W. (2020). Potential distribution areas of long-footed Kiwifruit in China and their response to climate change based on MaxEnt model. *J. Sichuan Agric. Univ.* 38, 755–763.

Ye, X. M., Chen, F. S., and Sun, R. X. (2019). Prediction of potential suitable distribution areas for Choerospondias axillaris based on MaxEnt model. *Acta Agric. Univ. jiangxiensis.* 41, 440–446.

Yixin, D. (2021). "Simulation of landscape evolution dynamics in the little xinganling marsh wetland [PhD thesis]," (Harbin: Harbin Normal University).

Zhang, H., Zhao, H., and Wang, H. (2020). Potential geographical distribution of Populus euphratica in China under future climate change scenarios based on Maxent model. *Acta Ecol. Sin.* 40 (18), 6552–6563.

Zhang, K., Yao, L., Meng, J., and Tao, J. (2018). Maxent modeling for predicting the potential geographical distribution of two peony species under climate change. *Sci. Total Environ.* 634, 1326–1334. doi:10.1016/j.scitotenv.2018.04.112

Zhang, L., Jing, Z., Li, Z., Liu, Y., and Fang, S. (2019). Predictive modeling of suitable habitats for Cinnamomum Camphora (L.) presl using maxent model under climate change in China. *Int. J. Environ. Res. Public Health* 16 (17), 3185. doi:10.3390/ijerph16173185

Zhang, X., Mao, R., Gong, C., Qiao, T., and Song, C. (2014). $CO_2$ evolution from standing litter of the emergent macrophyte Deyeuxia angustifolia in the Sanjiang Plain, Northeast China. *Ecol. Eng.* 63, 45–49. doi:10.1016/j.ecoleng.2013.12.002

Zhang, Y., Jin, R., Zhu, W., Zhang, D., and Zhang, X. (2020). Impacts of land use changes on wetland ecosystem services in the Tumen River basin. *Sustainability* 12, 9821. doi:10.3390/su12239821

Zhao, Y., Liao, J., Bao, X., and Ma, M. (2021). Soil seed bank dynamics are regulated by bird diversity and soil moisture during alpine wetland degradation. *Biol. Conserv.* 263, 109360. doi:10.1016/j.biocon.2021.109360

Zheng, X. J., Sun, P., Zhu, W. H., Xu, Z., Fu, J., Man, W. D., et al. (2017). Landscape dynamics and driving forces of wetlands in the Tumen River Basin of China over the past 50 years. *Landsc. Ecol. Eng.* 13 (2), 237–250. doi:10.1007/s11355-016-0304-8

Zhou, R. C., Wang, H. T., and Ni, H. W. (1992). Study on wet grassland in Sanjiang Plain. *Land Nat. Resour. Res.* 01, 43–47.

Zhu, W., Miao, C., and Zheng, X. (2014). Study on ecological safety evaluation and warning of wetlands in Tumen River watershed based on 3S technology. *Acta Ecol. Sin.* 34, 1379–1390.

frontiers | Frontiers in Ecology and Evolution

TYPE Original Research
PUBLISHED 20 September 2022
DOI 10.3389/fevo.2022.1002397



OPEN ACCESS

EDITED BY
Chuanyu Gao,
Northeast Institute of Geography and Agroecology (CAS), China

REVIEWED BY
Rongshuo Cai,
Third Institute of Oceanography, State Oceanic Administration, China
Xiangrui Meng,
Changchun Normal University, China
Bing Zhang,
Tianjin Normal University, China

*CORRESPONDENCE
Fengqin Yan
yanfq@lreis.ac.cn

SPECIALTY SECTION
This article was submitted to Conservation and Restoration Ecology, a section of the journal Frontiers in Ecology and Evolution

RECEIVED 25 July 2022
ACCEPTED 24 August 2022
PUBLISHED 20 September 2022

CITATION
Yan F (2022) Effects of climate changes on net primary productivity variation in the marsh area of the Sanjiang Plain. *Front. Ecol. Evol.* 10:1002397. doi: 10.3389/fevo.2022.1002397



# Effects of climate changes on net primary productivity variation in the marsh area of the Sanjiang Plain

Fengqin Yan[1,2]*

[1]State Key Laboratory of Resources and Environmental Information System, Institute of Geographic Sciences and Natural Resources Research, Chinese Academy of Sciences, Beijing, China, [2]College of Resources and Environment, University of Chinese Academy of Sciences, Beijing, China

The Sanjiang Plain includes the largest freshwater marsh in China, playing an important role in regional carbon cycle. As an important indicator of carbon cycle, the net primary productivity (NPP) is a crucial index for estimating the carbon storage of marshy wetlands. Investigating the association between climate factors and NPP variation quantitatively is of great significance for estimating carbon sequestration of marsh. Based on NPP data and climatic data from 1954 to 2014, the spatiotemporal change of NPP in marsh area was analyzed and its association with climate factors was investigated in the Sanjiang Plain in this study. The results indicated that the NPP showed an increase trend in the marsh area of the Sanjiang Plain in the past six decades. Temperate growth made the largest contribution to the NPP increase among the main climate factors in the last six decades, followed by $CO_2$ concentration. Solar Radiation had the largest explanatory power on the spatial distribution of NPP among three climate factors before 1985. After 1985, temperature played an important role in leading the NPP distribution. Results also showed that the explanatory power of interactions between climate factors was stronger than that of single factor. Our results highlight the asymmetric effects of interactions between climate factors on marsh vegetation, which should be adequately considered in estimating carbon sequestration in marsh area in the Sanjiang Plain.

KEYWORDS

**net primary productivity, marsh, the Sanjiang Plain, climate change, geographical detection method**

## Introduction

Wetlands are regions with low-level water, which are usually covered by vegetation during growing season (Vivian et al., 2014; Marthews et al., 2022). As the kidneys of the Earth, wetlands play an important role in biogeochemical cycle (Tercero et al., 2017; Xiao et al., 2019; Deng et al., 2022). Wetlands provide a lot of ecosystem service values

for mankind such as water conservation, biodiversity maintenance, coastal protection, water purification and flood mitigation (Yan and Zhang, 2019; Thomaz, 2021; Monge-Salazar et al., 2022; Tong et al., 2022). It is estimated that wetlands store 20–30% of the earth's carbon soil pool while covering only approximately 5–8% of the world's land surface (Mitsch and Gosselink, 2000; Roulet, 2000). Wetlands are good natural environments for separating and storing carbon from the atmosphere, due to their anoxic and humid conditions (O'Connor et al., 2010; Dargie et al., 2017). Net primary productivity (NPP) refers to the difference between the total amount of organic matter accumulated by green vegetation in the ecosystem through photosynthesis and the cumulative respiration per unit time. NPP, a significant indicator of carbon cycle, is the basis of the energy and material cycle of the ecosystem, which is related to the carbon fixation capacity of the ecosystem (Brouwers and Coops, 2016; Xiao et al., 2019). Studies have indicated that climate variation can influence vegetation coverage, growth conditions and growing season duration, leading to NPP variation and the subsequent carbon cycle (Brouwers and Coops, 2016; Li et al., 2018; Sun et al., 2022). Therefore, it is of great significance to investigate the effects of climate change on NPP variation in wetland areas quantitatively.

As one of the driving factors of vegetation growth (Schimel et al., 2000; Cao et al., 2022b; Ren et al., 2022), climate is influenced by land use and land cover changes (LUCC), and vice versa. Generally, climate warming enhances vegetation growth globally, with negative impacts in low latitudes (Shestakova et al., 2019; Madani et al., 2021; Cao et al., 2022b; Chen et al., 2022; Qiu et al., 2022). Additionally, increased precipitation would promote vegetation growth in water-limited regions. Accordingly, vegetation greening could produce biophysical feedback to climate, such as increase of evapotranspiration, surface cooling (Davin and de Noblet-Ducoudre, 2010). Climate changes are expected to act critical roles in the spatiotemporal patterns of vegetation growth. Previous studies usually focus on the response of vegetation growth on single climate factor (Brouwers and Coops, 2016; Madani et al., 2021; Chen et al., 2022), ignoring the response of vegetation growth on interactions between the dominate climate factors.

Although the effects of climate changes on vegetation NPP variation have become hot topics in the field of global change, most of which focus on forest, agriculture or grassland ecosystems (Schimel et al., 2000; Zarei et al., 2021; Cao et al., 2022a; Ji et al., 2022). Few studies investigated the response of NPP variation to climate change in wetland ecosystem, which has a unique environmental condition (Mao et al., 2014; Caplan et al., 2015; Wang et al., 2022). Due to the anoxic and humid condition, there are obvious differences in the effect of climate change on vegetation between wetland and other ecosystems (Zhang et al., 2016; Shen et al., 2019; Wang et al., 2022). Marsh is the main type of wetlands, playing an important role in carbon sequestration (Shen et al., 2021). Therefore, clarifying the effect of climate change on marsh NPP is crucial for assessing regional carbon storage and understanding carbon cycle. However, the quantitative association between climate change and NPP variation in marsh area remains poorly understood.

The Sanjiang Plain includes the largest freshwater marsh distribution area in China, which has also experienced intense human activities in the past decades (Wang et al., 2015; Yan, 2020). As a dominant type of wetlands in the Sanjiang Plain, marsh provides important ecosystem services (Wang et al., 2015; Yan and Zhang, 2019). And vegetation is crucial for carbon sequestration in the Sanjiang plain marshy wetland. Liu et al. (2015) estimated the NPP changes of Calamagrostis Angustifolia marsh at Fujin City in the Sanjiang Plain under IPCC SRES emission scenarios and found that increase of $CO_2$ concentration and temperature have a positive impact on the vegetation growth of wetland vegetation (Liu et al., 2015). Additionally, the effect of precipitation on NPP vegetation was more significant than that of temperature. Mao et al. (2014) found that human activities caused a loss of 84 gC $m^{-2}$ $yr^{-1}$ in marsh NPP during 2000–2011 in Northeast China (Mao et al., 2014); Wang et al. (2009) suggested that land use and land cover (LUCC) is the main factor affecting vegetation NPP in the Sanjiang Plain from 2000 to 2015 (Wang et al., 2009). Considering that climate factors are also important factors, it is necessary to investigate the response of marshy wetland NPP on climate changes in the Sanjiang Plain for a long-time.

To address these knowledge gaps, we investigated the association between climate change and NPP variation quantitatively in the Sanjing marsh area in the past six decades. Firstly, I analyzed the spatiotemporal changes in NPP and climate factors. Secondly, the association between climate changes and NPP changes was explored quantitatively. Lastly, the response of NPP distribution on climate factors and climate interactions were estimated quantitatively in two stages: stage I (1954–1985) and stage II (1986–2014).

# Materials and methods

## Study area

The Sanjiang Plain (**Figure 1**) is located in the northeastern part of Heilongjiang Province, from 45°01′05"N to 48°27′56" N and from 130°13′10"E to 135°05′26"E, with a total area of about 108,900 $km^2$ (Yan and Zhang, 2019). The Sanjiang Plain consists of the alluvial deposits of three rivers (the Amur, Ussuri, and Songhua rivers), and is the largest distribution of freshwater marsh in China. The Sanjiang Plain consists of 23 counties, namely Fuyuan, Tongjiang, Hegang, Luobei, Suibin, Fujin, Raohe, Huachuan, Jixian, Youyi, Tangyuan, Jiamusi, Shuangyashan, Baoqing, Hulin, Yilan, Huainan, Qitaihe, Boli, Mishan, Jixi, Jidong, and Mulin. The study area in this study

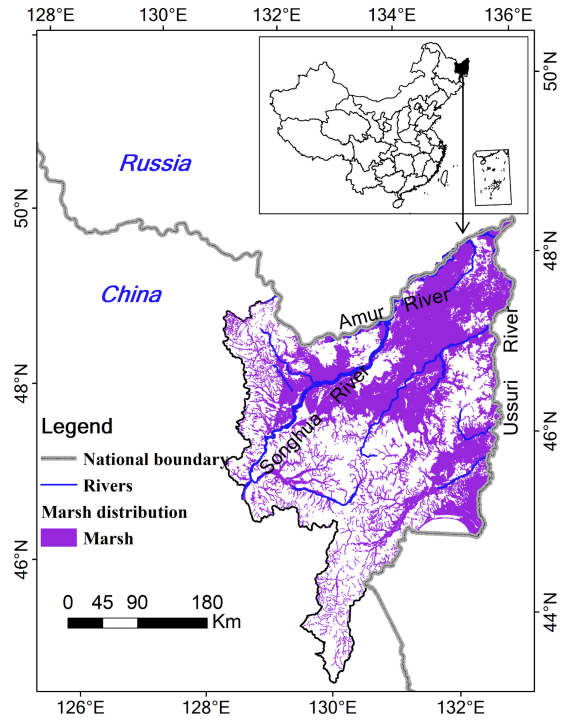


FIGURE 1
Location map of study area.

concentrates on the marsh wetland distribution area and its associated land use/cover changes (based on the marsh distribution in 1954).

## Data and methods

The climatic data (1954–2014) in this study include average temperature, precipitation and solar radiation. The meteorological data were obtained from the meteorological station data of China National Meteorological Data Sharing Center. A total of 10 meteorological data were selected, 7 of which are within the Three Rivers Plain and 3 outside the region. Using Kriging interpolation by ArcGIS software, combined with Fortran programming, the meteorological station data was interpolated into raster format with a resolution of 2 km × 2 km. The $CO_2$ concentration data was download from the Carbon Dioxide Information Analysis Center (CDIAC), whose website is: https://cdiac.ess-dive.lbl.gov/.

The NPP data was obtained from previous publication (Yan, 2017), which was produced by Dynamic Land Ecosystem Model. DLEM comprehensively considers the influence of carbon nitrogen coupling on carbon cycle and is well-evaluated in global and regional scale including China, United States and India etc. In the DLEM model, NPP was defined as the difference between gross primary productivity (GPP) and plant autotrophic respiratory consumption (RA).

$$NPP = GPP - R_A \quad (1)$$

The simulation of GPP (Unit: g $Cm^{-2}day^{-1}$) is based on the improved Farquar model (Farquhar et al., 1980), and the canopy is divided into sunlit and shaded layers.

$$GPP_{sun} = 12.01 \times 10^{-6} \times A_{sun} \times plai_{sun} \times dayl \times 3,600 \quad (2)$$

$$GPP_{shade} = 12.01 \times 10^{-6} \times A_{shade} \times plai_{shade} \times dayl \times 3,600 \quad (3)$$

$$GPP = GPP_{sun} + GPP_{shade} \quad (4)$$

Where $GPP_{sun}$ and $GPP_{shade}$ represent the GPP of sunlit and shaded canopy, respectively. $A_{sun}$ and $A_{shade}$ are the assimilation rates while $plai_{sun}$ and $plai_{shade}$ are the indices of sunlit and shaded canopy, respectively. *dayl* represents the daily daytime length.

The $plai_{sun}$ and $plai_{shade}$ *are* calculated as followed:

$$plai_{sun} = 1 - EXP(-proj_{LAI}) \quad (5)$$

$$plai_{shade} = proj_{LAI} - plai_{sun} \quad (6)$$

$proj_{LAI}$ is the leaf carbon content (g C $m^{-2}$) multiplied by the specific leaf area (SLA) of different vegetation function type. DLEM sets the carbon assimilation rate as the minimum of three limiting rates ($w_c$,$w_j$,$w_e$). For the $C_3$ species,they represent the assimilation rates limited by the efficiency of the photosynthetic enzymes system, available light photosynthetically active radiation (PAR) and transport of photosynthetic products, respectively. For the C3 species,$w_e$ is the assimilation rates limited by PEP carboxylase.

$$R_A = Mr + Gr \quad (7)$$

*Mr* and *Gr* denote maintenance and growth respiration, respectively. In the DLEM,25% of GPP is considered to be used as *Gr*.

$$G_r = 0.25 \times GPP \quad (8)$$

The *Mr* of different plants (leaf, sapwood, fine root and coarse foot) is estimated as follows:

$$Mr_i = rf \times R_{coeff\_i} \times f(T) \times N_i \quad (9)$$

Where *i* is the carbon pool of different plants. $Mr_i$ is the maintenance respiration of different carbon pools. R*f* denotes growing phase. It is defined as 0.5 in non-growing season and 1 in growing season. The growing season and non-growing season

are defined according to the vegetation phenology observed by satellite.; $R_{coeff\_i}$ is the respiration coefficient of different plant function types. $N_i$(g N $m^{-2}$)is the nitrogen content of different pools and *f(T)* is a temperature factor.

$$f(T) = e^{308.56 \times \left(\frac{1}{56.02} - \frac{1}{T+46.02}\right)} \quad (10)$$

T is the daily average temperature of the aboveground carbon pools (i.e., leaf and sapwood), or the soil temperature of the underground carbon pool (i.e., coarse roots and fine roots).

The LUCC data were obtained from remote sensing images. LUCC in 1976 was dominated by Landsat MSS imagery with a spatial resolution of 80 m. LUCC in 1986/2000/2010 were dominated by Landsat TM imagery while LUCC in 2015 was obtained from Landsat OIL imagery, with a spatial resolution of 30 m. Remote sensing imagery for the Landsat series is available on the USGS website.[1] LUCC data since 1976 were obtained based on a uniform set of standard processes (Liu et al., 2002, 2010). The land use data in 1954 were reconstructed from the Cellular Automata (CA) model (Yan and Zhang, 2019). To reduce post-classification error, LUCC maps were produced by comparing Landsat imagery between different years (Liu et al., 2003, 2014). The accuracies of the LUCC data interpretation were verified by comparing with a large number of field surveys with historical records, including aerial films, statistical yearbooks, etc. (Liu et al., 2002, 2003, 2014).

The Pearson Correlation Coefficient was used to detect the correlation between NPP increase and four climate factors (solar radiation, average temperature, precipitation and $CO_2$ concentration).

$$r = \frac{\Sigma (x - \bar{x})(y - \bar{y})}{\sqrt{\sum (x - \bar{x})^2 \sum (y - \bar{y})^2}} \quad (11)$$

Where r denotes the Pearson Correlation Coefficient. $\bar{x}$ and $\bar{y}$ are the average values of $x$ and $y$, respectively.

The Geographical Detection Method (GDM) was used to estimate the association between climatic factors and the spatial heterogeneity of NPP quantitatively in this study. GDM is a kind of variance analysis, which can detect spatial heterogeneity and potential factors (Wang et al., 2010). The GDM can identify the factors influence stratified heterogeneity without requiring a linear hypothesis. The GDM method has been widely used in many aspects including natural sciences, social sciences, environmental sciences and human health (Zhang and Zhao, 2018; Bai et al., 2019; Zhao et al., 2020b; Chang et al., 2022a; Guo et al., 2022). GDM includes four parts, namely, factor detector, interaction detector, ecological detector a; 43nd risk detector. The factor detector detects the magnitude of the influence of different environmental factors on the spatial variation of NPP. The interaction detector can reveal the interaction between different factors, that is evaluate the change of explanatory power when different factors interact in pairs. The higher the value of q, the greater the influence, and the expression is as follows (Wang et al., 2010):

$$q = 1 - \frac{\sum_{h=1}^{L} N_h \sigma_h^2}{N\sigma^2} = 1 - \frac{SSW}{SST} \quad (12)$$

$$SSW = \sum_{h=1}^{L} N_h \sigma_h^2 \quad (13)$$

where q ($\in$[0,1]) is the explanatory power of different factors and h is the classification of the impact factors. $N_h$ and N are, respectively, the layer h and the number of samples in the whole region; ${\sigma_h}^2$ and $\sigma^2$ are the variances of the *Y*-values for stratum h and the whole region, respectively. SSW and SST are the sum of within Sum of Squares and Total Sum of Squares, respectively. In this study, solar radiation, average temperature and precipitation are selected as influencing factors, and these the numerical variables are divided into 9 types by using the Natural Breaks classification method. Since the atmospheric $CO_2$ concentration was uniform spatially in the same year, it was not considered in the analysis of influencing factors of spatial differentiation.

# Results

## Net primary productivity changes

### Temporal change analysis

The total NPP in the Sanjiang Plain marshy area showed an increasing trend generally, with a decreasing trend in the 1950s. The statistical analysis of the data shows that the total NPP in the study area increased from 29.99 Tg Cyr-1 in the 1950s to 30.94 Tg Cyr-1 in the 2010s (**Figure 2**), with an increase of 3.2%. The highest value of the total NPP occurred in 2014 while the lowest value was in 1964.

The NPP changes between different decades were also analyzed (**Figure 2**). The total NPP showed a decreasing trend between the 1950s and 1960s, with a decrease of approximately 3.12 TgC. During the 1960s–1970s, the total NPP increased by 0.81 Tg C while it increased by 1.21 TgC between 1970s and 1980s. The increase of NPP during the 1980s–1990s was nearly same as that of the 1970s–1980s. The NPP increased by approximately 0.63 TgC and 0.21 TgC during the 1990s–2000s and 2000s–2010s, respectively.

### Spatial change analysis

In this study, the spatial distribution of NPP in the marshy areas of the study area during the 1950s and 2010s and its difference in the marshy areas of the study area were analyzed (**Figure 3**). The results showed that the NPP in the marshy

1 https://www.usgs.gov/

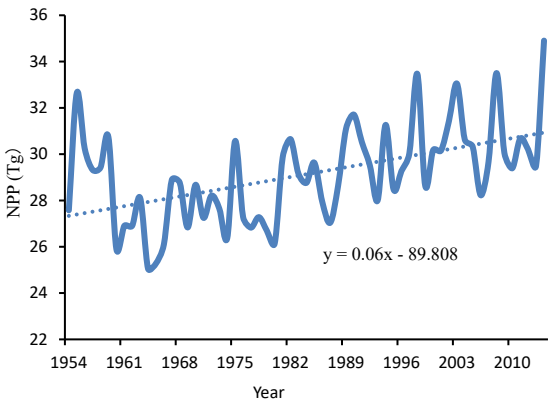


FIGURE 2
Temporal changes of net primary productivity since 1954 in the marsh area of the Sanjiang Plain.

wetlands of the Sanjiang Plain was mostly between 300 and 400 gC/m$^{-2}$/yr. And the average NPP values in the southern part of the study area are greater than those in the northern part. In areas where marshy wetland was not been disturbed, the mean marsh NPP values tend to decrease. Additionally, NPP tends to decrease in areas where marsh were transformed into dry farmland, bare land and water body while NPP tends to increase in areas where marsh were transformed into woodland and paddy fields.

## Changes of other environmental variables

The average temperature in the Sanjiang Plain has shown an increasing trend over the past 60 years or so (Figure 4). The highest temperature in the study area occurred in 2007 (4.78°C) while the lowest temperature occurred in 1969 (1.03°C), with a mean increase rate of approximately 0.23°C/10a. Between 1954 and 2014, the average temperature in the Sanjiang Plain was 3.3°C, with a relatively high inter-annual variability. The mean temperature between 1954 and 1985 was 2.88°C while that between 1985 and 2014 was 3.75°C.

During the period 1954–2014, the average annual precipitation in the Sanjiang Plain was 577.41 mm/year (Figure 5), with a relatively high inter-annual variability. Statistical data indicates that the maximum annual precipitation can reach to 810.52 mm (1994) while the minimum can reach to 396.94 mm (1976). There was a weak increasing trend in general during the past six decades in the Sanjiang Plain.

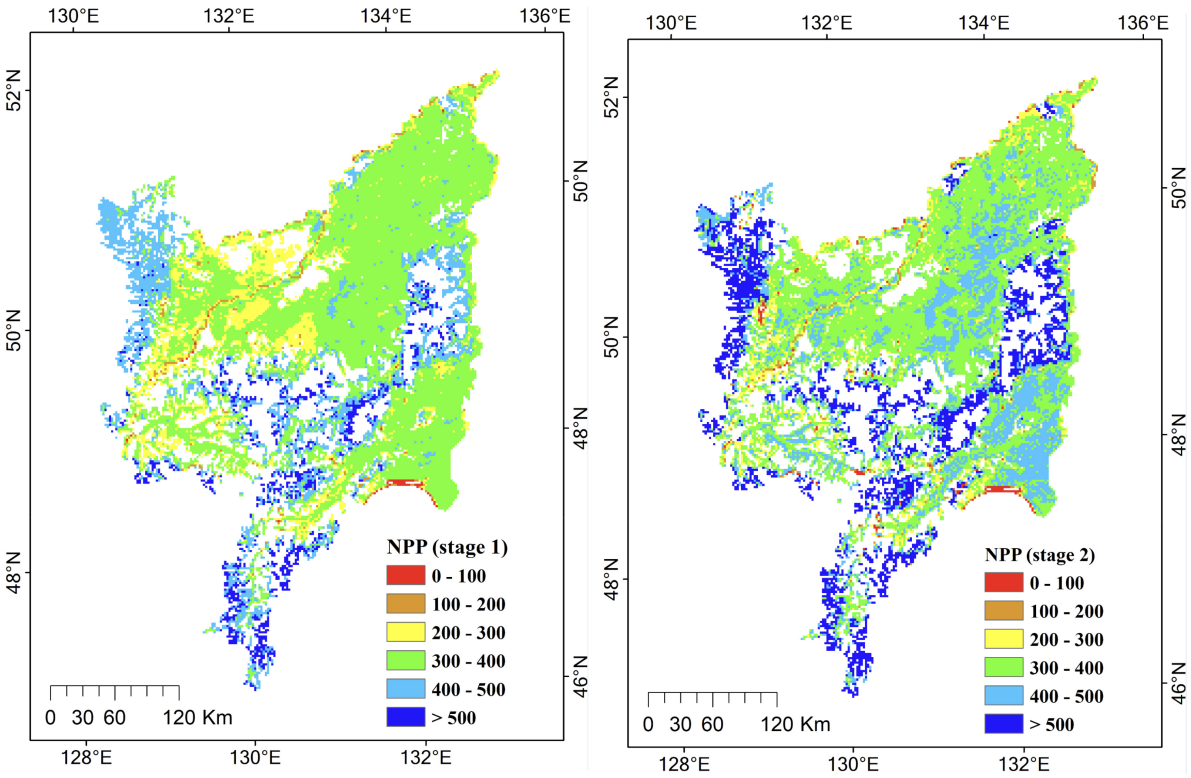


FIGURE 3
Spatial changes of net primary productivity since 1954 in the marsh area of the Sanjiang Plain (unit: gC/m$^{-2}$/yr).

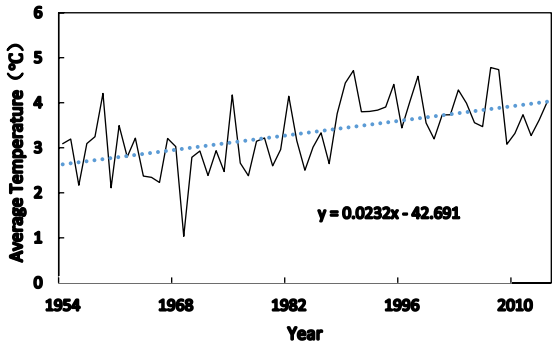


FIGURE 4
Changes of average temperature since 1954 in the Sanjiang Plain.

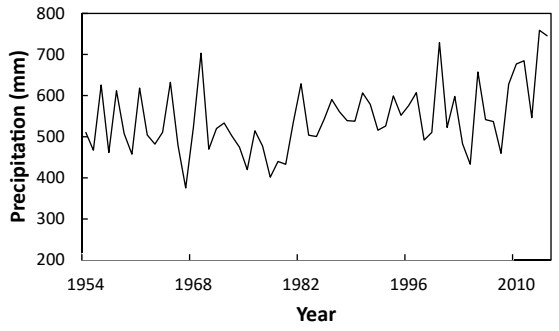


FIGURE 5
Changes of precipitation since 1954 in the Sanjiang Plain.

This study mapped the interannual variation of solar radiation in the Sanjiang Plain during the period 1954–2014 (as shown in Figure 6). Statistical analysis of the data shows that solar radiation in the Sanjiang Plain has generally shown a weak fluctuating growth trend over the past 60 years. The maximum solar radiation can reach to 168.08 W/m$^2$ (1986) while the minimum solar radiation was 156.93 W/m$^2$ (1971). There is no obvious trend in the annual solar radiation variation in the Sanjiang Plain, with a decreasing trend after an increasing trend.

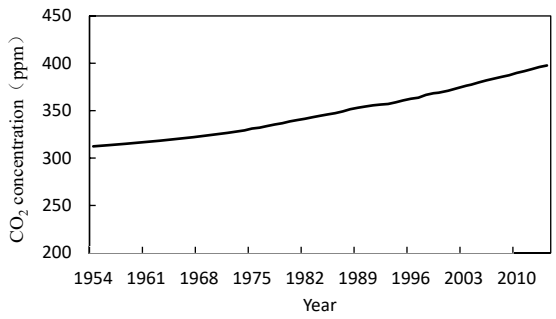


FIGURE 7
Changes of $CO_2$ concentration since 1954 in the Sanjiang Plain.

TABLE 1 The correlation coefficient between NPP and different climate factors.

| | Solar radiation | Temperature | Precipitation | $CO_2$ |
|---|---|---|---|---|
| *R* | 0.1266 | 0.6988 | 0.1703 | 0.5442 |

This study mapped the annual variation of $CO_2$ concentration in the Sanjiang Plain from 1954 to 2014 (as shown in Figure 7). Statistical analysis indicates that $CO_2$ concentration in the Sanjiang showed an obvious growth trend over the past 60 years, with an increase value of 85.3 ppm.

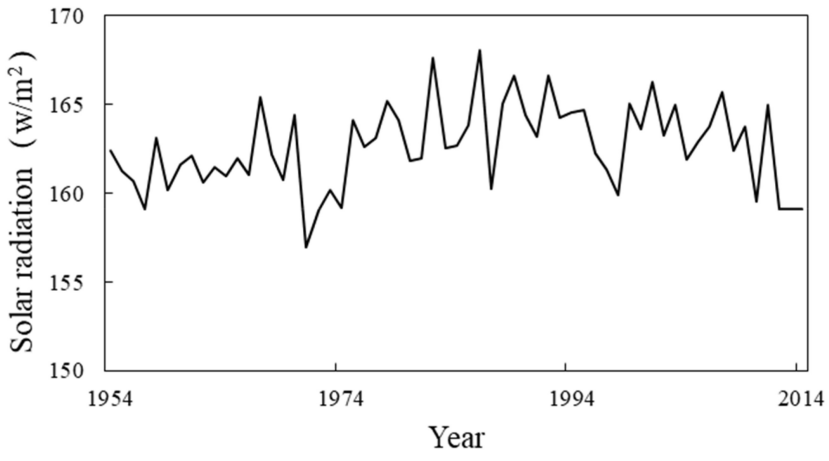


FIGURE 6
Changes of solar radiation since 1954 in the Sanjiang Plain.

It increased from 312.4 ppm in 1954 to 397.7 ppm in 2014, increasing by 21.45% in the last six decades.

## Relationship between net primary productivity and climate factors

### Correlation analysis

This study detected the correlation between NPP and different climate factors during the past six decades (as shown in **Table 1**). Results indicate that the average temperature had the largest correlation with NPP (0.6988) among four climate factors, followed by $CO_2$ (0.5442). The correlation coefficient between NPP and other two factors were relatively small, with a value of 0.1703 (precipitation) and 0.1266 (solar radiation), respectively. Results show that temperature made a great contribution to NPP increase in the marsh area in the Sanjiang Plain from 1954 to 2014. The increase of temperature promoted NPP growth.

### Influencing factors of spatial heterogeneity

The explanatory power of the main climate factors to the spatial heterogeneity of NPP in two stages was detected by the GDM method. A total of 19,466 sampling points in the study area were chosen as sampling points. The *p*-values of the explanatory power of each factor on the spatial heterogeneity of NPP were less than 0.001, indicating that the *q*-values of each climate factor were statistically significant (as shown in **Table 2**). Result indicated that solar radiation had the largest explanatory power in stage I (1954–1985) while temperature had the largest in stage II (1986–2014). The explanatory power of precipitation was the least both in stage I (1954–1985) and stage II (1986–2014). The explanatory power of each climate factor on spatial heterogeneity of NPP in stage I (1954–1985) was larger than that in stage II (1986–2014).

This study also analyzed the explanatory power of interactions between different climate factors on spatial heterogeneity of NPP (as shown in **Table 3**). Results indicated that the explanatory power of interactions between climate factors was stronger than that of single factor. In stage I, the explanatory powers of interaction between solar radiation and precipitation reached to 0.3634, which is more than twice that of the single factor. The explanatory power of the interaction between temperature and precipitation was 0.2958 while that of temperature and solar radiation was 0.2705, both of which are much larger than that of single factor. In stage II, the explanatory powers of interaction between solar radiation and precipitation reached to 0.2475, which is more than three times that of the single factor. The explanatory power of the interaction between temperature and precipitation was 0.2050 while that of temperature and solar radiation was 0.1943, both of which are much larger than single factor.

# Discussion

## The effect of climate changes on net primary productivity variation

The effect of temperature increase on NPP has two aspects: positive effect and negative effect (Brouwers and Coops, 2016; Madani et al., 2021; Ji et al., 2022). On one hand, temperature increase can prolong the growing season and enhance the efficiency of photosynthesis, thereby increasing NPP (Madani et al., 2021; Ji et al., 2022). On the other hand, it can increase water consumption and cause drought, leading to a negative effect on NPP growth (Osborne et al., 2000; Bilgili et al., 2020). Results indicate that the annual average temperature in Sanjiang Plain showed an upward trend. And there was a consistency between the growth trend of NPP and that of temperature, which shows that the increase of temperature has a positive effect on the growth of NPP in Sanjiang plain at middle and high latitudes. Global NPP is increased under the influence of climate warming generally, with NPP decreased in low latitudes and increased in middle and high latitudes (Hou et al., 2013; Tum et al., 2016; Gang et al., 2017; Yin et al., 2020). This study confirms that climate warming promotes the growth of NPP in middle and high latitudes. The influence of climate warming on NPP changes is manifested in two aspects. On the one hand, climate warming can directly affect photosynthesis and change NPP (Madani et al., 2021). On the other hand, climate warming can change the mineralization rate of soil nitrogen and soil water content, thus indirectly affecting NPP (Wan et al., 2005). The promotion of climate warming on NPP in Sanjiang Plain may be due to the promotion of vegetation fixation of more $CO_2$ under warming conditions, and the promotion of soil nitrogen mineralization rate. Although climate warming will reduce soil water content to a certain extent, which will lead to the decline of NPP. However, the study area is located in the humid area, which is less sensitive to the negative effect of water consumption caused by the rise of temperature than the arid/semi-arid area. In general, the increase of NPP caused by the increase of photosynthesis and soil nitrogen mineralization rate in the study area exceeded the decrease of NPP caused by the decrease of soil water content. Additionally, in the middle and high latitudes of the northern hemisphere, climate warming will prolong the vegetation growth season and increase vegetation activities, thus promoting the growth of NPP.

In the past 60 years, the increase of atmospheric $CO_2$ concentration has promoted the growth of NPP in the study area. As an important material of photosynthesis, $CO_2$ directly participates in photosynthesis and thus directly associated with vegetation NPP (Amthor, 1995; Running et al., 2000). The increase of atmospheric $CO_2$ concentration will increase the $CO_2$ flux of roots and the carbon supply of microorganisms, increase the demand for water and nitrogen in the process

TABLE 2 The explanatory power *q*-value of climate factors on the spatial heterogeneity of NPP.

| Stage | Explanatory power | Solar radiation | Precipitation | Temperature |
|---|---|---|---|---|
| Stage I | *q* | 0.1777 | 0.0988 | 0.1399 |
| | *P* | 0.000 | 0.000 | 0.000 |
| Stage II | *q* | 0.08228 | 0.0524 | 0.1166 |
| | *P* | 0.000 | 0.000 | 0.000 |

TABLE 3 The interaction between different climate factors.

| Stage | Explanatory power | Solar radiation | Precipitation | Temperature |
|---|---|---|---|---|
| | Solar radiation | 0.1777 | | |
| Stage I | Precipitation | 0.3634 | 0.0988 | |
| | Temperature | 0.2705 | 0.2958 | 0.1399 |
| | Solar radiation | 0.08228 | | |
| Stage II | Precipitation | 0.2475 | 0.0524 | |
| | Temperature | 0.1943 | 0.2050 | 0.1166 |

of plant photosynthesis, and lead to the enhancement of vegetation activities, thus promoting the increase of NPP (Amthor, 1995; Reich et al., 2006). Additionally, the change of $CO_2$ concentration can disturb the earth's radiation balance and affect the change of climate factors such as temperature, precipitation and relative humidity (Pörtner et al., 2005; Reich et al., 2006). The change of these climate factors will also have an impact on the NPP changes. Many studies have also indicated that the increase of $CO_2$ concentration can promote NPP growth (Amthor, 1995; Cao and Woodward, 1998; Schimel et al., 2000).

In the past 60 years, precipitation changes have promoted the growth of NPP in the study area. Wetlands are often characterized by perennial or seasonal ponding. If the precipitation is low, it will obviously have an important impact on their vegetation growth (Liu et al., 2015). This study finds that the annual average value of NPP in the years with higher precipitation (greater than average precipitation) is 29.59 TG c/yr, while the annual average value of NPP in the years with lower precipitation (greater than average precipitation) is 29.34 tgc/yr, which is lightly less than that in the years with higher precipitation. This is not completely consistent with previous studies. For example, Wang et al. (2011) pointed that the NPP of Qixinghe marshy wetland in Sanjiang Plain was negatively correlated with the annual precipitation (Wang et al., 2011). Because the water resources in this region were relatively sufficient, the better coordination of hydrothermal conditions in years with relatively dry climate led to the increase of vegetation evaporation and photosynthesis, as well as increasing accumulation of dry matter. This may be because the marshy wetland area in this study includes not only the original marsh, but also the areas that have been converted to other land use types. Vegetation growth has a strong association with solar radiation (Moreau et al., 2003; Fang et al., 2019; Zhou et al., 2021), but previous study paid less attention on effects of solar radiation on NPP variation of marsh area. This study indicated that radiation growth enhanced NPP increase in the past six decades, which is consistent with previous studies. And solar radiation also influenced the spatial heterogeneity of NPP, especially in stage I. Although the precipitation had the least explanatory power on the spatial heterogeneity of NPP, its interaction with solar radiation had the largest explanatory power both in two stages. Additionally, this study indicated that explanatory power of interactions between two climate factors was stronger than that of single factor. Therefore, asymmetric effects of interactions between climate factors on vegetation NPP should be given more attention in the future.

TABLE 4 The area (thousand ha) and percentage changes of marsh during 1954–2015 in the Sanjiang Plain.

| Year | 1954 | 1976 | 1986 | 2000 | 2015 |
|---|---|---|---|---|---|
| Area | 3770.12 | 2446.11 | 1119.14 | 1040.76 | 778.18 |
| Percentage | 34.71% | 22.52% | 10.30% | 9.58% | 7.17% |

## The effect of land cover changes on net primary productivity variation

In the past six decades, marsh in the Sanjiang Plain has been cultivated drastically. The marsh area decreased from 3770.12 in 1954 to 778.18 thousand ha in 2015, with the percentage decreased from 34.71% of the total area in 1954 to 7.17% in 2015 (**Table 4**). From 1954 to 1986, the percentage of marsh in the Sanjiang Plain decreased by 24.40%, with the value much larger than that between 1986 and 2015. The area of marsh decreased by 79.4% since 1954 in the Sanjiang Plain, with a value

about 2.99 million ha. Only 14% of the original marshy wetland was preserved in the last six decades. And 46% of the original marsh transformed to paddy filed while 27% of that converted to dry farmland. Large area of marsh has been reclaimed into dry farmland and then paddy field in the past six decades, leading to NPP changes. Landscape index analysis shows that the landscape fragmentation of marsh increased since the 1950s in the Sanjiang Plain (Yan and Zhang, 2019; Yan, 2020), also influencing carbon cycle and NPP changes. Previous studies indicated that LUCC in the Sangjiang Plain decreased NPP changes (Wang et al., 2009; Dong et al., 2015). The study of Sanjiang Plain from 2000 to 2005 showed that LUCC is the main factor affecting vegetation NPP, which directly leads to changes in regional NPP (Wang et al., 2009). Although NPP showed a general increasing trend in the Sanjiang Plain during 2000–2010, LUCC played a negative role in the NPP growth (Dong et al., 2015).

LUCC is an important reason that affects the carbon cycle process of terrestrial ecosystem and causes the change of carbon budget (Li et al., 2014; Chang et al., 2022b). On one hand, LUCC can directly affect the carbon cycle process by changing the vegetation types (Li et al., 2014). On the other hand, LUCC can cause changes in N deposition and $CO_2$ concentration, and then indirectly affect the carbon cycle process (Li et al., 2014; Lu et al., 2016; Zhao et al., 2020a). The research on the change of carbon budget caused by LUCC shows that the transformation between forest loss and urbanization usually reduced the carbon budget and farmland expansion can increase carbon budget in some regions (Hu and Wang, 2008; Fu et al., 2009; Yu et al., 2009; Chang et al., 2022b; Zhuang et al., 2022). For example, Yu et al. (2009) found that urbanization in Shenzhen city during 1999–2005 caused a loss of 321.51 Gg carbon. The increase of dry farmland decreased NPP in the Sanjiang plian from 2000 to 2010 (Dong et al., 2015). Study in Guangzhou indicated that conversion from wood grassland, shrublands/forests to croplands and the urban led to a large loss of NPP (Fu et al., 2013). In the past 60 years, the overall situation of LUCC in the study area is the large area loss of marsh, forest and grassland. LUCC in the marsh area in the past 60 years has a negative effect on NPP growth in the Sanjiang Plain. In the future, samples can be taken in areas where the marsh area that has not been reclaimed to exclude the impact of LUCC. Additionally, LUCC can influence temperature, precipitation, and radiation etc. (Davin and de Noblet-Ducoudre, 2010; Li et al., 2014; Cao et al., 2021). Therefore, the interactions between climate factors and LUCC should be paid more attention in the future.

## Conclusion

In our study, NPP increase was observed in the Sanjiang Plain in both stages (1954–1985 and 1986–2014) in the past six decades. Temperature had the largest correlation with NPP trends among four climate factors, followed by $CO_2$. Solar Radiation had the largest explanatory power on the spatial heterogeneity of NPP among three climate factors before 1985. After 1985, temperature played an important role in leading the spatial heterogeneity of NPP. The explanatory power of precipitation changes was relatively smaller than other two factor on NPP changes between two stages. However, the explanatory power of its interactions with solar radiation was much stronger than that of single factor. Future study should pay more attention to the interactions between climate factors as well as the interactions between different factors. Our results suggest the importance of association between climate factors and NPP variations for predicting marsh carbon storage variation.

## Data availability statement

The original contributions presented in this study are included in the article/supplementary material, further inquiries can be directed to the corresponding author.

## Author contributions

FY contributed to conception and design of the study, organized the database, performed the statistical analysis, wrote the first draft of the manuscript, and wrote sections of the manuscript.

## Funding

This research was funded by the National Natural Science Foundation of China (grant no. 41901383).

## Conflict of interest

The author declares that the research was conducted in the absence of any commercial or financial relationships that could be construed as a potential conflict of interest.

## Publisher's note

# References


Amthor, J. S. (1995). Terrestrial higher-plant response to increasing atmospheric [CO2] in relation to the global carbon cycle. *Glob. Change Biol.* 1, 243–274. doi: 10.1111/j.1365-2486.1995.tb00025.x

Bai, L., Jiang, L., Yang, D. Y., and Liu, Y. B. (2019). Quantifying the spatial heterogeneity influences of natural and socioeconomic factors and their interactions on air pollution using the geographical detector method: A case study of the Yangtze River Economic Belt, China. *J. Clean. Prod.* 232, 692–704. doi: 10.1016/j.jclepro.2019.05.342

Bilgili, B. C., Ersahin, S., Kavakligil, S. S., and Oner, N. (2020). Net primary productivity of a mountain forest ecosystem as affected by climate and topography. *Cerne* 26, 356–368. doi: 10.1590/01047760202026032730

Brouwers, N. C., and Coops, N. C. (2016). Decreasing net primary production in forest and shrub vegetation across southwest Australia. *Ecol. Indic.* 66, 10–19. doi: 10.1016/j.ecolind.2016.01.010

Cao, S. P., Zhang, L. F., He, Y., Zhang, Y. L., Chen, Y., Yao, S., et al. (2022b). Effects and contributions of meteorological drought on agricultural drought under different climatic zones and vegetation types in Northwest China. *Sci. Total Environ.* 821:153270. doi: 10.1016/j.scitotenv.2022.153270

Cao, D., Zhang, J. H., Han, J. Q., Zhang, T., Yang, S. S., Wang, J. W., et al. (2022a). Projected increases in global terrestrial net primary productivity loss caused by drought under climate change. *Earths Future* 10:e2022EF002681. doi: 10.1029/2022EF002681

Cao, F., Dan, L., Ma, Z., and Gao, T. (2021). The impact of land use and land cover change on regional climate over East Asia during 1980–2010 using a coupled model. *Theor. Appl. Climatol.* 145, 549–565. doi: 10.1007/s00704-021-03629-6

Cao, M., and Woodward, F. I. (1998). Net primary and ecosystem production and carbon stocks of terrestrial ecosystems and their responses to climate change. *Glob. Change Biol.* 4, 185–198. doi: 10.1046/j.1365-2486.1998.00125.x

Caplan, J. S., Hager, R. N., Megonigal, J. P., and Mozdzer, T. J. (2015). Global change accelerates carbon assimilation by a wetland ecosystem engineer. *Environ. Res. Lett.* 10:115006. doi: 10.1088/1748-9326/10/11/115006

Chang, J. J., Gong, L., Zeng, F. J., Xue, J., Mao, D. L., Cao, Y. X., et al. (2022a). Using hydro-climate elasticity estimator and geographical detector method to quantify the individual and interactive impacts on NDVI in oasis-desert ecotone. *Stoch. Environ. Res. Risk Assess.* 2022, 1–18. doi: 10.1007/s00477-022-02184-4

Chang, X. Q., Xing, Y. Q., Wang, J. Q., Yang, H., and Gong, W. S. (2022b). Effects of land use and cover change (LUCC) on terrestrial carbon stocks in China between 2000 and 2018. *Resour. Conserv. Recycl.* 182:106333. doi: 10.1016/j.resconrec.2022.106333

Chen, Z. T., Liu, H. Y., Xu, C. Y., Wu, X. C., Liang, B. Y., Cao, J., et al. (2022). Deep learning projects future warming-induced vegetation growth changes under SSP scenarios. *Adv. Clim. Change Res.* 13, 251–257. doi: 10.1016/j.accre.2022.01.007

Dargie, G. C., Lewis, S. L., Lawson, I. T., Mitchard, E. T. A., Page, S. E., Bocko, Y. E., et al. (2017). Age, extent and carbon storage of the central Congo Basin peatland complex. *Nature* 542, 86–90. doi: 10.1038/nature21048

Davin, E. L., and de Noblet-Ducoudre, N. (2010). Climatic impact of global-scale deforestation: Radiative versus nonradiative processes. *J. Clim.* 23, 97–112. doi: 10.1175/2009JCLI3102.1

Deng, J. M., Xiao, T. F., Fan, W. J., Ning, Z. P., and Xiao, E. Z. (2022). Relevance of the microbial community to Sb and as biogeochemical cycling in natural wetlands. *Sci. Total Environ.* 818:151826. doi: 10.1016/j.scitotenv.2021.151826

Dong, G., Bai, J., Yang, S., Wu, L., Cai, M., Zhang, Y., et al. (2015). The impact of land use and land cover change on net primary productivity on China's Sanjiang Plain. *Environ. Earth Sci.* 74, 2907–2917. doi: 10.1007/s12665-015-4318-6

Fang, H. L., Baret, F., Plummer, S., and Schaepman-Strub, G. (2019). An overview of global leaf area index (LAI): methods, products, validation, and applications. *Rev. Geophys.* 57, 739–799. doi: 10.1029/2018RG000608

Farquhar, G. D., von Caemmerer, S., and Berry, J. A. (1980). A biochemical model of photosynthetic $CO_2$ assimilation in leaves of C3 species. *Planta* 149, 78–90.

Fu, C., Yu, G. R., Fang, H. J., and Wang, Q. F. (2009). Effects of land use and cover change on terrestrial carbon balance of China. *Prog. Geogr.* 31, 88–96.

Fu, Y., Lu, X., Zhao, Y., Zeng, X., and Xia, L. (2013). Assessment impacts of weather and land use/land cover (LULC) change on Urban vegetation net primary productivity (NPP): A case study in Guangzhou, China. *Remote Sens.* 5, 4125–4144. doi: 10.3390/rs5084125

Gang, C. C., Zhang, Y. Z., Wang, Z. Q., Chen, Y. Z., Yang, Y., Li, J. L., et al. (2017). Modeling the dynamics of distribution, extent, and NPP of global terrestrial ecosystems in response to future climate change. *Glob. Planet. Change* 148, 153–165. doi: 10.1016/j.gloplacha.2016.12.007

Guo, G. H., Li, K., Zhang, D. G., and Lei, M. (2022). Quantitative source apportionment and associated driving factor identification for soil potential toxicity elements via combining receptor models, SOM, and geo-detector method. *Sci. Total Environ.* 830:154721. doi: 10.1016/j.scitotenv.2022.154721

Hou, S. S., Lei, L. P., and Zeng, Z. C. (2013). The response of global net primary productivity (NPP) to CO2 increasing and climate change: Evaluation of coupled model simulations. *J. Food Agric. Environ.* 11, 937–944.

Hu, H. F., and Wang, G. G. (2008). Changes in forest biomass carbon storage in the South Carolina Piedmont between 1936 and 2005. *Forest Ecol. Manag.* 255, 1400–1408. doi: 10.1016/j.foreco.2007.10.064

Ji, Y. H., Zhou, G. S., Wang, S. D., and Zhao, J. (2022). Warm-Wet climate trend enhances net primary production of the main ecosystems in China during 2000-2021. *Atmosphere* 13:738. doi: 10.3390/atmos13050738

Li, B. B., Fang, X. Q., Ye, Y., and Zhang, X. Z. (2014). Carbon emissions induced by cropland expansion in Northeast China during the past 300 years. *Sci. China Earth Sci.* 57, 2259–2268. doi: 10.1007/s11430-014-4894-4

Li, Y. N., Shao, L. Y., Yan, Z. M., Hou, H. H., Tang, Y., and Large, D. J. (2018). Net primary productivity and its control of the Middle Jurassic peatlands: An example from the southern Junggar coalfield. *Sci. China Earth Sci.* 61, 1633–1643. doi: 10.1007/s11430-017-9263-4

Liu, J. Y., Deng, X. Z., Liu, M. L., and Zhang, S. W. (2002). Study on the spatial patterns of land-use change and analyses of driving forces in Northeastern China during 1990-2000. *Chin. Geogr. Sci.* 12, 299–308. doi: 10.1007/s11769-002-0033-9

Liu, J. Y., Kuang, W. H., Zhang, Z. X., Xu, X. L., Qin, Y. W., Ning, J., et al. (2014). Spatiotemporal characteristics, patterns, and causes of land-use changes in China since the late 1980s. *J. Geogr. Sci.* 24, 195–210. doi: 10.1007/s11442-014-1082-6

Liu, J. Y., Liu, M. L., Zhuang, D. F., Zhang, Z. X., and Deng, X. Z. (2003). Study on spatial pattern of land-use change in China during 1995-2000. *Sci. China Ser. D Earth Sci.* 46, 373–384.

Liu, J. Y., Zhang, Z. X., Xu, X. L., Kuang, W. H., Zhou, W. C., Zhang, S. W., et al. (2010). Spatial patterns and driving forces of land use change in China during the early 21st century. *J. Geogr. Sci.* 20, 483–494. doi: 10.1007/s11442-010-0483-4

Liu, X., Wang, Y. Y., and Fan, Y. Q. (2015). Risk assessment of net primary productivity for wetland under climate change scenario: A case study of the *Calamagrostis angustifolia* wetland at Fujin in Sanjiang Plain, Northeast China. *China Environ. Sci.* 35, 3762–3770.

Lu, X. H., Jiang, H., Zhang, X. Y., and Jin, J. X. (2016). Relationship between nitrogen deposition and LUCC and its impact on terrestrial ecosystem carbon budgets in China. *Sci. China Earth Sci.* 59, 2285–2294. doi: 10.1007/s11430-015-5277-0

Madani, N., Parazoo, N. C., Kimball, J. S., Reichle, R. H., Chatterjee, A., Watts, J. D., et al. (2021). The impacts of climate and wildfire on ecosystem gross primary productivity in Alaska. *J. Geophys. Res. Biogeosci.* 126:e2020JG006078. doi: 10.1029/2020JG006078

Mao, D. H., Wang, Z. M., Li, L., Song, K. S., and Jia, M. M. (2014). Quantitative assessment of human-induced impacts on marshes in Northeast China from 2000 to 2011. *Ecol. Eng.* 68, 97–104. doi: 10.1016/j.ecoleng.2014.03.010

Marthews, T. R., Dadson, S. J., Clark, D. B., Blyth, E. M., Hayman, G. D., Yamazaki, D., et al. (2022). Inundation prediction in tropical wetlands from JULES-CaMa-Flood global land surface simulations. *Hydrol. Earth Syst. Sci.* 26, 3151–3175. doi: 10.5194/hess-26-3151-2022

Mitsch, W. J., and Gosselink, J. G. (2000). The value of wetlands: Importance of scale and landscape setting. *Ecol. Econ.* 35, 25–33. doi: 10.1016/S0921-8009(00)00165-8

Monge-Salazar, M. J., Tovar, C., Cuadros-Adriazola, J., Baiker, J. R., Montesinos-Tubee, D. B., Bonnesoeur, V., et al. (2022). Ecohydrology and ecosystem services of a natural and an artificial bofedal wetland in the central Andes. *Sci. Total Environ.* 838:155968. doi: 10.1016/j.scitotenv.2022.155968

Moreau, S., Bosseno, R., Gu, X. F., and Baret, F. (2003). Assessing the biomass dynamics of Andean bofedal and totora high-protein wetland grasses from NOAA/AVHRR. *Remote Sens. Environ.* 85, 516–529. doi: 10.1016/S0034-4257(03)00053-1

O'Connor, F. M., Boucher, O., Gedney, N., Jones, C. D., Folberth, G. A., Coppell, R., et al. (2010). Possible role of wetlands, permafrost, and methane hydrates in the methane cycle under future climate change: A review. *Rev. Geophys.* 48:RG4005. doi: 10.1029/2010RG000326

Osborne, C. P., Mitchell, P. L., Sheehy, J. E., and Woodward, F. I. (2000). Modelling the recent historical impacts of atmospheric CO2 and climate change on Mediterranean vegetation. *Glob. Change Biol.* 6, 445–458. doi: 10.1046/j.1365-2486.2000.00336.x

Pörtner, H. O., Langenbuch, M., and Michaelidis, B. (2005). Synergistic effects of temperature extremes, hypoxia, and increases in CO2 on marine animals: From Earth history to global change. *J. Geophys. Res.* 110:C09S10. doi: 10.1029/2004JC002561

Qiu, B. W., Ye, Z. Y., Chen, C. C., Tang, Z. H., Chen, Z. Q., Huang, H. Y., et al. (2022). Dense canopies browning overshadowed by global greening dominant in sparse canopies. *Sci. Total Environ.* 826:154222. doi: 10.1016/j.scitotenv.2022.154222

Reich, P. B., Hungate, B. A., and Luo, Y. (2006). Carbon-nitrogen interactions in terrestrial ecosystems in response to rising atmospheric carbon dioxide. *Annu. Rev. Ecol. Evol. Syst.* 37, 611–636. doi: 10.1146/annurev.ecolsys.37.091305.110039

Ren, Z. G., Tian, Z. H., Wei, H. T., Liu, Y., and Yu, Y. P. (2022). Spatiotemporal evolution and driving mechanisms of vegetation in the Yellow River Basin, China during 2000-2020. *Ecol. Indic.* 138:108832. doi: 10.1016/j.ecolind.2022.108832

Roulet, N. T. (2000). Peatlands, carbon storage, greenhouse gases, and the Kyoto Protocol: Prospects and significance for Canada. *Wetlands* 20, 605–615. doi: 10.1672/0277-5212(2000)020[0605:PCSGGA]2.0.CO;2

Running, S. W., Thornton, P. E., Nemani, R., and Glassy, J. M. (2000). "Global terrestrial gross and net primary productivity from the earth observing system," in *Methods in ecosystem science*, eds O. E. Sala, R. B. Jackson, H. A. Mooney, and R. W. Howarth (New York, NY: Springer), 44–57. doi: 10.1007/978-1-4612-1224-9_4

Schimel, D., Melillo, J., Tian, H. Q., McGuire, A. D., Kicklighter, D., Kittel, T., et al. (2000). Contribution of increasing CO2 and climate to carbon storage by ecosystems in the United States. *Science* 287, 2004–2006. doi: 10.1126/science.287.5460.2004

Shen, X. J., Liu, B. H., Jiang, M., Wang, Y. J., Wang, L., Zhang, J. Q., et al. (2021). Spatiotemporal change of Marsh vegetation and its response to climate change in China From 2000 to 2019. *J. Geophys. Res. Biogeosci.* 126:e2020JG006154. doi: 10.1029/2020JG006154

Shen, X. J., Liu, B. H., Xue, Z. S., Jiang, M., Lu, X. G., and Zhang, Q. (2019). Spatiotemporal variation in vegetation spring phenology and its response to climate change in freshwater marshes of Northeast China. *Sci. Total Environ.* 666, 1169–1177. doi: 10.1016/j.scitotenv.2019.02.265

Shestakova, T. A., Gutierrez, E., Valeriano, C., Lapshina, E., and Voltas, J. (2019). Recent loss of sensitivity to summer temperature constrains tree growth synchrony among boreal Eurasian forests. *Agric. Forest Meteorol.* 268, 318–330. doi: 10.1016/j.agrformet.2019.01.039

Sun, H. Z., Chen, Y. B., Xiong, J. N., Ye, C. H., Yong, Z. W., Wang, Y., et al. (2022). Relationships between climate change, phenology, edaphic factors, and net primary productivity across the Tibetan Plateau. *Int. J. Appl. Earth Observ. Geoinform.* 107:102708. doi: 10.1016/j.jag.2022.102708

Tercero, M. D., Alvarez-Rogel, J., Conesa, H. M., Parraga-Aguado, I., and Gonzalez-Alcaraz, M. N. (2017). Phosphorus retention and fractionation in an eutrophic wetland: A one-year mesocosms experiment under fluctuating flooding conditions. *J. Environ. Manag.* 190, 197–207. doi: 10.1016/j.jenvman.2016.12.060

Thomaz, S. M. (2021). Ecosystem services provided by freshwater macrophytes. *Hydrobiologia* 2021, 1–21. doi: 10.1007/s10750-021-04739-y

Tong, L. L., Mao, X. F., Song, X. H., Wei, X. Y., Tang, W. J., Deng, Y. F., et al. (2022). PSR-BP neural network-based health assessment of the Huangshui Plateau Urban Wetlands in China. *Front. Ecol. Evol.* 10:866597. doi: 10.3389/fevo.2022.866597

Tum, M., Zeidler, J. N., Gunther, K. P., and Esch, T. (2016). Global NPP and straw bioenergy trends for 2000-2014. *Biomass Bioenergy* 90, 230–236. doi: 10.1016/j.biombioe.2016.03.040

Vivian, L. M., Godfree, R. C., Colloff, M. J., Mayence, C. E., and Marshall, D. J. (2014). Wetland plant growth under contrasting water regimes associated with river regulation and drought: implications for environmental water management. *Plant Ecol.* 215, 997–1011. doi: 10.1007/s11258-014-0357-4

Wan, S., Hui, D., Wallace, L., and Luo, Y. (2005). Direct and indirect effects of experimental warming on ecosystem carbon processes in a tallgrass prairie. *Glob. Biogeochem. Cycles* 19:GB2014. doi: 10.1029/2004GB002315

Wang, F., Gao, Y. G., and Bai, M. Q. (2011). Impact of climate change on natural vegetation net primary productivity in Qixing River Wetland ecosystem from 1961-2008. *Chin. Agric. Sci. Bull.* 27, 257–262.

Wang, J. F., Li, X. H., Christakos, G., Liao, Y. L., Zhang, T., Gu, X., et al. (2010). Geographical detectors-based health risk assessment and its application in the neural tube defects study of the Heshun Region, China. *Int. J. Geogr. Inf. Sci.* 24, 107–127. doi: 10.1080/13658810802443457

Wang, Y. J., Shen, X. J., Jiang, M., Tong, S. Z., and Lu, X. G. (2022). Daytime and nighttime temperatures exert different effects on vegetation net primary productivity of marshes in the western Songnen Plain. *Ecol. Indic.* 137:108789. doi: 10.1016/j.ecolind.2022.108789

Wang, Z. M., Guo, Z. X., Song, K. S., Liu, D. W., Zhang, B., Zhang, S. Q., et al. (2009). Effects of land use/cover change on net primary productivity of Sanjiang Plain, during 2000-2005. *J. Nat. Resour.* 24, 136–146.

Wang, Z. M., Mao, D. H., Li, L., Jia, M. M., Dong, Z. Y., Miao, Z. H., et al. (2015). Quantifying changes in multiple ecosystem services during 1992-2012 in the Sanjiang Plain of China. *Sci. Total Environ.* 514, 119–130. doi: 10.1016/j.scitotenv.2015.01.007

Xiao, D. R., Deng, L., Kim, D. G., Huang, C. B., and Tian, K. (2019). Carbon budgets of wetland ecosystems in China. *Glob. Change Biol.* 25, 2061–2076. doi: 10.1111/gcb.14621

Yan, F. Q. (2017). *Spatial and temporal variation of net primary productivity of the Sanjiang plain and its influencing factors doctor*. Beijing: University of Chinese Academy of Sciences.

Yan, F. Q. (2020). Large-scale marsh loss reconstructed from satellite data in the small Sanjiang plain since 1965: Process, pattern and driving force. *Sensors* 20:1036. doi: 10.3390/s20041036

Yan, F. Q., and Zhang, S. W. (2019). Ecosystem service decline in response to wetland loss in the Sanjiang Plain, Northeast China. *Ecol. Eng.* 130, 117–121. doi: 10.1016/j.ecoleng.2019.02.009

Yin, S. Y., Wu, W. J., Zhao, X. J., Gong, C., Li, X. W., and Zhang, L. (2020). Understanding spatiotemporal patterns of global forest NPP using a data-driven method based on GEE. *PLoS One* 15:e0230098. doi: 10.1371/journal.pone.0230098

Yu, D., Shao, H., Shi, P., Zhu, W., and Pan, Y. (2009). How does the conversion of land cover to urban use affect net primary productivity? A case study in Shenzhen city, China. *Agric. Forest Meteorol.* 149, 2054–2060. doi: 10.1016/j.agrformet.2009.07.012

Zarei, A., Chemura, A., Gleixner, S., and Hoff, H. (2021). Evaluating the grassland NPP dynamics in response to climate change in Tanzania. *Ecol. Indic.* 125:107600. doi: 10.1016/j.ecolind.2021.107600

Zhang, X. L., and Zhao, Y. (2018). Identification of the driving factors' influences on regional energy-related carbon emissions in China based on geographical detector method. *Environ. Sci. Pollut. Res.* 25, 9626–9635. doi: 10.1007/s11356-018-1237-6

Zhang, Z. S., Craft, C. B., Xue, Z. S., Tong, S. Z., and Lu, X. G. (2016). Regulating effects of climate, net primary productivity, and nitrogen on carbon sequestration rates in temperate wetlands, Northeast China. *Ecol. Indic.* 70, 114–124. doi: 10.1016/j.ecolind.2016.05.041

Zhao, Y. J., Deng, Q. Y., Lin, Q., Zeng, C. Y., and Zhong, C. (2020b). Cadmium source identification in soils and high-risk regions predicted by geographical detector method. *Environ. Pollut.* 263:114338. doi: 10.1016/j.envpol.2020.114338

Zhao, J., Cohen, J. B., Chen, Y. T., Cui, W. H., Cao, Q. Q., Yang, T. F., et al. (2020a). High-resolution spatiotemporal patterns of China's FFCO2 emissions under the impact of LUCC from 2000 to 2015. *Environ. Res. Lett.* 15:044007. doi: 10.1088/1748-9326/ab6edc

Zhou, Y. Y., Yue, D. X., Li, C., Mu, X. L., and Guo, J. J. (2021). Identifying the spatial drivers of net primary productivity: A case study in the Bailong River Basin, China. *Glob. Ecol. Conserv.* 28:e01685. doi: 10.1016/j.gecco.2021.e01685

Zhuang, Q. W., Shao, Z. F., Li, D. R., Huang, X., Cai, B. W., Altan, O., et al. (2022). Unequal weakening of urbanization and soil salinization on vegetation production capacity. *Geoderma* 411:115712. doi: 10.1016/j.geoderma.2022.115712

frontiers | Frontiers in Ecology and Evolution

TYPE Original Research
PUBLISHED 21 September 2022
DOI 10.3389/fevo.2022.1005677



OPEN ACCESS

EDITED BY
Chuanyu Gao,
Northeast Institute of Geography and Agroecology (CAS), China

REVIEWED BY
Jiang Bao Xia,
Binzhou University, China
Hongli Song,
Linyi University, China

*CORRESPONDENCE
JunBao Yu
yu.junbao@gmail.com

SPECIALTY SECTION
This article was submitted to Conservation and Restoration Ecology, a section of the journal Frontiers in Ecology and Evolution

RECEIVED 28 July 2022
ACCEPTED 05 September 2022
PUBLISHED 21 September 2022

CITATION
Wang XH, Zou YH, Zhu T, Guan B, Yang JS and Yu JB (2022) The effects of hydrological connectivity blocking on *Suaeda salsa* development in the Yellow River Delta, China. *Front. Ecol. Evol.* 10:1005677. doi: 10.3389/fevo.2022.1005677



# The effects of hydrological connectivity blocking on *Suaeda salsa* development in the Yellow River Delta, China

XueHong Wang[1,2], YuHan Zou[1,2], Tao Zhu[1,2], Bo Guan[1,2], JiSong Yang[1,2] and JunBao Yu[1,2]*

[1]The Institute for Advanced Study of Coastal Ecology, Ludong University, Yantai, Shandong, China, [2]Key Laboratory of Ecological Restoration and Conservation of Coastal Wetlands in Universities of Shandong, Ludong University, Yantai, Shandong, China

Blocking of hydrological connectivity could greatly impact the sediment deposition process and change water and salinity conditions, which in turn affect plant germination, growth, and development in delta wetlands. A 2-year experiment, which included the effects of soil burial, water, and salinity on germination, growth, and production, was conducted to examine the function of hydrological connectivity blocking on the development of *Suaeda salsa*, a halophyte species. The results demonstrated that soil burial, water, and salinity all had significant effects on seed germination, plant growth, and production ($p < 0.05$). Seed germination decreased as soil buried depth increased (< 4 cm), and seeds did not germinate successfully when the buried depth was > 4 cm. Seed germination was the highest at 0 cm burial. However, moderate burial was beneficial for seedling emergence; therefore, the survival rate was the lowest when seeds were distributed at the surface (0 cm). Water and salinity both significantly affected the germination, growth, and productivity of *S. salsa*. Moderate salinity (10–20 g/kg) and fluctuating water (0–10 cm water depth) were suitable for seed germination and plant growth. Low salinity (< 10 g/kg), High salinity (>20 g/kg), drought, and high water levels (long-term flooding with water depth > 10 cm) were not conducive to the growth of *S. salsa*, and biomass and seed yield were also reduced. As a halophyte, salinity that is too low or too high is unsuitable for *S. salsa* population. Water and salinity also significantly affected *S. salsa* population ($p < 0.05$). In particular, water can offset the hazards of high salt concentrations. Blocking of hydrological connectivity can influence seed germination, yield, and vitality. In this case, *S. salsa* may have died out from the coastal wetland due to the lack of hydrological connectivity restoration.

KEYWORDS

**hydrological connectivity blocking, seed germination, seed yield and vitality, *Suaeda salsa*, the Yellow River Delta**

# Introduction

Hydrologic connectivity is a hydrologic process that supports the transfer of mass and energy between or among different water bodies and/or locations (soils, atmosphere, and vegetation) across a landscape (Lexartza-Artza and Wainwright, 2009; Bracken et al., 2013). Complete hydrological connectivity cannot only promote the cycle of energy and nutrients but also provide important habitats for animals and plants (Covino, 2017; Shao et al., 2019; Zheng et al., 2022). Wetland ecosystems with good hydrological connections can keep nutrients in the water body relatively stable in a mutable external environment and play a significant role in maintaining biodiversity (Noe et al., 2019; Norton et al., 2022). Hydrological connectivity is particularly important in delta wetlands, with intense interactions between saline and fresh water (Liu et al., 2020; Cui et al., 2022). In this context, delta wetlands are not only the habitat of many migratory waterfowl and are important for the protection base of biodiversity, but they also provide a buffer zone to maintain the dynamic balance of sea and land. They play a unique role in the material cycle, energy flow, and information transmission between rivers and oceans (Liu et al., 2021).

*Suaeda salsa* community is the main vegetation and the only pioneer plant in the salt marsh in the Yellow River Delta (YRD), China. It is mainly distributed in the transitional zone from land to beach, and provides an important habitat for birds and macrobenthos (Yu et al., 2012). Seed germination of *S. salsa* is highly susceptible to environmental factors such as water depth, salinity, and burial depth (Yu et al., 2012; Wang F. et al., 2015; Müller et al., 2019. Therefore, the distribution and growth of *S. salsa* may be vulnerable to changes in hydrological connectivity. In recent years, due to climate change and human activities such as roads and dams, the hydrological connectivity of the Yellow River has been seriously affected, the sediment transport process has been blocked, and the water-salt-sediment environment of coastal wetlands has also changed significantly (Wang S. et al., 2015; Saunders et al., 2016; Li et al., 2021). The amount of sediment entering the sea has decreased by 89% over the past 50 years, which has decreased the deposition rate of the YRD. Siltation and erosion in the estuary area have been altered, the amount of fresh water and salt water decreased dramatically, and soil salinity increased accordingly (Wang S. et al., 2015; Xue et al., 2022). Consequently, the salt marsh habitats of the YRD had deteriorated or many vegetation types had dried out (Liu, 2020). At the same time, the area of *S. salsa* shows a decreasing trend since 2006, and the dominance degree of *S. salsa* is decreasing continuously and the degree of fragmentation is severe (Zhang et al., 2022). Therefore, analyzing the ecological effects of dialectical hydrological connectivity on the development of *S. salsa* is of great significance.

Once hydrological connectivity blocking occurs in a delta, its effects on *S. salsa* community are unpredictable; hence, a greenhouse experiment was conducted to test it. In this experiment, seed germination and growth of *S. salsa* were subjected to different conditions that represent the situation of hydrological connectivity blocking. The purpose of the study was to solve those questions: (1) Do the hydrological connectivity blocking have negative or positive effect on *S. salsa* development? (2) What is the way that hydrological connectivity blocking affects *S. salsa* development? The results can provide valuable implications for the management of hydrological system and the restoration of degraded wetlands in the YRD.

# Materials and methods

## Site description

The study area is located in the YRD (118°3381811°2081, 37°353781°12378118y Dongying City, Shandong Province, China. The study area has a warm temperate continental monsoon climate, with distinctive seasons and rainy summers. The average annual temperature is 12.1°C. The frost-free period lasts 196 d per year in this region. The annual average rainfall in the study area is 551.6 mm, whereas the annual average evaporation is 1,962 mm. Approximately 70% of the precipitation occurs from June to August. Surface water in this area is mainly affected by precipitation and upriver water, particularly by the water-sediment regulation of the Yellow River at the end of June since 2002. The main soil types are tidal and salt soil. *S. salsa* and *Phragmites australis* are dominant species in the YRD (Guan et al., 2020).

## Experiment design

### Seed preparation

Fully developed seeds of *S. salsa* local genotypes were collected in October 2019 from the YRD National Natural Reserve. All seeds were kept under dark and dry conditions at 4°C until the start of the germination experiments. Soil for the experiment was collected from a depth of 20 cm near the YRD in 2019. All experiments were conducted in a greenhouse located at Ludong University, China. At the beginning of the experiment, seeds were surface-sterilized in an aqueous solution of 0.1% $KMnO_4$ for 10 min to avoid fungal attack, and subsequently rinsed with distilled water before being used in seed germination experiments.

#### Experiment 1: Effects of soil burial depth on seed germination in 2019

Germination experiments at different buried depths were conducted in a barrel (radius: 5 cm and height: 15 cm). Seeds were germinated at 0 cm (M0), 1 cm (M1), 2 cm (M2), 4 cm (M4), and 6 cm (M6) buried depths, respectively. The

soil was collected from the YRD. The salinity, water content, bulk density, electrical conductivity and pH of the initial experimental soils were 1.12 g/kg, 27.18%, 1.09 g/cm$^3$, 478 μm/cm, and 8.92, respectively. For each treatment, there were three replicates of 50 seeds each. During seed germination in buried soil, seeds were irrigated with distilled water to maintain saturation. All seeds were subjected to an alternating diurnal regime of 12 h of light at 25°C and 12 h of darkness at 15°C for 21 days. Seeds were considered germinated when the radicle protruded 1 mm from seed coat. Germination was recorded daily for 14 days, and seedling survival was recorded at the end of the experiment. The entire experiment lasted 4 weeks.

### Experiment 2: Effects of water and salt on germination and growth of *Suaeda salsa* in 2019

After the burial experiment, *S. salsa* seeds were planted in a barrel (radius: 15 cm and height: 35 cm) at a depth of 1 cm (according to the result of the soil burial experiment) to investigate the effects of the water-salt gradient on their germination and growth. The experiment began with three water treatments [long-term flooding (5–15 cm, F), periodic flooding (0–10 cm, S), and long-term drought (drought to saturated, D)], and four salinity treatments (i.e., 0, 10, 20, and 30 g/kg) in an orthogonal design. Salinity was controlled by adding a sea salt solution (obtained from seawater), in which $Na^+$ and $Cl^-$ were the most important ions (**Table 1**). Treatment D was carried out every 7 d. Treatment S was injected twice daily, and water was emptied after 2 h of water injection. Water control of the F treatment was performed every 2 d. Percent germination was recorded every day. A seed was considered germinated when the coleoptiles were elongated to 1 mm. The entire experiment lasted 16 weeks, and height, density, biomass, content of $Na^+$ and $Cl^-$ in each part were recorded and examined at the end.

### Experiment 3: Germination of seeds produced in experiment 2 in 2020

Germination experiments were conducted in a dish (radius: 5 cm). Seeds were germinated under saturated conditions at 10 g/kg salinity (the ideal germination condition). In this experiment, all seeds produced in experiment 2 were used in this experiment without replicates. During seed germination, the seeds were irrigated with distilled water to maintain moisture. The experiment lasted for 21 days. Percent germination was recorded daily. Seeds were considered germinated when the coleoptiles were elongated to 1 mm.

TABLE 1 Concentrations of main salt ions in the Yellow River Delta (Unit: mg/kg).

| $Na^+$ | $Mg^{2+}$ | $K^+$ | $Ca^{2+}$ | $Cl^-$ | $HCO^{3-}$ | $SO_4^{2-}$ | $CO_3^{2-}$ |
|---|---|---|---|---|---|---|---|
| 387,210 | 510 | 66.5 | 1232.5 | 433,100 | 175,680 | 4115.5 | 0 |

## Data analysis

Statistical analyses were performed using SPSS 20 and Origin 9.2. One-way analysis of variance (ANOVA) was used to determine the effects of burial depth, water regime, and salinity on the germination and growth of *S. salsa*. To meet the assumptions of homoscedasticity, some growth and photosynthetic parameters were log-transformed or square-root transformed. Before the analyses, graphs with residuals were applied to examine the rationality of the model assumptions and the reliability of the data. Multiple comparisons of means were performed using Duncan's test; different letters in **Figures 1**, **2** indicate significant differences at a significance level of 0.05. Values represent the mean ± SE of three replicates.

# Results

## Effects of soil burial on the germination and survival of *Suaeda salsa*

Analysis of differences indicated that soil burial depth had significant negative effects on germination percent ($p < 0.01$). As the burial depth increased, the seed germination percent decreased gradually (**Figure 1A**). Seed germination percent was the highest at M0. When the burial depth was ≥ 4 cm, there was no seed germination. However, the seedling survival percent changed significantly (**Figure 1B**). The survival percent at M1 was the highest, followed by the germination rates at M2 and M0 treatments. The survival percent were not significantly different between burial depths of M1 and M2.

## Effects of water depth and salinity on the germination and survival of *Suaeda salsa*

Although *S. salsa* is a halophyte, salinity and water both showed significant effects on its germination and growth ($p < 0.01$). The germination percent of *S. salsa* decreased as soil salinity increased, and high salinity was detrimental for seed germination. After 4-week growth, the seedling survival percent was slightly lower than the seed germination percent in all treatments (**Figures 2A,B**). Water significantly affected germination of *S. salsa* ($p < 0.01$). At the period of seed germination, the germination percent was higher in F and S, especially in S. In treatment D, the seed germination percent was the lowest, even at 0 g/kg salinity. In treatment S, except for the 30 g/kg salinity, the seed germination percent were similar. In treatment F, the seed germination percent at 10 g/kg salinity was the highest, even at 30 g/kg salinity, and the germination percent was up to 30%. Subjected to treatments S and D, the

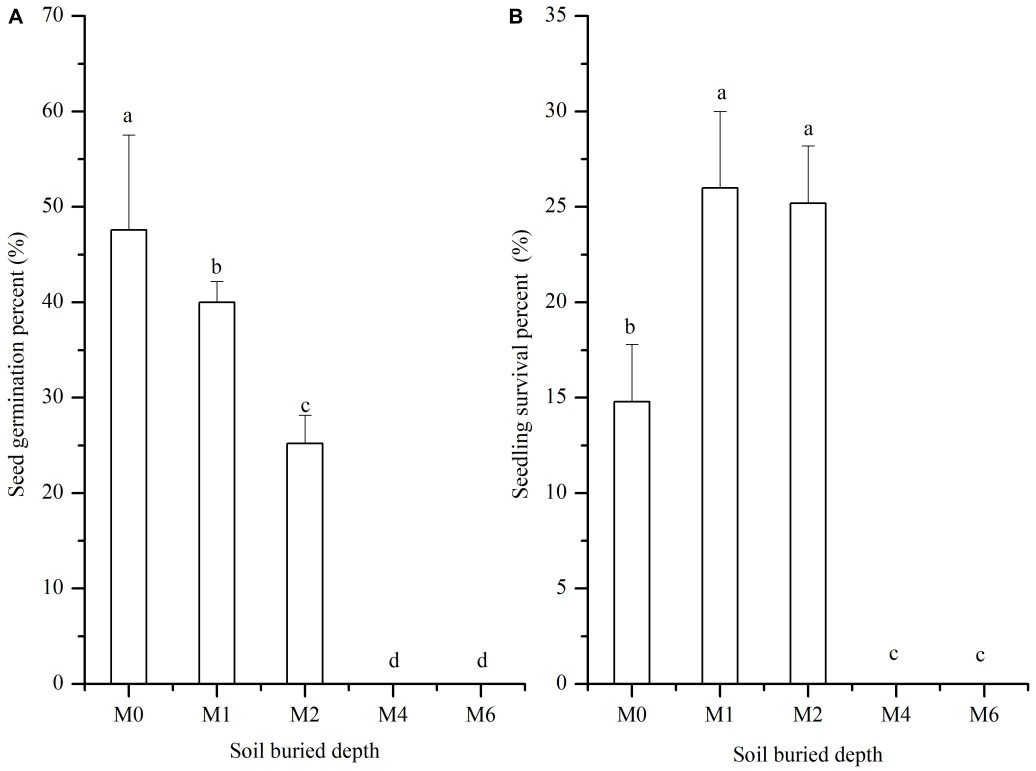


FIGURE 1
Seed germination of *S. salsa* subjected to different soil burial depths. **(A)** Seed germination percent (%) and **(B)** seedling survival rate subjected to 0 cm (M0), 1 cm (M1), 2 cm (M2), 4 cm (M4), and 6 cm (M6) buried depths. Different letters indicate significant differences in different buried depth. The data was 0 at M4 and M6.

seedling survival percent did not decrease much more than the germination percent. The S treatment was the most ideal one for *S. salsa* under medium and low salinity conditions (salinity was $\leq$ 20 g/kg). The F treatment ($\leq$ 15 cm) was suitable for *S. salsa* growth at lower salinity.

## Effects of water and salt on the growth of *Suaeda salsa*

Water and salinity had significant complex effects on the growth of S. salsa. Medium to low salinity ($\leq$ 20 g/kg) and moderate water (periodic flooding at 0–10 cm) were beneficial to the growth of S. salsa (Table 2). Drought and high salinity (salinity was $>$ 30 g/kg) were detrimental to the growth of *S. salsa*. In the F and D treatment, the height was the highest at 0 g/kg, and the density and total biomass were the highest at 10 g/kg. While in the S treatment, the height and total biomass were the highest at 10 g/kg, and the density was the highest at 0 g/kg. In all treatment, biomass at 10 g/kg salinity was the highest, and biomass was mainly distributed in stems and leaves. In the D treatment, by contrast, root biomass accounted for most of the total biomass. Results of water content were interesting. Salt tolerance gradually increased as water conditions improved. In D treatment, water content was the most at 10 g/kg salinity. In F and S treatment, water content was the most at 20 or 30 g/kg salinity. Multi-way variance analysis indicated that the effects of water are the first priority in salt habitats, and the combined effect of salt and water is also important in regulating *S. salsa* growth.

$Na^+$ and $Cl^-$ were similarly distributed in each treatment, with the leaf content being the highest, followed by that in the stems and roots (Figures 3A–F). In the 0 salinity treatment, $Na^+$ and $Cl^-$ were more evenly distributed in the root-stem-leaf. In the same salinity value, content of $Na^+$ was the highest in the S treatment, followed by that in the stems and roots in F and D treatments, respectively. The difference in $Cl^-$ concentration in each treatment was not significant. In the same water regime, contents of $Na^+$ and $Cl^-$ increased as salinity increased.

## Effects of water-salt treatments on the seed yield and vitality

Seeds are the foundation of the establishment and development of plant communities; therefore, seed yield

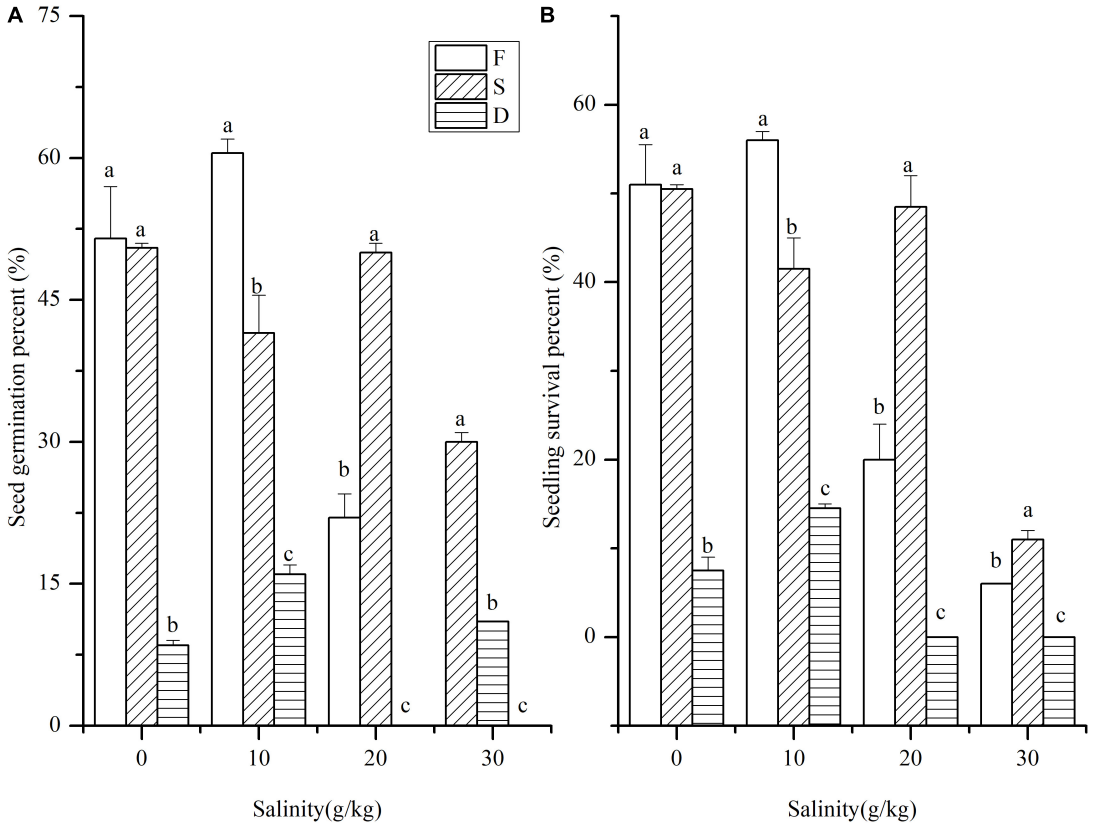


FIGURE 2
Seed germination of *S. salsa* subjected to salt and water treatments. **(A)** Seed germination percent and **(B)** seedling survival percent subjected to water and salt treatment (long-term flooding (5–15 cm, F), periodic flooding (0–10 cm, S), and long-term drought (drought to saturated, D). Different letters indicate significant differences in different water treatments at the same salinity. The data was 0 at D treatment in salinity values of 20 and 30 (g/kg).

and vitality are deemed as the preconditions of vegetation establishment and development. There was no seed production in the 0 g/kg and highsalt treatments (except for S30, **Table 3**). Seeds were produced at F10, S10, D10, F20, and S20 treatment. In the following year, the germination rates of seeds produced in the S10, F10, S20, and F20 treatments were higher than that in the D treatment. Although seeds were produced in the S30 treatment, their germination rate was 0%.

## Discussion

Germination and seedling emergence are critical stages in the life cycle of plants, particularly for annual halophytes, since they determine whether they can be established in variable environments (salt marshes or deserts) (Merino-Martín et al., 2017; Duan et al., 2018; Müller et al., 2019). In delta wetlands, the mutable deposition process, water regime (timing, duration, and depth), and soil salinity are outstanding environmental problems resulting from lack of hydrological connectivity (Dou et al., 2016). Therefore, adequate hydrological connectivity often determines the growth and distribution of plants. Once hydrological connectivity is blocked, the water cycle process changes, affecting the sediment deposition process and soil salinity, and finally affecting seed germination and plant growth (Wang S. et al., 2015).

Because of the interaction of fresh and saltwater, the sediment thickness in the YRD is variable. Seed germination is regulated by burial depth during the process of deposition (Mou and Sun, 2011). However, the effects were two-sided. Moderate buried depths could generally stimulate more germination and seeding than surface deposition of seed, because burial provides a moist environment around seeds and prevents them from desiccation (Sun et al., 2010). Excessive sediment may prevent seedling sprouting and affect survival because the emergence cannot reach the sediment surface or the seeds are unable to germinate due to lack of oxygen, light, and temperature fluctuation (Sun et al., 2010; Wu et al., 2013). In our study, the initial germination rate decreased and was negatively correlated with burial depth. A large percentage of seedlings emerged at shallow burial depths ($\leq$ 2 cm), but deep burials ($>$ 2 cm) significantly reduced seedling

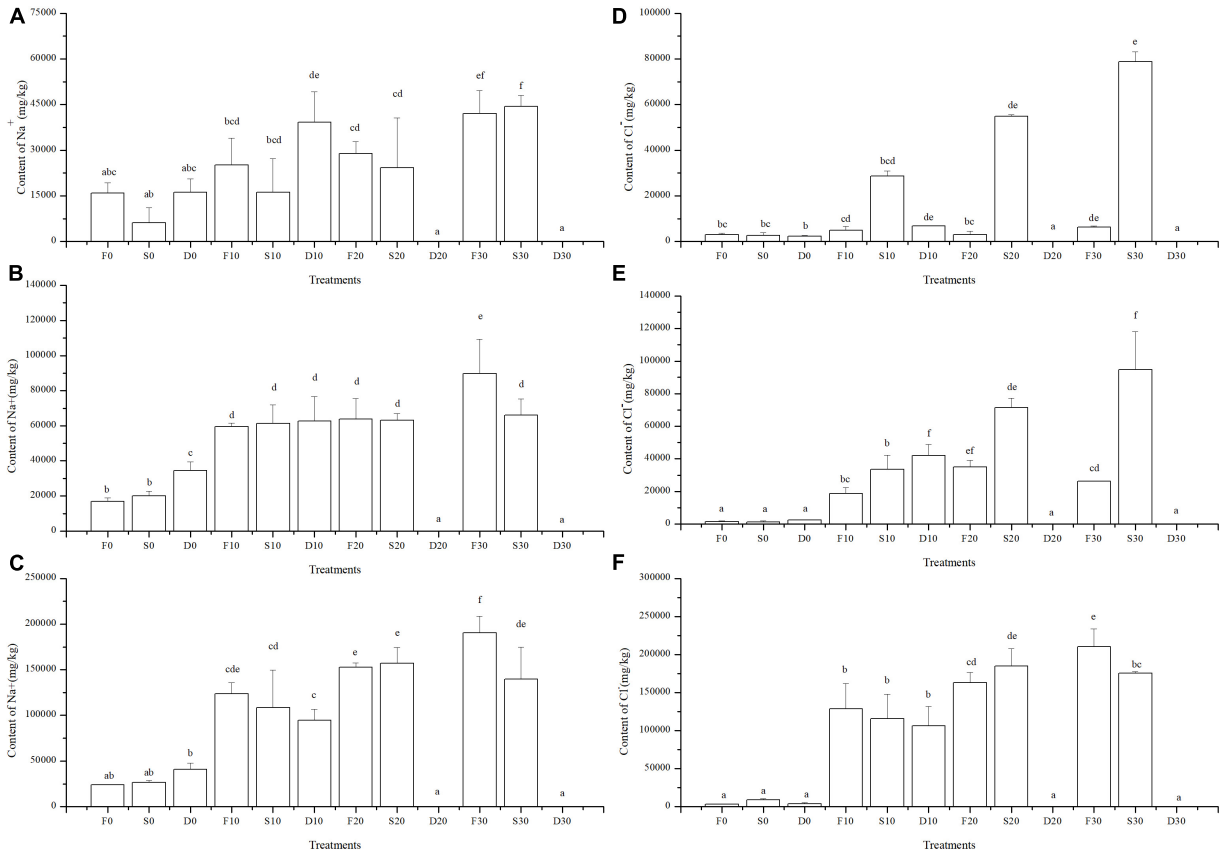


FIGURE 3
$Na^+$ and $Cl^-$ distribution in each part of *S. salsa* subjected to salt and water treatments. **(A)** Content of $Na^+$ in the root, **(B)** Content of $Na^+$ in the stem, **(C)** Content of $Na^+$ in the root, **(D)** Content of $Cl^-$ in the root, **(E)** Content of $Cl^-$ in the stem, and **(F)** Content of $Cl^-$ in the root. The data was 0 in D20 and D30.

emergence. Similar relationships have also been recorded in other studies. The survival of seedlings is important for plant development. Many studies have indicated that germination rate determines colonization rate. However, many seedling emergences could not successfully colonize the site because of the effects of environmental factors (Duan et al., 2018). In our experiment, although initial germination was the highest at a burial depth of 0 cm, the final survival rate was the lowest. The final survival rate was the highest at 1 cm burial depth, with lower mortality of initial emergences. Mortality was lowest at a buried depth of 2 cm, but the initial germination rate was also low. This result is similar to those of Mou's findings (Mou and Sun, 2011). The most probable factors that could influence the germination and survival of *S. salsa* may be the micro-environmental factors surrounding the seeds, such as temperature, humidity, oxygen, and light (Müller et al., 2019). Different burial depths would substantially change these micro-environmental factors and significantly affect seed germination (Limón and Peco, 2016). Under surface conditions, poor water and temperature retention can result in high seedling emergence mortality. Instead, a moderate buried depth could maintain a high seedling emergence survival with suitable influences of micro-environment factors (Soares et al., 2021).

Due to the interaction of fresh water and saline water, water logging and salt content are considered the two key environmental factors for plant establishment, succession, and productivity in the delta wetlands (Hou et al., 2020; Chen et al., 2022; Hussain et al., 2022). Waterlogging stress decreases the availability of carbon dioxide for salt marsh plants while also rendering oxygen levels deficient in the soils. Simultaneously, water influences plant growth through nutrient uptake *via* restricted transpiration rates and membrane permeability (Wang and Jiang, 2007). Furthermore, excess salinity from seawater affects plant growth *via* both osmotic stress and ionic toxicity (Wang F. et al., 2015; Louati et al., 2018). In our study, low water and low salinity showed significant positive effects on seed germination, seedling growth, and productivity. High water and salinity negatively affect seed germination and plant growth, and the effects of drought are

TABLE 2 Growth characteristics of *S. salsa* subjected to water [long-term flooding (5–15 cm, F), periodic flooding (0–10 cm, S), and long-term drought (drought to saturated, D)] and salt treatments.

| | Water regime | Salinity (g/kg) | | | |
|---|---|---|---|---|---|
| | | 0 | 10 | 20 | 30 |
| Height (cm) | F | 54.8 ± 3.31a | 45 ± 7.35b | 48.4 ± 3.50ab | 22.4 ± 4.50c |
| | S | 47.2 ± 4.92b | 57.6 ± 3.77a | 32.4 ± 1.85c | 29.8 ± 2.79c |
| | D | 29 ± 2.00a | 25.6 ± 3.26b | 0.00 ± 0.00c | 0.00 ± 0.00c |
| Density (plant/pot) | F | 51.00 ± 4.50a | 56.00 ± 1.00a | 20.00 ± 4.00b | 6.00 ± 0.00c |
| | S | 50.50 ± 0.50a | 41.50 ± 3.50b | 48.50 ± 3.50a | 11.00 ± 1.00c |
| | D | 7.50 ± 1.50b | 14.50 ± 0.50a | 0.00 ± 0.00c | 0.00 ± 0.00c |
| Total dry biomass (g/pot) | F | 49.12 ± 6.55c | 128.68 ± 1.68a | 106.74 ± 5.84b | 41.76 ± 1.00c |
| | S | 56.64 ± 2.76b | 121.12 ± 25.74a | 49.60 ± 20.93b | 49.80 ± 3.77b |
| | D | 5.69 ± 0.48b | 38.10 ± 0.40a | 0.00 ± 0.00c | 0.00 ± 0.00c |
| Dry biomass of root (g/pot) | F | 2.84 ± 0.13b | 5.18 ± 0.10a | 2.73 ± 0.17b | 1.94 ± 0.01c |
| | S | 3.68 ± 0.16b | 13.22 ± 0.49a | 2.06 ± 0.22bc | 1.60 ± 0.14c |
| | D | 1.39 ± 0.40b | 4.52 ± 0.33 | 0.00 ± 0.00c | 0.00 ± 0.00c |
| Dry biomass of stem (g/pot) | F | 17.92 ± 2.67c | 45.06 ± 1.48a | 26.24 ± 3.64b | 13.22 ± 0.46c |
| | S | 19.72 ± 1.37b | 41.01 ± 12.19a | 18.42 ± 2.94b | 12.29 ± 1.01b |
| | D | 1.67 ± 0.26b | 6.30 ± 0.17a | 0.00 ± 0.00c | 0.00 ± 0.00c |
| Dry biomass of leaf (g/pot) | F | 28.36 ± 3.76b | 78.45 ± 0.87a | 77.78 ± 4.85a | 26.60 ± 0.56b |
| | S | 33.25 ± 1.66b | 66.89 ± 15.20a | 29.12 ± 17.89b | 35.91 ± 3.50b |
| | D | 2.63 ± 0.16b | 27.28 ± 0.42a | 0.00 ± 0.00c | 0.00 ± 0.00c |
| Total water content (%) | F | 53.83 ± 0.17c | 64.22 ± 0.74b | 72.65 ± 2.52a | 70.78 ± 0.50a |
| | S | 60.14 ± 0.76c | 63.77 ± 0.93c | 70.27 ± 3.69 | 77.95 ± 1.43a |
| | D | 22.27 ± 0.66b | 40.83 ± 0.42a | 0.00 ± 0.00c | 0.00 ± 0.00c |
| Water content of root (%) | F | 8.61 ± 0.85c | 41.73 ± 2.37a | 15.31 ± 0.47b | 14.58 ± 1.73b |
| | S | 7.81 ± 0.76c | 35.37 ± 1.09a | 11.41 ± 0.29b | 12.89 ± 1.72b |
| | D | 28.27 ± 5.29a | 26.48 ± 1.54a | 0.00 ± 0.00b | 0.00 ± 0.00b |
| Water content of stem (%) | F | 45.33 ± 1.93d | 50.54 ± 1.13c | 57.29 ± 0.78b | 62.61 ± 0.86a |
| | S | 47.81 ± 2.66c | 56.43 ± 1.94b | 60.52 ± 1.50b | 70.58 ± 1.64a |
| | D | 18.38 ± 0.66b | 27.15 ± 0.99a | 0.00 ± 0.00c | 0.00 ± 0.00c |
| Water content of leaf (%) | F | 63.79 ± 0.69c | 73.55 ± 0.52b | 79.72 ± 2.45a | 78.94 ± 0.20a |
| | S | 73.19 ± 0.79b | 74.17 ± 1.19b | 82.29 ± 2.45a | 83.35 ± 1.83a |
| | D | 22.12 ± 1.06b | 46.35 ± 0.27 | 0.00 ± 0.00c | 0.00 ± 0.00c |

The lower case letters indicate significant differences at $p < 0.05$.

similar. Our results are agreed with formers' result, in which no matter single effect or integrated effects of salinity and waterlogging could restricted plant growth, and could reduce plant height and leaf area (Merino-Martín et al., 2017; Lu et al., 2022). As a halophyte, *S. salsa* thrives in the presence of NaCl. At lower salinity levels, *S. salsa* can absorb $Na^+$ and $Cl^-$ and store them in the vacuoles to lower the plant water potential, thereby improving its ability to absorb water from the soil (Song et al., 2011). In addition, salinity could enhance ATPase and PPase activities, which endows *S. salsa* with more energy to transfer $Na^+$ and $Cl^-$ to vacuoles (Zhang et al., 2010). However, at higher salinity levels, increasing osmotic stress and ionic toxicity would retard the absorption of water and nutrients, and subsequently weaken the photosynthesis and metabolic activity (Li et al., 2022). In this study, $Na^+$ was mainly distributed in the leaves and stems. The $Cl^-$ species were mainly distributed in the leaves, and in the 0-salt treatment, $Cl^-$ was more evenly distributed in the root-stem-leaf. This is in agreement with Zhang's study, which indicated that waterlogging can increase $Na^+$ and $Cl^-$ concentrations in the leaves.

Studies have shown that salt and waterlogging significantly affect seed yield and quality (Wang F. et al., 2015; Li et al., 2020; Meng et al., 2022). Greater water depth and longer flooding time had a higher impact on the yield, and the yield reduction rate was significantly positively correlated with flooding depth and time (Duan et al., 2018). No significant correlations were found between the seed quality and waterlogging. Salt greatly reduces the seed yield of non-halophytes, particularly of some important cash crops (Yadav et al., 2011) and non-halophytes

TABLE 3 Seed production of *S. salsa* subjected to water [long-term flooding (5–15 cm, F), periodic flooding (0–10 cm, S), and long-term drought (drought to saturated, D)] and salt treatment (0, 10, 20, and 30 g/kg).

| | Seed produced (Yes/No) | Seed quantity | Seed germination rate in the next year (%) |
|---|---|---|---|
| F0 | No | 0 | 0 |
| S0 | No | 0 | 0 |
| D0 | No | 0 | 0 |
| F10 | Yes | 516 | 93 |
| S10 | Yes | 621 | 99 |
| D10 | Yes | 98 | 28 |
| F20 | Yes | 246 | 62 |
| S20 | Yes | 407 | 71 |
| D20 | No | 0 | 0 |
| F30 | No | 0 | 0 |
| S30 | Ye | 23 | 0 |
| D30 | No | 0 | 0 |

show significant yield reductions in soils with increasing salinity (Galvan-Ampudia and Testerink, 2011). However, moderate salinity significantly promotes the reproductive growth of halophytes (*S. salsa*) and increases their number of flowers, number of seeds, and quality (Guo et al., 2018). The seed vitality of halophytes was significantly higher than that under non-saline conditions. In this study, seed yield and vitality at salinities of 10 and 20‰ were better than those at a salinity that was too low or high. Seed yield and vitality in the S and F treatments were better than those in the D treatment.

## Conclusion

In delta wetlands, hydrological connectivity blocking could result in the modification of sediment processes, water regimes, and salinity values, which would further alter the germination, seedling, and growth of *S. salsa*. In this study, we found that blocked ephemeral hydrological connectivity may favor *S. salsa* germination and growth owing to changes in water and salinity. Blocking short-term hydrological connectivity is suitable for *S. salsa* growth and development. However, blocking long-term hydrological connectivity (inundation, drought, or excess salinity) is harmful for *S. salsa* growth. The effects of long-term blocking of hydrological connectivity on the *S. salsa* population were reflected in the seed yield and quality; long-term blocking sharply reduced the seed yield and vitality. Overall, the findings of this study provide a scientific basis for the protection and restoration of hydrological connectivity and *S. salsa* habitats in delta wetlands.

## Data availability statement

The original contributions presented in this study are included in the article/supplementary material, further inquiries can be directed to the corresponding author.

## Ethics statement

Authors state that the research was conducted according to ethical standards.

## Author contributions

XW, JSY, and JBY contributed to the conception of the study. YZ and TZ performed the experiment and helped to perform the data analyses. XW and BG contributed significantly to analysis, manuscript preparation, performed the data analyses, and wrote the manuscript. JSY and JBY helped to perform the analysis with constructive discussions. All authors contributed to the article and approved the submitted version.

## Funding

This work was supported by the Key Program from the National Natural Science Foundation of China (U2006215 and U1806218) and the National Natural Science Foundation of China (42171111 and 41871087).

## Acknowledgments

We thank Editage (www.editage.com) for English language editing.

## Conflict of interest

The authors declare that the research was conducted in the absence of any commercial or financial relationships that could be construed as a potential conflict of interest.

## Publisher's note

All claims expressed in this article are solely those of the authors and do not necessarily represent those of their affiliated organizations, or those of the publisher, the editors and the reviewers. Any product that may be evaluated in this article, or claim that may be made by its manufacturer, is not guaranteed or endorsed by the publisher.

# References


Bracken, L. J., Wainwright, J., Ali, G. A., Tetzlaff, D., Smith, M. W., Reaney, S. M., et al. (2013). Concepts of hydrological connectivity: Research approaches, pathways and future agendas. *Earth Sci. Rev.* 119, 17–34. doi: 10.1016/j.earscirev.2013.02.001

Chen, P., Xia, J. B., Ma, H. S., Gao, F. L., Dong, M. M., Xing, X. S., et al. (2022). Analysis of spatial distribution pattern and its influencing factors of the Tamarix chinensis population on the beach of the muddy coastal zone of Bohai Bay. *Ecol. Indic.* 140:109016. doi: 10.1016/j.ecolind.2022.109016

Covino, T. (2017). Hydrologic connectivity as a framework for understanding biogeochemical flux through watersheds and along fluvial networks. *Geomorphology* 277, 133–144. doi: 10.1016/j.geomorph.2016.09.030

Cui, Y., Zhang, Y. H., Zhou, S. J., Pan, Y. Y., Wang, R. Q., Li, Z., et al. (2022). Cracks and root channels promote both static and dynamic vertical hydrological connectivity in the Yellow River Delta. *J. Clean Prod.* 367, 132972.

Dou, P., Cui, B. S., Xie, T., Dong, D. Z., and Gu, B. H. (2016). Macrobenthos Diversity Response to Hydrological Connectivity Gradient. *Wetlands* 36, 45–55. doi: 10.1007/s13157-014-0580-8

Duan, H. M., Ma, Y. C., Liu, R. R., Li, Q., Yang, Y., and Song, J. (2018). Effect of combined waterlogging and salinity stresses on euhalophyte suaeda glauca. *Plant Physiol. Biochem.* 127, 231–237. doi: 10.1016/j.plaphy.2018.03.030

Galvan-Ampudia, C. S., and Testerink, C. (2011). Salt stress signals shape the plant root. *Curr. Opin. Plant Biol.* 14, 296–302. doi: 10.1016/j.pbi.2011.03.019

Guan, B., Zhang, H. X., Wang, X. H., Yang, S. S., Chen, M., Hou, A. X., et al. (2020). Salt is a main factor shaping community composition of arbuscular mycorrhizal fungi along a vegetation successional series in the Yellow River Delta. *Catena* 185:104318. doi: 10.1016/j.catena.2019.104318

Guo, J. R., Li, Y. D., Han, G. L., Song, J., and Wang, B. S. (2018). NaCl markedly improved the reproductive capacity of the euhalophyte Suaeda salsa. *Funct. Plant Biol.* 45, 350–361. doi: 10.1071/FP17181

Hou, W. H., Zhang, R. J., Xi, Y. B., Liang, S. X., and Sun, Z. C. (2020). The role of waterlogging stress on the distribution of salt marsh plants in the Liao River estuary wetland. *Glob. Ecol. Conserv.* 23:e01100. doi: 10.1016/j.gecco.2020.e01100

Hussain, T., Asrar, H., Li, J. S., Feng, X. H., Gul, B., and Liu, X. J. (2022). The presence of salts in the leaf exudate improves the photosynthetic performance of a recreto-halophyte. *Tamarix chinensis*. *Environ. Exp. Bot.* 199:104896.

Lexartza-Artza, I., and Wainwright, J. (2009). Hydrological connectivity: Linking concepts with practical implications. *Catena* 79, 146–152. doi: 10.1016/j.catena.2009.07.001

Li, K. L., Li, Y. D., Guo, J. R., and Wang, B. S. (2020). Preliminary study on na+-mediated improvement of seed yield in euhalophyte Suaeda salsa *(in chinese)*. *J. Plant Ecol.* 56, 49–56. doi: 10.13592/j.cnki.ppj.2019.0544

Li, Q., Liu, R., Li, Z. H., Fan, H., and Song, J. (2022). Positive effects of NaCl on the photoreaction and carbon assimilation efficiency in Suaeda salsa. *Plant Physiol. Bioch.* 177, 32–37. doi: 10.1016/j.plaphy.2022.02.019

Li, Y. F., Xu, J. Y., Wright, A., Qiu, C. Q., Wang, C., and Liu, H. Y. (2021). Integrating two aspects analysis of hydrological connectivity based on structure and process to support muddy coastal restoration. *Ecol. Indic.* 133:108416. doi: 10.1016/j.ecolind.2021.108416

Limón, Á, and Peco, B. (2016). Germination and emergence of annual species and burial depth: Implications for restoration ecology. *Acta Oecol.* 71, 8–13. doi: 10.1016/j.actao.2016.01.001

Liu, J. K. (2020). *Hydrological connectivity and its influence on vegetation in the coast wetland in the yellow river delta*. Beijing: Beijing Forestry University.

Liu, J. K., Cui, B. S., Zhang, Z. M., and Zhang, M. X. (2021). Scale effects of structural hydrological connectivity in coastal wetlands in the Yellow River Delta*(in chinese)*. *Acta Ecol. Sin.* 41, 3745–3754.

Liu, J., Engel, B. A., Zhang, G. F., Wang, Y., Wu, Y. N., Zhang, M. X., et al. (2020). Hydrological connectivity: One of the driving factors of plant communities in the Yellow River Delta. *Ecol. Indic.* 112:106150. doi: 10.1016/j.ecolind.2020.106150

Louati, D., Majdoub, R., Rigane, H., and Abida, H. (2018). Effects of irrigating with Saline Water on Soil Salinization (Eastern Tunisia). *Arabian J. Sci. Eng.* 43, 3793–3805. doi: 10.1007/s13369-018-3215-1

Lu, X. B., Liu, R., Liu, H. Q., Wang, T., Li, Z. H., Zhang, L. P., et al. (2022). Experimental evidence from Suaeda glauca explains why the species is not naturally distributed in non-saline soils. *Sci. Total Environ.* 817:153028. doi: 10.1016/j.scitotenv.2022.153028

Meng, Y., Weng, W. A., Chen, L., Hu, Q., Xing, Z. P., Wei, H. Y., et al. (2022). Effects of water-saving irrigation on grain yield and quality: A meta-analysis. *Sci. Agric. Sin.* 55, 2121–2134.

Merino-Martín, L., Courtauld, C., Commander, L., Turner, S., Lewandrowski, W., and Stevens, J. (2017). Interactions between seed functional traits and burial depth regulate germination and seedling emergence under water stress in species from semi-arid environments. *J. Arid Environ.* 147, 25–33. doi: 10.1016/j.jaridenv.2017.07.018

Mou, X. J., and Sun, Z. G. (2011). Effects of sediment burial disturbance on seedling emergence and growth of Suaeda salsa in the tidal wetlands of the Yellow River estuary. *J. Exp. Mar. Biol. Ecol.* 409, 99–106. doi: 10.1016/j.jembe.2011.08.006

Müller, F. L., Raitt, L. M., Cyster, L. F., Cupido, C. F., Samuels, M. I., Chimphango, S. B. M., et al. (2019). The effects of temperature, water availability and seed burial depth on seed germination and seedling establishment of Calobota sericea (Fabaceae). *S. Afr. J. Bot.* 121, 224–229. doi: 10.1016/j.sajb.2018.11.012

Noe, G. B., Boomer, K., Gillespie, J. L., Hupp, C. R., Martin-Alciati, M., Floro, K., et al. (2019). The effects of restored hydrologic connectivity on floodplain trapping vs. Release of phosphorus, nitrogen, and sediment along the Pocomoke River, Maryland USA. *Ecol. Eng.* 138, 334–352. doi: 10.1016/j.ecoleng.2019.08.002

Norton, A. J., Rayner, P. J., Wang, Y.-P., Parazoo, N. C., Baskaran, L., Briggs, P. R., et al. (2022). Hydrologic connectivity drives extremes and high variability in vegetation productivity across Australian arid and semi-arid ecosystems. *Remote Sens Environ*. 272:112937. doi: 10.1016/j.rse.2022.112937

Saunders, M. I., Brown, C. J., Foley, M. M., Febria, C. M., Albright, R., Mehling, M. G., et al. (2016). Human impacts on connectivity in marine and freshwater ecosystems assessed using graph theory: A review. *Mar. Freshw. Res.* 67, 277–290. doi: 10.1071/mf14358

Shao, X., Fang, Y., Jawitz, J. W., Yan, J., and Cui, B. S. (2019). River network connectivity and fish diversity. *Sci. Total Environ.* 689, 21–30. doi: 10.1016/j.scitotenv.2019.06.340

Soares, V. C., Scremin-Dias, E., Felipe, D. L., Damasceno-Junior, G. A., Pott, A., and Lima, L. B. (2021). Fire has little to no effect on the enhancement of germination, but buried seeds may survive in a Neotropical wetland. *Flora* 278:151801. doi: 10.1016/j.flora.2021.151801

Song, J., Shi, G. W., Gao, B., Fan, H., and Wang, B. S. (2011). Waterlogging and salinity effects on two Suaeda salsa populations. *Physiol. Plant.* 141, 343–351. doi: 10.1111/j.1399-3054.2011.01445.x

Sun, Z. G., Mou, X. J., Lin, G., Wang, L., Song, H., and Jiang, H. (2010). Effects of sediment burial disturbance on seedling survival and growthof Suaeda salsa in the tidal wetland of the Yellow River estuary. *Plant Soil.* 337, 457–468. doi: 10.1007/s11104-010-0542-8

Wang, F., Xu, Y. G., Wang, S., Shi, W. W., Liu, R. R., Feng, G., et al. (2015). Salinity affects production and salt tolerance of dimorphic seeds of Suaeda salsa. *Plant Physiol. Biochem.* 95, 41–48. doi: 10.1016/j.plaphy.2015.07.005

Wang, K. H., and Jiang, Y. W. (2007). Waterlogging tolerance of kentucky bluegrass cultivars. *Hort Sci.* 42, 386–390.

Wang, S., Fu, B. J., Piao, S. L., Lü, Y. H., Philippe, C., Feng, X. M., et al. (2015). Reduced sediment transport in the Yellow River due to anthropogenic changes. *Nat. Geosci.* 9, 38–41. doi: 10.1038/ngeo2602

Wu, J., Cui, N. X., and Cheng, S. P. (2013). Effects of sediment anoxia on growth and root respiratory metabolism of. *Ecol. Eng.* 53, 194–199. doi: 10.1016/j.ecoleng.2012.12.043

Xue, S., Jian, H., Yang, F., Liu, Q., and Yao, Q. (2022). Impact of water-sediment regulation on the concentration and transport of dissolved heavy metals in the middle and lower reaches of the Yellow River. *Sci. Total Environ.* 806:150535. doi: 10.1016/j.scitotenv.2021.150535

Yadav, S., Irfan, M., Ahmad, A., and Hayat, S. (2011). Causes of salinity and plant manifestations to salt stress: A review. *J. Environ. Biol.* 32, 667–685.

Yu, J. B., Wang, X. H., Ning, K., Li, Y. Z., Wu, H. F., Fu, Y. Q., et al. (2012). Effects of Salinity and Water Depth on Germination of Phragmites australis in Coastal Wetland of the Yellow River Delta. *Clean Soil Air Water* 40, 1154–1158. doi: 10.1002/clen.201100743

Zhang, C. Y., Chen, S. L., Li, P., and Liu, Q. L. (2022). Spatiotemporal dynamic remote sensing monitoring of typical wetland vegetation in the current Huanghe River estuary reserve. *Acta Oceanol. Sin.* 44, 125–136.

Zhang, S. R., Song, J., Wang, H., and Feng, G. (2010). Effect of salinity on seed germination, ion content and photosynthesis of cotyledons in halophytes or xerophyte growing in Central Asia. *J. Plant Ecol.* 3, 259–267. doi: 10.1093/jpe/rtq005

Zheng, P., Jiang, X. M., Shu, F. Y., Li, Z. F., Zhang, S. J., and Alahuhta, J. (2022). Loss of lateral hydrological connectivity impacts multiple facets of molluscan biodiversity in floodplain lakes. *J. Environ. Manage* 320:115885. doi: 10.1016/j.jenvman.2022.115885

frontiers | Frontiers in Environmental Science

TYPE Original Research
PUBLISHED 21 September 2022
DOI 10.3389/fenvs.2022.992690



OPEN ACCESS

EDITED BY
He Yixin,Chengdu Institute of Biology (CAS), China

REVIEWED BY
Bo Kang,
Hefei University of Technology, China
Zihao Wen,
Institute of Hydrobiology (CAS), China

*CORRESPONDENCE
Paige D. Kowal,
p_kowal@ducks.ca

SPECIALTY SECTION
This article was submitted to Conservation and Restoration Ecology, a section of the journal Frontiers in Environmental Science

RECEIVED 12 July 2022
ACCEPTED 22 August 2022
PUBLISHED 21 September 2022

CITATION
Kowal PD, Badiou P, Emery RB, Goldsborough LG, Wrubleski DA, Armstrong LM and Page B (2022), Improvements in water clarity and submersed aquatic vegetation cover after exclusion of invasive common carp from a large freshwater coastal wetland, Delta Marsh, Manitoba.
*Front. Environ. Sci.* 10:992690.
doi: 10.3389/fenvs.2022.992690



# Improvements in water clarity and submersed aquatic vegetation cover after exclusion of invasive common carp from a large freshwater coastal wetland, Delta Marsh, Manitoba

Paige D. Kowal[1]*, Pascal Badiou[1], Robert B. Emery[1], L. Gordon Goldsborough[2], Dale A. Wrubleski[1], Llwellyn M. Armstrong[1] and Bryan Page[1]

[1]Institute for Wetland and Waterfowl Research, Ducks Unlimited Canada, Stonewall, MB, Canada, [2]Biological Sciences, University of Manitoba, Winnipeg, MB, Canada

Once introduced to shallow aquatic ecosystems common carp (*Cyprinus carpio*) often degrade habitat, negatively impacting the native organisms that rely on these systems. Detrimental effects often observed following the introduction of carp include a reduction in water clarity as bottom sediments become disturbed and resuspended and phytoplankton blooms become more severe and frequent. This results in a reduction of submersed aquatic vegetation (SAV), the effects of which are felt across multiple trophic levels. We sought to limit large carp (>70 mm maximum body width) access to a culturally and biologically significant 18,500 ha freshwater coastal wetland located in Manitoba, Canada to restore pre-carp conditions which were characterized by clear water and abundant SAV. In winter 2012–2013, exclusion structures were built to limit access by large carp to Delta Marsh during the spring and summer. A monitoring program (2009–2018) compared marsh conditions before and after carp exclusion. Water clarity improved following carp exclusion, largely driven by a reduction of inorganic suspended solids (ISS) rather than phytoplankton biomass, indicating that maintaining clear water conditions might be supplemented by reductions in nutrient export from agricultural areas adjacent to the marsh. The decrease in ISS and phytoplankton varied spatially, with the greatest change observed in the westernmost area of the marsh which is more sheltered compared to the large open bays characterizing eastern areas of the marsh. SAV doubled in percent cover through the 6 years of monitoring post-carp exclusion and SAV cover and species richness in the marsh was comparable to what was present in the early 1970s when there was also partial carp exclusion. Similar to water clarity, the increase in SAV cover was most significant in sheltered areas of the marsh. Our results suggest that excluding large carp can improve water clarity, SAV cover, and SAV species richness in large freshwater wetlands, benefiting waterfowl and other species.

KEYWORDS

coastal wetland, freshwater marsh, common carp, invasive species, biomanipulation, water clarity, submersed aquatic vegetation

## Introduction

Water clarity and submersed aquatic vegetation (SAV) play important roles in aquatic ecosystems. High water clarity promotes SAV growth by allowing increased light penetration through the water column (Robel 1961; Hanson and Butler 1994). Areas with healthy SAV communities have greater fish species richness and diversity and serve as spawning, refuge, and feeding habitat (Randall et al., 1996; Weaver et al., 1997; Cvetkovic et al., 2010; Miller et al., 2018). Associated invertebrates are food sources for both fish and waterfowl (Bartonek and Hickey 1969; Keast 1984; DuBowy 1985; Hann 1995), and the vegetative parts are consumed by some waterfowl species (Collias and Collias 1963; DuBowy 1985). SAV in turn helps maintain a clear water state through several pathways: by reducing sediment and nutrient resuspension by wave action (Hamilton and Mitchell 1996; Horppila and Nurminen 2005), acting as refuge for zooplankton that consume phytoplankton (Scheffer 1999; Celewicz-Goldyn and Kuczynska-Kippen 2017), competing with phytoplankton for nutrients (van Donk et al., 1990), and potentially limiting algae growth through allelopathy (Körner and Nicklish 2002; Hilt and Gross 2008).

In many parts of the world, and particularly in North American shallow aquatic ecosystems, invasive common carp (*Cyprinus carpio*; hereafter, carp) negatively impact water clarity and SAV assemblages by resuspending bottom sediments and lowering light penetration (Badiou and Goldsborough 2010; Kaemingk et al., 2016), and through physical disturbance of SAV during feeding and spawning (Tryon 1954; Crivelli 1983). Carp absence-presence studies in shallow aquatic ecosystems have demonstrated a switch from a clear water, SAV dominated phase to a turbid, phytoplankton dominated phase (Lougheed et al., 1998; Zambrano and Hinojosa 1999; Bajer et al., 2009). Other studies have documented an opposite shift from a turbid to a clear water state after benthivorous fish (especially carp) have been removed or partially excluded, triggering increased growth, extent, and diversity of SAV species (Meijer et al., 1990; Ivey et al., 1998; Schrage and Downing 2004; Kaemingk et al., 2016). The first recorded appearance of carp in the wild in Manitoba, Canada was in the Red River at Lockport in 1938 (Hinks 1943). Carp are believed to have first appeared at Lake Manitoba and Delta Marsh in the late 1940s (Atton 1959; Swain 1979). By the early 1960s, large spring runs of carp were observed at the channels connecting Delta Marsh to Lake Manitoba.

Delta Marsh in western Canada (50.19875, -98.20478), is one of North America's largest freshwater coastal wetlands covering 18,500 ha (Watchorn et al., 2012). A forested beach ridge separates Delta Marsh and Lake Manitoba. Four channels transect the ridge, connecting the marsh to the lake, and water flows between marsh and lake are dynamic and driven by the prevailing winds (Aminian 2015). Marsh water quality is influenced by lake water inputs and runoff from the surrounding watershed, with less mixing and dilution of marsh water during periods of low water levels and runoff (Bortoluzzi 2013). Water clarity is generally low, with an average turbidity range of 12–45 nephelometric turbidity units (NTU) and total suspended solids range from 10 to 100 mg/L (Hnatiuk 2006; Bortoluzzi 2013). The marsh water is brackish, with a conductivity range of 1,600–2,640 µS/cm (Bortoluzzi 2013). As with Lake Manitoba, Delta Marsh water is typically alkaline (Bortoluzzi 2013).

Historically, Delta Marsh had abundant and diverse emergent and SAV assemblages (Hinks and Fryer 1936) which helped support populations of breeding and migrating waterbirds. However, over the last 50+ years the marsh had become turbid and SAV cover decreased by > 50% (Goldsborough and Wrubleski 2001). Concerns over decreasing SAV and the effect on higher trophic levels prompted several SAV mapping surveys at the marsh, the first occurring in 1974 (Anderson and Jones 1976). Further decreases in SAV areal extent documented in surveys in 1997 and 2009–2010, decreasing water clarity, and a series of studies examining the impacts of carp on Delta Marsh using a combination of mesocosm and whole ecosystem manipulation experiments (Evelsizer and Turner 2006; Hnatiuk 2006; Badiou and Goldsborough 2010, 2015; Hertam 2010) led researchers to conclude carp were largely responsible for the deteriorating conditions observed at the marsh. Numerous other studies have found that carp are particularly detrimental to coastal wetlands and shallow lakes (Lougheed et al., 2004; Schrage and Downing 2004; Bajer et al., 2009). Additionally, other stressors such as the regulation of Lake Manitoba water levels beginning in 1961, the increasing enrichment of the marsh by nutrients from domestic sewage, agricultural manures, and fertilizers (through direct runoff and diversion of flood waters from the Assiniboine River through operation of the Portage Diversion), and expansion of hybrid cattail (*Typha* x *glauca*) have also contributed to the declining health of the marsh (Wrubleski et al., 2016). There may also be synergistic effects between carp and these stressors. For example, the presence of carp is believed to amplify eutrophication in aquatic ecosystems (Drenner et al., 1998) and biomanipulation has been proposed as an effective way to mitigate eutrophication in wetland systems (Angeler et al., 2003).

To address the adverse effects caused by carp we initiated a project to exclude large carp (>70 mm maximum body width) from Delta Marsh with the objective of improving waterfowl

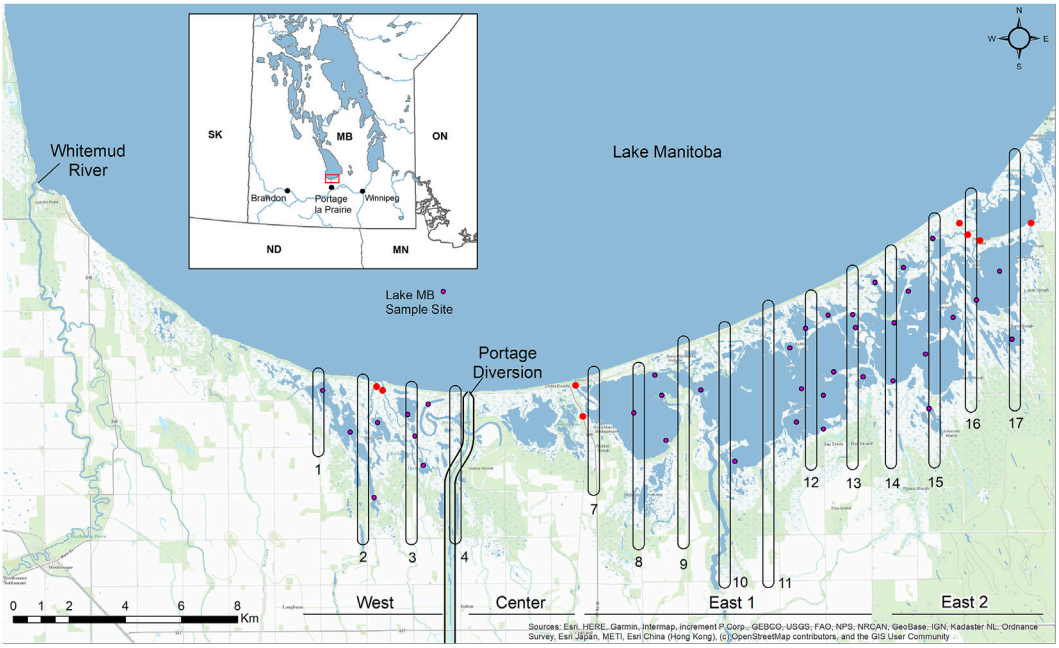


FIGURE 1
Location of water clarity sampling sites (purple dots) in the west, east 1, and east 2 units at Delta Marsh (37), and at Lake Manitoba (1). Red circles are locations of carp exclusion structures; numbered rounded rectangles are submersed aquatic vegetation mapping transects. The inset figure shows the location of Delta Marsh (red bounding box) within Manitoba.

habitat. In winter 2012–2013, exclusion structures were built on channels connecting Lake Manitoba to Delta Marsh. Fish, including carp, overwinter in the lake and migrate into the marsh each spring (Lapointe 1986). The exclusion structures were fitted with removable screens with 70 mm spacing between vertical steel bars. Screens are positioned several weeks after the start of fish migration to allow early arriving native fish access to the marsh, but prior to the peak of carp migration. The screens are removed in mid-July. We monitored water clarity and SAV cover at Delta Marsh pre-(2009, 2010, 2012) and post-(2013–2018) carp exclusion. We hypothesized that water clarity, SAV cover and species richness would increase following the exclusion of large carp from the marsh.

# Methods

## Site description

Delta Marsh is divided into three main units by anthropogenic structures (Figure 1). The Portage Diversion isolates the west marsh from the other units. This 29 km long channel was completed in 1970 and is used to divert flood waters from the Assiniboine River north into Lake Manitoba. Five kilometers east of the diversion is Provincial Road 240 which divides the center and east marsh. The east marsh makes up the largest portion of Delta Marsh and from Provincial Road 240 it stretches approximately 19 km northeastward along the south shore of Lake Manitoba (Figure 1). For increased spatial resolution the east marsh was analyzed as two separate units (east 1 and east 2). The division between these two units occurs at a natural and nearly mid-way point of the east marsh where water movement is constricted through several small channels (Figure 1). Carp were excluded from all but the most northeasterly large bay of the marsh (Figure 1).

## Delta Marsh water clarity data

Water sampling occurred at 37 sites (Figure 1) during May to July 2009, 2010, and 2012–2018, the period corresponding to when carp exclusion screens would have been in place post-carp exclusion. Each site was sampled approximately every two to three weeks, with three to seven sample rounds completed each year. Sampling was avoided when wind speed exceeded 30 km/h. Measurements included water depth (cm) and surface water temperature (°C), and integrated water samples of the uppermost 1 m of the water column were collected using an acrylic tube inserted vertically into the water column. Samples were kept in a cooler until they could be processed.

Water samples were processed the same day at a field laboratory and analyzed for specific conductance (μS/cm; YSI 85 probe and meter [YSI Inc., Yellow Springs, OH]), total (TSS) and inorganic (ISS) suspended solids (mg/L), and total chlorophyll and chlorophyll-a (μg/L). Known volumes of the water samples were filtered through a vacuum pump and pre-weighed Whatman GF/C 42.5 mm filter paper then dried at 100°C in a drying oven for 24 h and weighed for TSS; filters were then placed in a furnace at 600°C for 1 h and weighed again for ISS. As a proxy for phytoplankton biomass, total chlorophyll (chlorophyll-a + phaeophytin; μg/L) pigment absorbance was measured after filtering a second portion of the water samples through the vacuum pump and a Whatman GF/C 42.5 mm filter. Each filter was then placed in a 7 ml glass vial and frozen for 24 h before 5 ml of 90% methanol was added, after which the vials were placed in a dark drawer for another 24 h; the liquid was pipetted from the vials to a cuvette and analyzed for chlorophyll-a in a spectrophotometer at 665nm and 750nm. The cuvettes were then acidified with one drop of 0.01N hydrochloric acid; after an hour the cuvettes were analyzed for phaeophytin in the spectrophotometer at wavelengths of 665nm and 750nm. Chlorophyll-a, phaeophytin, and total chlorophyll concentrations were calculated based on absorbance readings at wavelength values of 665 nm and 750 nm (Marker et al., 1980).

## Lake Manitoba data

Lake Manitoba water chemistry data (conductivity [μS/cm], ammonia [$NH_3$, mg/L], total nitrogen [TN, mg/L], and total phosphorous [TP, mg/L]) were obtained from Manitoba Environment, Climate and Parks. Water quality samples were collected at a sampling station (MB05LLS013; Manitoba Environment, Climate and Parks) located in the south basin of the lake, approximately 3.5 km north of Delta Marsh (Figure 1).

We summed daily volumes ($m^3$/day) of water discharging from two main tributaries to the Lake Manitoba south basin: the Whitemud River and the Portage Diversion (Figure 1). Daily volumes were downloaded from the Water Survey of Canada (gauges 05LL002 and 05LL019, respectively). Daily volumes (January 1$^{st}$–December 31$^{st}$; 2009–2018) were summed to obtain total annual water volume discharge ($m^3$).

## Water clarity data analysis

Delta Marsh water clarity was compared pre- and post-carp exclusion, and between the west, east 1, and east 2 units in the marsh. We used ISS and total chlorophyll as separate water clarity response variables in two modelling efforts to separate the inorganic and algal contributors to suspended solids. Generalized linear mixed models (log link function and gamma distribution; SAS Institute, Inc., Cary, NC) were used to model ISS and total chlorophyll as a function of period (pre- or post-carp exclusion), unit (east 1, east 2, west; Figure 1), unit*period, and a number of covariates known to affect water clarity (Meijer et al., 1990; Chow-Fraser 1999, 2006; Beaulieu et al., 2013), including: year-varying annual Lake Manitoba total discharge loading (Portage Diversion + Whitemud River); year- and sample round-varying Lake Manitoba conductivity, total chlorophyll, $NH_3$, TN, TP, and water level; site-varying relative exposure index (REI); site- and year-varying Julian date of sampling; Delta Marsh water depth, water temperature, total chlorophyll, chlorophyll-a, windspeed effects, resuspension potential, and conductivity.

Random effects of site, year, and site*year were also included to account for repeated sampling both within and across years. The covariate REI was calculated to characterize the exposure of each site to wind generated waves (Keddy 1982):

$$\mathbf{REI} = \sum_{i=1}^{X} (\boldsymbol{V_i} \times \boldsymbol{P_i} \times \boldsymbol{F_i})$$

where $i$ is $i$th compass heading (X = 1 to 36; every 10° starting at 0°); $V$ is mean wind speed from the $i$th direction; $P$ is proportion with which wind occurred from the $i$th direction; and $F$ is effective fetch distance from the $i$th direction. We summarized mean wind speed and wind direction frequency from data collected every 15 min during May to July over a 5-year period, 2014–2018, at a weather station located at the SE corner of the marsh (50.19946, -98.08638). We used geospatial models (see Rohweder et al., 2012) to calculate effective fetch distances.

To model increases or decreases in ISS and in total chlorophyll that might lag behind rising or falling wind speeds we included lagged wind speed and resuspension potential covariates over nine-time intervals: at the time of sampling, and averaged over the preceding 1, 3, 6, 9, 12, 18, 24, and 36 hourly intervals. We used hourly wind speed and wind direction data from Environment and Climate Change Canada's (ECCC) Portage Southport weather station (Station ID: 5012324; station located 30.1 km south of the center of Delta Marsh). When wind speed and wind direction values were missing, we substituted data from ECCC's Portage Southport A or Delta Marsh CS stations. Several sources (Carper and Bachmann 1984; Booth et al., 2000; Bajkiewicz-Grabowska et al., 2016) have validated shallow water wave theory that when water depth is less than half the wavelength, the wave orbital motion beneath the water surface interacts with the bottom sediments, at which point sediment resuspension is likely. Resuspension potential is described as:

$$\boldsymbol{Resuspension\ Potential} = \left(\frac{\boldsymbol{Wavelength}}{\boldsymbol{2}}\right) \Big/ \boldsymbol{Water\ Depth}$$

Modeling subsets were run to identify the optimum time interval at which to model lagged wind speed and resuspension potential. REI was also considered as a candidate to represent windspeed effects. Fixed effects of unit, period, unit*period, REI,

and random effects of site, year, and site*year were included in all of these competing models and the effects of windspeed and resuspension potential were added one-at-a-time. Best approximating models (identified as minimizing AIC) were used for identifying a best time interval scale for representing windspeed and resuspension potential.

Since resuspension potential incorporates wind speed and water depth, two full model simplification paths were explored including either the best time interval effects of (i) wind speed and water depth or (ii) resuspension potential, with all the other variables described previously. To facilitate model convergence independent variables were scaled by orders of magnitude. REI was retained in all model runs as it characterizes the wind exposure of each water sampling site, which influences water clarity at varying degrees spatially across Delta Marsh. The effects of unit, period, and unit*period were retained as these were the effects of primary interest. Full models were sequentially simplified by removing the effects with the smallest Wald-statistics (Wood et al., 2008) and all models were ranked by AIC to identify the best approximating and competing models (identified as those within 2 ΔAIC units and structurally simpler than the top model [Arnold 2010]). Ratios of estimated marginal means (EMMs) were used to determine if there were overall or unit specific differences in ISS and total chlorophyll between pre- and post-carp exclusion.

## Submersed aquatic vegetation data

SAV beds at Delta Marsh were mapped between July and September 1974, 1997, 2009–2010 (this survey spanned two field seasons), 2014, and 2016–2018. Watercraft were used in all years to ground-truth vegetation bed perimeters. The extent of SAV beds were mapped, and SAV species were recorded and assigned to either single or mixed species assemblages. Survey methods used in 1974 (Anderson and Jones 1976) and 1997 (D. Wrubleski and M. Anderson, Ducks Unlimited Canada, unpublished report) combined the use of aerial photographs and ground truthing. Due to turbid conditions a garden rake was dragged along the marsh bottom to delineate vegetation bed perimeters in 1997 and 2009–2010 (M. Baschuk and D. Wrubleski, unpublished report). Aerial photographs were not used in the 2009–2010 and 2014 SAV surveys due to turbid conditions which limited vegetation bed interpretation. Vegetation beds were drawn on paper maps in the field. A handheld data collector (Trimble Juno; Trimble Navigation Ltd., Sunnyvale, CA) was also used in 2014. All paper maps were later digitized using ArcGIS (ESRI, Inc., Redland, CA). In 2016–2018 polygons and points representing SAV beds were recorded using a tablet running ESRI's Collector for ArcGIS software connected to a GPS receiver. Points were created for small SAV beds measuring approximately 4 $m^2$. During data processing, point locations were buffered 1 m on all sides resulting in polygons 4 $m^2$. SAV beds smaller than 4 $m^2$ were not mapped.

In 1974, 1997, 2009–2010, and 2014 SAV distribution was mapped across the entire east marsh; in 2010 the west marsh was also included. In 2016–2018 only areas falling under 400 m wide survey transects (hereafter, SAV mapping transects; Figure 1) were mapped in both the east and west marsh. In order to standardize the comparison of SAV among years, we only included survey data within SAV mapping transects 1–4 and 7–17 within the carp exclusion zone (Figure 1).

## Submersed aquatic vegetation data analysis

We assigned each SAV record to one of ten treatments based on marsh unit and SAV survey year(s): 1) west, late pre-carp exclusion (2010), 2) west, late post-carp exclusion (2016–2018), 3) east 1, early pre-carp exclusion (1974), 4) east 1, late pre-carp exclusion (1997 and 2009–2010), 5) east 1, early post-carp exclusion (2014), 6) east 1, late post-carp exclusion (2016–2018), 7) east 2, early pre-carp exclusion (1974), 8) east 2, late pre-carp exclusion (1997 and 2009–2010), 9) east 2, early post-carp exclusion (2014), and 10) east 2, late post-carp exclusion (2016–2018). We specify pre- and post-carp exclusion here in the context of the current carp exclusion project, as in the 1970s there was also carp exclusion. For each treatment we calculated the estimated percent areal cover of total SAV and of the three most common SAV species found at Delta Marsh (*Ceratophyllum demersum* [coontail], *Myriophyllum sibiricum* [northern watermilfoil], and *Stuckenia pectinata* [sago pondweed]) as the proportion of SAV areal extent to open water area. As mixed species bed assemblage classifications were not consistent among years we summed, by species, the areal extent of vegetation beds with any occurrence of that species to facilitate within-species comparisons. The data were treated as pseudo-binomial, and a generalized linear model (SAS PROC GLIMMIX; using a logit link function, binomial distribution, and allowing for overdispersion) was used to obtain log-odds estimates of SAV cover as a function of treatment. Odds ratio contrasts of estimated marginal means (EMMs) were used to identify whether the differences in total and species-specific SAV percent areal coverage were significant among treatments.

# Results

## Water clarity

The effects of average wind speed and resuspension potential over the preceding 18 h advanced to the ISS full model reduction sets. The best approximating reduced model for ISS included effects of unit, period, unit*period, Lake Manitoba (LKMB) $NH_3$, Delta Marsh (DM) chlorophyll-a, total chlorophyll, REI, and average wind speed over the preceding 18 h. A competing model

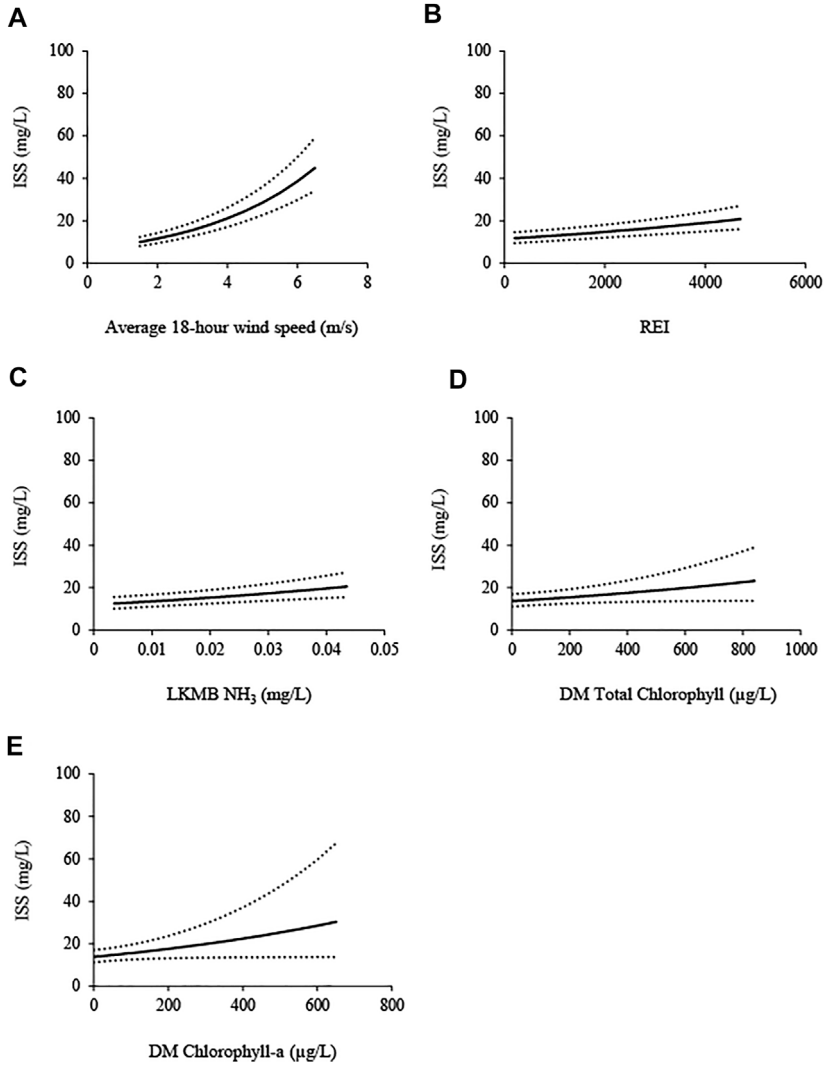


FIGURE 2
Inorganic suspended solids (ISS; mg/L) in the Delta Marsh (DM) carp exclusion zone (west, east 1, and east 2 units), 2009, 2010, and 2012–2018, modeled in relation to: **(A)** average wind speed over the preceding 18 hours (average 18-h wind speed; m/s), **(B)** relative exposure index (REI), **(C)** Lake Manitoba (LKMB) ammonia ($NH_3$; mg/L), **(D)** DM total chlorophyll (µg/L), and **(E)** DM chlorophyll-a (µg/L). 95% confidence intervals (±; dotted lines) are shown. Each covariate effect was isolated by setting all other covariates to their mean values, averaging over unit*period effects and setting random effects of site, year, and site*year to zero.

(ΔAIC = 1.74) included all effects in the best approximating model except DM chlorophyll-a. ISS was positively correlated with the effects (β, ± SE), in descending order of strength, of average windspeed over the preceding 18 h (0.301, ± 0.025), REI (0.128, ± 0.027), LKMB $NH_3$ (12.4, ± 3.40), DM total chlorophyll (0.063, ± 0.032), and DM chlorophyll-a (0.121, ± 0.063; Figure 2).

The effects of average windspeed in the preceding 36 h and resuspension potential over the preceding 24 h advanced to the full model reduction sets for total chlorophyll. The best approximating model included effects of unit, period, unit*period, DM water temperature, Julian date, ISS, REI, and conductivity, and LKMB conductivity, $NH_3$, TN, TP, and total discharge. There were no competing models. As REI was imprecisely estimated (i.e., the ratio of the estimated effect to standard error was < ~2) we did not plot or interpret this effect. Effects (β, ± SE) that were positively correlated with total chlorophyll, in descending order of strength, were: DM water temperature (0. 743, ± 0. 075), Julian date (1.029, ± 0.107), and ISS (0.922, ± 0.133), LKMB conductivity (0.203, ± 0.033), $NH_3$ (14.6, ± 3.54), and TN (0.289, ± 0.079). Effects that were negatively correlated with total chlorophyll, in descending order of strength, were: DM conductivity (-0.091, ± 0.022), LKMB total discharge (-0.023, ± 0.008) and TP (-2.51, ± 0.911; Figure 3).

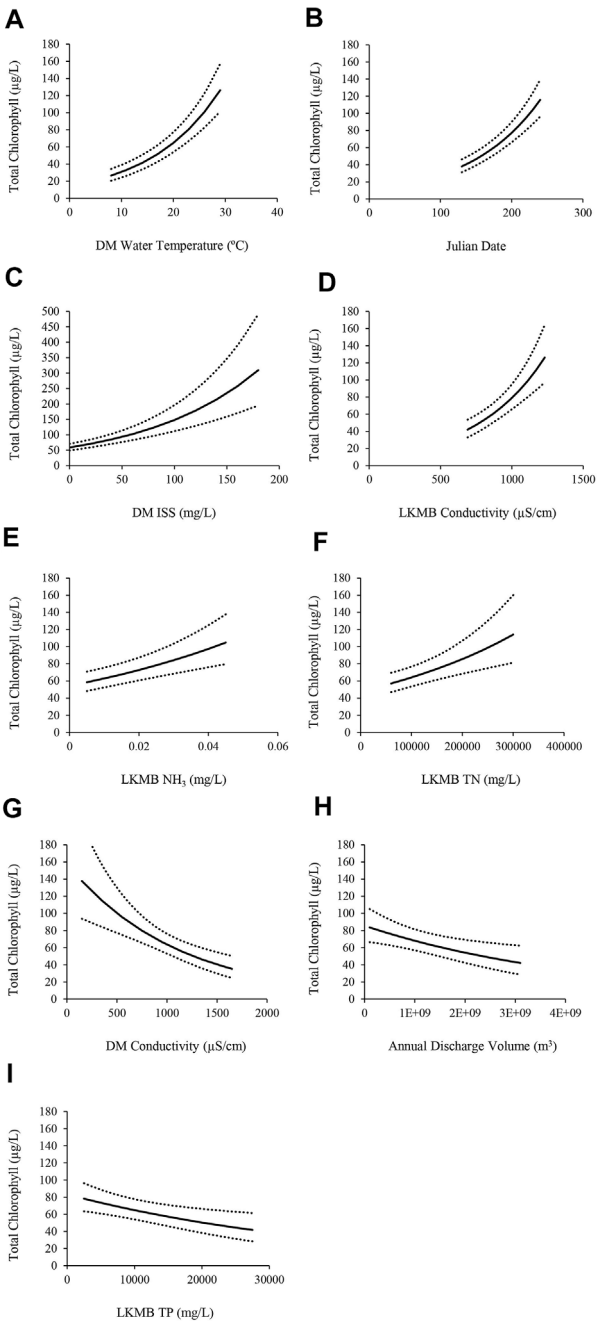


FIGURE 3
Total chlorophyll (µg/L) in the Delta Marsh (DM) carp exclusion zone (west, east 1, and east 2 units), 2009, 2010, and 2012–2018, modeled in relation to: **(A)** DM water temperature (°C), **(B)** Julian date (days), **(C)** DM inorganic suspended solids (ISS; mg/L), **(D)** Lake Manitoba (LKMB) conductivity (µS/cm), **(E)** LKMB ammonia ($NH_3$; mg/L), **(F)** LKMB total nitrogen (TN; mg/L), **(G)** DM conductivity (µS/cm), **(H)** Total annual discharge volume ($m^3$) into LKMB, and **(I)** LKMB total phosphorus (TP; mg/L). 95% confidence intervals (± dotted lines) are shown. Each covariate effect was isolated by setting all other covariates to their mean values, averaging over unit*period effects and setting random effects of site, year, and site*year to zero.

Estimated means ratios indicate there was an overall marginal decline (-32%) in ISS pre-to post-carp exclusion (Table 1). The magnitude of decline in ISS was spatially dependent, with a significantly larger decrease in the west marsh unit (-59%) relative to inconclusive changes in the east 1 (-10%) and east 2 units (-14%; Table 1 and Figure 4). Tests of statistical significance of changes in total chlorophyll were inconclusive, although there was evidence of an overall decline (-22%) pre-to post-carp exclusion, but no evidence of a difference between marsh units (Table 1; Figure 4).

## Submersed aquatic vegetation

Overall in the east marsh carp exclusion zone the areal extent of SAV declined between mapping surveys conducted in 1974 and 1997, and increased with each survey between 2014 and 2018 (Figure 5). In the west marsh, SAV areal extent increased since the pre-carp exclusion survey in 2010 (Figure 5).

There were no significant differences in total SAV percent cover (hereafter, SAV cover) between treatment periods in the west and east 1 marsh units (Table 2; Figure 6A). Total SAV cover in the late post-treatment period was significantly greater in the west and east 2 units versus the east 1 unit, and in the east 2 unit declined significantly by one third between the early pre- and late pre-treatment periods. SAV cover in the east 2 marsh unit significantly tripled between the late pre- and late post-treatment periods, and significantly increased between early post- and late post-treatment periods (Table 2; Figure 6A).

The same contrasts of odds ratios for total SAV cover (see Table 2) were assessed for each of the three dominant SAV species. There were no significant changes in *C. demersum* cover between treatment periods; however, there were significant cover differences between marsh units in the late pre-treatment period; cover was nearly 15 times greater in the west versus the east 1 unit (Figure 6B). In the late post-treatment period, *C. demersum* cover was greatest in the east 2 versus the west and east 1 units (Figure 6B). In the late pre-treatment period *M. sibiricum* cover was low in all marsh units (Figure 6C). *M. sibiricum* cover increased in all units after carp were excluded. In the late post-treatment period, *M. sibiricum* cover was greatest in the east 2 unit, followed in descending order by the west and east 1 units (Figure 6C). *S. pectinata* was the dominant SAV species, making up the majority of the total SAV cover in almost all treatment periods and marsh units (Figure 6D). While *S. pectinata* cover in the east 2 unit declined between the early pre- and early post-treatment periods, before increasing in the late post-treatment period, the changes were not statistically significant (Figure 6D). The increase in *S. pectinata* cover in the west unit was also not statistically significant. *S. pectinata* cover in east 1 remained consistently lower after the early pre-

TABLE 1 Tests of contrasts in inorganic suspended solids (ISS) and total chlorophyll (TChl) within the carp exclusion zone during May to July by treatment period [pre- (2009, 2010, and 2012) and post- (2013–2018) carp exclusion] and marsh unit (west, east 1, east 2), Delta Marsh, Manitoba. Contrasts are statistically significant (bold) when 95% confidence intervals exclude 1.00 (CL = confidence limit).

| Contrast | Estimated Ratio[a] | (Lower 95% CL, Upper 95% CL) |
|---|---|---|
| ISS overall post- vs. pre- | 0.68 | (0.45, 1.02) |
| **ISS west post- vs. pre-** | **0.41** | **(0.25, 0.65)** |
| ISS east 1 post- vs. pre- | 0.90 | (0.59, 1.38) |
| ISS east 2 post- vs. pre- | 0.86 | (0.55, 1.33) |
| ISS change in east 1 vs. change in east 2 | 1.06 | (0.79, 1.40) |
| **ISS change[b] in west vs. change in east 1** | **0.45** | **(0.33, 0.63)** |
| **ISS change in west vs. change in east 2** | **0.48** | **(0.34, 0.67)** |
| TChl overall post- vs. pre- | 0.79 | (0.57, 1.11) |
| TChl west post- vs. pre- | 0.80 | (0.54, 1.19) |
| TChl east 1 post- vs. pre- | 0.80 | (0.56, 1.14) |
| TChl east 2 post- vs. pre- | 0.78 | (0.54, 1.13) |
| TChl change in east 1 vs. change in east 2 | 1.03 | (0.78, 1.34) |
| TChl change in west vs. change in east 1 | 1.00 | (0.74, 1.36) |
| TChl change in west vs. change in east 2 | 1.03 | (0.75, 1.42) |

[a]The ratios between estimated marginal means (EMMs) for ISS and TChl (e.g., ISS, Post-EMM/Pre-EMM). In computing EMMs, all quantitative covariates in the best approximating models were set to mean values.
[b]A contrast of the temporal changes in two different regions (e.g., ISS west post-vs. pre-/ISS east 1 post-vs. pre-).

treatment period. In the late post-treatment period, *S. pectinata* cover was significantly greater in the west and east 2 units as compared to the east 1 unit (Figure 6D). Other species-specific contrasts were not statistically significant, possibly due in some cases to extremely low cover values, high relative variability in cover among SAV mapping transects and treatment periods, or possibly as a result of how we summed mixed species bed areal extents.

While the increase in SAV percent cover was significant in the west unit post-carp exclusion, we observed a decrease in *S. pectinata* areal extent in the west unit in 2018 (Figure 5). In late July and early August 2018, extensive beds of SAV, primarily composed of *S. pectinata*, were observed in the west unit (P. Kowal, personal observation). However, many vegetation beds had disappeared when the SAV was mapped 15–17 August.

We recorded changes in the dominance and number of SAV species within the marsh between treatment periods. During the pre- and early post-treatment periods the dominant SAV species in the east marsh was *S. pectinata*; *M. sibiricum* was the dominant species in the east marsh in the late post-treatment period (Figure 6). In the west marsh, *S. pectinata* was the dominant SAV species across pre- and post-treatment periods (Figure 6). Six SAV species were identified at Delta Marsh in 2014, four in 2016, and eight in 2017 and 2018. Records of sparse occurrences of some species in 2016 were lost, and therefore our estimates of species richness are conservative for that year. *Potamogeton pusillus* (small pondweed) and *Sparganium eurycarpum* (giant bur-reed) were detected in 2017 and 2018 after last being observed in 1997. In 2017, *Chara*, a genus of charophyte green algae characteristic of clear water habitats, was observed for the first time in recent years, in the east 2 unit.

## Discussion

Biomanipulation, through removal or exclusion, has been widely used to successfully reduce carp biomass in small lakes (Sorensen Bajer, 2020) and shown to result in significant water quality improvements such as reduced turbidity, decreases in chlorophyll-a, and increased SAV (Schrage and Downing 2004; Kaemingk et al., 2016; Jůza 2019; Huser et al., 2022). However, most attempts to regulate invasive carp populations have been largely applied to smaller (<250 ha), isolated water bodies with limited hydrological connections (Lougheed et al., 2004). For the most part, carp biomanipulation has been achieved through physical removal via harvest fishing (Bajer et al., 2011) and specialized traps (Stuart et al., 2011), water level drawdowns (Verrill and Berry 1995), chemical/biological removal mechanisms such as rotenone (Schrage and Downing 2004; Bonneau and Scarnecchia 2015), use of the koi herpes virus (McColl et al., 2007), and daughterless carp genetic manipulation (Brown and Gilligan 2014). However, physical removal is often only successful in the short term with carp populations usually rebounding quickly (Tempero et al., 2019) and chemical/biological removal is not feasible and is challenging within existing regulatory frameworks on large interconnected systems with important commercial and indigenous fisheries such as the Delta Marsh-Lake Manitoba system. Our research

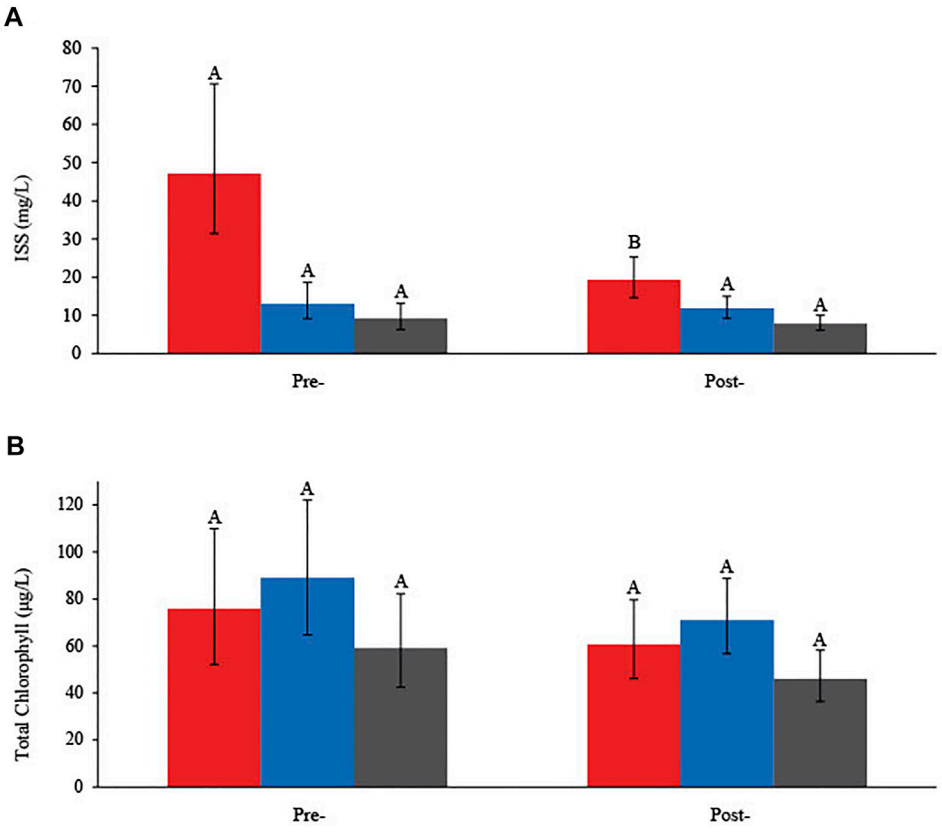


FIGURE 4
**(A)** Estimated marginal means (EMMs) of **(A)** inorganic suspended solids (ISS; mg/L) and **(B)** total chlorophyll (µg/L), with 95% confidence intervals, in the west (red), east 1 (blue), and east 2 (grey) units pre- (2009, 2010, and 2012) and post- (2013–2018) carp exclusion, Delta Marsh, Manitoba. Different letters (A and B) indicate a statistical difference between periods (pre- or post-carp exclusion) within the same marsh unit.

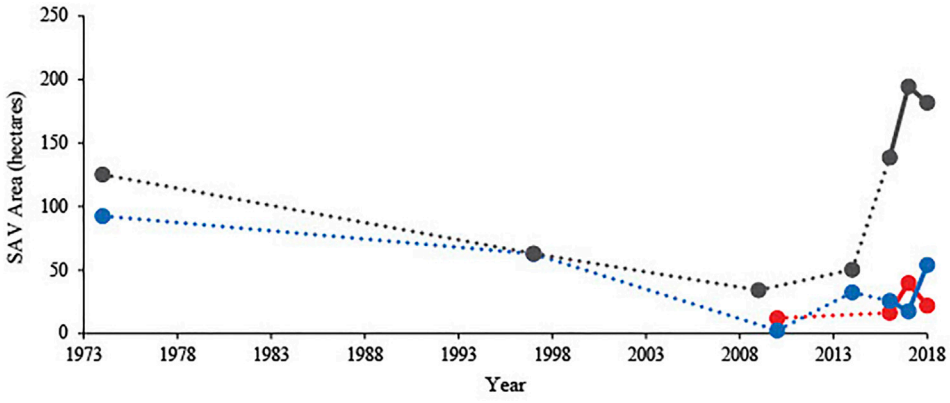


FIGURE 5
Total areal extent (ha) of submersed aquatic vegetation (SAV) in SAV mapping transects 1–4 in the west (red), 7–13 in the east 1 (blue), and 14–17 in the east 2 (grey) carp-exclusion zones, 1974, 1997, 2009, 2010, 2014, and 2016–2018, Delta Marsh, Manitoba. Dotted lines connect non-consecutive survey years; solid lines connect consecutive survey years.

TABLE 2 Tests of contrasts in total submersed aquatic vegetation (SAV) estimated percent cover between treatment period: early pre-carp exclusion [1974]; late pre-carp exclusion [1997 and 2009–2010]; early post-carp exclusion [2014]; late post-carp exclusion [2016–2018], and marsh unit (west, east 1, east 2), Delta Marsh, Manitoba. Contrasts are statistically significant (bold) when 95% confidence intervals exclude 1.00 (CL = confidence limit).

| Contrast | Estimated odds Ratio[a] | (Lower 95% CL, upper 95% CL) |
|---|---|---|
| west, post- vs. pre- | 2.21 | (0.72, 6.78) |
| east 1, late post- vs. late pre- | 1.06 | (0.37, 3.09) |
| east 1, late post- vs. early pre- | 0.38 | (0.13, 1.07) |
| east 1, early post- vs. late pre- | 1.03 | (0.25, 4.33) |
| east 1, early post- vs. early pre- | 0.37 | (0.09, 1.51) |
| east 1, late pre- vs. early pre- | 0.36 | (0.11, 1.14) |
| east 1, late post- vs. early post- | 1.03 | (0.27, 3.95) |
| **east 2, late post- vs. late pre-** | **4.31** | **(1.64, 11.3)** |
| east 2, late post- vs. early pre- | 1.30 | (0.49, 3.47) |
| east 2, early post- vs. late pre- | 0.79 | (0.17, 3.70) |
| east 2, early post- vs. early pre- | 0.24 | (0.05, 1.12) |
| **east 2, late pre- vs. early pre-** | **0.30** | **(0.09, 0.99)** |
| **east 2, late post- vs. early post-** | **5.46** | **(1.37, 21.7)** |
| **late post-, west vs. east 1** | **6.84** | **(2.99, 15.6)** |
| late post-, west vs. east 2 | 0.84 | (0.43, 1.67) |
| **late post-, east 2 vs. east 1** | **8.11** | **(3.57, 18.4)** |
| late pre-, west vs. east 1 | 3.29 | (0.89, 12.2) |
| late pre-, west vs. east 2 | 1.65 | (0.44, 6.10) |
| late pre-, east 2 vs. east 1 | 2.00 | (0.61, 6.54) |
| early pre-, east 2 vs. east 1 | 2.38 | (0.74, 7.68) |
| early post-, east 2 vs. east 1 | 1.54 | (0.27, 8.78) |

[a]The ratios between odds of total SAV estimated percent cover (e.g., odds of west unit SAV cover, late post-/late pre-).

demonstrates that limiting access of large carp using exclusion structures, specifically during the spawning season, can improve water clarity and SAV cover in a large freshwater coastal wetland.

Post-carp exclusion we measured increases in water clarity, and SAV cover and species richness. We saw spatially variable increases in SAV cover post-carp exclusion which were accompanied by spatially variable decreases in ISS and to a lesser extent total chlorophyll, similar to results of other carp removal studies (Hanson and Butler 1994; Schrage and Downing 2004). Increased water clarity and SAV cover can arise through several synergistic mechanisms. Increased water clarity allows deeper light penetration which enhances SAV growth (Robel 1961; Lougheed et al., 1998). Increased SAV cover results in less wind and wave action; thus lowering sediment disturbance and resuspension, further increasing water clarity and SAV growth (Bachmann et al., 2000; Cho 2007; Van Zuidam and Peeters 2015). Hanson and Butler (1994) found that an initial increase in water clarity after fish removal was caused by increased zooplankton grazing during the growing season which allowed for the establishment of SAV; subsequent water clarity improvements were maintained by SAV lowering sediment resuspension and algal biomass. The changes in SAV cover and ISS following carp exclusion at Delta Marsh were significantly greater in the west unit compared to the east 1 and 2 units. The east 1 unit has larger, more exposed bays than the east 2 unit, and both units are more open and exposed than the west unit and this may explain why the effects of carp exclusion on ISS were muted in the east units relative to the west unit. This is supported by average 18 h wind speeds and REI being the two strongest environmental predictors of ISS at Delta Marsh. The simultaneous existence of both turbid and clear water states within one shallow aquatic system is possible depending on the degree of exposure and presence of SAV (Scheffer et al., 1994), especially in a system as large and complex as Delta Marsh. The exclusion of carp appears to have resulted in less resuspension of sediment early in the growing season, allowing SAV cover to expand compared to years when carp had free access to the marsh. The exclusion of carp also likely reduced physical disturbance of SAV. Furthermore, benthivorous fish like carp are also known to reduce the erosion resistance of sediment which enhances sediment resuspension by wave action (Scheffer et al., 2003), lowering the capacity for SAV establishment. The changes in water clarity and SAV we observed suggest that the exclusion of

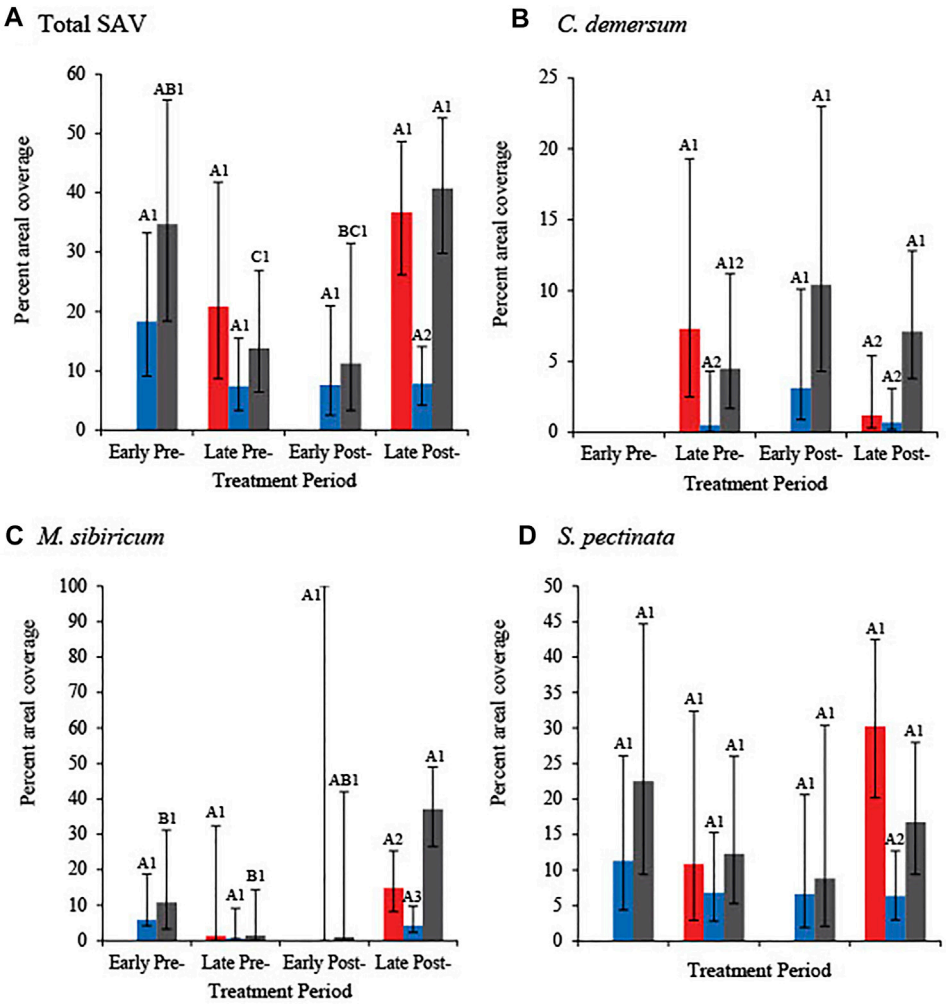


FIGURE 6
Percent cover and 95% confidence intervals of **(A)** total submersed aquatic vegetation (SAV) and the three most common SAV species [**(B)** *Ceratophyllum demersum*, **(C)** *Myriophyllum sibiricum*, and **(D)** *Stuckenia pectinata*] in SAV mapping transects and 1–4 in the west (red), 7–13 in the east 1 (blue), and 14–17 in the east 2 (grey) carp exclusion units, Delta Marsh, Manitoba. Treatment periods are defined as: early pre-carp exclusion (1974), late pre-carp exclusion (1997, 2009–2010), early post-carp exclusion (2014), and late post-carp exclusion (2016–2018). Percent cover included homogenous vegetation beds and mixed species bed assemblages where each species occurred. Different letters **(A–C)** indicate a statistical difference between treatment periods within the same species and unit. Different numbers (1–3) indicate a statistical difference between units within each SAV group (total SAV or species) and treatment period.

carp coupled with the wind sheltered hydrogeomorphic nature of the west unit allowed for a rapid recovery in both water clarity and SAV there.

Historically, sago pondweed was a dominant species in Delta Marsh, and was very important as a food source to waterfowl (Anderson and Low 1976; Gordon 1985). Thus, there is significant interest in its response to carp exclusion. Anderson (1978) found that the distribution of *S. pectinata* at the marsh was highly correlated to site exposure and our observations regarding site exposure support this. The large exposed bays of the east 1 unit have seen greater shoreline and island erosion compared to the other marsh units (Wrubleski et al., 2016), and since the early 1970s. *S. pectinata* has remained consistently low in that unit. While the increase in SAV percent cover, primarily consisting of *S. pectinata*, was significantly greater in the west unit post-carp exclusion we observed a decrease in SAV areal extent in 2018 there that we speculate was due to early senescence caused by extremely low water levels, wave action, and grazing by waterfowl.

The exclusion of large carp from Delta Marsh resulted in increased water clarity and SAV cover and species richness despite carp exclusion coinciding with some of the highest water levels recorded on this system since the 1960s as a result of major flooding events in 2011 (Blais et al., 2016) and

2014 (Ahmari et al., 2016). Because increased water levels often decrease SAV abundance (Robel 1961; Scheffer et al., 1992) we expect that the exclusion of carp from Delta Marsh will result in greater water clarity and SAV cover under more normal water levels. Furthermore, these improvements have occurred during a period when Lake Manitoba, and Delta Marsh itself have experienced increased nutrient loading as a result of frequent operation of the Portage Diversion, which is the single largest input of nutrients to Lake Manitoba when it is in operation (Page 2011). Warm water temperatures and high nutrient availability in the water column promote blue-green algae growth which restricts water transparency (Kosten et al., 2012; Beaulieu et al., 2013). Nutrient loading can also mimic the detrimental impact of carp presence by promoting phytoplankton growth, possibly overriding the effects of carp on water quality in nutrient rich water (Badiou and Goldsborough 2015). Because benthivorous fish, like carp are known to interact synergistically with nutrient loading to increase phytoplankton biomass (Drenner et al., 1998), it is possible that our carp exclusion project is also helping to mitigate the impacts of high nutrient loading into Delta Marsh.

While the exclusion of large carp resulted in increased water clarity and SAV cover (this study) and increased use by diving ducks (Bortolotti et al., 2022—submitted), maintaining these conditions in light of other stressors being experienced at Delta Marsh such as increasing nutrient loading, stabilized water levels, and invasive hybrid cattail will necessitate ongoing monitoring and assessment of marsh conditions. Of these stressors, focusing on managing nutrient inputs from the agriculturally dominated portions of the Delta Marsh watershed should be investigated as a supplementary mechanism for sustaining and potentially improving conditions that favor water clarity and increased SAV cover over time.

## Data availability statement

The raw data supporting the conclusions of this article will be made available by the authors, without undue reservation.

## Author contributions

PK, PB, RE conceived and designed the analysis. PK, RE, LG collected the data. PK, RE, BP, DW, and LG contributed data or analysis tools. PK, RE, and BP organized the database. LA performed statistical analyses. PK wrote the first draft of the manuscript. PB wrote sections of the manuscript. All authors contributed to manuscript revision, read, and approved the submitted version.

## Funding

This project was funded by Ducks Unlimited Canada, the United States Fish and Wildlife Service through the North American Wetlands Conservation Act, Manitoba Department of Natural Resources and Northern Development, Wildlife Habitat Canada, as well as grants and funds from numerous individuals and foundations. Research was conducted under Manitoba Fisheries Branch Scientific Collection permits, and Manitoba Wildlife Management Area Use permits. Delta Marsh is located within the traditional territory of the Anishinaabe and Dakota Peoples, and on the homeland of the Métis Nation. In the spirit of reconciliation, we respectfully acknowledge these Nations as the original caretakers of this land.

## Acknowledgments

S. Witherly provided GIS support for submersed aquatic vegetation mapping and analyses. We thank the numerous research technicians and volunteers involved in the monitoring program for their hard work. Much of the data used in this paper was generated by the “Restoring the Tradition at Delta Marsh” project.

## Conflict of interest

The authors declare that the research was conducted in the absence of any commercial or financial relationships that could be construed as a potential conflict of interest.

## Publisher’s note



## References

Ahmari, H., Blais, E.-L., and Greshuk, J. (2016). The 2014 flood event in the Assiniboine River Basin: Causes, assessment and damage. *Can. Water Resour. J./ Revue Can. des ressources hydriques* 41, 85–93. doi:10.1080/07011784.2015.1070695

Aminian, P. (2015). Manitoba: University of Manitoba. [master’s thesis]. [Winnipeg, (MB)] http://hdl.handle.net/1993/31013.Hydrodynamic modelling of Delta Marsh and simplified methods of discharge estimation for discontinuous inland coastal wetlands.

Anderson, M. G. (1978). Distribution and production of sago pondweed (*Potamogeton Pectinatus* L.) on a northern prairie marsh. *Ecology* 59, 154–160. doi:10.2307/1936642

Anderson, M. G., and Jones, R. E. (1976). *Submerged aquatic vascular plants of east Delta Marsh*. Winnipeg, MB, Canada: Manitoba Department of Renewable Resources and Transportation Services.

Anderson, M. G., and Low, J. B. (1976). Use of sago pondweed by waterfowl on the Delta marsh, Manitoba. *J. Wildl. Manage.* 40, 233–242. doi:10.2307/3800420

Angeler, D. G., Chow-Fraser, P., Hanson, M. A., Sánchez-Carrillo, S., and Zimmer, K. D. (2003). Biomanipulation: A useful tool for freshwater wetland mitigation? *Freshw. Biol.* 48 (12), 2203–2213. doi:10.1046/j.1365-2427.2003.01156.x

Arnold, T. W. (2010). Uninformative parameters and model selection using Akaike's Information Criterion. *J. Wildl. Manage* 74, 1175–1178. doi:10.1111/j.1937-2817.2010.tb01236.x

Atton, F. M. (1959). The invasion of Manitoba and Saskatchewan by carp. *Trans. Am. Fish. Soc.* 88, 203–205. doi:10.1577/1548-8659(1959)88

Bachmann, R. W., Hoyer, M. V., and Canfield, D. E., Jr. (2000). The potential for wave disturbance in shallow Florida lakes. *Lake Reserv. Manag.* 16, 281–291. doi:10.1080/07438140009354236

Badiou, P. H. J., and Goldsborough, L. G. (2010). Ecological impacts of an exotic benthivorous fish in large experimental wetlands, Delta Marsh, Canada. *Wetlands* 30, 657–667. doi:10.1007/s13157-010-0071-5

Badiou, P. H. J., and Goldsborough, L. G. (2015). Ecological impacts of an exotic benthivorous fish, the common carp (*Cyprinus carpio* L.), on water quality, sedimentation, and submerged macrophyte biomass in wetland mesocosms. *Hydrobiologia* 755, 107–121. doi:10.1007/s10750-015-2220-6

Bajer, P. G., Chizinski, C. J., and Sorensen, P. W. (2011). Using the Judas technique to locate and remove wintertime aggregations of invasive common carp. *Fish. Manag. Ecol.* 18, 497–505. doi:10.1111/j.1365-2400.2011.00805.x

Bajer, P. G., Sullivan, G., and Sorensen, P. W. (2009). Effects of a rapidly increasing population of common carp on vegetative cover and waterfowl in a recently restored Midwestern shallow lake. *Hydrobiologia* 632, 235–245. doi:10.1007/s10750-009-9844-3

Bajkiewicz-Grabowska, E., Markowski, M., and Lemańczyk, K. (2016). Application of geoinformation techniques to determine zones of sediment resuspension induced by wind waves in lakes (using two lakes from Northern Poland as examples). *Limnol. Rev.* 16, 3–14. doi:10.2478/limre-2016-0001

Bartonek, J. C., and Hickey, J. J. (1969). Food habits of canvasbacks, redheads, and lesser scaup in Manitoba. *Condor* 71, 280–290. doi:10.2307/1366304

Beaulieu, M., Pick, F., and Gregory-Eaves, I. (2013). Nutrients and water temperature are significant predictors of cyanobacterial biomass in a 1147 lakes data set. *Limnol. Oceanogr.* 58, 1736–1746. doi:10.4319/lo.2013.58.5.1736

Blais, E.-L., Greshuk, J., and Stadnyk, T. (2016). The 2011 flood event in the Assiniboine River basin: Causes, assessment and damages. *Can. Water Resour. J./Revue Can. des ressources hydriques* 41, 74–84. doi:10.1080/07011784.2015.1046139

Bonneau, J. L., and Scarnecchia, D. L. (2015). Response of benthic macroinvertebrates to carp (*Cyprinus carpio*) biomanipulation in three tributaries of a eutrophic, great plains reservoir, USA. *Trans. Kans. Acad. Sci.* 118, 13–26. doi:10.1660/062.118.0103

Booth, J. G., Miller, R. L., McKee, B. A., and Leathers, R. A. (2000). Wind-induced bottom sediment resuspension in a microtidal coastal environment. *Cont. Shelf Res.* 20, 785–806. doi:10.1016/s0278-4343(00)00002-9

Bortoluzzi, T. (2013). Manitoba: University of Manitoba. [dissertation]. [Winnipeg (MB)] http://hdl.handle.net/1993/19686.Spatial and temporal patterns in the hydrology, water chemistry and algal nutrient status of Delta Marsh, as influenced by the hydrology of adjoining Lake Manitoba.

Brown, P., and Gilligan, D. (2014). Optimizing an integrated pest-management strategy for a spatially structured population of common carp (*Cyprinus carpio*) using meta-population modelling. *Mar. Freshw. Res.* 65, 538–550. doi:10.1071/MF13117

Carper, G. L., and Bachmann, R. W. (1984). Wind resuspension of sediments in a prairie lake. *Can. J. Fish. Aquat. Sci.* 41, 1763–1767. doi:10.1139/f84-217

Celewicz-Goldyn, S., and Kuczynska-Kippen, N. (2017). Ecological value of macrophyte cover in creating habitat for microalgae (diatoms) and zooplankton (rotifers and crustaceans) in small field and forest water bodies. *PLoS ONE* 12 (5), e0177317. doi:10.1371/journal.pone.0177317

Cho, H. J. (2007). Effects of prevailing winds on turbidity of a shallow estuary. *Int. J. Environ. Res. Public Health* 4, 185–192. doi:10.3390/ijerph2007040014

Chow-Fraser, P. (2006) Development of the wetland water quality index for assessing the quality of Great Lakes coastal wetlands. in T. Simon and T. P. Stewart, editors. *Coastal wetlands of the laurentian great lakes: Health, habitat and indicators*. Authorhouse Press, Bloomington, IN, USA. http://greatlakeswetlands.ca/publications/development-of-the-water-quality-index-wqi-to-assess-effects-of-basin-wide-land-use-alteration-on-coastal-marshes-of-the-laurentian-great-lakes/ (Accessed 2 January 2020).

Chow-Fraser, P. (1999). Seasonal, interannual, and spatial variability in the concentrations of total suspended solids in a degraded coastal wetland of Lake Ontario. *J. Gt. Lakes. Res.* 25, 799–813. doi:10.1016/S0380-1330(99)70778-1

Collias, N. E., and Colias, E. C. (1963). Selective feeding by wild ducklings of different species. *Wilson Bull.* 75, 6–14. doi:10.1016/0003-3472%2858%2990066-6

Crivelli, A. J. (1983). The destruction of aquatic vegetation by carp. *Hydrobiologia* 106, 37–41. doi:10.1007/bf00016414

Cvetkovic, M., Wei, A., and Chow-Fraser, P. (2010). Relative importance of macrophyte community versus water quality variables for predicting fish assemblages in coastal wetlands of the Laurentian Great Lakes. *J. Gt. Lakes. Res.* 36, 64–73. doi:10.1016/j.jglr.2009.10.003

Drenner, R. W., Gallo, K. L., Baca, R. M., and Smith, J. D. (1998). Synergistic effects of nutrient loading and omnivorous fish on phytoplankton biomass. *Can. J. Fish. Aquat. Sci.* 55, 2087–2096. doi:10.1139/f98-095

DuBowy, P. J. (1985). Feeding ecology and behavior of postbreeding male blue-winged teal and northern shovelers. *Can. J. Zool.* 63, 1292–1297. doi:10.1139/z85-194

Evelsizer, V. D., and Turner, A. M. (2006). Species-specific responses of aquatic macrophytes to fish exclusion in a prairie marsh: A manipulative experiment. *Wetlands* 26, 430–437. doi:10.1672/0277-5212(2006)26[430

Goldsborough, L. G., and Wrubleski, D. A. (2001) The decline of Delta Marsh, an internationally significant wetland in south-central Manitoba. In Sixth Prairie Conservation and Endangered Species Conference.

Gordon, D. H. (1985) Postbreeding ecology of male mallards on the Delta marsh, Manitoba. [PhD dissertation]. [East Lansing, (MI)]: Michigan State University, Michigan.

Hamilton, D. P., and Mitchell, S. F. (1996). An empirical model for sediment resuspension in shallow lakes. *Hydrobiologia* 317, 209–220. doi:10.1007/BF00036471

Hann, B. J. (1995). Invertebrate associations with submersed aquatic plants in a prairie wetland. *Univ. Manit. Field Stn.* 30, 78–84.

Hanson, M. A., and Butler, M. G. (1994). Responses of plankton, turbidity, and macrophytes to biomanipulation in a shallow prairie lake. *Can. J. Fish. Aquat. Sci.* 51, 1180–1188. doi:10.1139/f94-117

Hertam, S. C. (2010). The effects of common carp (*Cyprinus carpio* L.) on water quality, algae and submerged vegetation in Delta Marsh. Manitoba: University of Manitoba. Manitoba. [master's thesis]. [Winnipeg (MB)] http://hdl.handle.net/1993/4207.

Hilt, S., and Gross, E. M. (2008). Can allelopathically active submerged macrophytes stabilize clear-water states in shallow lakes? *Basic Appl. Ecol.* 9, 422–432. doi:10.1016/j.baae.2007.04.003

Hinks, D., and Fryer, R. (1936). *Aquatic plant survey 1936*. Manitoba: Manitoba Department of Mines and Natural Resources Government Report.

Hinks, D. (1943). *The fishes of Manitoba*. Winnipeg, MB, Canada: Department of Mines and Natural Resources.

Hnatiuk, S. D. (2006). Manitoba: University of Manitoba. [master's thesis]. [Winnipeg (MB)] http://hdl.handle.net/1993/7963. Experimental manipulation of ponds to determine the impact of common carp (*Cyprinus carpio* L.) in Delta Marsh, Manitoba: Effects on water quality, algae, and submersed vegetation.

Horppila, J., and Nurminen, L. (2005). Effects of different macrophyte growth forms on sediment and P resuspension in a shallow lake. *Hydrobiologia* 545, 167–175. doi:10.1007/s10750-005-2677-9

Huser, B. J., Bajer, P. G., Kittelson, S., Christenson, S., and Menken, K. (2022). Changes to water quality and sediment phosphorus forms in a shallow, eutrophic lake after removal of common carp (*Cyprinus carpio*). *Inland Waters* 12, 33–46. doi:10.1080/20442041.2020.1850096

Ivey, G. L., Cornely, J. E., and Ehlers, B. D. (1998). Carp impacts on waterfowl at malheur national Wildlife refuge. https://pdfs.semanticscholar.org/ed90/29bf2c4472074571d7af729dc4483c10ed9e.pdf (Accessed May 24, 2019).Oregon. Transactions of the 63rd North American Wildlife and Natural Resources Conference.

Jůza, T., Duras, J., Blabolil, P., Sajdlová, Z., Hess, J., Chocholoušková, Z., et al. (2019). Recovery of the Velky Bolevecky pond (Plzen, Czech Republic) via biomanipulation–key study for management. *Ecol. Eng.* 136, 167–176. doi:10.1016/j.ecoleng.2019.06.025

Kaemingk, M. A., Jolley, J. C., Paukert, C. P., Willis, D. W., Henderson, K., Holland, R. S., et al. (2016). Common carp disrupt ecosystem structure and function through middle-out effects. *Mar. Freshw. Res.* 68, 718–731. doi:10.1071/MF15068

Keast, A. (1984). The introduced aquatic macrophyte, *Myriophyllum spicatum*, as habitat for fish and their invertebrate prey. *Can. J. Zool.* 62, 1289–1303. doi:10.1139/z84-186

Keddy, P. A. (1982). Quantifying within-lake gradients of wave energy: Interrelationships of wave energy, substrate particle size and shoreline plants in Axe Lake, Ontario. *Aquat. Bot.* 14, 41–58. doi:10.1016/0304-3770(82)90085-7

Körner, S., and Nicklisch, A. (2002). Allelopathic growth inhibition of selected phytoplankton species by submerged macrophytes. *J. Phycol.* 38, 862–871. doi:10.1046/j.1529-8817.2002.t01-1-02001.x

Kosten, S., Huszar, V. L., Bécares, E., Costa, L. S., van Donk, E., Hansson, L. A., et al. (2012). Warmer climates boost cyanobacterial dominance in shallow lakes. *Glob. Chang. Biol.* 18, 118–126. doi:10.1111/j.1365-2486.2011.02488.x

Lapointe, G. D. (1986). St. Paul, (MN): University of Minnesota. [master's thesis].Fish movement and predation on macroinvertebrates in a lakeshore marsh.

Lougheed, V. L., Crosbie, B., and Chow-Fraser, P. (1998). Predictions on the effect of common carp (*Cyprinus carpio*) exclusion on water quality, zooplankton, and submergent macrophytes in a Great Lakes wetland. *Can. J. Fish. Aquat. Sci.* 55, 1189–1197. doi:10.1139/f97-315

Lougheed, V. L., Theÿsmeÿer, T., and Chow-Fraser, P. (2004). Carp exclusion, food-web interactions, and the restoration of Cootes Paradise Marsh. *J. Gt. Lakes. Res.* 30, 44–57. doi:10.1016/S0380-1330(04)70328-7

Marker, A. F. H., Nusch, E. A., Rai, H., and Riemann, B. (1980). The measurement of photosynthetic pigments in freshwaters and standardization of methods: Conclusions and recommendations. *Arch. Für Hydrobiol.* 14, 91–106.

McColl, K. A., Sunarto, A., Williams, L. M., and Crane, M. St.J. (2007). Koi herpes virus: Dreaded pathogen or white knight? *Aquac. Health Int.* 9, 4–6. http://hdl.handle.net/102.100.100/127764?index=1.

Meijer, M. L., de Haan, M. W., Breukelaar, A. W., and Buiteveld, H. (1990). Is reduction of the benthivorous fish an important cause of high transparency following biomanipulation in shallow lakes? *Hydrobiologia* 200/201, 303–315. doi:10.1007/BF02530348

Miller, J. W., Kocovsky, P. M., Wiegmann, D., and Miner, J. G. (2018). Fish community responses to submerged aquatic vegetation in Maumee Bay, western Lake Erie. *North Am. J. Fish. manage.* 38, 623–629. doi:10.1002/nafm.10061

Page, E. C. M. (2011). Manitoba: University of Manitoba. [master's thesis]. [Winnipeg (MB)] http://hdl.handle.net/1993/4831.A water quality assessment of Lake Manitoba, a large shallow lake in central Canada.

Randall, R. G., Minns, C. K., Cairns, V. W., and Moore, J. E. (1996). The relationship between an index of fish production and submerged macrophytes and other habitat features at three littoral areas in the Great Lakes. *Can. J. Fish. Aquat. Sci.* 53, 35–44. doi:10.1139/f95-271

Robel, R. J. (1961). Water depth and turbidity in relation to growth of sago pondweed. *J. Wildl. Manage.* 25, 436–438. doi:10.2307/3798837

Rohweder, J., Rogala, J. T., Johnson, B. L., Anderson, D., Clark, S., Chamberlin, F., et al. (2012). Application of wind fetch and wave models for habitat rehabilitation and enhancement projects – 2012 update. *Contract Rep. Prep. U.S. Army Corps Engineers' Up. Miss. River Restor. – Environ. Manag. Program.* 1–52.

Scheffer, M., de Redelijkheid, M. R., and Noppert, F. (1992). Distribution and dynamics of submerged vegetation in a chain of shallow eutrophic lakes. *Aquat. Bot.* 42, 199–216. doi:10.1016/0304-3770(92)90022-B

Scheffer, M., Portielje, R., and Zambrano, L. (2003). Fish facilitate wave resuspension of sediment. *Limnol. Oceanogr.* 48, 1920–1926. doi:10.4319/lo.2003.48.5.1920

Scheffer, M. (1999). The effect of aquatic vegetation on turbidity; how important are the filter feeders? *Hydrobiologia* 408/409, 307–316. doi:10.1023/a:1017011320148

Scheffer, M., van den Berg, M., Breukelaar, A., Breukers, C., Coops, H., Doef, R., et al. (1994). Vegetated areas with clear water in turbid shallow lakes. *Aquat. Bot.* 49, 193–196. doi:10.1016/0304-3770(94)90038-8

Schrage, L. J., and Downing, J. A. (2004). Pathways of increased water clarity after fish removal from Ventura Marsh; a shallow, eutrophic wetland. *Hydrobiologia* 511, 215–231. doi:10.1023/B:HYDR.0000014065.82229.c2

Sorensen, P. W., and Bajer, P. G. (2020). Case studies demonstrate that common carp can be sustainably reduced by exploiting source-sink dynamics in Midwestern lakes. *Fishes* 5, 36. doi:10.3390/fishes5040036

Stuart, I. G., Williams, A., McKenzie, J., and Holt, T. (2011). Managing a migratory pest species: A selective trap for common carp. *N. Am. J. Fish. Manag.* 26, 888–893. doi:10.1577/M05-205.1

Swain, D. P. (1979). Biology of the carp (*Cyprinus carpio*) in North America and its distribution in Manitoba, North Dakota and neighbouring U.S. waters. Manitoba Winnipeg, MB, Canada: Manitoba Department of Natural Resources. Manuscript Report 79–73.

Tempero, G. W., Hicks, B. J., Ling, N., Morgan, D., Daniel, A. J., Özkundakci, D., et al. (2019). Fish community responses to invasive fish removal and installation of an exclusion barrier at Lake Ohinewai, Waikato. *N. Z. J. Mar. Freshw. Res.* 53, 397–415. doi:10.1080/00288330.2019.1579101

Tryon, C. A. (1954). The effect of carp exclosures on growth of submerged aquatic vegetation in Pymatuning Lake, Pennsylvania. *J. Wildl. Manage.* 18, 251–254. doi:10.2307/3797722

van Donk, E., Grimm, M. P., Gulati, R. D., and Klein Breteler, J. P. G. (1990). Whole-lake food-web manipulation as a means to study community interactions in a small ecosystem. *Hydrobiologia* 200/201, 275–289. doi:10.1007/BF02530346

Van Zuidam, B. G., and Peeters, E. T. H. M. (2015). Wave forces limit the establishment of submerged macrophytes in large shallow lakes. *Limnol. Oceanogr.* 60, 1536–1549. doi:10.1002/lno.10115

Verrill, D. D., and Berry, C. R. (1995). Effectiveness of an electrical barrier and lake drawdown for reducing common carp and bigmouth buffalo abundances. *N. Am. J. Fish. Manage.* 15, 137–141. doi:10.1577/1548-8675(1995)015%3C0137

Watchorn, K. E., Goldsborough, G. L., Wrubleski, D., and Mooney, B. G. (2012). A hydrogeomorphic inventory of coastal wetlands of the Manitoba great lakes: Lakes Winnipeg, Manitoba, and Winnipegosis. *J. Gt. Lakes. Res.* 38 (3), 115–122. doi:10.1016/j.jglr.2011.05.008

Weaver, M. J., Magnuson, J. J., and Murray, C. K. (1997). Distribution of littoral fishes in structurally complex macrophytes. *Can. J. Fish. Aquat. Sci.* 54, 2277–2289. doi:10.1139/f97-130

Wood, A. M., White, I. R., and Royston, P. (2008). How should variable selection Be performed with multiply imputed data? *Stat. Med.* 27, 3227–3246. doi:10.1002/sim.3177

Wrubleski, D., Badiou, P., and Goldsborough, G. (2016). "Coastal wetlands of Manitoba's great lakes (Canada)," in *The wetland book*. Editors C. Finlayson, G. Milton, R. Prentice, and N. Davidson (Dordrecht: Springer). doi:10.1007/978-94-007-6173-5_190-1

Zambrano, L., and Hinojosa, D. (1999). Direct and indirect effects of carp (*Cyprinus carpio* L.) on macrophyte and benthic communities in experimental shallow ponds in central Mexico. *Hydrobiologia* 408/409, 131–138. doi:10.1007/978-94-017-2986-4_13

frontiers | Frontiers in Environmental Science

TYPE Review
PUBLISHED 04 October 2022
DOI 10.3389/fenvs.2022.942788



OPEN ACCESS

EDITED BY
Chuanyu Gao,
Northeast Institute of Geography and Agroecology (CAS), China

REVIEWED BY
Liang Yang,
Northeast Institute of Geography and Agroecology (CAS), China
Miriam Groß-Schmölders,
University of Basel, Switzerland

*CORRESPONDENCE
Samuel Obeng Apori,
d21125192@mytudublin.ie
Furong Tian,
furong.tian@tudublin.ie

SPECIALTY SECTION
This article was submitted to Conservation and Restoration Ecology, a section of the journal Frontiers in Environmental Science

RECEIVED 13 May 2022
ACCEPTED 04 July 2022
PUBLISHED 04 October 2022

CITATION
Apori SO, Mcmillan D, Giltrap M and Tian F (2022), Mapping the restoration of degraded peatland as a research area: A scientometric review.
*Front. Environ. Sci.* 10:942788.
doi: 10.3389/fenvs.2022.942788



# Mapping the restoration of degraded peatland as a research area: A scientometric review

Samuel Obeng Apori[1,2]*, Douglas Mcmillan[1,3], Michelle Giltrap[1,4] and Furong Tian[1,4]*

[1]School of Food Science Environmental Health, Technological University Dublin, Dublin, Ireland, [2]Environmental Sustainability and Health Institute, Technological University Dublin, Dublin, Ireland, [3]Green Restoration Ireland Cooperative Society Ltd., Carlow, Ireland, [4]FOCAS Research Institute, Technological University Dublin, Dublin, Ireland

Degraded peatland has reduced many ecosystem services, such as water quality and quantity, biodiversity, carbon storage, climate regulations, and other cultural benefits. Therefore, several initiatives for the restoration of degraded peatland (RDP) have attempted to restore the ecosystem processes, productivity, and services of the degraded peatland to its original natural condition. Notwithstanding the popularity of RDP research among researchers and industry practitioners, a quantitative technique to map a comprehensive survey of the intellectual core and the general body landscape of knowledge on RDP research does not exist. In this study, a scientometric analysis was employed to analyze 522 documents using VOSviewer and CiteSpace. The Web of Science database was used to retrieve bibliographic records using the advanced search "TS (topic) = ('drained peatland restoration' OR 'drained bog restoration' OR 'drained mire restoration' OR degraded peatland restoration' OR 'degraded bog restoration' OR 'drained peatland reclamation' OR 'drained bog restoration' OR' degraded peatland reclamation' OR 'degraded bog reclamation' OR' drained mire restoration' OR 'degraded mire reclamation' OR 'degraded fen restoration' OR 'drained fen reclamation'). "The outcome sought to provide relevant information in RDP research, such as (i) publication trends, (ii) research outlets, (iii) most influential keywords, (iv) most influential institutions and authors, and (v) top influential countries active in RDP research. In addition, four clusters were identified to ascertain the central theme of RDP research, in which cluster one is linked to the central research theme-" impact of drainage on peatland ecosystem services; cluster two focused on the impact of peatland restoration on greenhouse gas emissions; cluster three is associated with peatland restoration and biogeochemical properties; and cluster four is related to peatland restoration and species richness. A new research hotspot, such as soil respiration, was identified via the keywords with the strongest citation bursts. This study will provide various stakeholders (e.g., industry, journal editors, policymakers, and researchers) with an instinctive understanding of the research status and the development frontier of RDP research.

KEYWORDS

**peatland restoration, degraded peatland, scientometric, publication trend analysis, greenhouse gas, drainage**

# 1 Introduction

Peatlands are found in an estimated 180 countries (Parish et al., 2008), covering 4.23 million km$^2$, or 2.84% of the global land area. They play a significant role in mediating the ecosystem functions, such as carbon storage, rich biodiversity, water retention and water quality, and livelihood (Joosten, 2009; Xu et al., 2018).

Nevertheless, most countries have degraded more than half of their original peatland coverage for agriculture and energy. One of the major causes of degradation of peatlands is the drainage for timber production, affecting approximately 15 million hectares in the northern boreal subarctic regions (Strack et al., 2008). It has been estimated that 50 million ha (13%) of peatlands have been directly altered by human land use in most European countries (Lappalainen 1996; Strack et al., 2008; Tanneberger and Wichtmann 2011). For example, Germany has degraded more than 85% of its original peatlands, an estimated 930,000 ha of drained peatlands (Joosten et al., 2017). In Ireland, peat soils cover 21% of the total land area, with a total peatland area of 1,564,650 hectares, but it is estimated that only 10% of raised bogs and 28% of blanket bogs are in a natural state (Pike, 2021). Peatlands make up 12% of the Southeast Asia, estimated to be around 27 million peatlands (Joosten et al., 2017). However, out of 27 million hectares of peatland, 12 million hectares (45%) are currently degraded. For example, in the past 15 years, it has been estimated that 3 million hectares of Indonesia's peatlands have been burned to make way for farming and logging. In Scotland, 70% of blanket bogs and 90% of raised bogs have been damaged.

Degraded peatland has reduced many ecosystem functions, such as water quality and quantity, biodiversity, and climate regulations (Bonn et al., 2016). Many studies have indicated that huge amounts of carbon have been emitted into the atmosphere due to peatland deforestation and degradation, draining, and repeated fires (Ballhorn et al., 2009; Jaenicke et al., 2010; Hooijer et al., 2014). The removal of above- and below-ground biomass, peat decomposition and oxidation caused by drainage, and peat combustion are all major sources of carbon loss and $CO_2$ emissions into the atmosphere. Meanwhile, the application of N fertilizers on degraded peatland acts as a source of $N_2O$ emission, especially when nitrogen fertilizers have been added to promote agricultural productivity (Dohong et al., 2017; Mishra et al., 2021). Tree harvesting by clear-cutting on drained peatland has also been reported to enhance the leaching of dissolved organic C (DOC), dissolved organic N (DON), and mineral N to surface waters and the nearest catchment in a boreal peatland (Könönen et al., 2018). The clear-cutting of trees exposes the peat surfaces to direct sunlight, which and stimulates the decomposition of the drier peat through increased aerobic mineralization, causing high concentrations of DOC and associated watercolor to upland and seminatural catchments (Hooijer et al., 2014). Therefore, several restorations of degraded peatland (RDP) initiative has been attempted to restore the ecosystem processes, productivity, and services of the degraded peatland to its original natural condition (Haapalehto et al., 2011; Bonn et al., 2014).

RDP research has received considerable attention from researchers but is not limited to industry practitioners, with several researchers publishing traditional review papers from different aspects to summarize its development and effectiveness. Several review studies have made significant contributions to the RDP research discourse (Prince et al., 2003; Andersen et al., 2017; Chimner et al., 2017; Dohong et al., 2018; Leifeld and Menichetti, 2018; Harrison et al., 2020). Regardless, using the traditional reviews has some limitations because it has been qualitative and is subjected to manual evaluation according to the researcher's experience, which has been disparaged for irreproducibility and predilection to subjective biases (Hammersley, 2001; Yu and Liao, 2016).

According to Markoulli et al. (2017), traditional reviews seek to investigate the "trees," but do not provide a wide overview of the "forest." In addition, most existing review work has narrowed perspectives focusing on specificity, limiting aspects of RDP research. For example, Yuwati et al. (2021) review work focused on the restoration of degraded tropical peatland in Indonesia, while Dohong et al. (2017) study focused on a review of the drivers of tropical peatland degradation in South-East Asia. However, to the best of our knowledge, the existing literature on RDP is restricted to specific locations and review studies that provide a complete insight into RDP using the quantitative technique are inadequately examined. To fill this gap, the present study employs analytical algorithms to map a comprehensive survey of the intellectual core and the landscape of the general body of knowledge on RDP research. Specifically, a scientometric analysis was examined to evaluate the intellectual discourse and landscape of the general body of knowledge of (i) publication trend of RDP; (ii) country's co-authorship analysis, keywords co-occurrence analysis, research outlet analysis and document citation analysis, and (iii) a comprehensive discussion on key themes using the keywords co-occurrence analysis.

## 1.1 World peatland coverage

Peatlands are a distinctive wetland type that are characterized by the accumulation of partially decayed organic matter, resulting in the formation of peat layers (Likens, 2009). To date, there is no accepted standard definition of "peat" and "peatland," with different interest groups often using their definitions for peatland. For example, Burton & Hodgson (1987) define peat or peatland as > 50% OM, measured as a loss on ignition, while Joosten and Clarke (2002) determined peatland or peat as sedentarily accumulated material which consists of about 30% (dry mass) of dead organic material. In Ireland, 45-cm thick peat moss is considered a peatland, while

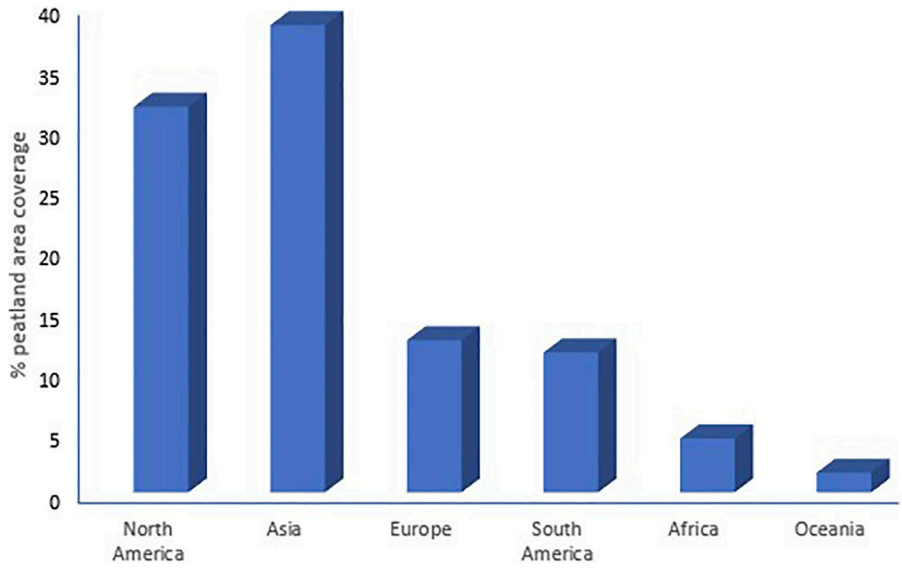


FIGURE 1
Percentage of the world's peatland coverage. Data used was retrieved from PEATMAP (Xu et al., 2018). As a result, 4.23 million km$^2$ was used as the total global peatland area coverage.

Germany's minimum thickness is approximately 30 cm (Steffens, 1996).

Peatlands cover 2.84% of the global land area, mainly in the mid-high latitudes of the Northern Hemisphere, with Canada containing 27% of the world's peatlands and is the second country with the most peatlands after Russia (Xu et al., 2018). Bogs and fens are the dominant peatland types in Canada. Bogs cover 67% ($762 \times 10^3$ km$^2$) of the total peatland area and fens cover 32% ($367 \times 10^3$ km$^2$), while marshes and swamps cover the remaining 1% (Tarnocai, 2006). Boreal (and polar), temperate, and tropical zone contribute about 83.3%, 4.0, and 12.7%, respectively, to the total peatland coverage (Leifeld and Menichetti, 2018). Active peat formation is found in the moist temperate climates predominate in the northern areas of the circumboreal taiga zone of coniferous forests, Finland, Alaska, and Canada (Tarnocai and Stolbovoy, 2006). The percentages of the global breakdown of peatland area coverage (4.23 million km$^2$) are shown in Figure 1, with the highest and the lowest percentage of peatland coverage from Asia and the Ocean, respectively.

In addition, peatlands are predominant outside the boreal zone proper in Ireland, Scotland, Germany, southwest Sweden, and northern Poland, northern Minnesota, and the Everglades of Florida (Sjörs, 1980). Canada contains an estimated of 27% of the world's peatlands and is the country with the most peatlands after Russia. Generally, peatlands are widespread in Asia, North America, Europe, and South America (FAO, 2012).

## 1.2 Types of peatland

Peatland formation results from flooding or waterlogged conditions, which results in the inhibition of organic materials decompositions, specifically plant material, due to the oxygen diffusion being impeded by the flooding conditions (Dise, 2009). There are many different ways of classifying peatland based on the purposes of the classifications. Recently, peat-forming systems have been classified into two broad peat-forming types based on the hydrogenetic type: the ombrogenous (nutrient-poor bogs) and geogenous bogs (fen), which differ in vegetation cover, water availability, and nutrient supply, geography and climate, and many more (Flores-Moreno et al., 2016). Water availability on peatland surfaces is significant for the distribution of vegetation, biomass productivity, nutrient transfer, decomposition, and preservation of organic matter in the peatland types. Nutrients (chemical elements, compounds, and metals) supplied to the peatland stimulate the growth metabolism of plants, either positively or negatively affecting the biodiversity, thereby influencing the type of peatland form (Lamers et al., 2012).

Topography and climate conditions are factors that cannot be ignored during peatland formation because they affect the productivity of the ecosystem by influencing the phytosociology, biomass production, energy flux, plant dynamics, and soil and nutrient cycling (Graniero and Price, 1999). For example, herbaceous plant remains in the temperate climatic region produce fibric to hemic peats during decomposition; while in the humid climatic region highly decayed woody plant remains

produce hemic to sapric peats, influencing the nutrient flux and types of peat form (Flores, 2014).

Ombrogenous peatlands (bog) receive water and nutrients from the atmosphere because they are isolated from the groundwater. They are found mainly in the temperate and the tropics region, with differing peatland types, vegetation cover, peat depth, and topography (Joosten & Clarke, 2002; Lavoie et al., 2005a). Unlike fen, ombrogenous bog depends only on rainfall for water and nutrient supplies, which influence the vegetation and the plant biomass cover. This results in the formation of an above-ground biomass, which is known as raised or blanket bogs (Nykänen et al., 1998: Flores, 2014).

A raised bog is characterized by complex structures of organic debris reaching an estimated thickness of 12 m, comprising three sediments stratigraphy, namely a basal tier of the bog formed under minerotrophic groundwater, sub-surface, and upper tiers (Hammond, 1981). In addition, the layers formed in the raised bog consist of a loose living moss at the surface, dead moss, and a partially decomposed peat that retards evapotranspiration during the intense temperature rise, hence protecting the bog from water loss (Minayeva and Sirin, 2011). Raised bogs consist of low concentrations of dissolved nutrients and low pH (<5.0) with *sphagnum mosses*, but can also contain patches of sedge (*Carex* sp.), small shrubs, and trees (Bubier et al., 1995).

A blanket bog consists of peat in a moderately deep accumulation of 2.6 m thick that is deposited on gentle to steep slopes (Hammond, 1981), having a low pH (<5.0), and a predominate vegetation cover of Vaccinium *myrtillus, t'mpetrum nigrum*, and *Diplophyllum_albican*. The onset of the blanket bog formation is closely correlated with climatic deterioration within the post-glacial period. Its formation is controlled by climatic factors such as rainfall (>1,250 mm), high atmospheric humidity, and topography (Hammond, 1981). The topography influences the flow of nutrients leached by rain and the vegetation distribution, as reported by Hammond (1981). The high acidity of ombrotrophic bogs originates from their organic acids, predominately fulvic and humic acid, and the sequestration of cations in peat. Generally, the pH of the blanket and the raised bogs is dependent on the carboxylic acid (R–COOH) content of dissolved organic matter (DOM) originating in the peat, ion exchange with living plants (e.g., bryophytes), and the nutrient content received from their atmosphere (Sjörs and Gunnarsson, 2002).

Fens are wetlands with accumulated peat of 40 cm thick, receiving water and nutrients from rainfall, inflowing streams, and groundwater, making them fertile for plant growth compared to the ombrogenous peatlands. The enriched water from the inflowing streams and the surrounding watershed provides an array of minerals for a diverse plant community and stimulates the degree of oxygenation to the organic substrate, thereby accelerating peat decomposition (Miettinen & Liew, 2010). The formation of geogenous bogs occurs at raised bogs bases (ombrogenous bogs) and the central plain, in river valleys, and poorly drained hollows adjacent to raised bogs. The fens are characterized by acidic to alkaline water ranging from 4.5 to 7.5, with brown mosses and herbaceous plants as the common vegetation (Crum, & Planisek, 1992). The high pH of the fen is due to the input of water and minerals from the ground, overland runoff, and the nearby watershed serving as a source of more mineral-derived alkalinity and higher pH (Bridgham et al., 1999). With increasing pH, Sjörs (1950) subdivided fen into acidic fens, intermediate fens, and rich fens. Sjörs and Gunnarsson (2002) conclude that the high pH of an intact or undisturbed fen peatland is due to the release of bicarbonate and carbonate from the groundwater to buffer the pH of the fen.

## 1.3 Effect of degraded peatland on ecological functions

The impact of peatlands that have been degraded or disturbed has changed in physical characteristics, biology, and chemistry, resulting in a loss of the ecological function of the peat, putting environmental and social-economic development at risk (Maftu'ah et al., 2019). Some of the repercussions of disturbing peatland include hydrophobicity, increased soil acidity, and decreased total organic carbon (TOC) and total organic nitrogen (TON) (Anshari 2010). Irreversible drying conditions indicate degraded peat features (Salmah et al., 1991). According to Valat et al. (1991), the hydrophobic character of peat soil is caused by: the presence of humic acid, which is naturally hydrophobic because its particles are covered by wax; the presence of non-polar groups, such as ethyl, methyl, and temporary aromatic compounds, which cause the hydrophilic group to decrease; and the absorption of hydrophobic substances, such as oil, fat, and N-organic fractions on the surface of the humic fraction. Soil hydrophobicity can aid in evaluating soil quality and fertility factors (Matejková and Simon, 2012). According to Maftu'ah et al. (2019), soil water content at the study site showed a substantial variation. Compared to natural peatlands and agricultural land, there was a considerable decrease in water content in degraded peatlands, reaching more than 3 times lower.

Soil pH in degraded peatlands is 3.62, whereas in agricultural soils it is 4.70 (Maftu'ah et al., 2019). According to Maftu'ah et al. (2019), the overall pH of soil differed significantly. Ion $H^+$ and $Al^{3+}$ were the main sources of the low pH in the peat in the examined area (Maftu'ah et al., 2019). The dissociation of organic acids, specifically plant-derived acids, which are usually dominated by fulvic and humic acid in peat was the source of the $H^+$ ion. Organic acids play a significant role in peat soil's low pH. Carboxylates (R-COOH) and phenols ($C_6H_4OH$) are the most abundant reactive groups in decomposed organic matter, and they dominate the exchange complex. Strong organic acids can dissociate and produce enormous amounts of ions. The

presence of Al ions is also a source of higher acidity (Maftu'ah et al., 2019).

In an experiment, disturbed or degraded peatlands had the highest total N values, while natural peatlands had the lowest (Maftu'ah et al., 2019). This happens because plant materials contribute to organic matter in the soil, and natural peatlands have low decomposition rates, which may help maintain high organic matter (Maftu'ah et al., 2019). Because bog drainage has been demonstrated to boost production rates, dissolved organic carbon (DOC) concentrations are a particular concern in degraded peatlands (Bussell et al., 2010). This could be due to increased microbial activity and phenolic component breakdown caused by oxygenation (Fenner and Freeman, 2011) and changes in peat structure (Minkkinen and Laine, 1998; Holden, 2005). Other nutrients, such as nitrogen (N) and phosphorus (P), which are held in substantial amounts in the upper layers of peat soils are also prone to losses as a result of oxygenation and subsequent mineralization (Miller et al., 1996; Tiemeyer et al., 2007).

Peatland is one of the World Wildlife Fund's internationally important ecological regions (Brooks et al., 2006). The majority of wild animals and flora have been known to thrive in this location due to ideal habitats (e.g., fertile soil, rainforest, and a favorable environment) (Adesiji, et al., 2015). According to Parish and Looi (1999), agricultural development causes peatland removal, which results in a loss of biodiversity and habitat for some indigenous flora and wildlife. Prior to the invasion of peatlands for logging and expansion of oil palm plantations, there was a high level of vegetation and fauna (Adesiji, et al., 2015).

Emissions from degraded peatlands are estimated at 2 gigatonnes of CO 2e annually, due to peatland deforestation and degradation, draining, and repeated fires (Zheng et al., 2021). The removal of above- and below-ground biomass, peat decomposition and oxidation caused by drainage, and peat combustion are all major sources of carbon loss and $CO_2$ emissions; Hooijer et al., 2012; Hooijer et al., 2006). Draining peatland for large-scale agriculture and industrial plantations has been a global concern in recent decades due to significant $CO_2$ emissions from peat oxidation and decomposition, which contribute to global climate change (Hooijer et al., 2012; Biancalani and Avagyan, 2014).

# 2 Methodology

This current study employs analytical algorithms that are known as scientometrics to detect the intellectual structure of RDP by analyzing the major topic studied, and the connections among researchers and major studies (Nikolenko et al., 2017). Scientometric is a subset of informetric analysis process and visualization of bibliometric data of a particular research theme. This method is useful for visualizing significant patterns and trends in RDP research discourse. Scientometric studies produce an authentic and less skewed result that is not influenced by any individual's or author's perspective (Martinez et al., 2019; Şenel, 2019; Baker et al., 2021). Furthermore, it provides solutions to the difficulties experienced by scholars doing traditional reviews and connects journals, keywords, writers, publications, and nations within a specific study topic (Darko et al., 2020; Zhang et al., 2021). Therefore, this study uses maps and bibliometric data to quantify research trends and highlight research hotspots in the RDP research discourse.

## 2.1 Data collection and search strategy

The Web of Science (WOS) database was selected to retrieve bibliography information of documents in RDP research. The WOS was chosen for the data collection because its research entails over 3,300 carefully selected publishers and over 12,000 high-impact journals, indexed in the database since 1900 (Li et al., 2021). The data used for this study was extracted on 15 January 2022, from the online library of the Technological University Dublin using the advanced search "TS (topic) = ('drained peatland restoration' OR 'drained bog restoration' OR 'drained mire restoration' OR degraded peatland restoration' OR 'degraded bog restoration' OR 'drained peatland reclamation' OR 'drained bog restoration' OR 'degraded peatland reclamation' OR 'degraded bog reclamation' OR 'drained mire restoration' OR 'degraded mire reclamation' OR 'degraded fen restoration' OR 'drained fen reclamation'). If the defined terms appeared in the title, keywords, or abstracts, then the documents would be identified. In addition, data refinement techniques were employed such that the "document type" was limited to "review" and "article" only, while the language type was limited to English only and the "timespan" was set to "1945 to 2021." As a result, 522 documents were retrieved by keyword based-bibliometric for the scientometric analysis. Retrieved documents from the WOS database were then saved in "plain text" with "full record and cited references".

## 2.2 Science mapping

Scientometric techniques such as network construction through keywords co-occurrence analysis, document co-citation analysis, citation burst analysis, outlets direct citation analysis, and co-authorship analysis were carried out *via* VOSviewer and CiteSpace. Vosviewer and the CiteSpace were selected as science mapping tools to analyze the retrieved bibliographic data in the RDP research discourse. Vosviewer is a software tool that offers basic functionality for producing, visualizing, and exploring bibliometric networks (Van Eck & Waltman, 2020).

The output of the VOSviewer is a distance-based map that consists of nodes and edges, whereas the node size reveals the frequency of occurrence of a topic in the abstract and titles of

published documents in relation to specific research topics and the edges indicate the relations among the nodes, strength, and weight of the relations (Perianes-Rodriguez et al., 2016; Oraee et al., 2017). In addition, the total length strength is attributed to the strength of the relationship between nodes, as reported in Elisha and Viljoen (2021), while a link referred to a connection or a relationship between two items.

Fractional counting was selected to create the distance-based map. The idea of selecting fractional counting is to decrease the influence of documents having many authors such that the co-authorship link strength between two authors is evaluated not only by the number of documents co-authored by the authors but also by the total number of authors of each of the co-authored documents (Van Eck & Waltman, 2013).

Similarly, to the VOSviewer, the CiteSpace also performs visual analytic functions of science mapping, as reported in Chen (2006). In this study, burst detection in CiteSpace was used to provide evidence of which keywords have frequently been cited within RDP research. The burst detection in CiteSpace is based on Kleinberg's algorithm (Kleinberg, 2002).

### 2.2.1 Keywords co-occurrence analysis

Keywords represent a published document's content or the core theme of a research paper, (Cobo et al., 2011; Van Eck & Waltman, 2014; Shrivastava, & Mahajan, 2016). According to Su and Lee (2010), keyword analysis offers an opportunity to ascertain the central theme of particular research topics (Chen et al., 2021; Van Eck and Waltman, 2014; Hosseini et al., 2018: van Eck et al., 2010). To compute the visualization of the keywords, all keywords were used rather than the author's keywords. According to Hosseini et al. (2018), using all keywords for mapping-based studies produces a large number of terms that are not solely dependent on authors' experience and knowledge in choosing appropriate research keywords. All of our keywords have been widely used in several science mapping-based studies (Ravikumar et al., 2015; Williams et al., 2016; Zhang et al., 2017; Fridell et al., 2020). A total of 2,578 keywords were obtained from the WOS database using the fractional counting methodology. Regarding the "minimum number of occurrences" for a keyword to be included in the network, a value of 9 was selected, and the inclusion criterion was met by 103 of the 2,578 keywords.

### 2.2.2 Outlets direct citation analysis

Outlets' direct citation analysis can be significant to researchers in identifying the best journals for their research publication (Hosseini et al., 2018). Furthermore, according to Guidry et al. (2004) and Darko et al. (2019), performing outlets' direct citation analysis assists the journal editors in making adjustments to the goals and objectives of their journals, and assists institutions/libraries in optimizing the resources allocation for investing in journals. A total of 181 sources were obtained from the WOS database using the fractional counting methodology. The "minimum number of documents of a source" and the "minimum number of citations of a source" were set to 5 and 60, respectively. Of the 180 sources found, 20 items met the threshold and were added to the resultant network for the outlet's direct citation analysis in RDP research.

### 2.2.3 Document citation networks in RDP

Document citation analysis helps to reveal the intuition of the structure of a scientific knowledge domain. The concept of citation has been used as a research method to measure the degree of relationship between documents and the impact of the publication. Therefore, citation analysis of documents was computed to analyze the citations of documents in the RDP research domain. A total of 522 documents were reported using the fractional counting methodology. The minimum number of citations of the documents" was set to 70. Of the 522 documents found, 18 items met the threshold and were added to the resultant network.

### 2.2.4 Co-authorship analysis

Co-authorship networks can evaluate scientific collaboration networks. The minimum number of documents of an author and citations were set to 7 and 40, respectively. Of the 1,366 authors, only 15 authors met the threshold and were added to the resultant network.

### 2.2.5 Active countries in the RDP research

The significance of determining the most active countries in the RDP research domain is to enhance future collaboration, specialties, and expertise, and can promote the exchange of technologies and innovation among countries, as reported in Wuni et al. (2019). The resultant network was generated by setting the minimum number of documents and the citation of a country to 11 and 20, respectively. Of the 51 countries of RDP research discourse, 12 met the threshold.

## 3 Results and discussion

### 3.1 Publication trend of RDP research

The RDP literature data retrieved from WOS revealed that RDP research began in 1991, based on our search keywords, as seen in Figure 2. The first study was conducted by Van Diggelen et al. (1991), who analyzed the hydro-ecology of the fen system at Leiper Posse in eastern Germany. Poddubny and Galat conducted the second study, which was published in the Regulated Rivers: Research & Management journal. Poddubny and Galat's (1995) research, which was titled "Habitat associations of upper Volga River fishes: effects of reservoirs", recommended that the restoration of degraded bog areas or flood plains can enhance the diversity and productivity of fishes in the upper Volga River. This indicates that RDP research has been around since 1991.

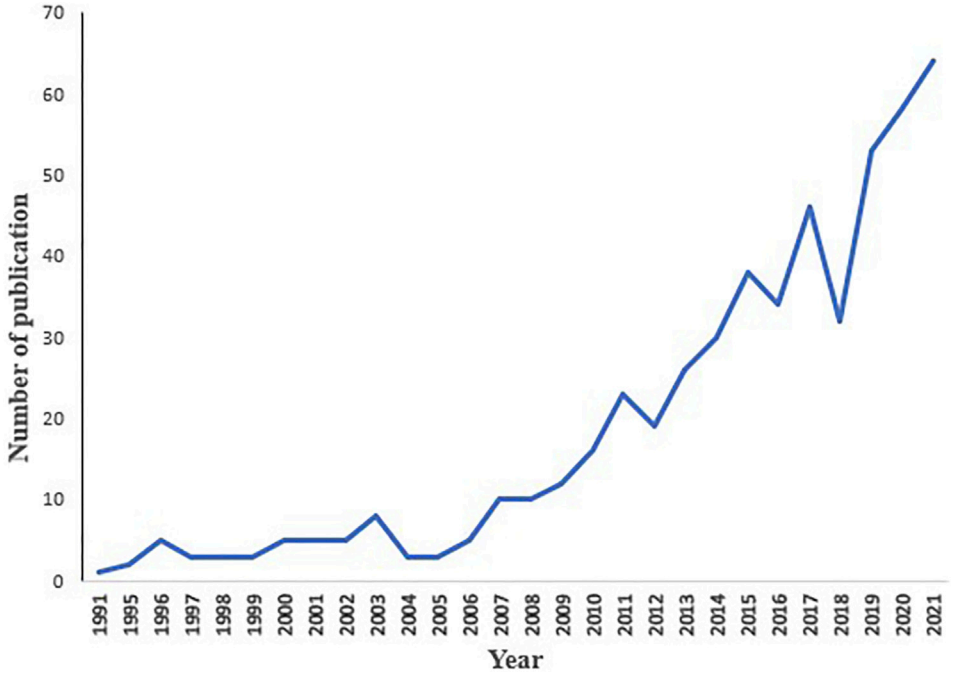


FIGURE 2
Trends in the RDP publication from 1991 to 2021.

Figure 2 shows the publication trend of RDP from 1991 to 2021. The number of documents published increased from 1 document in 1991 to 61 documents in 2021. Figure 2 shows an exponential increase of published documents over the reported period (1991–2021), which may probably be due to the world recognition of the significance of RDP research in the enhancement of ecosystem services. Examples of ecosystem services indicators that have been reported to enhance after the restoration of degraded peatland from 1991 to 2021 include atmospheric $CO_2$ sequestration (Waddington and Warner, 2001), vegetation (Tuittila et al., 2000), organic carbon (Wallage et al., 2006), porewater (Meissner et al., 2003) and so on. A steady and tremendous increase in RDP research was observed from 2012 to 2015, with a sharp decrease in 2016. Unexpectedly, there was an increase in published documents from 2019 to 2021.

The rising importance of RDP research agrees with Andersen et al.'s (2017) and Waddington et al.'s (2010) findings that most countries have degraded more than half of their original peatland coverage for agriculture and energy use, resulting in greenhouse gas emissions. Therefore, RDP research aims to decrease greenhouse gas emissions and enhance on-farm biodiversity conservation and other environmental-related issues. For example, Chapman et al. (2012) emphasized that integrating RDP as mitigation measures for reducing greenhouse gas (GHG) in Scotland could provide up to 2.7 Mt $CO_2$-eq savings per year. A similar observation was made in Ireland that restoring degraded peatland through rewetting could reduce $CO_2$ emissions by enhancing C sequestration, as Wilson et al. (2012) and Wilson et al. (2013) reported.

An overview of the RPD is presented in Table 1. As observed in Table 1, the total number of citations increased from 1991 to 2021. However, a slight fluctuation of citations per published document is seen with the highest total times cited observed in 2021. Therefore, based on search keywords in this study, it can be deduced that since RDP started in 1991, there have been 522 published documents, achieving total times cited of 10,480 in the RDP research field.

## 3.2 Structure of the body of knowledge in RDP: Research outlet, keywords co-occurrence analysis, and document citation analysis

### 3.2.1 Keywords co-occurrence analysis

The keywords co-occurrence network analysis helps to group the keywords into different clusters. Four clusters were obtained entailing 74 nodes, 2,730 links and a total link strength of 1,242.50, as seen in Figure 3, depicting the major keywords and their inter-relatedness

TABLE 1 Characteristics by year of publications of the RDP, from 1991 to 2021.

| Published Year | Total publications (TC) | Total times cited (TP) | TC/TP | % Total Publication |
|---|---|---|---|---|
| 1991 | 1 | 0 | 0 | 0.2 |
| 1992 | * | * | * | 0 |
| 1993 | * | * | * | 0 |
| 1994 | * | * | * | 0 |
| 1995 | 2 | 2 | 1 | 0.4 |
| 1996 | 5 | 17 | 3 | 1.0 |
| 1997 | 3 | 12 | 4 | 0.6 |
| 1998 | 3 | 26 | 9 | 0.6 |
| 1999 | 3 | 38 | 13 | 0.6 |
| 2000 | 5 | 35 | 7 | 1.0 |
| 2001 | 5 | 61 | 12 | 1.0 |
| 2002 | 5 | 53 | 11 | 1.0 |
| 2003 | 8 | 78 | 10 | 1.5 |
| 2004 | 3 | 72 | 24 | 0.6 |
| 2005 | 3 | 90 | 30 | 0.6 |
| 2006 | 5 | 108 | 22 | 1.0 |
| 2007 | 10 | 110 | 11 | 1.9 |
| 2008 | 10 | 115 | 12 | 1.9 |
| 2009 | 12 | 162 | 14 | 2.3 |
| 2010 | 16 | 246 | 15 | 3.1 |
| 2011 | 23 | 255 | 11 | 4.4 |
| 2012 | 19 | 295 | 16 | 3.6 |
| 2013 | 26 | 377 | 15 | 5.0 |
| 2014 | 30 | 508 | 17 | 5.7 |
| 2015 | 38 | 561 | 15 | 7.3 |
| 2016 | 34 | 786 | 23 | 6.5 |
| 2017 | 46 | 801 | 17 | 8.8 |
| 2018 | 32 | 902 | 28 | 6.1 |
| 2019 | 53 | 1,082 | 20 | 10.2 |
| 2020 | 58 | 1,330 | 23 | 11.1 |
| 2021 | 64 | 1,603 | 25 | 12.3 |

*No publication found.

of the current RDP research. The colors of each node indicate the different clusters to which the terms belong. A term was assigned to each cluster to provide in-depth interpretation and understanding of the central research theme within the RDP.

#### 3.2.1.1 Cluster #1

Keywords explaining peatland drainage impact are classified into cluster one, represented in yellow, containing drainage, climate change, hydrology, water, hydraulic conductivity, and fire (Figure 3). The analysis of all keywords revealed that the keywords in cluster one are linked to the central research theme "impact of drainage on peatland ecosystem services," which suggests that peatland drainage is a major threat to peatland degradation.

Peatland formation results from flooding or waterlogged conditions, which results in the inhibition of organic materials decompositions, specifically plant materials, due to the oxygen diffusion being impeded by the flooding conditions (Dise, 2009). As a result, peatland drainage is being done by constructing drainage canals to lower the groundwater table, which allows peatland conversion to various land uses such as agriculture, plantation, forestry, and mining (Jaenicke et al., 2010; Rydin et al., 2013). However, the depletion of the groundwater leads to peat oxidation, consolidation, and shrinkage resulting in peat subsidence, carbon emissions, and increased fire hazards, all of which exacerbate climate change (Hooijer et al., 2012; Dohong et al., 2017).

The peatland drainage issues are closely tied to climate change consequences, which is a major environmental

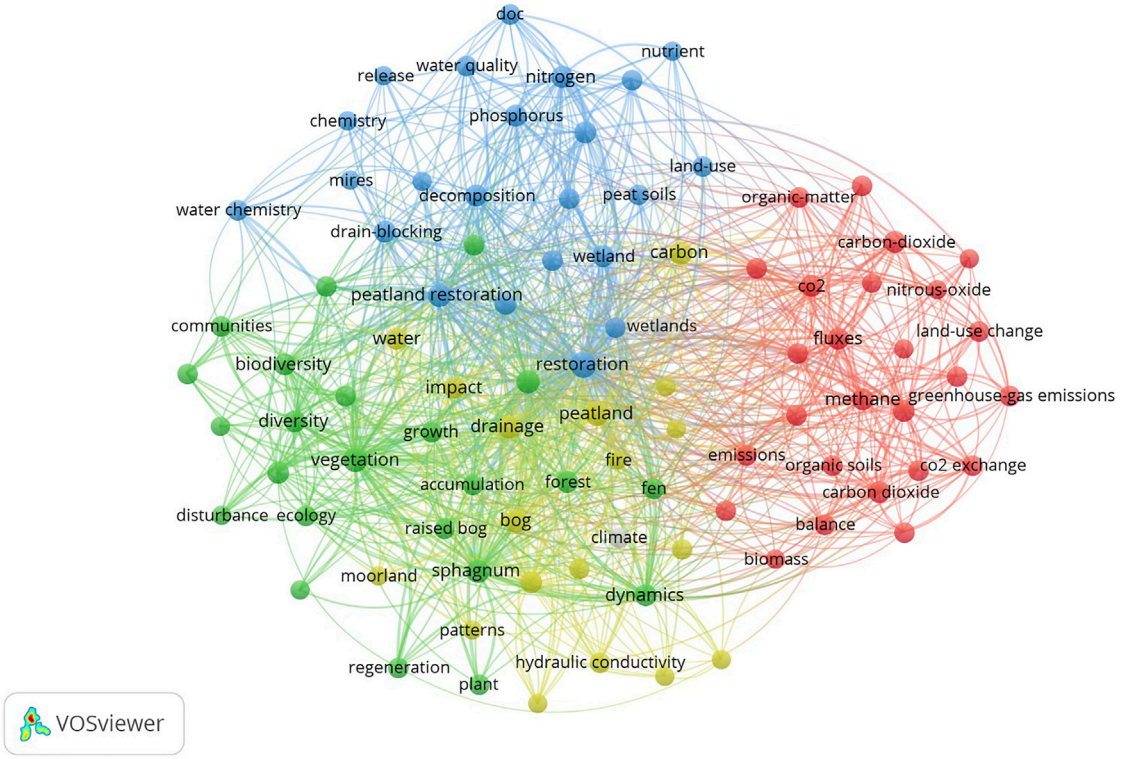


FIGURE 3
Main areas of RDP (co-occurrence network of keywords).

phenomenon (Prévost et al., 1999; Waddington and Price, 2000; Holden et al., 2004; Joosten, 2009; Hooijer et al., 2012). Therefore, there is no doubt that RDP research has been focused on how drainage affects climate change, water chemistry, and hydrology, serving as the justification for the RDP according to the keywords seen in cluster 1. In cluster one, drainage has the highest keyword occurrence and strong links to climate change and other keywords, which implies that drainage significantly impacts climate change.

Notwithstanding the less coverage of peatland worldwide, it plays a significant role in mediating fluxes of carbon dioxide ($CO_2$), methane ($CH_4$) and nitrous oxide ($N_2O$) between soil and the atmosphere (Martikainen et al., 1993). Peatland drainage stimulates soil aeration and oxygen concentrations, facilitating the growth and activity of aerobic microbes resulting in soil organic carbon decomposition, and thereby reversing the carbon flux into a net $CO_2$ emission into the atmosphere (Nykänen et al., 1998; Blodau, 2002; Smith, & Conen, 2004; Ojanen et al., 2013). The aeration created by the drainage stimulates the nitrification process, increasing the emission of $N_2O$, especially in the minerotrophic peatlands (Aerts & Ludwig 1997; Gao et al., 2014; Hribljan et al., 2014; Wang et al., 2017; Liimatainen et al., 2018). Mikaloff Fletcher and Schaefer (2019) predicted that the emission effects from drained peatlands in 2020–2100 entail 12%–41% of the remaining GHG emission budget. Also, runoff from drained peat through the drainage channels has known to cause degradation of water catchments and their downstream quality (Skaggs et al., 1994; Prévost et al., 1999; Piirainen et al., 2013; Kaila et al., 2016; Nieminen et al., 2017a; Nieminen et al., 2017b). Peatland drainage results in higher DOC concentrations in surface and pore water and increases DOC export into nearby streams (Strack et al., 2008). Marttila et al. (2018) observed high concentrations of nutrients and suspended sediment, mainly dissolved nitrogen and phosphorus, were found in headwater streams in catchments containing drained peatland, which agrees with similar studies reported by Mattsson et al. (2003) and Nieminen et al. (2017b).

In addition, the biogeochemical properties of peatland that have been affected by drainage are organic matter decomposition and fractions, soil respiration, soil enzymes, elemental concentration, microbial degradation, peat humification, and so on (Moore and Basiliko, 2006; Olde Venterink et al., 2009; Macrae et al., 2013; Hulatt et al., 2014; Brown et al., 2015; Krüger et al., 2015; Harris et al., 2020; Xu et al., 2021). In addition, studies on the impact of peatland drainage on the vegetation cover have been conducted by Ramchunder et al. (2009) and Haapalehto

et al. (2011). For example, Stewart & Lance (1991) reported a complete disappearance of *Sphagnum capillifolium* on 20 years of drained raised bog. Wilson et al. (2010) studied the effect of drainage on the plant species abundance within a Welsh blanket peatland. They reported a less abundance of peat-forming plant species, specifically *Eriophorum angustifolium.*

#### 3.2.1.2 Cluster #2

The second cluster (red portion of Figure 3) focuses on the impact of peatland restoration on GHG emissions, specifically $N_2O$, $CO_2$, and $CH_4$ emissions. Despite peatlands covering about 3% of the Earth's surface, they store ~644 Gt of C and 8–15 Gt N of the terrestrial biosphere (Turetsky et al., 2015; Leifeld and Menichetti, 2018; Ahmad et al., 2020). Currently, drainage accounts for ~10% of global peatlands degradation, transforming them from a net sink to a net source of GHG (Knox et al., 2015; Leifeld and Menichetti, 2018).

The consequences of drainage to stimulate GHG emissions into the atmosphere facilitated the need for peatland protection and restoration as proximate mitigation measures (Wilson et al., 2015). Dohong et al. (2018) review the techniques for effective tropical peatland restoration. According to Dohong et al. (2018), hydrological restoration through peatland rewetting has effectively reduced GHG emissions from degraded peatland. According to Strack and Zuback (2013), rewetting of degraded peatland reduced $CO_2$ emission through the reduction of peat mineralization, as well as negligible $N_2O$ emissions as a result of lowering the availability of mineral nitrogen in saturated conditions.

The hydrological restoration of degraded peatland involves a process that is known as rewetting/reflooding (O'Brien et al., 2007). Rewetting is the process whereby deliberately introduced ditches or gullies are blocked to reduce the surface runoff outflow or allow water levels within the peat to return to their natural state (Ahmad et al., 2020). The significance of peatland rewetting is to enhance the peat's hydrological properties by raising the groundwater table so that the hydrological properties of the drained peatland are recovered and stabilized as close as possible to its pre-logging and pre-drainage hydrological conditions (Page et al., 2009a; Panda et al., 2012).

Several studies observed that rewetting of drained peatland stimulates $CO_2$-C sink functions immediately (Tuittila et al., 1999; Zeng & Gao, 2016; Cui et al., 2017). This happens because rewetting reduces the diffusive oxygen supply in the peatland, thereby creating an anaerobic environment, which in turn inhibits the organic matter and the litter decomposition, resulting in soil organic matter accumulation and the formation of peat layer (partially decomposed organic matter) (Herbst et al., 2011; Kim et al., 2011). However, the rewetting of degraded peatland stimulates the $CH_4$ gases because the resulting anoxic conditions created by the rewetting are conducive to methanogenesis. Vanselow-Algan et al. (2015), Hahn et al. (2015) reported a methane emission of 148 g CH4 $m^{-2}$ $yr^{-1}$ and 260 g CH4 $m^{-2}$ $yr^{-1}$, respectively exceeding the default IPCC emission factor for rewetted drained peatland in the temperate region (29 g $CH_4$ $m^{-2}$ $yr^{-1}$). Kandel et al. (2019) observed an increase in $CH_4$ emission after 12 years of rewetting compared to the undrained site. They attributed their findings to the decomposition of above-ground biomass under inundated soil surface conditions.

Therefore, restoration management intended to reduce $CO_2$ and $CH_4$ emissions should prevent on-site above-ground biomass deposition combined with site inundation (Kandel et al., 2019). $N_2O$ emission reduction from rewetted peatlands is due to the raising of the groundwater table, thereby inhibiting nitrification and the denitrification process (Oktarita et al., 2017; Pärn et al., 2018). However, the resulting GHG fluxes from rewetted peatland may differ due to temperature, vegetation cover, growing season length, microbial community composition, biogeochemistry, previous land-use history, prevailing biomass species, and site (Renou-Wilson et al., 2014; Wrage-Mönnig et al., 2018).

#### 3.2.1.3 Cluster #3

Cluster 3 (blue) is associated with peatland restoration and biogeochemical properties, specifically DOC. The keywords that are found in cluster 3 are phosphorus, nitrogen, carbon, water quality, water table, decomposition, dissolved organic carbon, and drain blocking. Degraded peatland is known to have high nutrient content because the lower water tables of the drained peatland expose deeper peat to oxic conditions, resulting in the high decomposition of the organic matter/peat layers and nutrient mineralization in the peat matrix. The drained peatlands contribute to the loss of carbon through the aquatic fluxes of carbon (e.g., DOC) into downstream water bodies, as reported in Limpens et al. (2008).

Restoration of the degraded peatland will result in the inhibitory effects of low nutrient concentration and DOC transport. Hence, making RDP research target DOC due to its consequences (D'Andrilli et al., 2010; Tfaily et al., 2013). DOC transport from degraded peatland to nearby catchment causes organic and inorganic micropollutants, and enhances bacterial regrowth within water distribution systems (Holden, 2005; Gough et al., 2016). Haapalehto et al. (2014) reported long-term decreases in DOC and nutrient leaching but temporary increases in N and P for the first 5 years of degraded peatland restoration. In addition, major nutrient such as phosphorus and nitrogen content has been extensively studied in a restored peatland (Moore et al., 2005; Nieminen et al., 2017a; Munir et al., 2017; Salmon et al., 2021).

#### 3.2.1.4 Cluster #4

Cluster 4, represented in green, is related to peatland restoration and species richness, having keywords such as biodiversity, conservations, sphagnum, vegetation, plant, and so on. Since co-occurrence keywords are essential in reflecting and

TABLE 2 Top 25 most active keywords in the restoration of degraded peatland research.

| Keyword | Occurrences | Total link strength |
|---|---|---|
| Restoration | 179 | 175 |
| Vegetation | 108 | 107 |
| Peatlands | 69 | 68 |
| Drainage | 64 | 63 |
| Dynamics | 49 | 49 |
| Nitrogen | 49 | 48 |
| Water | 49 | 49 |
| Carbon | 46 | 46 |
| Bog | 44 | 43 |
| Sphagnum | 44 | 44 |
| Management | 40 | 39 |
| Diversity | 39 | 39 |
| Biodiversity | 36 | 36 |
| Fluxes | 35 | 35 |
| Rewetting | 35 | 35 |
| Wetlands | 35 | 33 |
| Hydrology | 33 | 33 |
| Phosphorus | 33 | 32 |
| Conservation | 32 | 32 |
| Impact | 32 | 32 |
| Wetland | 32 | 32 |
| Methane | 31 | 31 |
| Soil | 31 | 31 |
| Decomposition | 29 | 29 |
| Fen | 29 | 29 |

defining research contents, cluster 4, as seen in Figure 3, revealed degraded peatland restoration on the vegetation development. Peatland vegetation supports numerous invertebrates, birds, and bryophytes (Warner and Asada, 2006). Therefore, vegetation development on drained peatland has been an indicator to measure the success of peatland restoration (Richert et al., 2000; Tuittila et al., 2000; Van Dijk et al., 2007) because the vegetation response plays a significant role in the carbon and GHG budget of a peatland (Peacock et al., 2013). The vegetation development on restored sites depends on the water table, plant propagules, temperature, and the nutrient status of the site (Campbell and Rochefort, 2003; Strack et al., 2014).

Blocking drained ditches in drained peatland is frequently used to increase the water table (WT) to enhance the establishment of peat-forming plant species. Some peat-forming plant species that have been reported to have re-established after restoring degraded peatland are *Eriophorum vaginatum*, *Sphagnum cuspidatum*, and *Sphagnum auriculatum*, *Calluna vulgaris*, *Vaccinium myrtillus*, *Erica tetralix*, and *Empetrum nigrum* (Komulainen et al., 1998; Lavoie et al., 2005b). Peacock et al. (2013) reported that ditch blocking increased plant species richness in restored peatland; whereas *Eriophorum vaginatum* and *Eriophorum cuspidatum were* the primary colonizing species, with additional colonization by *Eriophorum angustifolium*, algae, and other sphagnum species.

Table 2 shows the top 25 most active keywords in the RDP research domain based on the numerical statistics of the variations in the node sizes and total link strength (co-occurrence connection or links) of the keywords. Out of 2,578 all keywords, the top five (5) most active keywords used in the RDP research domain are restoration, vegetation, peatland, drainage, and dynamics. Furthermore, co-occurrence keywords analysis was performed using cite space to investigate the topics receiving significant attention in the RDP research domain (Figure 4).

Figure 4 shows the burst time of most co-occurring keywords or research hotspots in the RDP research domain with the strongest citation bursts analysis using CiteSpace from 1991 to 2021. Citation burst illustrates evidence of which keywords have frequently been cited within the literature of a research theme/area, specifically growing topics or topics associated with surges in citations (Chen et al., 2014). Using the WOS dataset, 68 keywords had citation bursts, as seen in Figure 4, illustrating the top 25 keywords with the strongest citation bursts. The blue lines in the figure denote the time interval, whereas the red lines represent the time interval during which a subject was found to have a burst, indicating a citation burst event. The citation burst ranges from 5.42 to 2.33. The top five keywords having the strongest citation burst were diversity (burst strength, 5.42; 2014–2016), peatland (burst strength, 3.79; 2013–2016), land use (burst strength, 3.63; 2015–2016), water (burst strength, 3.27; 2006–2012), and drain blocking (burst strength, 3.22; 2014–2018). Furthermore, soil respiration (burst strength, 2.93; 2019–2021) is the most current burst, representing the emerging trend within the RDP research domain.

### 3.2.2 Research outlet: Outlets direct citation analysis

Figure 5 displays the network of the landmark research outlets in the RDP, consisting of 190 links and a total link strength of 3,264. Three clusters were formed, with different colors (i.e., red, green, and yellow) assigned to differentiate between journal clusters. Cluster 1 (blue) entails research outlets publishing articles focusing on the hydrology of peatland in RDP research. The research outlets found in cluster 1 are Science of the Total Environment, Hydrological Processes, Journal of Hydrology and Water Resources Research and so on. Cluster 2 (green) comprises research outlets Restoration Ecology, Biological Conversation, Applied Vegetation Science, Ecology and Evolution, and so on, which focus on vegetation and ecology RDP research. Cluster 3 (red) is composed of Mires and Peat, Wetlands

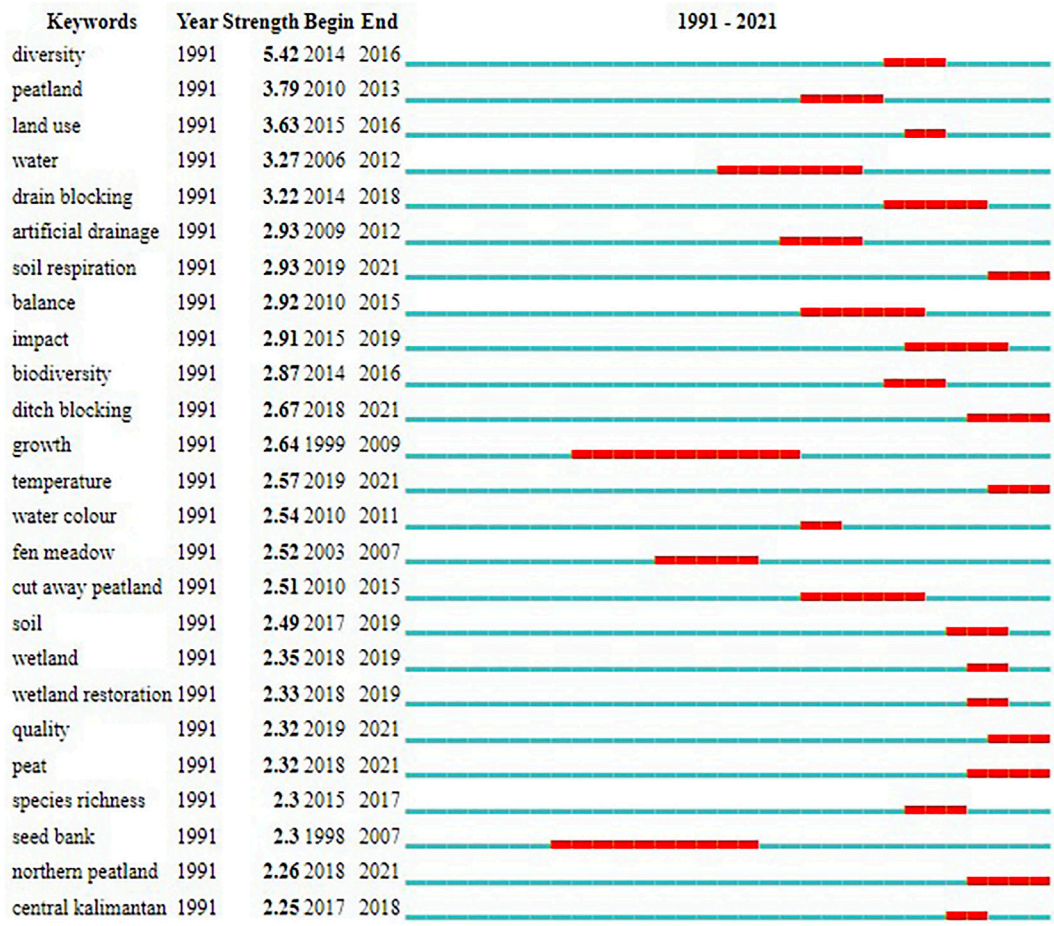


FIGURE 4
Top 25 keywords with the strongest citation bursts in the RDP (1991–2021).

Ecology and Management, Ecosystem, Ecological Engineering, Biogeoscience, and so on.

The top 20 research outlets with their quantitative measurement are presented in Table 3, with Mires and Peat recording the highest number of articles (40) in the RDP research domain. Mires and Peat is a peer-reviewed internet journal that publishes articles on mires, peatlands and peat-related research. It is published jointly by the International Peatland Society (IPS) and the International Mire Conservation Group (IMCG) (http://mires-and-peat.net/).

### 3.2.3 Document citation networks in RDP research

The resultant network of the document citation network analysis of RDP research comprises 101 links and 187.50 total links as displayed in Figure 6. From Figure 6, the top three cited articles include Leifeld and Menichetti (2018) "The underappreciated potential of peatlands in global climate change mitigation strategies." This article reveals that restoration of drained peatland drastically reduces the current annual GHG emission, which is 3.4 times less nitrogen costly, involving a much smaller land area demand than improving mineral soil carbon sequestration for mitigation of GHG emissions peat coverage areas. A review article titled "Hydrological processes in abandoned and restored peatlands: An overview of management approaches" which was written by Price et al. (2003), obtained a citation of 183, making them the second most cited article in the RDP research domain. Price et al. (2003) revealed that hydrological management increases hydrological functions, such as hydraulic conductivity, water retention capacity, vegetation development, and the specific yield of abandoned land peatland. Finally, the third most cited

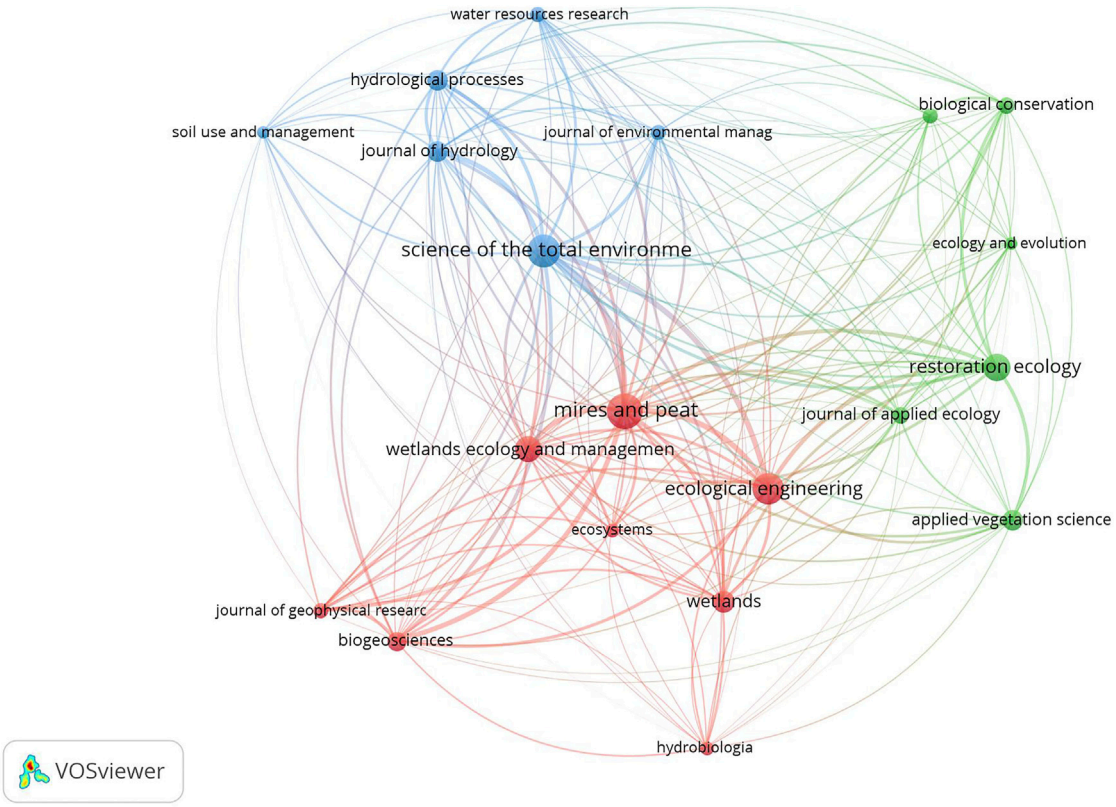


FIGURE 5
Network of the landmark research outlets in the RDP.

article was "Greenhouse gas balances of managed peatlands in the Nordic countries: Present knowledge and gaps" which was conducted by Maljanen et al. (2010). Another observation made from Table 4 suggests that the top three influential documents based on the citation index in the RDP research domain were literature review articles. A different trend was observed when evaluating the links among the top 13 articles. It was found that 22, 60, 80 and 60 of the 522 articles have cited Price et al. (2003), Maljanen et al. (2010)Leified et al. (2012), Knox et al. (2015), respectively. By analyzing the impact of rewetting on drained peatland, Komulainen et al. (1999) found that 2 years of rewetting stimulated carbon sequestration such that rewetted minerotrophic fen obtained $CO_2$-C balance ranged from 162 to 283 g $m^{-2}$, with dense *E. vaginatum* vegetation and a high-water table, while rewetted bog had $CO_2$-C balance varied from 54 to 101 g $m^{-2}$ having a high-water table and mire vegetation. Wuni et al. (2019) emphasized that the influence of articles can be assessed by their total citations, normalized citations, and links with other articles. Therefore, using the total citation approach, Table 4 summarizes the top 13 most influential research articles, with key findings, links, and citations.

## 3.3 Co-authorship and active countries in the RDP research

### 3.3.1 Co-authorship analysis

Scientific collaboration between researchers and institutions enhances knowledge exchange, innovation, and joint funding application (Hosseini et al., 2018). Only two clusters of productive and collaborative researchers were revealed, consisting of 105 links and a total link of 2,136, as illustrated in Supplementary Figure S1. Researchers such as Baird, Andy J., Peacock, Mike, Green, Sophie M., and Evans, Chris D. are found in cluster one (red). Cluster two (red) includes researchers such as Holden, Joseph and Evans, Martin G. Researchers such as Evans, Martin G and Holden, Joseph tend to collaborate more often in the RDP research (Evans et al., 1999; Holden et al., 2006). Supplementary Figure S1 suggests that Holden, Joseph; Kotiaho, Janne S., Vasander, Harri and Tahvanainen, Teemu are the top collaboratives researchers within the RDP research discourse. Using the citation index to measure the productivity of the top collaborative co-authors, Vasander, Harri and Holden, Joseph emerge as the top-cited authors within the RDP research domain, as seen in Supplementary Table S1.

TABLE 3 Research outlets in the restoration of degraded peatland research.

| Research outlet | No. of articles | Average citation | Total citations | Total link strength |
|---|---|---|---|---|
| Mires and peat | 40 | 8 | 311 | 929 |
| Science of the total environment | 35 | 20 | 683 | 811 |
| Ecological engineering | 30 | 15 | 444 | 646 |
| Restoration ecology | 24 | 14 | 346 | 490 |
| Wetlands ecology and management | 21 | 25 | 517 | 415 |
| Wetlands | 15 | 16 | 234 | 264 |
| Applied vegetation science | 14 | 22 | 309 | 215 |
| Hydrological processes | 13 | 13 | 172 | 324 |
| Journal of hydrology | 13 | 42 | 541 | 391 |
| Biogeosciences | 12 | 38 | 455 | 393 |
| Biological conservation | 9 | 12 | 111 | 194 |
| Journal of applied ecology | 9 | 37 | 336 | 178 |
| Forest ecology and management | 8 | 16 | 124 | 152 |
| Journal of environmental management | 8 | 16 | 129 | 202 |
| Journal of geophysical research-biogeosciences | 7 | 15 | 107 | 247 |
| Water resources research | 7 | 16 | 110 | 190 |
| Ecosystems | 6 | 52 | 314 | 182 |
| Hydrobiologia | 6 | 42 | 250 | 104 |
| Ecology and evolution | 5 | 19 | 93 | 109 |
| Soil use and management | 5 | 18 | 90 | 92 |

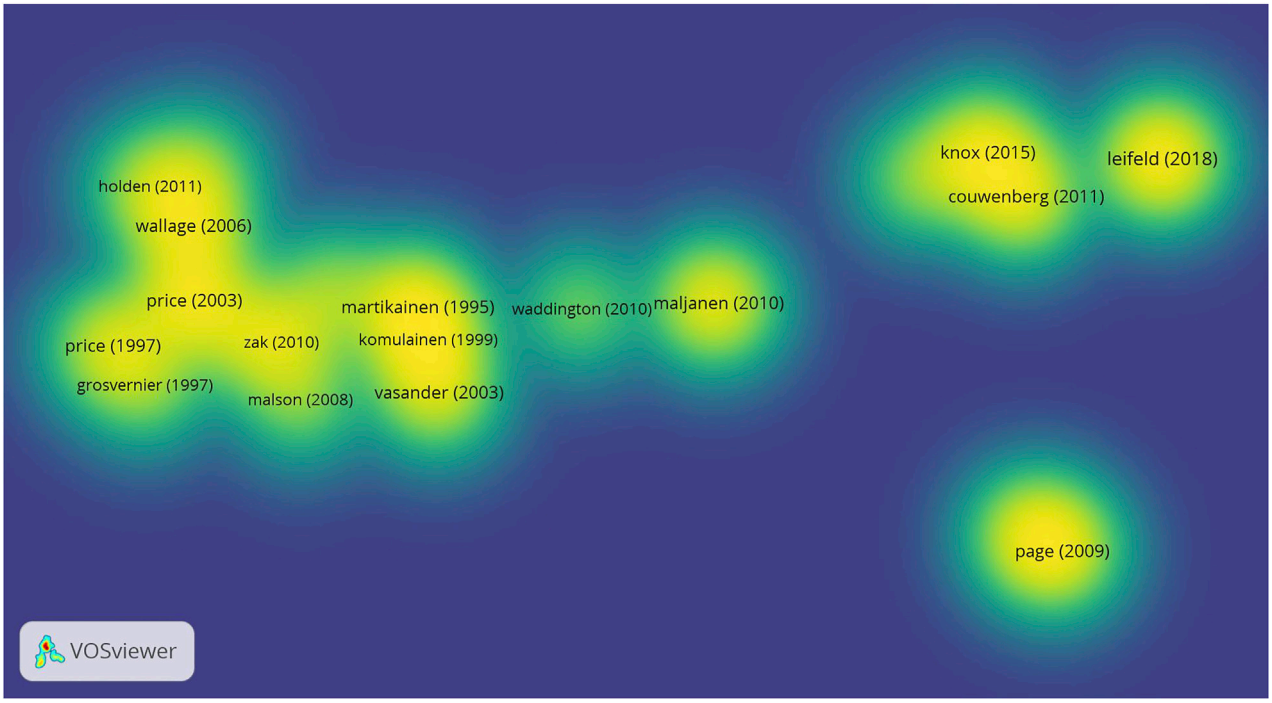


FIGURE 6
Density map of document citation network analysis.

TABLE 4 Highly cited document in the restoration of degraded peatland research domain.

| Article | Title | Citations | Total links | Research outlets | Type of articles | Key findings |
|---|---|---|---|---|---|---|
| Leifeld and Menichetti (2018) | The underappreciated potential of peatlands in global climate change mitigation strategies | 226 | 22 | Nature communication | Review | Restoration of drained peatland drastically reduces the current annual greenhouse gas emission, which is 3.4 times less nitrogen costly than improving mineral soil carbon sequestration for mitigation of greenhouse gas emission in peat coverage areas. |
| Price et al. (2003) | Hydrological processes in abandoned and restored peatlands: An overview of management approaches | 183 | 60 | Wetlands Ecology and Management | Review | The authors discovered that hydrological management options (e.g., blocking ditches, constructing bunds, reconfiguring the surface, and managing microclimate) increase the hydrological functions of abandoned land peatland. |
| Maljanen et al. (2010) | Greenhouse gas balances of managed peatlands in the Nordic countries—present knowledge and gaps | 183 | 80 | Biogeosciences | Review | Annual mean GHG balances ($CH_4$, $N_2O$ and $CO_2$ emissions) from agriculture managed peatland in the Nordic countries were 2,280 and 3,140 g $CO_2$ eq. $m^{-2}$ for areas drained for grass swards, cereals or those left fallow, respectively. The mean net GHG missions in abandoned and afforested agricultural peatlands recorded 1,580 and 500 g $CO_2$ eq.$m^{-2}$, respectively. |
| Knox et al. (2015) | Agricultural peatland restoration: effects of land-use change on greenhouse gas ($CO_2$ and $CH_4$) fluxes in the Sacramento-San Joaquin Delta | 178 | 60 | Global Change Biology | Research article | The conventional drained agricultural peatland used for pasture and corn production released 341 g C $m^2$ $yr^1$ as $CO_2$ and 11.4 g C $m^2$ $yr^1$ as $CH_4$, while flooded land-use types (a rice paddy and two restored wetlands) store up to 397 g C $m^2$ $yr^1$ but obtained a higher methane emission ranging from 39 to 53 g C $m^2$ $yr^1$, suggesting that rewetting of drained agriculture pet soils reduce soil subsidence and GHG emissions. |
| Martikainen (1995) | Change in fluxes of carbon dioxide, methane and nitrous oxide due to forest drainage of mire sites of different trophy | 160 | 11 | Plant and Soil | Research article | Drainage negatively affects the annual $CO_2$ and $N_2O$ emissions but decreases the emissions of $CH_4$ in a drained peatland. |
| Couwenberg et al. (2011) | Assessing greenhouse gas emissions from peatlands using vegetation as a proxy | 158 | 70 | Hydrobiologia | Research article | A water-level class, trophic state (C: N ratio), base richness (pH) and vegetation type were used as 'vegetation forms' as a comprehensive proxy for estimating baseline and project scenario greenhouse emissions from degraded peatland and thus emission reductions from rewetting. |
| Page (2009) | Restoration Ecology of Lowland Tropical Peatlands in Southeast Asia: Current Knowledge and Future Research Direction | 157 | 23 | Ecosystems | Review | The review reported that fire, exacerbated by drainage, is the principal driver of land-use change. In contrast, repeated and high-intensity fires lead to retrogressive succession towards non-forest communities in Kalimantan, Indonesia. Furthermore, the hydrological restoration through rewetting the drained peatland was identified as the key vegetation restoration and protecting the remaining peat carbon stocks. |
| Wosten (2008) | Peat–water interrelationships in a tropical peatland ecosystem in Southeast Asia | 146 | 4 | Catena | Research article | The hydropedological modelling approach was used to generate groundwater level prediction maps to study the peat-water interrelationships in a degraded tropical peatland. The model identified areas with good restoration |

(Continued on following page)

TABLE 4 (*Continued*) Highly cited document in the restoration of degraded peatland research domain.

| Article | Title | Citations | Total links | Research outlets | Type of articles | Key findings |
|---|---|---|---|---|---|---|
| | | | | | | potential based on predicted flooding depth and duration. The model predicted groundwater levels should be maintained between 40 cm below and 100 cm above the peat surface to prevent subsidence and fire during rewetting. |
| Price (1996) | Soil moisture, water tension, and water table relationships in a managed cutover bog | 142 | 16 | Journal of Hydrology | Research Article | The study compared the hydrological indicators between a natural bog, drained and harvested bog, and drained harvested bog with ditches blocked. Ditches block with mulching obtained high water table recessions similar to the natural site. However, the soil moisture obtained at the block site did not differ from the drain site. The site with ditches blocked observed higher greater water tension than the drained bog site. |
| Vasander et al. (2003) | Status and restoration of peatlands in northern Europe | 137 | 41 | Wetlands Ecology and Management | Review | Rewetting and ditch or drainage blocking were identified as restoration techniques developed for degraded peatland management in Estonia, Sweden, and Finland, specifically for nutrient-rich peatland. |
| Komulainen et al. (1999) | Restoration of drained peatlands in southern Finland: initial effects on vegetation change and CO2 balance | 121 | 47 | Journal of Applied Ecology | Research article | Two years of rewetting stimulate carbon sequestration such that rewetted minerotrophic fen obtained $CO^2$-C balance ranging from 162 to 283 g $m^{-2}$, with dense *E. vaginatum* vegetation and a high-water table while rewetted bog had $CO^2$-C balance varied from 54 to 101 g $m^{-2}$ having a high-water table and mire vegetation. |
| Jauhiainen et al. (2008) | Carbon dioxide and methane fluxes in drained tropical peat before and after hydrological restoration | 121 | 47 | Ecology | Research article | After restoration, the drained tropical peat forest showed higher annual minimum soil water table levels. However, the improvement of the peat hydrology did not instantly reduce $CO_2$ flux rates in forest sites. As a result, the cumulative $CO_2$ emissions of the tropical peat did not reflect the notable changes in the hydrological conditions before and after restoration. In addition, the methane emission from the rewetted peat did not differ from the drained peat. |
| Holden et al. (2001) | Water table dynamics in undisturbed drained and restored blanket peat | 106 | 48 | Journal of Hydrology | Research article | Water tables in undisturbed drained and restored blanket peats are more variable in order (drained > restored > intact) such that the mean water table depths over 18 months studied period were −5.8 cm at the intact site, −8.9 cm at the restored site and −11.5 cm at the drained sites. |

### 3.3.2 Active countries in the RDP research

Supplementary Figure S2 illustrates the most active countries in the RDP research discourse, with larger nodes indicating a high number of publications. Cluster one (blue) involves the countries of the United Kingdom, especially England, Scotland, and Wales, with England possessing the higher nodes. Cluster two (green) consists of Germany, Netherland, Poland, and Sweden, with Germany obtaining the higher nodes. The higher node obtained by Germany is not surprising because they have degraded more than 85% of its original peatlands, and hence restoration research options are now implemented to restore the degraded peatland to its original state. Cluster three (red) consists of five countries, with the highest nodes obtained by Finland. Based on this analysis, it can be revealed that about 26% (51 out of 195) of all countries are involved

TABLE 5 Active countries in the restoration of degraded peatland research.

| Country | Documents | Citations | Av. Citation | Total link strength |
|---|---|---|---|---|
| Sweden | 18 | 667 | 37 | 886 |
| Finland | 68 | 2053 | 30 | 1,837 |
| Canada | 46 | 1270 | 28 | 1875 |
| Netherlands | 47 | 1121 | 24 | 1,430 |
| England | 96 | 2005 | 21 | 3,976 |
| United States of America | 43 | 794 | 18 | 1,717 |
| Wales | 24 | 412 | 17 | 1,262 |
| Germany | 88 | 1498 | 17 | 3,179 |
| Indonesia | 40 | 675 | 17 | 1,629 |
| Poland | 34 | 465 | 14 | 1,480 |
| Scotland | 37 | 426 | 12 | 1,602 |
| China | 24 | 197 | 8 | 561 |

in RDP research. Supplementary Figure S2 reveals that RDP is conducted in countries with extensive peatland coverage. Regarding the strength of links, the strongest links were between the following pairs: England-Wales; England-Scotland; England-Finland; Germany-USA; and Canada-USA.

Table 5 shows the top 12 influential countries based on the number of articles, with England (96) obtaining the higher number of articles. The top three countries are England (96), Germany (88), and Finland (68). However, an inconsistent pattern is observed when ranking based on citations. Under this, Finland (2053), England (2005), and Germany (1,498) are the top influential countries in the RDP research domain. A slightly different ranking pattern is observed when using the average citation index, such that Sweden (37), Finland (30) and Canada (28) are the influential countries in the research domain.

## 4 Conclusion

This study reconnoiters the status and the global trends of RDP research using scientometric analysis. RDP research has tremendously increased in the last decade, resulting in numerous literature reviews being published. Nevertheless, this current study presents the first scientometric review of RDP research using 522 documents (research articles and literature review) retrieved from WOS database. The structure of the body of knowledge in RDP research was evaluated using the research outlet, keywords co-occurrence analysis, and document citation analysis. Specifically, the scientometric analysis of the RDP dataset discovered the following conclusions:

- Annual exponential growth in the number of publications in RDP research was observed.
- Four research themes were identified with the co-occurrence of keywords analysis, namely: (i) impact of drainage on peatland ecosystem services; (ii) impact of peatland restoration on GHG emissions; (iii) peatland restoration and biogeochemical properties; and (iv) peatland restoration and plant species richness.
- The top three keywords in RDP research having the strongest citation burst were diversity (burst strength, 5.42; 2014–2016), peatland (burst strength, 3.79; 2010–2013), and land use (burst strength, 3.27; 2014–2018).
- The most contributing research outlets of RDP research are Mires and Peat and the Science of the Total Environment.
- England and Germany are the most active countries in RDP research.
- It was found that 22, 60, 80, and 60 of the 522 articles have cited Price et al. (2003), Maljanen et al. (2010), Leified et al. (2012), Knox et al. (2015), respectively.

The current scientometric analysis is limited to certain keywords, TS (topic) = (‘drained peatland restoration’ OR ‘drained bog restoration’ OR ‘drained mire restoration’ OR degraded peatland restoration’ OR ‘degraded bog restoration’ OR ‘drained peatland reclamation’ OR ‘drained bog restoration’ OR ‘degraded peatland reclamation’ OR ‘degraded bog reclamation’ OR ‘drained mire restoration’ OR ‘degraded mire reclamation’ OR ‘degraded fen restoration’ OR ‘drained fen reclamation’) and the selected documents were limited to review and research articles only. In addition, only one database (WOS) was used for the extraction of the dataset, which may suffer from the intrinsic limitations of WOS’s coverage of publications. Due to these, this study might not fully capture the whole available literature on RDP. However, scientometric analysis of RDP research provides instinctive graphics for a research hotspot in RDP, and valuable information based on a comprehensive analysis of the research theme and future trends (Liu et al., 2019).

## Author contributions

Conceptualization, SA; Methodology, SA; Software, SA; Validation, SA; Formal analysis, SA; Investigation, DM; Resources, DM and FT; Data curation, SA; Writing—original draft preparation, SA; Writing—review and editing, MG, FT, and DM; Visualization, SA; Supervision, MG, FT, and DM; Project administration, MG, FT, and DM; Funding acquisition, FT. All authors have read and agreed to the published version of the manuscript.

## Funding

This research is supported by the Carbon Farming and Group Project Design for Peatlands under Agricultural Management project. The project is funded by European Innovation Partnerships from The Department of Agriculture, Food and the Marine (DAFM).

## Conflict of interest

Authors DM and MG were employed by the company Green Restoration Ireland Cooperative Society Ltd.

The remaining authors declare that the research was conducted in the absence of any commercial or financial relationships that could be construed as a potential conflict of interest.

## Publisher's note



## Supplementary material

The Supplementary Material for this article can be found online at: https://www.frontiersin.org/articles/10.3389/fenvs.2022.942788/full#supplementary-material

**SUPPLEMENTARY FIGURE S1**
Density Map of Co-Authorship Network.

**SUPPLEMENTARY FIGURE S2**
Network of most contributing countries in the RDP research.

## References

Adesiji, A. R., Mohammed, T. A., Nik Daud, N. N., Saari, M., Gbadebo, A. O., and Jacdonmi, I. (2015). Impacts of land-use change on peatland degradation: a review. *Ethiop. J. Environ. Stud. Manag.* 8, 225. doi:10.4314/ejesm.v8i2.11

Aerts, R., and Ludwig, F. (1997). Water-table changes and nutritional status affect trace gas emissions from laboratory columns of peatland soils. *Soil Biol. Biochem.* 29, 1691–1698. doi:10.1016/s0038-0717(97)00074-6

Ahmad, S., Liu, H., Günther, A., Couwenberg, J., and Lennartz, B. (2020). Long-term rewetting of degraded peatlands restores hydrological buffer function. *Sci. Total Environ.* 749, 141571. doi:10.1016/j.scitotenv.2020.141571

Andersen, R., Farrell, C., Graf, M., Muller, F., Calvar, E., Frankard, P., et al. (2017). An overview of the progress and challenges of peatland restoration in Western Europe. *Restor. Ecol.* 25 (2), 271–282. doi:10.1111/rec.12415

Anshari, G. Z., Afifudin, M., Nuriman, M., Gusmayanti, E., Arianie, L., Susana, R., et al. (2010). Drainage and land use impacts on changes in selected peat properties and peat degradation in West Kalimantan Province, Indonesia. *Biogeosciences* 7 (3), 3403–3419. doi:10.5194/bg-7-3403-2010

Baker, H. K., Kumar, S., and Pattnaik, D. (2021). Twenty-five years of the journal of corporate finance: A scientometric analysis. *J. Corp. Finance* 66, 101572. doi:10.1016/j.jcorpfin.2020.101572

Ballhorn, U., Siegert, F., Mason, M., and Limin, S. (2009). Derivation of burn scar depths and estimation of carbon emissions with LIDAR in Indonesian peatlands. *Proc. Natl. Acad. Sci. U. S. A.* 106 (50), 21213–21218. doi:10.1073/pnas.0906457106

Bhiry, N., Payette, S., and Robert, É. C. (2007). Peatland development at the arctic tree line (Québec, Canada) influenced by flooding and permafrost. *Quat. Res.* 67 (3), 426–437. doi:10.1016/j.yqres.2006.11.009

Biancalani, R., and Avagyan, A. (2014). *Towards climate-responsible peatlands management. Mitigation of climate change in agriculture series (MICCA)*. Rome, Italy: Food and Agriculture Organization of the United Nations, 9.

Blodau, C. (2002). Carbon cycling in peatlands A review of processes and controls. *Environ. Rev.* 10 (2), 111–134. doi:10.1139/a02-004

Bonn, A., Reed, M. S., Evans, C. D., Joosten, H., Bain, C., Farmer, J., et al. (2014). Investing in nature: Developing ecosystem service markets for peatland restoration. *Ecosyst. Serv.* 9, 54–65. doi:10.1016/j.ecoser.2014.06.011

Bonn, A., Allott, T., Evans, M., Joosten, H., and Stoneman, R. (2016). "Peatland restoration and ecosystem services: an introduction," in *Peatland restoration and ecosystem services: Science, policy and practice*. Cambridge, UK: Cambridge University Press, 1–16.

Bridgham, S. D., Pastor, J., Updegraff, K., Malterer, T. J., Johnson, K., Harth, C., et al. (1999). Ecosystem control over temperature and energy flux in northern peatlands. *Ecol. Appl.* 9 (4), 1345–1358. doi:10.1890/1051-0761(1999)009[1345:ecotae]2.0.co;2

Brooks, T. M., Mittermeier, R. A., da Fonseca, G. A., Gerlach, J., Hoffmann, M., Lamoreux, J. F., et al. (2006). Global biodiversity conservation priorities. *science* 313, 58–61. doi:10.1126/science.1127609

Brown, L. E., Holden, J., Palmer, S. M., Johnston, K., Ramchunder, S. J., and Grayson, R. (2015). Effects of fire on the hydrology, biogeochemistry, and ecology of peatland river systems. *Freshw. Sci.* 34 (4), 1406–1425. doi:10.1086/683426

Bubier, J. L., Moore, T. R., Bellisario, L., Comer, N. T., and Crill, P. M. (1995). Ecological controls on methane emissions from a northern peatland complex in the zone of discontinuous permafrost, Manitoba, Canada. *Glob. Biogeochem. Cycles* 9 (4), 455–470. doi:10.1029/95gb02379

Burton, R. G. O., and Hodgson, J. M. (1987). "Lowland peat in England and Wales," in *Soil survey technical monograph No.15* (UK: Harpenden), 146.

Bussell, J., Jones, D., Healey, J., and Pullin, A. (2010). *How do draining and re-wetting affect carbon stores and greenhouse gas fluxes in peatland soils*. CEE Rev. 08-012.

Campbell, D. R., Rochefort, L., and Lavoie, C. (2003). Determining the immigration potential of plants colonizing disturbed environments: The case of milled peatlands in Quebec. *J. Appl. Ecol.* 40 (1), 78–91. doi:10.1046/j.1365-2664.2003.00782.x

Chapman, S., Artz, R., and Donnelly, D. (2012). Carbon savings from peat restoration. *Clim. Change Enquiry* (1205–02), 1–17.

Chen, C. (2006). CiteSpace II: Detecting and visualizing emerging trends and transient patterns in scientific literature. *J. Am. Soc. Inf. Sci. Technol.* 57 (3), 359–377. doi:10.1002/asi.20317

Chen, H., Yang, G., Peng, C., Zhang, Y., Zhu, D., Zhu, Q., et al. (2014). The carbon stock of alpine peatlands on the Qinghai–Tibetan Plateau during the Holocene and their future fate. *Quater. Sci. Rev.* 95, 151–158. doi:10.1016/j.quascirev.2014.05.003

Chen, K., Wang, J., Yu, B., Wu, H., and Zhang, J. (2021). Critical evaluation of construction and demolition waste and associated environmental impacts: A scientometric analysis. *J. Clean. Prod.* 287, 125071. doi:10.1016/j.jclepro.2020.125071

Chimner, R. A., Cooper, D. J., Wurster, F. C., and Rochefort, L. (2017). An overview of peatland restoration in north America: Where are we after 25 years? *Restor. Ecol.* 25 (2), 283–292. doi:10.1111/rec.12434

Cobo, M. J., López-Herrera, A. G., Herrera-Viedma, E., and Herrera, F. (2011). Science mapping software tools: Review, analysis, and cooperative study among tools. *J. Am. Soc. Inf. Sci. Technol.* 62 (7), 1382–1402. doi:10.1002/asi.21525

Couwenberg, J., Thiele, A., Tanneberger, F., Augustin, J., Bärisch, S., Dubovik, D., et al. (2011). Assessing greenhouse gas emissions from peatlands using vegetation as a proxy. *Hydrobiologia* 674 (1), 67–89. doi:10.1007/s10750-011-0729-x

Crum, H., and Planisek, S. (1992). *A focus on peatlands and peat mosses*. Ann Arbor, MI: University of Michigan Press.

Cui, L., Kang, X., Li, W., Hao, Y., Zhang, Y., Wang, J., et al. (2017). Rewetting decreases carbon emissions from the Zoige alpine peatland on the Tibetan Plateau. *Sustainability* 9 (6), 948. doi:10.3390/su9060948

D'Andrilli, J., Chanton, J. P., Glaser, P. H., and Cooper, W. T. (2010). Characterization of dissolved organic matter in northern peatland soil porewaters by ultra high resolution mass spectrometry. *Org. Geochem.* 41 (8), 791–799. doi:10.1016/j.orggeochem.2010.05.009

Darko, A., Chan, A. P., Adabre, M. A., Edwards, D. J., Hosseini, M. R., and Ameyaw, E. E. (2020). Artificial intelligence in the AEC industry: Scientometric analysis and visualization of research activities. *Automation Constr.* 112, 103081. doi:10.1016/j.autcon.2020.103081

Darko, A., Chan, A. P., Huo, X., and Owusu-Manu, D. G. (2019). A scientometric analysis and visualization of global green building research. *Build. Environ.* 149, 501–511. doi:10.1016/j.buildenv.2018.12.059

Dise, N. B. (2009). Peatland response to global change. *Science* 326 (5954), 810–811. doi:10.1126/science.1174268

Dohong, A., Aziz, A. A., and Dargusch, P. (2017). A review of the drivers of tropical peatland degradation in South-East Asia. *Land use policy* 69, 349–360. doi:10.1016/j.landusepol.2017.09.035

Dohong, A., Abdul Aziz, A., and Dargusch, P. (2018). A review of techniques for effective tropical peatland restoration. *Wetlands* 38 (2), 275–292. doi:10.1007/s13157-018-1017-6

Elisha, I. L., and Viljoen, A. (2021). Trends in rooibos tea (aspalathus linearis) research (1994–2018): A scientometric assessment. *South Afr. J. Bot.* 137, 159–170. doi:10.1016/j.sajb.2020.10.004

Evans, M. G., Burt, T. P., Holden, J., and Adamson, J. K. (1999). Runoff generation and water table fluctuations in blanket peat: Evidence from UK data spanning the dry summer of 1995. *J. Hydrology* 221 (3-4), 141–160. doi:10.1016/s0022-1694(99)00085-2

FAO (2012). *Harmonized world soil database*. Version 1.2.

Fenner, N., and Freeman, C. (2011). Drought-induced carbon loss in peatlands. *Nat. Geosci.* 4, 895–900. doi:10.1038/ngeo1323

Flores, R. M. (2014). *Origin of coal as gas source and reservoir rocks.* Coal and coalbed gas. Amsterdam: Elsevier, 97–165.

Flores-Moreno, H., Reich, P. B., Lind, E. M., Sullivan, L. L., Seabloom, E. W., Yahdjian, L., et al. (2016). Climate modifies response of non-native and native species richness to nutrient enrichment. *Phil. Trans. R. Soc. B* 371 (1694), 20150273. doi:10.1098/rstb.2015.0273

Fridell, M., Edwin, S., Von Schreeb, J., and Saulnier, D. D. (2020). Health system resilience: What are we talking about? A scoping review mapping characteristics and keywords. *Int. J. Health Policy Manag.* 9 (1), 6–16. doi:10.15171/ijhpm.2019.71

Gao, Y., Chen, H., and Zeng, X. (2014). Effects of nitrogen and sulfur deposition on CH4 and N2O fluxes in high-altitude peatland soil under different water tables in the Tibetan Plateau. *Soil Sci. Plant Nutrit.* 60 (3), 404–410. doi:10.1080/00380768.2014.893812

Gough, R., Holliman, P. J., Fenner, N., Peacock, M., and Freeman, C. (2016). Influence of water table depth on pore water chemistry and trihalomethane formation potential in peatlands. *water Environ. Res.* 88 (2), 107–117. doi:10.2175/106143015x14362865227878

Graniero, P. A., and Price, J. S. (1999). The importance of topographic factors on the distribution of bog and heath in a Newfoundland blanket bog complex. *Catena* 36 (3), 233–254. doi:10.1016/s0341-8162(99)00008-9

Guidry, J. A., Guidry Hollier, B. N., Johnson, L., Tanner, J. R., and Veltsos, C. (2004). Surveying the cites: A ranking of marketing journals using citation analysis. *Mark. Educ. Rev.* 14 (1), 45–59. doi:10.1080/10528008.2004.11488853

Haapalehto, T., Kotiaho, J. S., Matilainen, R., and Tahvanainen, T. (2014). The effects of long-term drainage and subsequent Restoration on water table level and pore water chemistry in boreal peatlands. *J. Hydrology* 519, 1493–1505. doi:10.1016/j.jhydrol.2014.09.013

Haapalehto, T. O., Vasander, H., Jauhiainen, S., Tahvanainen, T., and Kotiaho, J. S. (2011). The effects of peatland restoration on water-table depth, elemental concentrations, and vegetation: 10 years of changes. *Restor. Ecol.* 19 (5), 587–598. doi:10.1111/j.1526-100x.2010.00704.x

Hahn, J., Köhler, S., Glatzel, S., and Jurasinski, G. (2015). Methane exchange in a coastal fen in the first year after flooding-a systems shift. *PloS one* 10 (10), e0140657. doi:10.1371/journal.pone.0140657

Hammersley, M. (2001). On 'systematic'reviews of research literatures: A 'narrative'response to Evans & benefield. *Br. Educ. Res. J.* 27 (5), 543–554. doi:10.1080/01411920120095726

Hammond, R. F. (1981). *The peatlands of Ireland*. Dublin: An Foras Taluntais, 60.

Harris, L. I., Moore, T. R., Roulet, N. T., and Pinsonneault, A. J. (2020). Limited effect of drainage on peat properties, porewater chemistry, and peat decomposition proxies in a boreal peatland. *Biogeochemistry* 151 (1), 43–62. doi:10.1007/s10533-020-00707-1

Harrison, M. E., Ottay, J. B., D'Arcy, L. J., Cheyne, S. M., Belcher, C., Cole, L., et al. (2020). Tropical forest and peatland conservation in Indonesia: Challenges and directions. *People Nat.* 2 (1), 4–28. doi:10.1002/pan3.10060

Herbst, M., Friborg, T., Ringgaard, R., and Soegaard, H. (2011). Interpreting the variations in atmospheric methane fluxes observed above a restored wetland. *Agric. For. Meteorology* 151 (7), 841–853. doi:10.1016/j.agrformet.2011.02.002

Holden, J., Chapman, P. J., and Labadz, J. C. (2004). Artificial drainage of peatlands: Hydrological and hydrochemical process and wetland restoration. *Prog. Phys. Geogr. Earth Environ.* 28 (1), 95–123. doi:10.1191/0309133304pp403ra

Holden, J., Evans, M. G., Burt, T. P., and Horton, M. (2006). Impact of land drainage on peatland hydrology. *J. Environ. Qual.* 35 (5), 1764–1778. doi:10.2134/jeq2005.0477

Holden, J., Burt, T. P., and Cox, N. J. (2001). Macroporosity and infiltration in blanket peat: The implications of tension disc infiltrometer measurements. *Hydrol. Process.* 15 (2), 289–303. doi:10.1002/hyp.93

Holden, J. (2005). Peatland hydrology and carbon release: Why small-scale process matters. *Phil. Trans. R. Soc. A* 363 (1837), 2891–2913. doi:10.1098/rsta.2005.1671

Hooijer, A., Silvius, M., Wosten, H., and Page, E. S. (2006). PEAT-CO2: Assessment of CO2 emissions from drained peatlands in SE Asia. Delft Hydraulics Report Q3943/2006. (36p.).

Hooijer, A., Page, S., Jauhiainen, J., Lee, W. A., Lu, X. X., Idris, A., et al. (2012). Subsidence and carbon loss in drained tropical peatlands. *Biogeosciences* 9 (3), 1053–1071. doi:10.5194/bg-9-1053-2012

Hooijer, A., Page, S., Navratil, P., Vernimmen, R., van der Vat, M., Tansey, K., et al. (2014). *Carbon emissions from drained and degraded peatland in Indonesia and emission factors for measurement, reporting and verification (MRV) of peatland greenhouse gas emissions–a summary of KFCP research results for practitioners*. Jakarta, Indonesia: IAFCP.

Hosseini, M. R., Martek, I., Zavadskas, E. K., Aibinu, A. A., Arashpour, M., and Chileshe, N. (2018). Critical evaluation of off-site construction research: A scientometric analysis. *Automation Constr.* 87, 235–247. doi:10.1016/j.autcon.2017.12.002

Hribljan, J. A., Kane, E. S., Pypker, T. G., and Chimner, R. A. (2014). The effect of long-term water table manipulations on dissolved organic carbon dynamics in a poor fen peatland. *J. Geophys. Res. Biogeosci.* 119, 577–595. doi:10.1002/2013jg002527

Hulatt, C. J., Kaartokallio, H., Asmala, E., Autio, R., Stedmon, C. A., Sonninen, E., et al. (2014). Bioavailability and radiocarbon age of fluvial dissolved organic matter (DOM) from a northern peatland-dominated catchment: Effect of land-use change. *Aquat. Sci.* 76 (3), 393–404. doi:10.1007/s00027-014-0342-y

Jaenicke, J., Wösten, H., Budiman, A., and Siegert, F. (2010). Planning hydrological restoration of peatlands in Indonesia to mitigate carbon dioxide emissions. *Mitig. Adapt. Strateg. Glob. Chang.* 15 (3), 223–239. doi:10.1007/s11027-010-9214-5

Jauhiainen, J., Limin, S., Silvennoinen, H., and Vasander, H. (2008). Carbon dioxide and methane fluxes in drained tropical peat before and after hydrological restoration. *Ecology* 89 (12), 3503–3514. doi:10.1890/07-2038.1

Joosten, H., and Clarke, D. (2002). *Wise use of mires and peatlands*. International Mire Conservation Group and International Peat Society, 304.

Joosten, H., Tanneberger, F., and Moen, A. (2017). *Mires and peatlands of Europe*.

Joosten, H. (2009). *The global peatland CO2 picture: Peatland status and drainage related emissions in all countries of the world*.

Kaila, A., Asam, Z., Koskinen, M., Uusitalo, R., Smolander, A., Kiikkilä, O., et al. (2016). Impact of re-wetting of forestry-drained peatlands on water quality—A laboratory approach assessing the release of P, N, Fe, and dissolved organic carbon. *Water Air Soil Pollut.* 227 (8), 1–15. doi:10.1007/s11270-016-2994-9

Kandel, T. P., Lærke, P. E., Hoffmann, C. C., and Elsgaard, L. (2019). Complete annual CO2, CH4, and N2O balance of a temperate riparian wetland 12 years after rewetting. *Ecol. Eng.* 127, 527–535. doi:10.1016/j.ecoleng.2017.12.019

Kim, D. G., Vargas, R., Bond-Lamberty, B., and Turetsky, M. R. (2011). Effects of soil rewetting and thawing on soil gas fluxes: A review of current literature and suggestions for future research. *Biogeosciences* 8 (5), 2459–2483. doi:10.5194/bg-9-2459-2012

Kleinberg, J. (2002). An impossibility theorem for clustering. *Adv. Neural Inform. Process. Syst.* 15.

Knox, S. H., Sturtevant, C., Matthes, J. H., Koteen, L., Verfaillie, J., and Baldocchi, D. (2015). Agricultural peatland restoration: Effects of land-use change on greenhouse gas (CO2 and CH4) fluxes in the sacramento-san joaquin delta. *Glob. Chang. Biol.* 21 (2), 750–765. doi:10.1111/gcb.12745

Komulainen, V. M., Nykänen, H., Martikainen, P. J., and Laine, J. (1998). Short-term effect of Restoration on vegetation change and methane emissions from peatlands drained for forestry in southern Finland. *Can. J. For. Res.* 28 (3), 402–411. doi:10.1139/x98-011

Komulainen, V. M., Tuittila, E. S., Vasander, H., and Laine, J. (1999). Restoration of drained peatlands in southern Finland: Initial effects on vegetation change and $CO_2$ balance. *J. Appl. Ecol.* 36 (5), 634–648. doi:10.1046/j.1365-2664.1999.00430.x

Könönen, M., Heinonsalo, J., Laiho, R., Kusin, K., Limin, S., and Vasander, H. (2018). Deforested and drained tropical peatland sites show poorer peat substrate quality and lower microbial biomass and activity than unmanaged swamp forest. *Soil Biol. Biochem.* 123, 229–241. doi:10.1016/j.soilbio.2018.04.028

Krüger, J. P., Leifeld, J., Glatzel, S., Szidat, S., and Alewell, C. (2015). Biogeochemical indicators of peatland degradation–a case study of a temperate bog in northern Germany. *Biogeosciences* 12 (10), 2861–2871. doi:10.5194/bg-12-2861-2015

Lamers, L. P., Van Diggelen, J. M., Op den Camp, H. J., Visser, E. J., Lucassen, E. C., Vile, M. A., et al. (2012). Microbial transformations of nitrogen, sulfur, and iron dictate vegetation composition in wetlands: A review. *Front. Microbiol.* 3, 156. doi:10.3389/fmicb.2012.00156

Lappalainen, E. (1996). *Global peat resources*.

Lavoie, C., Marcoux, K., Saint-Louis, A., and Price, J. S. (2005a). The dynamics of a cotton-grass (Eriophorum vaginatum L.) cover expansion in a vacuum-mined peatland, southern Québec, Canada. *Wetlands* 25 (1), 64–75. doi:10.1672/0277-5212(2005)025[0064:tdoace]2.0.co;2

Lavoie, M., Paré, D., Fenton, N., Groot, A., and Taylor, K. (2005b). Paludification and management of forested peatlands in Canada: A literature review. *Environ. Rev.* 13 (2), 21–50. doi:10.1139/a05-006

Leifeld, J., and Menichetti, L. (2018). The underappreciated potential of peatlands in global climate change mitigation strategies. *Nat. Commun.* 9 (1), 1071–1077. doi:10.1038/s41467-018-03406-6

Leifeld, J., Steffens, M., and Galego-Sala, A. (2012). Sensitivity of peatland carbon loss to organic matter quality. *Geophys. Res. Lett.* 39 (14). doi:10.1029/2012GL051856

Li, J., Goerlandt, F., and Reniers, G. (2021). An overview of scientometric mapping for the safety science community: Methods, tools, and framework. *Saf. Sci.* 134, 105093. doi:10.1016/j.ssci.2020.105093

Liimatainen, M., Voigt, C., Martikainen, P. J., Hytönen, J., Regina, K., Óskarsson, H., et al. (2018). Factors controlling nitrous oxide emissions from managed northern peat soils with low carbon to nitrogen ratio. *Soil Biol. Biochem.* 122, 186–195. doi:10.1016/j.soilbio.2018.04.006

Likens, G. E. (2009). *Encyclopedia of inland waters*. Elsevier.

Limpens, J., erendse, F., Blodau, C., Canadell, J. G., Freeman, C., Holden, J., et al. (2008). Peatlands and the carbon cycle: From local processes to global implications—a synthesis. *Biogeosciences* 5, 1475–1491. doi:10.5194/bg-5-1475-2008

Liu, Z., Lu, Y., and Peh, L. C. (2019). A review and scientometric analysis of global building information modeling (BIM) research in the architecture, engineering and construction (AEC) industry. *Buildings* 9 (10), 210. doi:10.3390/buildings9100210

Macrae, M. L., Devito, K. J., Strack, M., and Waddington, J. M. (2013). Effect of water table drawdown on peatland nutrient dynamics: Implications for climate change. *Biogeochemistry* 112 (1), 661–676. doi:10.1007/s10533-012-9730-3

Maftu'ah, E., Fahmi, A., and Hayati, A. (2019)). Changes in degraded peat land characteristic using FTIR-spectrocopy. *IOP Conf. Ser. Earth Environ. Sci.* 393, 012091. doi:10.1088/1755-1315/393/1/012091

Maljanen, M., Hytönen, J., and Martikainen, P. J. (2010). Cold-season nitrous oxide dynamics in a drained boreal peatland differ depending on land-use practice. *Canadian J. Forest Res.* 40 (3), 565–572.

Markoulli, M. P., Lee, C. I., Byington, E., and Felps, W. A. (2017). Mapping human resource management: Reviewing the field and charting future directions. *Hum. Resour. Manag. Rev.* 27 (3), 367–396. doi:10.1016/j.hrmr.2016.10.001

Martinez, S., del Mar Delgado, M., Marin, R. M., and Alvarez, S. (2019). Science mapping on the environmental footprint: A scientometric analysis-based review. *Ecol. Indic.* 106, 105543. doi:10.1016/j.ecolind.2019.105543

Martikainen, P. J., Nykänen, H., Crill, P., and Silvola, J. (1993). Effect of a lowered water table on nitrous oxide fluxes from northern peatlands. *Nature* 366 (6450), 51–53. doi:10.1038/366051a0

Martikainen, P. J., Nykänen, H., Alm, J., and Silvola, J. (1995). Change in fluxes of carbon dioxide, methane and nitrous oxide due to forest drainage of mire sites of different trophy. *Plant Soil* 168 (1), 571–577. doi:10.2307/42939899

Marttila, H., Karjalainen, S. M., Kuoppala, M., Nieminen, M. L., Ronkanen, A. K., Kløve, B., et al. (2018). Elevated nutrient concentrations in headwaters affected by drained peatland. *Sci. Total Environ.* 643, 1304–1313. doi:10.1016/j.scitotenv.2018.06.278

Matějková, Š., and Šimon, T. (2012). Application of FTIR spectroscopy for evaluation of hydrophobic/hydrophilic organic components in arable soil. *Plant Soil Environ.* 58 (4), 192–195. doi:10.17221/317/2011-pse

Mattsson, T., Finér, L., Kortelainen, P., and Sallantaus, T. (2003). Brook water quality and background leaching from unmanaged forested catchments in Finland. *Water, Air, Soil Pollut.* 147 (1), 275–298. doi:10.1023/a:1024525328220

Meissner, R., Rupp, H., and Leinweber, P. (2003). Re-wetting of fen soils and changes in water quality-experimental results and further research needs. *J. Water Land Dev.* 7, 75–91.

Miettinen, J., and Liew, S. C. (2010). Status of peatland degradation and development in Sumatra and Kalimantan. *Ambio* 39 (5), 394–401. doi:10.1007/s13280-010-0051-2

Mikaloff Fletcher, S. E., and Schaefer, H. (2019). Rising methane: A new climate challenge. *Science* 364, 932–933. doi:10.1126/science.aax1828

Miller, J., Anderson, H., Ray, D., and Anderson, A. (1996). Impact of some initial forestry practices on the drainage waters from blanket peatlands. *Forestry* 69 (3), 193–203. doi:10.1093/forestry/69.3.193

Minayeva, T. Y., and Sirin, A. A. (2012). Peatland biodiversity and climate change. *Biol. Bull. Rev.* 2 (2), 164–175. doi:10.1134/s207908641202003x

Minkkinen, K., and Laine, J. (1998). Effect of forest drainage on the peat bulk density of pine mires in Finland. *Can. J. For. Res.* 28, 178–186. doi:10.1139/x97-206

Mishra, S., Page, S. E., Cobb, A. R., Lee, J. S. H., Jovani-Sancho, A. J., Sjögersten, S., et al. (2021). Degradation of Southeast Asian tropical peatlands and integrated strategies for their better management and restoration. *J. Appl. Ecol.* 58 (7), 1370–1387. doi:10.1111/1365-2664.13905

Moore, T., and Basiliko, N. (2006). "Decomposition in boreal peatlands," in *Boreal peatland ecosystems* (Berlin, Heidelberg: Springer), 125–143.

Moore, T. R., Trofymow, J. A., Siltanen, M., Prescott, C., and Group, C. W. (2005). Patterns of decomposition and carbon, nitrogen, and phosphorus dynamics of litter in upland forest and peatland sites in central Canada. *Can. J. For. Res.* 35 (1), 133–142. doi:10.1139/x04-149

Munir, T. M., Khadka, B., Xu, B., and Strack, M. (2017). Mineral nitrogen and phosphorus pools affected by water table lowering and warming in a boreal forested peatland. *Ecohydrology* 10 (8), e1893. doi:10.1002/eco.1893

Nikolenko, S. I., Koltcov, S., and Koltsova, O. (2017). Topic modelling for qualitative studies. *J. Inform. Sci.* 43 (1), 88–102. doi:10.1177/0165551515617393

Nieminen, M., Sallantaus, T., Ukonmaanaho, L., Nieminen, T. M., and Sarkkola, S. (2017a). Nitrogen and phosphorus concentrations in discharge from drained peatland forests are increasing. *Sci. Total Environ.* 609, 974–981. doi:10.1016/j.scitotenv.2017.07.210

Nieminen, M., Sarkkola, S., and Laurén, A. (2017b). Impacts of forest harvesting on nutrient, sediment and dissolved organic carbon exports from drained peatlands: A literature review, synthesis and suggestions for the future. *For. Ecol. Manag.* 392, 13–20. doi:10.1016/j.foreco.2017.02.046

Nykänen, H., Alm, J., Silvola, J., Tolonen, K., and Martikainen, P. J. (1998). Methane fluxes on boreal peatlands of different fertility and the effect of long-term experimental lowering of the water table on flux rates. *Glob. Biogeochem. Cycles* 12 (1), 53–69. doi:10.1029/97gb02732

O'Brien, H., Labadz, J. C., and Butcher, D. P. (2007). *Review of blanket bog management and restoration. Nottingham Trent University research rep. (BD1241) to Defra*. London.

Ojanen, P., Minkkinen, K., and Penttilä, T. (2013). The current greenhouse gas impact of forestry-drained boreal peatlands. *For. Ecol. Manag.* 289, 201–208. doi:10.1016/j.foreco.2012.10.008

Oktarita, S., Hergoualc'h, K., Anwar, S., and Verchot, L. V. (2017). Substantial $N_2O$ emissions from peat decomposition and N fertilization in an oil palm plantation exacerbated by hotspots. *Environ. Res. Lett.* 12 (10), 104007. doi:10.1088/1748-9326/aa80f1

Olde Venterink, H., Kardel, I., Kotowski, W., Peeters, W., and Wassen, M. J. (2009). Long-term effects of drainage and hay-removal on nutrient dynamics and limitation in the Biebrza mires, Poland. *Biogeochemistry* 93 (3), 235–252. doi:10.1007/s10533-009-9300-5

Oraee, M., Hosseini, M. R., Papadonikolaki, E., Palliyaguru, R., and Arashpour, M. (2017). Collaboration in BIM-based construction networks: A bibliometric-qualitative literature review. *Int. J. Proj. Manag.* 35 (7), 1288–1301. doi:10.1016/j.ijproman.2017.07.001

Parish, F., and Looi, C. C. (1999). "Wetlands, biodiversity and climate change," in *Options and needs for enhanced linkage between the ramsar convention on wetlands, convention on biological diversity andUN framework convention on climate change* (Global Environment Network).

Parish, F., Sirin, A., Charman, D., Joosten, H., Minayeva, T., Silvius, M., et al. (2008). *Assessment on peatlands, biodiversity and climate change: Main report*. Wageningen: Global Environment Centre, Kuala Lumpur and Wetlands International.

Pärn, J., Verhoeven, J. T., Butterbach-Bahl, K., Dise, N. B., Ullah, S., Aasa, A., et al. (2018). Nitrogen-rich organic soils under warm well-drained conditions are global nitrous oxide emission hotspots. *Nat. Commun.* 9 (1), 1135–1138. doi:10.1038/s41467-018-03540-1

Peacock, M., Evans, C. D., Fenner, N., and Freeman, C. (2013). Natural revegetation of bog pools after peatland restoration involving ditch blocking—the influence of pool depth and implications for carbon cycling. *Ecol. Eng.* 57, 297–301. doi:10.1016/j.ecoleng.2013.04.055

Perianes-Rodriguez, A., Waltman, L., and Van Eck, N. J. (2016). Constructing bibliometric networks: A comparison between full and fractional counting. *J. Inf.* 10 (4), 1178–1195. doi:10.1016/j.joi.2016.10.006

Piirainen, S., Domisch, T., Moilanen, M., and Nieminen, M. (2013). Long-term effects of ash fertilization on runoff water quality from drained peatland forests. *For. Ecol. Manag.* 287, 53–66. doi:10.1016/j.foreco.2012.09.014

Pike, J. (2021). *Peat and peatlands*.

Poddubny, A. G., and Galat, D. L. (1995). Habitat associations of upper Volga River fishes: Effects of reservoirs. *Regul. Rivers Res. Mgmt.* 11 (1), 67–84. doi:10.1002/rrr.3450110107

Prévost, M., Plamondon, A. P., and Belleau, P. (1999). Effects of drainage of a forested peatland on water quality and quantity. *J. Hydrology* 214 (1-4), 130–143. doi:10.1016/s0022-1694(98)00281-9

Price, J. S. (1996). Hydrology and microclimate of a partly restored cutover bog. *Québec. Hydrol. Proc.* 10, 1263–1272. doi:10.1002/(SICI)1099-1085(199610)10:10<1263::AID-HYP458>3.0.CO;2–1

Price, J. S., Heathwaite, A. L., and Baird, A. J. (2003). Hydrological processes in abandoned and restored peatlands: An overview of management approaches. *Wetl. Ecol. Manag.* 11 (1–2), 65–83. doi:10.1023/A:1022046409485

Ramchunder, S. J., Brown, L. E., and Holden, J. (2009). Environmental effects of drainage, drain-blocking and prescribed vegetation burning in UK upland peatlands. *Prog. Phys. Geogr. Earth Environ.* 33 (1), 49–79. doi:10.1177/0309133309105245

Ravikumar, S., Agrahari, A., and Singh, S. N. (2015). Mapping the intellectual structure of scientometrics: A co-word analysis of the journal scientometrics (2005–2010). *Scientometrics* 102 (1), 929–955. doi:10.1007/s11192-014-1402-8

Renou-Wilson, F., Barry, C., Müller, C., and Wilson, D. (2014). The impacts of drainage, nutrient status and management practice on the full carbon balance of grasslands on organic soils in a maritime temperate zone. *Biogeosciences* 11 (16), 4361–4379. doi:10.5194/bg-11-4361-2014

Richert, M., Dietrich, O., Koppisch, D., and Roth, S. (2000). The influence of rewetting on vegetation development and decomposition in a degraded fen. *Restor. Ecol.* 8 (2), 186–195. doi:10.1046/j.1526-100x.2000.80026.x

Rieley, J. O., Wüst, R. A. J., Jauhiainen, J., Page, S. E., Wösten, J. H. M., Hooijer, A., et al. (2008). "Tropical peatlands: Carbon stores, carbon gas emissions and contribution to climate change processes," in *Peatlands and climate change* (Finland: International Peat Society), 148–181.

Rydin, H., Jeglum, J. K., and Bennett, K. D. (2013). *The biology of peatlands*, 2e. Oxford University Press.

Salmah, Z., Spoor, G., Zahari, A. B., and Welch, D. N. (1991). "Importance of water management in peat soil at farm level, level," in Proc. Of the inter. Trop. Peatland, May 6–10, 1991, Kuching, Sarawak, Malaysia. Editor B. Y. Aminuddin, et al. (MARDI-Dep. Agric.), 228–238.

Salmon, V. G., Brice, D. J., Bridgham, S., Childs, J., Graham, J., Griffiths, N. A., et al. (2021). Nitrogen and phosphorus cycling in an ombrotrophic peatland: A benchmark for assessing change. *Plant Soil* 466 (1), 649–674. doi:10.1007/s11104-021-05065-x

Şenel, E. (2019). Evolution of homeopathy: A scientometric analysis of global homeopathy literature between 1975 and 2017. *Complementary Ther. Clin. Pract.* 34, 165–173. doi:10.1016/j.ctcp.2018.11.018

Shrivastava, R., and Mahajan, P. (2016). Artificial intelligence research in India: A scientometric analysis. *Sci. Technol. Libr.* 35 (2), 136–151. doi:10.1080/0194262x.2016.1181023

Sirin, A., Minayeva, T., Vozbrannaya, A., and Bartalev, S. (2011). How to avoid peat fires? *Sci. Russ.* 2, 13–21.

Sjörs, H., and Gunnarsson, U. (2002). Calcium and pH in north and central Swedish mire waters. *J. Ecol.* 90, 650–657. doi:10.1046/j.1365-2745.2002.00701.x

Sjörs, H. (1980). Peat on earth: multiple use or conservation? *Ambio* 9 (6), 303–308. http://www.jstor.org/stable/4312610

Sjörs, H., and Sjors, H. (1950). On the relation between vegetation and electrolytes in north Swedish mire waters. *Oikos* 2 (2), 241–258. doi:10.2307/3564795

Skaggs, R. W., Breve, M. A., and Gilliam, J. W. (1994). Hydrologic and water quality impacts of agricultural drainage. *Crit. Rev. Environ. Sci. Technol.* 24 (1), 1–32. doi:10.1080/10643389409388459

Smith, K. A., and Conen, F. (2004). Impacts of land management on fluxes of trace greenhouse gases. *Soil use Manag.* 20 (2), 255–263. doi:10.1111/j.1475-2743.2004.tb00366.x

Spitzer, K., and Danks, H. V. (2006). Insect biodiversity of boreal peat bogs. *Annu. Rev. Entomol.* 51, 137–161. doi:10.1146/annurev.ento.51.110104.151036

Steffens, P. (1996). *Mires and peat resources in Germany*.

Stewart, A. J., and Lance, A. N. (1991). Effects of moor-draining on the hydrology and vegetation of northern Pennine blanket bog. *J. Appl. Ecol.* 28, 1105–1117. doi:10.2307/2404228

Strack, M., Waddington, J. M., Bourbonniere, R. A., Buckton, E. L., Shaw, K., Whittington, P., et al. (2008). Effect of water table drawdown on peatland dissolved organic carbon export and dynamics. *Hydrol. Process.* 22 (17), 3373–3385. doi:10.1002/hyp.6931

Strack, M., and Zuback, Y. C. A. (2013). Annual carbon balance of a peatland 10 yr following restoration. *Biogeosciences* 10 (5), 2885–2896. doi:10.5194/bg-10-2885-2013

Strack, M., Keith, A. M., and Xu, B. (2014). Growing season carbon dioxide and methane exchange at a restored peatland on the Western Boreal Plain. *Ecol. Eng.* 64, 231–239. doi:10.1016/j.ecoleng.2013.12.013

Su, H. N., and Lee, P. C. (2010). Mapping knowledge structure by keyword co-occurrence: A first look at journal papers in technology foresight. *Scientometrics* 85 (1), 65–79. doi:10.1007/s11192-010-0259-8

Tanneberger, F., and Wichtmann, W. (2011). *Carbon credits from peatland rewetting: Climate, biodiversity, land use*. Stuttgart: Schweizerbart Science Publishers.

Tarnocai, C., and Stolbovoy, V. (2006). Northern peatlands: Their characteristics, development and sensitivity to climate change. *Dev. earth Surf. Process.* 9, 17–51. doi:10.1016/S0928-2025(06)09002-X

Tarnocai, C. (2006). The effect of climate change on carbon in Canadian peatlands. *Glob. Planet. Change* 53 (4), 222–232. doi:10.1016/j.gloplacha.2006.03.012

Tfaily, M. M., Hamdan, R., Corbett, J. E., Chanton, J. P., Glaser, P. H., and Cooper, W. T. (2013). Investigating dissolved organic matter decomposition in northern peatlands using complimentary analytical techniques. *Geochimica Cosmochimica Acta* 112, 116–129. doi:10.1016/j.gca.2013.03.002

Tiemeyer, B., Frings, J., Kahle, P., Köhne, S., and Lennartz, B. (2007). A comprehensive study of nutrient losses, soil properties and groundwater concentrations in a degraded peatland used as an intensive meadow - implications for re-wetting. *J. Hydrol. X.* 345, 80–101. doi:10.1016/j.jhydrol.2007.08.002

Tuittila, E. S., Komulainen, V. M., Vasander, H., and Laine, J. (1999). Restored cut-away peatland as a sink for atmospheric CO2. *Oecologia* 120 (4), 563–574. doi:10.1007/s004420050891

Tuittila, E. S., Vasander, H., and Laine, J. (2000). Impact of rewetting on the vegetation of a cut-away peatland. *Appl. Veg. Sci.* 3 (2), 205–212. doi:10.2307/1478999

Turetsky, M. R., Benscoter, B., Page, S., Rein, G., Van Der Werf, G. R., and Watts, A. (2015). Global vulnerability of peatlands to fire and carbon loss. *Nat. Geosci.* 8 (1), 11–14. doi:10.1038/ngeo2325

Valat, B., Jouany, C., and Riviere, L. M. (1991). Characterization of the wetting properties of air-dried peats and composts. *Soil Sci.* 173 (5), 100–107. doi:10.1097/00010694-199108000-00006

Van Diggelen, R., Grootjans, A. P., Kemmers, R. H., Kooijman, A. M., Succow, M., De Vries, N. P. J., et al. (1991). Hydro-ecological analysis of the fen system Lieper Posse, eastern Germany. *J. Veg. Sci.* 2 (4), 465–476. doi:10.2307/3236028

Van Dijk, J., Stroetenga, M., Van Bodegom, P. M., and Aerts, R. (2007). The contribution of rewetting to vegetation restoration of degraded peat meadows. *Appl. Veg. Sci.* 10 (3), 315–324. doi:10.1111/j.1654-109x.2007.tb00430.x

Van Eck, N. J., and Waltman, L. (2013). 1. Leiden, 1–53. VOS viewer manual *Univeristeit Leiden,* 1.

Van Eck, N. J., and Waltman, L. (2014). "Visualising bibliometric networks," in *Measuring scholarly impact* (Cham: Springer), 285–320.

Van Eck, N. J., and Waltman, L. (2020). *VOSviewer manual: Manual for VOSviewer version 1.6. 15*. Leiden: Centre for Science and Technology Studies (CWTS) of Leiden University. https://www.vosviewer.com/documentation/Manual_VOSviewer_1.6.13.pdf

van Eck, N., Waltman, L., Noyons, E., and Buter, R. (2010). Automatic term identification for bibliometric mapping. *Scientometrics* 82 (3), 581–596. doi:10.1007/s11192-010-0173-0

Vanselow-Algan, M., Schmidt, S. R., Greven, M., Fiencke, C., Kutzbach, L., and Pfeiffer, E. M. (2015). High methane emissions dominated annual greenhouse gas balances 30 years after bog rewetting. *Biogeosciences* 12 (14), 4361–4371. doi:10.5194/bg-12-4361-2015

Vasander, H., Tuittila, E. S., Lode, E., Lundin, L., Ilomets, M., Sallantaus, T., et al. (2003). Status and restoration of peatlands in northern Europe. *Wetl. Ecol. Manag.* 11 (1), 51–63. doi:10.1023/a:1022061622602

Waddington, J. M., Strack, M., and Greenwood, M. J. (2010). Toward restoring the net carbon sink function of degraded peatlands: Short-term response in CO2 exchange to ecosystem-scale Restoration. *J. Geophys. Res.* 115 (G1), G01008. doi:10.1029/2009jg001090

Waddington, J. M., and Price, J. S. (2000). Effect of peatland drainage, harvesting, and Restoration on atmospheric water and carbon exchange. *Phys. Geogr.* 21 (5), 433–451. doi:10.1080/02723646.2000.10642719

Waddington, J. M., and Warner, K. (2001). Atmospheric CO2 sequestration in restored mined peatlands. *Ecoscience* 8 (3), 359–368. doi:10.1080/11956860.2001.11682664

Wallage, Z. E., Holden, J., and McDonald, A. T. (2006). Drain blocking: An effective treatment for reducing dissolved organic carbon loss and water discolouration in a drained peatland. *Sci. total Environ.* 367 (2-3), 811–821. doi:10.1016/j.scitotenv.2006.02.010

Wang, H., Yu, L., Zhang, Z., Liu, W., Chen, L., Cao, G., et al. (2017). Molecular mechanisms of water table lowering and nitrogen deposition in affecting greenhouse gas emissions from a Tibetan alpine wetland. *Glob. Chang. Biol.* 23, 815–829. doi:10.1111/gcb.13467

Warner, B. G., and Asada, T. (2006). Biological diversity of peatlands in Canada. *Aquatic Sci.* 68 (3), 240–253. doi:10.1007/s00027-006-0853-2

Williams, R., Runco, M. A., and Berlow, E. (2016). Mapping the themes, impact, and cohesion of creativity research over the last 25 years. *Creativity Res. J.* 28 (4), 385–394. doi:10.1080/10400419.2016.1230358

Wilson, D., Renou-Wilson, F., Farrell, C., Bullock, C., and Müller, C. (2012). "Carbon restore – The potential of Irish peatlands for carbon uptake and storage," in *Climate change research programme* (Johnstown Castle, Co. Wexford, Ireland: prepared for the Environmental Protection Agency). Report Series No.17.

Wilson, J. D., Anderson, R., Bailey, S., Chetcuti, J., Cowie, N. R., Hancock, M. H., et al. (2014). Modelling edge effects of mature forest plantations on peatland waders informs landscape-scale conservation. *J. Appl. Ecol.* 51, 204–213. doi:10.1111/1365-2664.12173

Wilson, D., Dixon, S. D., Artz, R. R. E., Smith, T. E. L., Evans, C. D., Owen, H. J. F., et al. (2015). Derivation of greenhouse gas emission factors for peatlands managed for extraction in the Republic of Ireland and the United Kingdom. *Biogeosciences* 12 (18), 5291–5308. doi:10.5194/bg-12-5291-2015

Wilson, L., Wilson, J., Holden, J., Johnstone, I., Armstrong, A., and Morris, M. (2010). Recovery of water tables in Welsh blanket bog after drain blocking: discharge rates, time scales and the influence of local conditions. *J. Hydrol.* 391 (3–4), 377–386. doi:10.1016/j.jhydrol.2010.07.042

Wösten, J. H. M., Clymans, E., Page, S. E., Rieley, J. O., and Limin, S. H. (2008). Peat–water interrelationships in a tropical peatland ecosystem in Southeast Asia. *Catena* 73 (2), 212–224. doi:10.1016/j.catena.2007.07.010

Wrage-Mönnig, N., Horn, M. A., Well, R., Müller, C., Velthof, G., and Oenema, O. (2018). The role of nitrifier denitrification in the production of nitrous oxide revisited. *Soil Biol. Biochem.* 123, A3–A16. doi:10.1016/j.soilbio.2018.03.020

Wuni, I. Y., Shen, G. Q., and Osei-Kyei, R. (2019). Scientometric review of global research trends on green buildings in construction journals from 1992 to 2018. *Energy Build.* 190, 69–85. doi:10.1016/j.enbuild.2019.02.010

Xu, J., Morris, P. J., Liu, J., and Holden, J. (2018). PEATMAP: Refining estimates of global peatland distribution based on a meta-analysis. *Catena* 160, 134–140. doi:10.1016/j.catena.2017.09.010

Xu, Z., Wang, S., Wang, Z., Dong, Y., Zhang, Y., Liu, S., et al. (2021). Effect of drainage on microbial enzyme activities and communities dependent on depth in peatland soil. *Biogeochemistry* 155 (3), 323–341. doi:10.1007/s10533-021-00828-1

Yu, D., and Liao, H. (2016). Visualization and quantitative research on intuitionistic fuzzy studies. *J. Intelligent Fuzzy Syst.* 30 (6), 3653–3663. doi:10.3233/ifs-162111

Yuwati, T. W., Rachmanadi, D., Turjaman, M., Indrajaya, Y., Nugroho, H. Y. S. H., Qirom, M. A., et al. (2021). Restoration of degraded tropical peatland in Indonesia: A review. *Land* 10 (11), 1170. doi:10.3390/land10111170

Zeng, X., and Gao, Y. (2016). Short-term effects of drying and rewetting on CO2 and CH4 emissions from high-altitude peatlands on the Tibetan Plateau. *Atmosphere* 7 (11), 148. doi:10.3390/atmos7110148

Zhang, Y., Huang, K., Yu, Y., and Yang, B. (2017). Mapping of water footprint research: A bibliometric analysis during 2006–2015. *J. Clean. Prod.* 149, 70–79.

Zhang, B., Ahmad, W., Ahmad, A., Aslam, F., and Joyklad, P. (2021). A scientometric analysis approach to analyse the present research on recycled aggregate concrete. *J. Build. Eng.* 46, 103679. doi:10.1016/j.jobe.2021.103679

Zheng, B., Ciais, P., Chevallier, F., Chuvieco, E., Chen, Y., and Yang, H. (2021). Increasing forest fire emissions despite the decline in global burned area. *Sci. Adv.* 7 (39), eabh2646. doi:10.1126/sciadv.abh2646

# Frontiers in
# Ecology and Evolution

**Ecological and evolutionary research into our natural and anthropogenic world**

This multidisciplinary journal covers the spectrum of ecological and evolutionary inquiry. It provides insights into our natural and anthropogenic world, and how it can best be managed.

---

## Discover the latest Research Topics

See more →

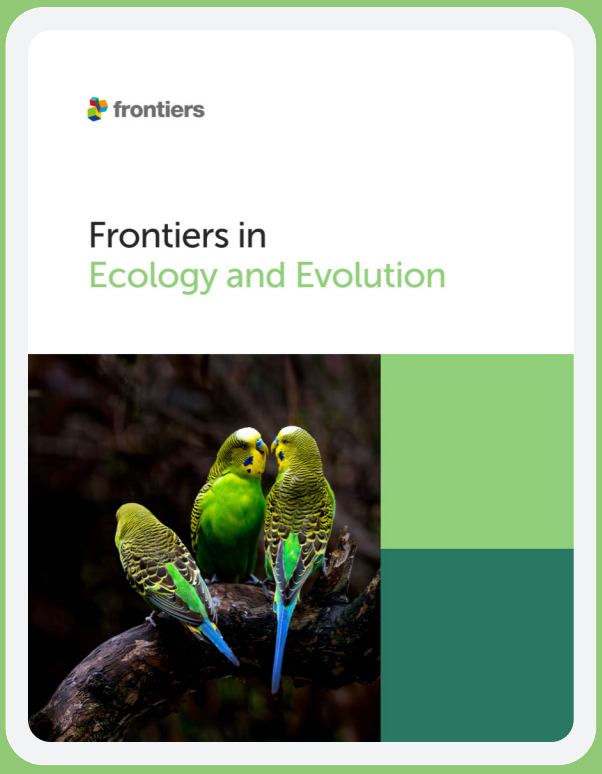


**Frontiers**

Avenue du Tribunal-Fédéral 34
1005 Lausanne, Switzerland
frontiersin.org

**Contact us**

+41 (0)21 510 17 00
frontiersin.org/about/contact